Model Calculations of the Atmospheric Effects of Supersonic Aviation Which Were Used in the IPCC Special Report on Aviation and the Global Atmosphere

Lead Author:
Debra Weisenstein, AER, Inc., U.S.A.

Technical Support:
Karen Sage, NASA Langley Research Center, U.S.A.
Donald Brown, NASA Langley Research Center, U.S.A.

Co-Authors:
Richard S. Eckman, NASA Langley Research Center, U.S.A.
Malcolm K.W. Ko, AER, Inc., U.S.A.

Contributors:
Steven L. Baughcum, Boeing Company, U.S.A.
Martyn Chipperfield, University of Cambridge, U.K.
Michael Gauss, University of Oslo, Norway
William L. Grose, NASA Langley Research Center, U.S.A.
Robert S. Harwood, University of Edinburgh, U.K.
Ivar Isaksen, University of Oslo, Norway
Charles H. Jackman, NASA Goddard Space Flight Center, U.S.A.
Douglas E. Kinnison, Lawrence Livermore National Laboratory, U.S.A.
Giovanni Pitari, University L'Aquila, Italy
Helen Rogers, University of Cambridge, U.K.
Courtney J. Scott, AER, Inc., U.S.A.
Peter F. Vohralik, CSIRO, Australia
Vicky West, University of Edinburgh, U.K.

May 1999

Rationale

This report is intended to expand upon the IPCC Special Report on Aviation and the Global Atmosphere. It provides additional detail regarding the supersonic emission scenario calculations presented in Chapter 4—Modeling the Future Atmosphere. Due to the space limitations in that document, detailed plots and discussion for a majority of the model calculations were omitted. This document is intended to fill that gap and has been compiled for two reasons: (1) to aid those called upon to review the IPCC Special Report, and (2) to archive and document the calculations performed by nine modeling groups for up to 50 scenarios each. This document does not attempt to provide a synthesis of the modeling results or draw conclusions regarding the impact of aircraft on the atmosphere. That function is provided by the IPCC report.

The model descriptions and model results presented in this document represent the state of those models in 1997 when the calculations were performed. Because models are continually evolving and undergoing further development, these results should be considered as a historical snapshot. Please do not cite results presented herein without first obtaining permission from the group which performed the calculations.

Contents

1 Model Descriptions **4**

1.1 Transport Formulation . . . 4

1.1.1 Domain and Resolution . . . 4

1.1.2 Temperature and Transport Parameters . . . 6

1.2 Chemistry Treatment . . . 11

1.2.1 Gas-phase Chemistry . . . 11

1.2.2 Heterogeneous Chemistry . . . 11

1.2.2.1 Reactions on Sulfate Aerosol . . . 11

1.2.2.2 Reactions on PSCs and Cold Sulfate Aerosol . . . 12

1.2.3 Chemistry Solvers . . . 14

1.3 Sources and Sinks for Some Species . . . 14

2 Emission Scenarios **22**

2.1 Fuel Use . . . 22

2.2 HSCT Emissions . . . 23

2.3 Sulfur Emission Scenarios . . . 24

3 Background Atmospheres **44**

3.1 Scenario D Results . . . 44

3.2 Scenario D3 Results . . . 96

3.3 Scenario D4 Results . . . 101

3.4 Scenario D5 Results . . . 111

3.5 Scenario D6 Results . . . 117

3.6 Scenario D7 Results . . . 123

3.7 Scenario D8 Results . . . 129

3.8 Scenario D9 Results . . . 133

3.9 Scenario F Results . . . 141

3.10 Scenario G Results . . . 145

4 HSCT Perturbations for 2015 **150**

4.1 H_2O Perturbations . . . 152

4.2 NO_y Perturbations . . . 175

4.3 O_3 Perturbations . . . 213

4.3.1 Base Scenarios (S1a-e,i,j) . . . 213

4.3.2 Scenarios with Sulfur Emissions (S1f-h,k,l) . . . 286

4.3.3 Scenarios with Modified Cruise Altitude (S2a-e) . . . 323

4.3.4 Scenarios with Enhanced Background Aerosol (S3a-f) . . . 353

4.3.5 Scenarios without PSC Formulations (S4a-c) . . . 391

4.3.6 Scenarios with Different Cl_y Loadings (S5a,b, S6a,b) . . . 404

4.3.7 Scenarios with Interactive Microphysics (S7a-d, S8a) . . . 425

5 HSCT Perturbations for 2050 **454**
5.1 H_2O Perturbations . . . 456
5.2 NO_y Perturbations . . . 460
5.3 O_3 Perturbations . . . 467
5.3.1 Base Scenarios (S9a,b,d,g) . . . 468
5.3.2 Scenarios with Sulfur Emissions (S9c,e,f,h) . . . 485
5.3.3 Scenarios with Modified Cruise Altitude (S10a-d) . . . 503
5.3.4 Scenarios with Modified Subsonic Fleets (S11a, S12a) . . . 520

Chapter 4

HSCT Perturbations for 2015

A total of 35 scenarios for the 2015 atmosphere were used in the IPCC supersonic aircraft assessment. Not all models performed all scenario calculations. The scenarios were chosen to explore the effects of parametric modifications in the HSCT aircraft fleet, such as EI(NO_x), fleet size, cruise altitude, EI(SO_2), and SO_2 gas-to-particle conversion fraction. The effect of modifications in the background atmosphere was also explored by varying the background aerosol surface area density, the chlorine loading level, the PSC parameterization, and the microphysical treatment. A summary of the scenarios considered, along with the scenario designations, for 2015 is given in Table 4.1. The reference atmosphere used for each scenario is listed in the table. Perturbations are given relative to the reference scenario, which includes identical boundary conditions and the same model formulation, but omits the HSCT fleet.

Table 4.1: Specifications for Supersonic Aircraft Emission Scenarios in 2015

Scenario	Cl_y (ppbv)	Fleet Size	EI(NO_x)	Cruise Altitude	SAD Description	Special	Ref. Atm.
S1a	3.0	500	5	Std	SA0	No H_2O	D
S1b	3.0	500	0	Std	SA0		D
S1c	3.0	500	5	Std	SA0		D
S1d	3.0	500	10	Std	SA0		D
S1e	3.0	500	15	Std	SA0		D
S1f	3.0	500	5	Std	SA1		D
S1g	3.0	500	10	Std	SA1		D
S1h	3.0	500	5	Std	SA3		D
S1i	3.0	1000	5	Std	SA0		D
S1j	3.0	1000	10	Std	SA0		D
S1k	3.0	500	5	Std	SA5		D
S1l	3.0	500	5	Std	SA7		D
S2a	3.0	500	5	+2 km	SA0		D
S2b	3.0	500	5	-2 km	SA0		D
S2c	3.0	500	10	-2 km	SA0		D
S2d	3.0	500	15	-2 km	SA0		D
S2e	3.0	1000	5	-2 km	SA0		D
S3a	3.0	500	0	Std	4xSA0		D3
S3b	3.0	500	5	Std	4xSA0		D3
S3c	3.0	500	10	Std	4xSA0		D3
S3d	3.0	500	15	Std	4xSA0		D3
S3e	3.0	500	5	Std	4xSA0+(SA1-SA0)		D3
S3f	3.0	500	5	Std	4xSA0+(SA3-SA0)		D3
S4a	3.0	500	0	Std	SA0	No PSCs	D4
S4b	3.0	500	5	Std	SA0	No PSCs	D4
S4c	3.0	500	5	Std	SA0	No PSCs, No H_2O	D4
S5a	1.0	500	5	Std	SA0		D5
S5b	1.0	500	5	Std	SA1		D5
S6a	4.0	500	5	Std	SA0		D6
S6b	4.0	500	5	Std	SA1		D6
S7a	3.0	500	5	Std	50% Particles	Microphysics	D7
S7b	3.0	500	5	+2 km	50% Particles	Microphysics	D7
S7c	3.0	500	5	-2 km	50% Particles	Microphysics	D7
S7d	3.0	500	10	Std	50% Particles	Microphysics	D7
S8a	3.0	500	5	Std	100% Particles	Microphysics	D8

4.1 H_2O Perturbations

Because EI(H_2O) is invariant, only modifications in fleet size and cruise altitude impact the HSCT perturbation to stratospheric water vapor. Figure 4.1 shows the change in H_2O in ppmv for June due to emission of H_2O by a fleet of 500 HSCT aircraft operating in 2015 (Scenario S1c). The maximum perturbation is located in the northern hemisphere lower stratosphere for all models. The LARC model produces the smallest maximum perturbations to H_2O of 0.2 ppmv. However, this model does not calculate H_2O mixing ratios in the stratosphere, but instead solves for the HSCT-emitted H_2O as a separate species and adds the perturbation to the otherwise fixed background H_2O. All other models calculate maximum H_2O perturbations of between 0.4 ppmv and 0.6 ppmv with the CSIRO, SCTM1, and SLIMCAT models at the lower end of this range. Differences in the way the models treat tropospheric H_2O has an impact on these calculated perturbations. Some models fix H_2O in the entire troposphere, while others fix H_2O only in the lower troposphere.

Vertical profiles of H_2O perturbation at 45^oN, the equator, and 45^oS are shown in Figures 4.2-4.4 for Scenario S1c. Profiles of all models are included in each plot to allow easy comparison. The GSFC model calculates the greatest perturbation in H_2O in the middle and upper stratosphere (above 25 km) at all latitudes and also the largest perturbation in the lower stratosphere at 45^oN. This indicates that the GSFC model has the longest residence time for the aircraft-emitted H_2O. The AER, UNIVAQ, and LLNL models have lower stratospheric H_2O perturbations at 45^oN only slightly less than the GSFC model, but much lower perturbations in the middle and upper stratosphere. The SCTM1 model calculates the lowest H_2O perturbation in the middle and upper stratosphere at all latitudes. The SLIMCAT model, though it has one of the lower perturbations at 45^oN in the lower stratosphere, has a perturbation in the middle stratosphere at the equator and 45^oS comparable with the GSFC model. This model must have a long stratospheric residence time for emitted H_2O, but rapidly transports the emitted material out of the northern hemisphere lower stratosphere.

Increases in H_2O due to emission by a fleet of 1000 HSCT aircraft in 2015 (Scenario S1i) are shown in Figure 4.5 for June conditions. Vertical profiles of this perturbation at 45^oN, the equator, and 45^oS are shown in Figures 4.6-4.8. Because the 1000 HSCT fleet is not simply scaled from the 500 HSCT fleet, but represents a different economic projection, the geographical distribution of emissions is different. This is apparent in the GSFC model results at 45^oN, which peak at 18 km for the 500 aircraft fleet and at 20 km for the 1000 aircraft fleet.

Scenario S2a represents a 500 aircraft HSCT fleet with cruise altitude adjusted upward by 2 km. H_2O perturbations for this scenario are shown in Figure 4.9 for June conditions of 2015. While the quantity of emitted H_2O is identical to that from Scenario S1c, the perturbation to H_2O is enhanced by 30-100%, depending on the model. The stratospheric residence time of emitted materials is considerably enhanced at higher emission altitudes relative to lower altitudes.

Vertical profiles of H_2O perturbation at 45^oN, the equator, and 45^oS are shown in Figures 4.10-4.12 for Scenario S2a. Compared with similar figures for Scenario S1c (Figures 4.2-4.4), it can be seen the the maximum perturbation at 45^oN occurs at 20-22 km rather than 18-20 km, and the relative perturbations between models are somewhat different. At 45^oN, the peak perturbation in the GSFC model is 30% greater than any other model for Scenario S2a, but only 15% greater than any other model for Scenario S1c.

Scenario S2b represents a 500 aircraft HSCT fleet with cruise altitude adjusted downward by 2 km. Figure 4.13 shows perturbations in H_2O for June conditions in 2015 from this emission scenario. The H_2O perturbations are reduced by 40-60% relative to the S1c-D scenario because the emissions are closer to the tropopause and more readily removed from the stratosphere. The maximum perturbations at 45^oN are 0.2 ppmv for the AER, CSIRO, and THINAIR models; 0.4 ppmv for the GSFC and LLNL models; and 0.5 ppmv for the UNIVAQ model.

Vertical profiles of H_2O perturbation at 45^oN, the equator, and 45^oS are shown in Figures 4.14-4.16 for Scenario S2b. Maximum perturbation at 45^oN occurs at 16 km for this scenario. The UNIVAQ model calculated the largest perturbation in the 12-20 km altitude region. The GSFC and UNIVAQ models calculate much larger perturbations than the other models from 8-12 km. Perturbations in the upper stratosphere are only 0.1-0.2 ppmv at 45^oN and 0.1 ppmv at the equator and 45^oS.

Figure 4.17 shows H_2O perturbations from Scenario S2e-D, representing 1000 HSCT aircraft operating at 2 km below the nominal cruise altitude. The perturbation is roughly linear with fleet size (compare with Scenario S2b). Compared with Scenario S1i (same fleet size but different cruise altitude), the H_2O

perturbations are reduced by 50% for the AER and CSIRO models and by 30% for the GSFC and LLNL models due to the lowered cruise altitude. Vertical profiles of the H_2O perturbation at 45^oN, the equator, and 45^oS are shown in Figures 4.18-4.20 for this scenario.

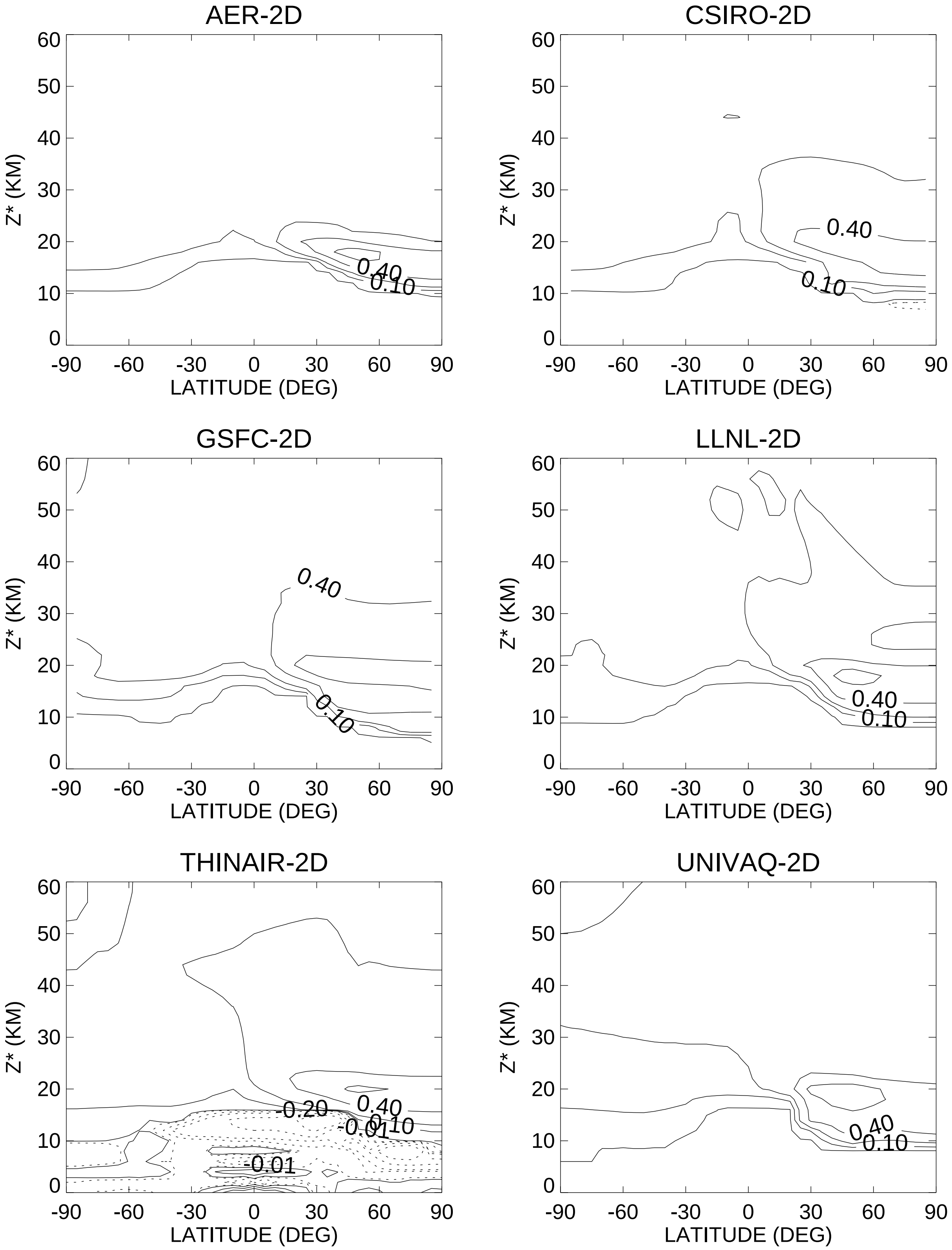

Figure 4.1: Calculated perturbation to H_2O (ppmv) as a function of latitude and altitude in June of 2015 due to H_2O emissions from a fleet of 500 HSCT aircraft under Scenario S1c relative to Scenario D. Contours are -0.6, -0.4, -0.2, -0.1, -0.01, 0.01, 0.1, 0.2, 0.4, 0.6 ppmv.

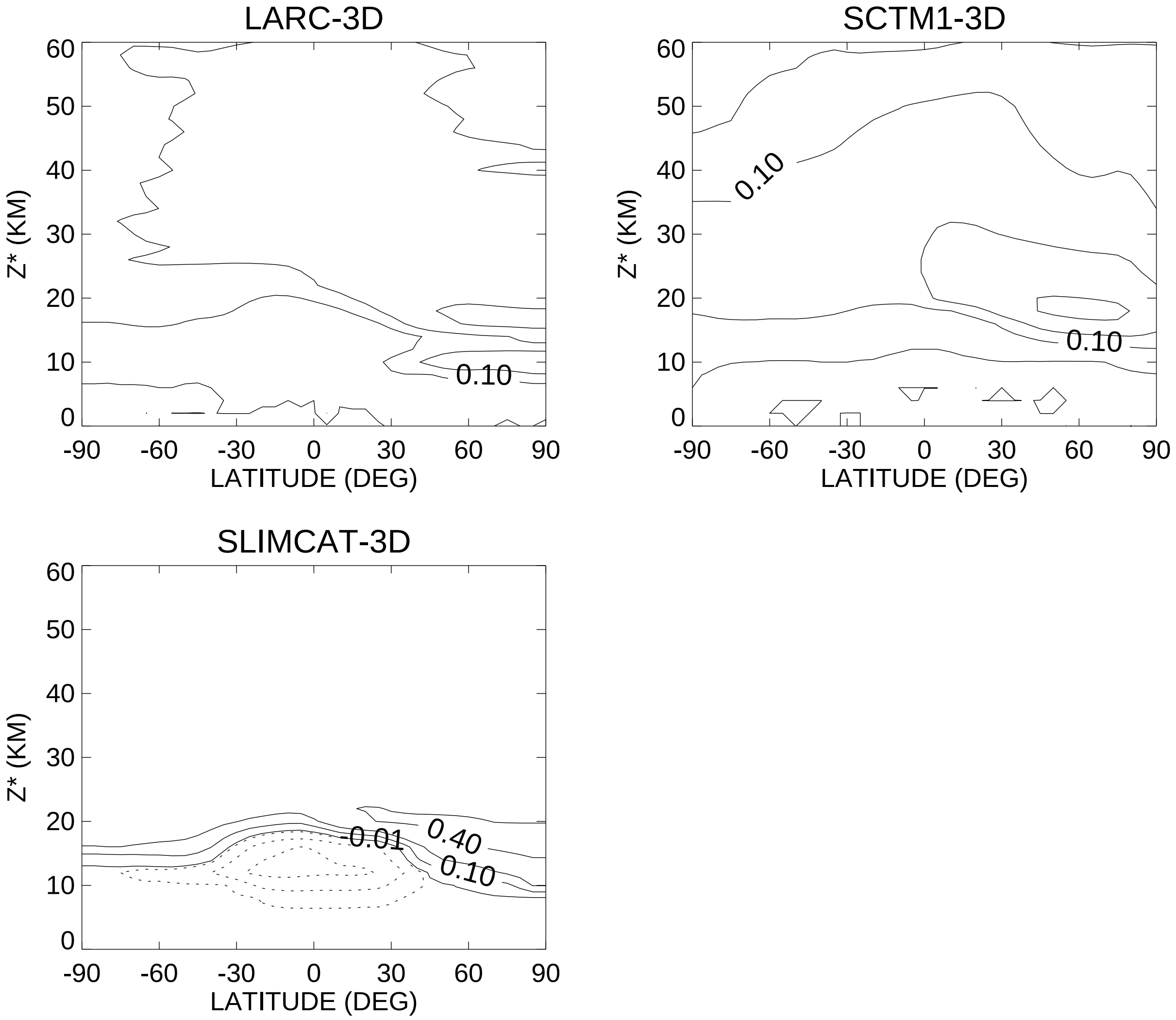

Figure 4.1: continued

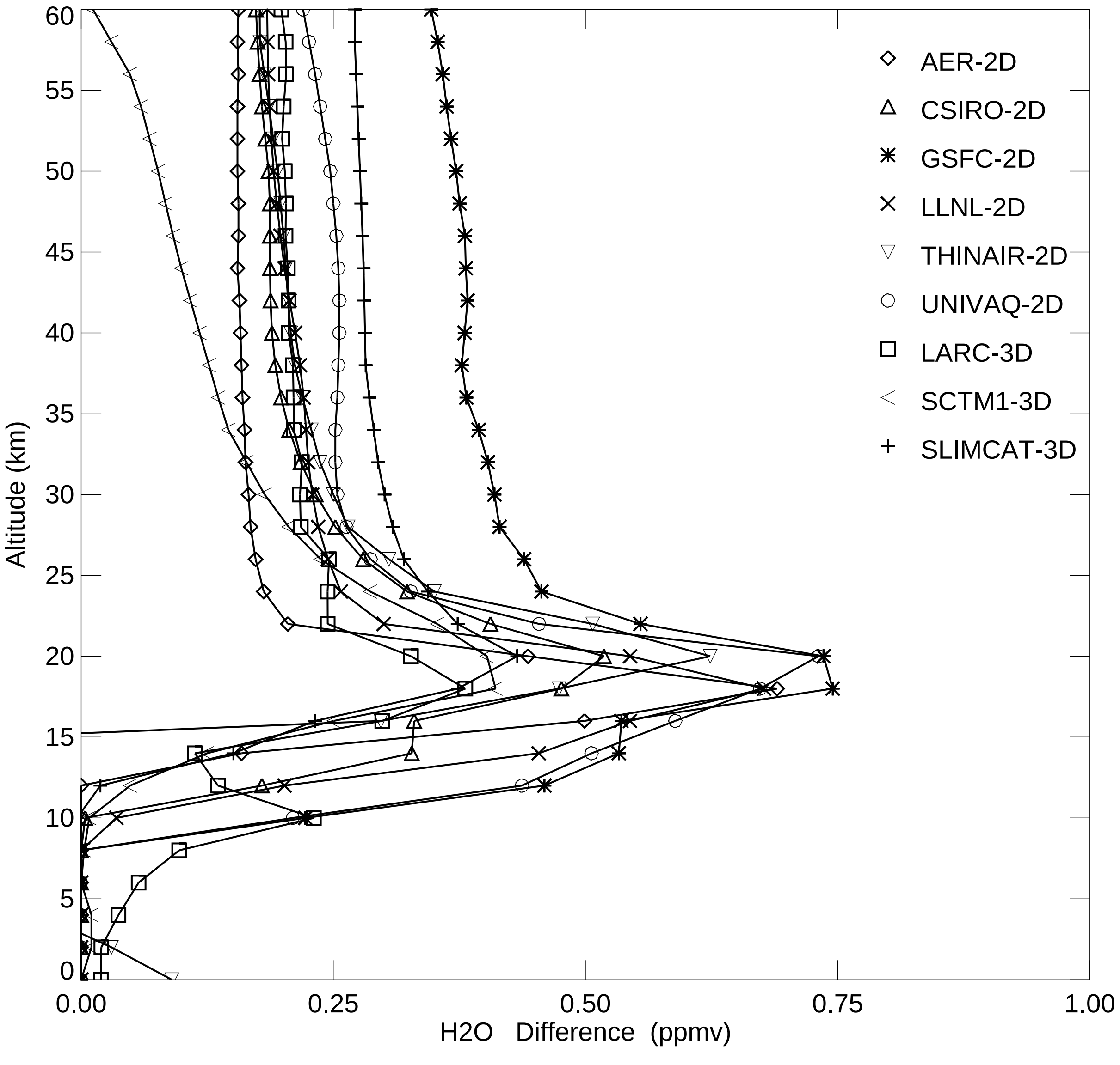

Figure 4.2: Calculated perturbations to H_2O (ppmv) as a function of altitude at 45^{o}N in June of 2015 due to H_2O emissions from a fleet of 500 HSCT aircraft under Scenario S1c relative to Scenario D.

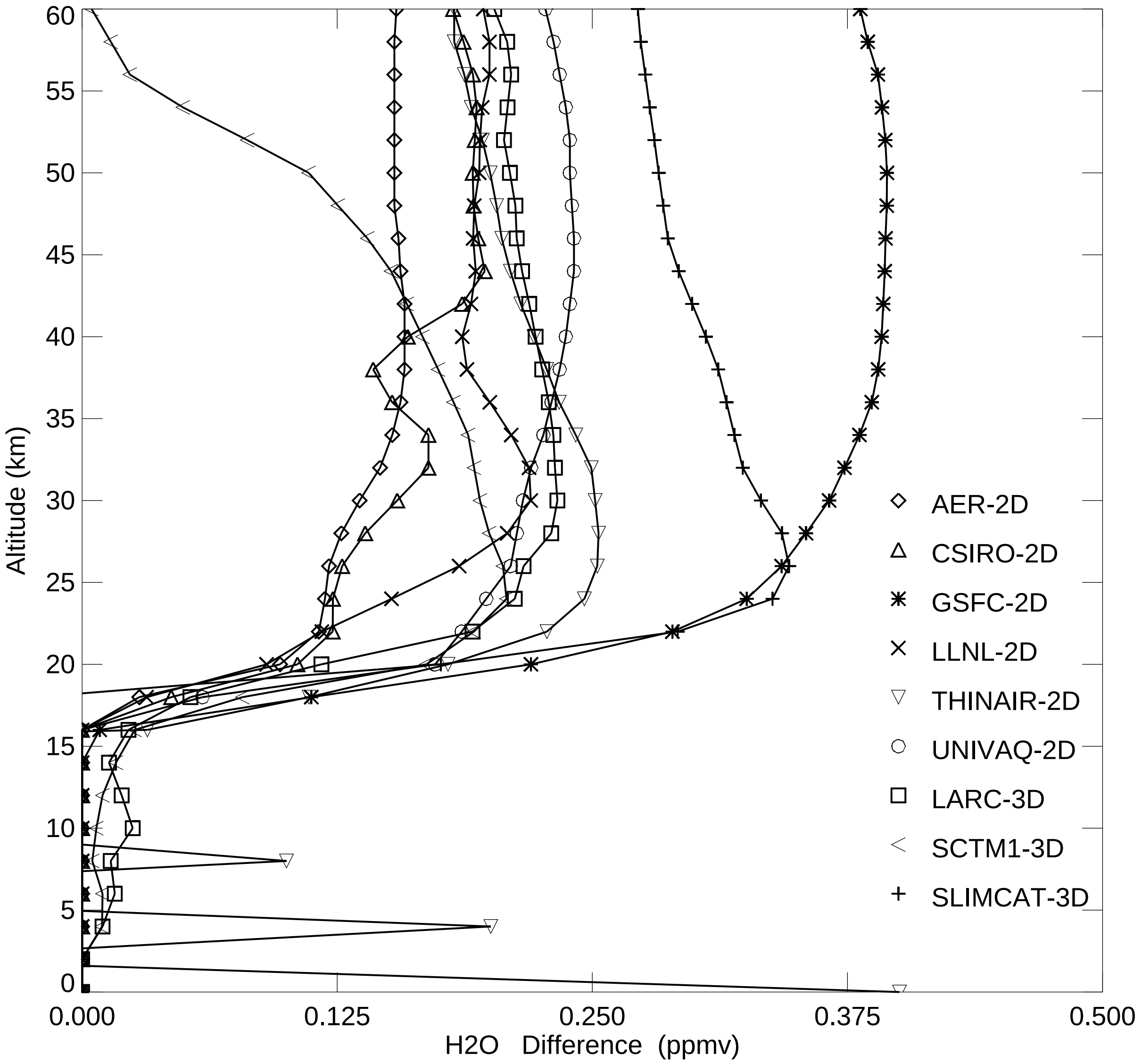

Figure 4.3: Calculated perturbations to H_2O (ppmv) as a function of altitude at the equator in June of 2015 due to H_2O emissions from a fleet of 500 HSCT aircraft under Scenario S1c relative to Scenario D.

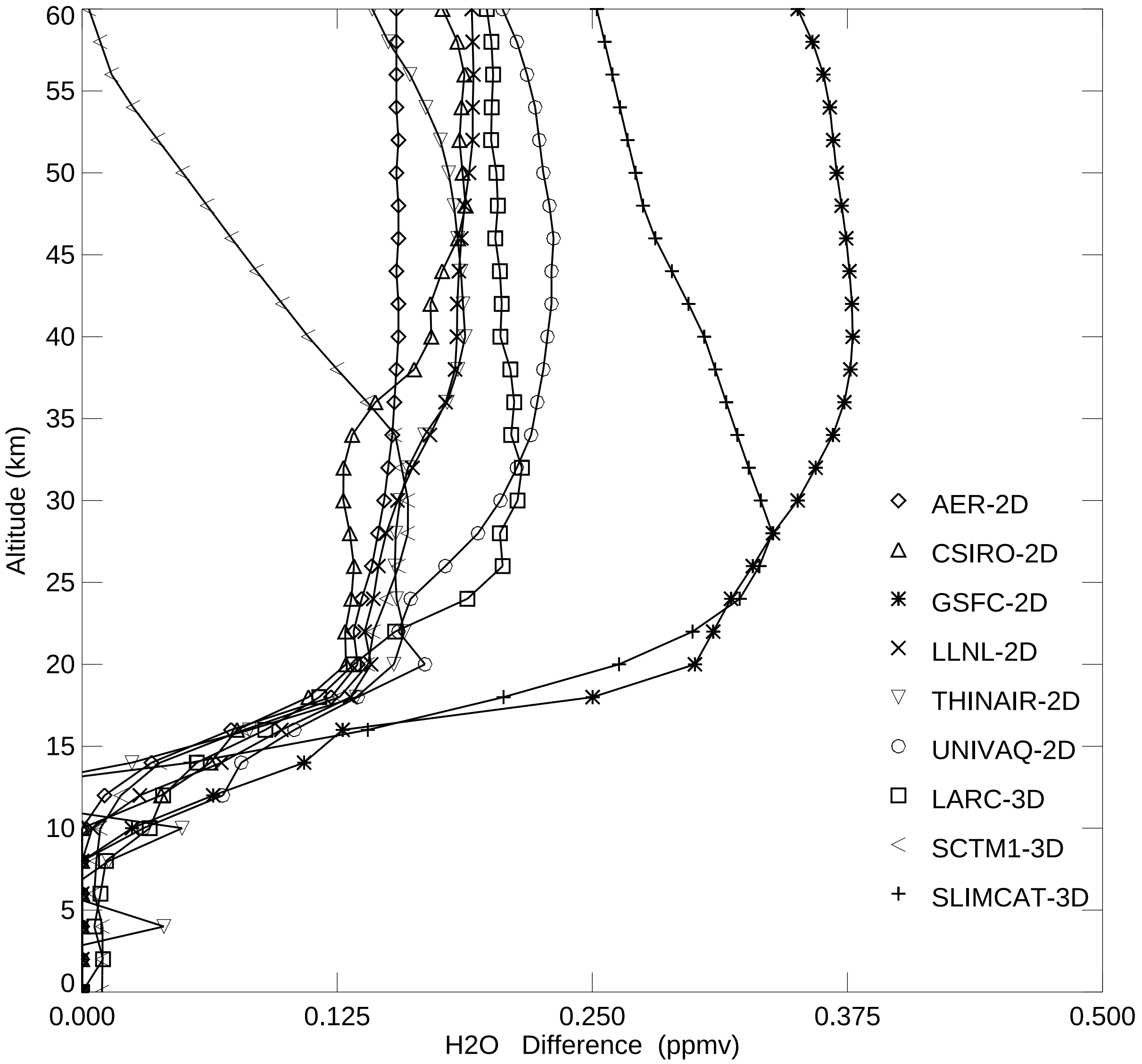

Figure 4.4: Calculated perturbations to H_2O (ppmv) as a function of altitude at 45^{o}S in June of 2015 due to H_2O emissions from a fleet of 500 HSCT aircraft under Scenario S1c relative to Scenario D.

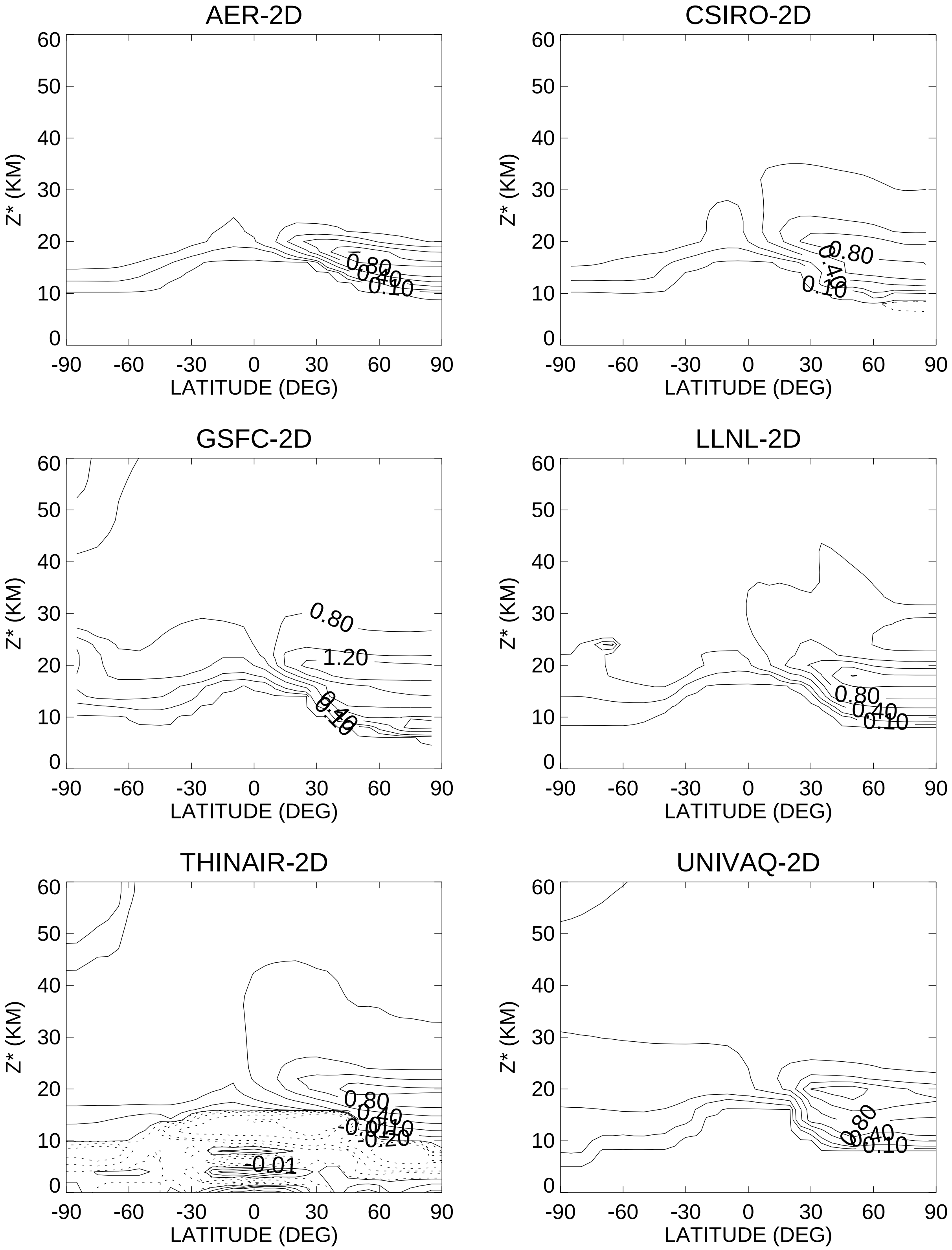

Figure 4.5: Calculated perturbations to H_2O (ppmv) as a function of latitude and altitude in June of 2015 due to H_2O emissions from a fleet of 1000 HSCT aircraft under Scenario S1i relative to Scenario D. Contours are -0.6, -0.4, -0.2, -0.1, -0.01, 0.01, 0.1, and 0.2 to 1.2 by 0.2 ppmv.

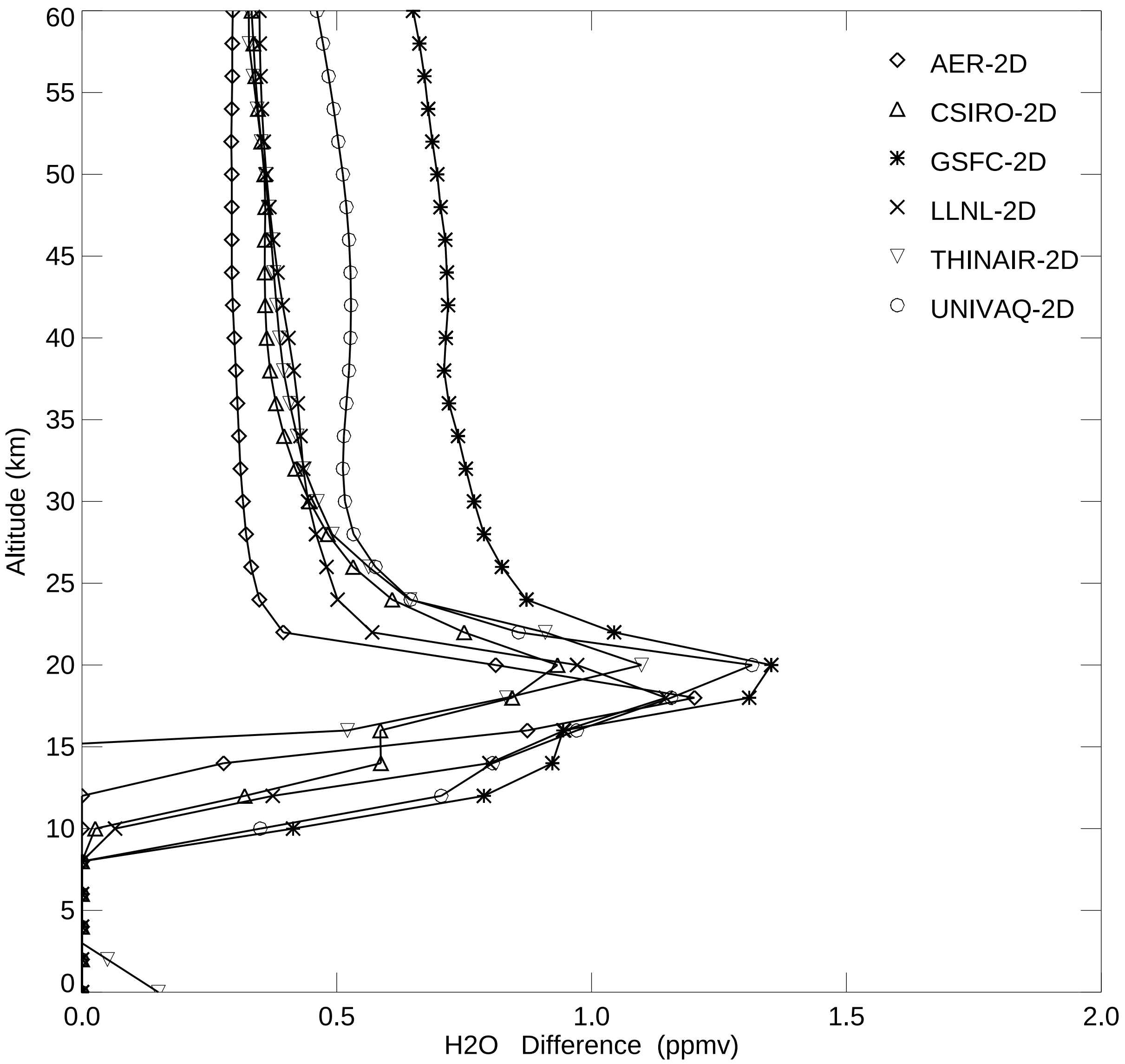

Figure 4.6: Calculated perturbations to H_2O (ppmv) as a function of altitude at 45^{o}N in June of 2015 due to H_2O emissions from a fleet of 1000 HSCT aircraft under Scenario S1i relative to Scenario D.

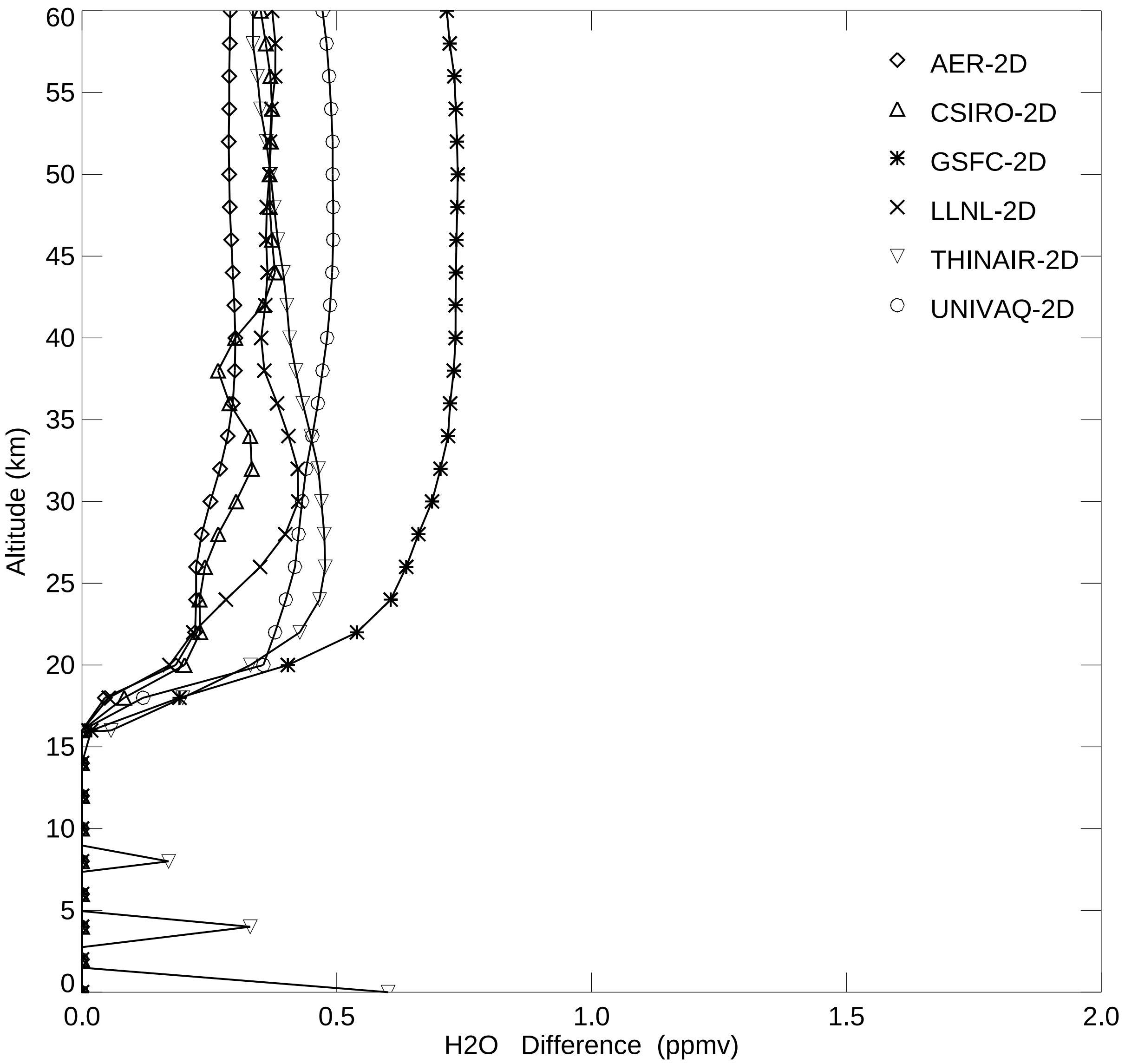

Figure 4.7: Calculated perturbations to H_2O (ppmv) as a function of altitude at the equator in June of 2015 due to H_2O emissions from a fleet of 1000 HSCT aircraft under Scenario S1i relative to Scenario D.

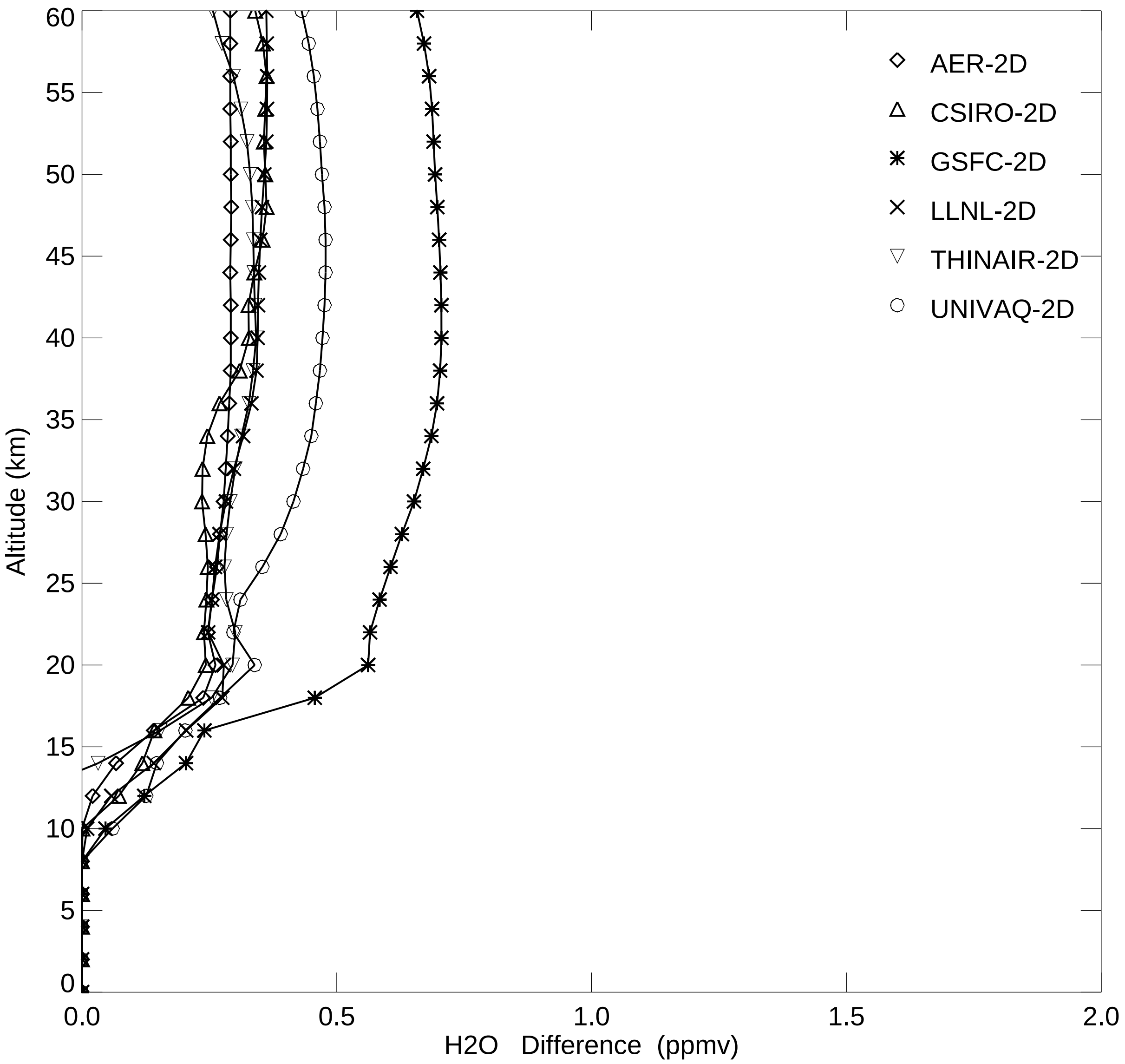

Figure 4.8: Calculated perturbations to H_2O (ppmv) as a function of altitude at 45°S in June of 2015 due to H_2O emissions from a fleet of 1000 HSCT aircraft under Scenario S1i relative to Scenario D.

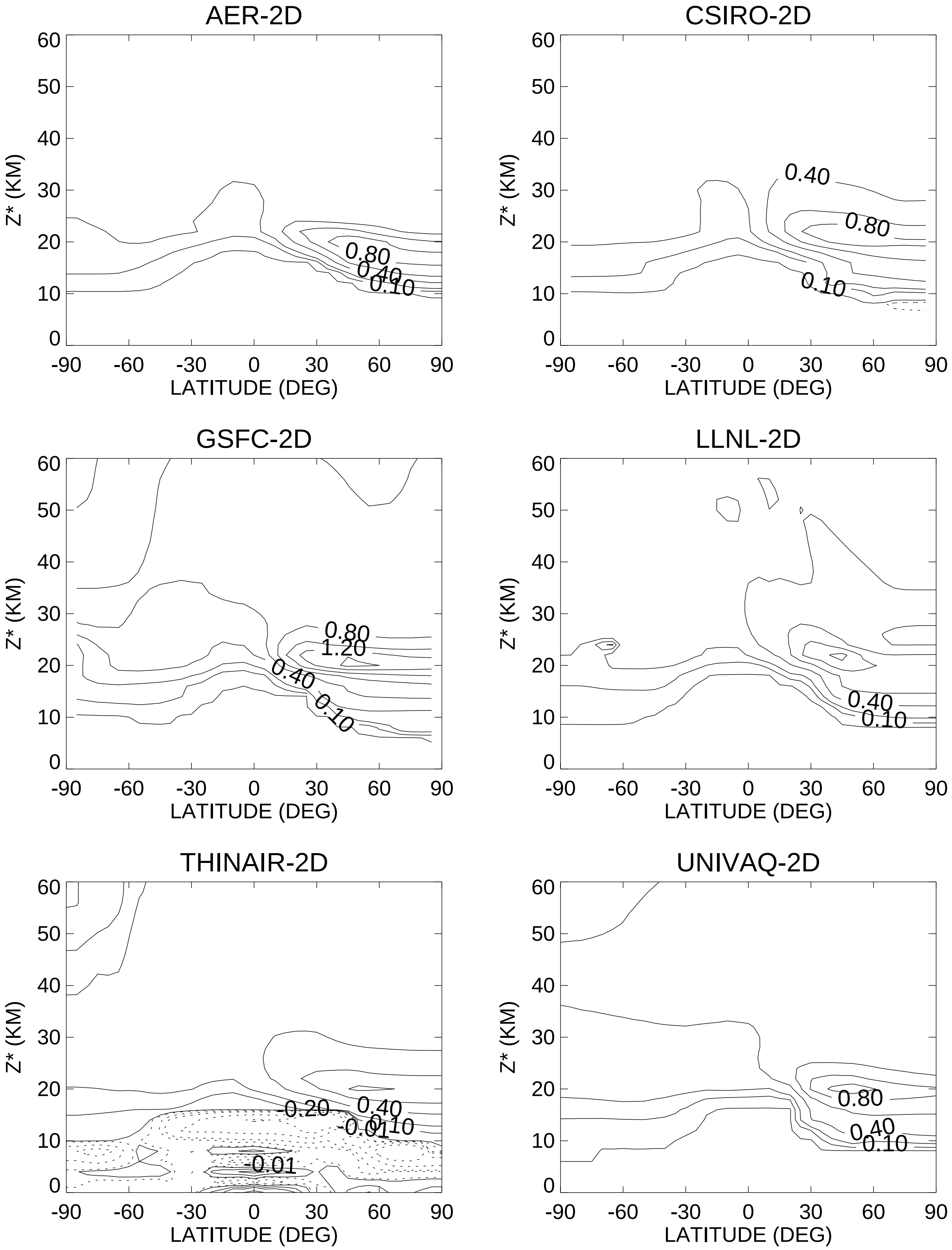

Figure 4.9: Calculated perturbations to H_2O (ppmv) as a function of latitude and altitude in June of 2015 due to H_2O emissions from a fleet of 500 HSCT aircraft operating at 2 km above nominal cruise altitude under Scenario S2a relative to Scenario D. Contours are -0.6, -0.4, -0.2, -0.1, -0.01, 0.01, 0.1, and 0.2 to 1.4 by 0.2 ppmv.

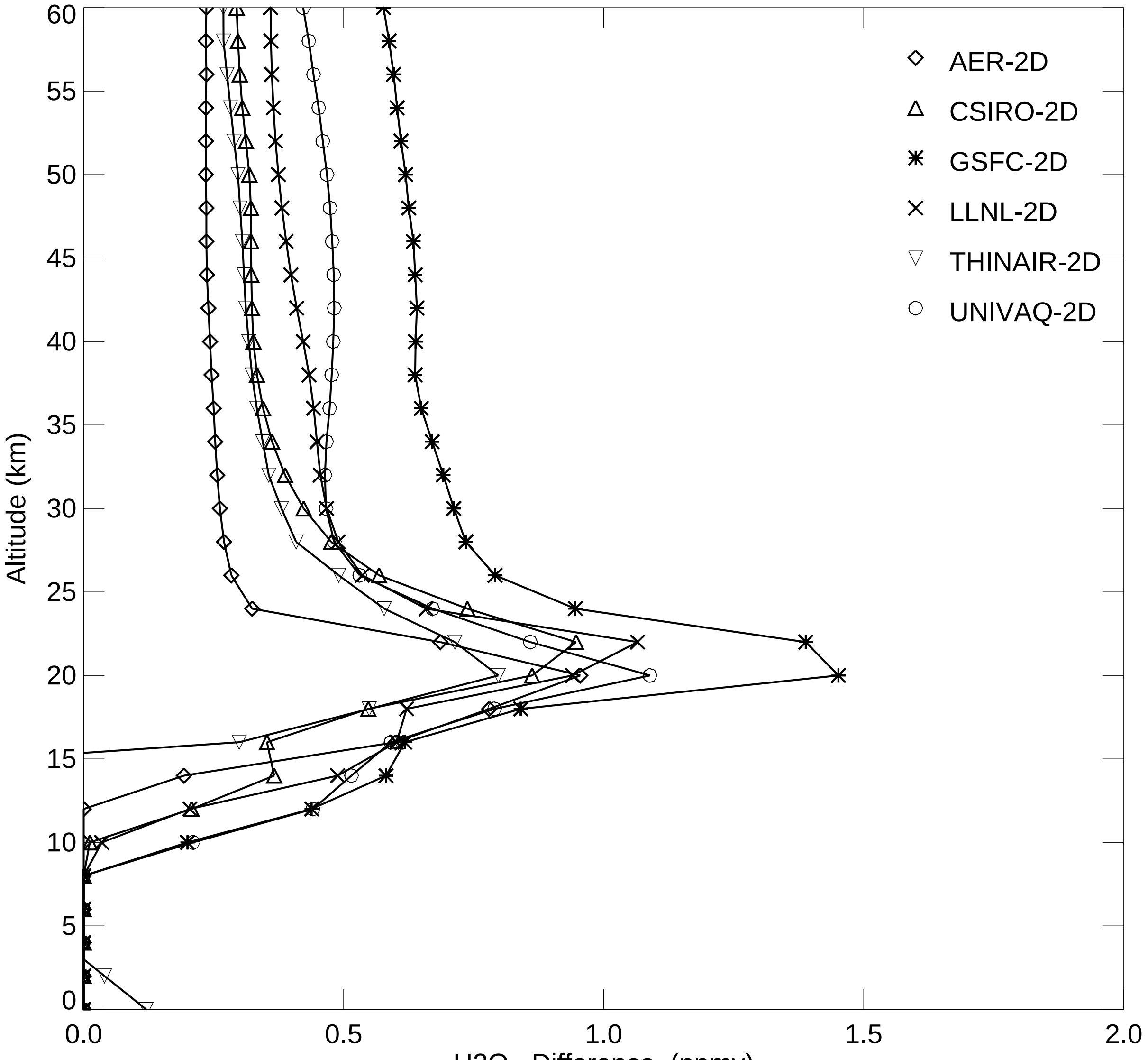

Figure 4.10: Calculated perturbations to H_2O (ppmv) as a function of altitude at 45^{o}N in June of 2015 due to H_2O emissions from a fleet of 500 HSCT aircraft operating at 2 km above nominal cruise altitude under Scenario S2a relative to Scenario D.

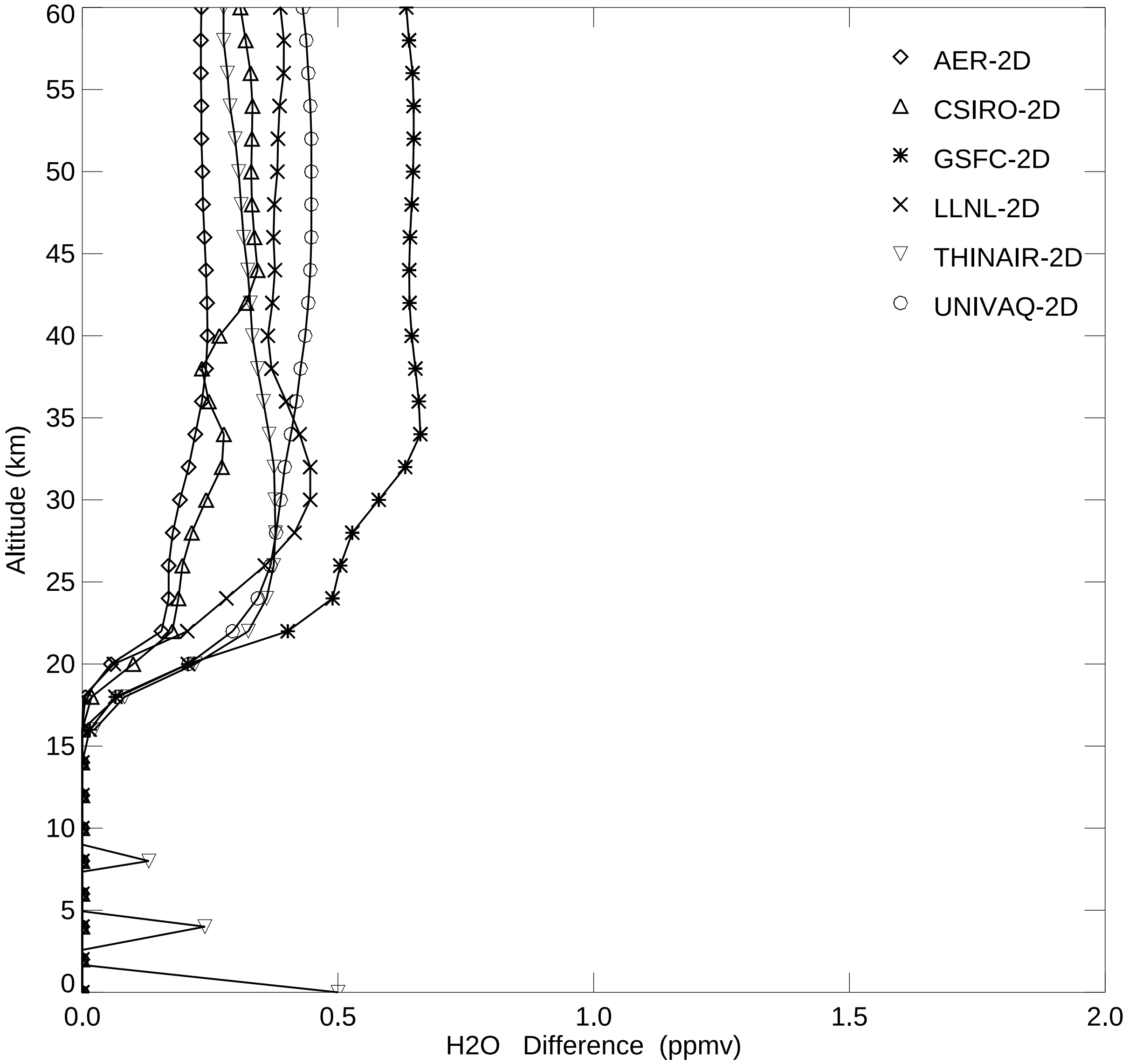

Figure 4.11: Calculated perturbations to H_2O (ppmv) as a function of altitude at the equator in June of 2015 due to H_2O emissions from a fleet of 500 HSCT aircraft operating at 2 km above nominal cruise altitude under Scenario S2a relative to Scenario D.

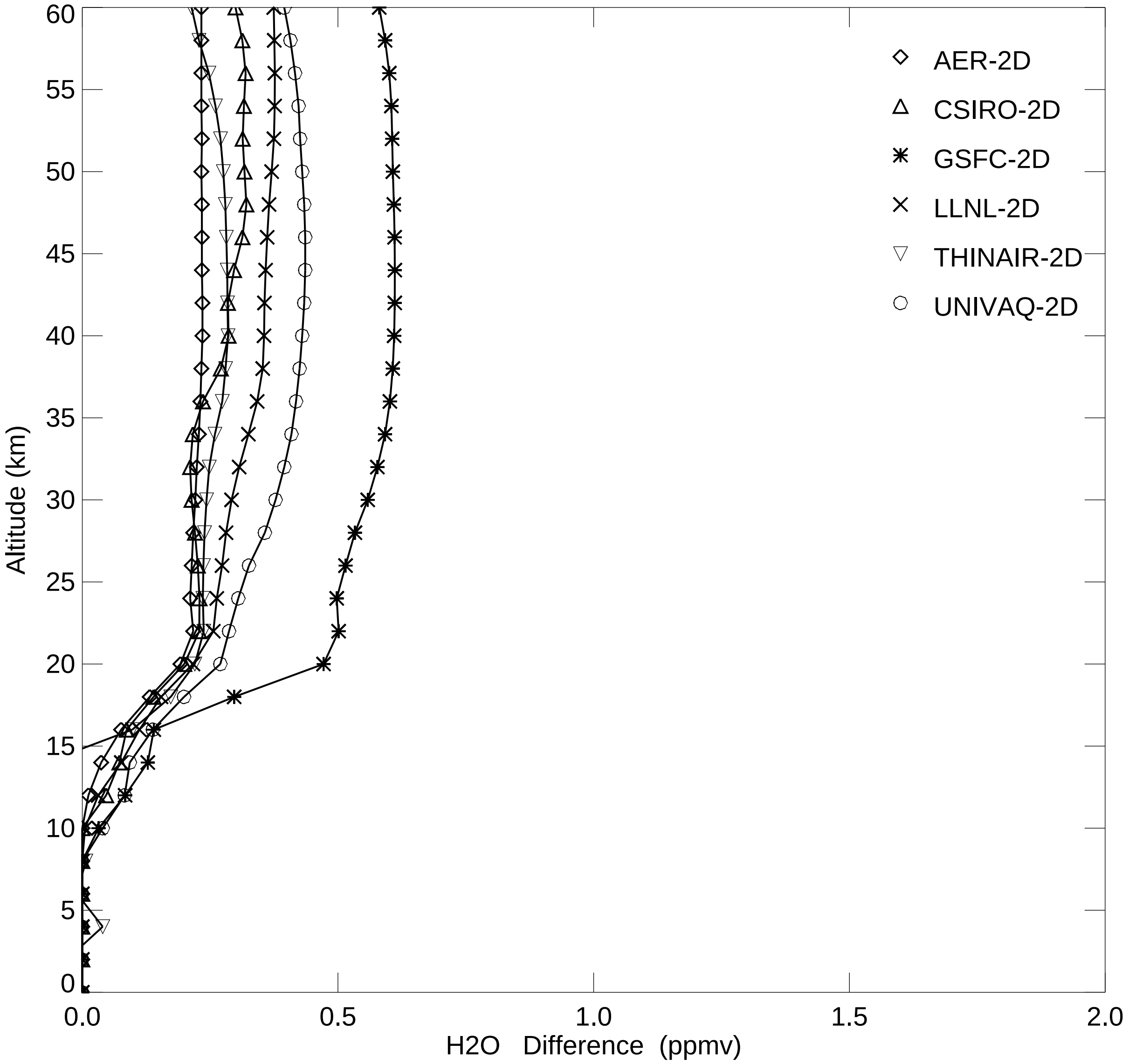

Figure 4.12: Calculated perturbations to H_2O (ppmv) as a function of altitude at 45^{o}S in June of 2015 due to H_2O emissions from a fleet of 500 HSCT aircraft operating at 2 km above nominal cruise altitude under Scenario S2a relative to Scenario D.

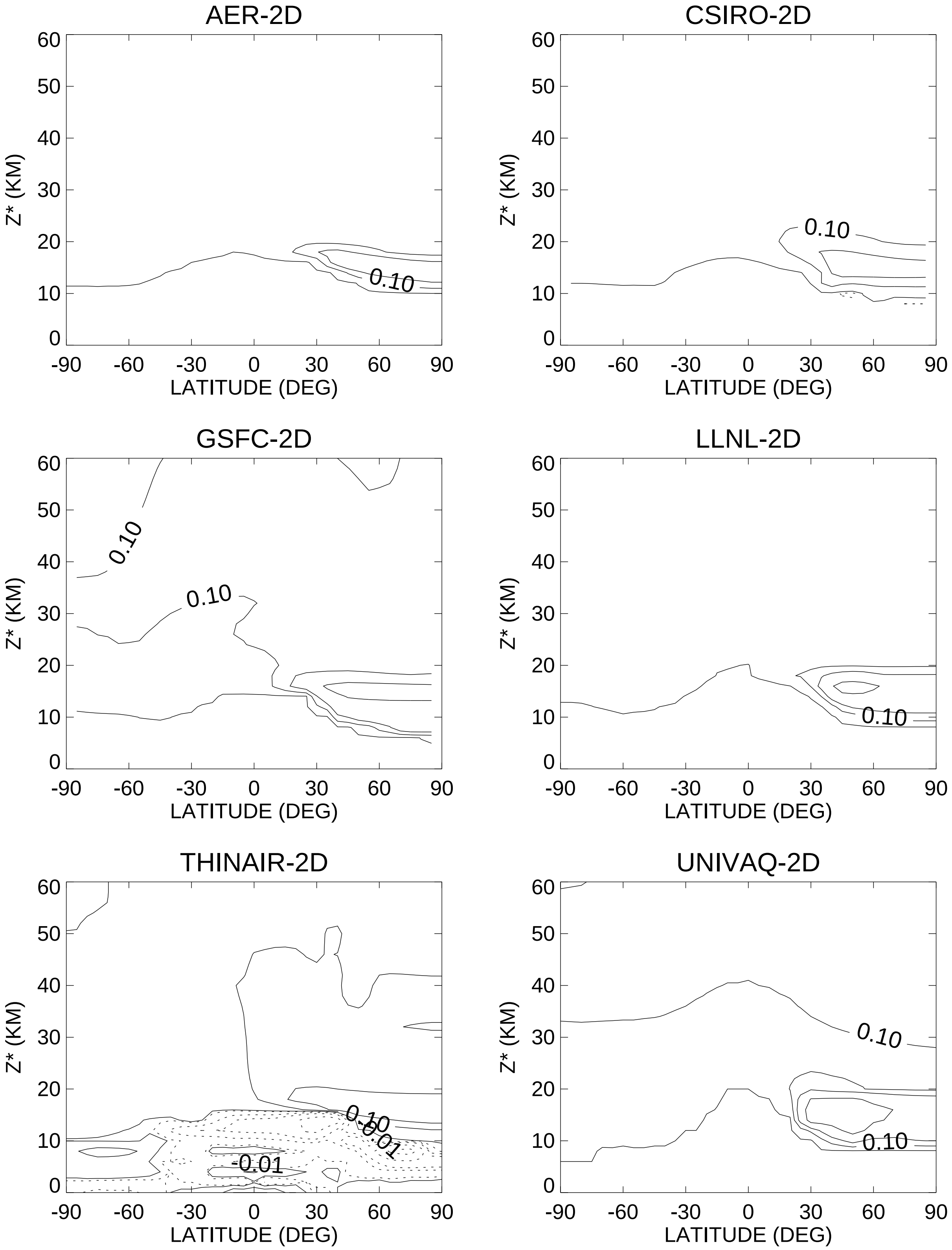

Figure 4.13: Calculated perturbations to H_2O (ppmv) as a function of latitude and altitude in June of 2015 due to H_2O emissions from a fleet of 500 HSCT aircraft operating at 2 km below nominal cruise altitude under Scenario S2b relative to Scenario D. Contours are -0.4, -0.2, -0.1, -0.01, 0.01, 0.1, 0.2, 0.4 ppmv.

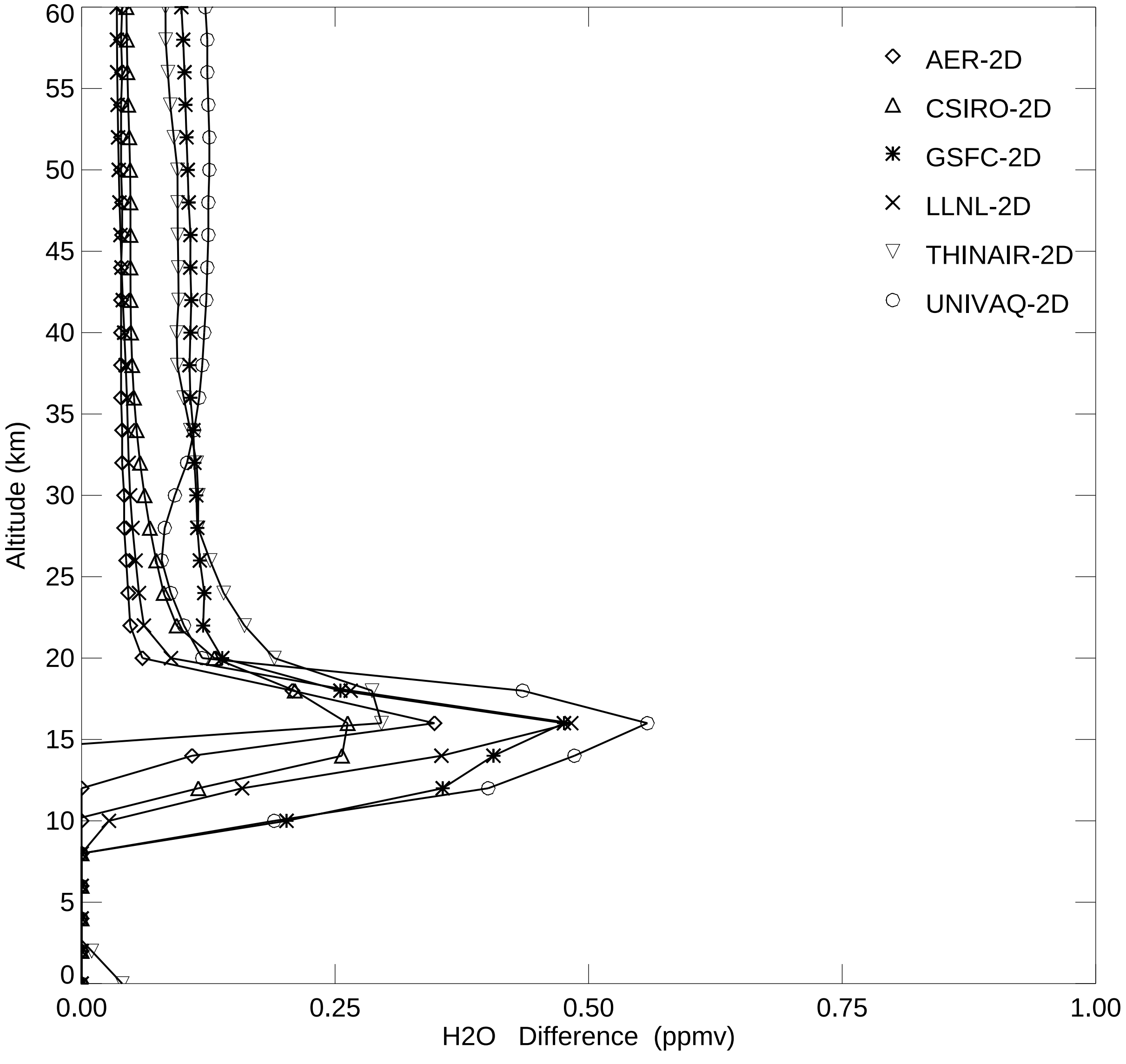

Figure 4.14: Calculated perturbations to H_2O (ppmv) as a function of altitude at 45^{o}N in June of 2015 due to H_2O emissions from a fleet of 500 HSCT aircraft operating at 2 km below nominal cruise altitude under Scenario S2b relative to Scenario D.

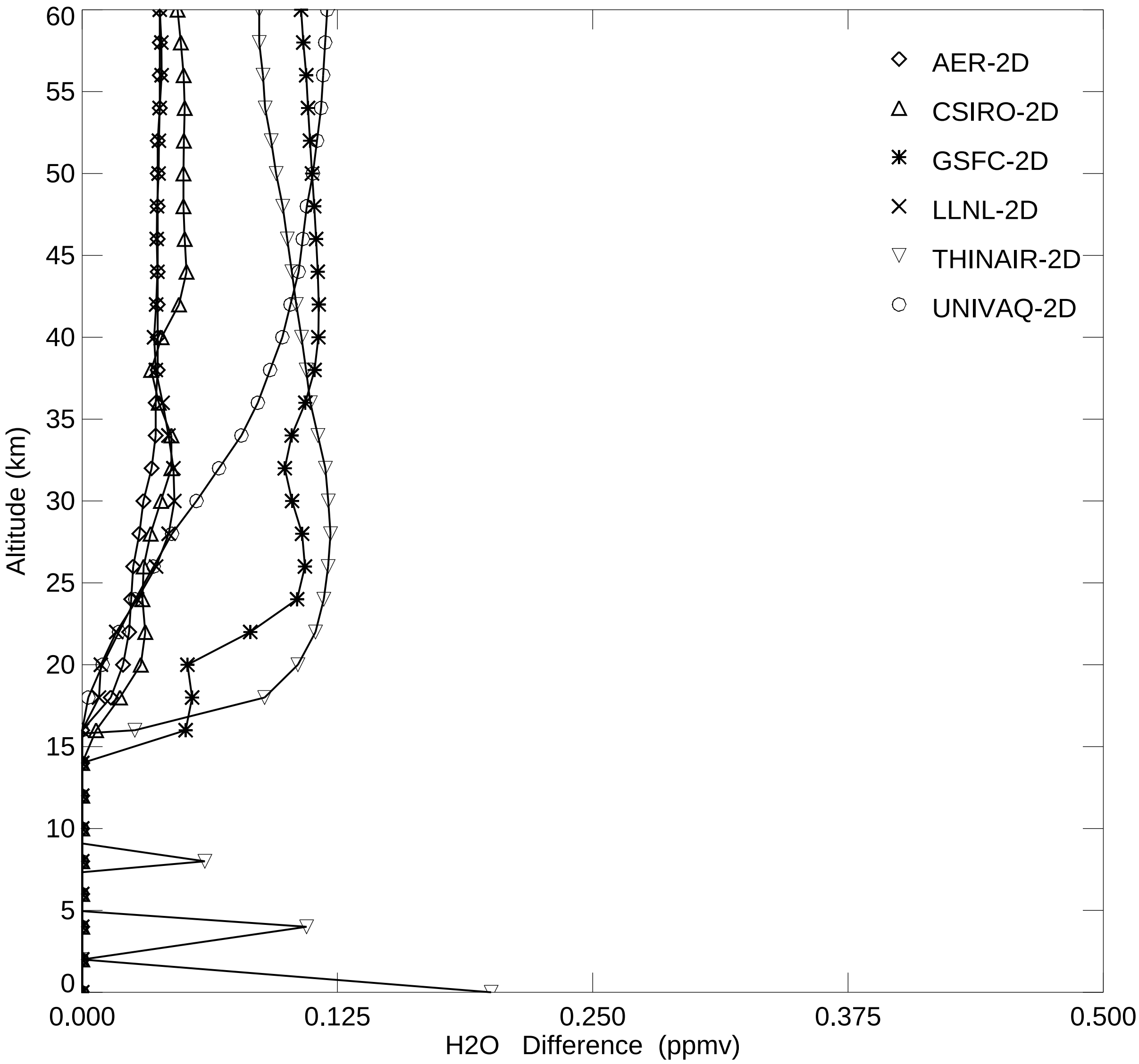

Figure 4.15: Calculated perturbations to H_2O (ppmv) as a function of altitude at the equator in June of 2015 due to H_2O emissions from a fleet of 500 HSCT aircraft operating at 2 km below nominal cruise altitude under Scenario S2b relative to Scenario D.

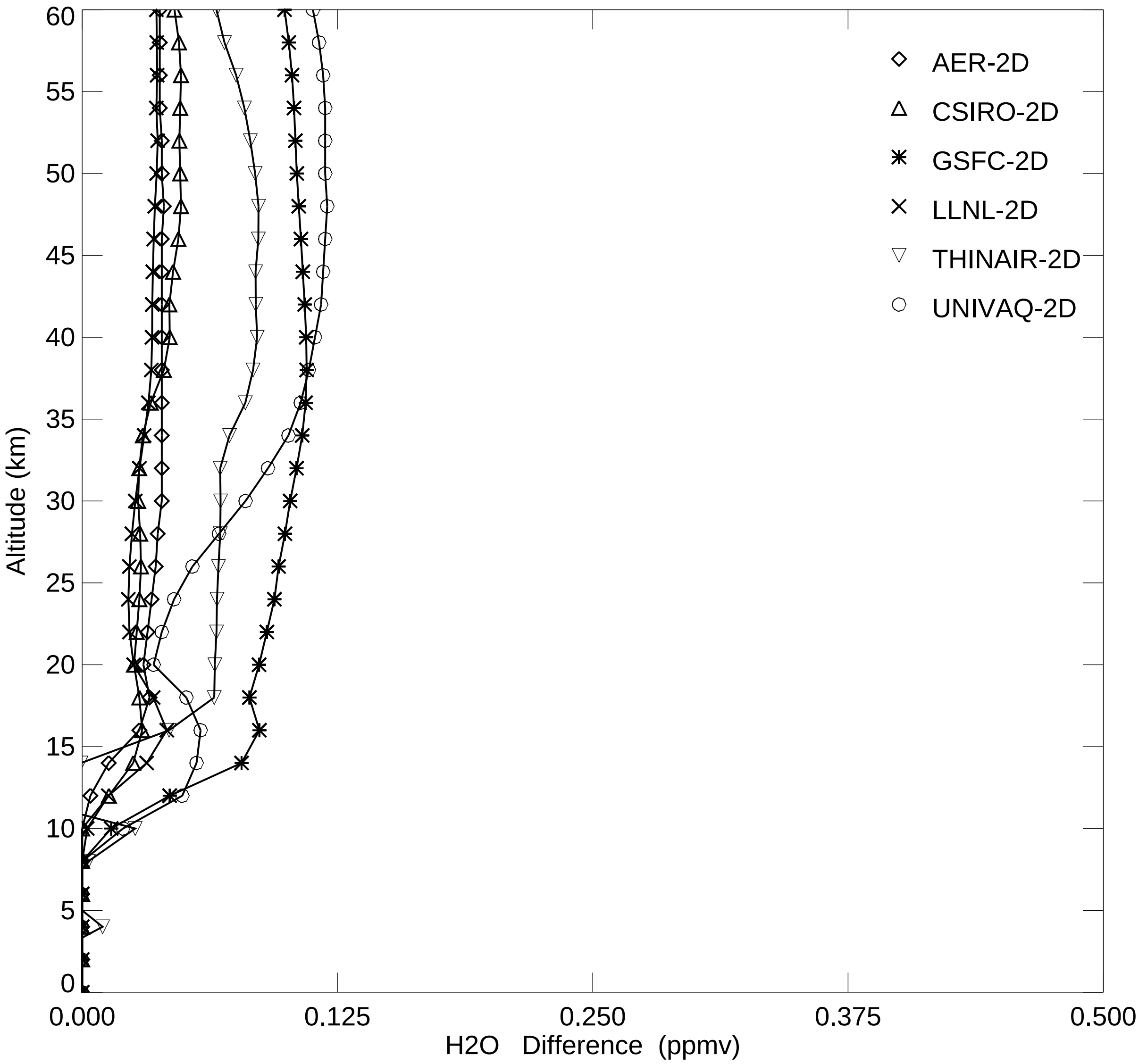

Figure 4.16: Calculated perturbations to H_2O (ppmv) as a function of altitude at 45^{o}S in June of 2015 due to H_2O emissions from a fleet of 500 HSCT aircraft operating at 2 km below nominal cruise altitude under Scenario S2b relative to Scenario D.

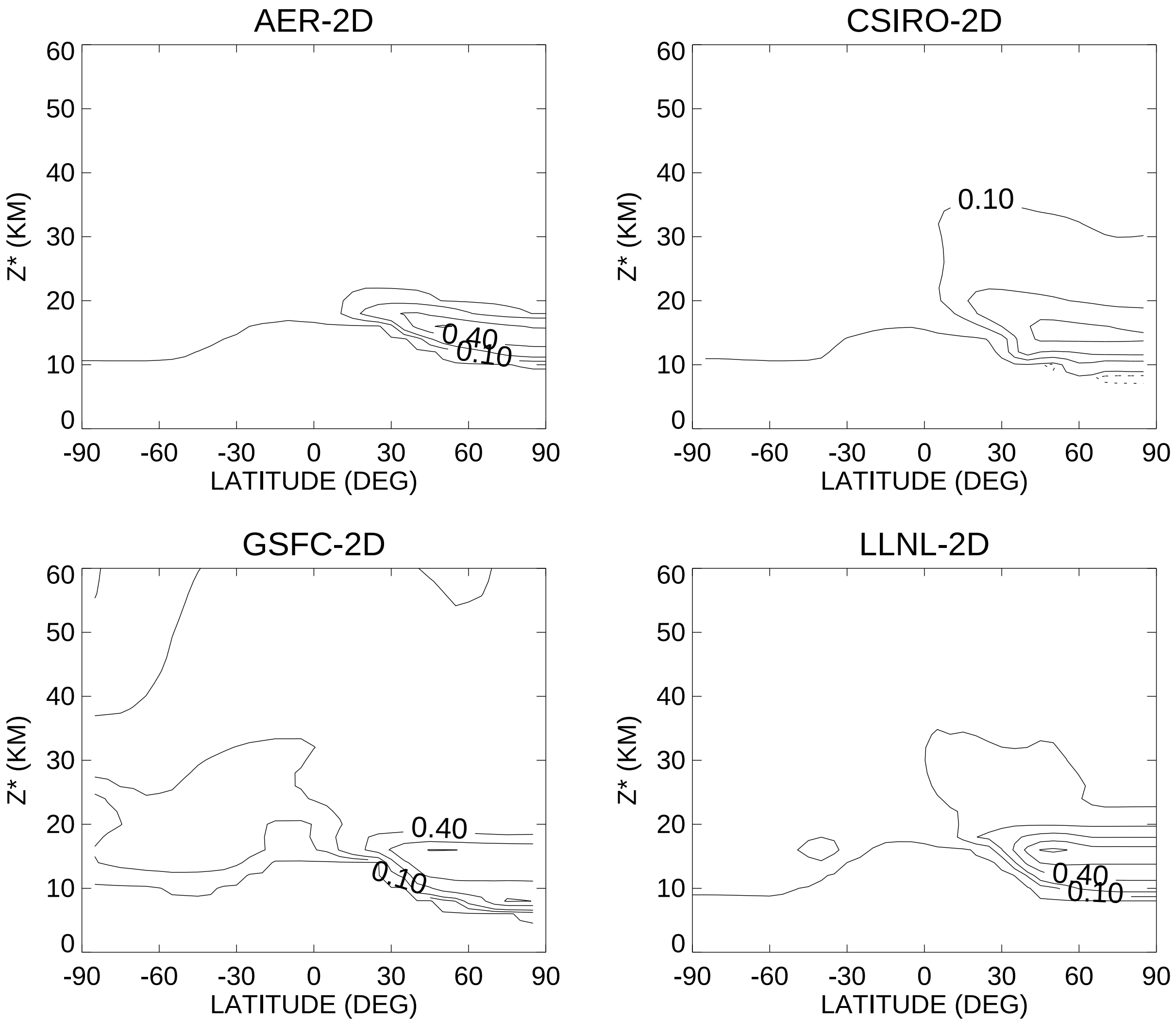

Figure 4.17: Calculated perturbations to H_2O (ppmv) as a function of latitude and altitude in June of 2015 due to H_2O emissions from a fleet of 1000 HSCT aircraft operating at 2 km below nominal cruise altitude under Scenario S2e relative to Scenario D. Contours are -0.01, 0.01, 0.1, 0.2, 0.4, 0.6, 0.8 ppmv.

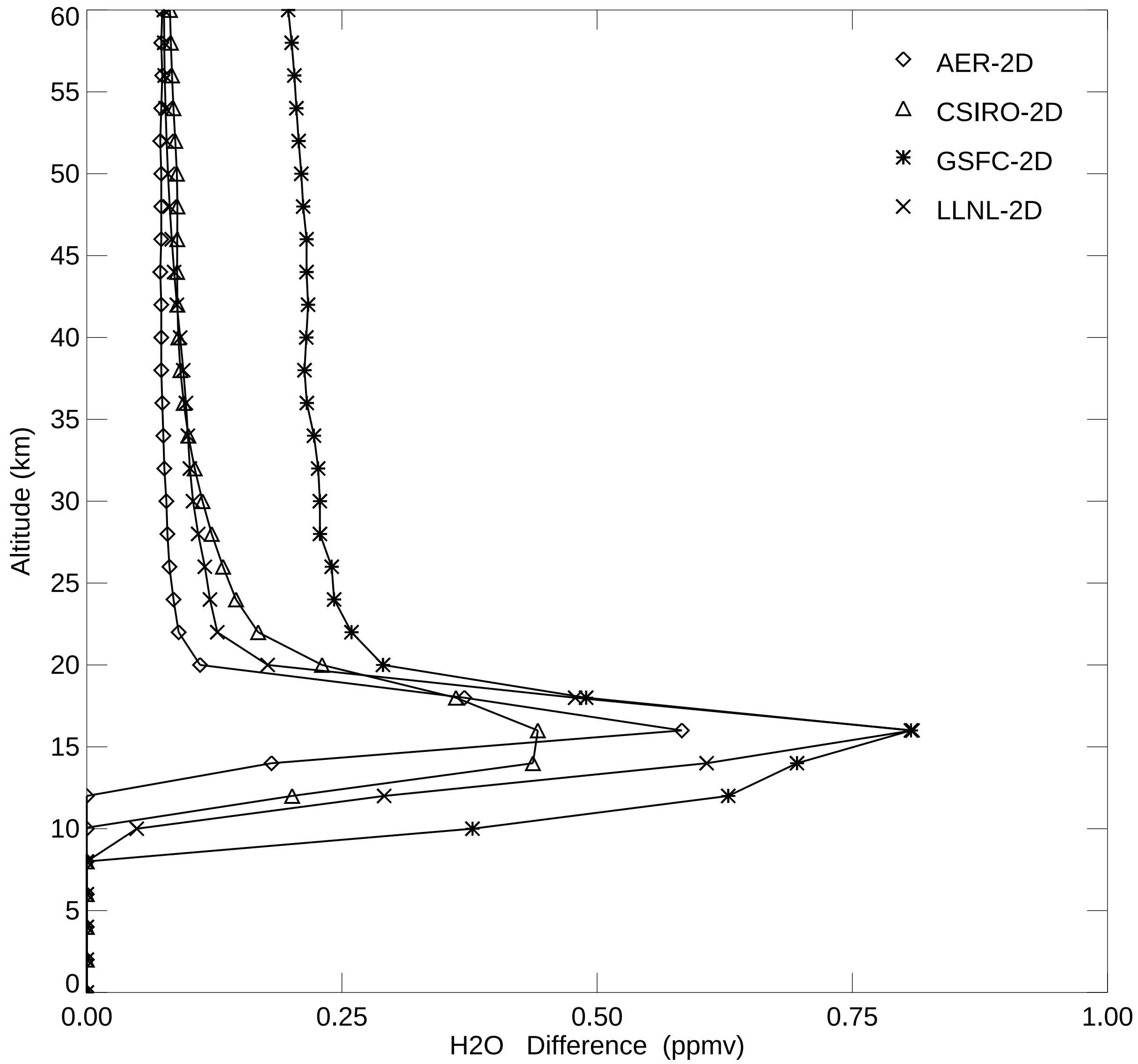

Figure 4.18: Calculated perturbations to H_2O (ppmv) as a function of altitude at 45^oN in June of 2015 due to H_2O emissions from a fleet of 1000 HSCT aircraft operating at 2 km below nominal cruise altitude under Scenario S2e relative to Scenario D.

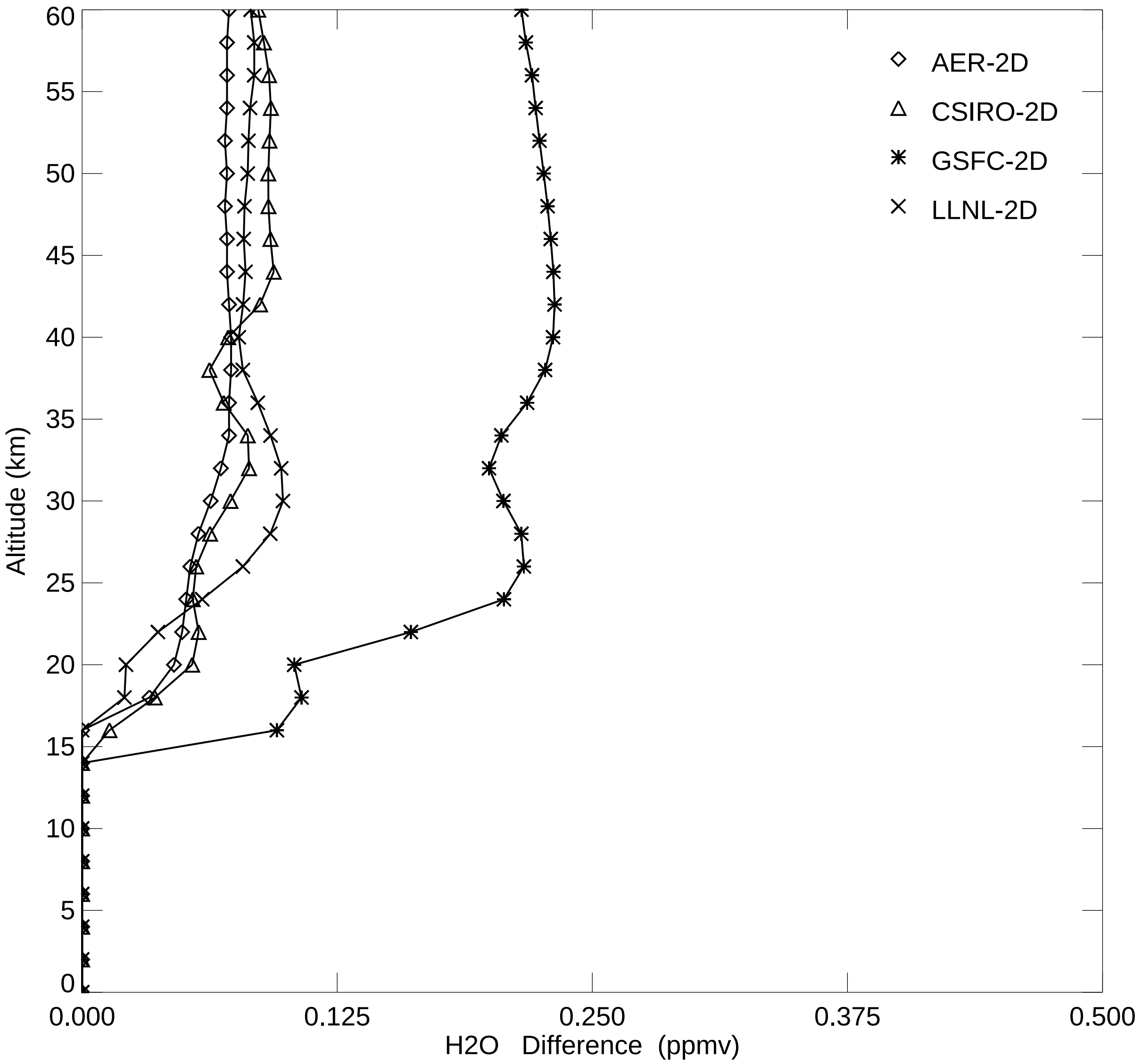

Figure 4.19: Calculated perturbations to H_2O (ppmv) as a function of altitude at the equator in June of 2015 due to H_2O emissions from a fleet of 1000 HSCT aircraft operating at 2 km below nominal cruise altitude under Scenario S2e relative to Scenario D.

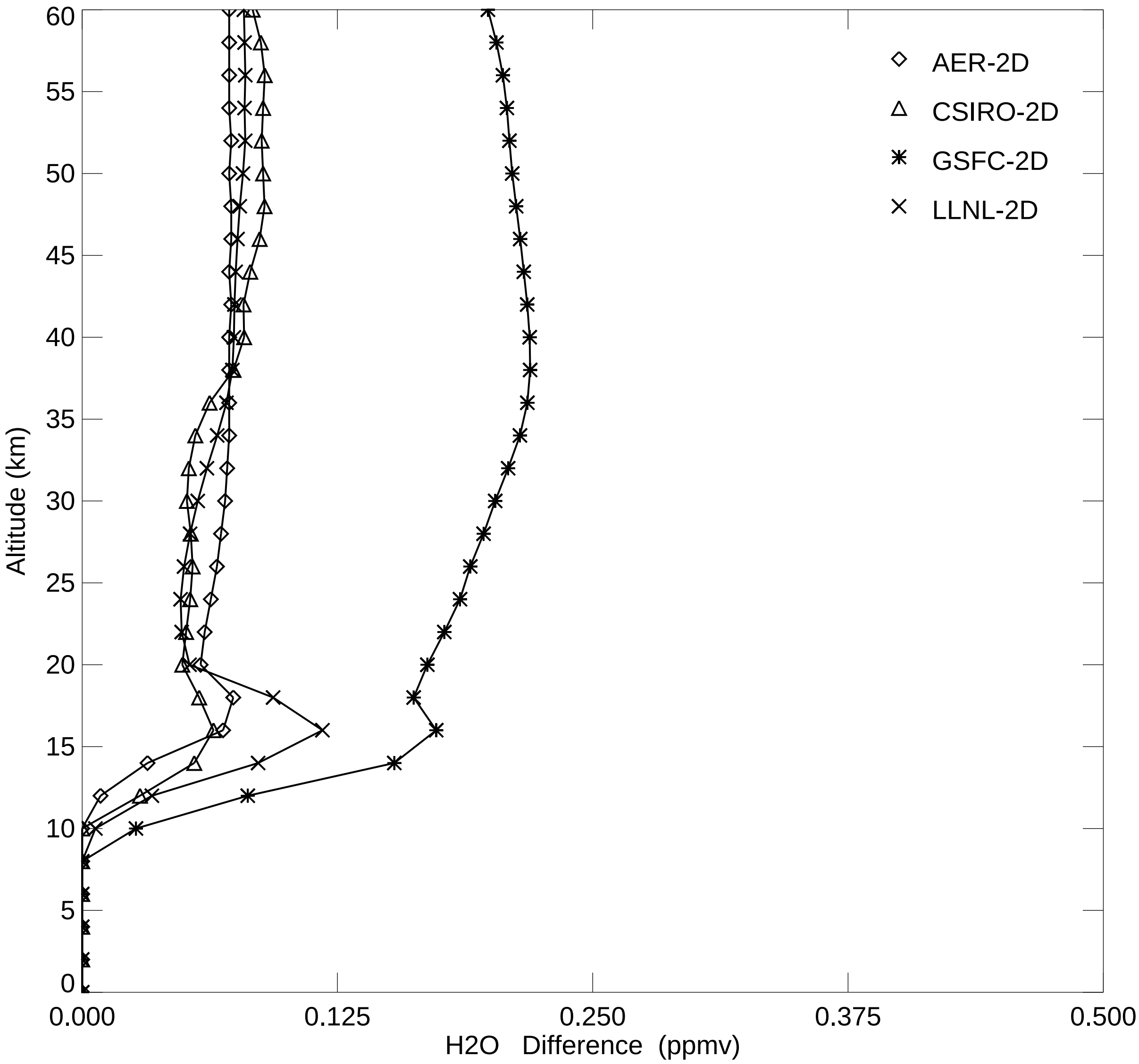

Figure 4.20: Calculated perturbations to H_2O (ppmv) as a function of altitude at 45^oS in June of 2015 due to H_2O emissions from a fleet of 1000 HSCT aircraft operating at 2 km below nominal cruise altitude under Scenario S2e relative to Scenario D.

4.2 NO_y Perturbations

Because the NO_x emission index for future HSCT engines is not known with certainty, this parameter is treated parametrically in these scenarios. The NO_x emission index is varied from 5 to 15 gm (NO_2) per kg fuel burned to cover the likely range of future engines. The engineering goal for the HSCT program is a NO_x EI of 5, so this is treated as the standard case. Other emission indices, including zero, are used to study the sensitivity of the ozone response to this parameter. Variations in fleet size and cruise altitude also modify the atmosphere's response to NO_x emissions.

The perturbations to NO_y due to aircraft emissions of NO_x under Scenario S1c are shown in Figure 4.21. This scenario represents 500 HSCT aircraft operating in 2015 with EI(NO_x)=5. Figures 4.22-4.24 show vertical profiles of NO_y perturbation at 45°N, the equator, and 45°S in June of 2015 for the same scenario. The maximum perturbation varies from 0.6 ppbv to 1.2 ppbv at 45°N, with the GSFC model calculating the largest perturbation. Some models show negative perturbations near the south pole in June due to denitrification reactions occurring on polar stratospheric clouds in this region. These models include AER, GSFC, LLNL, and UNIVAQ.

There is a factor of two variation in calculated NO_y perturbation among the models at 45°N in the lower stratosphere. The intermodel variability becomes a factor of 3 at the equator and a factor of 4-5 at 45°S. Though the GSFC model shows the largest perturbation at 45°N, the SLIMCAT model show a much greater perturbation at 45°S. At the equator, SLIMCAT shows the largest perturbation below 27 km, while GSFC and THINAIR have larger perturbations above 30 km. The AER model shows the smallest perturbation in the 22-35 km region at all latitudes.

NO_y perturbations with EI(NO_x)=10 and 500 HSCT aircraft (Scenario S1d) are shown in Figure 4.25. The perturbations are roughly twice the magnitude of those for EI(NO_x)=5. Figures 4.26-4.28 show profiles of NO_y perturbation for this scenario. Notice that the calculated perturbations for the THINAIR model from Scenario S1d have different profile shapes than the perturbations from Scenario S1c. Because the THINAIR model calculated temperature and wind fields interactively, calculated perturbations do not simply scale with EI(NO_x) for this model.

Figure 4.29 shows NO_y perturbations for a 500 aircraft fleet with EI(NO_x)=15 (Scenario S1e). Only 6 models performed calculations for this scenario. Maximum NO_y perturbations are greater than 2 ppbv in the northern hemisphere lower stratosphere for all models, and greater than 3 ppbv for GSFC. This can be compared to background NO_y concentrations of 6-10 ppbv in the same region. Vertical profiles of NO_y perturbation are shown in Figures 4.30-4.32.

With a fleet of 1000 HSCTs and EI(NO_x)=5, the total NO_x emitted is somewhat less than with the 500 HSCT fleet and EI(NO_x)=10. The geographical distribution of fuel use is somewhat different also. The NO_y perturbations for this scenario (S1i) are shown in Figure 4.33. Vertical profiles of NO_y perturbation at 45°N, the equator, and 45°S are shown in Figures 4.34-4.36. Maximum perturbations at 45°N range from 1.5 to 2.1 ppbv.

Scenario S1j represents a fleet of 1000 HSCT aircraft with EI(NO_x)=10. NO_y perturbations from this scenario are shown in Figure 4.37 as functions of latitude and altitude and in Figures 4.38-4.40 as functions of altitude at 45°N, the equator, and 45°S. Maximum NO_y perturbations range from 3.0 ppbv to 4.3 ppbv.

Several scenarios were used to examine the impact of aircraft emissions at different cruise altitudes. Scenario S2a assumes that the HSCT cruise altitude is shifted 2 km above the nominal cruise altitude of 18-20 km. Scenarios S2b-S2e assume that the HSCT cruise altitude is shifted 2 km below the nominal cruise altitude. As with the H_2O perturbation, emission at higher altitudes increases the perturbation while emission at lower altitudes decreases the perturbation.

NO_y perturbations for Scenario S2a, with 500 aircraft cruising at 20-22 km with EI(NO_x)=5, are shown in Figures 4.41-4.44. Increases relative to Scenario S1c range from 30% to 90% in the northern hemisphere lower stratosphere. Figures 4.45-4.48 show NO_y perturbations with 500 aircraft, EI(NO_x)=5, and a cruise altitude of 16-18 km. In this case, decreases in the perturbation relative to Scenario S1c range from 20% to 55%.

Scenario S2c represents 500 aircraft cruising at 2 km below the nominal cruise altitude with EI(NO_x)=10. NO_y perturbations from this scenario are shown in Figure 4.49. For the four models which calculated this scenario, the NO_y perturbation is found to be double that for Scenario S2b. The GSFC model also calculated the scenario with EI(NO_x)=15 for the same fleet size and cruise altitude (Scenario S2d). This result is shown in Figure 4.50.

Figures 4.51-4.54 show results for Scenario S2e with 1000 HSCT aircraft cruising at 2 km below nominal cruise altitude with EI(NO_x)=5. NO_y perturbations are 70-90% greater than those from Scenario S2b. Maximum perturbations range from 0.75 ppbv to 1.5 ppbv.

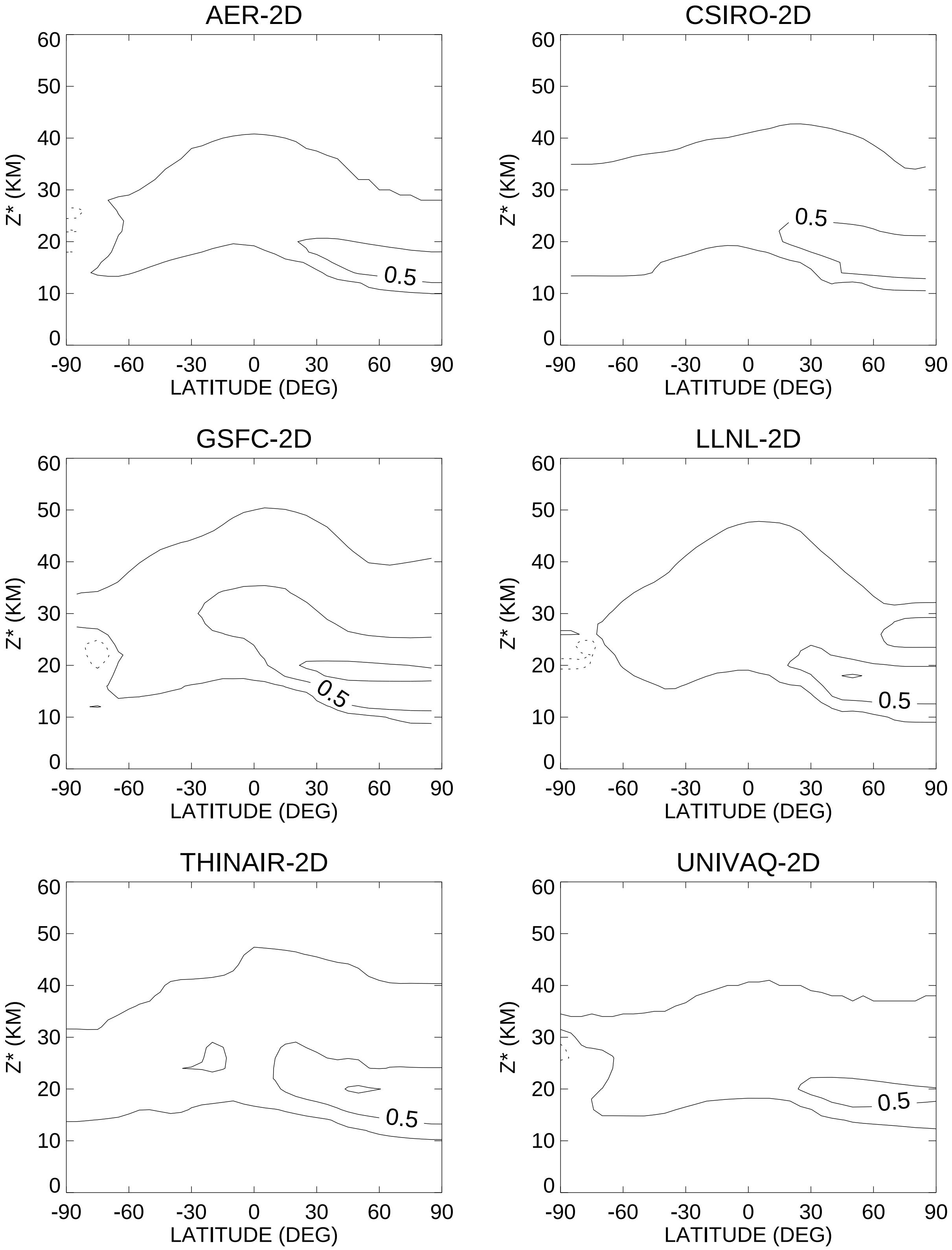

Figure 4.21: Calculated perturbations to NO_y (ppbv) as a function of latitude and altitude in June of 2015 due to NO_x emissions from a fleet of 500 HSCT aircraft with $EI(NO_x)=5$ under Scenario S1c relative to Scenario D. Contours are -1, -0.5, 0, 0.5, 1.0 ppbv.

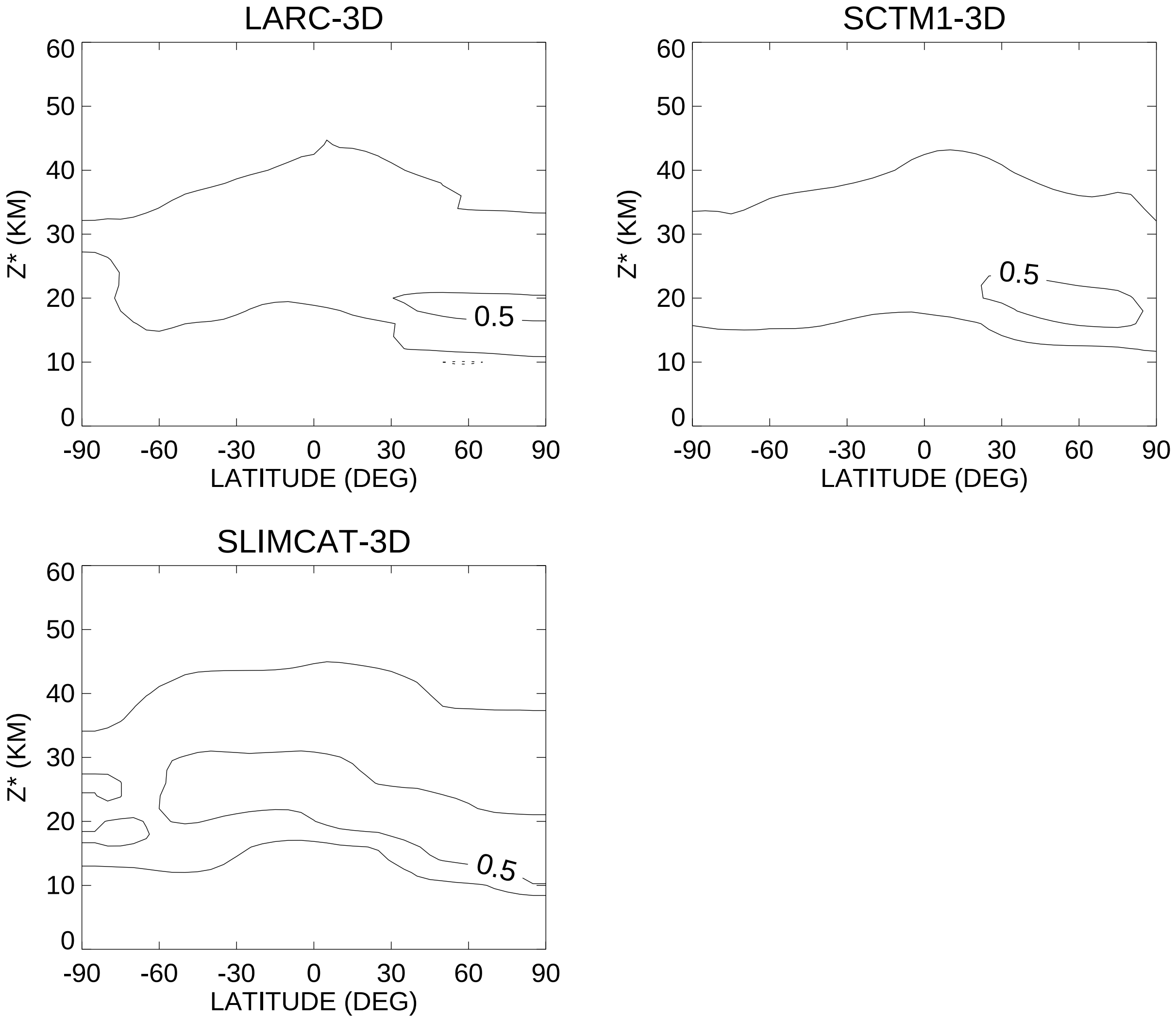

Figure 4.21: continued

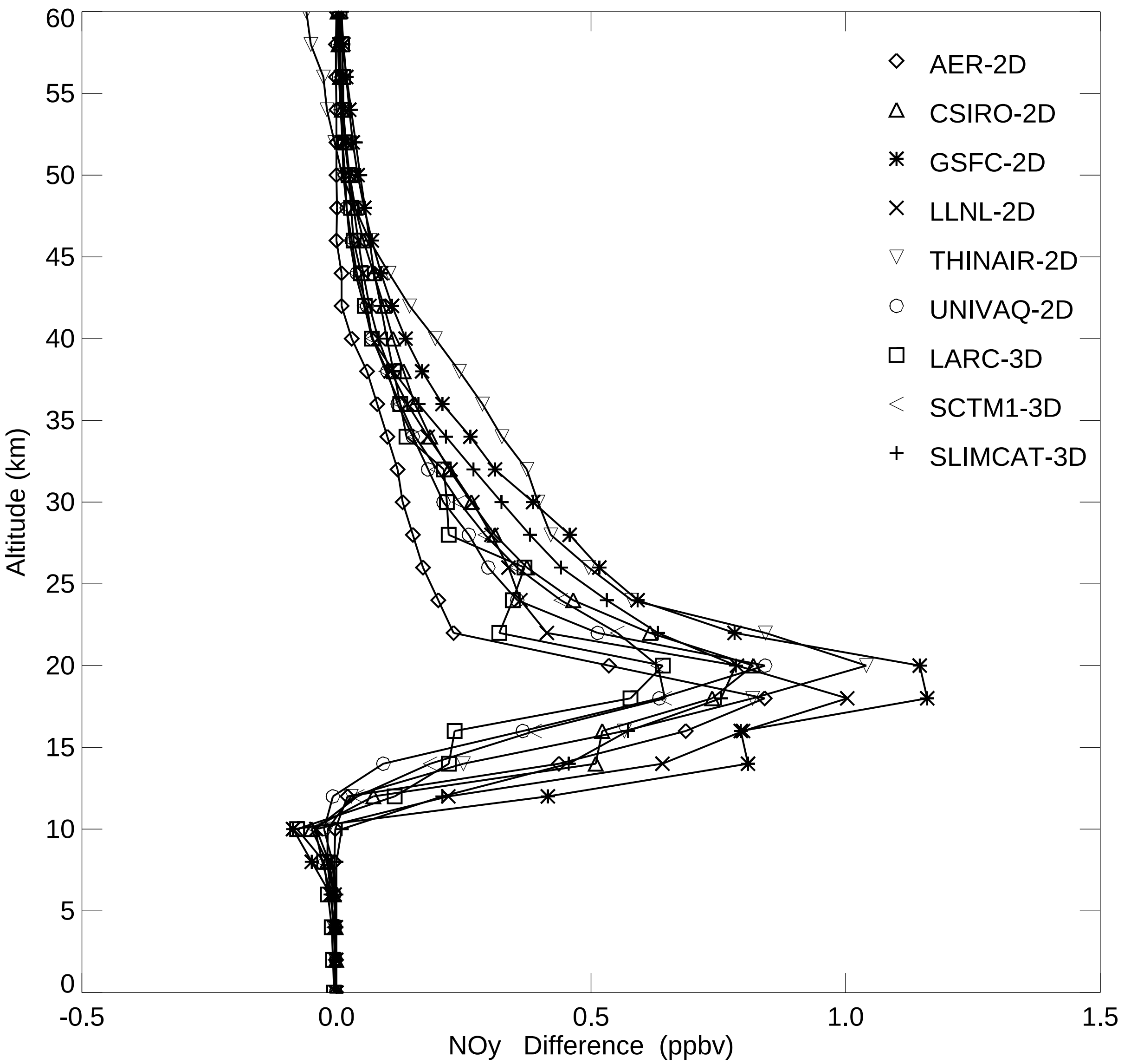

Figure 4.22: Calculated perturbations to NO_y (ppbv) as a function of altitude at 45°N in June of 2015 due to NO_x emissions from a fleet of 500 HSCT aircraft with EI(NO_x)=5 under Scenario S1c relative to Scenario D.

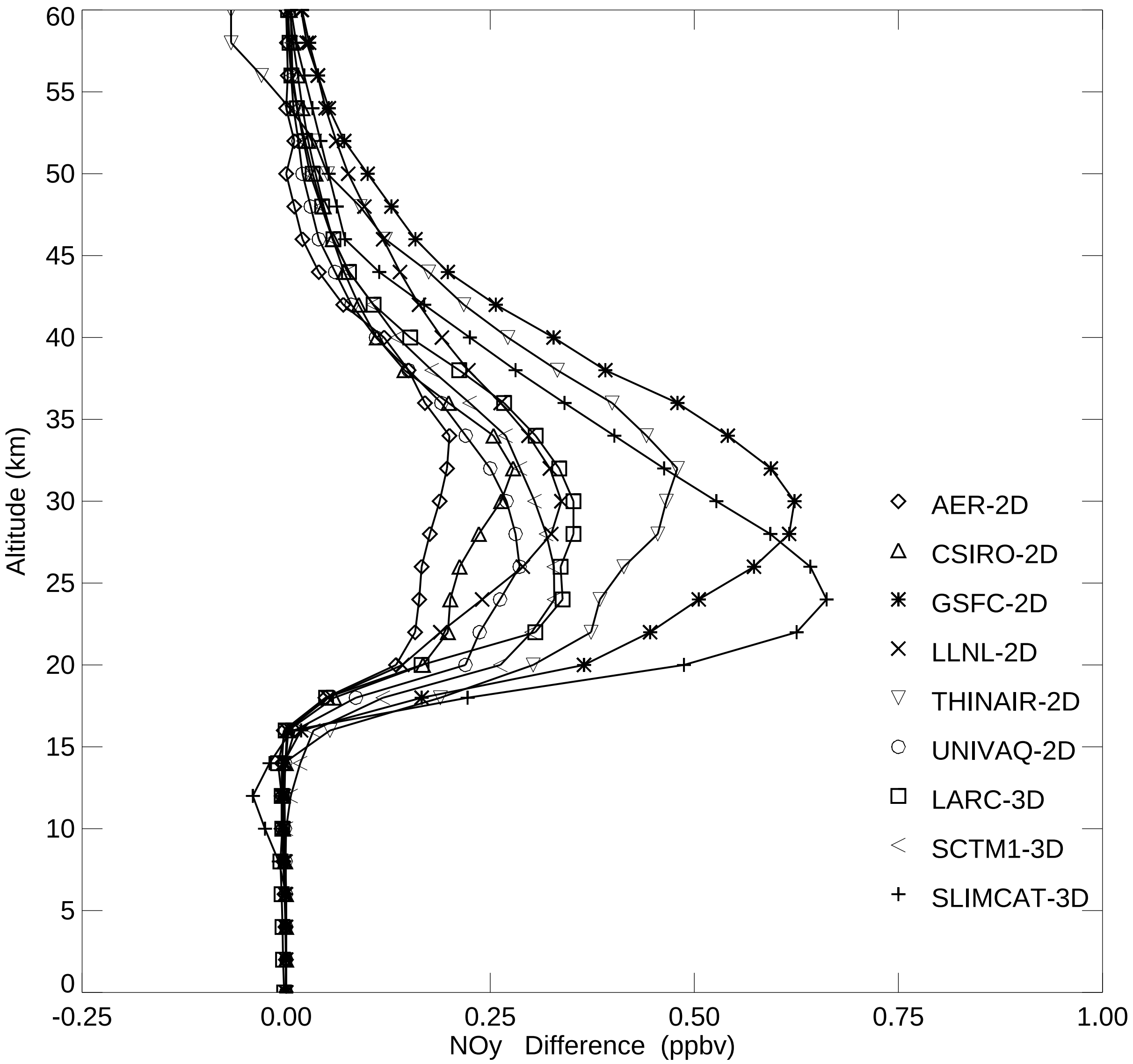

Figure 4.23: Calculated perturbations to NO_y (ppbv) as a function of altitude at the equator in June of 2015 due to NO_x emissions from a fleet of 500 HSCT aircraft with $EI(NO_x)=5$ under Scenario S1c relative to Scenario D.

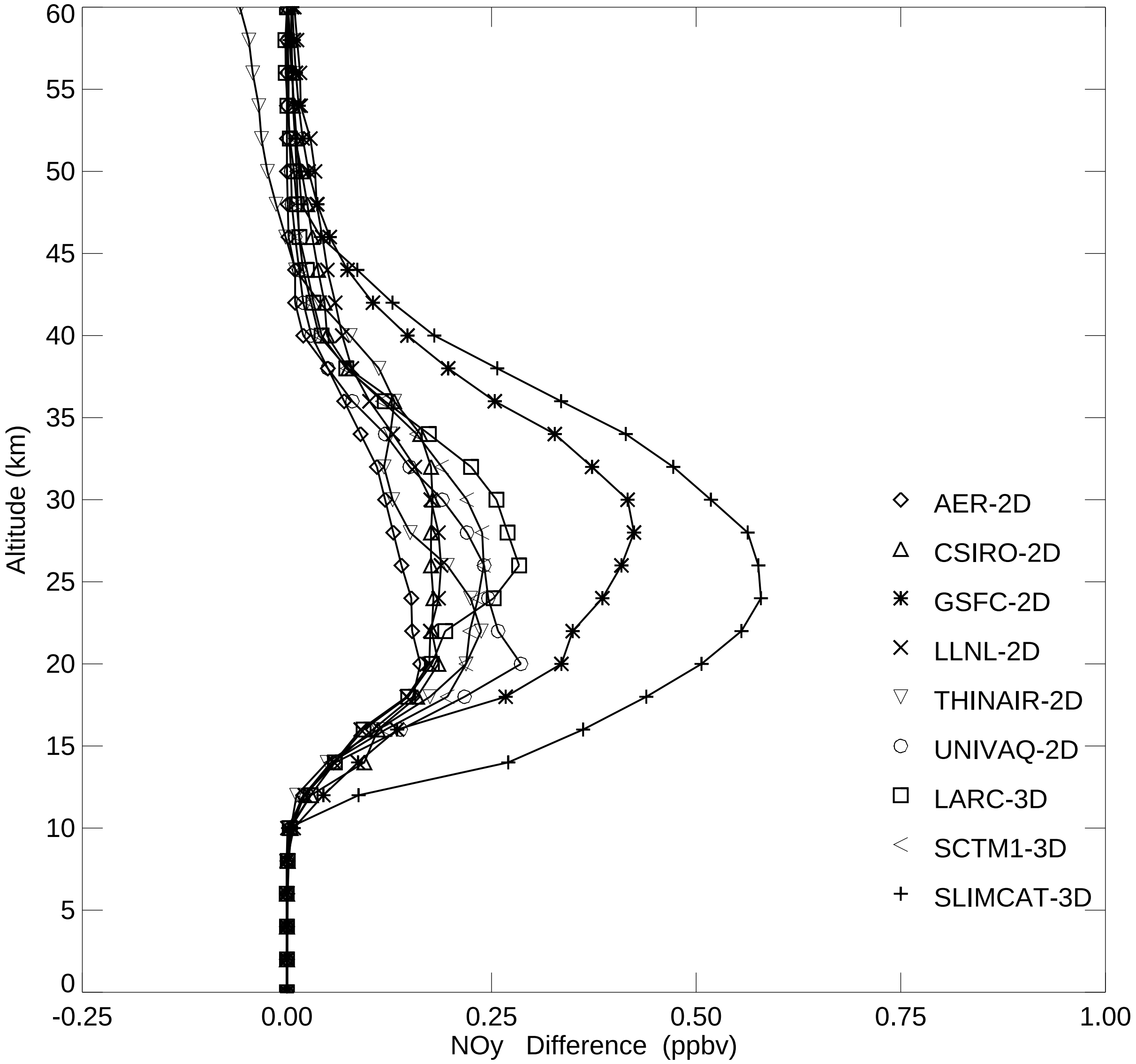

Figure 4.24: Calculated perturbations to NO_y (ppbv) as a function of altitude at 45^oS in June of 2015 due to NO_x emissions from a fleet of 500 HSCT aircraft with $EI(NO_x)=5$ under Scenario S1c relative to Scenario D.

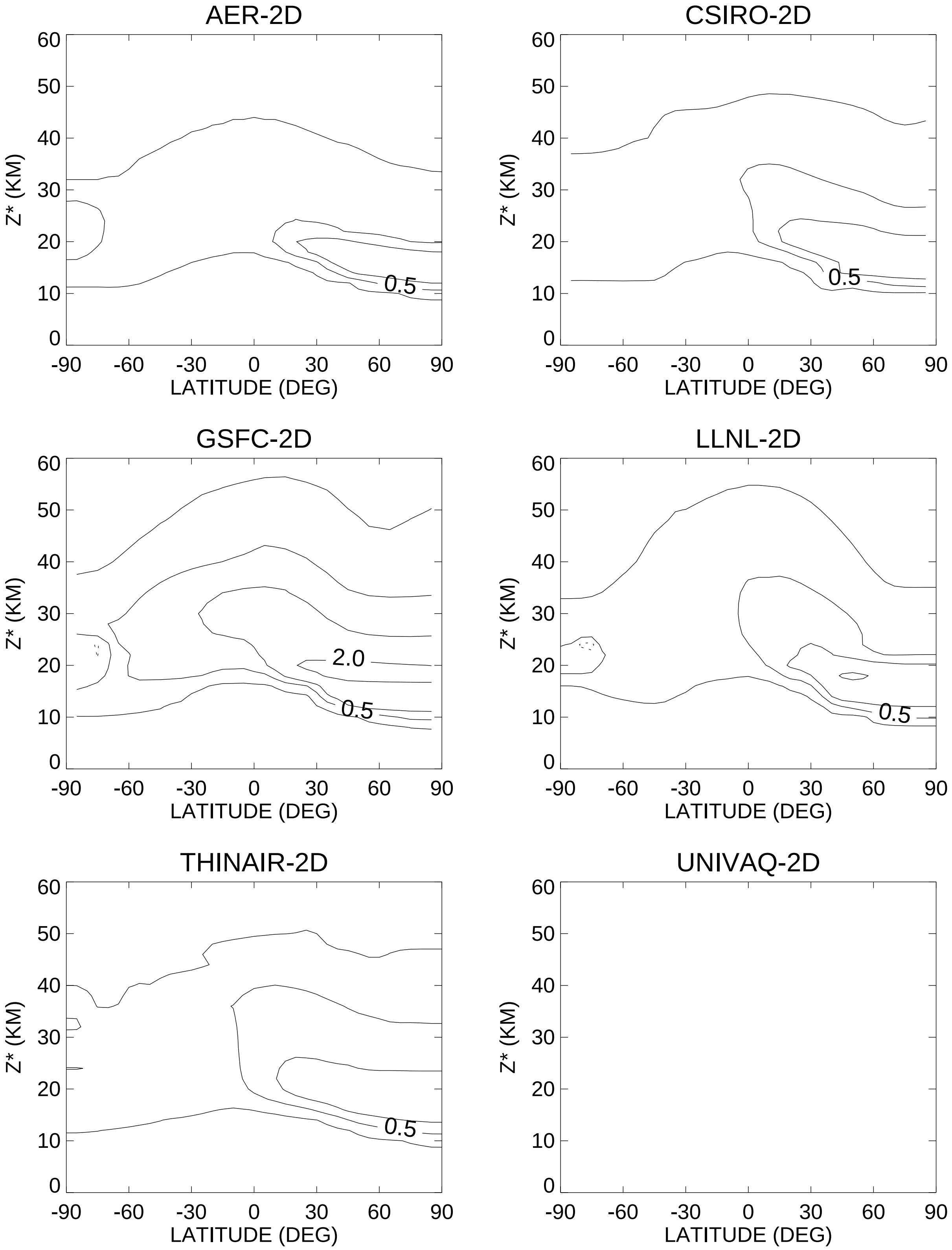

Figure 4.25: Calculated perturbations to NO_y (ppbv) as a function of latitude and altitude in June of 2015 due to NO_x emissions from a fleet of 500 HSCT aircraft with EI(NO_x)=10 under Scenario S1d relative to Scenario D. Contours are -0.5, 0, 0.5, 1.0, 2.0 ppbv.

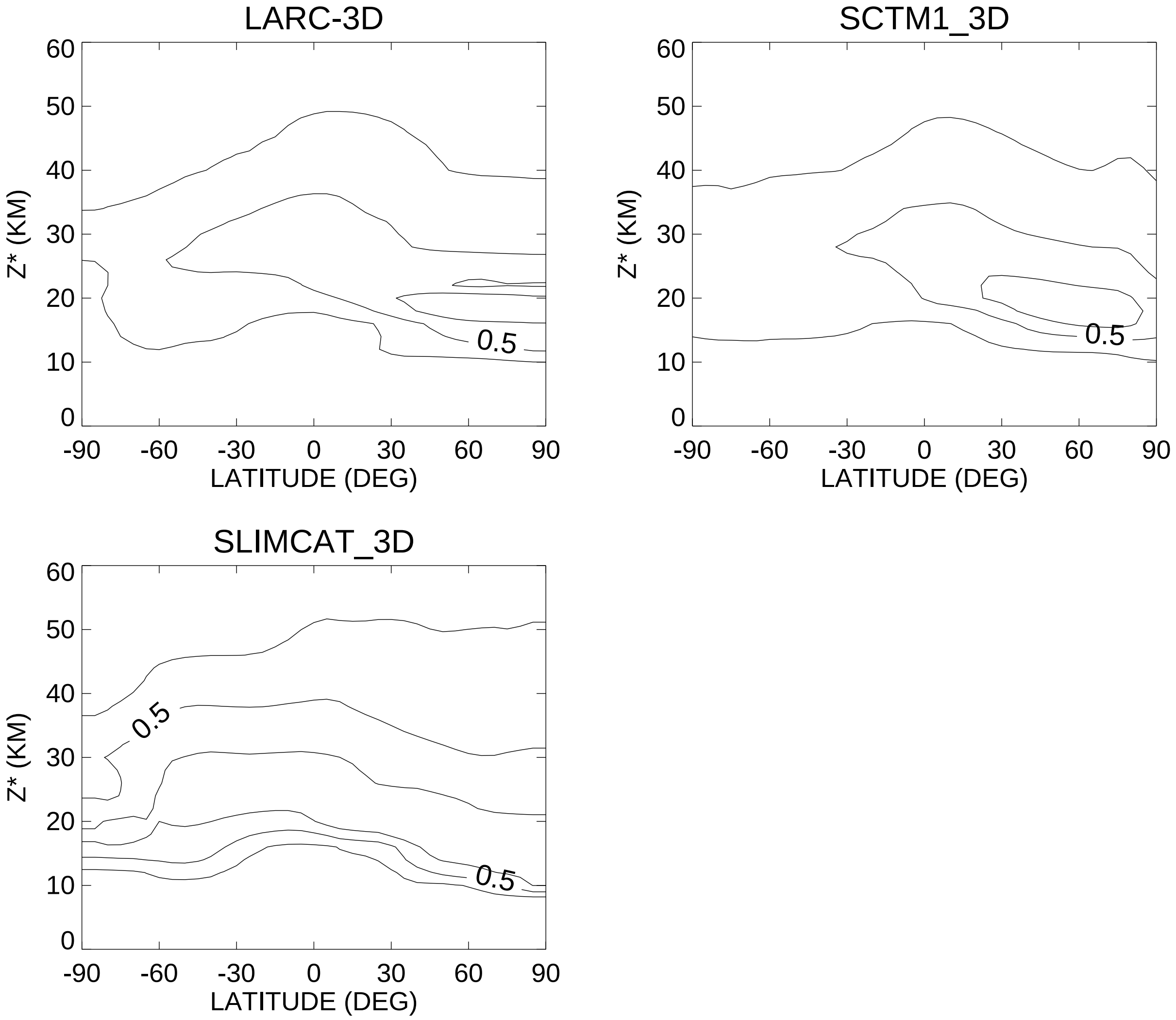

Figure 4.25: continued

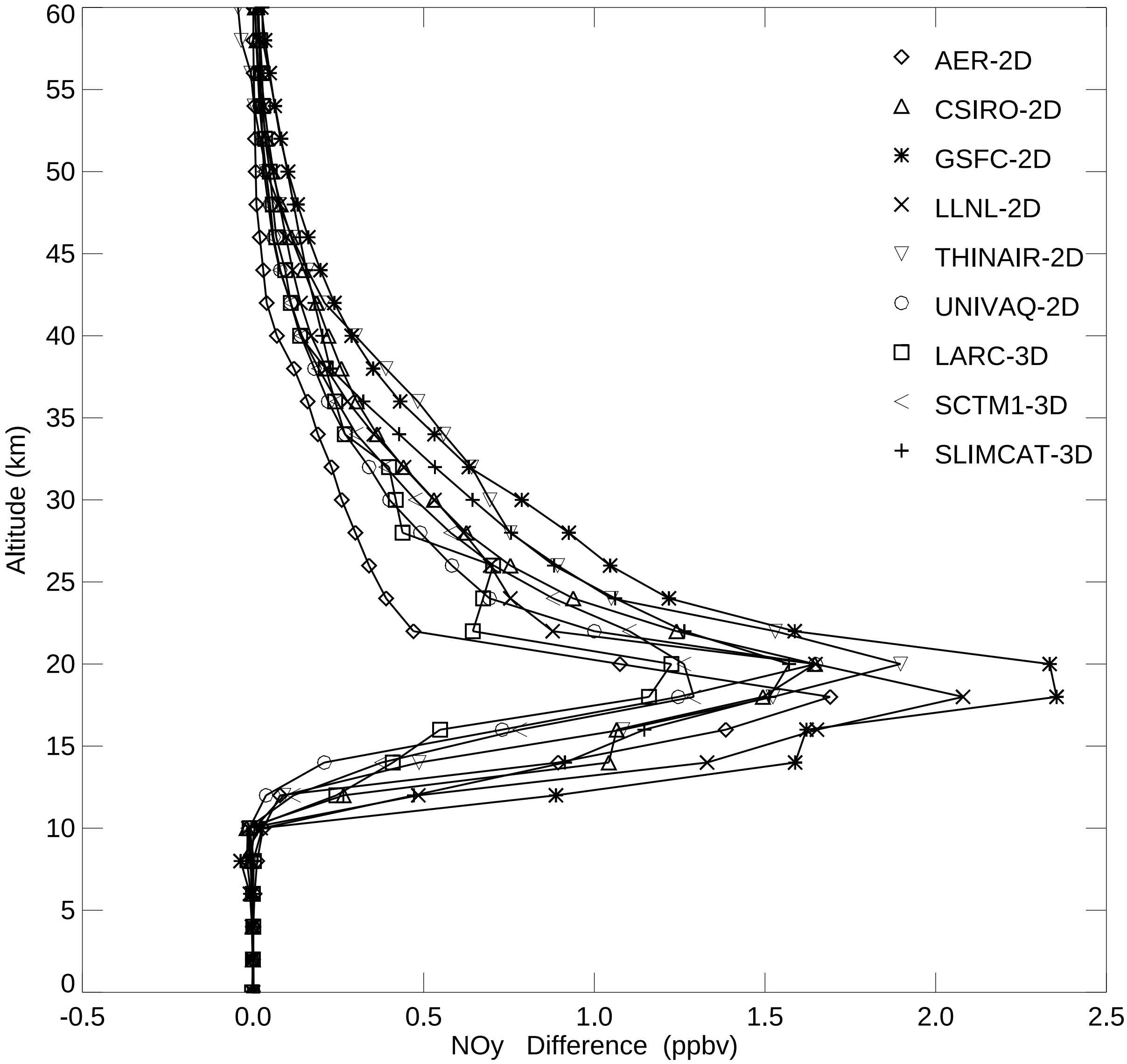

Figure 4.26: Calculated perturbations to NO_y (ppbv) as a function of altitude at 45^{o}N in June of 2015 due to NO_x emissions from a fleet of 500 HSCT aircraft with EI(NO_x)=10 under Scenario S1d relative to Scenario D.

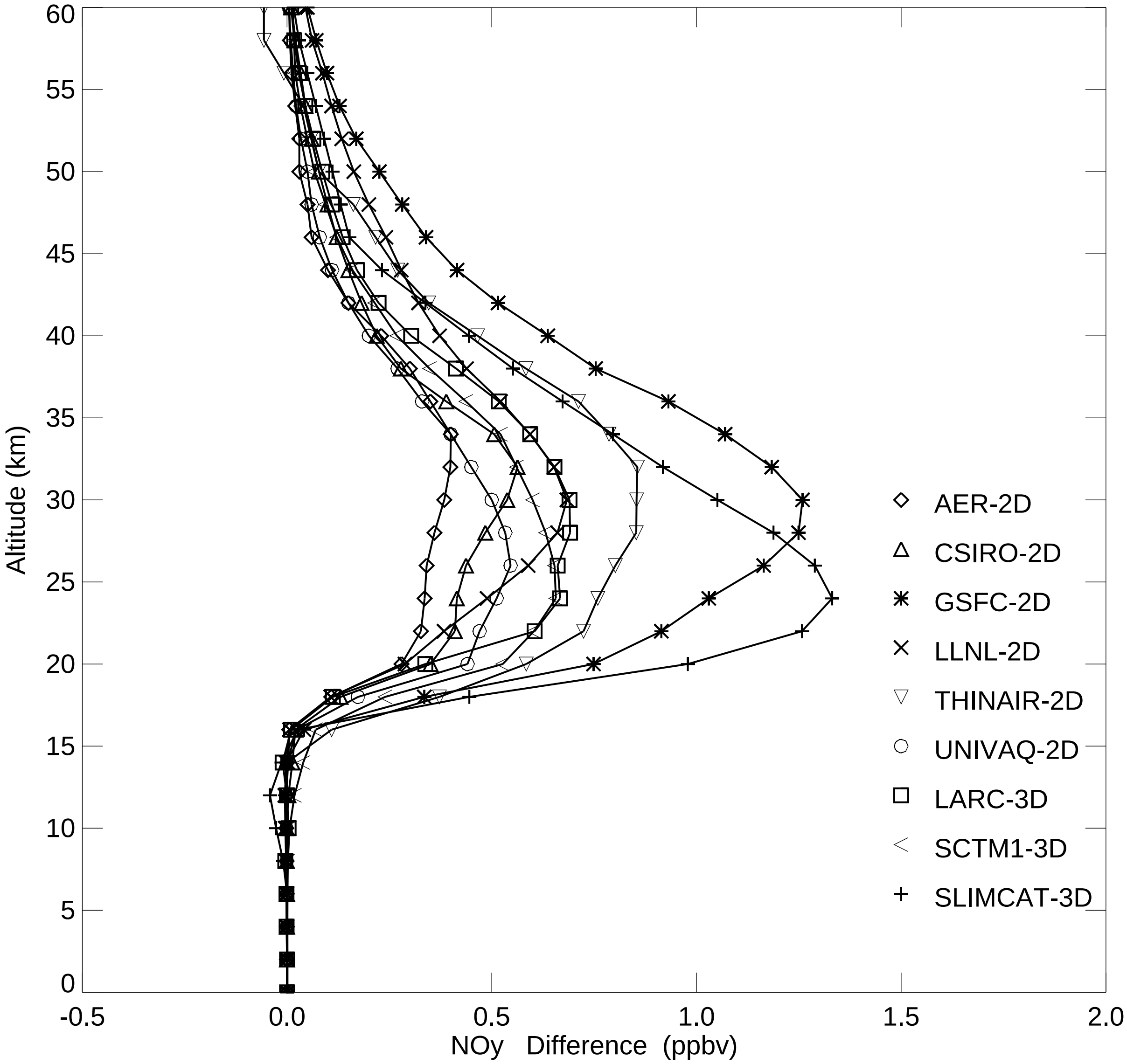

Figure 4.27: Calculated perturbations to NO_y (ppbv) as a function of altitude at the equator in June of 2015 due to NO_x emissions from a fleet of 500 HSCT aircraft with EI(NO_x)=10 under Scenario S1d relative to Scenario D.

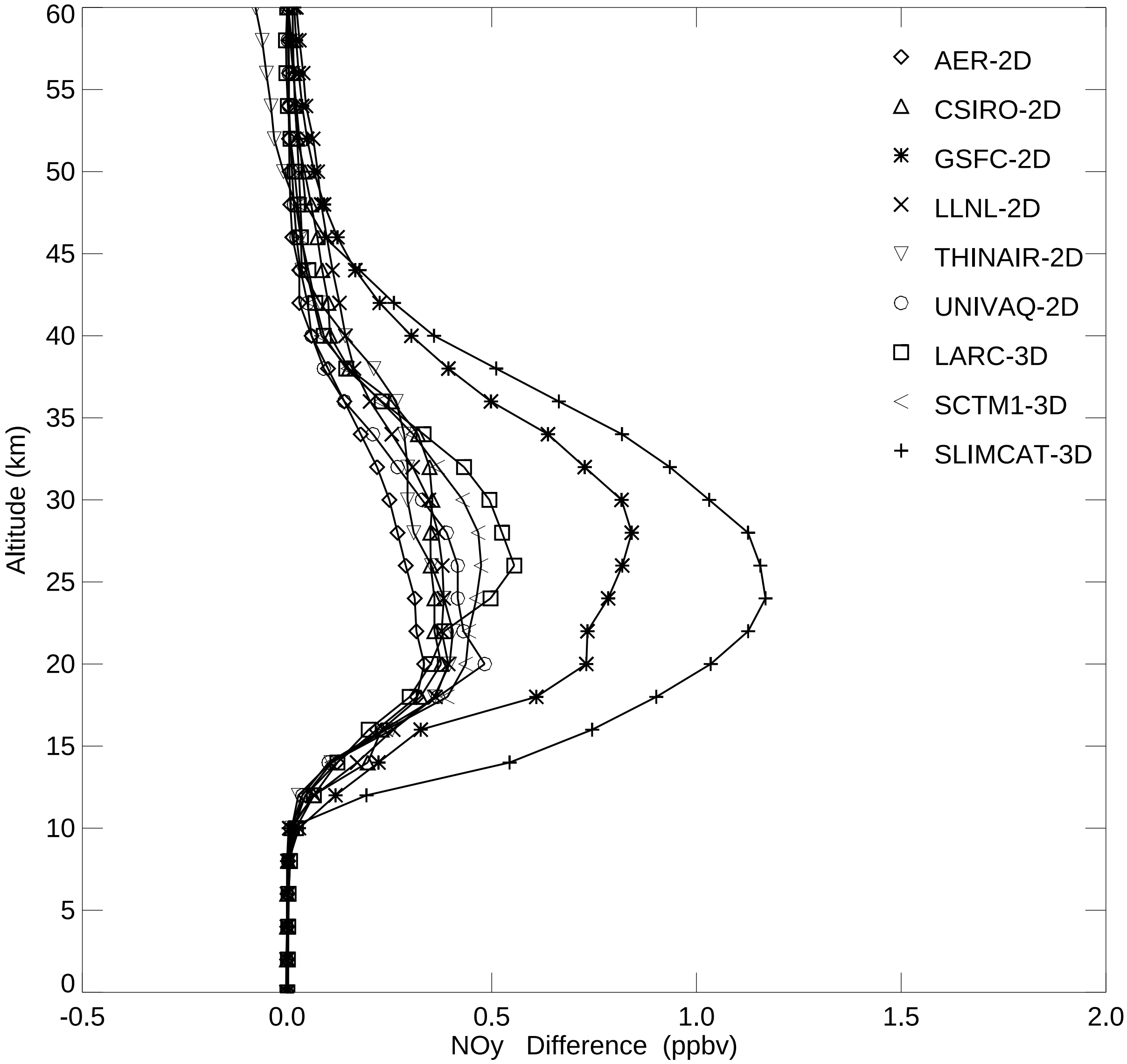

Figure 4.28: Calculated perturbations to NO_y (ppbv) as a function of altitude at 45^{o}S in June of 2015 due to NO_x emissions from a fleet of 500 HSCT aircraft with EI(NO_x)=10 under Scenario S1d relative to Scenario D.

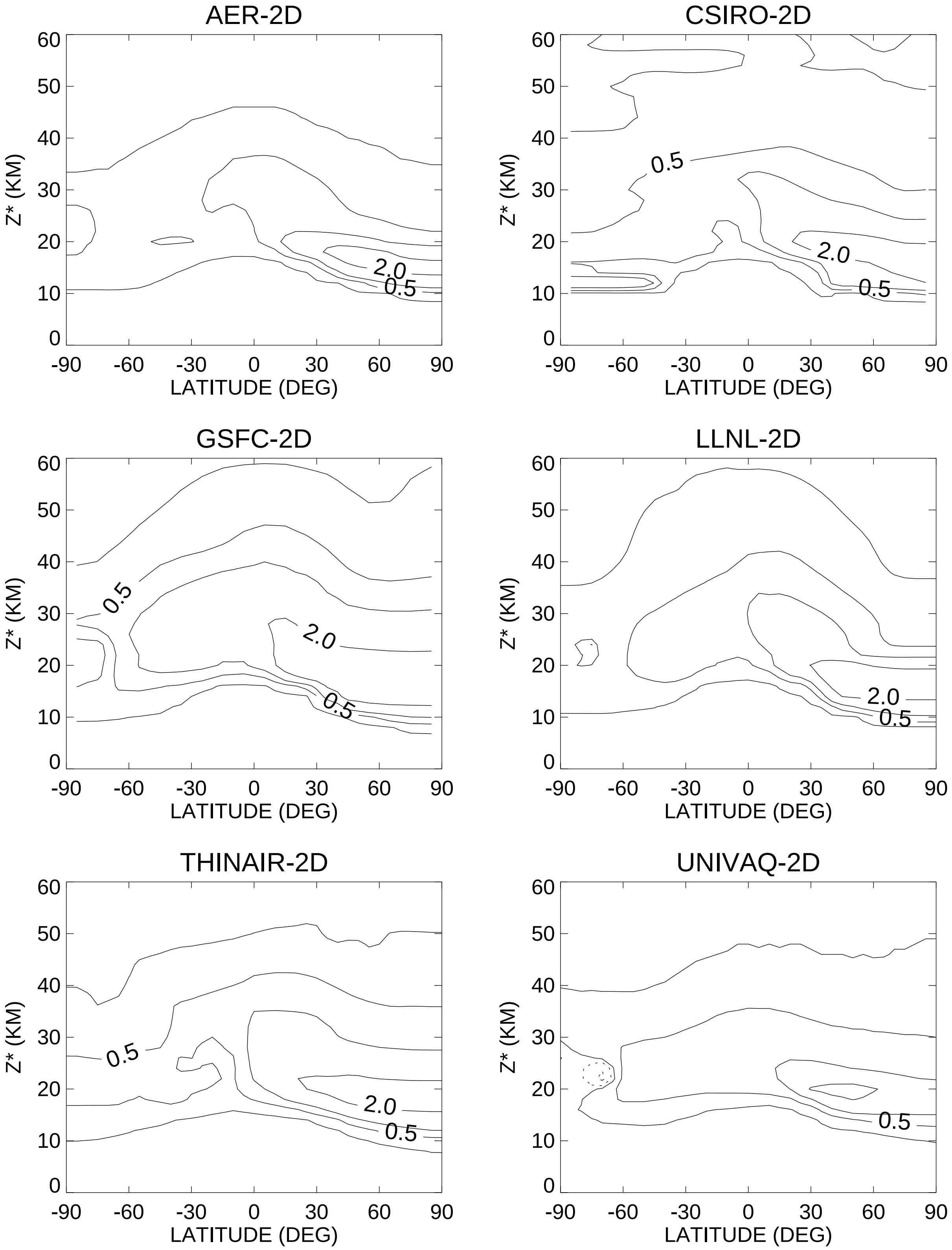

Figure 4.29: Calculated perturbations to NO_y (ppbv) as a function of latitude and altitude in June of 2015 due to NO_x emissions from a fleet of 500 HSCT aircraft with EI(NO_x)=15 under Scenario S1e relative to Scenario D. Contours are -1.0, -0.5, -0.1 0, 0.1, 0.5, 1, 2, 3 ppbv.

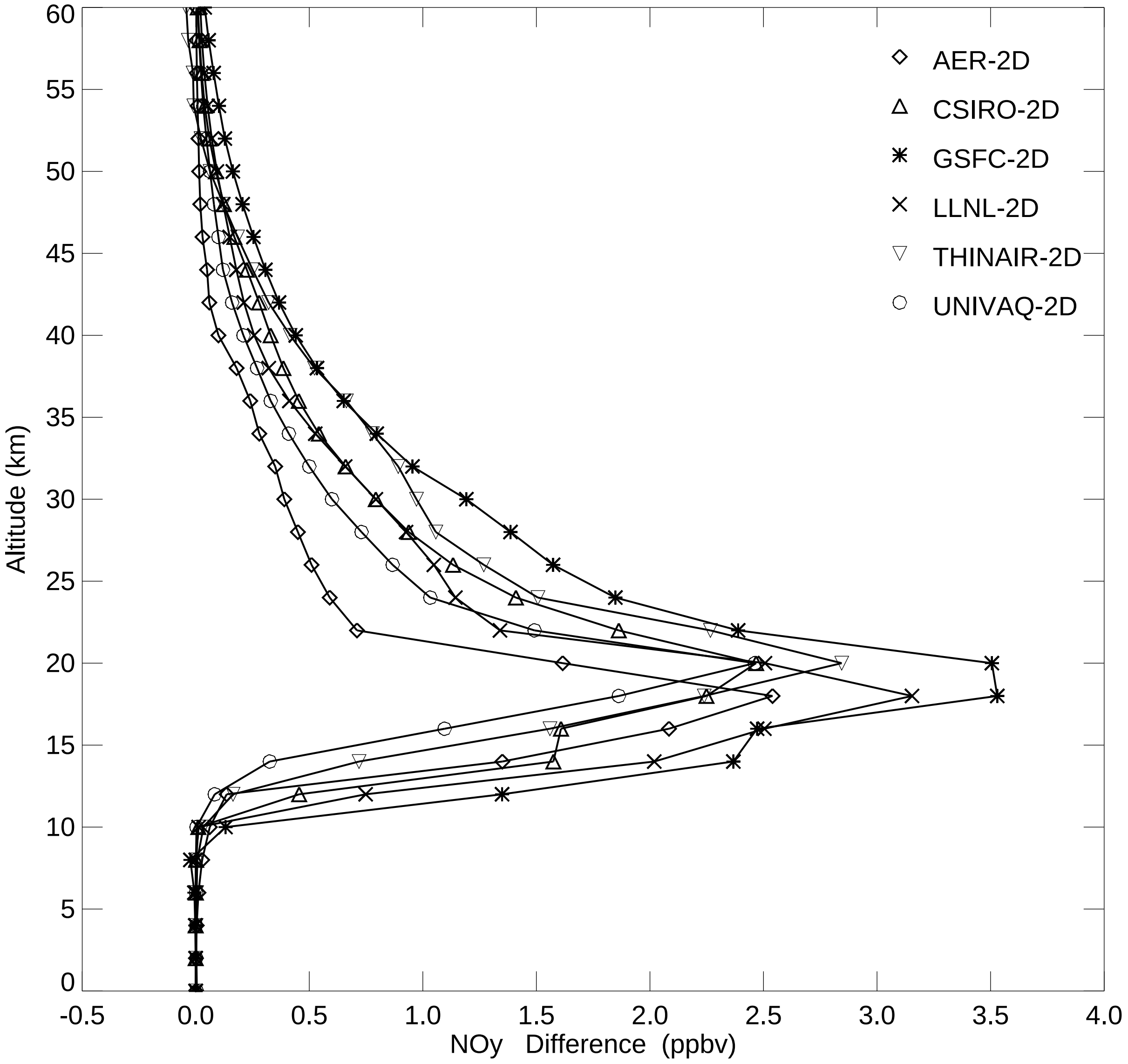

Figure 4.30: Calculated perturbations to NO_y (ppbv) as a function of altitude at 45^{o}N in June of 2015 due to NO_x emissions from a fleet of 500 HSCT aircraft with EI(NO_x)=15 under Scenario S1e relative to Scenario D.

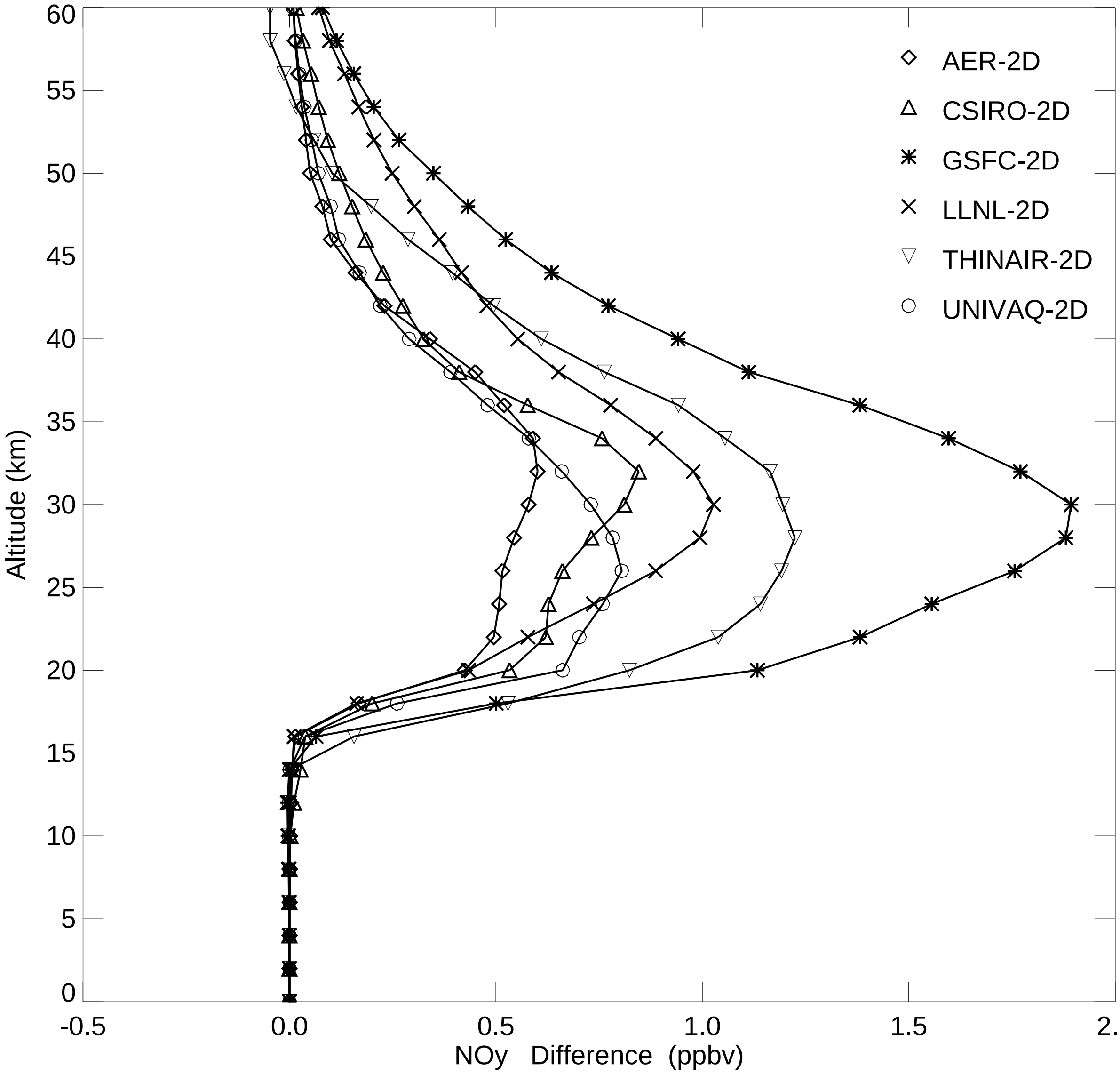

Figure 4.31: Calculated perturbations to NO_y (ppbv) as a function of altitude at the equator in June of 2015 due to NO_x emissions from a fleet of 500 HSCT aircraft with $EI(NO_x)=15$ under Scenario S1e relative to Scenario D.

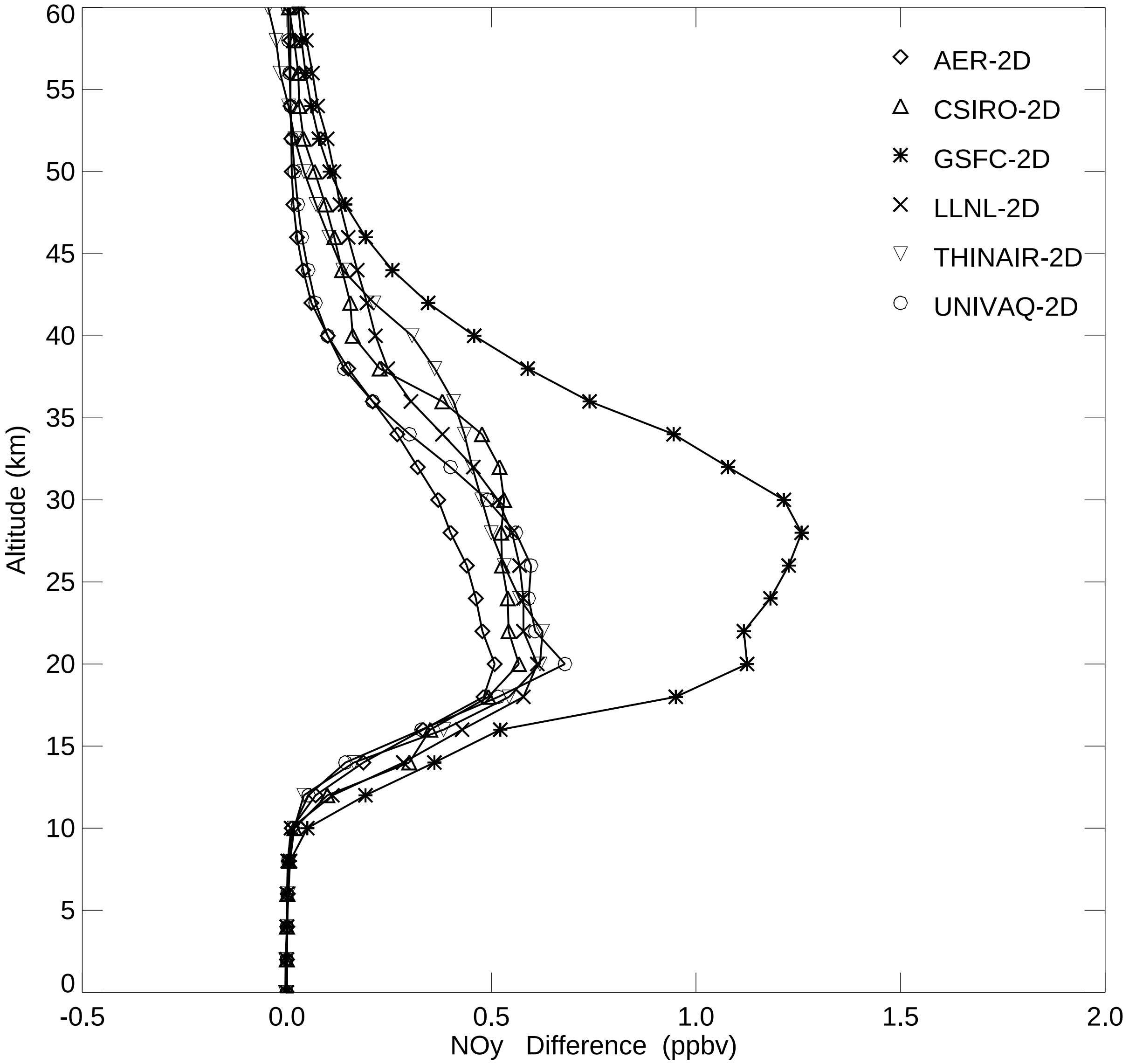

Figure 4.32: Calculated perturbations to NO_y (ppbv) as a function of altitude at 45^{o}S in June of 2015 due to NO_x emissions from a fleet of 500 HSCT aircraft with EI(NO_x)=15 under Scenario S1e relative to Scenario D.

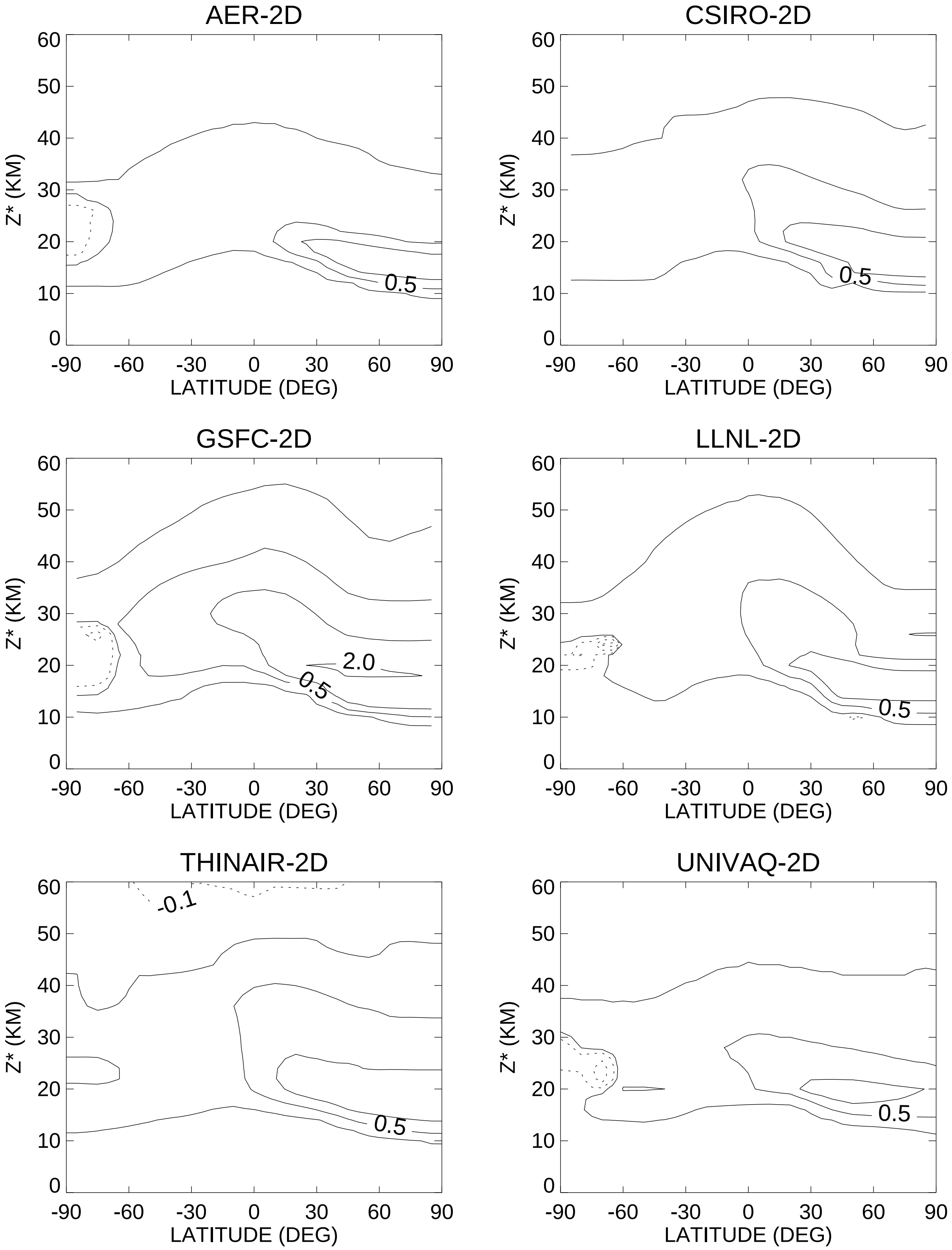

Figure 4.33: Calculated perturbations to NO_y (ppbv) as a function of latitude and altitude in June of 2015 due to NO_x emissions from a fleet of 1000 HSCT aircraft with $EI(NO_x)=5$ under Scenario S1i relative to Scenario D. Contours are -1.0, -0.5, 0, 0.5, 1.0, 2.0 ppbv.

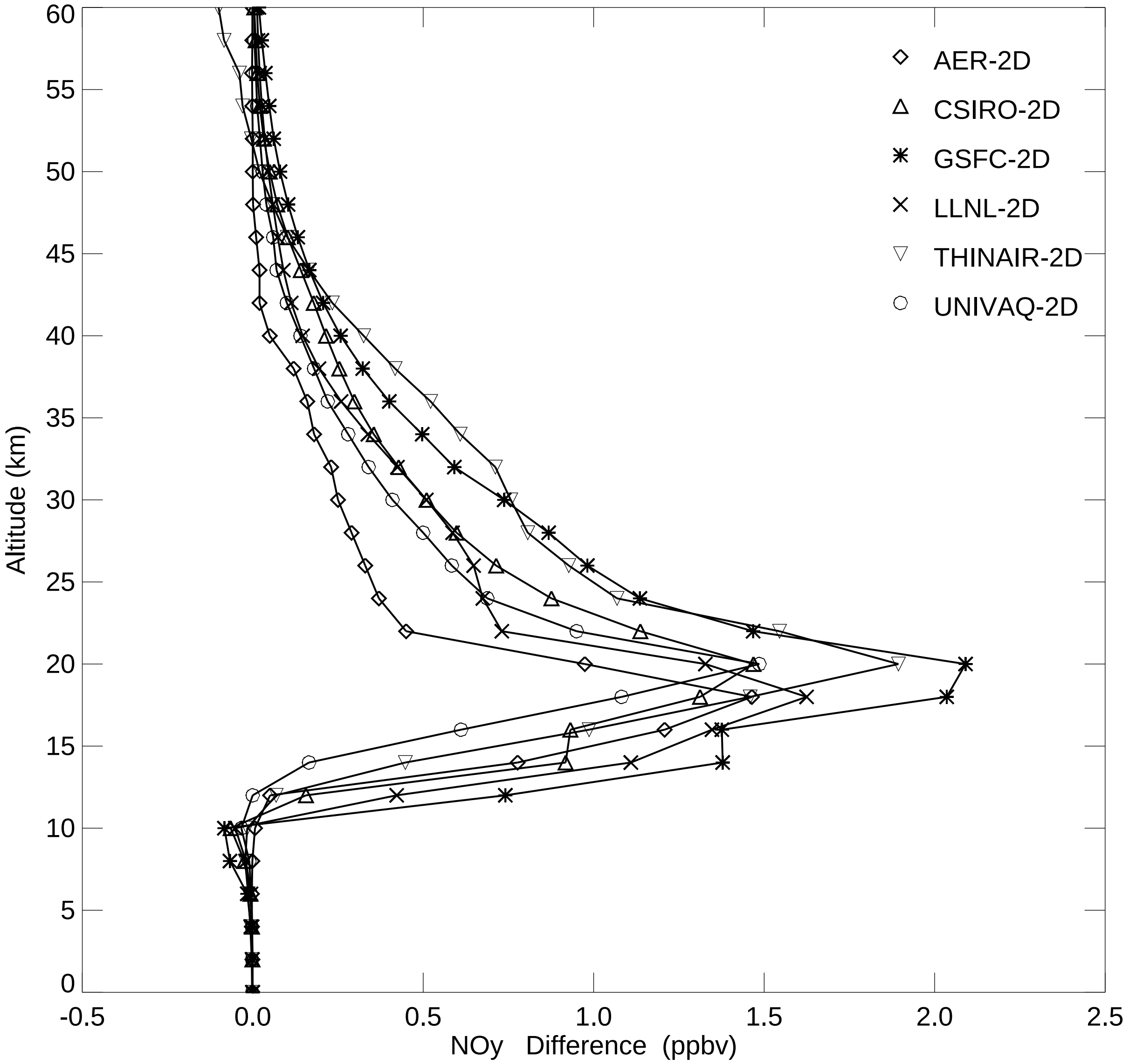

Figure 4.34: Calculated perturbations to NO_y (ppbv) as a function of altitude at 45^{o}N in June of 2015 due to NO_x emissions from a fleet of 1000 HSCT aircraft with EI(NO_x)=5 under Scenario S1i relative to Scenario D.

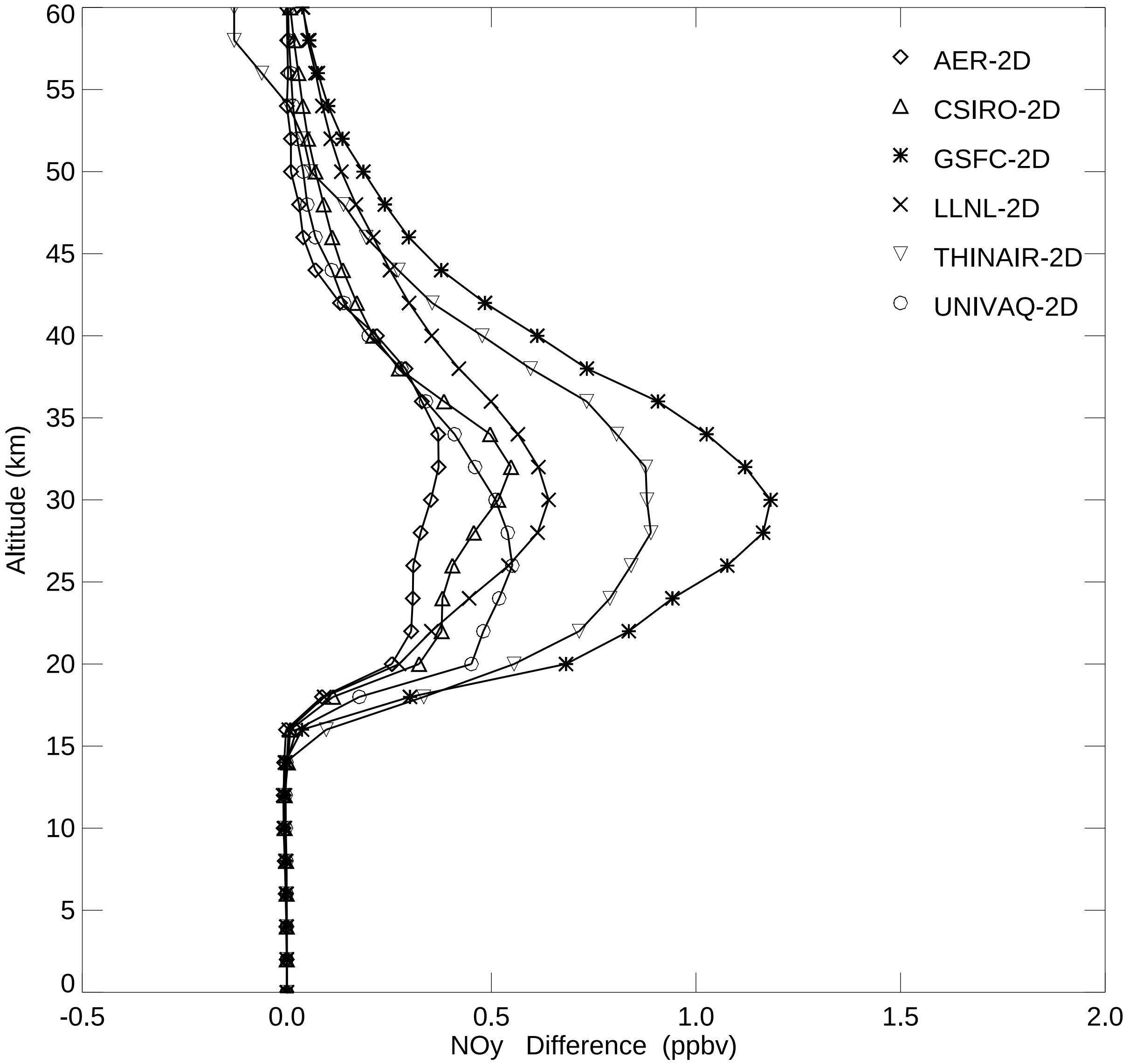

Figure 4.35: Calculated perturbations to NO_y (ppbv) as a function of altitude at the equator in June of 2015 due to NO_x emissions from a fleet of 1000 HSCT aircraft with $EI(NO_x)=5$ under Scenario S1i relative to Scenario D.

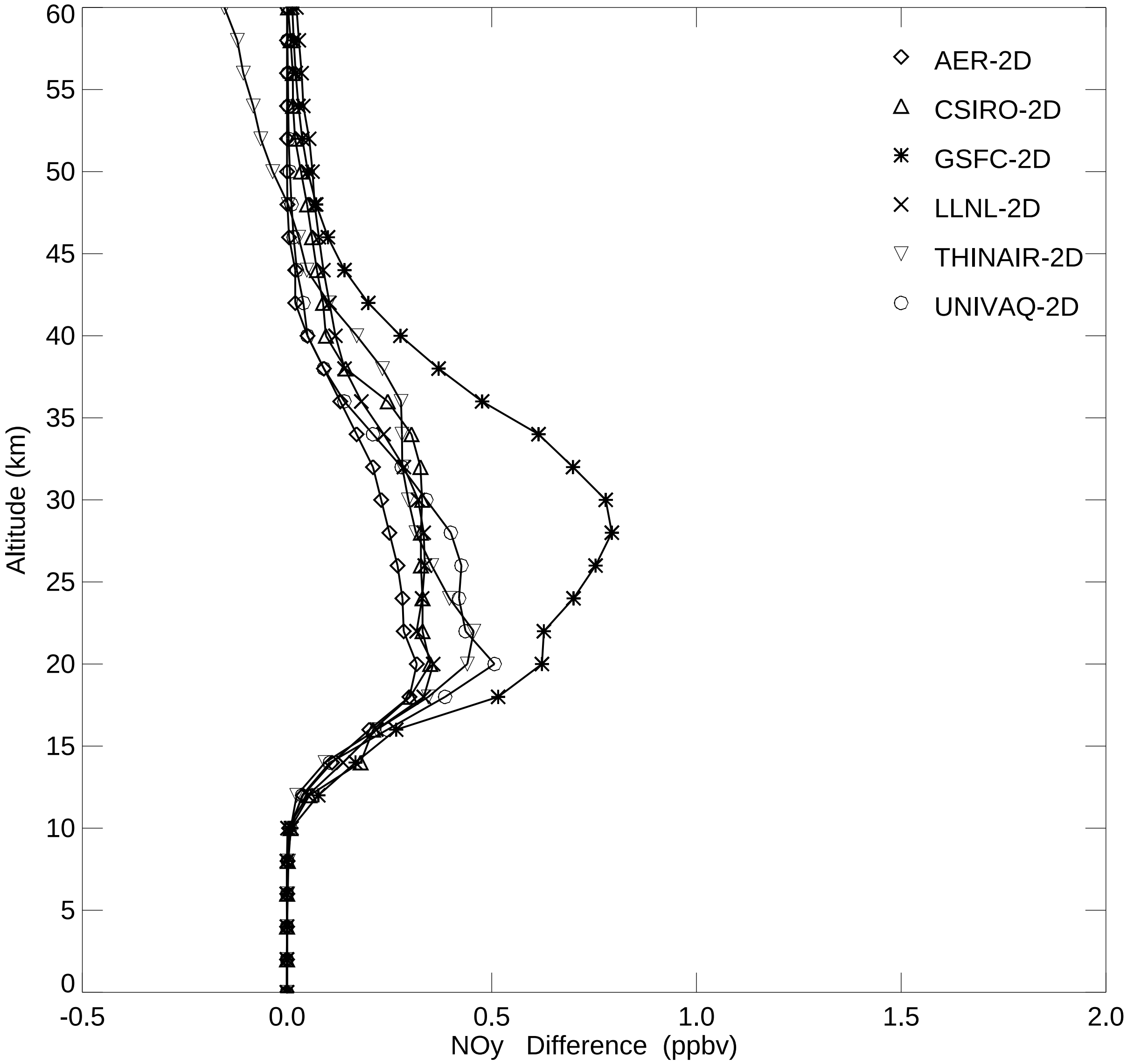

Figure 4.36: Calculated perturbations to NO_y (ppbv) as a function of altitude at 45^{o}S in June of 2015 due to NO_x emissions from a fleet of 1000 HSCT aircraft with EI(NO_x)=5 under Scenario S1i relative to Scenario D.

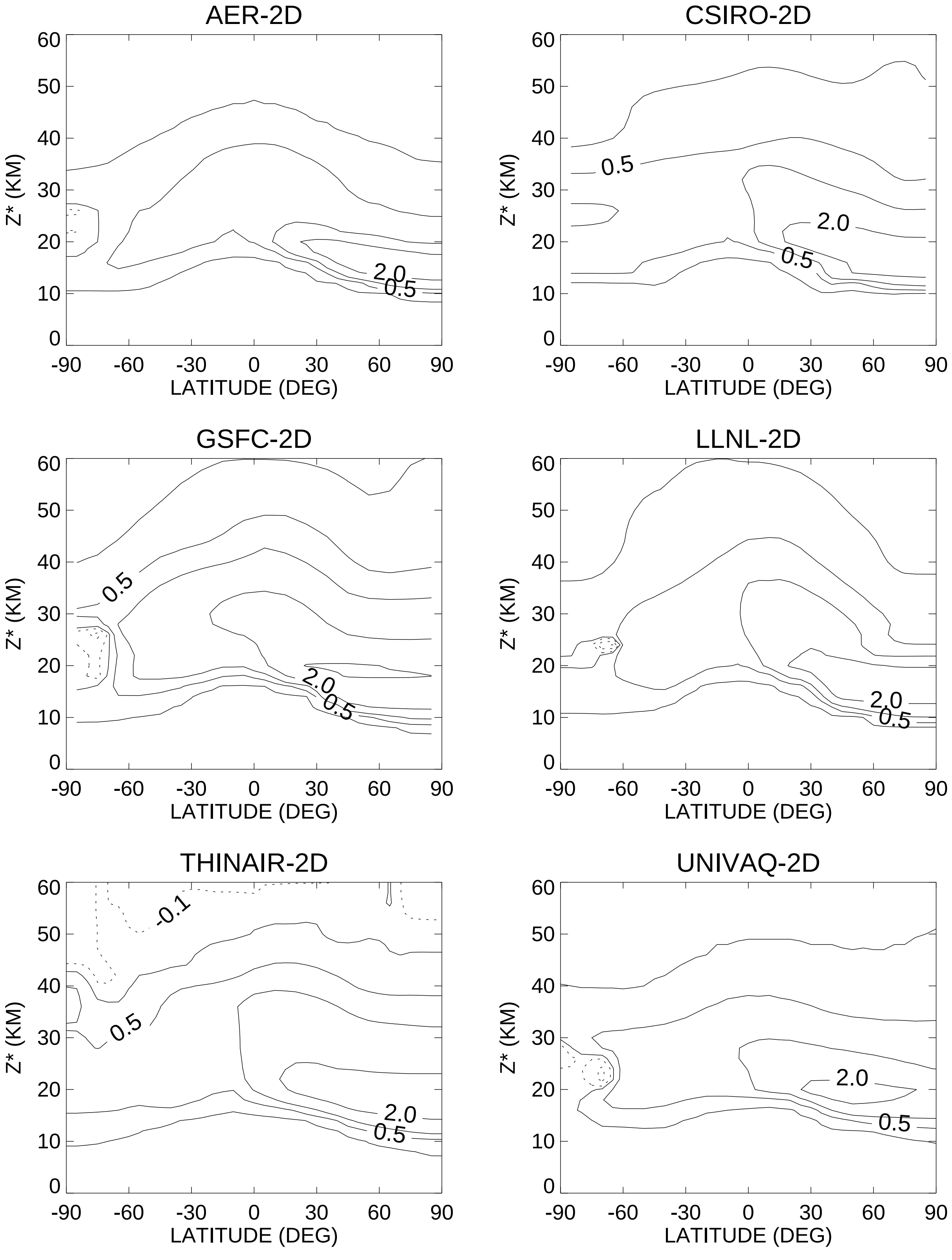

Figure 4.37: Calculated perturbations to NO_y (ppbv) as a function of latitude and altitude in June of 2015 due to NO_x emissions from a fleet of 1000 HSCT aircraft with EI(NO_x)=10 under Scenario S1j relative to Scenario D. Contours are -1, -0.5, -0.1, 0, -.1, 0.5, 1, 2, 3, 4 ppbv.

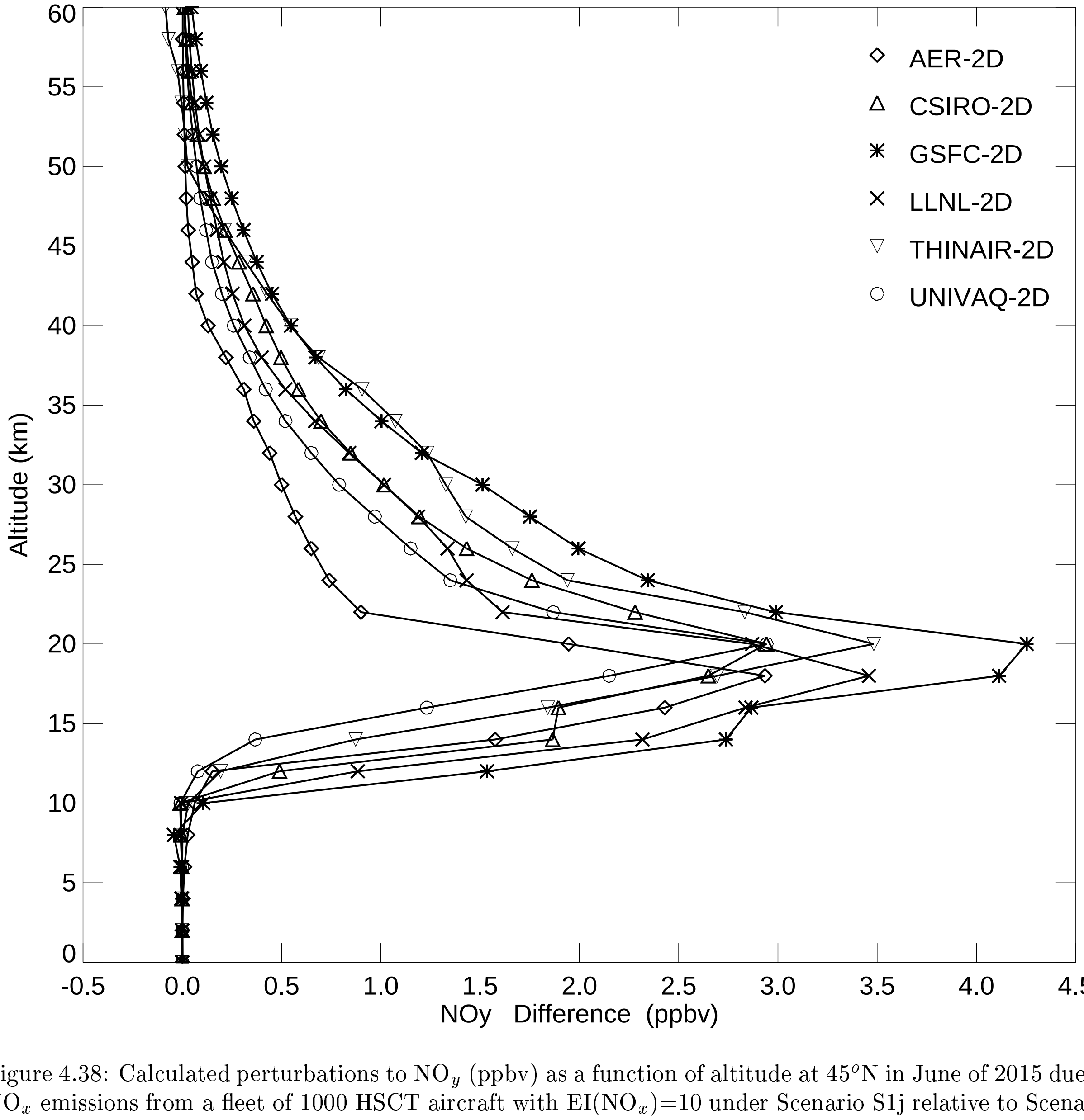

Figure 4.38: Calculated perturbations to NO_y (ppbv) as a function of altitude at 45^oN in June of 2015 due to NO_x emissions from a fleet of 1000 HSCT aircraft with $EI(NO_x)$=10 under Scenario S1j relative to Scenario D.

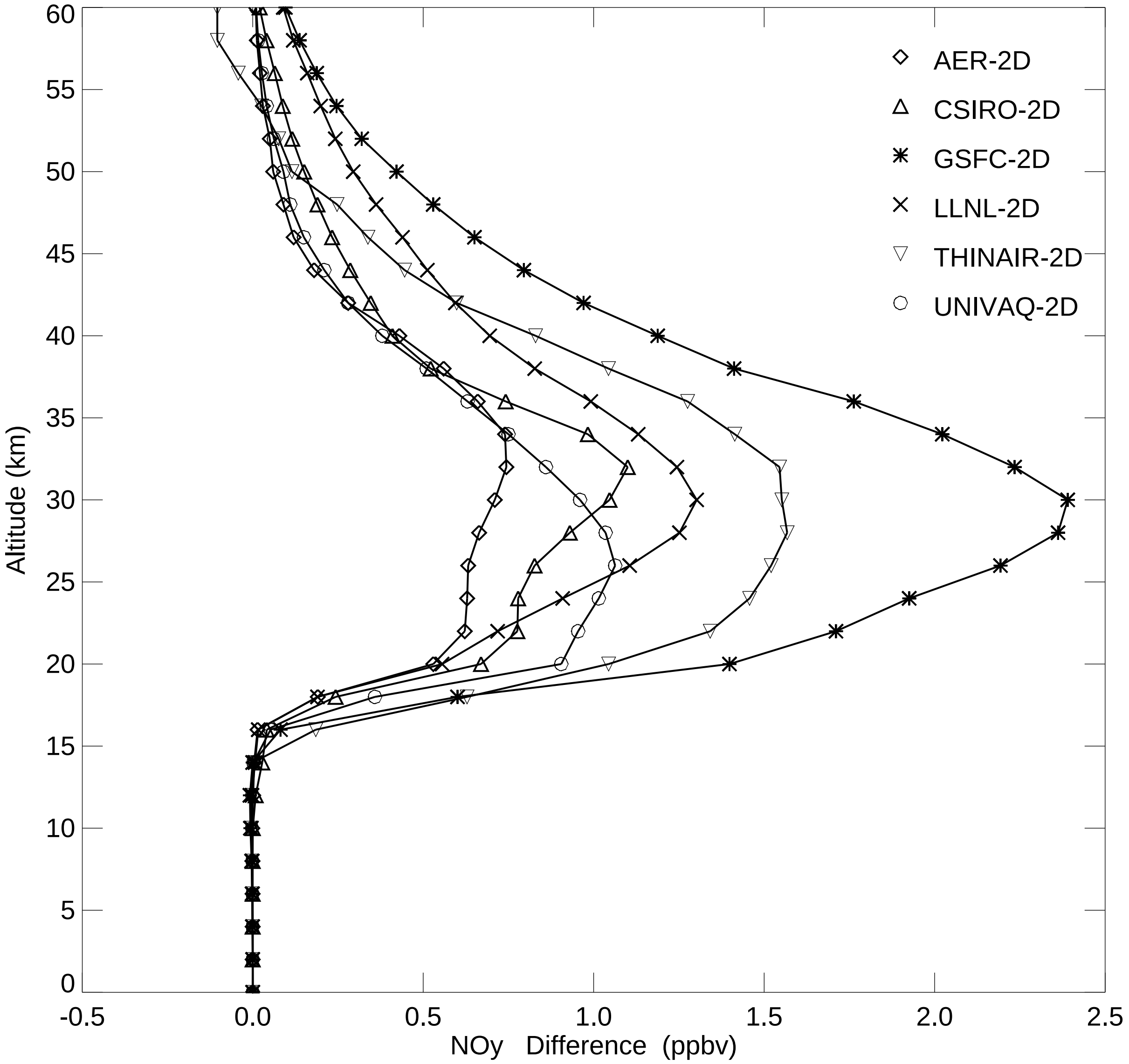

Figure 4.39: Calculated perturbations to NO_y (ppbv) as a function of altitude at the equator in June of 2015 due to NO_x emissions from a fleet of 1000 HSCT aircraft with EI(NO_x)=10 under Scenario S1j relative to Scenario D.

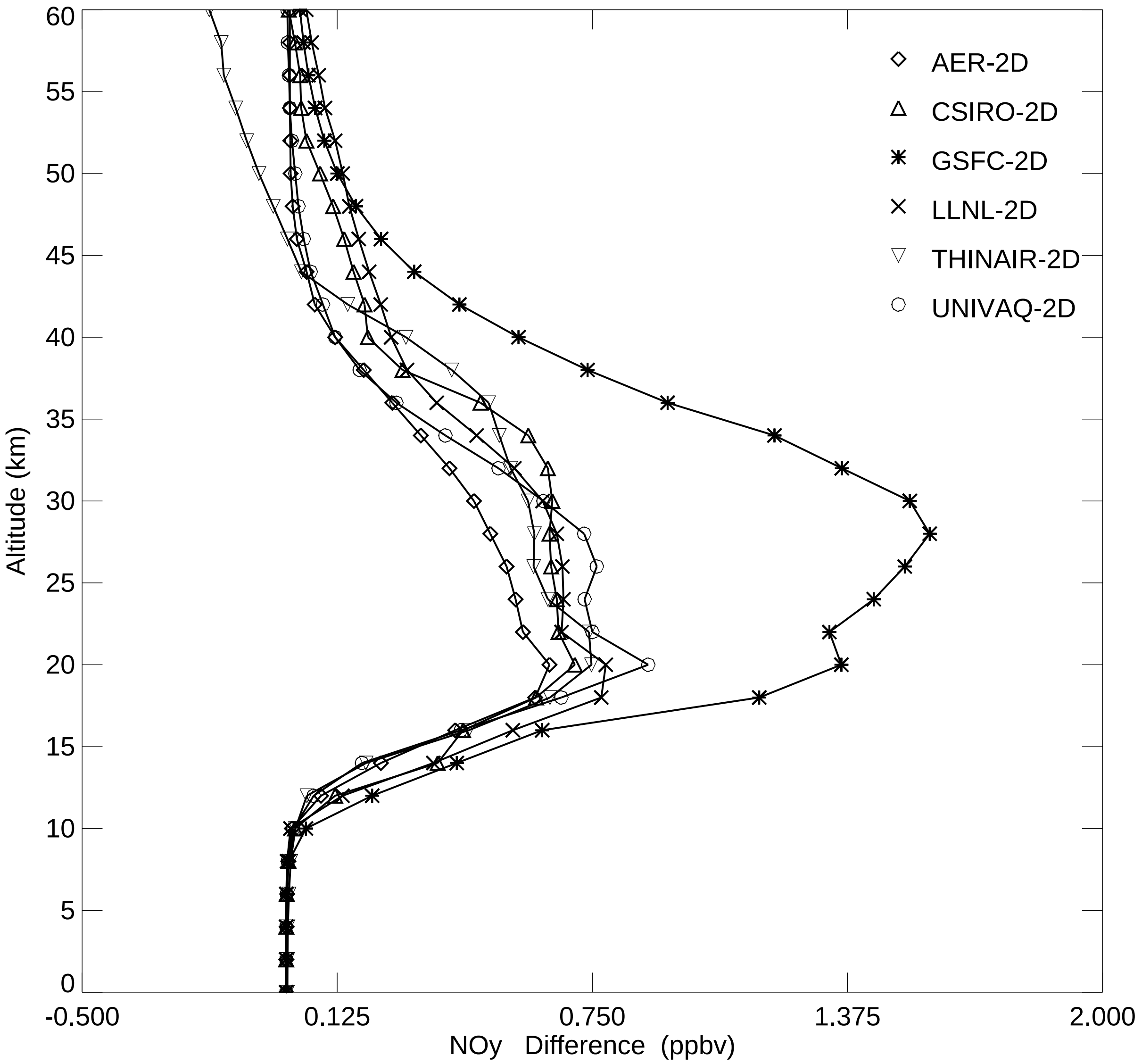

Figure 4.40: Calculated perturbations to NO_y (ppbv) as a function of altitude at 45^{o}S in June of 2015 due to NO_x emissions from a fleet of 1000 HSCT aircraft with EI(NO_x)=10 under Scenario S1j relative to Scenario D.

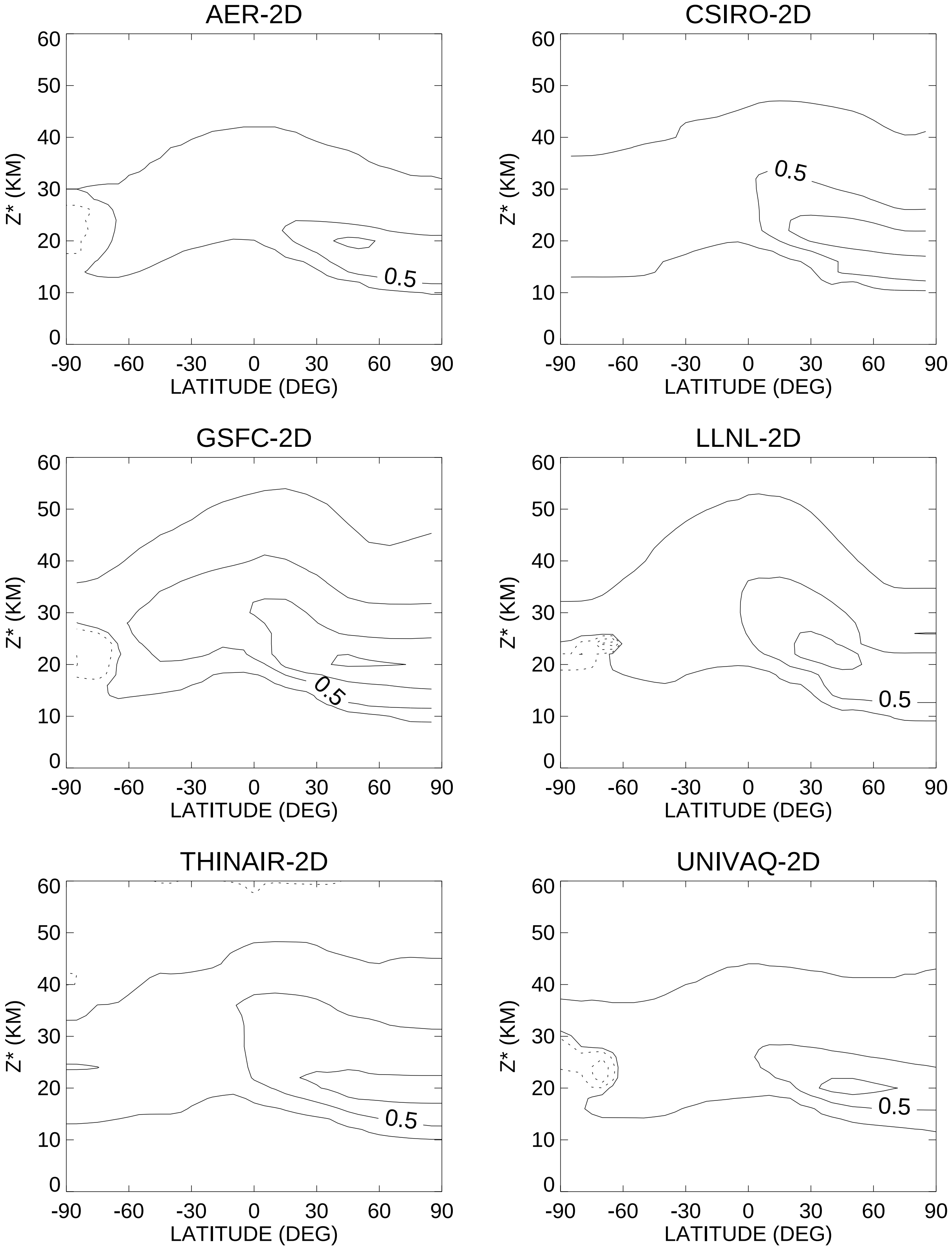

Figure 4.41: Calculated perturbations to NO_y (ppbv) as a function of latitude and altitude in June of 2015 due to NO_x emissions from a fleet of 500 HSCT aircraft operating at 2 km above nominal cruise altitude with EI(NO_x)=5 under Scenario S2a relative to Scenario D. Contours are -1.0, -0.5, 0, 0.5, 1.0, 2.0 ppbv.

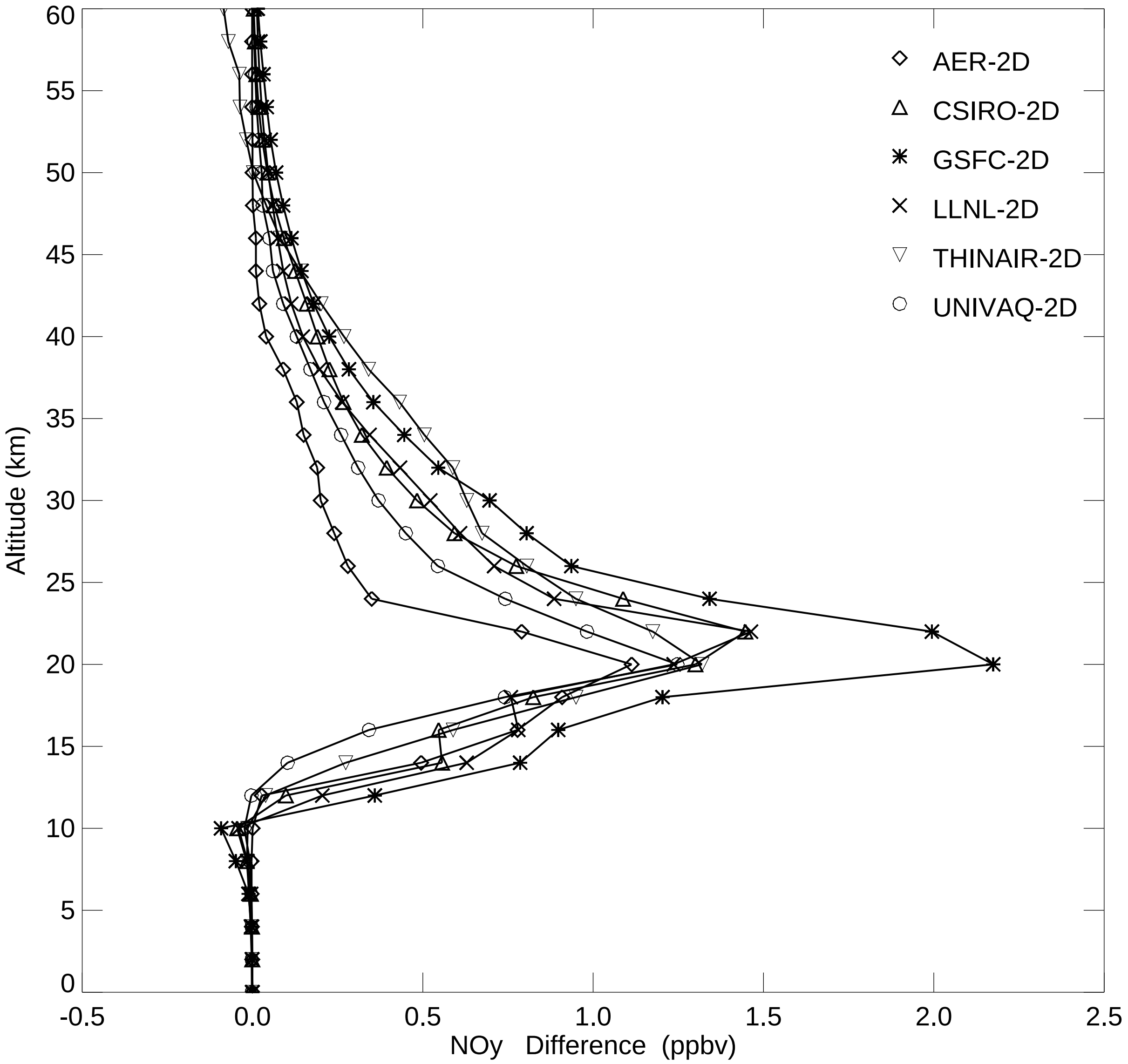

Figure 4.42: Calculated perturbations to NO_y (ppbv) as a function of altitude at 45°N in June of 2015 due to NO_x emissions from a fleet of 500 HSCT aircraft operating at 2 km above nominal cruise altitude with $EI(NO_x)$=5 under Scenario S2a relative to Scenario D.

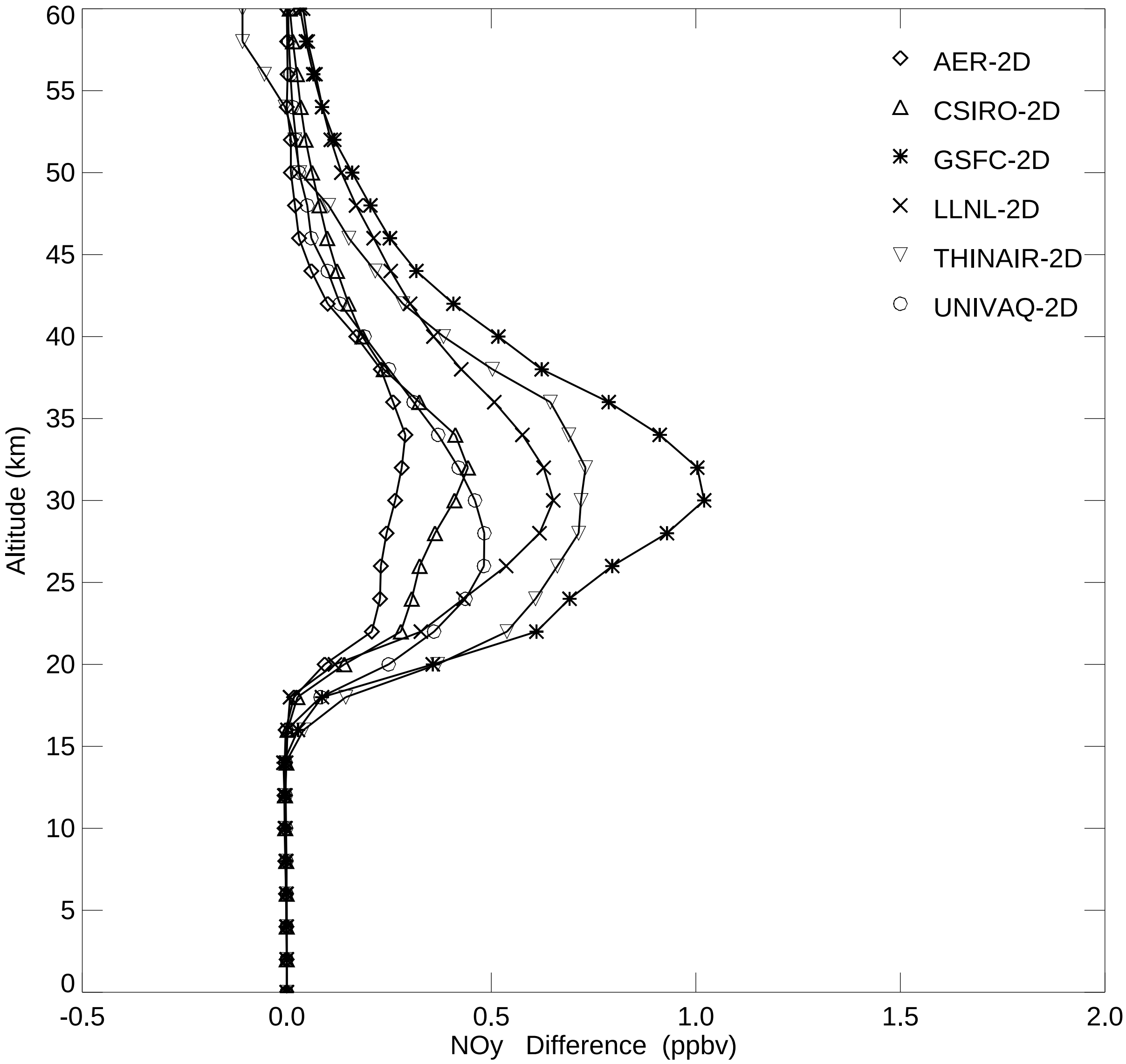

Figure 4.43: Calculated perturbations to NO_y (ppbv) as a function of altitude at the equator in June of 2015 due to NO_x emissions from a fleet of 500 HSCT aircraft operating at 2 km above nominal cruise altitude with $EI(NO_x)=5$ under Scenario S2a relative to Scenario D.

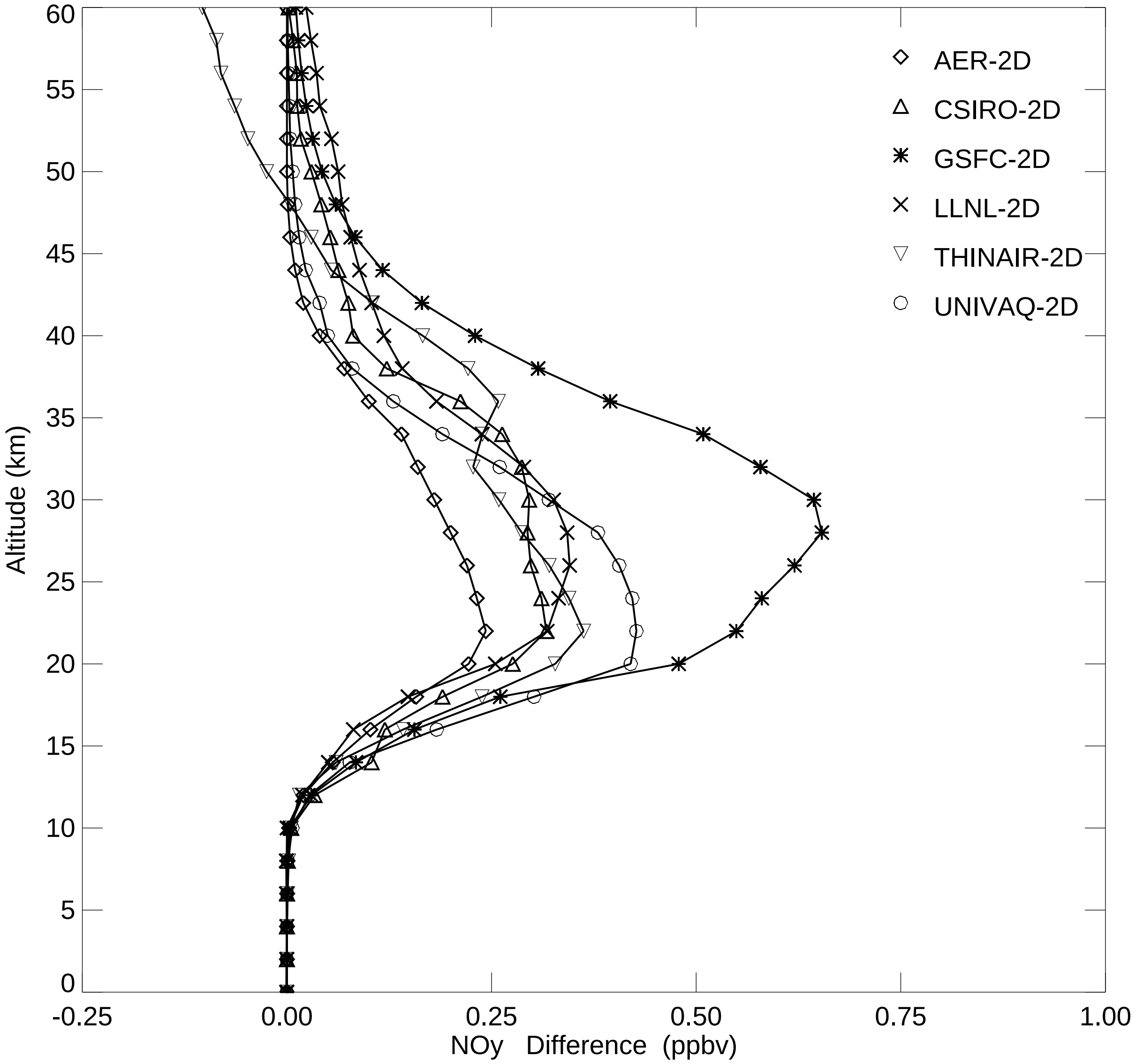

Figure 4.44: Calculated perturbations to NO_y (ppbv) as a function of altitude at 45^oS in June of 2015 due to NO_x emissions from a fleet of 500 HSCT aircraft operating at 2 km above nominal cruise altitude with $EI(NO_x)$=5 under Scenario S2a relative to Scenario D.

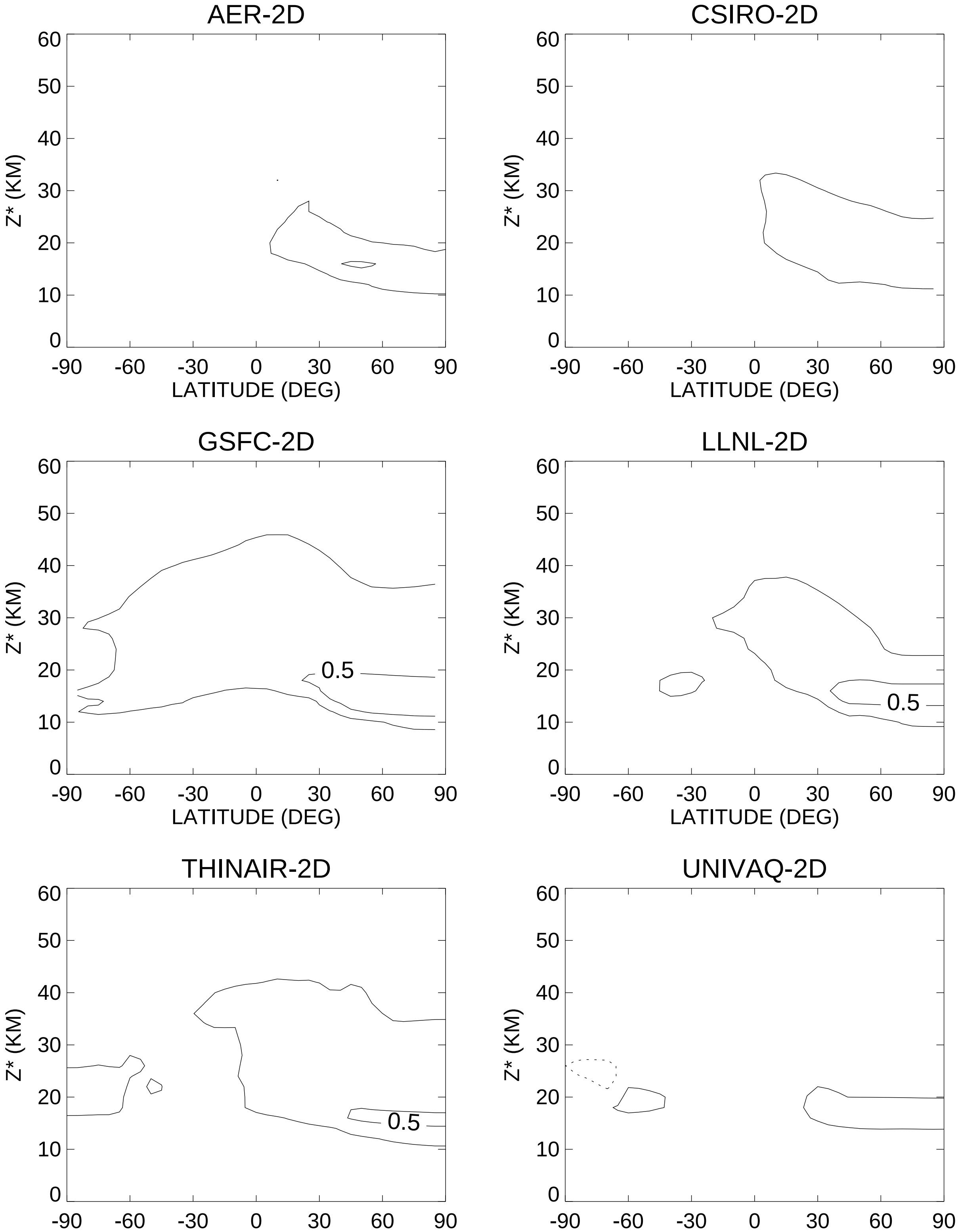

Figure 4.45: Calculated perturbations to NO_y (ppbv) as a function of latitude and altitude in June of 2015 due to NO_x emissions from a fleet of 500 HSCT aircraft operating at 2 km below nominal cruise altitude with $EI(NO_x)$=5 under Scenario S2b relative to Scenario D. Contours are -0.1, 0, 0.1, 0.25, 0.5, 0.75 ppbv.

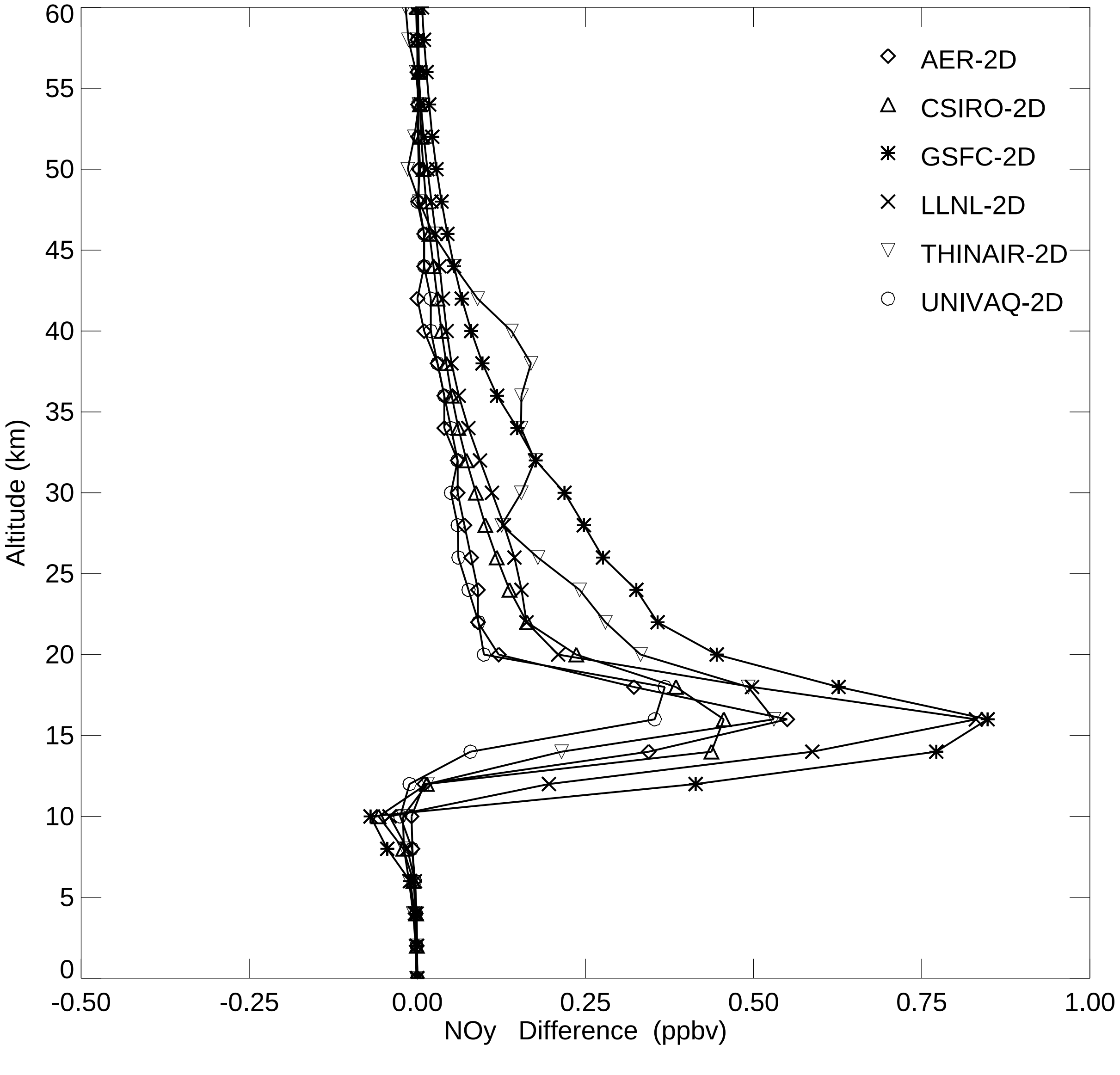

Figure 4.46: Calculated perturbations to NO_y (ppbv) as a function of altitude at 45^{o}N in June of 2015 due to NO_x emissions from a fleet of 500 HSCT aircraft operating at 2 km below nominal cruise altitude with $EI(NO_x)=5$ under Scenario S2b relative to Scenario D.

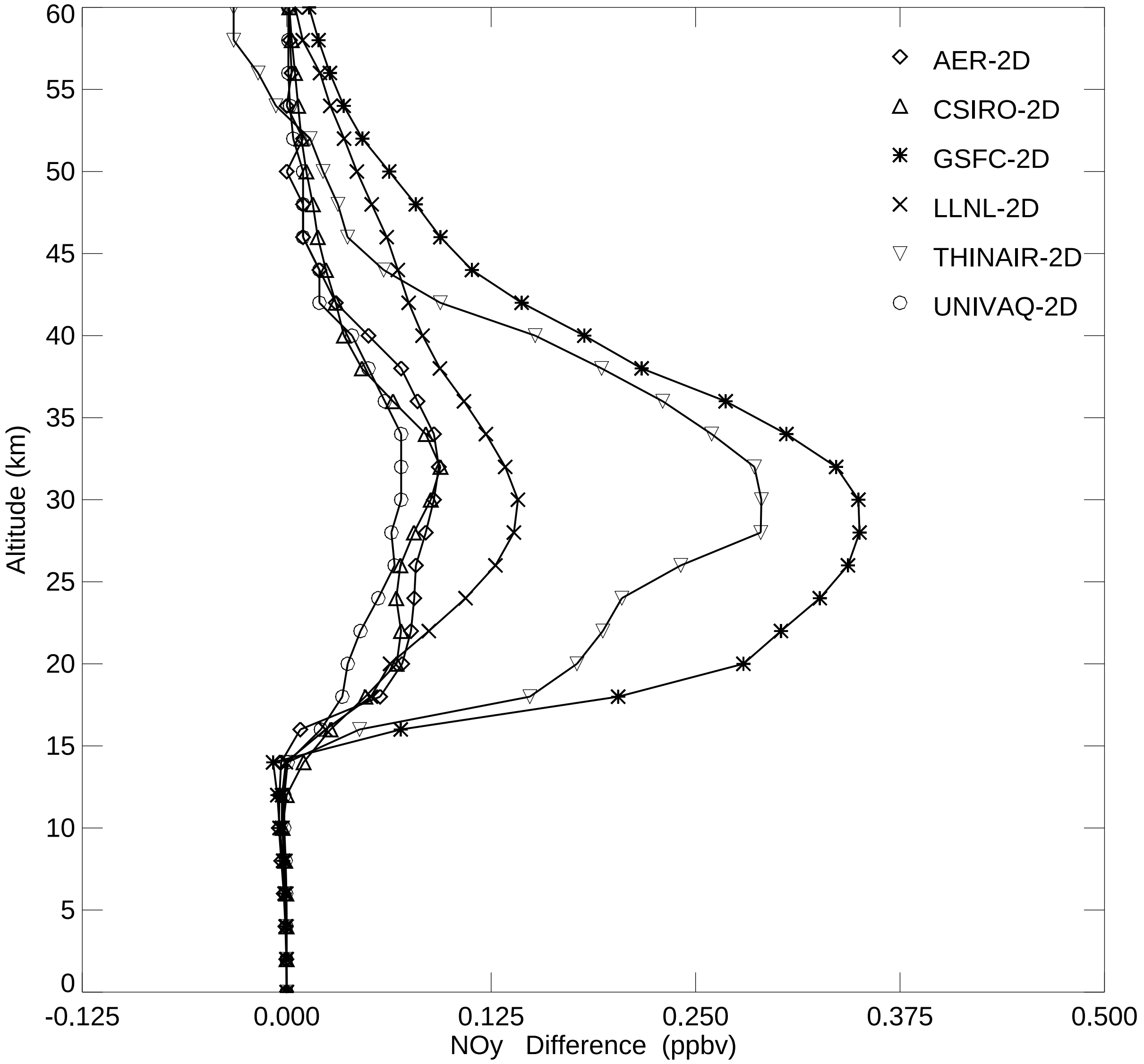

Figure 4.47: Calculated perturbations to NO_y (ppbv) as a function of altitude at the equator in June of 2015 due to NO_x emissions from a fleet of 500 HSCT aircraft operating at 2 km below nominal cruise altitude with EI(NO_x)=5 under Scenario S2b relative to Scenario D.

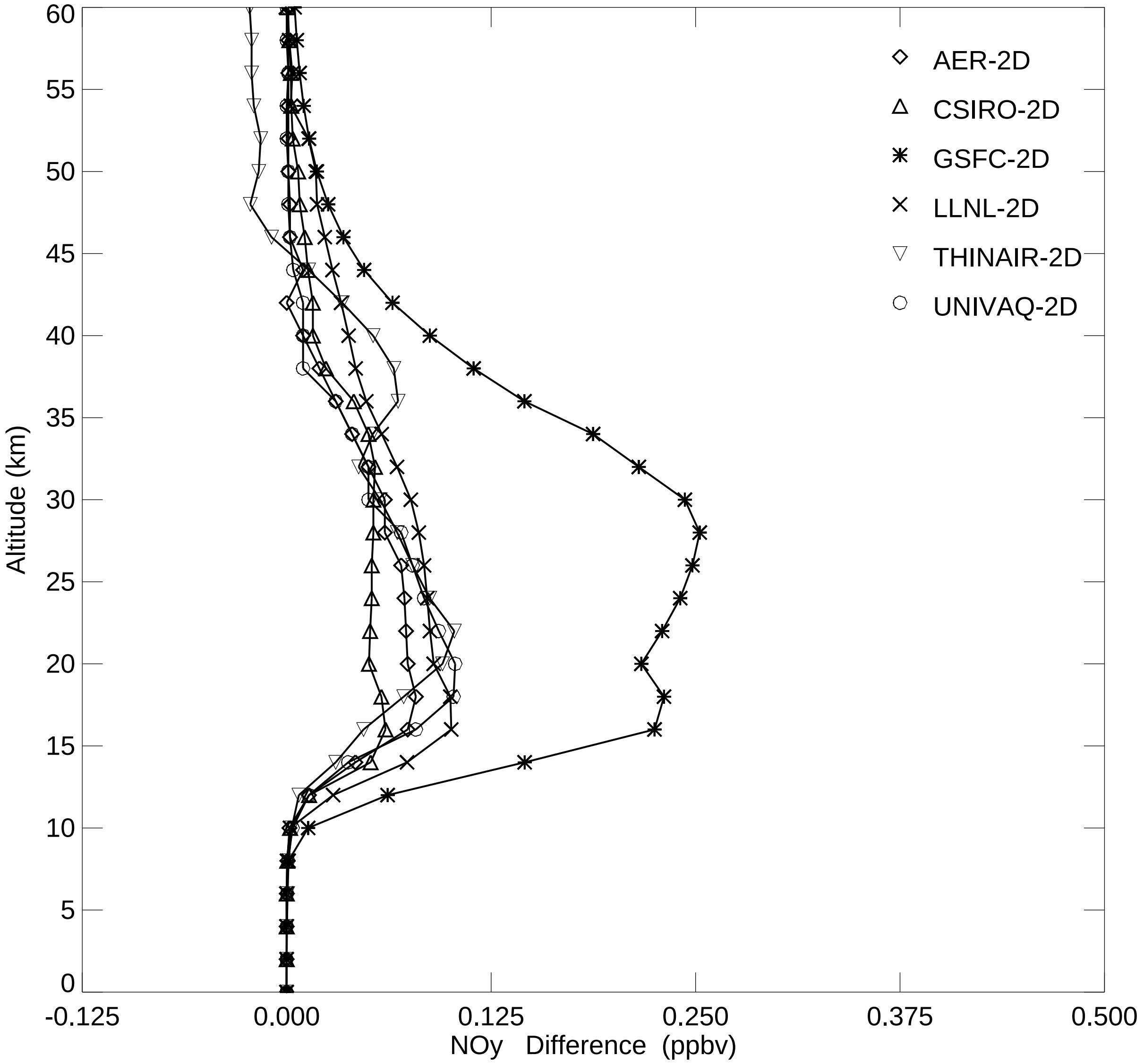

Figure 4.48: Calculated perturbations to NO_y (ppbv) as a function of altitude at 45^{o}S in June of 2015 due to NO_x emissions from a fleet of 500 HSCT aircraft operating at 2 km below nominal cruise altitude with EI(NO_x)=5 under Scenario S2b relative to Scenario D.

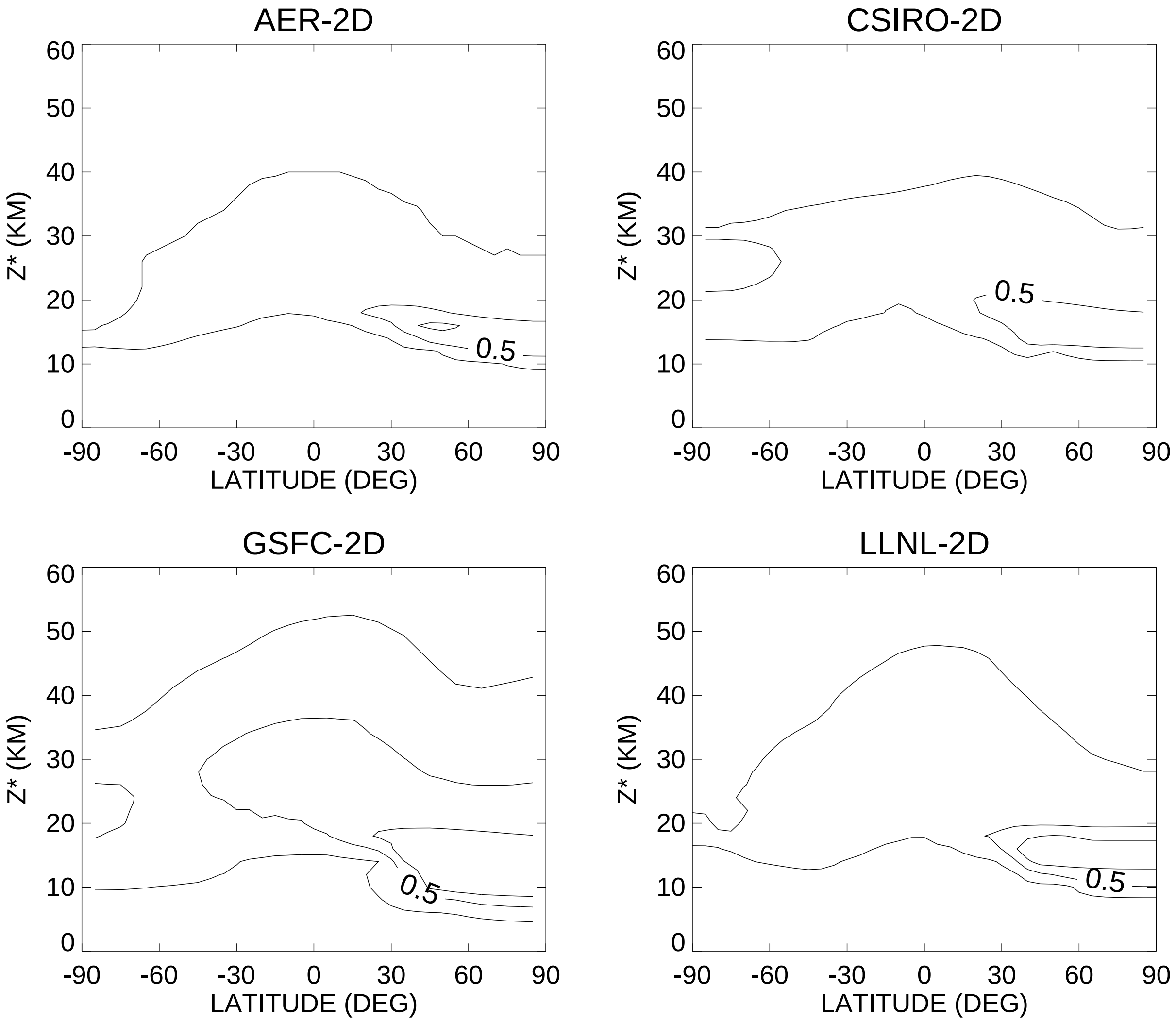

Figure 4.49: Calculated perturbations to NO_y (ppbv) as a function of latitude and altitude in June of 2015 due to NO_x emissions from a fleet of 500 HSCT aircraft operating at 2 km below nominal cruise altitude with EI(NO_x)=10 under Scenario S2c relative to Scenario D. Contours are 0, 0.5, 1.0 ppbv.

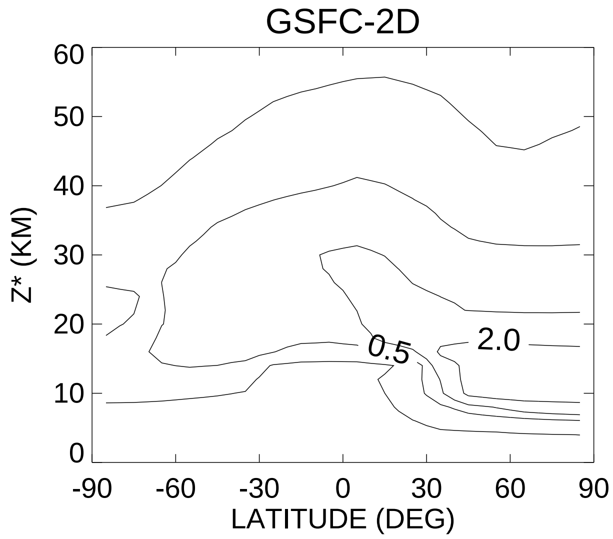

Figure 4.50: Calculated perturbations to NO_y (ppbv) as a function of latitude and altitude in June of 2015 due to NO_x emissions from a fleet of 500 HSCT aircraft operating at 2 km below nominal cruise altitude with EI(NO_x)=15 under Scenario S2d relative to Scenario D. Contours are 0, 0.5, 1.0, 2.0 ppbv.

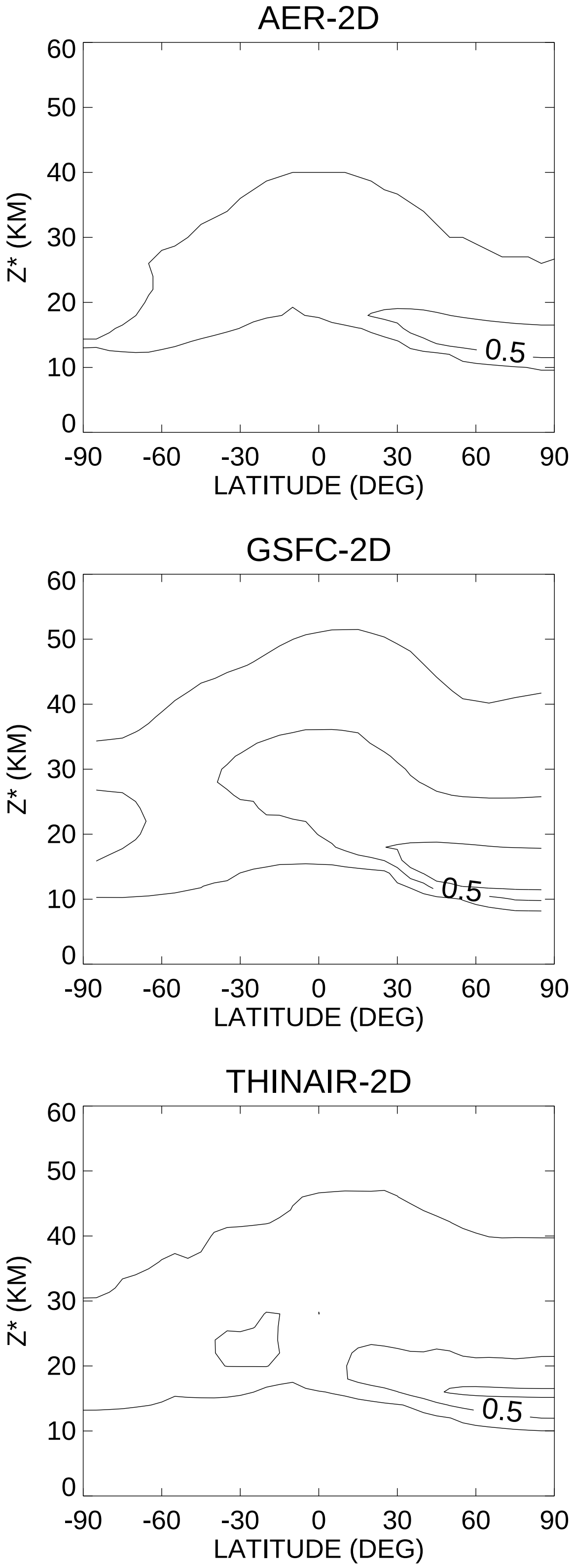

Figure 4.51: Calculated perturbations to NO_y (ppbv) as a function of latitude and altitude in June of 2015 due to NO_x emissions from a fleet of 1000 HSCT aircraft operating at 2 km below nominal cruise altitude with EI(NO_x)=5 under Scenario S2e relative to Scenario D. Contours are 0, 0.5, 1.0 ppbv.

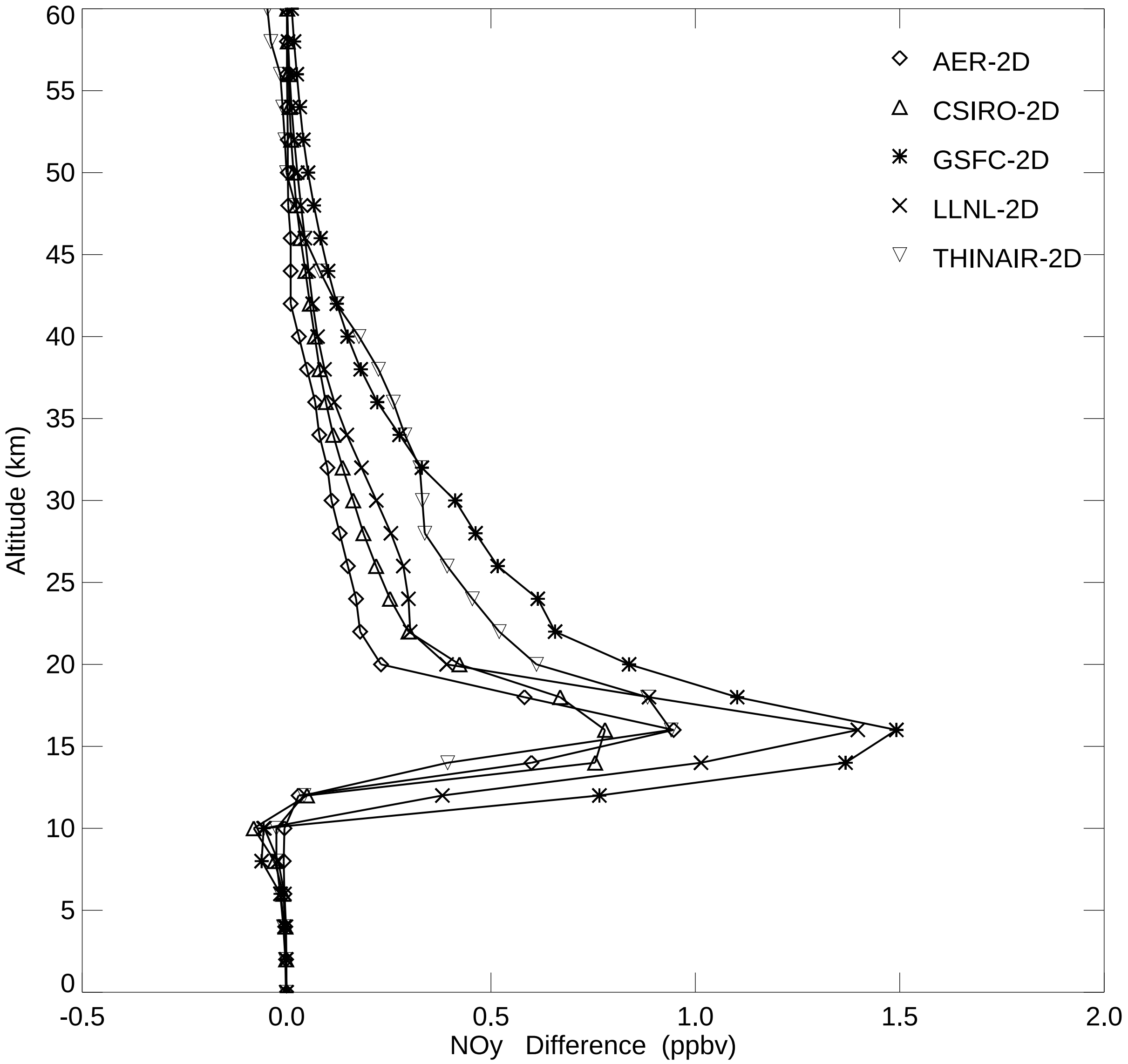

Figure 4.52: Calculated perturbations to NO_y (ppbv) as a function of altitude at 45°N in June of 2015 due to NO_x emissions from a fleet of 1000 HSCT aircraft operating at 2 km below nominal cruise altitude with $EI(NO_x)$=5 under Scenario S2e relative to Scenario D.

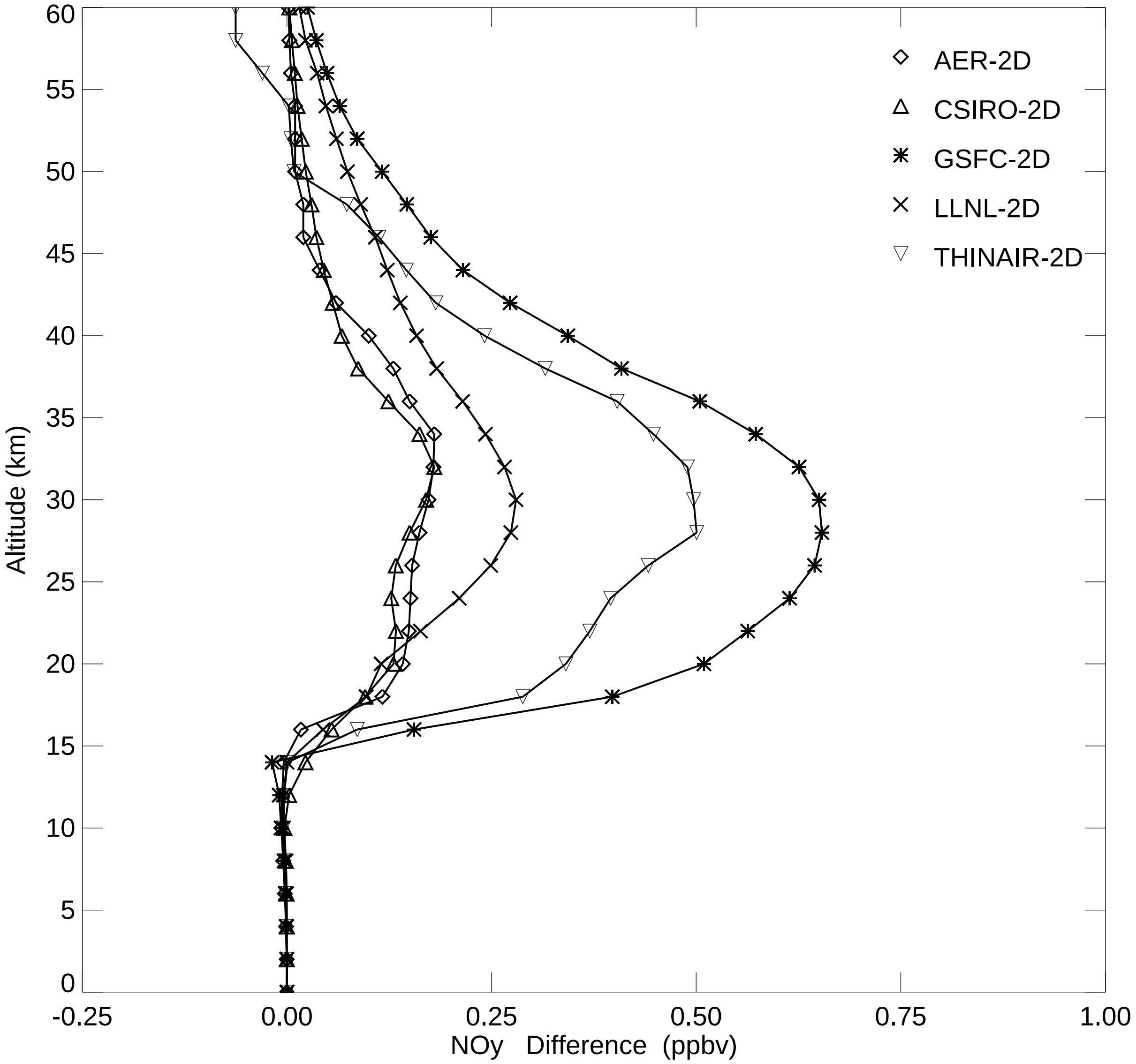

Figure 4.53: Calculated perturbations to NO_y (ppbv) as a function of altitude at the equator in June of 2015 due to NO_x emissions from a fleet of 1000 HSCT aircraft operating at 2 km below nominal cruise altitude with $EI(NO_x)=5$ under Scenario S2e relative to Scenario D.

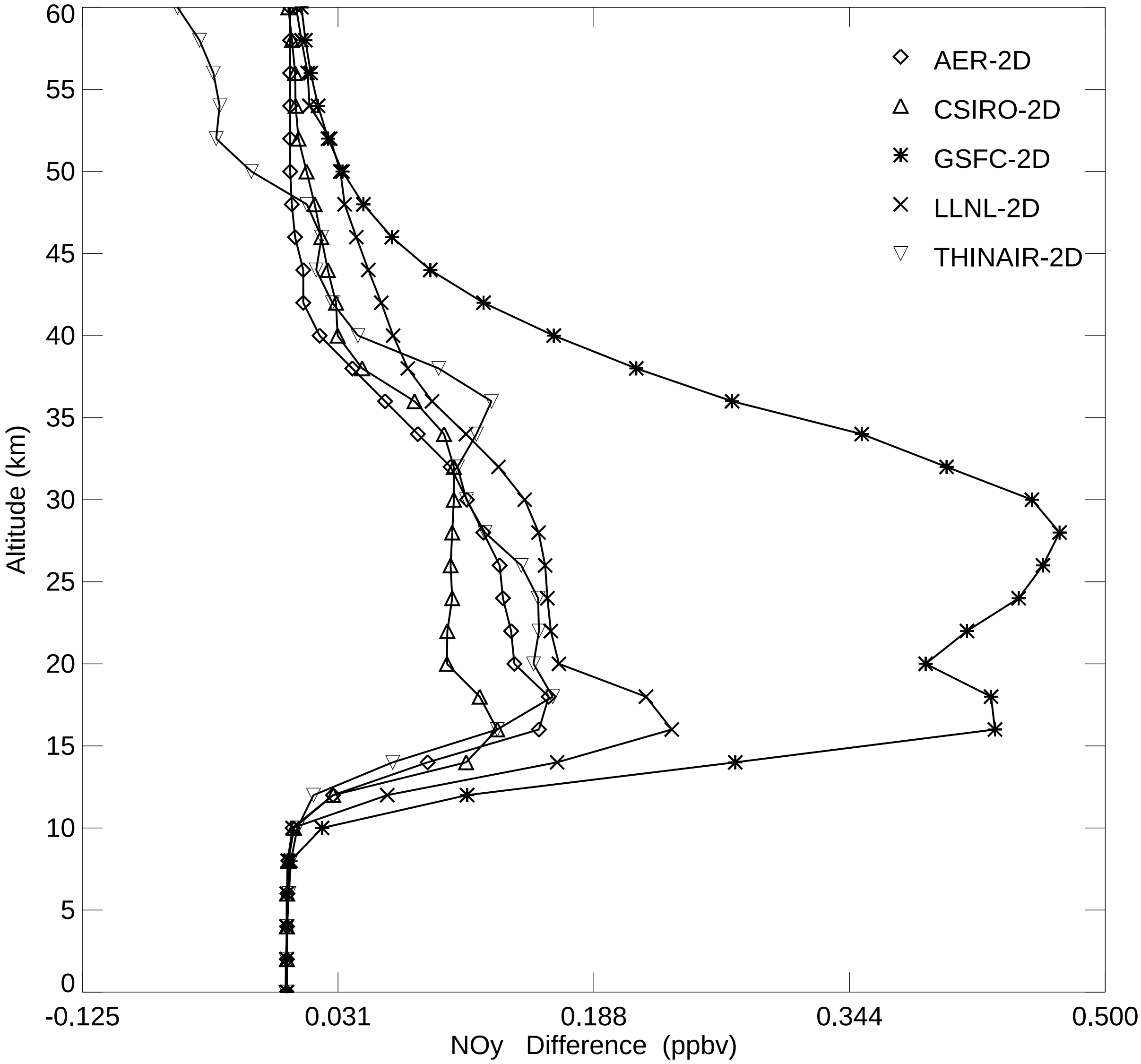

Figure 4.54: Calculated perturbations to NO_y (ppbv) as a function of altitude at 45^{o}S in June of 2015 due to NO_x emissions from a fleet of 1000 HSCT aircraft operating at 2 km below nominal cruise altitude with EI(NO_x)=5 under Scenario S2e relative to Scenario D.

4.3 O_3 Perturbations

Changes in ozone are related to changes in ultra-violet radiation reaching the ground. Changes in ozone would also be expected to modify the climate. Thus predicted changes in ozone are the most important results provided in Chapter 4 of IPCC. A synopsis of calculated ozone column changes is listed in Table 4.2 for the northern and southern hemispheres for each model for all of the 2015 scenarios. In the following sections, changes in ozone are plotted for each scenario. Changes in ozone as a function of altitude and latitude are shown for March, June, and October. These months were chose to present both polar regions in their respective springtimes, since the northern and southern polar regions often respond differently to perturbations in H_2O and NO_y. This is due to the colder temperatures in the southern polar region, which allows for PSC occurrence and denitrification/dehydration to occur continuously throughout the winter season.

4.3.1 Base Scenarios (S1a-e,i,j)

This set of scenarios is represented by the designations S1a-S1e and S1i-S1j. These scenarios represent variations in EI(NO_x), variations in fleet size, and sensitivity to H_2O emissions. The background atmosphere for all these scenario is D, the 2015 atmosphere with subsonic aircraft and nonvolcanic levels of sulfate aerosol (SA0). Scenarios S1a-S1e assume 500 HSCT aircraft and use the SA0 sulfate surface area density, ie. they assume no emission of sulfur from HSCT aircraft in the stratosphere. Scenarios S1i and S1j assume 1000 HSCT aircraft with EI(NO_x) of 5 or 10 and no sulfur emissions.

Scenario S1a includes NO_x emissions with emission index 5, but no emissions of H_2O. This scenario is provided as a sensitivity study to help separate the impact of NO_x and H_2O on stratospheric ozone. It is completely unrealistic, however, to assume that the aircraft engines could emit no H_2O. The change in March ozone mixing ratio in percent relative to Scenario D is shown in Figure 4.55. Most models show ozone decreases in the stratosphere above 20-30 km and in parts of the troposphere. Ozone increases are found in the lowermost stratosphere and parts of the troposphere due to smog reactions involving NO_x. Changes in zonal-mean ozone are less than 1% for most models over most of the domain. Zonal-mean ozone changes for June are shown in Figure 4.56 and for October in Figure 4.57. The GSFC model shows substantial ozone increases in the southern polar region in October due to HSCT emission of NO_x. Figures 4.58, 4.59, and 4.60 show vertical profiles of ozone change at 45^{o}N, the equator, and 45^{o}S, respectively, with all models shown in a single plot. Percentage changes in zonal-mean column ozone for Scenario S1a relative to Scenario D are shown in Figure 4.61. Calculated changes in ozone column for this scenario are quite small, though the SCTM1 model calculates depletions of 0.5% for northern polar regions in summer and fall.

Scenario S1b represents HSCT emissions with EI(NO_x)=0, ie. only emission of H_2O is included. Figures 4.62-4.64 show ozone change as a function of latitude and altitude for Scenario S1b relative to Scenario D for March, June, and October. S1b shows much larger ozone depletions than S1a, indicating that H_2O emissions have a larger impact on ozone than NO_x emissions at EI(NO_x)=5. Emission of H_2O leads to ozone depletion below 20 km and above 35 km. Upper stratospheric ozone depletion ranges from 0.5 to 2% in direct correlation to the amount of H_2O accumulated in this region. Depletion in the lower stratosphere ranges from 0.5 to 3% for most models and seasons, though GSFC shows 10% depletion in October near the south pole. Changes in ozone as a function of altitude at 45^{o}N, the equator, and 45^{o}S for June are shown in Figures 4.65-4.67. Perturbation to total ozone as a function of latitude and season are shown in Figure 4.68. Of the six models which calculated this scenario, three predict ozone depletions of 0.5% or more in parts of the northern hemisphere. The GSFC and LLNL models also predicts substantial depletion in the southern hemisphere (-4% maximum for GSFC, -1.4% for LLNL).

The case with both H_2O and NO_x emissions is represented by Scenario S1c, with 500 HSCT aircraft, EI(NO_x)=5, and no sulfur emissions. All 9 models performed this calculation. Changes in ozone for Scenario S1c relative to Scenario D are shown in Figures 4.69, 4.70, and 4.71 for March, June, and October, respectively. Changes in ozone as a function of altitude at 45^{o}N, the equator, and 45^{o}S are shown in Figures 4.72-4.74. All models show a positive ozone response in the tropical lower stratosphere, with the UNIVAQ model shows the largest positive response there. The LARC model shows a substantial positive response in the northern hemisphere lower stratosphere and upper troposphere as well. The GSFC model shows the largest ozone perturbations above 35 km and in the southern hemisphere lower stratosphere at all

Table 4.2: Annual Average Ozone Column Perturbations (in percent) for Each Model for the Northern Hemisphere (top number) and Southern Hemisphere (bottom number) in 2015

Scen -ario	Fleet Size	EI NO_x	SAD Desc.	Special	AER	GSFC	UNI-VAQ	LLNL	CSI -RO	THIN -AIR	SLIM -CAT	SCT -M1	LARC
S1a	500	5	SA0	No H_2O	-0.07	-0.1	0.2	-0.01	-0.09	-	-0.2	-0.2	-
					-0.03	0.03	0.1	0.1	-0.07	-	-0.09	-0.007	-
S1b	500	0	SA0		-0.6	-0.4	-0.4	-0.3	-0.2	-	-0.6	-	-
					-0.3	-0.8	-0.2	-0.3	-0.07	-	-0.7	-	-
S1c	500	5	SA0		-0.3	-0.4	-0.002	-0.2	-0.2	-0.2	-0.4	-0.3	-0.05
					-0.1	-0.8	0.02	-0.2	-0.1	-0.2	-0.6	-0.1	-0.1
S1d	500	10	SA0		-0.3	-0.6	0.2	-0.3	-0.3	-0.5	-0.5	-0.5	0.07
					-0.1	-0.7	0.1	-0.1	-0.2	-0.3	-0.7	-0.1	-0.03
S1e	500	15	SA0		-0.3	-0.8	0.4	-0.4	-0.5	-0.9	-	-	-
					-0.05	-0.7	0.2	-0.01	-0.3	-0.5	-	-	-
S1f	500	5	SA1		-1.0	-1.1	-0.4	-0.7	-0.5	-	-	-	-0.4
					-0.4	-1.1	-0.1	-0.5	-0.1	-	-	-	-0.3
S1g	500	10	SA1		-0.8	-1.1	-0.2	-0.7	-0.5	-	-	-	-
					-0.3	-1.0	-0.01	-0.4	-0.2	-	-	-	-
S1h	500	5	SA3		-1.1	-1.3	-0.5	-0.8	-0.5	-	-	-	-
					-0.4	-1.2	-0.2	-0.6	-0.1	-	-	-	-
S1i	1000	5	SA0		-0.7	-0.9	-0.06	-0.5	-0.5	-0.4	-	-	-
					-0.3	-1.4	0.005	-0.3	-0.2	-0.3	-	-	-
S1j	1000	10	SA0		-0.7	-1.4	0.1	-0.7	-0.7	-1.1	-	-	-
					-0.2	-1.4	0.2	-0.2	-0.3	-0.6	-	-	-
S1k	500	5	SA5		-0.8	-0.7	-0.2	-0.5	-0.4	-	-	-	-
					-0.3	-0.9	-0.05	-0.3	-0.1	-	-	-	-
S1l	500	5	SA7		-0.6	-	-	-	-	-	-	-	-
					-0.3	-	-	-	-	-	-	-	-
S2a	500	5	SA0	Cruise +2 km	-0.7	-1.0	-0.1	-0.6	-0.6	-0.3	-	-	-
					-0.2	-1.2	-0.06	-0.3	-0.2	-0.2	-	-	-
S2b	500	5	SA0	Cruise -2 km	-0.1	-0.09	0.01	-0.05	-0.05	-0.09	-	-	-
					-0.04	-0.2	0.03	-0.01	-0.03	-0.09	-	-	-
S2c	500	10	SA0	Cruise -2 km	-0.1	0.1	-	-0.03	-0.003	-	-	-	-
					-0.1	-0.06	-	0.07	-0.03	-	-	-	-
S2d	500	15	SA0	Cruise -2 km	-	0.3	-	-	-	-	-	-	-
					-	0.07	-	-	-	-	-	-	-
S2e	1000	5	SA0	Cruise -2 km	-0.3	-0.2	-	-0.1	-0.09	-0.2	-	-	-
					-0.2	-0.4	-	-0.02	-0.05	-0.2	-	-	
S3a	500	0	4xSA0		-0.5	-0.5	-0.4	-0.4	-0.3	-	-	-	-
					-0.2	-0.7	-0.1	-0.3	-0.1	-	-	-	-
S3b	500	5	4xSA0		-0.2	-0.04	0.07	-0.2	-0.09	-	-	-	-
					-0.09	-0.5	0.06	-0.2	-0.09	-	-	-	-
S3c	500	10	4xSA0		0.04	0.2	0.4	0.001	0.03	-	-	-	-
					0.02	-0.4	0.2	-0.04	-0.08	-	-	-	-
S3d	500	15	4xSA0		0.2	0.4	0.6	0.09	0.09	-	-	-	-
					0.1	-0.3	0.3	0.07	-0.07	-	-	-	-
S3e	500	5	4xSA0+		-0.5	-0.4	-0.09	-0.3	-0.2	-	-	-	-
			SA1-SA0		-0.2	-0.6	-0.01	-0.3	-0.1	-	-	-	-
S3f	500	5	4xSA0+		-0.6	-0.5	-0.2	-0.4	-0.3	-	-	-	-
			SA3-SA0		-0.2	-0.7	-0.02	-0.3	-0.1	-	-	-	-
S4a	500	0	SA0	No PSCs	-0.5	-0.4	-0.3	-	-0.2	-	-	-	-
					-0.3	-0.3	-0.1	-	-0.07	-	-	-	-
S4b	500	5	SA0	No PSCs	-0.2	-0.4	0.02	-	-0.2	-	-	-	-
					-0.1	-0.3	0.001	-	-0.1	-	-	-	-
S4c	500	5	SA0	No PSCs	-0.1	-0.2	0.3	-	-0.09	-	-	-	-
				No H_2O	-0.1	-0.02	0.1	-	-0.07	-	-	-	-
S5a	500	5	SA0	Cl_y=	-0.3	-0.5	-0.006	-	-	-	-	-	-
				1.0 ppbv	-0.1	-0.5	-0.02	-	-	-	-	-	-
S5b	500	5	SA1	Cl_y=	-0.5	-0.7	-0.3	-	-	-	-	-	-
				1.0 ppbv	-0.2	-0.7	-0.1	-	-	-	-	-	-
S6a	500	5	SA0	Cl_y=	-0.4	-0.4	0.03	-	-	-	-	-	-
				4.0 ppbv	-0.1	-0.8	-0.01	-	-	-	-	-	-
S6b	500	5	SA1	Cl_y=	-1.0	-1.1	-0.4	-	-	-	-	-	-
				4.0 ppbv	-0.4	-1.0	-0.2	-	-	-	-	-	-
S7a	500	5	50%	Microphysics	-1.0	-	-0.5	-	-	-	-	-	-
			Part.		-0.4	-	-0.3	-	-	-	-	-	-
S7b	500	5	50%	Microphysics	-1.4	-	-0.7	-	-	-	-	-	-
			Part.	Cruise +2 km	-0.5	-	-0.4	-	-	-	-	-	-
S7c	500	5	50%	Microphysics	-0.6	-	-0.2	-	-	-	-	-	-
			Part.	Cruise -2 km	-0.3	-	-0.1	-	-	-	-	-	-
S7d	500	10	50%	Microphysics	-0.9	-	-0.2	-	-	-	-	-	-
			Part.		-0.4	-	-0.2	-	-	-	-	-	-
S8a	500	5	100%	Microphysics	-1.1	-	-0.5	-	-	-	-	-	-
			Part.		-0.5	-	-0.3	-	-	-	-	-	-

seasons. Changes in total ozone as a function of latitude and season are shown in Figure 4.75. Most models show a slightly smaller ozone column response with NO_x and H_2O emissions than with H_2O emission alone. Changes in total ozone in June as a function of latitude only are shown in Figure 4.76, with all models plotted together. Hemispheric average ozone changes, which are listed in Table 4.2, range from ~0% to -0.4% in the northern hemisphere and from ~0% to -0.8% in the southern hemisphere.

Scenario S1d is similar to S1c but with EI(NO_x)=10. Changes in ozone as a function of latitude and altitude for March, June, and October are shown in Figures 4.77, 4.78, and 4.79. Vertical profiles of ozone change are shown in Figures 4.80, 4.81, and 4.82 for 45°N, the equator, and 45°S in June. Compared with Scenario S1c, most models show additional ozone depletion in the northern hemisphere middle and high latitudes between 20 and 35 km. Most models also show less ozone depletion, or a greater ozone increase, in the southern hemisphere below 20 km. Figure 4.83 shows changes in total ozone for this scenario. The CSIRO, THINAIR and SCTM1 models show larger total ozone depletion in Scenario S1d than in Scenario S1c. The UNIVAQ and LARC models shows a more positive ozone response, while the GSFC and LLNL models show more depletion in the northern hemisphere and less depletion in the southern hemisphere. AER show little change in column ozone depletion between Scenarios S1d and S1c.

Scenario S1e is similar to S1d and S1c but with EI(NO_x)=15. The model results continue the pattern seen between Scenarios S1c and S1d. The additional NO_x produced additional ozone depletion in the northern hemisphere middle and high latitudes between 20 and 35 km, and less ozone depletion in the southern hemisphere below 20 km. These results can be seen in Figures 4.84-4.89. Changes in total ozone for Scenario S1e are shown in Figure 4.90. Changes in total ozone in June as a function of latitude only are shown in Figure 4.91, with all models plotted together. The CSIRO, GSFC, and LLNL models show more northern hemisphere ozone depletion than for Scenario S1d. Only the CSIRO and THINAIR models show more ozone depletion in the southern hemisphere. The UNIVAQ model shows a more positive ozone response in both hemispheres.

Sensitivity to aircraft NO_x emissions is shown graphically in Figures 4.92 and 4.93, which plot annual average hemispheric ozone perturbation as a function of EI(NO_x) for 500 HSCT aircraft, background surface area of SA0, and no sulfur emissions. Scenarios S1b-S1e are included. For the northern hemisphere (Figure 4.92), all models show similar or less ozone depletion as the EI(NO_x) varies from 0 to 5, indicating that emission of H_2O from the aircraft plays the dominant role in ozone depletion. The UNIVAQ model shows the largest positive sensitivity in this range, while the AER and SLIMCAT models also show a positive sensitivity. The THINAIR, LARC, and SCTM1 models did not calculate the EI(NO_x)=0 case. Between EI(NO_x)=5 and EI(NO_x)=15, the GSFC, LLNL, CSIRO, THINAIR, AND SLIMCAT models show increased ozone depletion at greater EI(NO_x). The AER model shows little sensitivity to EI(NO_x) in this range, and the UNIVAQ and LARC models show less ozone depletion at greater EI(NO_x). Notice also that the range of calculated ozone perturbations among the models is narrower for smaller EI(NO_x). In the southern hemisphere (Figure 4.93), sensitivities are smaller because of the smaller amount of emitted material released or transported to the southern hemisphere. GSFC and SLIMCAT have substantially larger calculated ozone depletions in the southern hemisphere than other models, but this ozone depletion is insensitive to EI(NO_x).

Scenarios S1i and S1j include 1000 HSCT aircraft, with EI(NO_x)=5 for S1i and EI(NO_x)=10 for S1j. Figures 4.94, 4.95, and 4.96 show ozone percent changes as a function of latitude and altitude for March, June, and October for Scenario S1i relative to Scenario D. Compared with Scenario S1c, all models show substantially more ozone depletion at all seasons for extratropical latitudes. The tropical lower stratosphere shows a greater ozone increase due to the self-healing effect from ozone depletion at higher altitudes. Vertical profiles of ozone changes for Scenario S1i are shown in Figures 4.97, 4.98, and 4.99 for June at 45°N, the equator, and 45°S. Changes in total ozone for Scenario S1i relative to Scenario D are shown in Figure 4.100. Ozone column changes are substantially larger than for Scenario S1c. They are also substantially larger than for Scenario S1d, which has similar NO_x emissions but half the H_2O emissions, indicating the important role of H_2O emissions from HSCT aircraft in future ozone depletion. The THINAIR model differs from the rest in that S1d shows more ozone depletion than S1i, ie. the relative roles of NO_x and H_2O differ from the other models.

Changes in ozone for March, June, and October from Scenario S1j relative to Scenario D are shown in Figures 4.101, 4.102, and 4.103. Ozone depletion above 20 km is enhanced above that from Scenario S1i, while below 20 km, ozone depletion is reduced. Vertical profiles of ozone changes for Scenario S1j are shown in Figures 4.104, 4.105, and 4.106 for June at 45°N, the equator, and 45°S. Changes in total ozone for

Scenario S1j relative to Scenario D are shown in Figure 4.107. Northern hemisphere total ozone depletion is enhanced relative to Scenario S1i in the GSFC, LLNL, CSIRO, and THINAIR models, unchanged in the AER model, and reduced in the UNIVAQ model. In the southern hemisphere, ozone depletion is reduced in the AER, LLNL and UNIVAQ models and enhanced in the CSIRO and THINAIR models relative to Scenario S1i. The GSFC model obtains about the same southern hemisphere ozone depletion for S1j as for S1i.

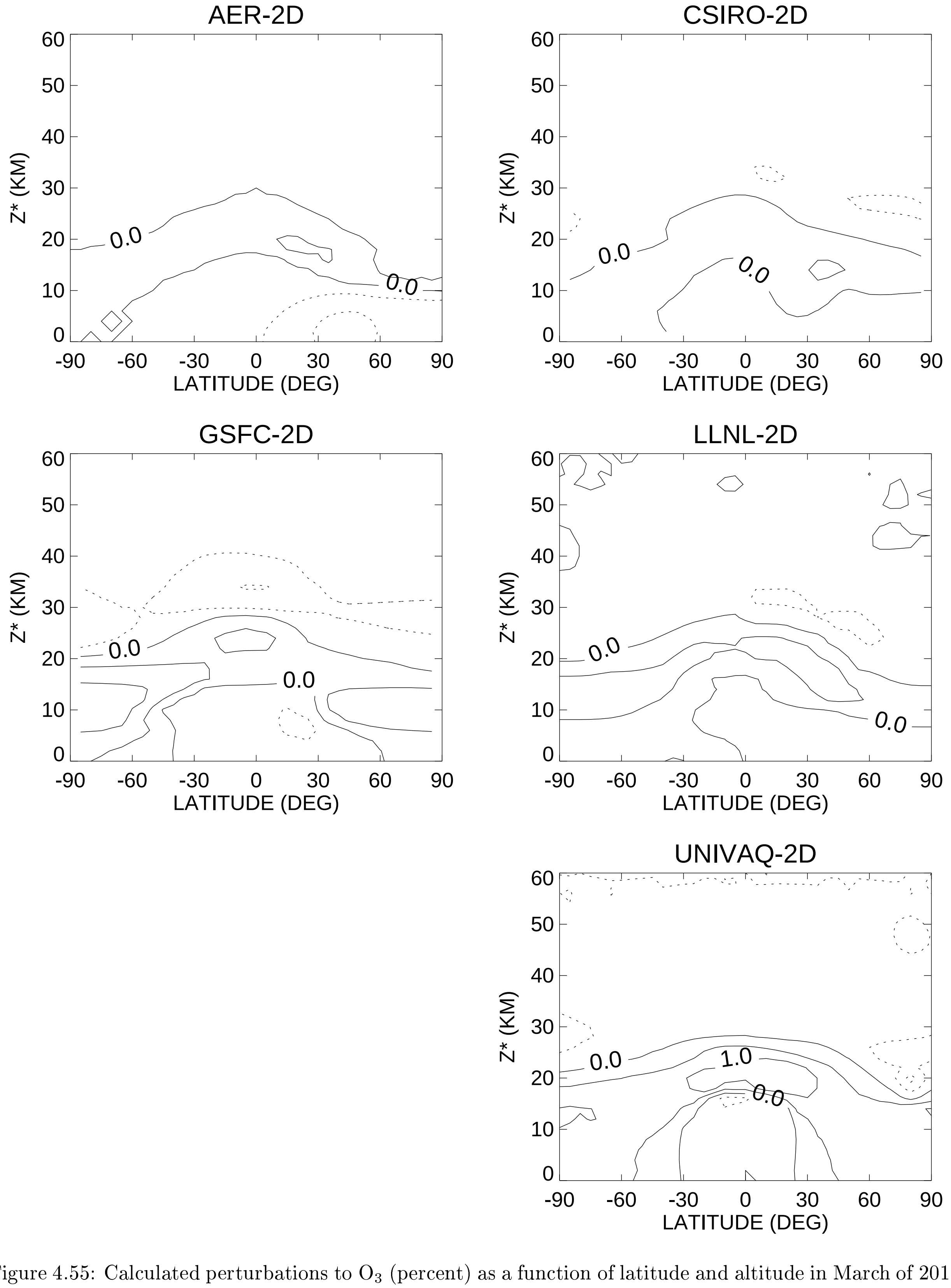

Figure 4.55: Calculated perturbations to O_3 (percent) as a function of latitude and altitude in March of 2015 due to emissions from a fleet of 500 HSCT aircraft with EI(NO_x)=5 and no H_2O emissions under Scenario S1a relative to Scenario D. Contours are -1, -0.5, 0, 0.5, 1.

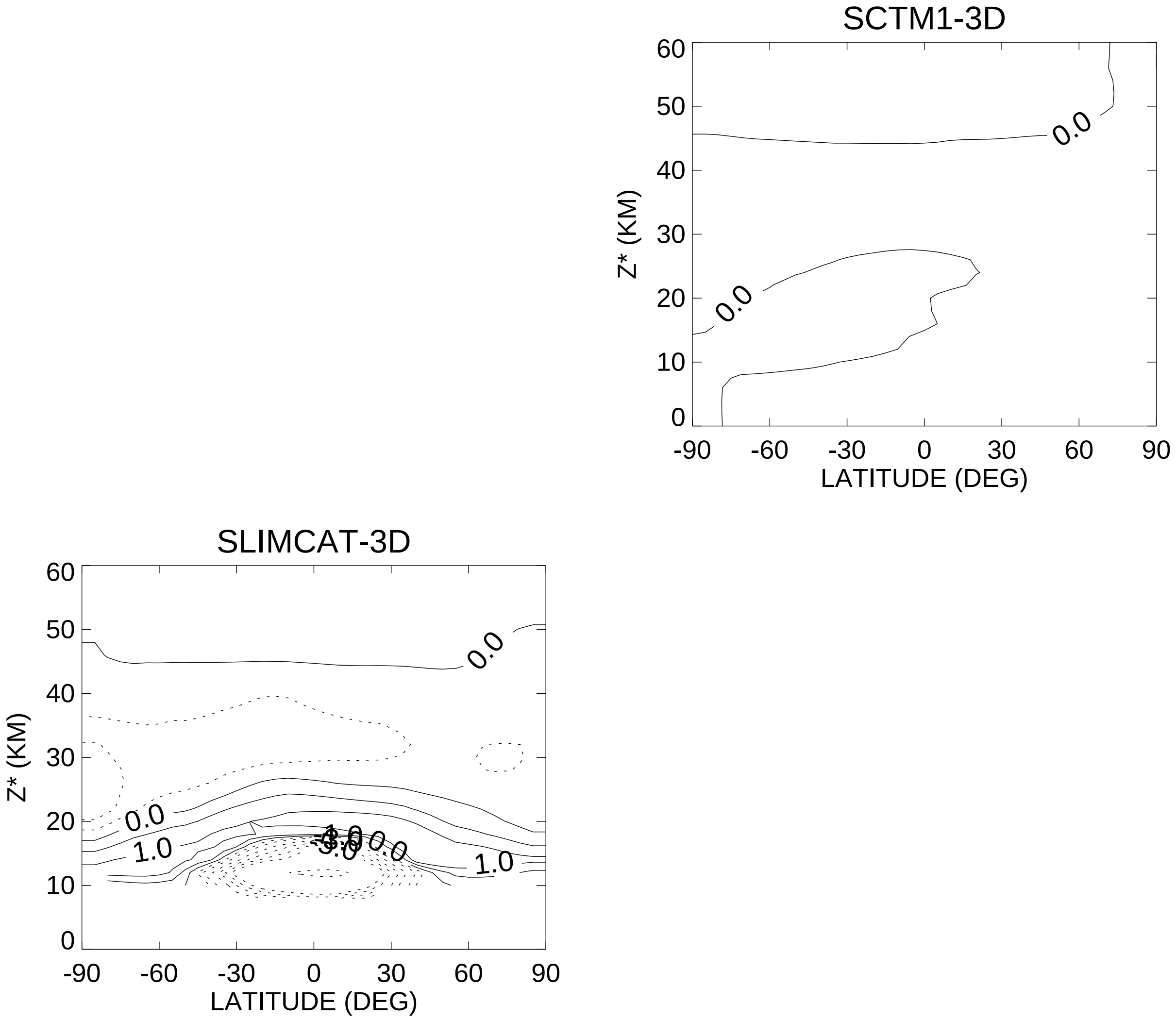

Figure 4.55: continued

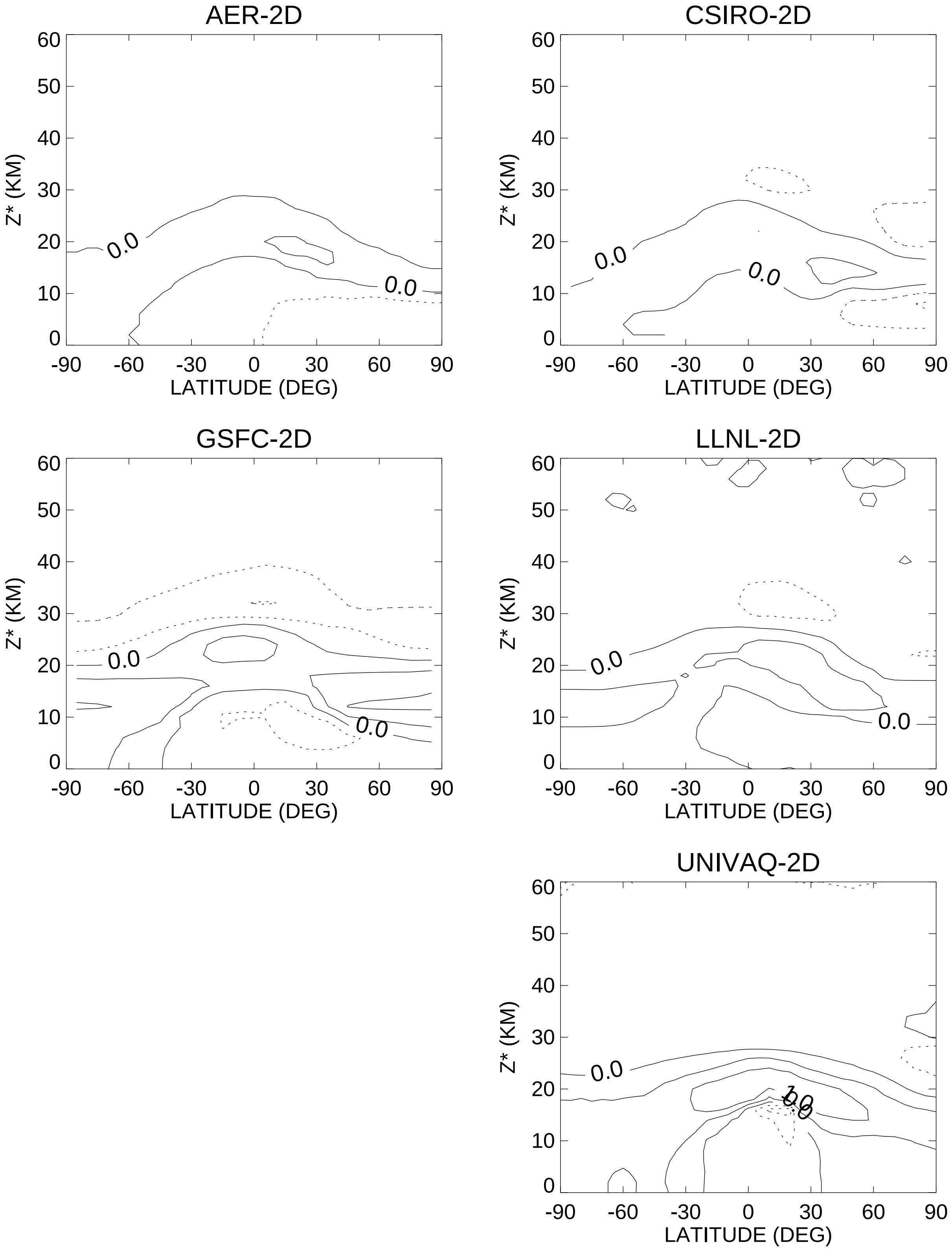

Figure 4.56: Calculated perturbations to O_3 (percent) as a function of latitude and altitude in June of 2015 due to emissions from a fleet of 500 HSCT aircraft with $EI(NO_x)=5$ and no H_2O emissions under Scenario S1a relative to Scenario D. Contours are -1, -0.5, 0, 0.5, 1.

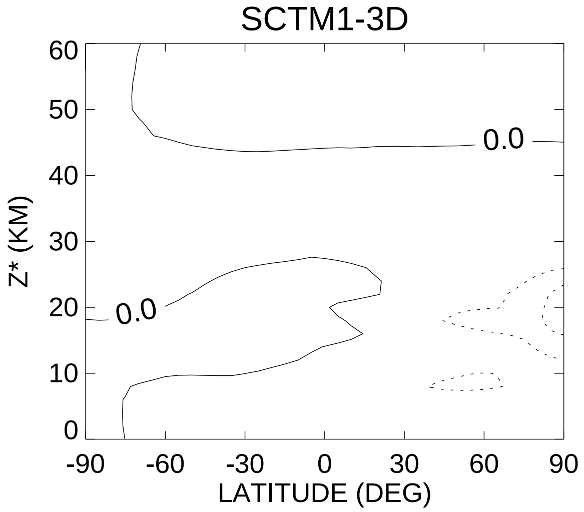

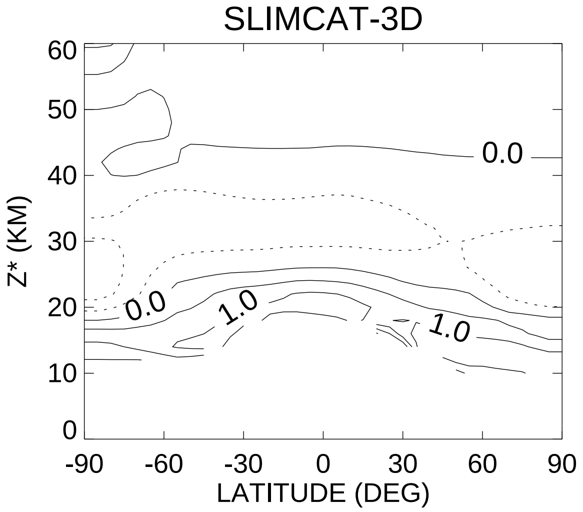

Figure 4.56: continued

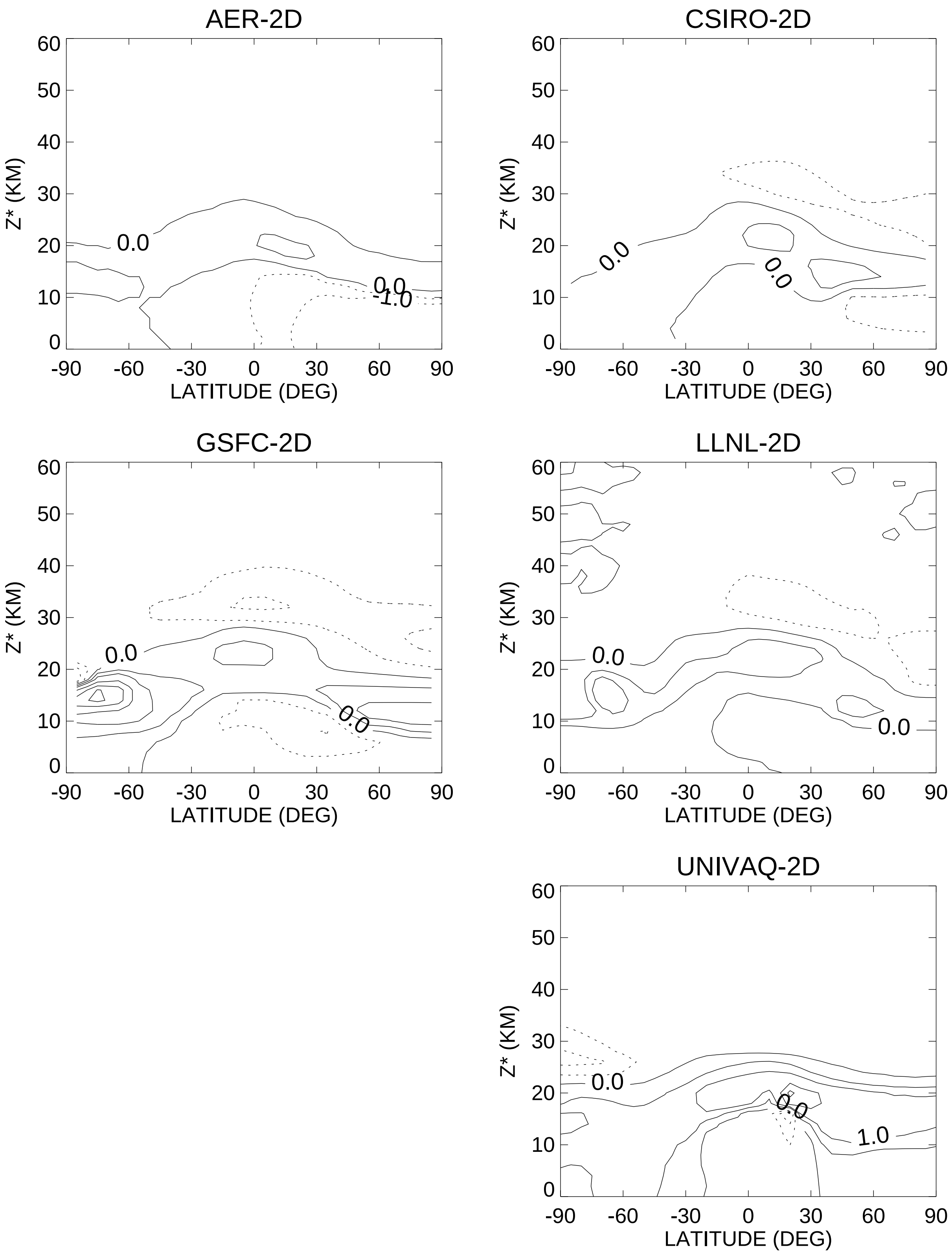

Figure 4.57: Calculated perturbations to O_3 (percent) as a function of latitude and altitude in October of 2015 due to emissions from a fleet of 500 HSCT aircraft with EI(NO_x)=5 and no H_2O emissions under Scenario S1a relative to Scenario D. Contours are -1, -0.5, 0, 0.5, 1, 2, 3.

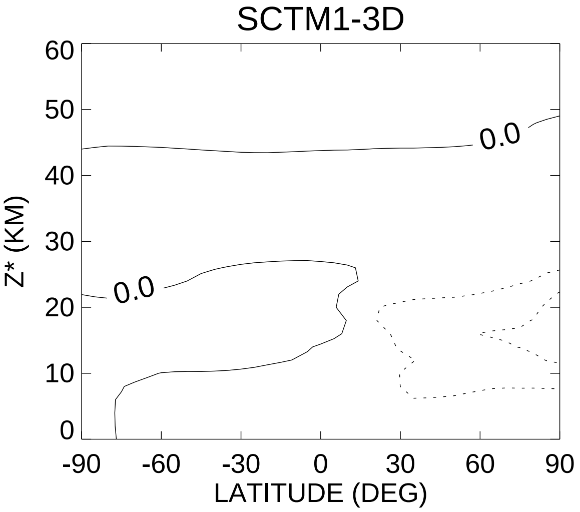

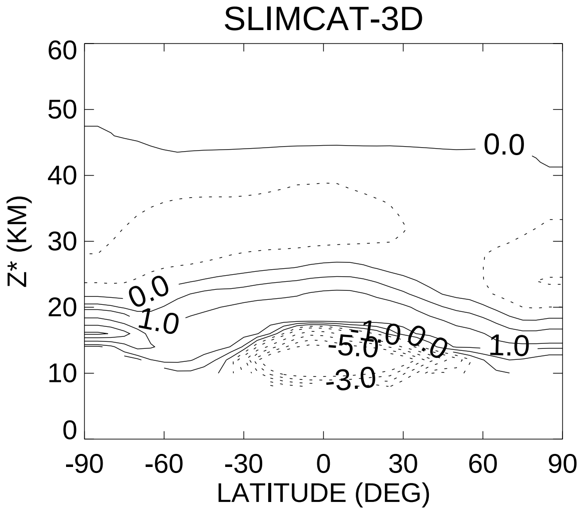

Figure 4.57: continued

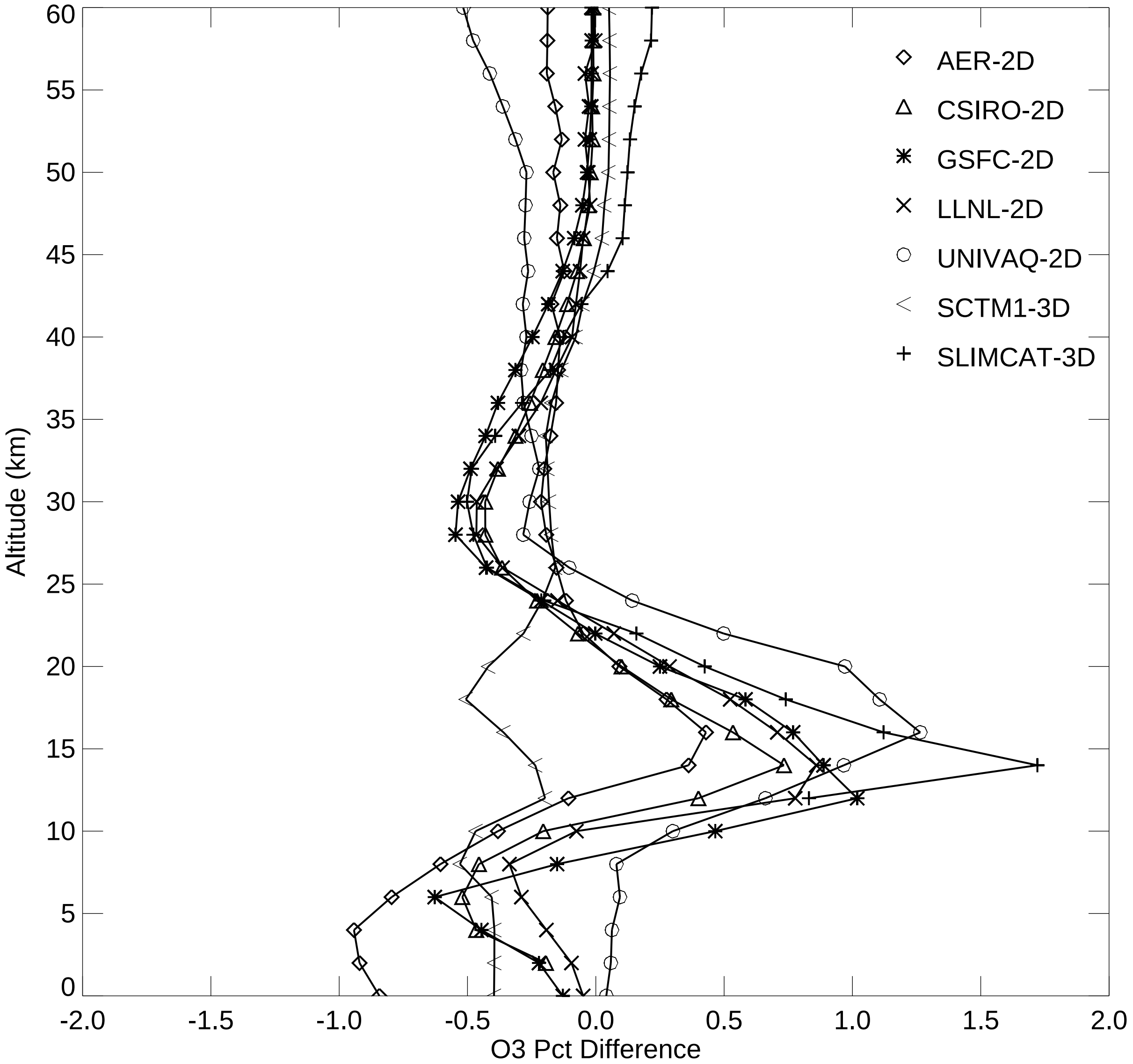

Figure 4.58: Calculated perturbations to O_3 (percent) as a function of altitude at 45^oN in June of 2015 due to emissions from a fleet of 500 HSCT aircraft with $EI(NO_x)=5$ and no H_2O emissions under Scenario S1a relative to Scenario D.

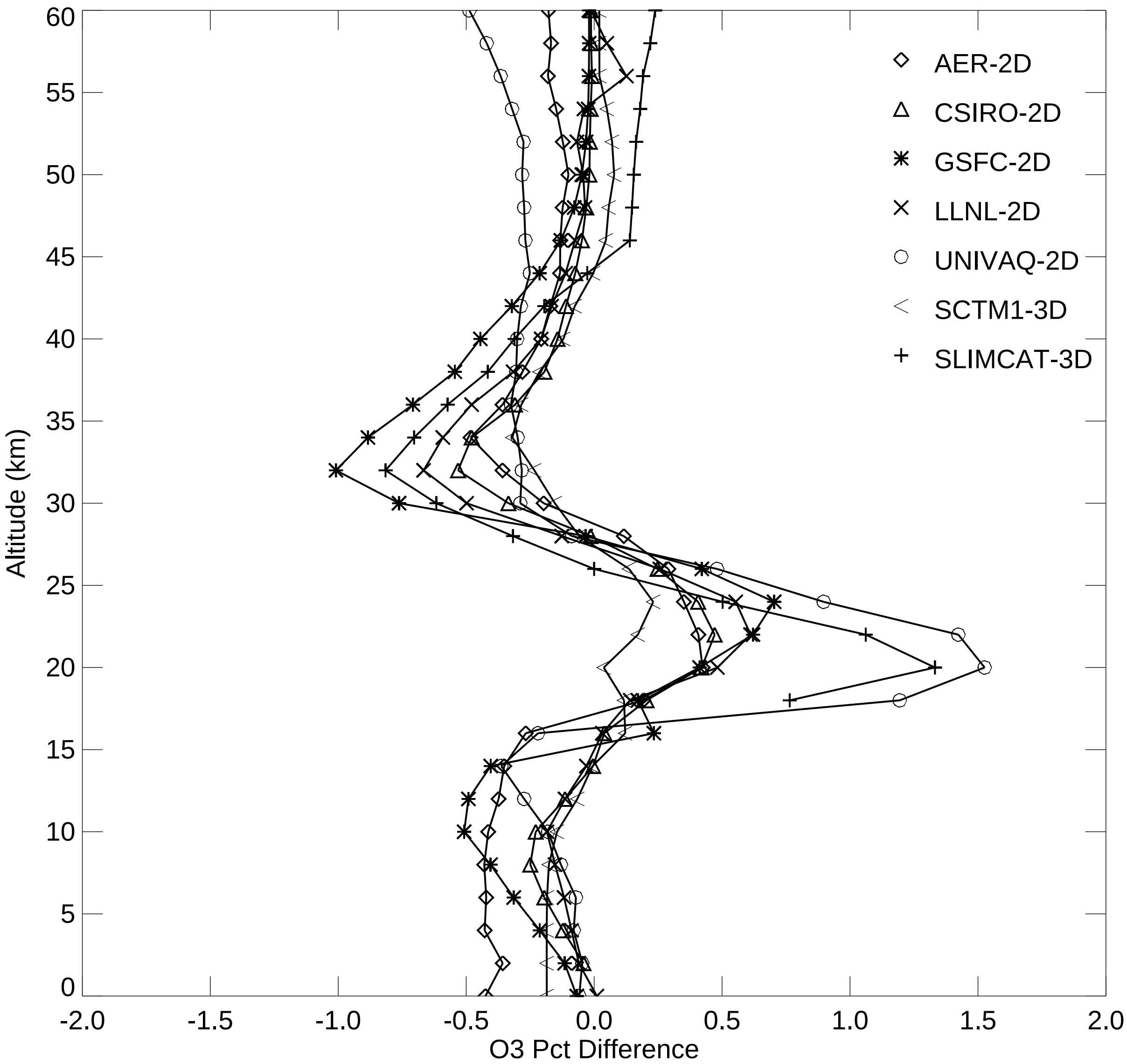

Figure 4.59: Calculated perturbations to O_3 (percent) as a function of altitude at the equator in June of 2015 due to emissions from a fleet of 500 HSCT aircraft with $EI(NO_x)=5$ and no H_2O emissions under Scenario S1a relative to Scenario D.

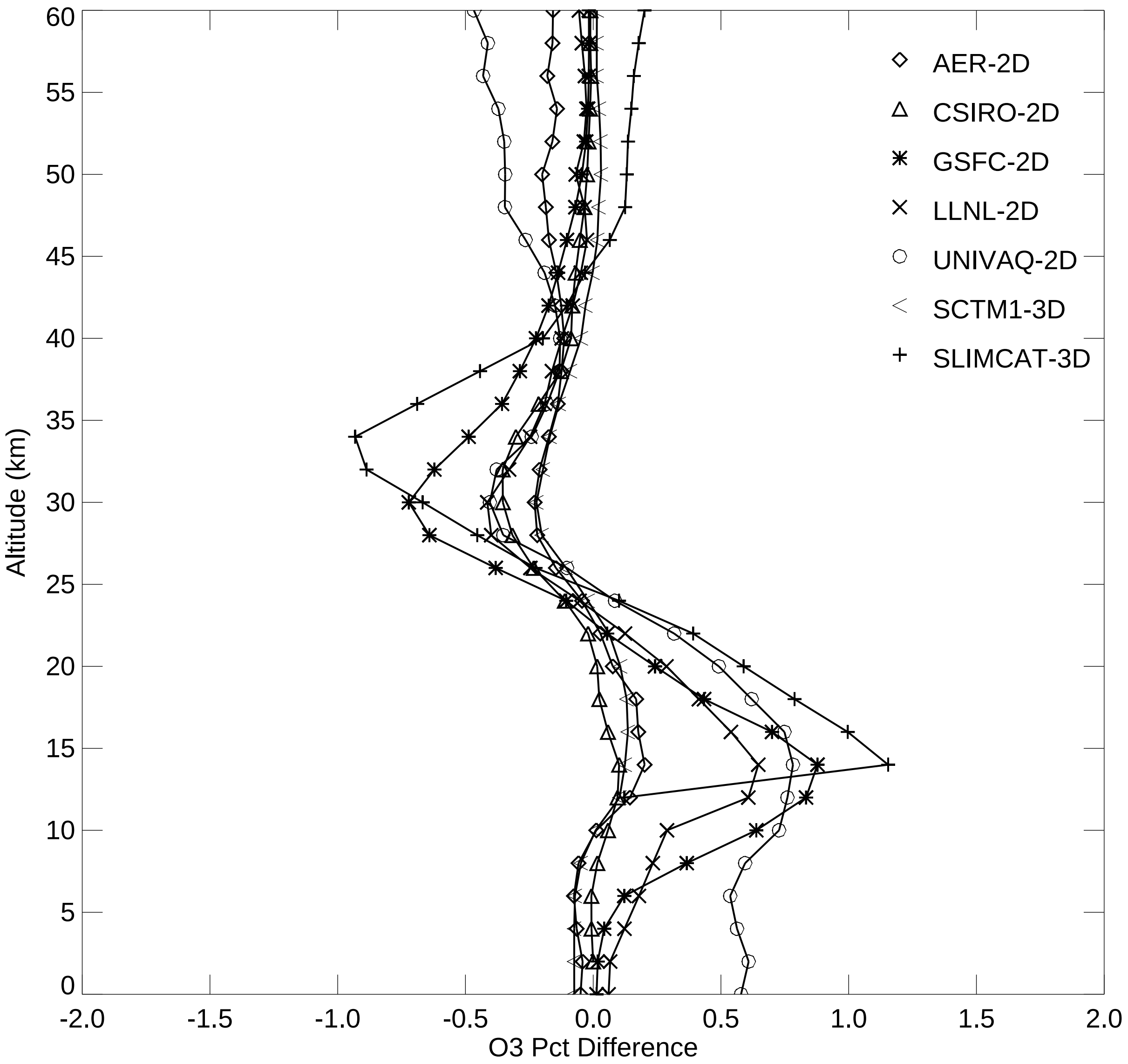

Figure 4.60: Calculated perturbations to O_3 (percent) as a function of altitude at 45^{o}S in June of 2015 due to emissions from a fleet of 500 HSCT aircraft with EI(NO_x)=5 and no H_2O emissions under Scenario S1a relative to Scenario D.

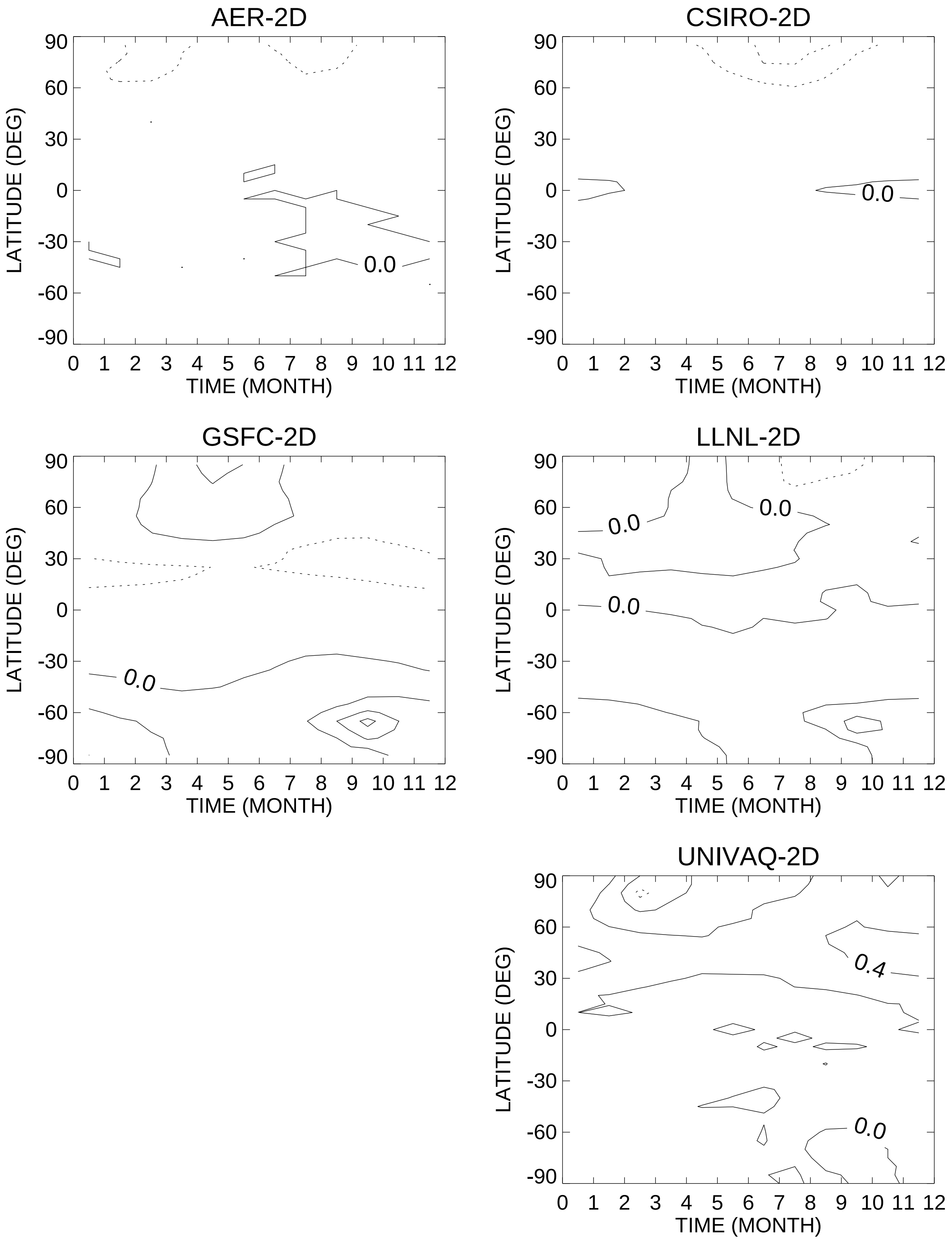

Figure 4.61: Calculated perturbations to column O_3 (percent) as a function of latitude and season in 2015 due to emissions from a fleet of 500 HSCT aircraft with EI(NO_x)=5 and no H_2O emissions under Scenario S1a relative to Scenario D. Contours are -1.2 to 0.6 by 0.2.

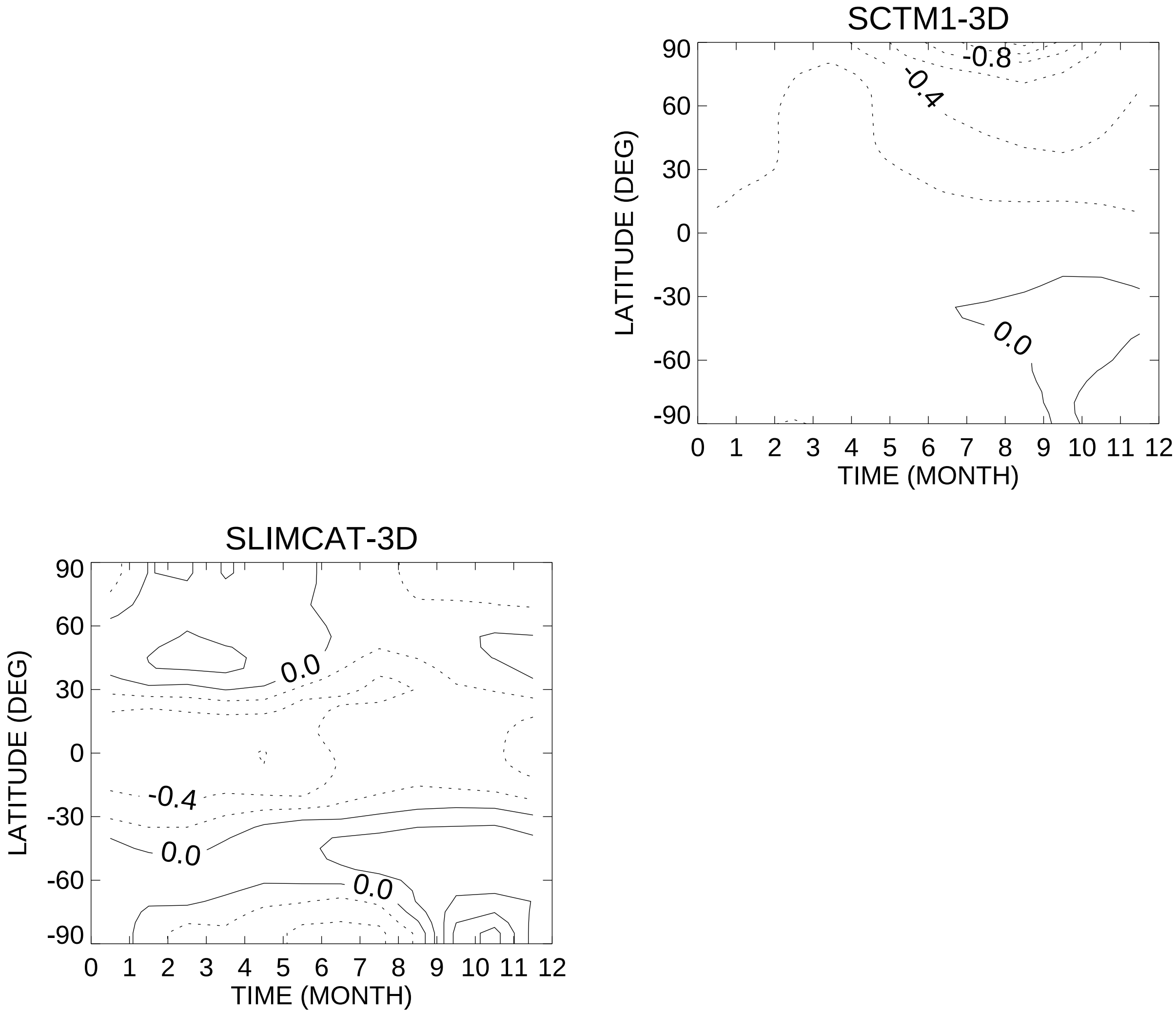

Figure 4.61: continued

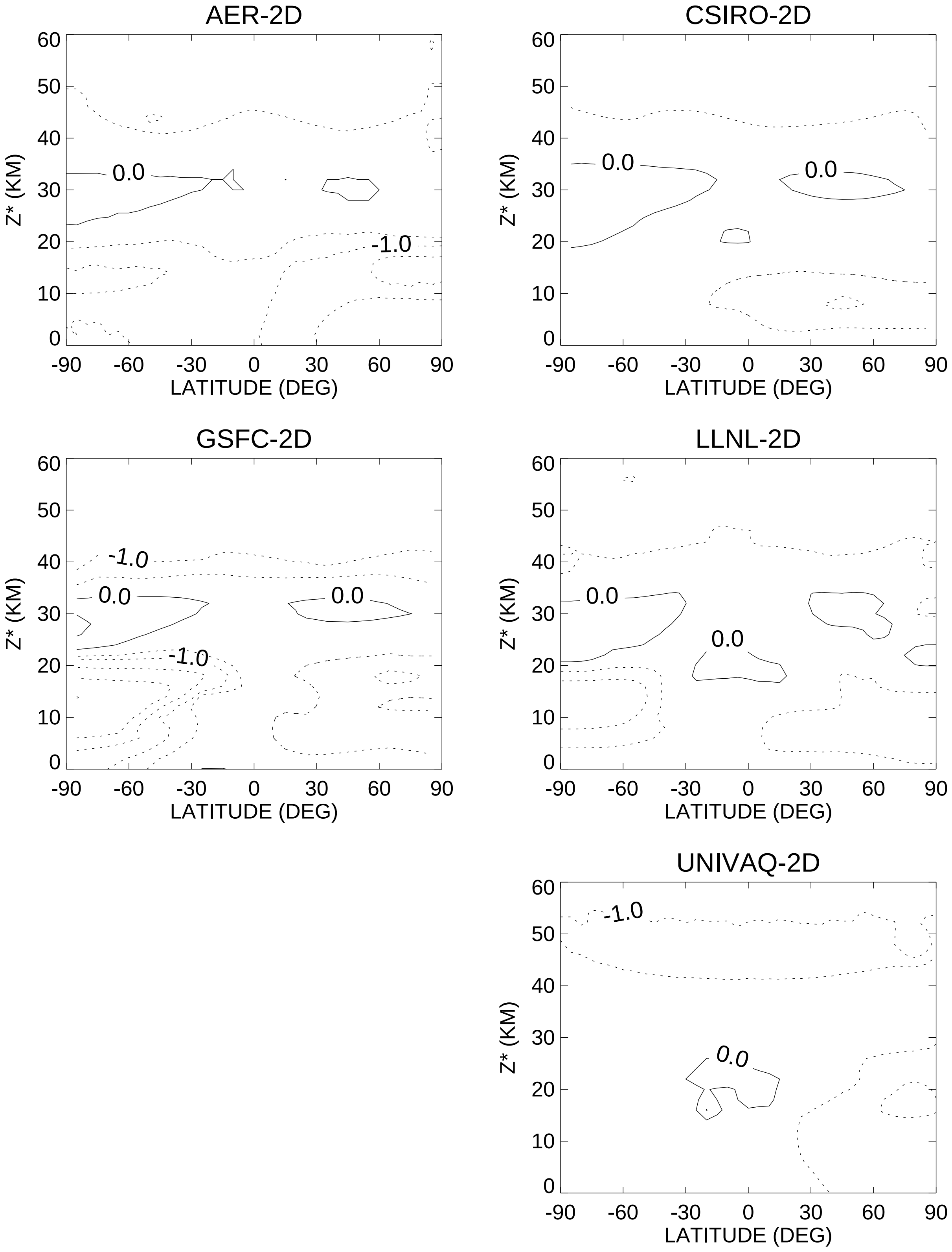

Figure 4.62: Calculated perturbations to O_3 (percent) as a function of latitude and altitude in March of 2015 due to emissions from a fleet of 500 HSCT aircraft with $EI(NO_x)=0$ under Scenario S1b relative to Scenario D. Contours are -3, -2, -1, -0.5, 0, 0.5.

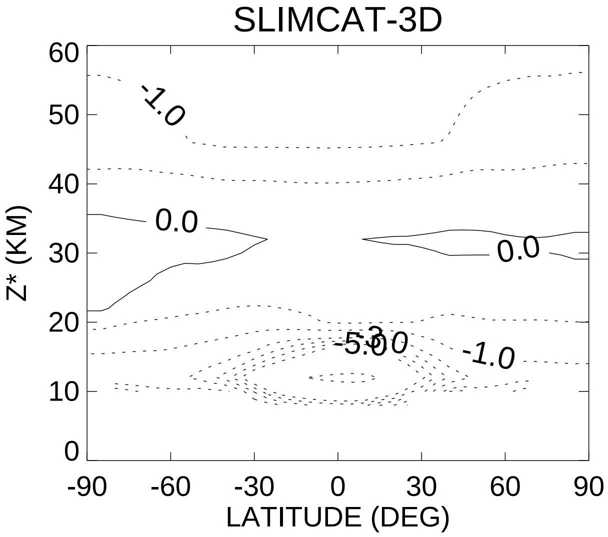

Figure 4.62: continued

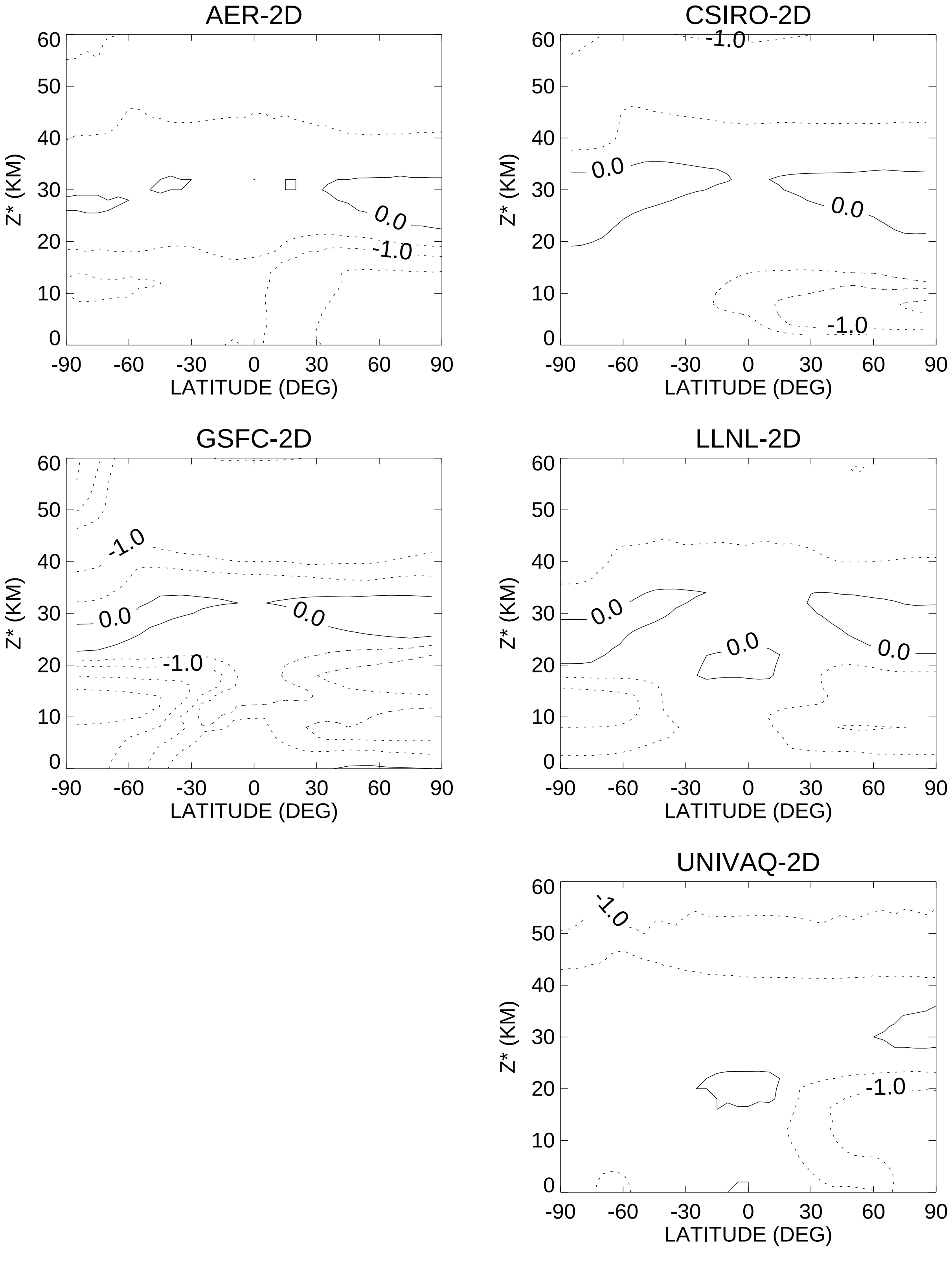

Figure 4.63: Calculated perturbations to O_3 (percent) as a function of latitude and altitude in June of 2015 due to emissions from a fleet of 500 HSCT aircraft with EI(NO_x)=0 under Scenario S1b relative to Scenario D. Contours are -3, -2, -1, -0.5, 0.

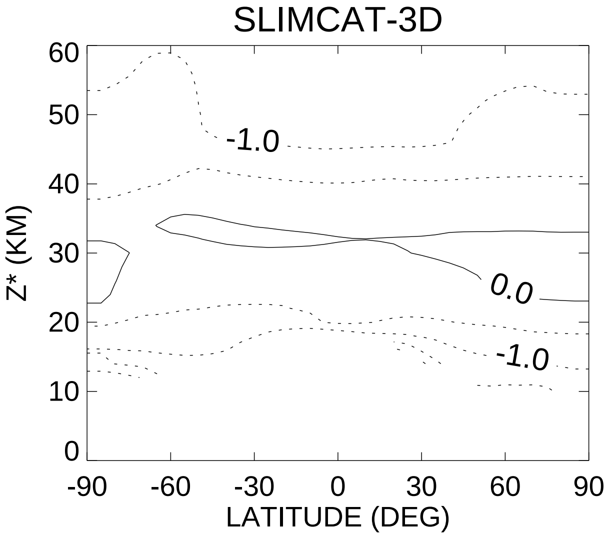

Figure 4.63: continued

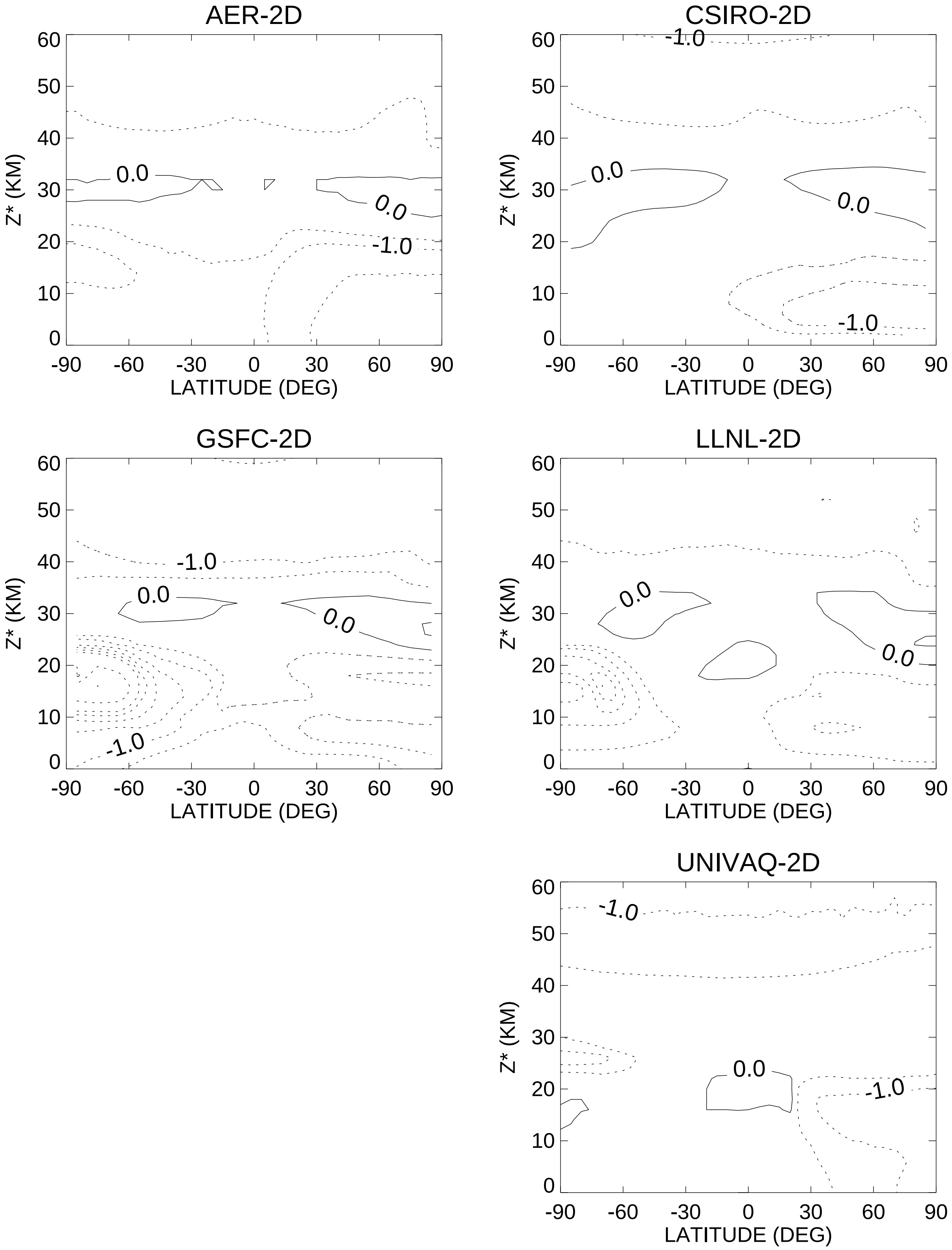

Figure 4.64: Calculated perturbations to O_3 (percent) as a function of latitude and altitude in October of 2015 due to emissions from a fleet of 500 HSCT aircraft with $EI(NO_x)=0$ under Scenario S1b relative to Scenario D. Contours are -15, -10, -5, -4, -3, -2, -1, -0.5, 0, 0.5.

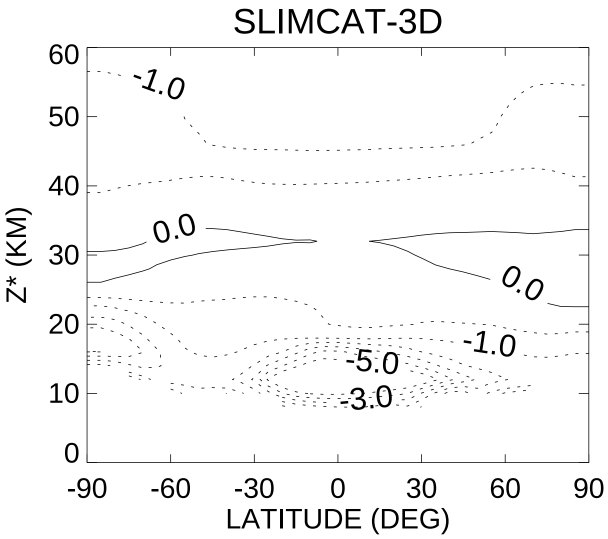

Figure 4.64: continued

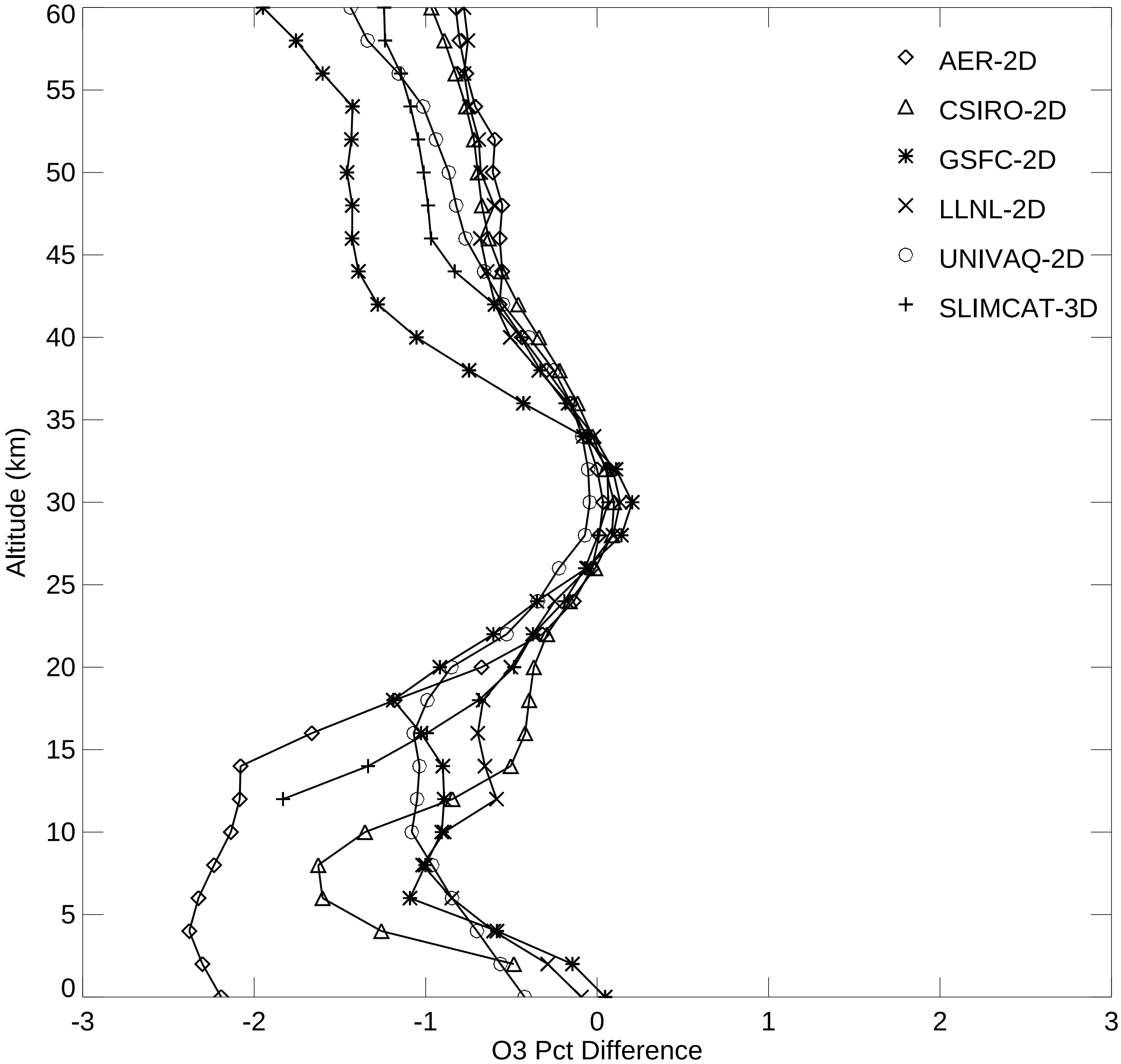

Figure 4.65: Calculated perturbations to O_3 (percent) as a function of altitude at 45^{o}N in June of 2015 due to emissions from a fleet of 500 HSCT aircraft with EI(NO_x)=0 under Scenario S1b relative to Scenario D.

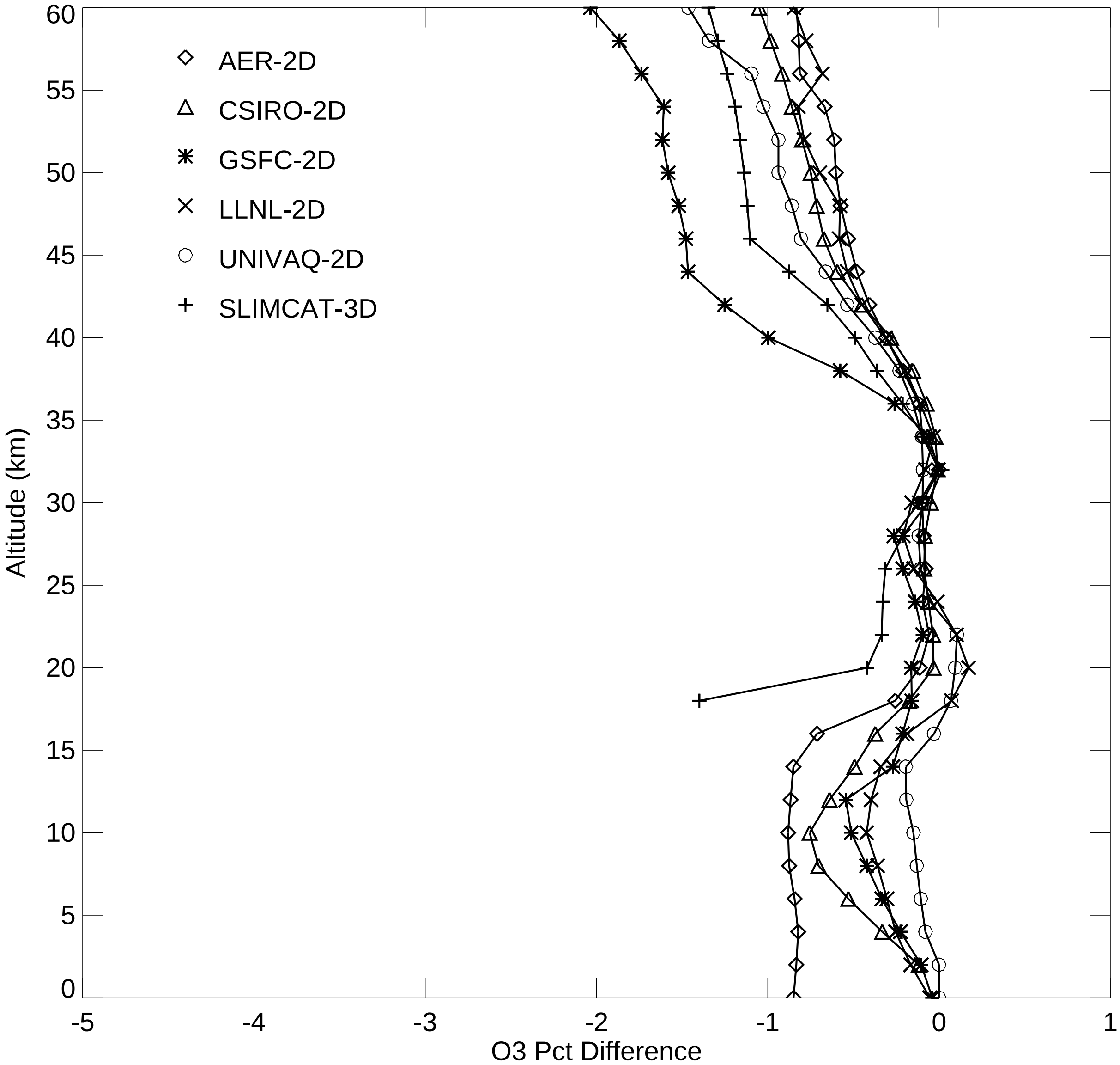

Figure 4.66: Calculated perturbations to O_3 (percent) as a function of altitude at the equator in June of 2015 due to emissions from a fleet of 500 HSCT aircraft with $EI(NO_x)=0$ under Scenario S1b relative to Scenario D.

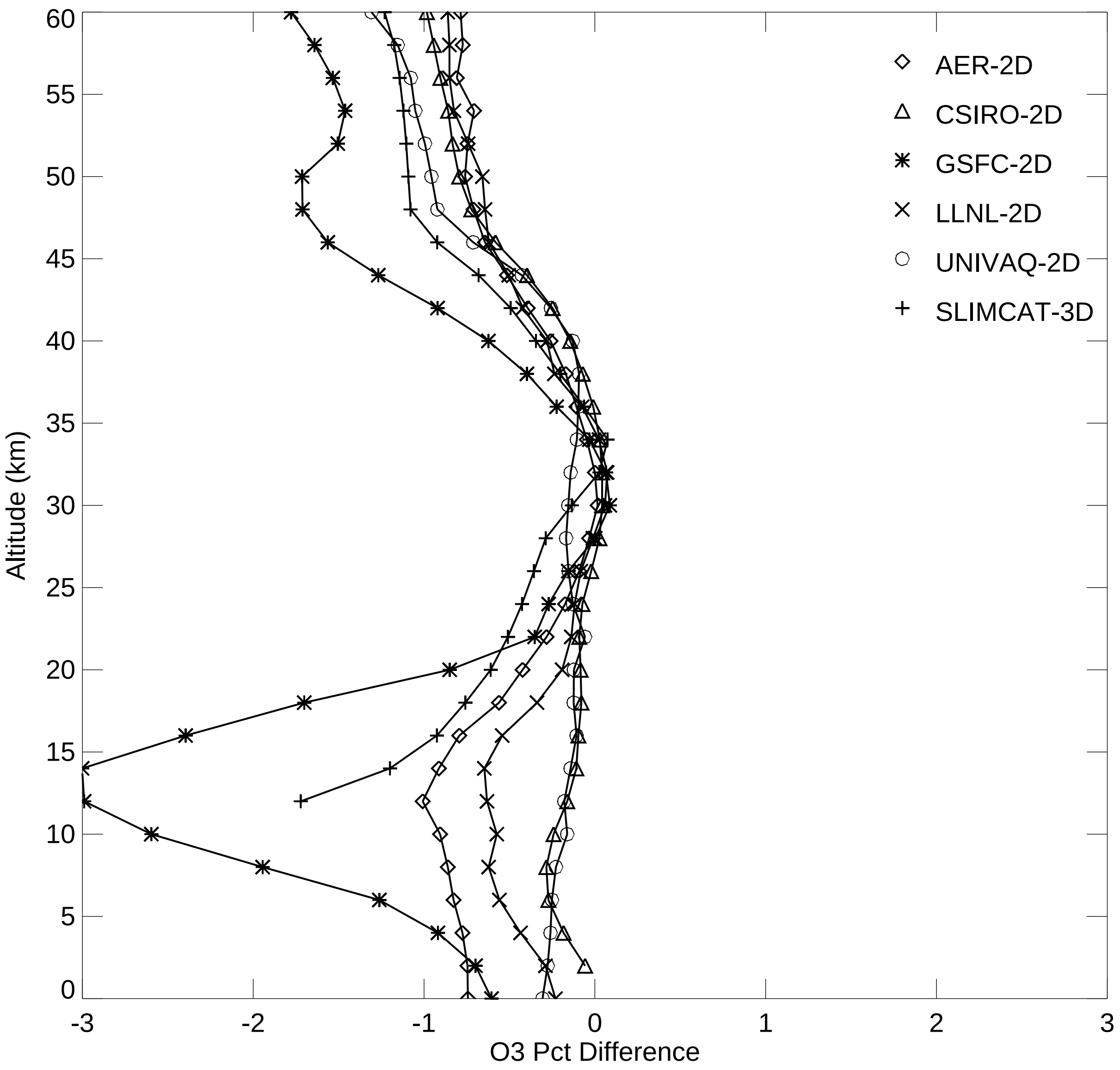

Figure 4.67: Calculated perturbations to O_3 (percent) as a function of altitude at 45^oS in June of 2015 due to emissions from a fleet of 500 HSCT aircraft with EI(NO_x)=0 under Scenario S1b relative to Scenario D.

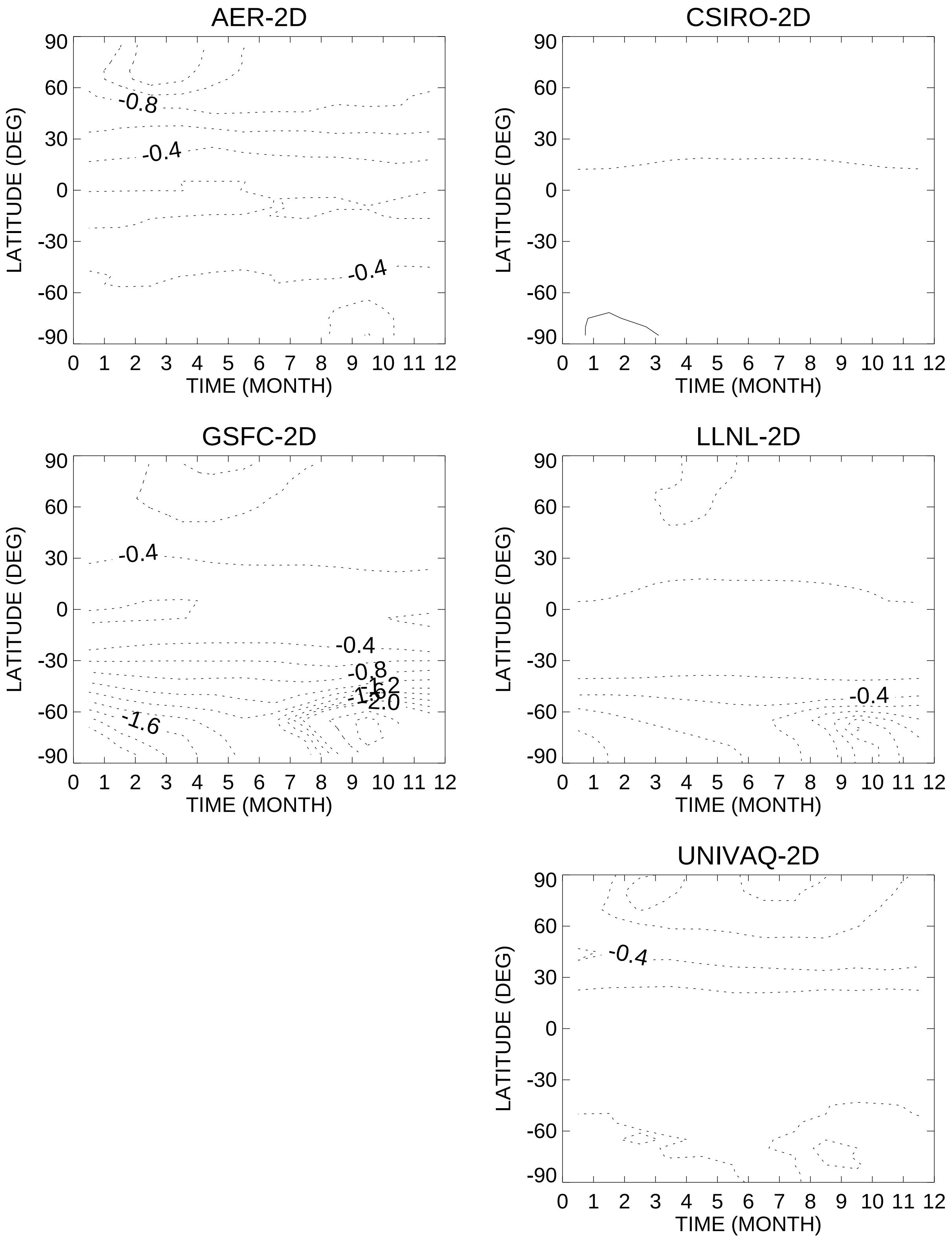

Figure 4.68: Calculated perturbations to column O_3 (percent) as a function of latitude and season in 2015 due to emissions from a fleet of 500 HSCT aircraft with EI(NO_x)=0 under Scenario S1b relative to Scenario D. Contours are -4, -3, and -2.0 to 0 by 0.2.

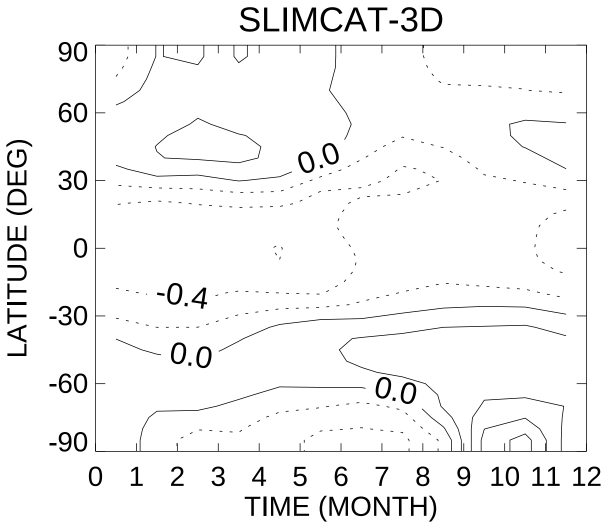

Figure 4.68: continued

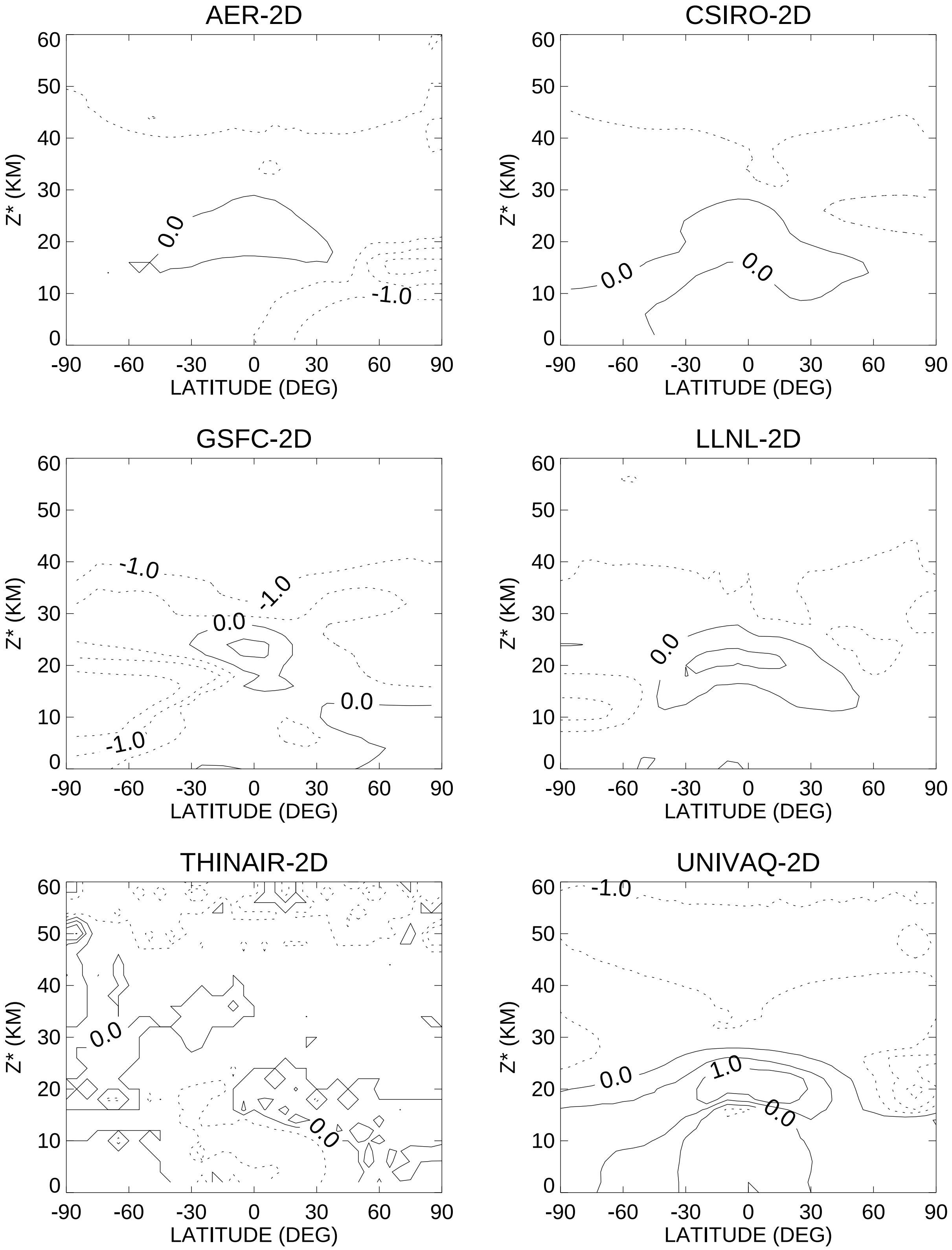

Figure 4.69: Calculated perturbations to O_3 (percent) as a function of latitude and altitude in March of 2015 due to emissions from a fleet of 500 HSCT aircraft with EI(NO_x)=5 under Scenario S1c relative to Scenario D. Contours are -10, -5, -4, -3, -2, -1, -0.5, 0, 0.5, 1.

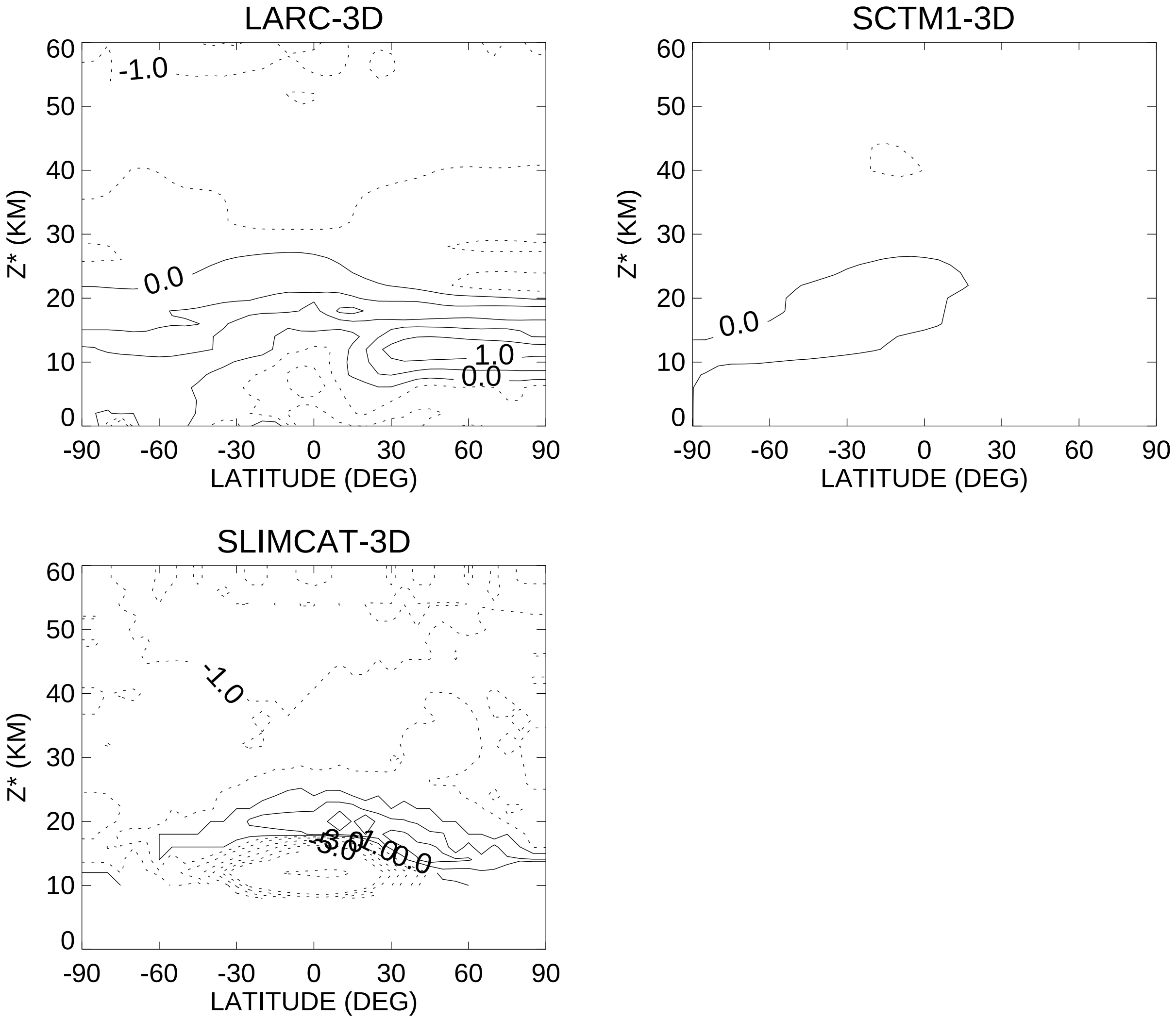

Figure 4.69: continued

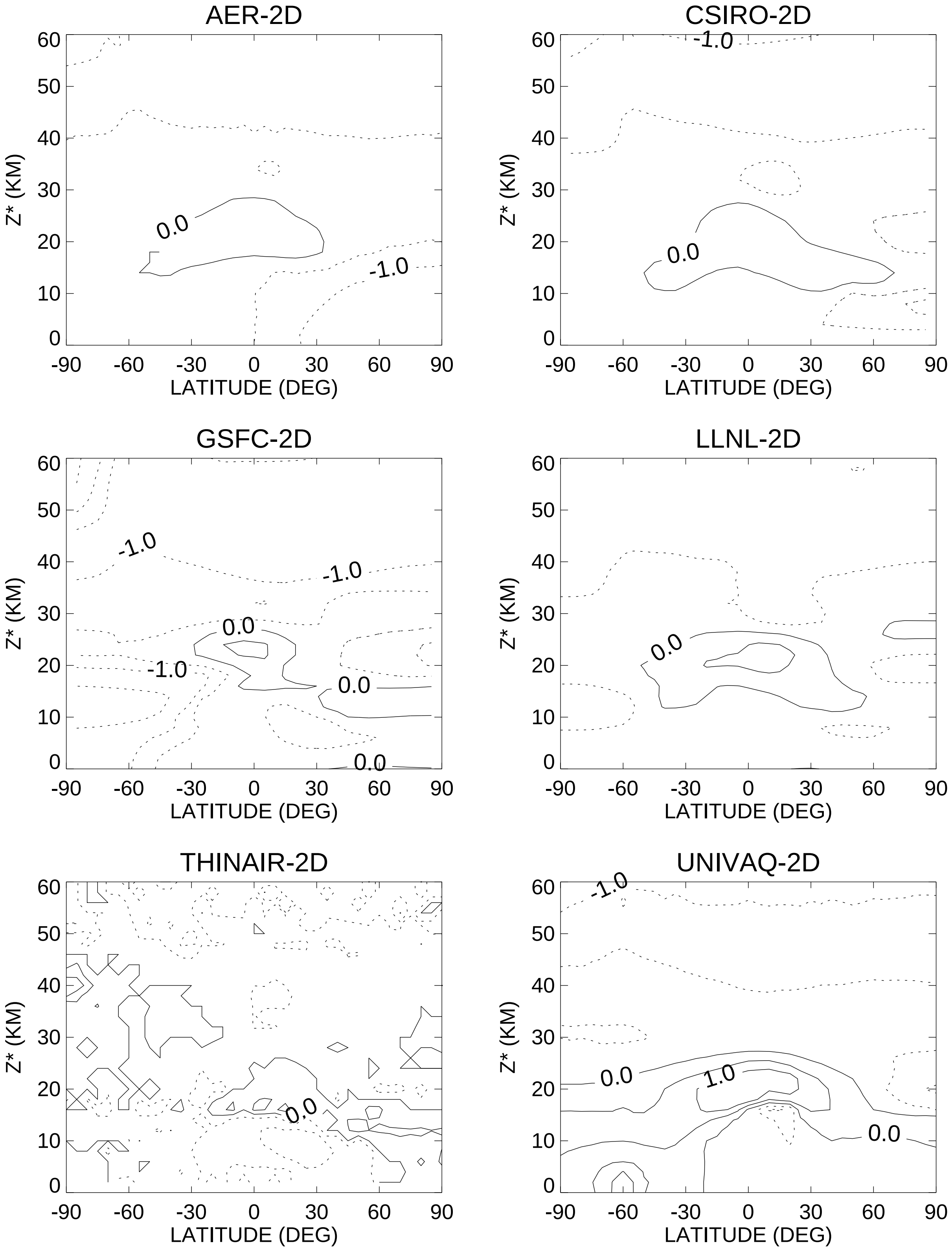

Figure 4.70: Calculated perturbations to O_3 (percent) as a function of latitude and altitude in June of 2015 due to emissions from a fleet of 500 HSCT aircraft with EI(NO_x)=5 under Scenario S1c relative to Scenario D. Contours are -10, -5, -4, -3, -2, -1, -0.5, 0, 0.5, 1, 2.

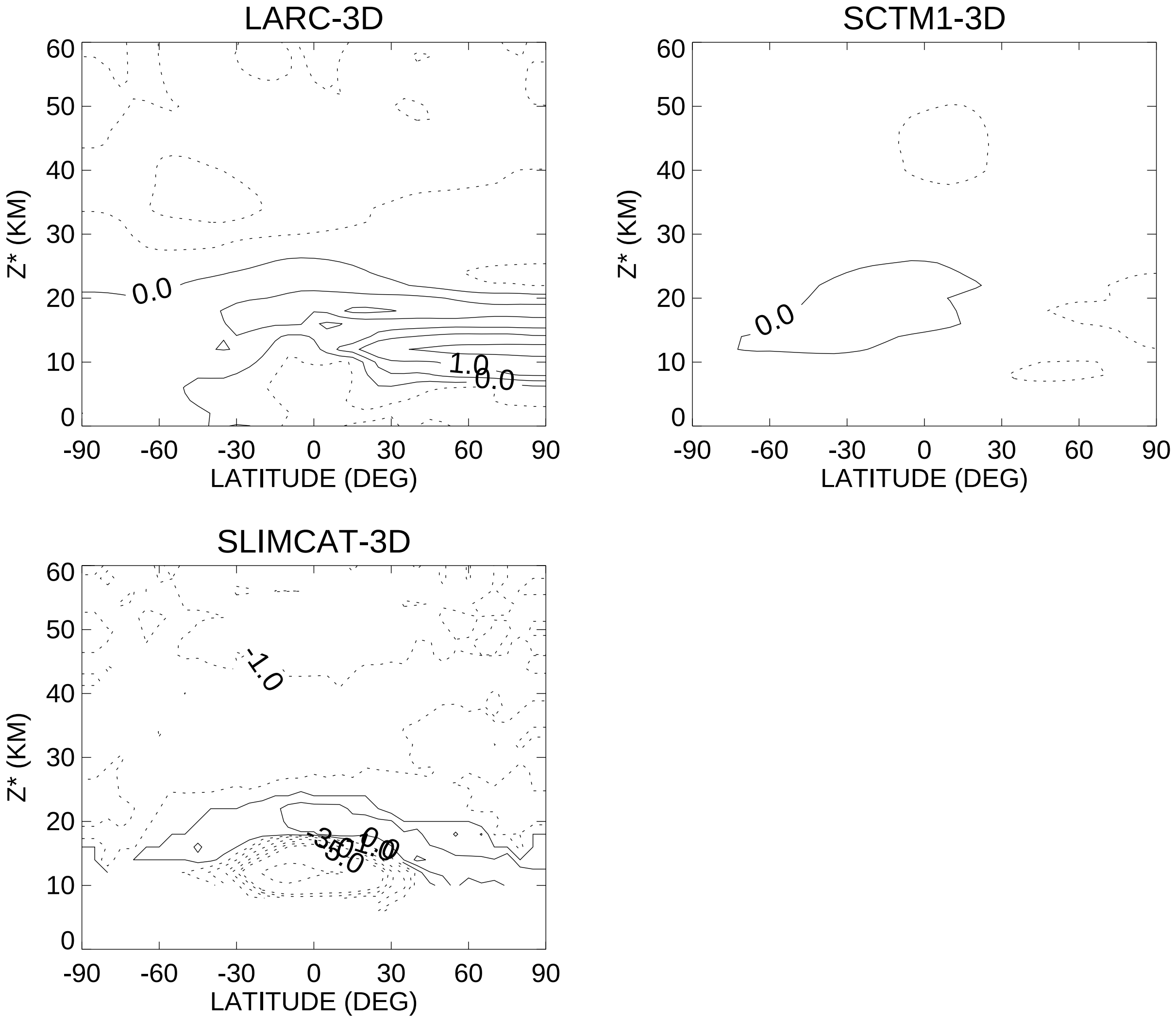

Figure 4.70: continued

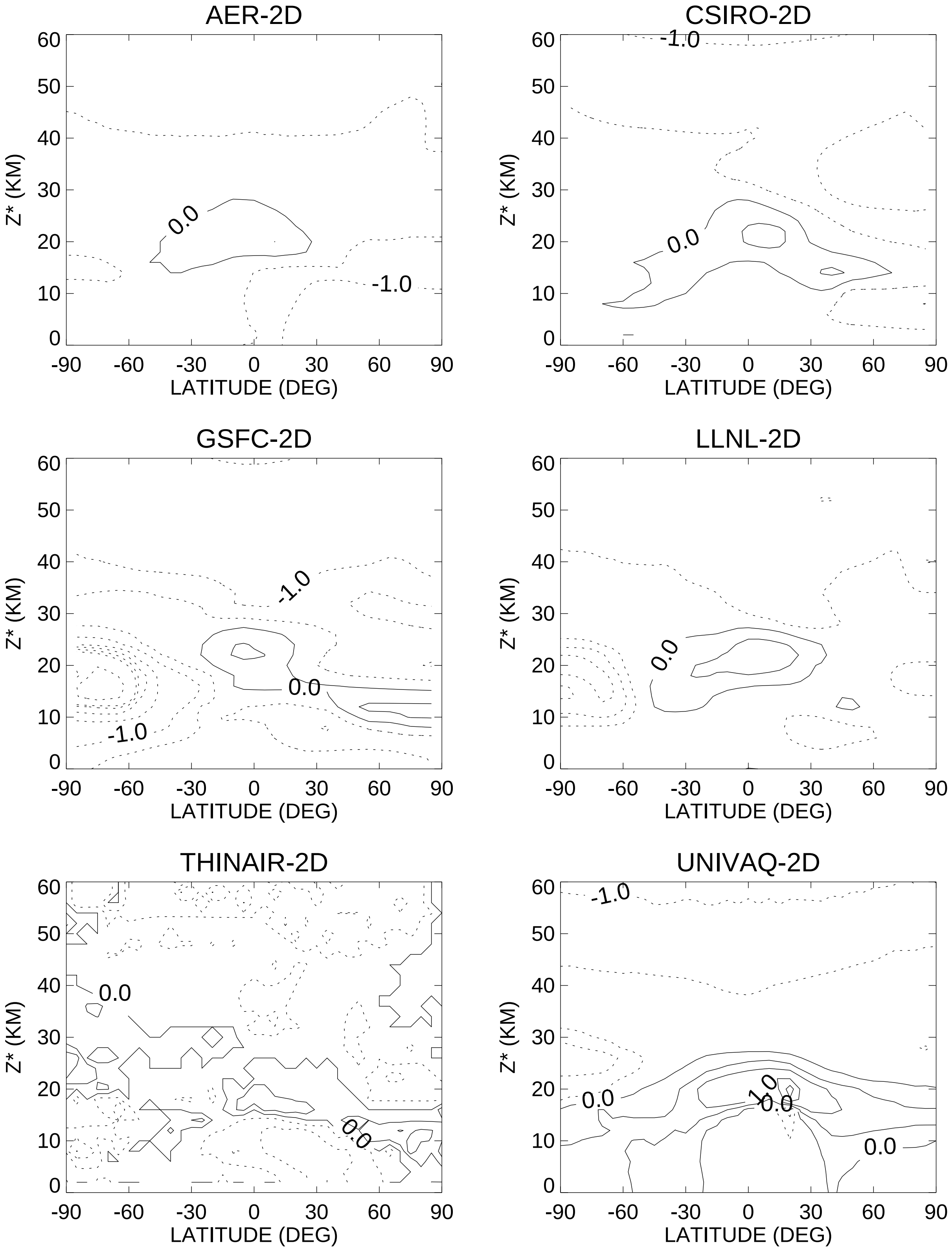

Figure 4.71: Calculated perturbations to O_3 (percent) as a function of latitude and altitude in October of 2015 due to emissions from a fleet of 500 HSCT aircraft with $EI(NO_x)=5$ under Scenario S1c relative to Scenario D. Contours are -10, -5, -4, -3, -2, -1, -0.5, 0, 0.5, 1, 2, 3.

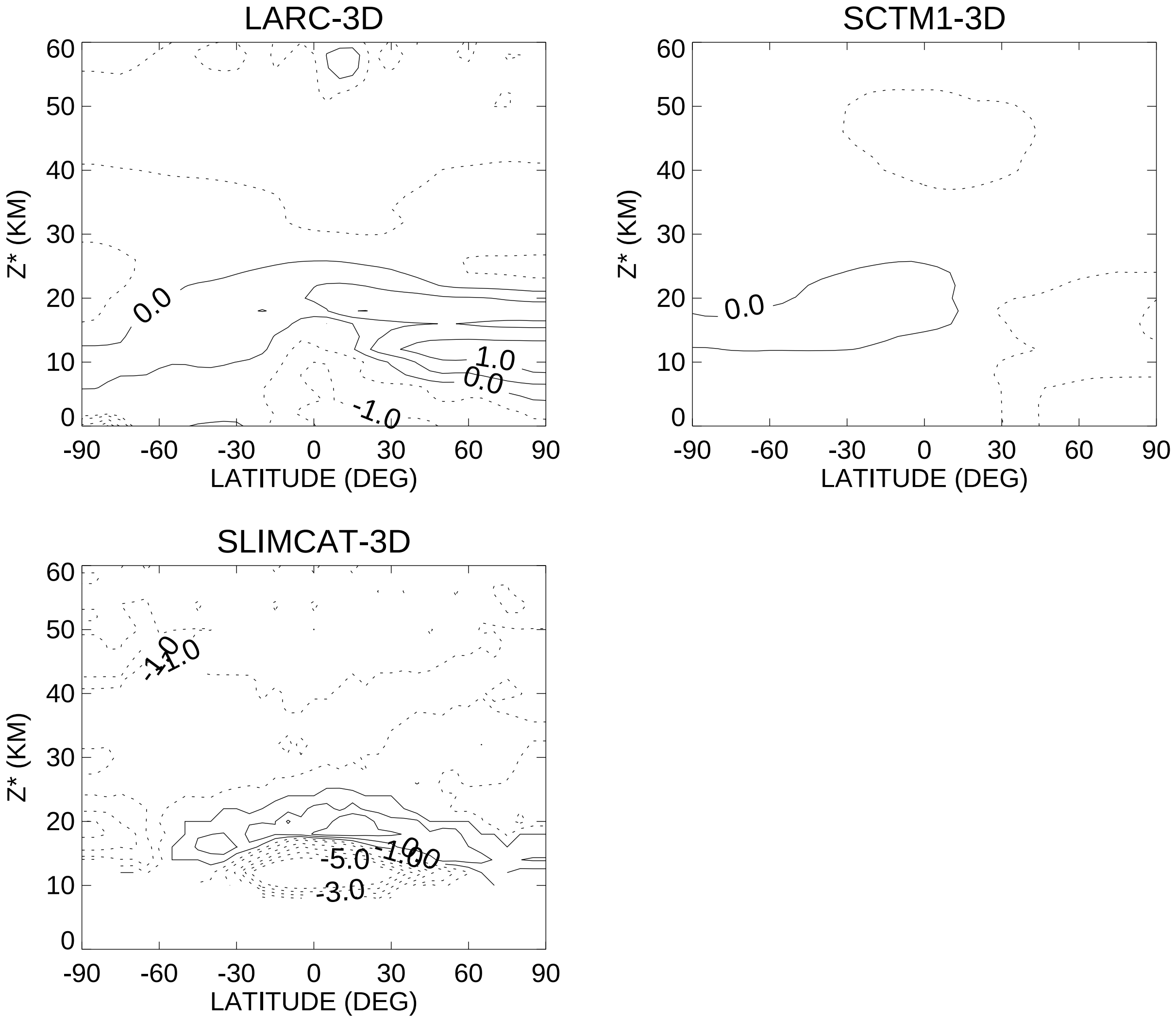

Figure 4.71: continued

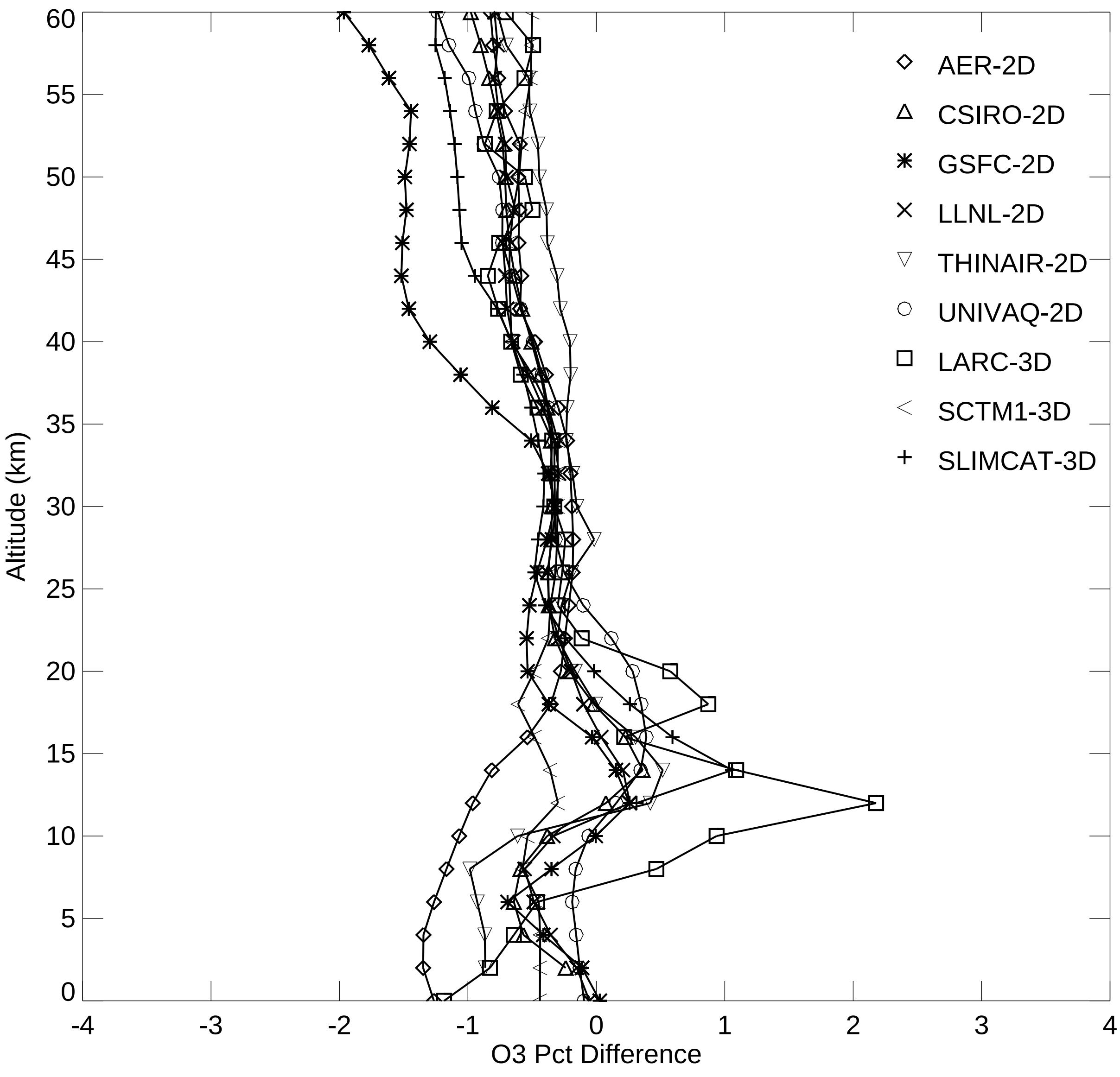

Figure 4.72: Calculated perturbations to O_3 (percent) as a function of altitude at 45^oN in June of 2015 due to emissions from a fleet of 500 HSCT aircraft with EI(NO_x)=5 under Scenario S1c relative to Scenario D.

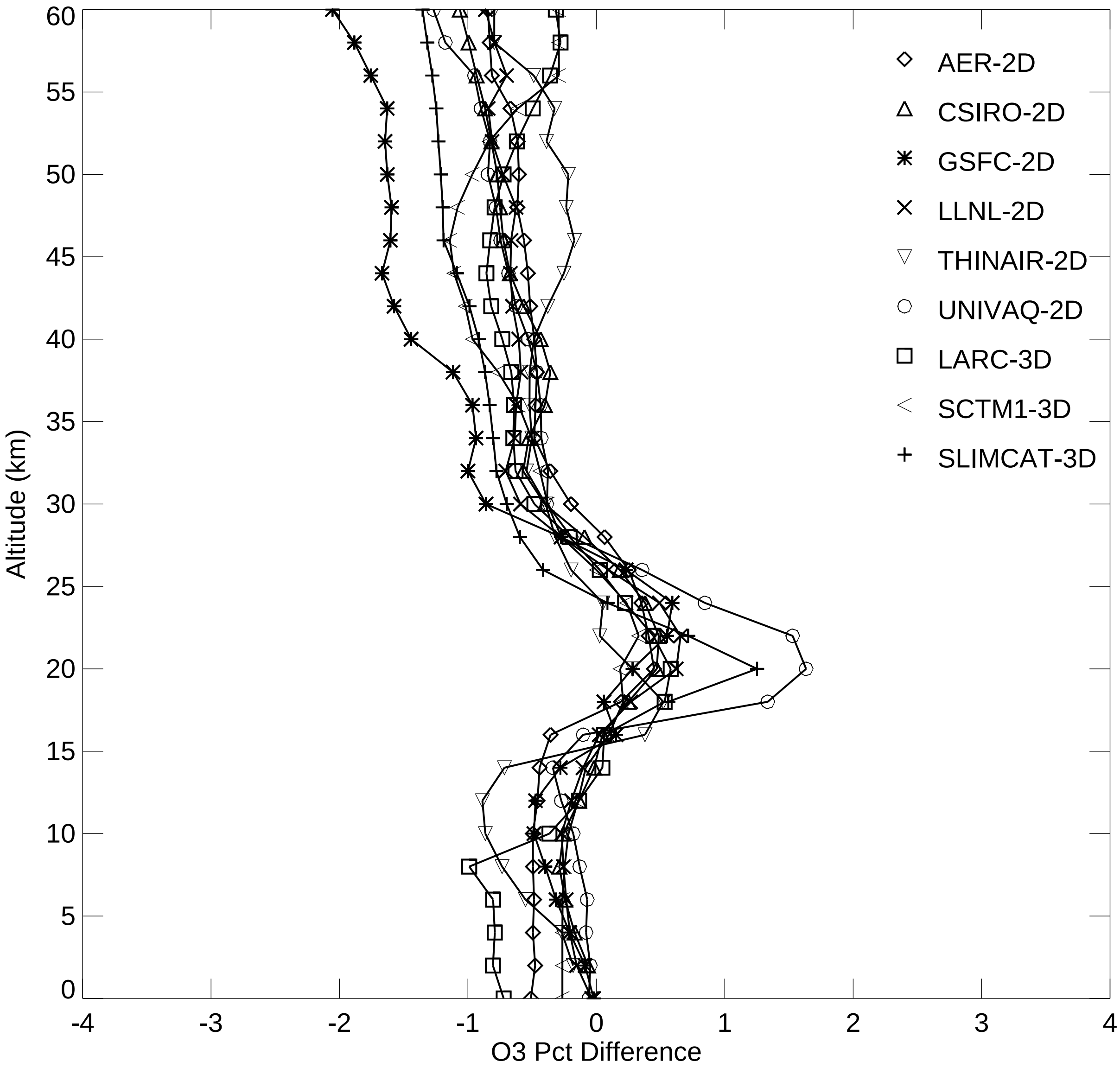

Figure 4.73: Calculated perturbations to O_3 (percent) as a function of altitude at the equator in June of 2015 due to emissions from a fleet of 500 HSCT aircraft with $EI(NO_x)=5$ under Scenario S1c relative to Scenario D.

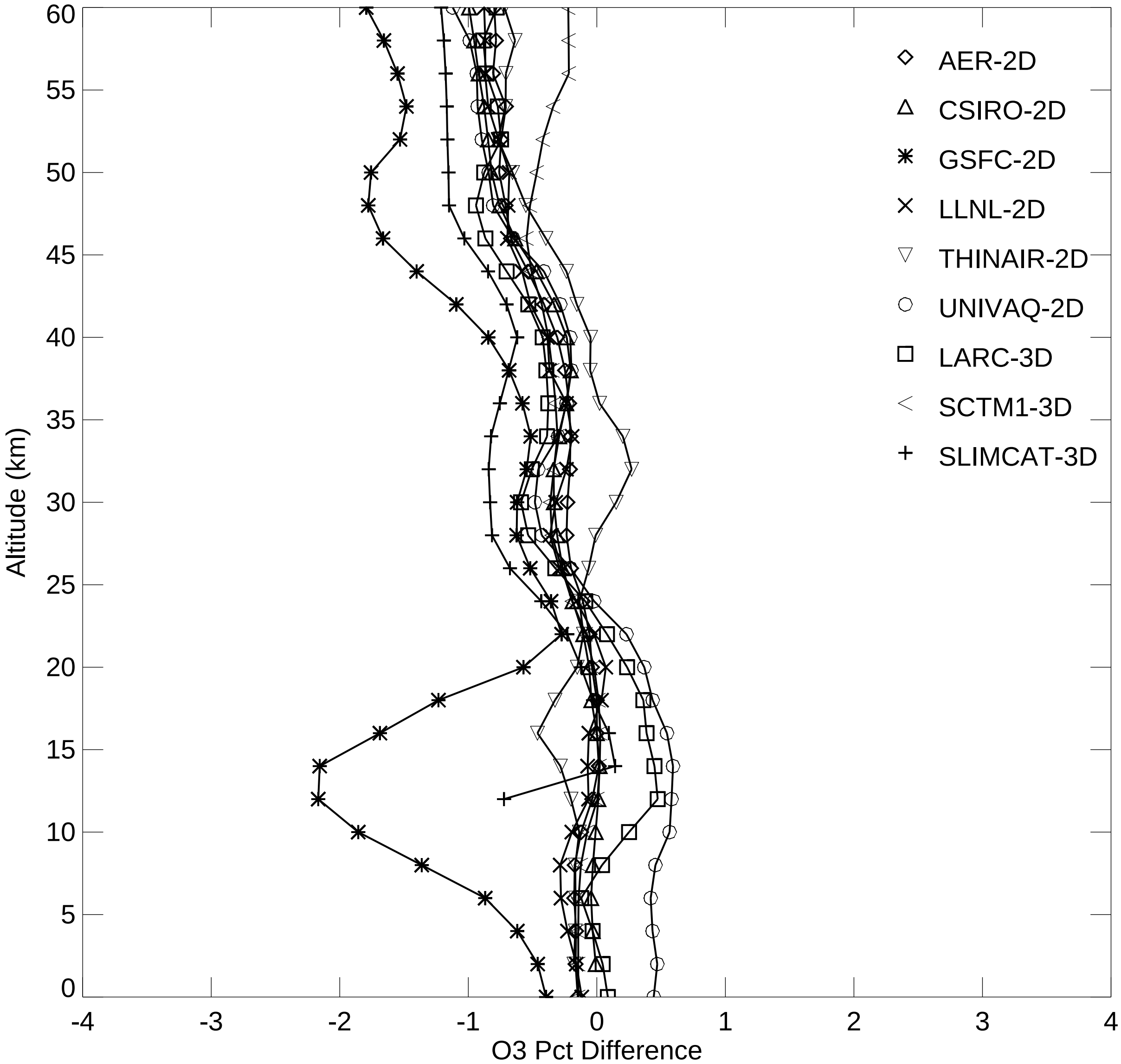

Figure 4.74: Calculated perturbations to O_3 (percent) as a function of altitude at 45^oS in June of 2015 due to emissions from a fleet of 500 HSCT aircraft with EI(NO_x)=5 under Scenario S1c relative to Scenario D.

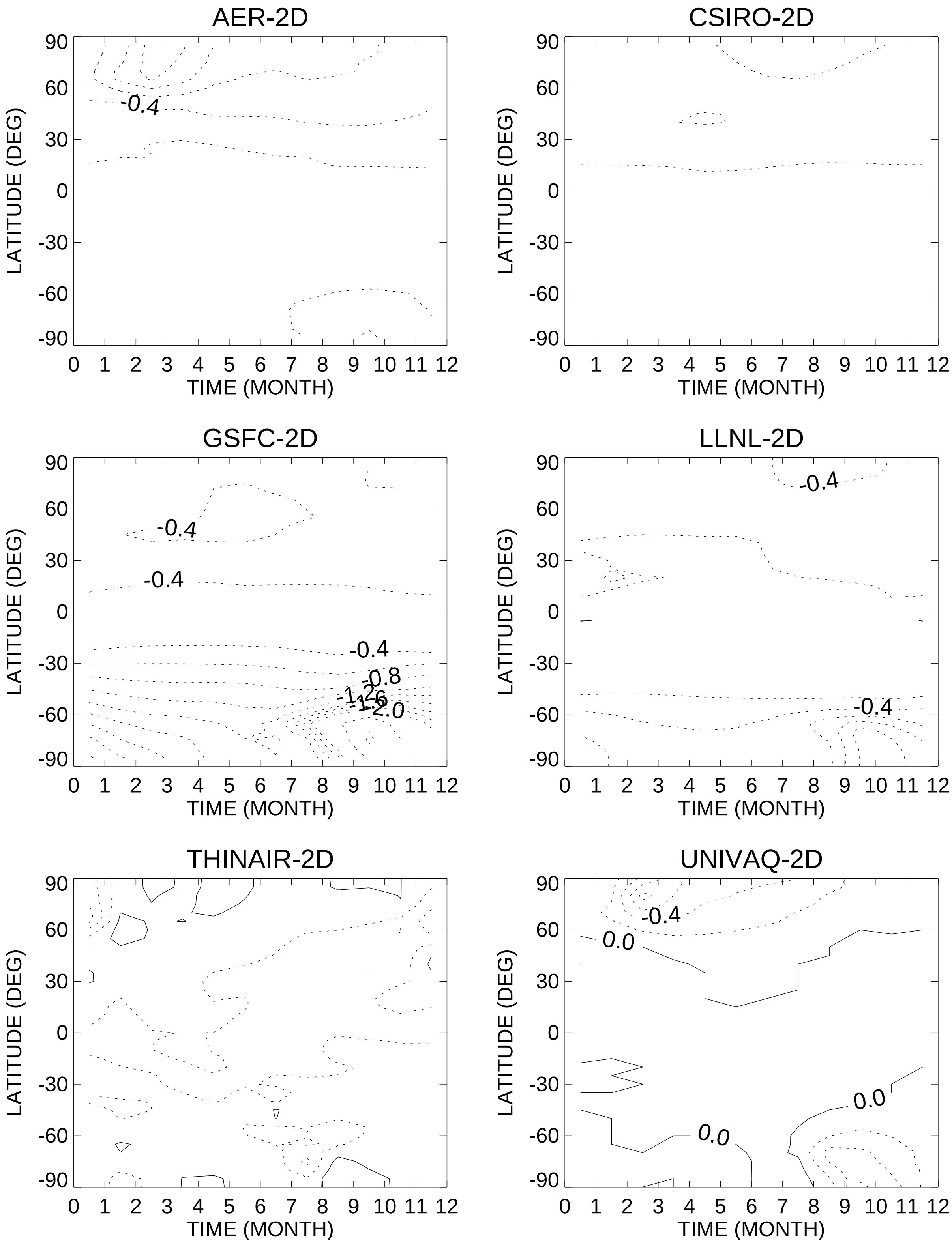

Figure 4.75: Calculated perturbations to column O_3 (percent) as a function of latitude and season in 2015 due to emissions from a fleet of 500 HSCT aircraft with EI(NO_x)=5 under Scenario S1c relative to Scenario D. Contours are -4, -3, and -2.0 to 0.2 by 0.2.

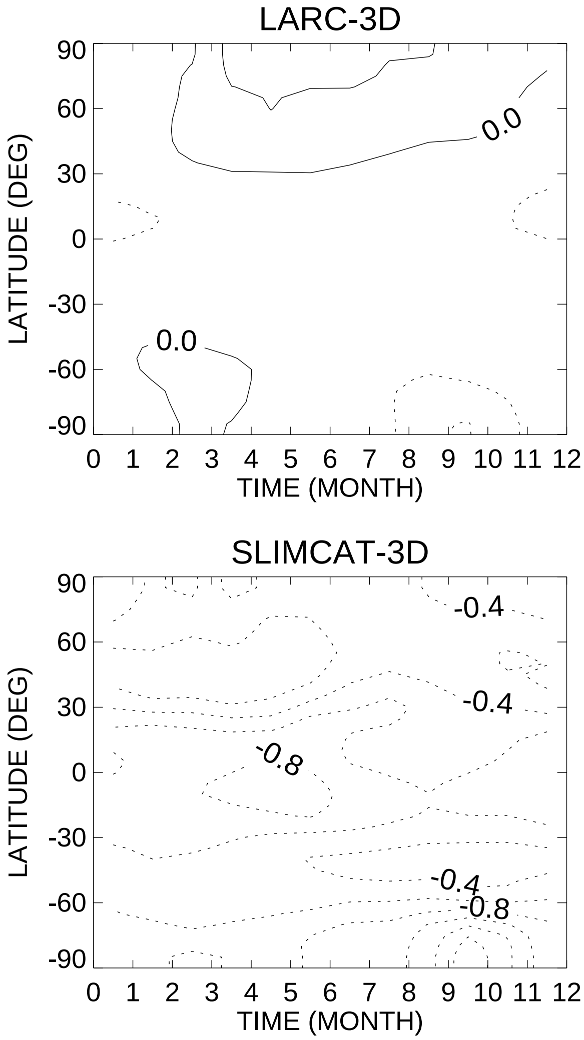

Figure 4.75: continued

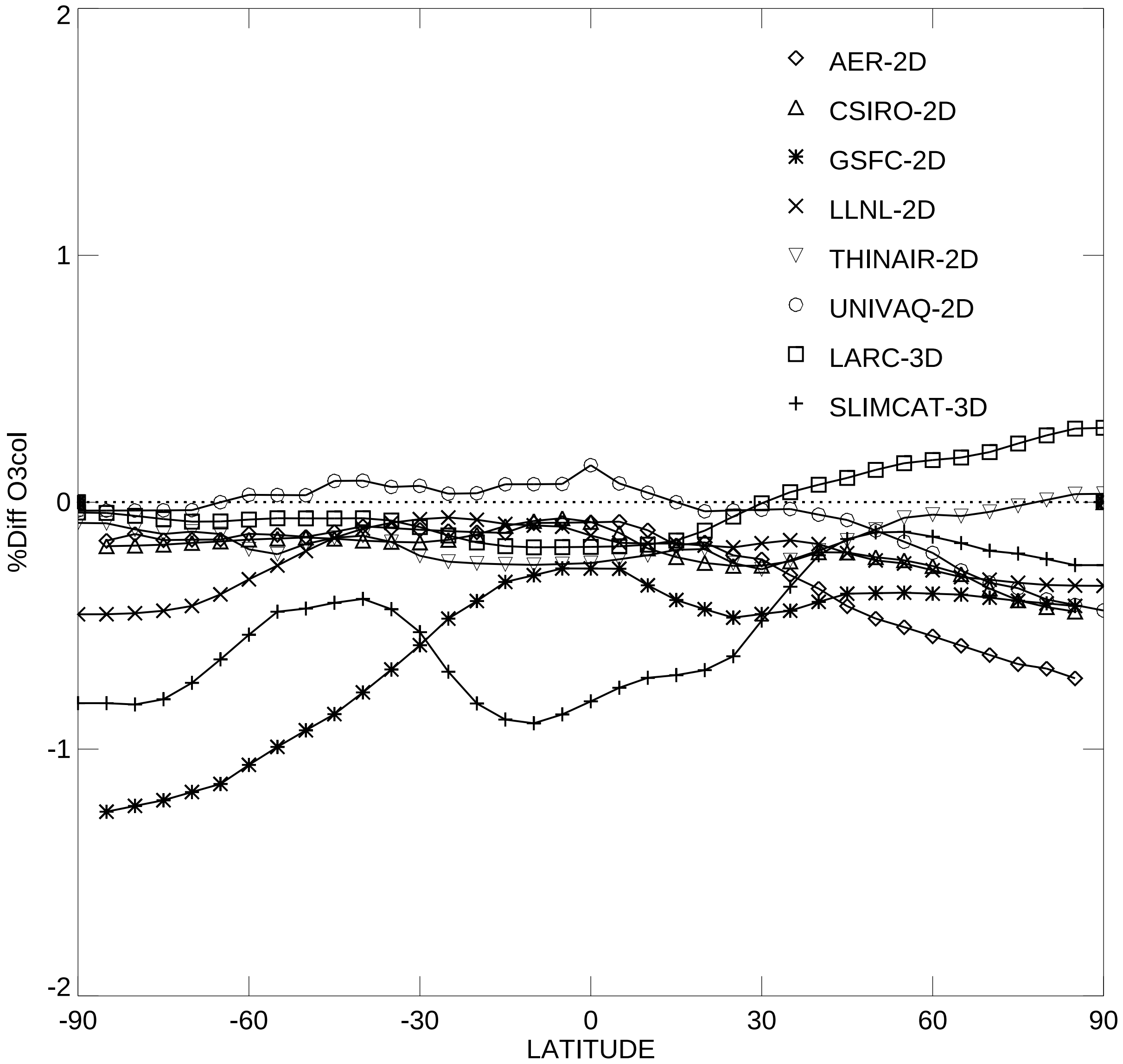

Figure 4.76: Calculated perturbations to total O_3 (percent) in June as function of latitude due to emissions from a fleet of 500 HSCT aircraft operating in 2015 (Scenario S1c - Scenario D) with $EI(NO_x)$=5.

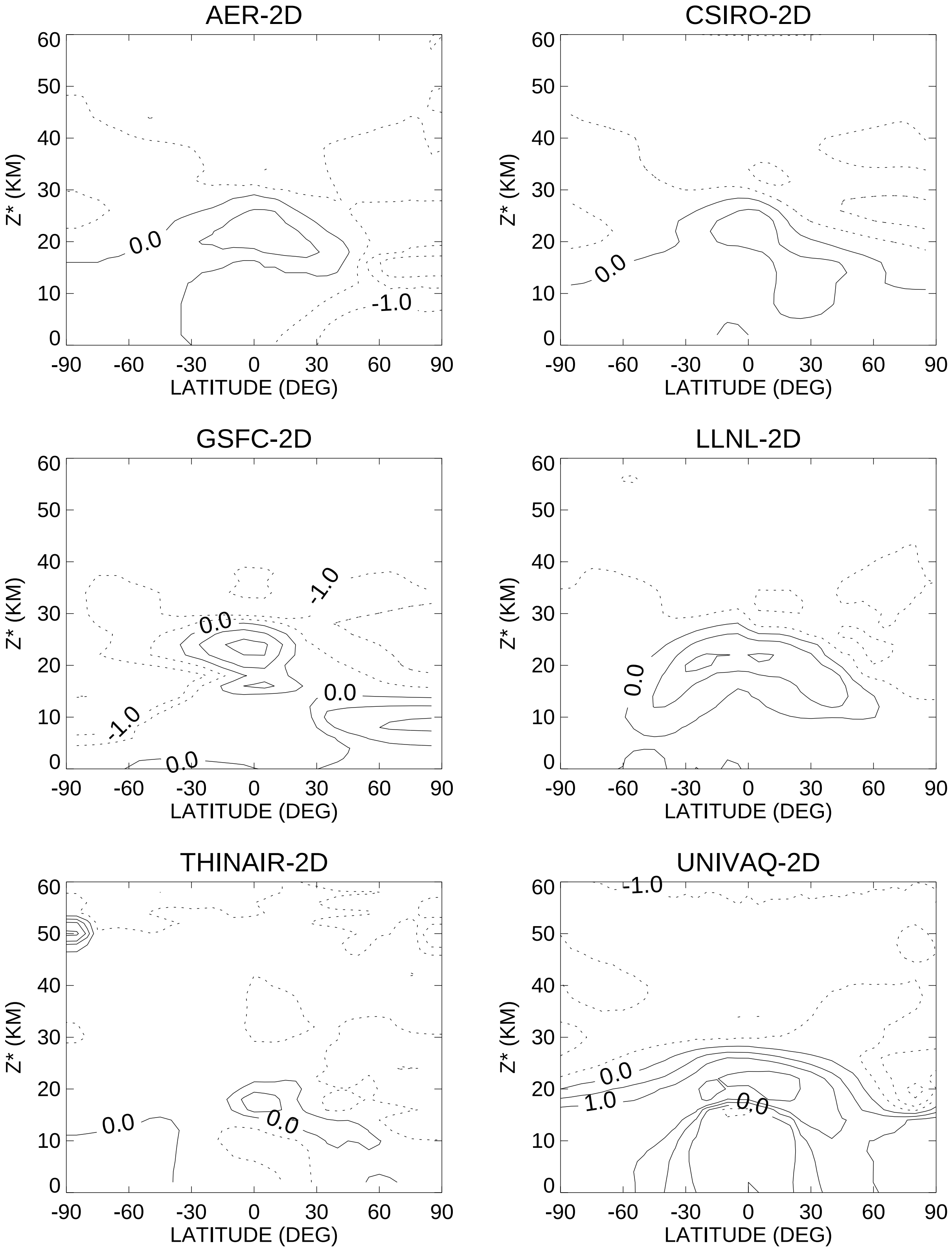

Figure 4.77: Calculated perturbations to O_3 (percent) as a function of latitude and altitude in March of 2015 due to emissions from a fleet of 500 HSCT aircraft with EI(NO_x)=10 under Scenario S1d relative to Scenario D. Contours are -2, -1, -0.5, 0, 0.5, 1, 2, 3.

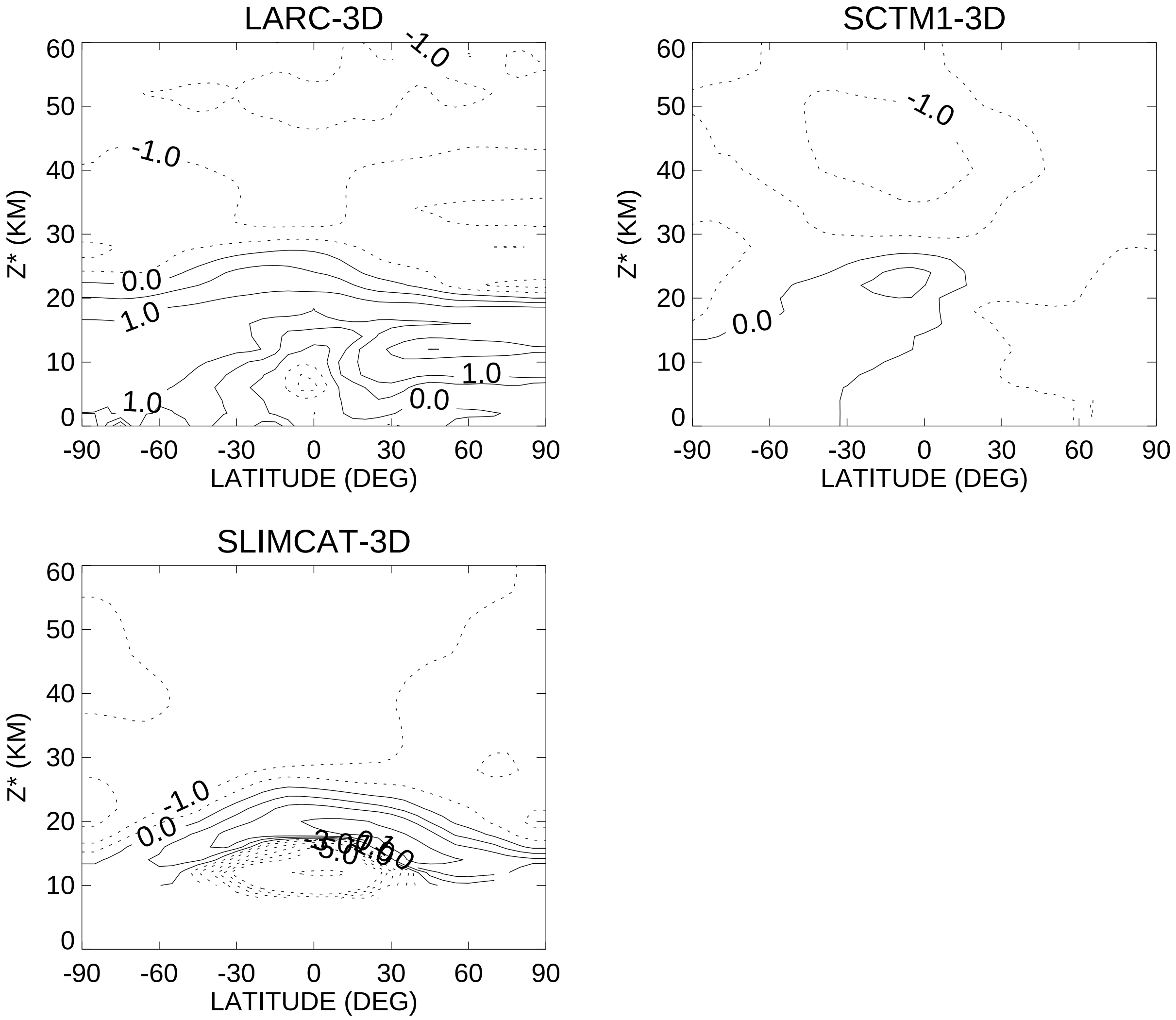

Figure 4.77: continued

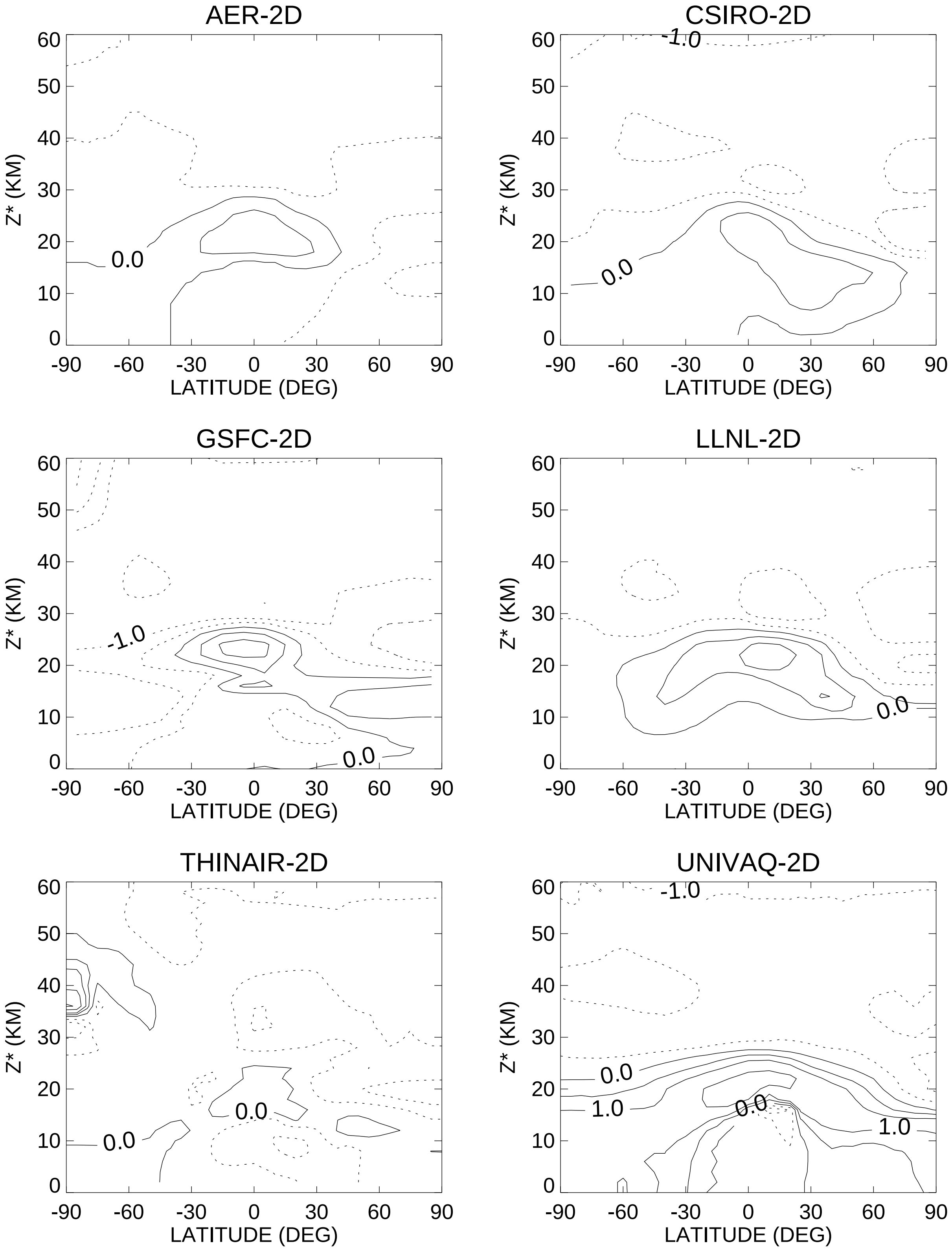

Figure 4.78: Calculated perturbations to O_3 (percent) as a function of latitude and altitude in June of 2015 due to emissions from a fleet of 500 HSCT aircraft with EI(NO_x)=10 under Scenario S1d relative to Scenario D. Contours are -2, -1, -0.5, 0, 0.5, 1, 2, 3, 4.

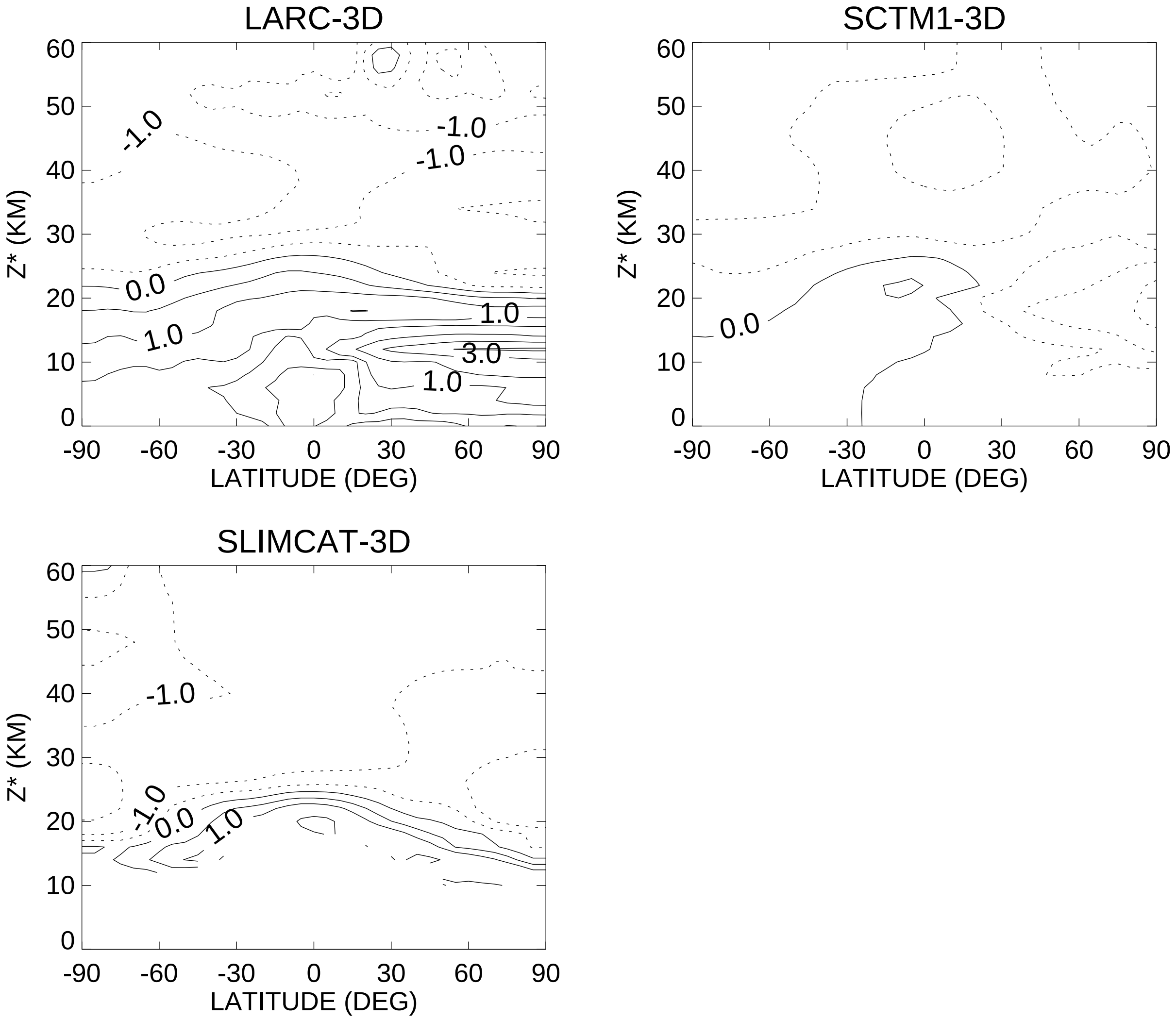

Figure 4.78: continued

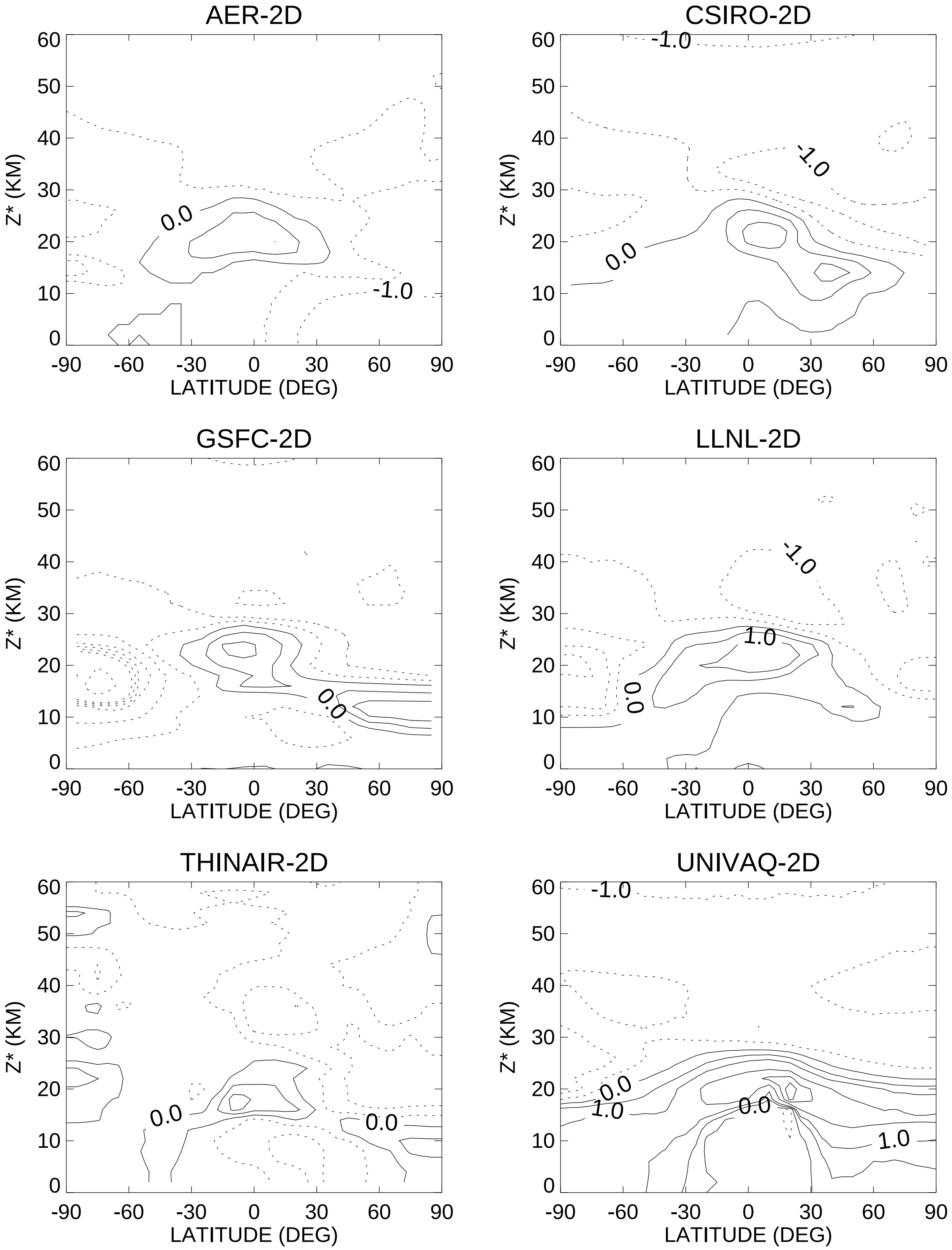

Figure 4.79: Calculated perturbations to O_3 (percent) as a function of latitude and altitude in October of 2015 due to emissions from a fleet of 500 HSCT aircraft with $EI(NO_x)=10$ under Scenario S1d relative to Scenario D. Contours are -10, -5, -4, -3, -2, -1, -0.5, 0, 0.5, 1, 2, 3, 4.

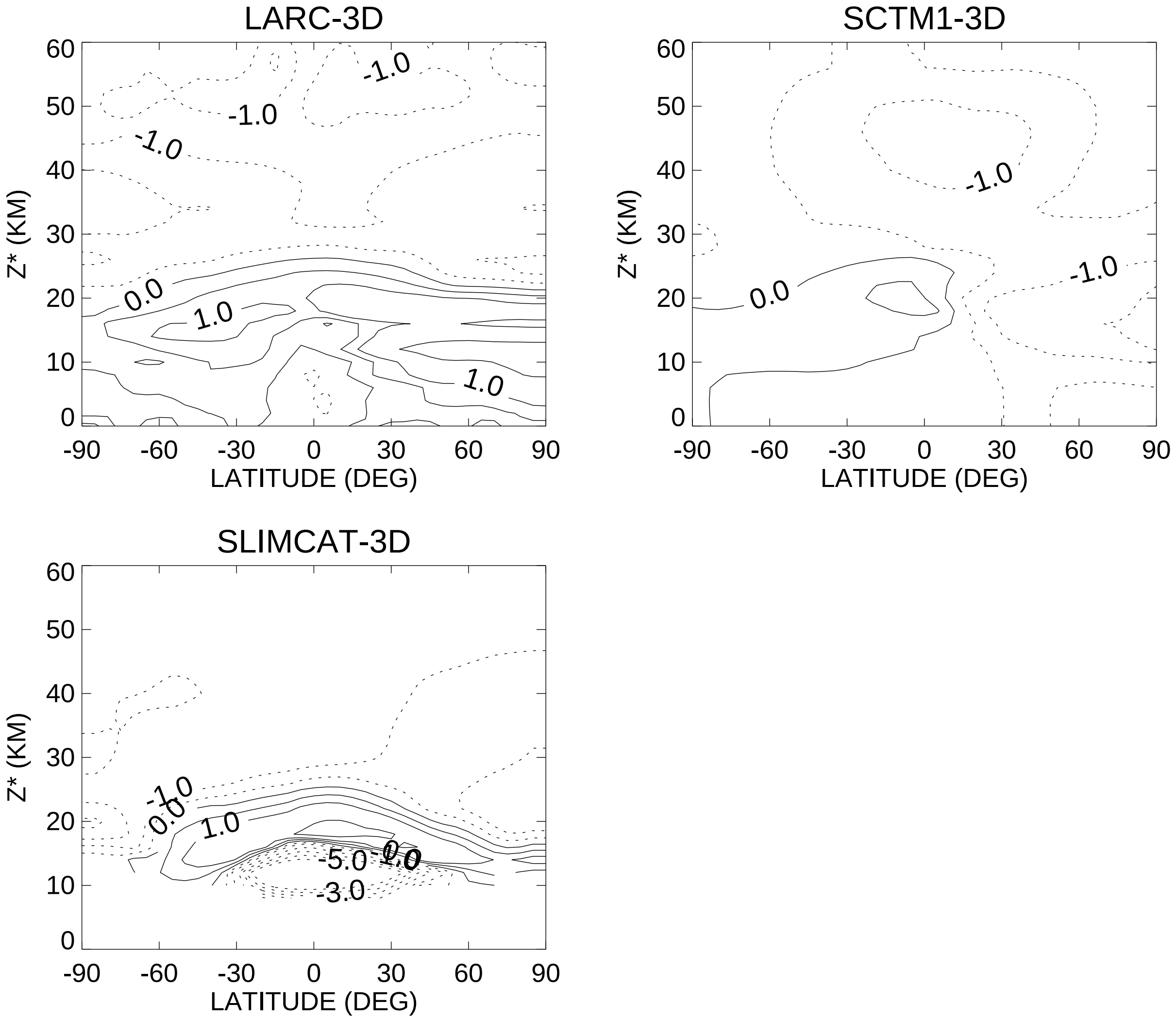

Figure 4.79: continued

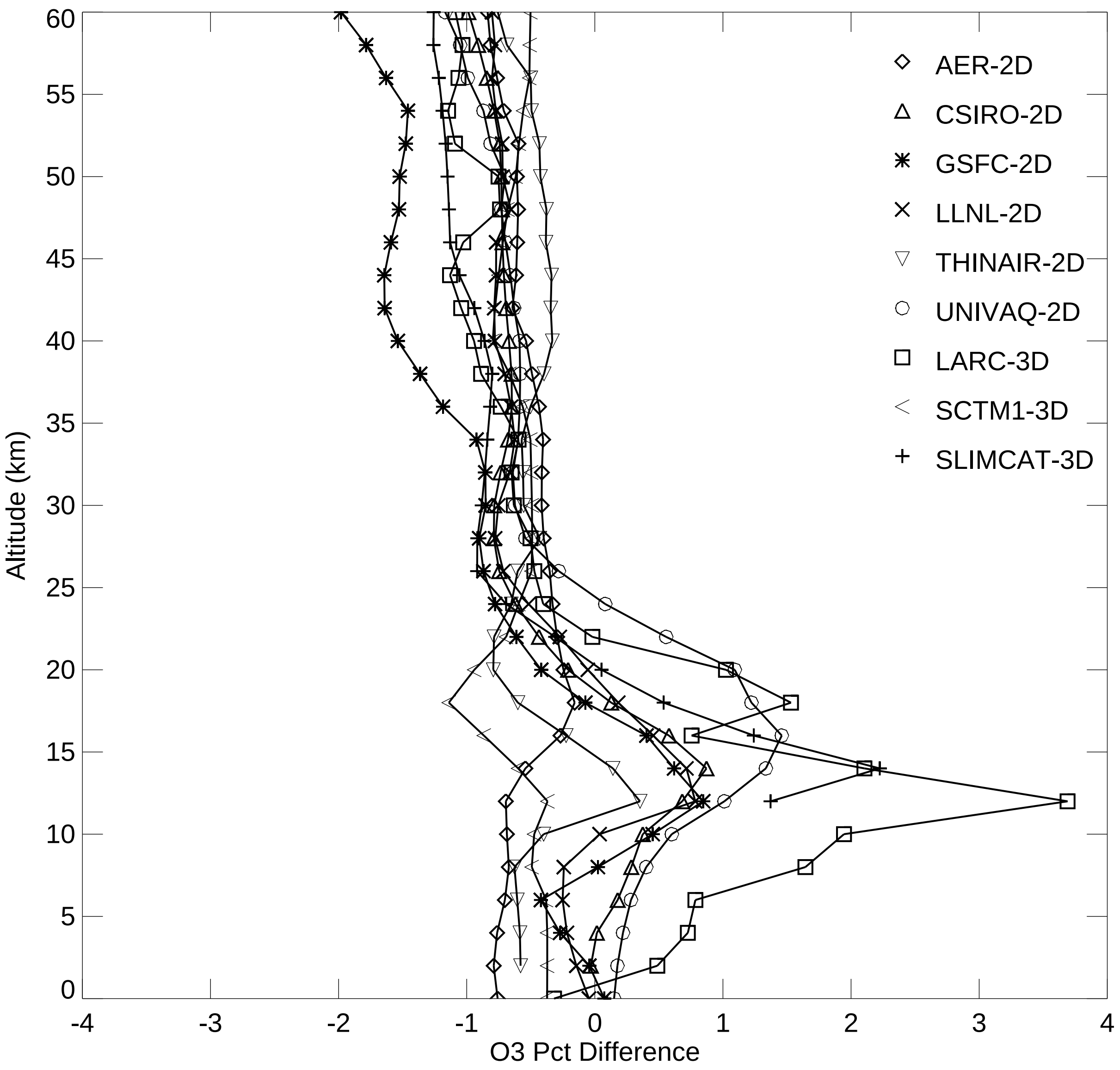

Figure 4.80: Calculated perturbations to O_3 (percent) as a function of altitude at 45^{o}N in June of 2015 due to emissions from a fleet of 500 HSCT aircraft with EI(NO_x)=10 under Scenario S1d relative to Scenario D.

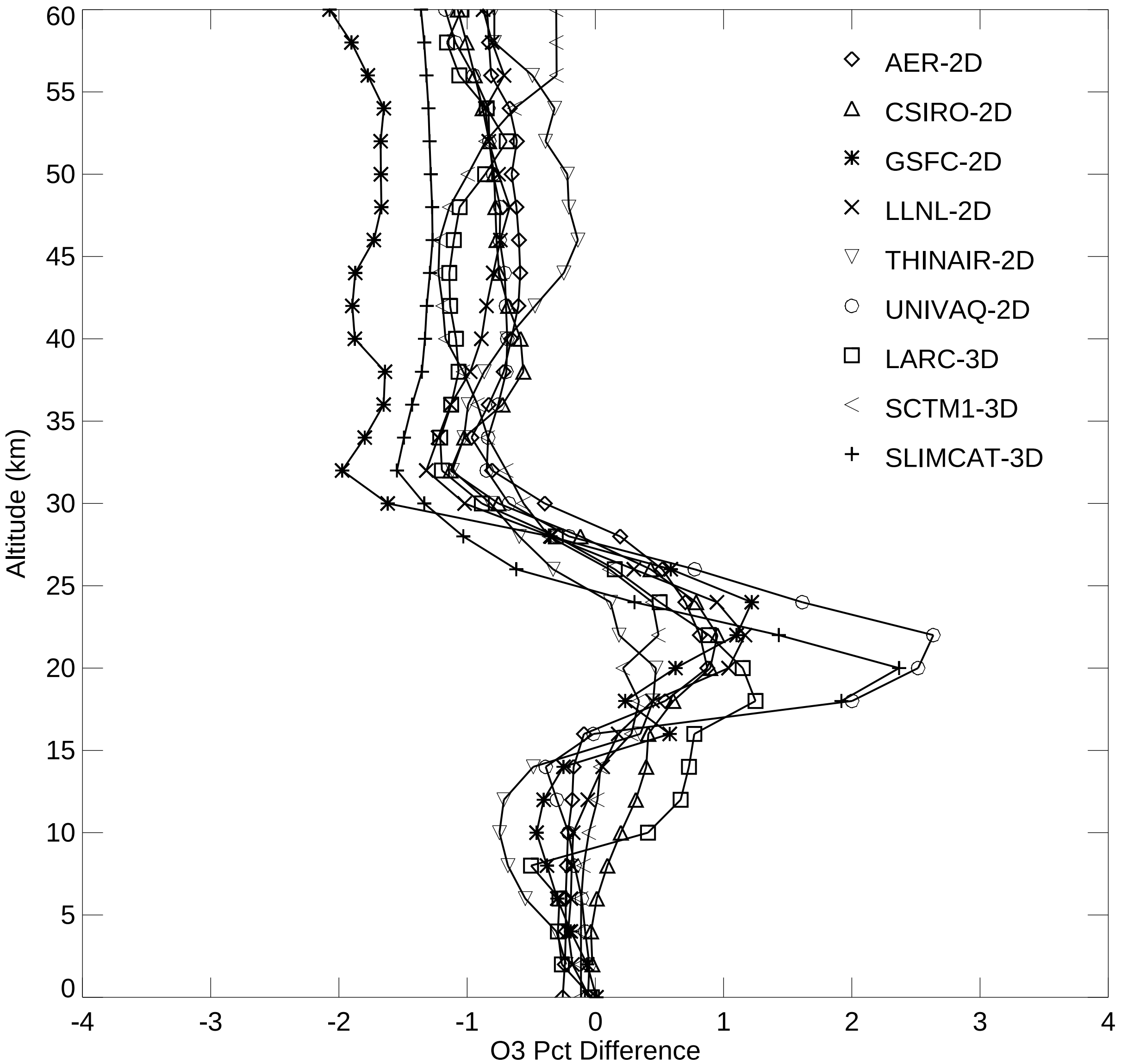

Figure 4.81: Calculated perturbations to O_3 (percent) as a function of altitude at the equator in June of 2015 due to emissions from a fleet of 500 HSCT aircraft with $EI(NO_x)=10$ under Scenario S1d relative to Scenario D.

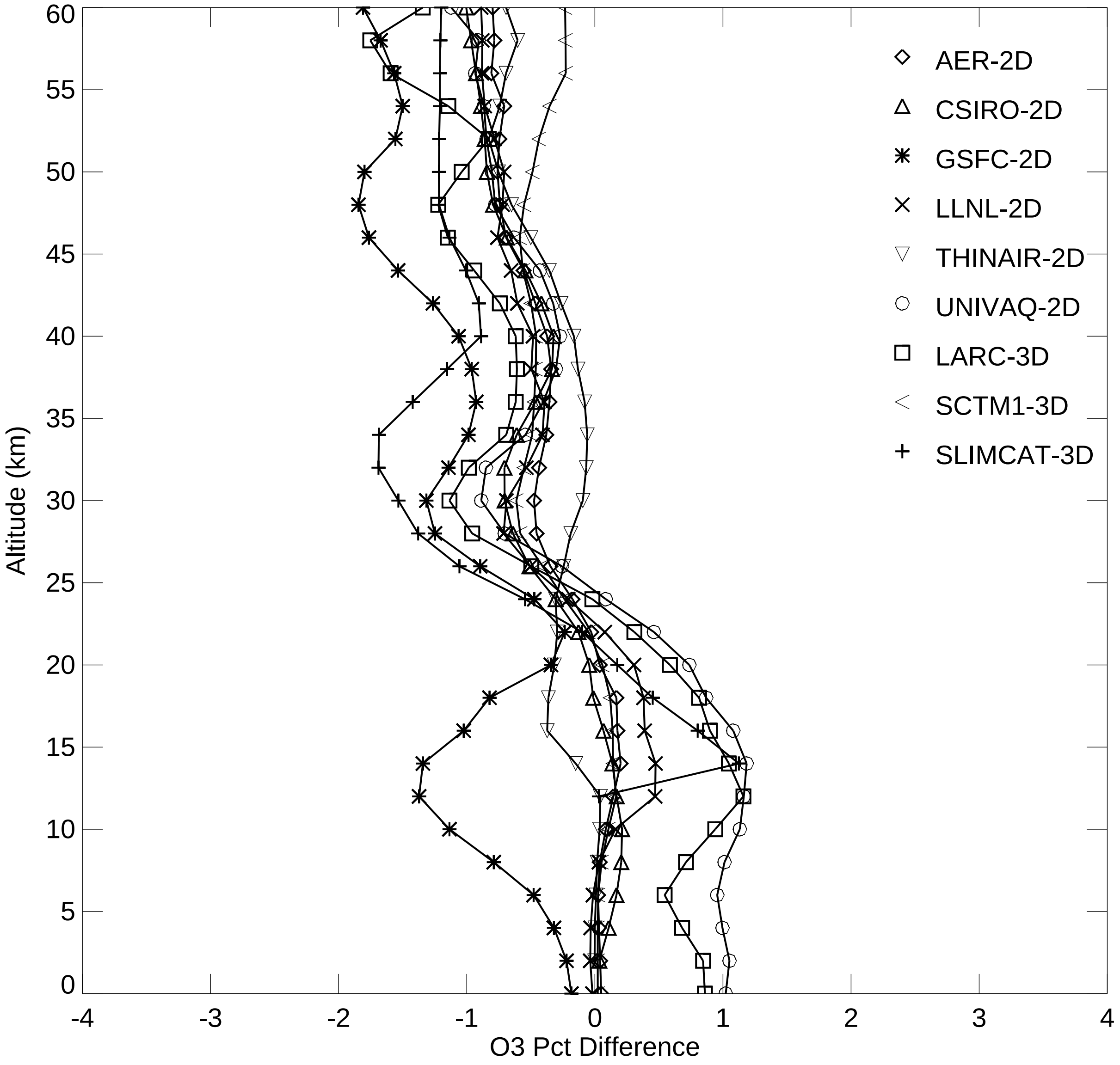

Figure 4.82: Calculated perturbations to O_3 (percent) as a function of altitude at 45^oS in June of 2015 due to emissions from a fleet of 500 HSCT aircraft with EI(NO_x)=10 under Scenario S1d relative to Scenario D.

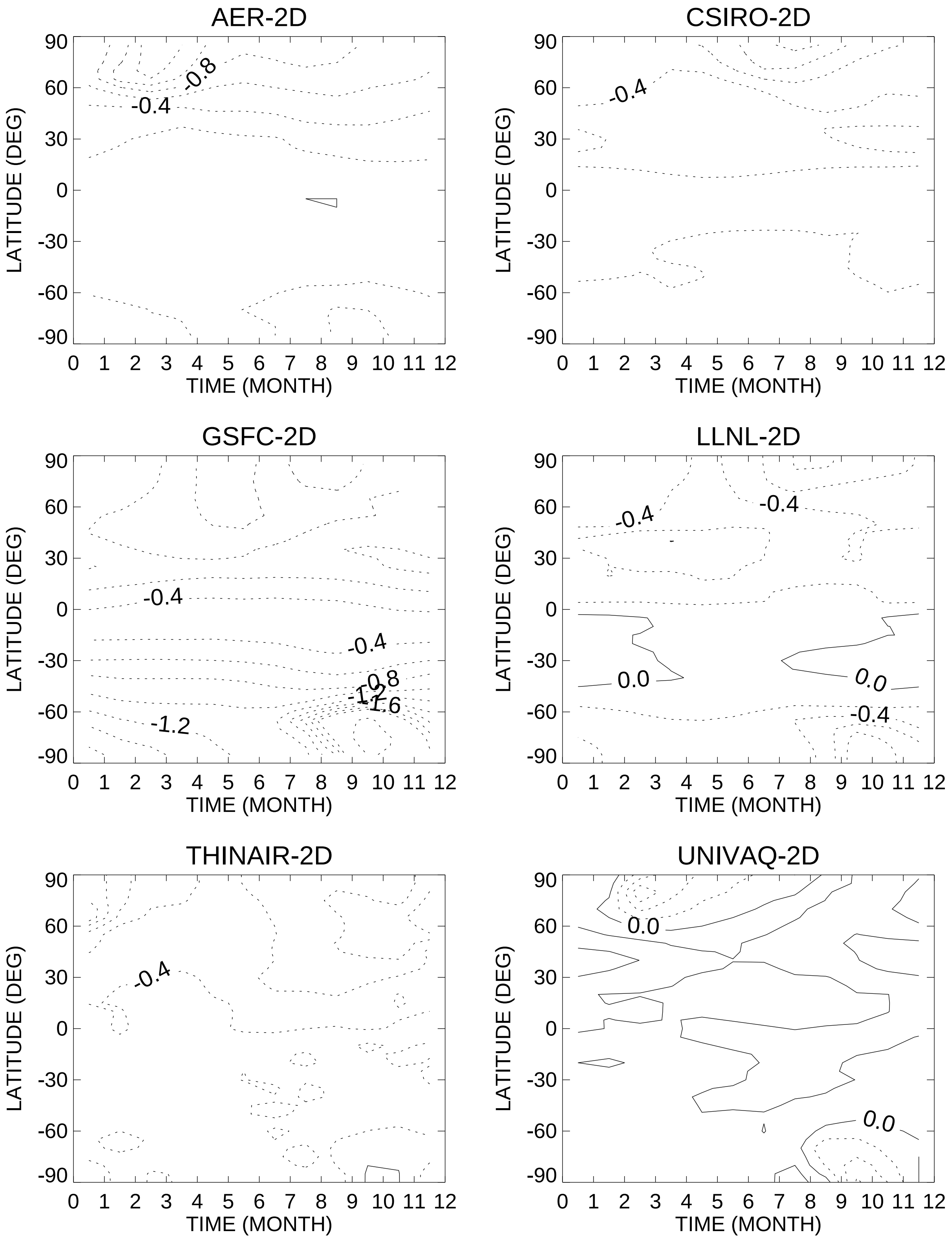

Figure 4.83: Calculated perturbations to column O_3 (percent) as a function of latitude and season in 2015 due to emissions from a fleet of 500 HSCT aircraft with $EI(NO_x)=10$ under Scenario S1d relative to Scenario D. Contours are -3 and -2.0 to 0.6 by 0.2.

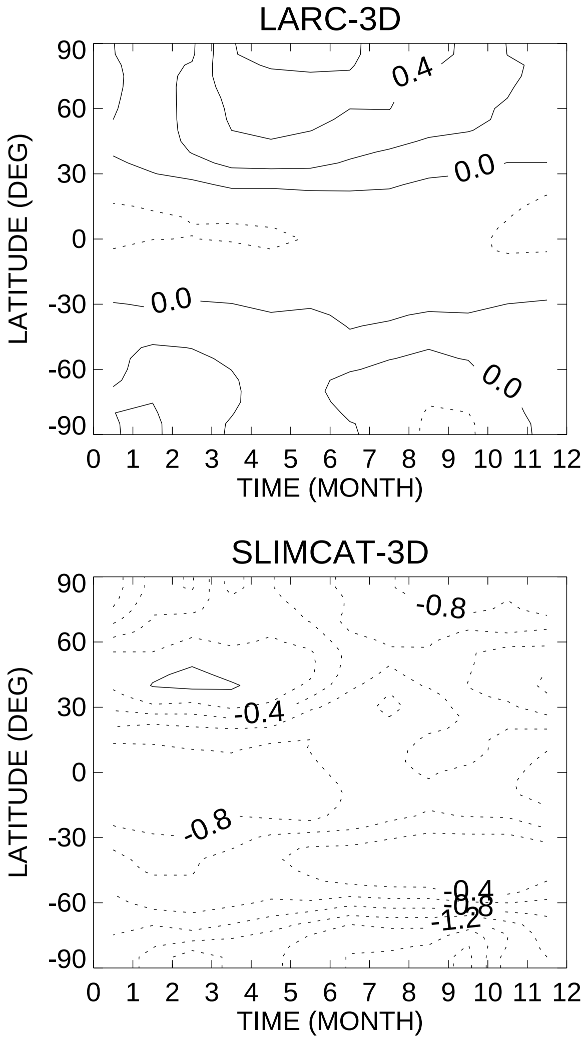

Figure 4.83: continued

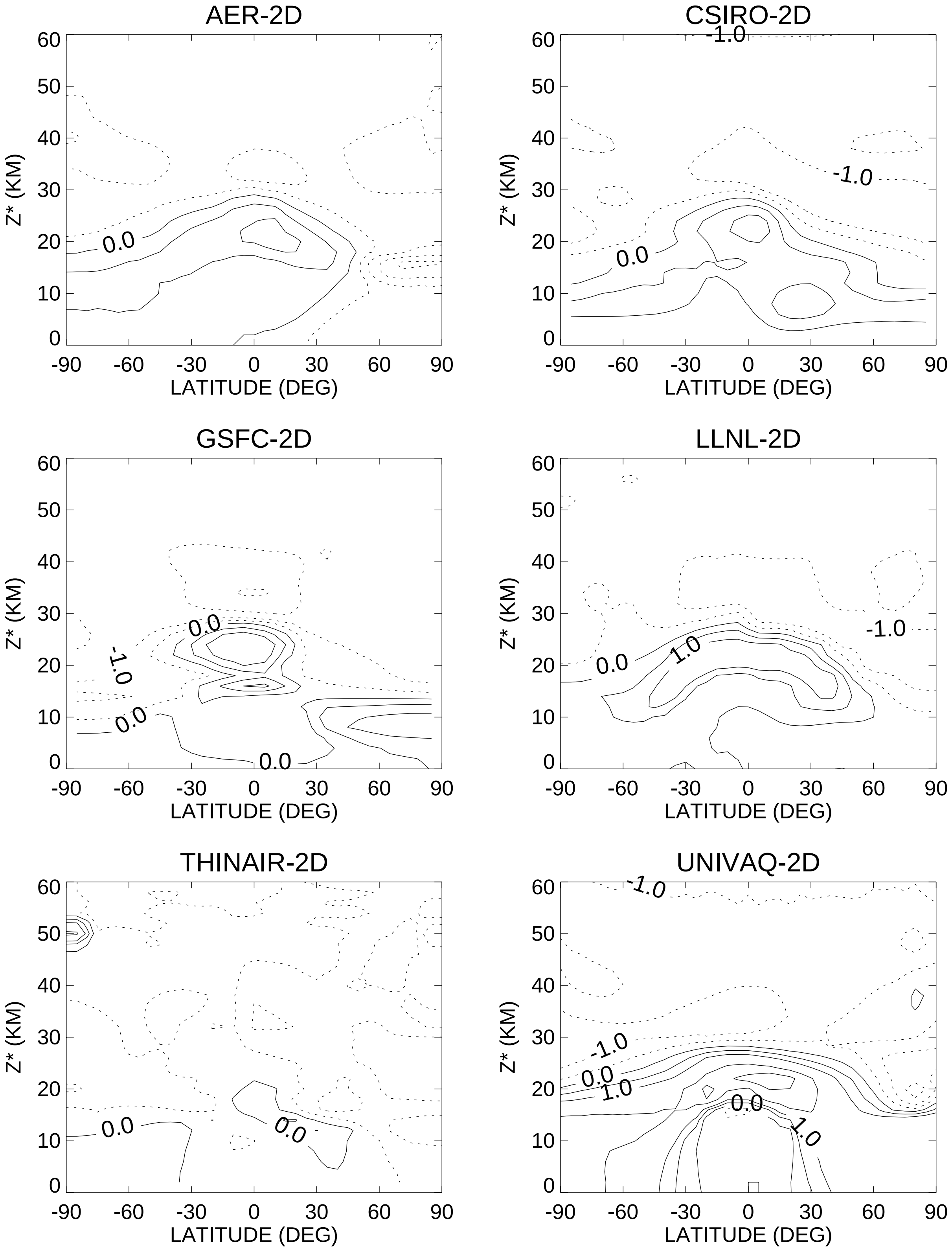

Figure 4.84: Calculated perturbations to O_3 (percent) as a function of latitude and altitude in March of 2015 due to emissions from a fleet of 500 HSCT aircraft with EI(NO_x)=15 under Scenario S1e relative to Scenario D. Contours are -3, -2, -1, -0.5, 0, 0.5, 1, 2, 3.

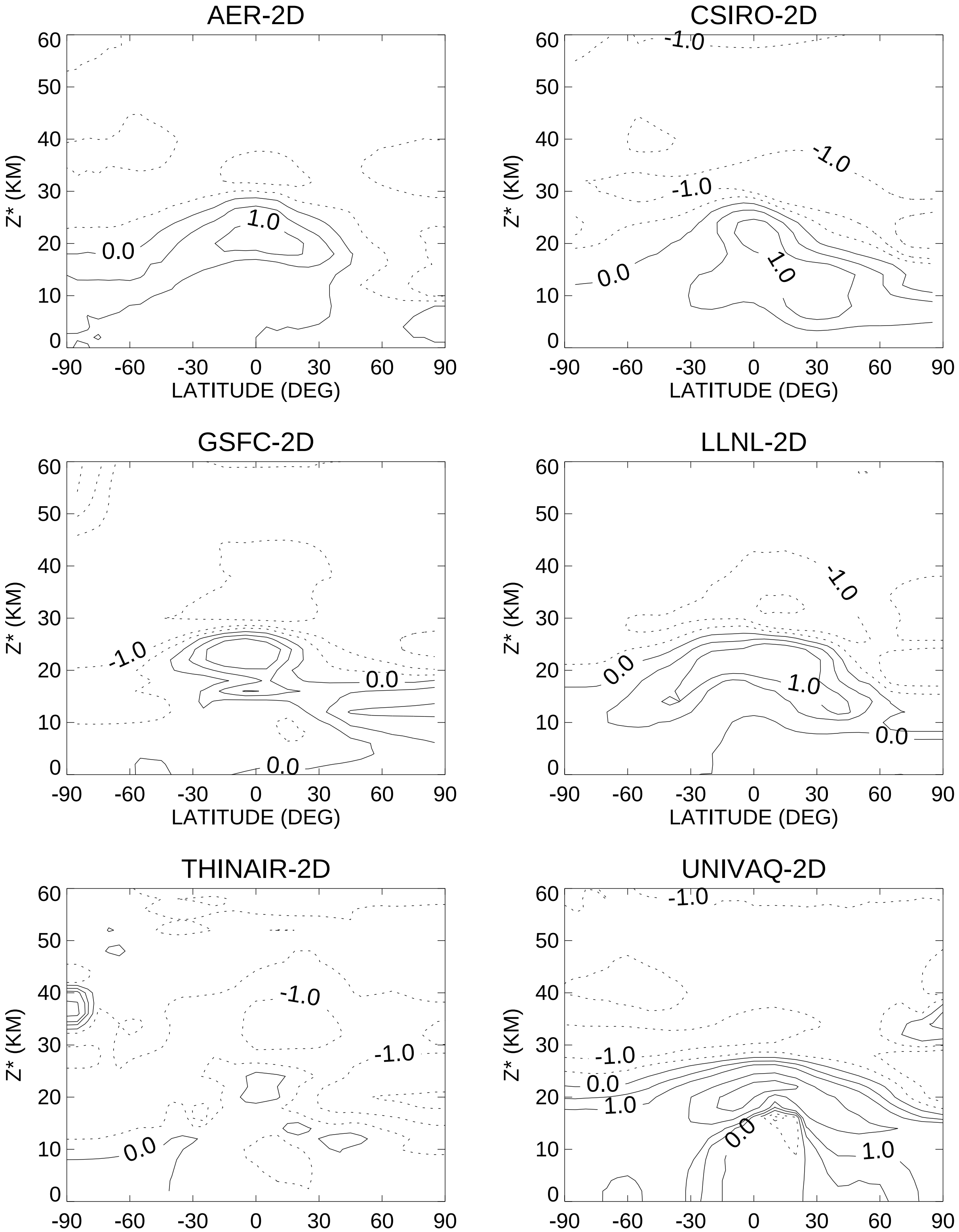

Figure 4.85: Calculated perturbations to O_3 (percent) as a function of latitude and altitude in June of 2015 due to emissions from a fleet of 500 HSCT aircraft with EI(NO_x)=15 under Scenario S1e relative to Scenario D. Contours are -2, -1, -0.5, 0, 0.5, 1, 2, 3.

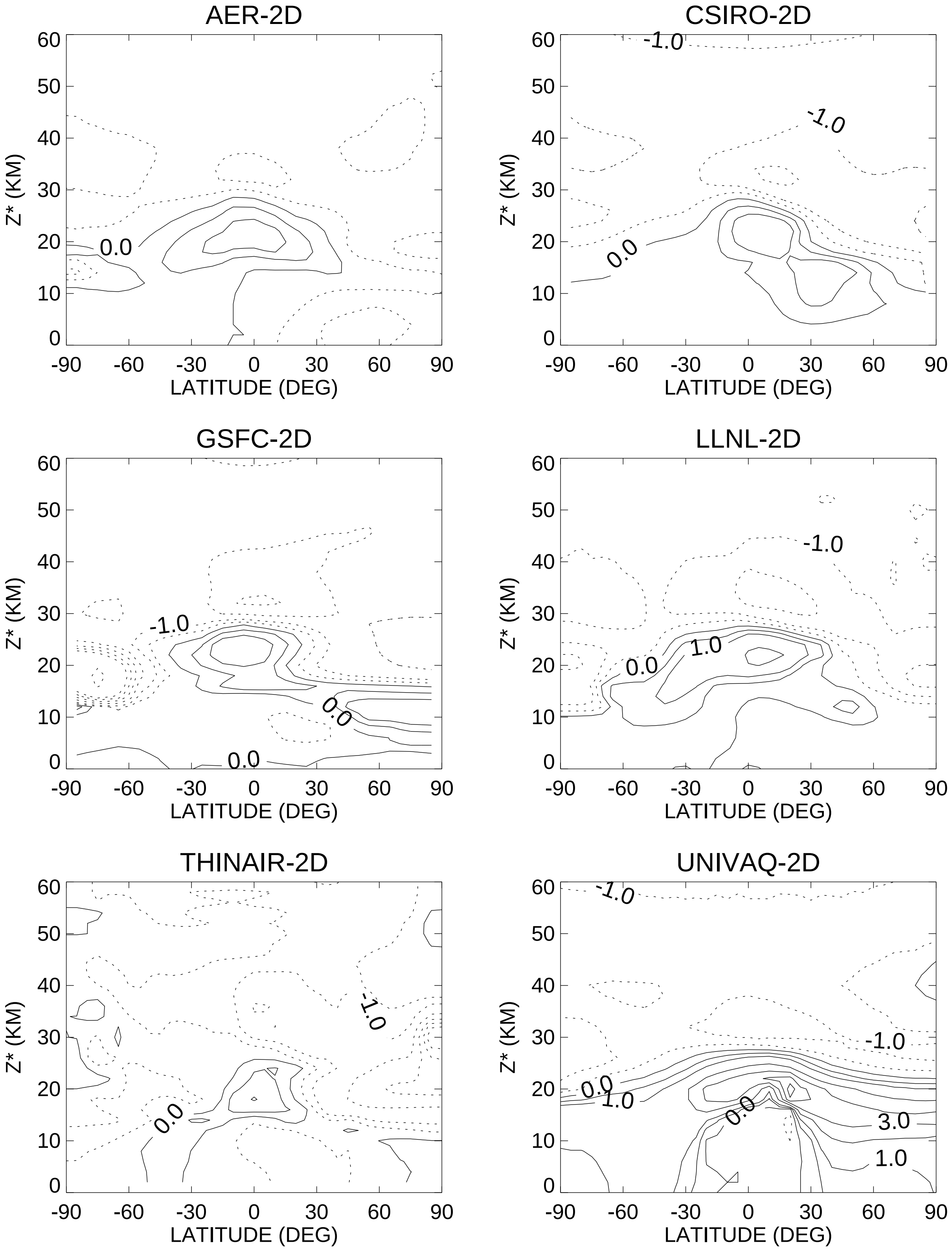

Figure 4.86: Calculated perturbations to O_3 (percent) as a function of latitude and altitude in October of 2015 due to emissions from a fleet of 500 HSCT aircraft with $EI(NO_x)$=15 under Scenario S1e relative to Scenario D. Contours are -10, -5, -4, -3, -2, -1, -0.5, 0, 0.5, 1, 2, 3, 4, 5.

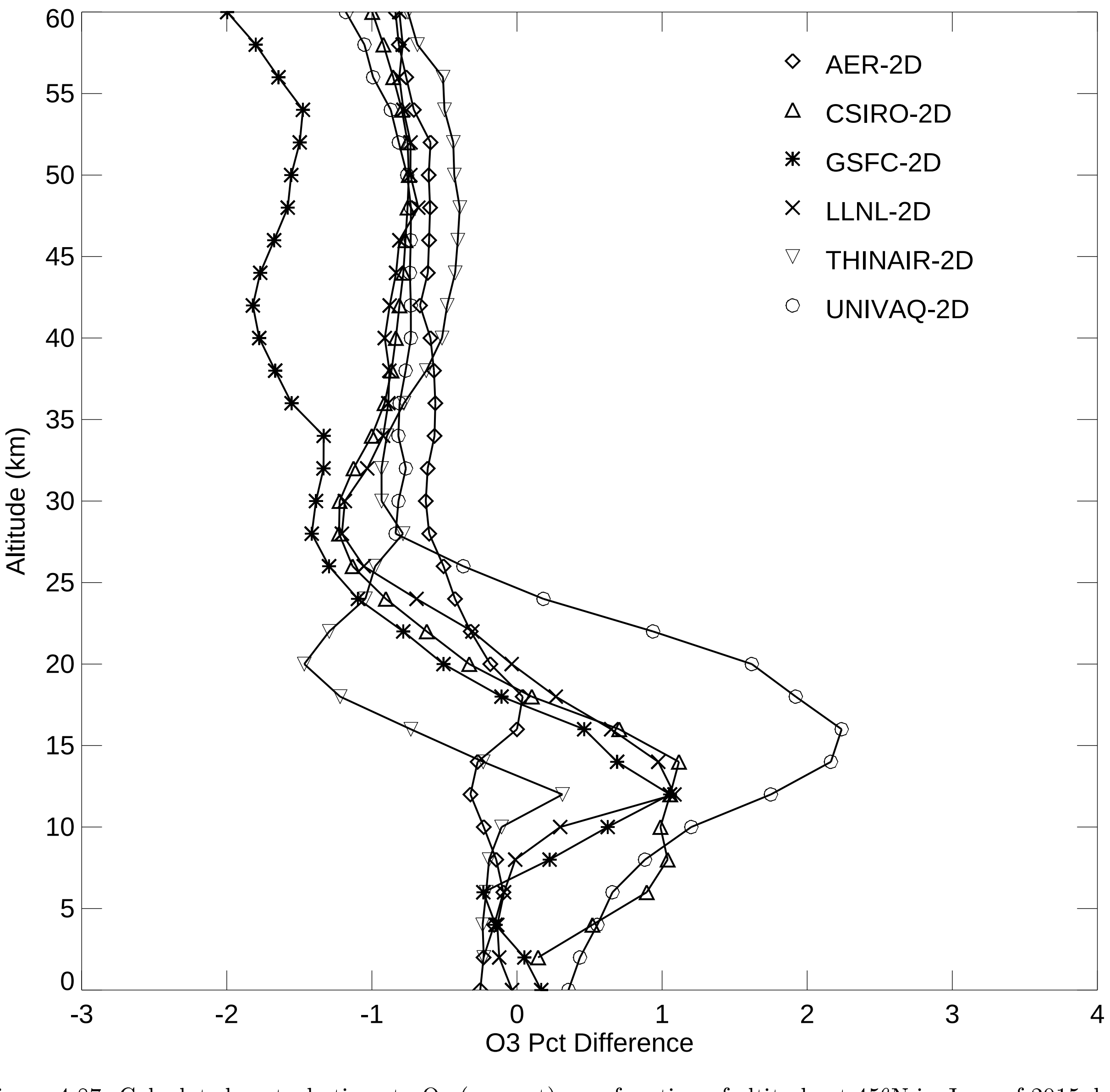

Figure 4.87: Calculated perturbations to O_3 (percent) as a function of altitude at 45^oN in June of 2015 due to emissions from a fleet of 500 HSCT aircraft with $EI(NO_x)$=15 under Scenario S1e relative to Scenario D.

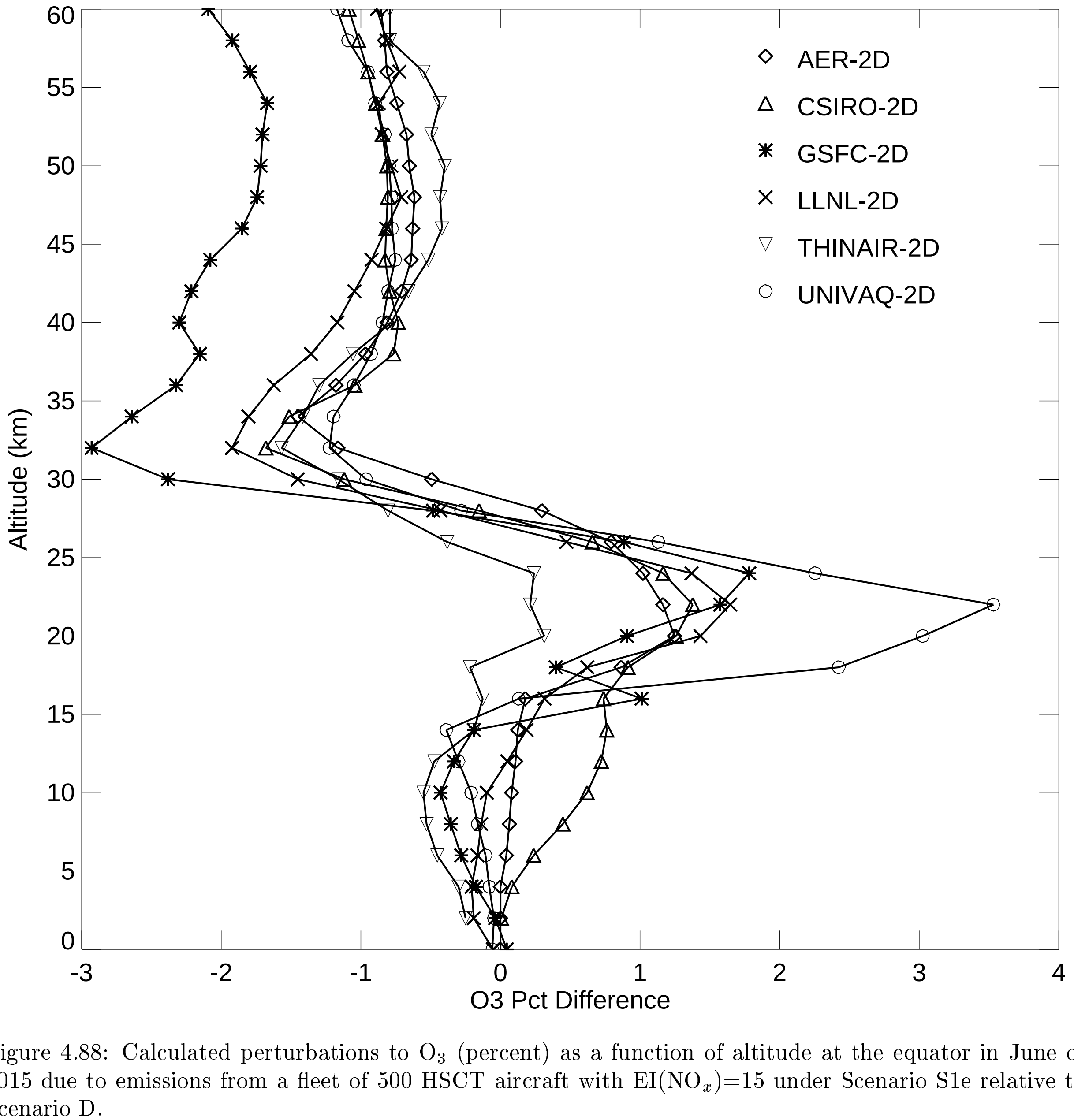

Figure 4.88: Calculated perturbations to O_3 (percent) as a function of altitude at the equator in June of 2015 due to emissions from a fleet of 500 HSCT aircraft with $EI(NO_x)=15$ under Scenario S1e relative to Scenario D.

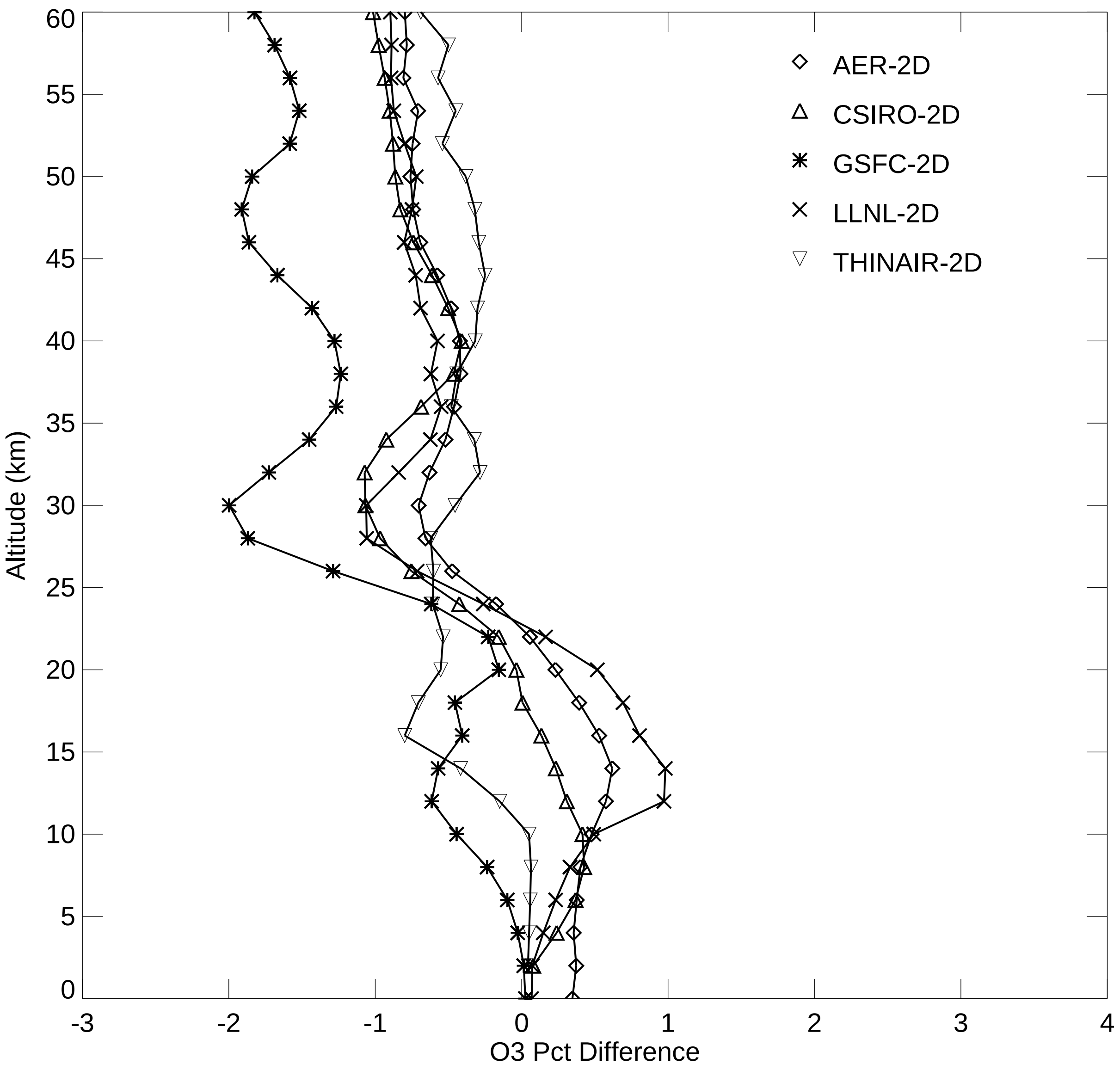

Figure 4.89: Calculated perturbations to O_3 (percent) as a function of altitude at 45^oS in June of 2015 due to emissions from a fleet of 500 HSCT aircraft with EI(NO_x)=15 under Scenario S1e relative to Scenario D.

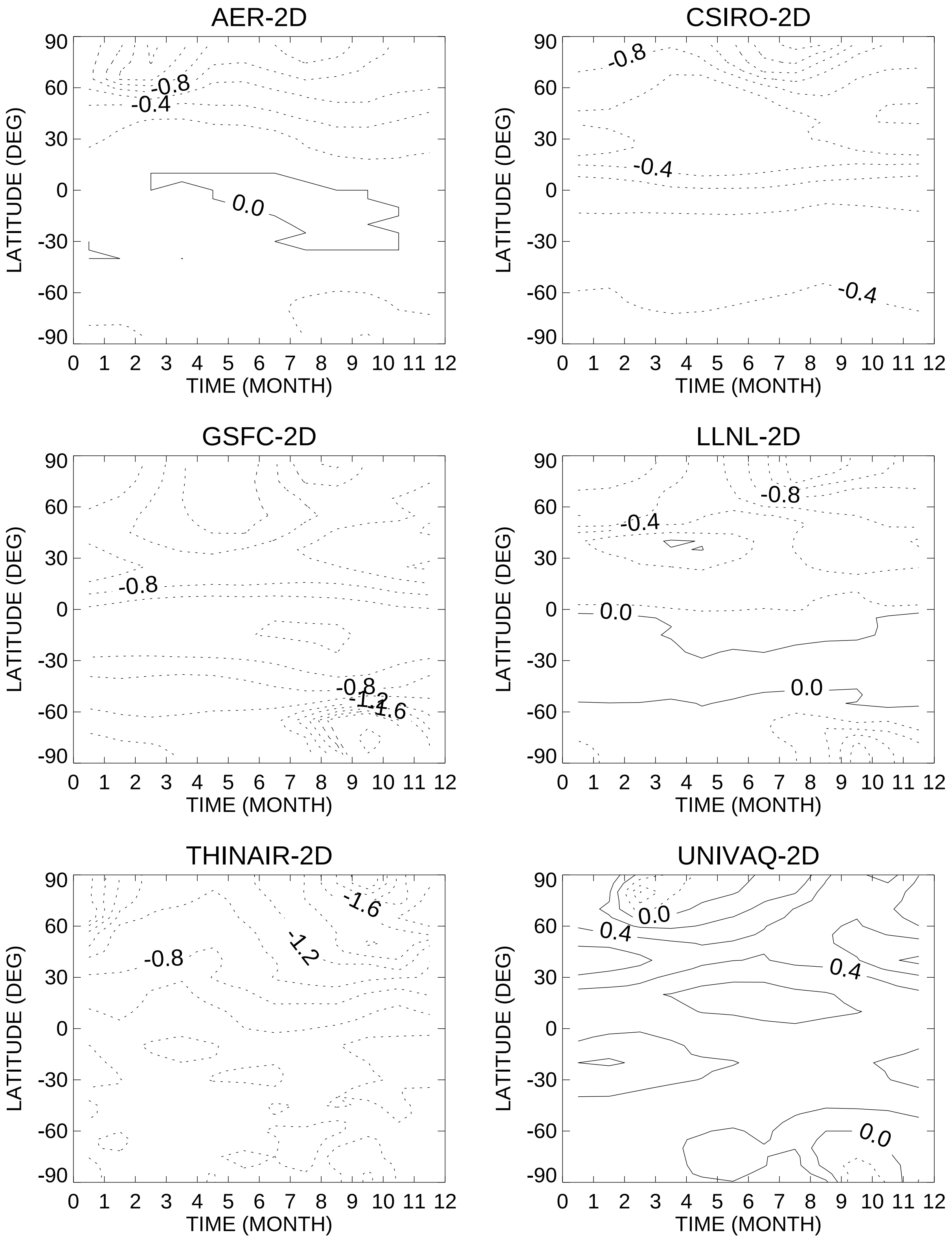

Figure 4.90: Calculated perturbations to column O_3 (percent) as a function of latitude and season in 2015 due to emissions from a fleet of 500 HSCT aircraft with $EI(NO_x)=15$ under Scenario S1e relative to Scenario D. Contours are -3 and -2.0 to 0.6 by 0.2.

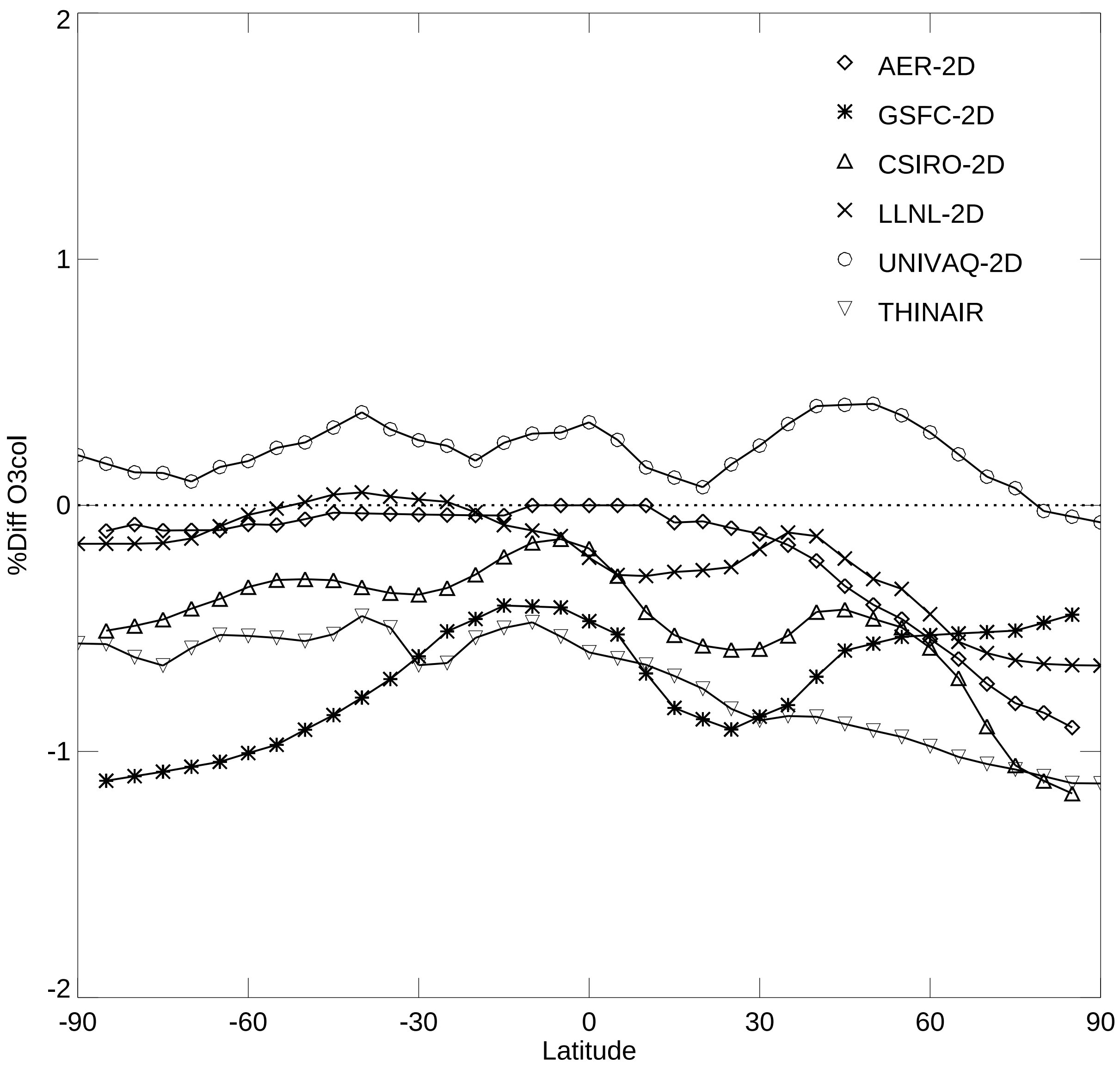

Figure 4.91: Calculated perturbations to total O_3 (percent) in June as a function of latitude due to emissions from a fleet of 500 HSCT aircraft operating in 2015 (Scenario S1e - Scenario D) with EI(NO_x)=15.

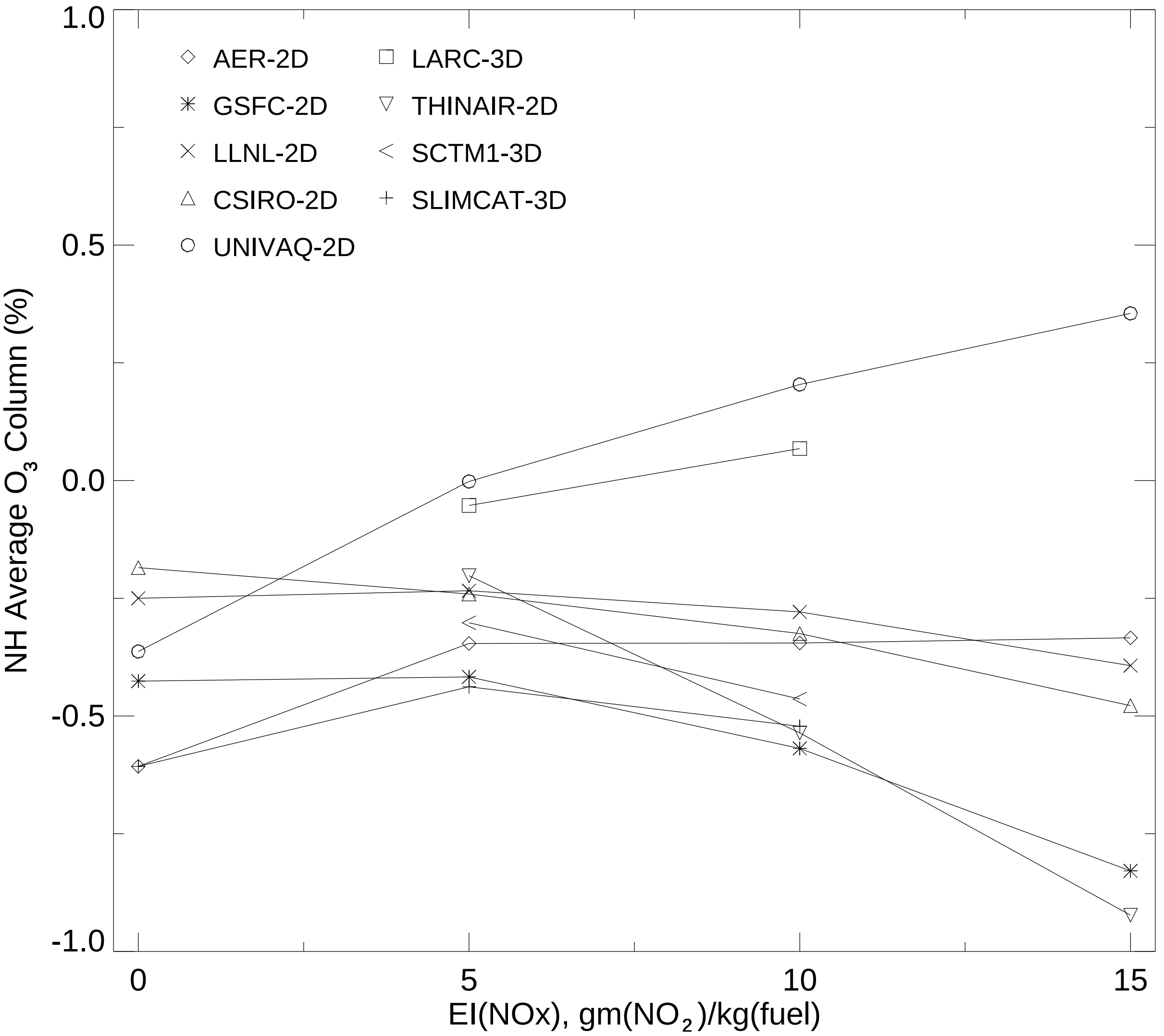

Figure 4.92: Northern hemisphere annual average total O_3 column change (percent) as a function of $\mathrm{EI(NO}_x)$ for an HSCT fleet of 500 aircraft operating in 2015 with SA0 sulfate surface area density.

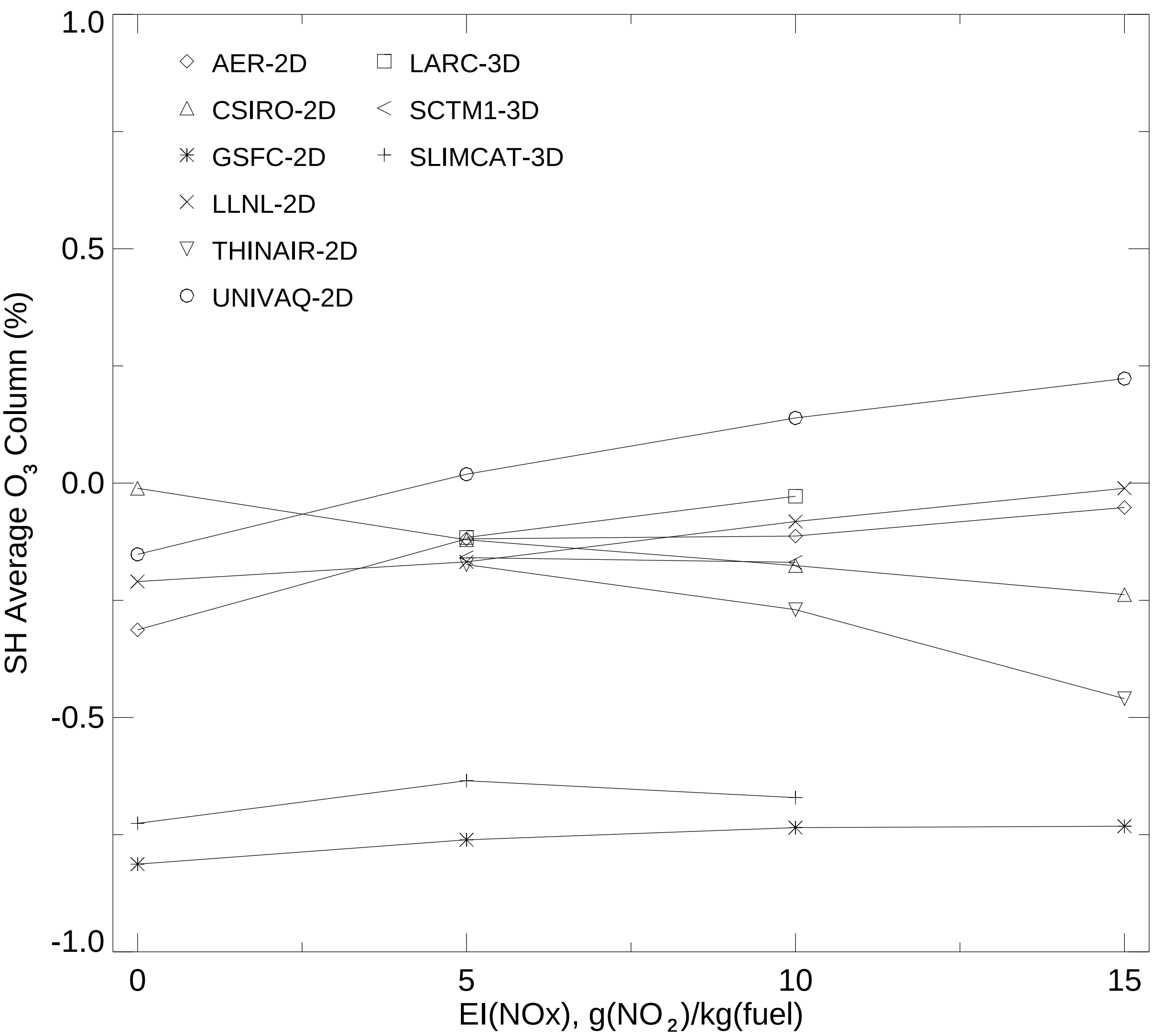

Figure 4.93: Southern hemisphere annual average total O_3 column change (percent) as a function of EI(NO_x) for an HSCT fleet of 500 aircraft operating in 2015 with SA0 sulfate surface area density.

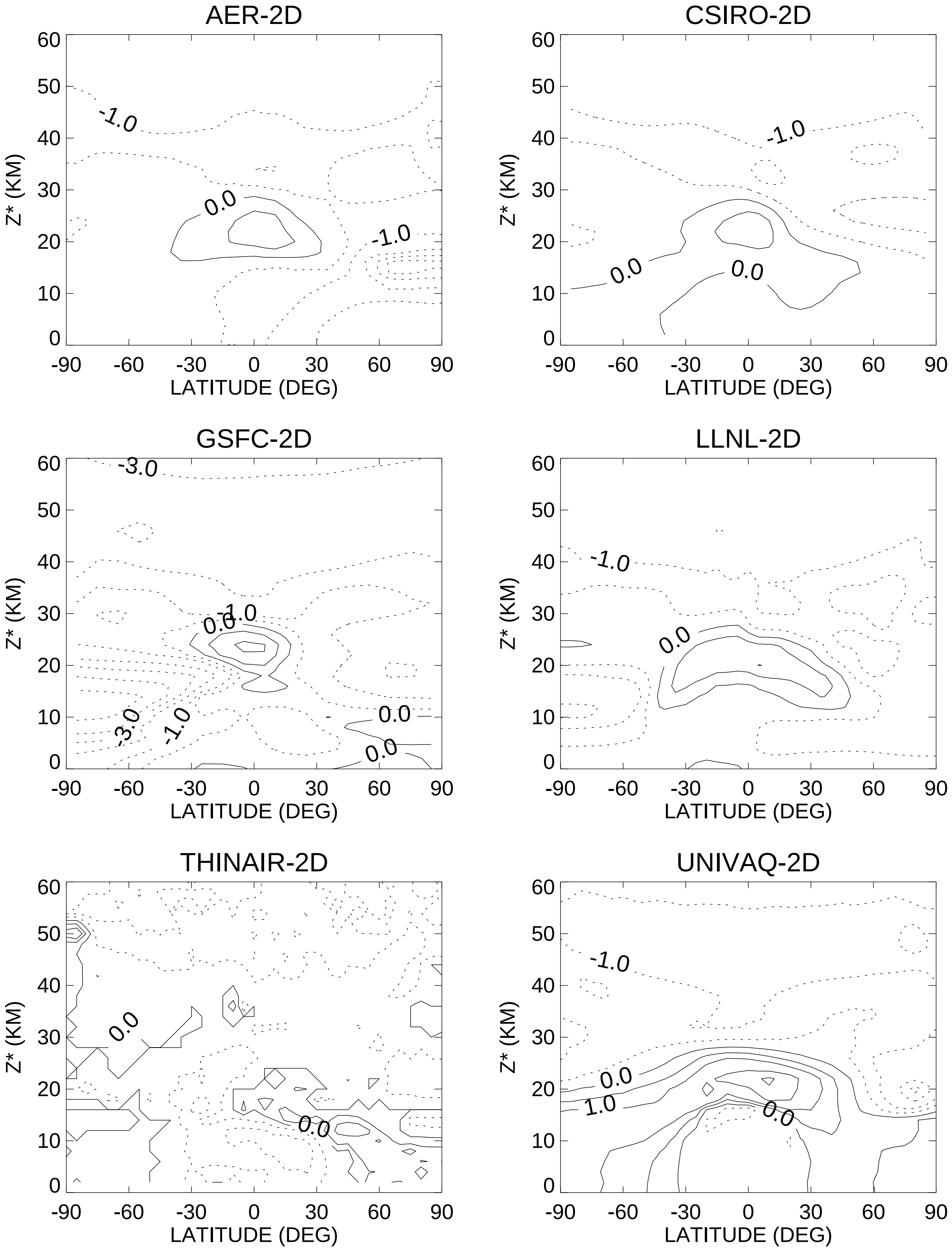

Figure 4.94: Calculated perturbations to O_3 (percent) as a function of latitude and altitude in March of 2015 due to emissions from a fleet of 1000 HSCT aircraft with EI(NO_x)=5 under Scenario S1i relative to Scenario D. Contours are -5, -4, -3, -2, -1, -0.5, 0, 0.5, 1, 2, 3.

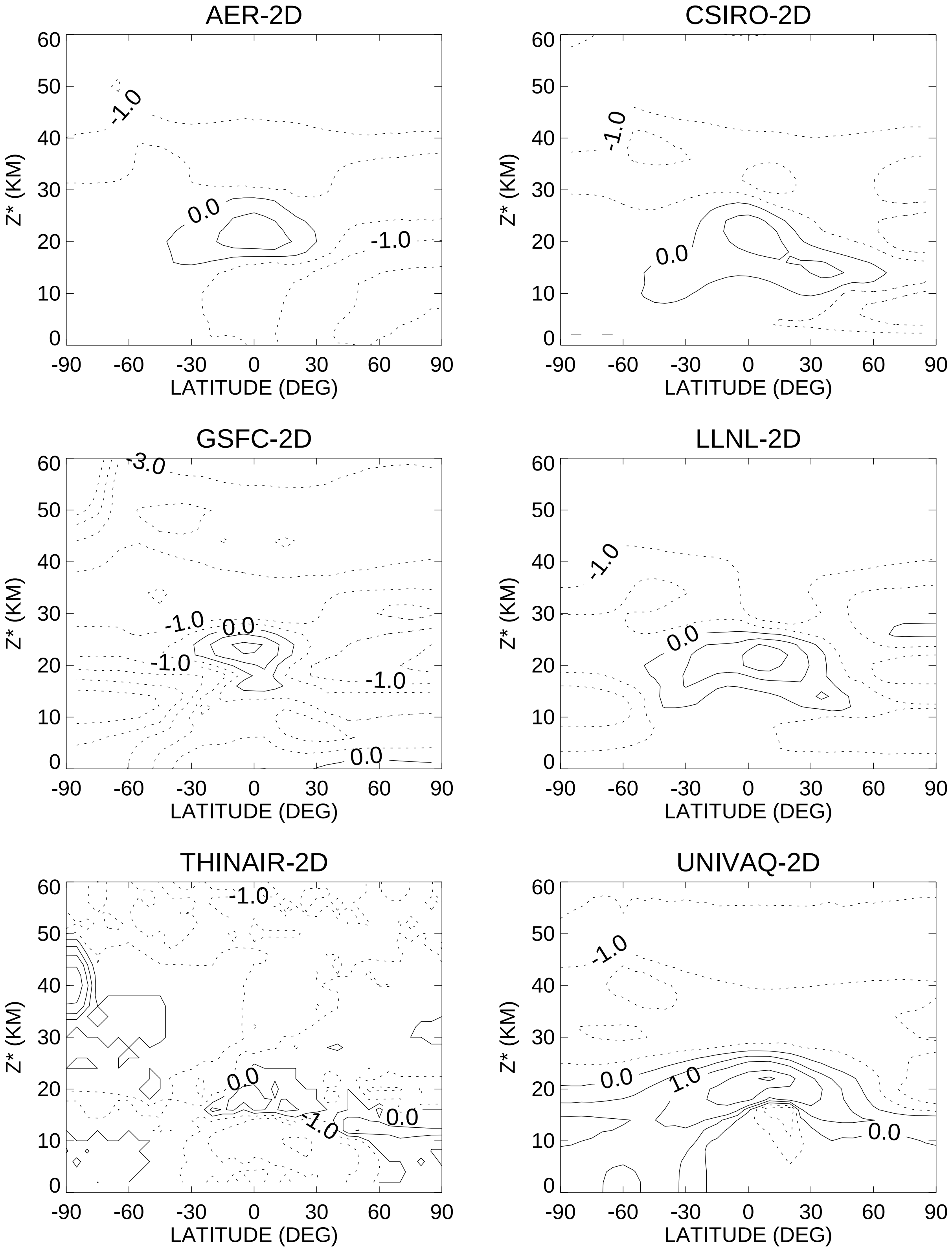

Figure 4.95: Calculated perturbations to O_3 (percent) as a function of latitude and altitude in June of 2015 due to emissions from a fleet of 1000 HSCT aircraft with EI(NO_x)=5 under Scenario S1i relative to Scenario D. Contours are -4, -3, -2, -1, -0.5, 0, 0.5, 1, 2, 3.

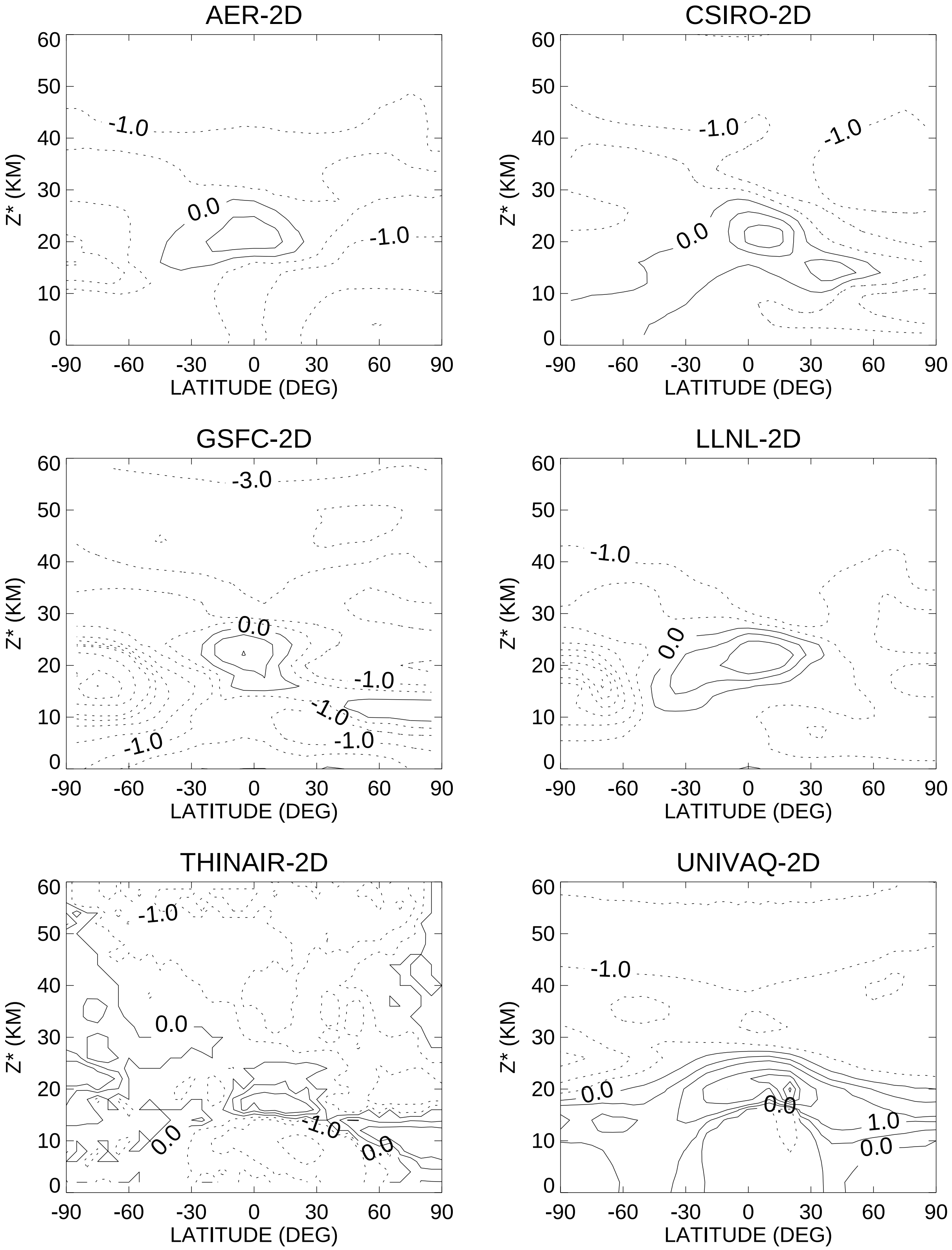

Figure 4.96: Calculated perturbations to O_3 (percent) as a function of latitude and altitude in October of 2015 due to emissions from a fleet of 1000 HSCT aircraft with $EI(NO_x)=5$ under Scenario S1i relative to Scenario D. Contours are -20, -15, -10, -5, -4, -3, -2, -1, -0.5, 0, 0.5, 1, 2, 3, 4, 5.

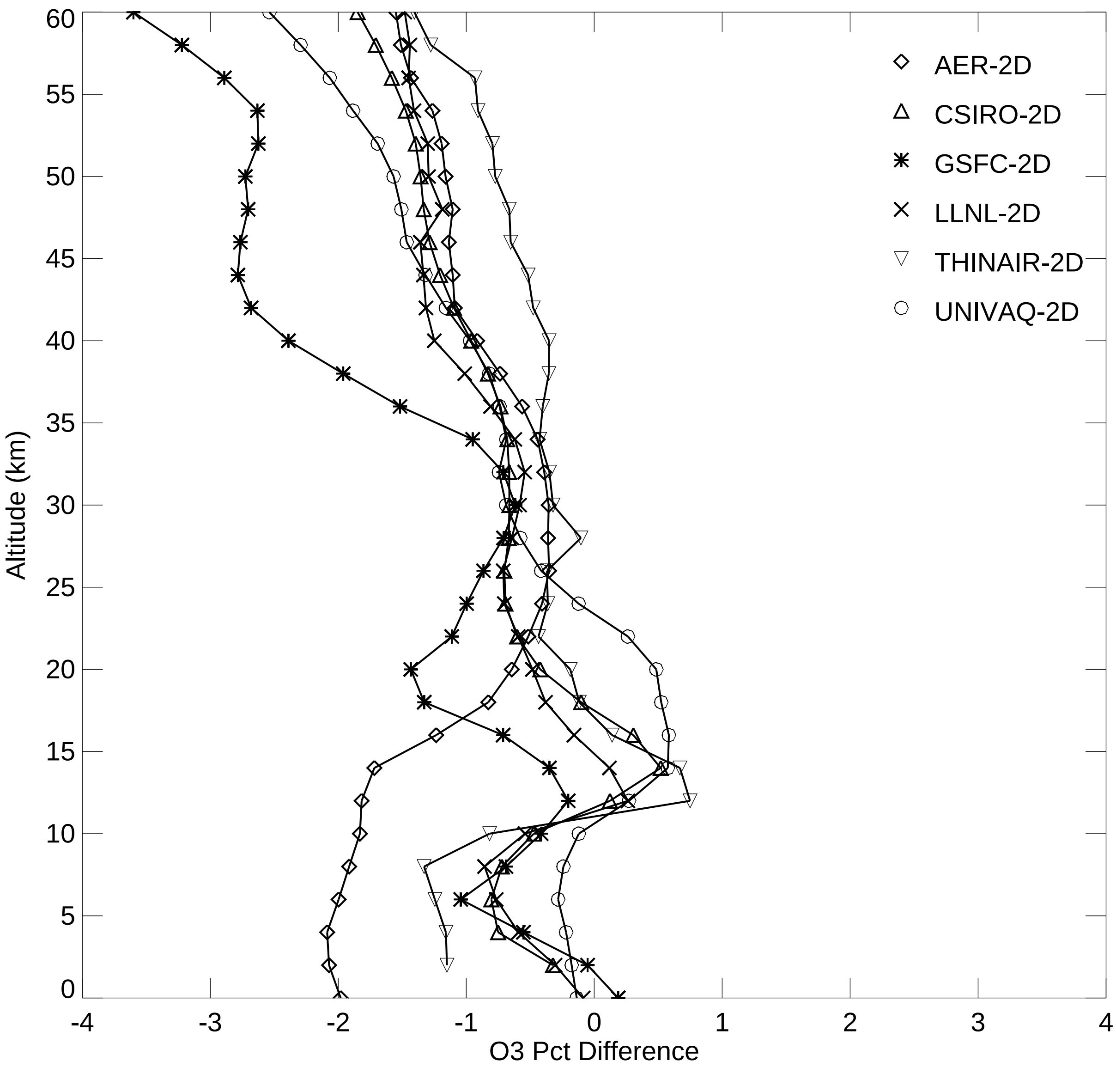

Figure 4.97: Calculated perturbations to O_3 (percent) as a function of altitude at 45^oN in June of 2015 due to emissions from a fleet of 1000 HSCT aircraft with EI(NO_x)=5 under Scenario S1i relative to Scenario D.

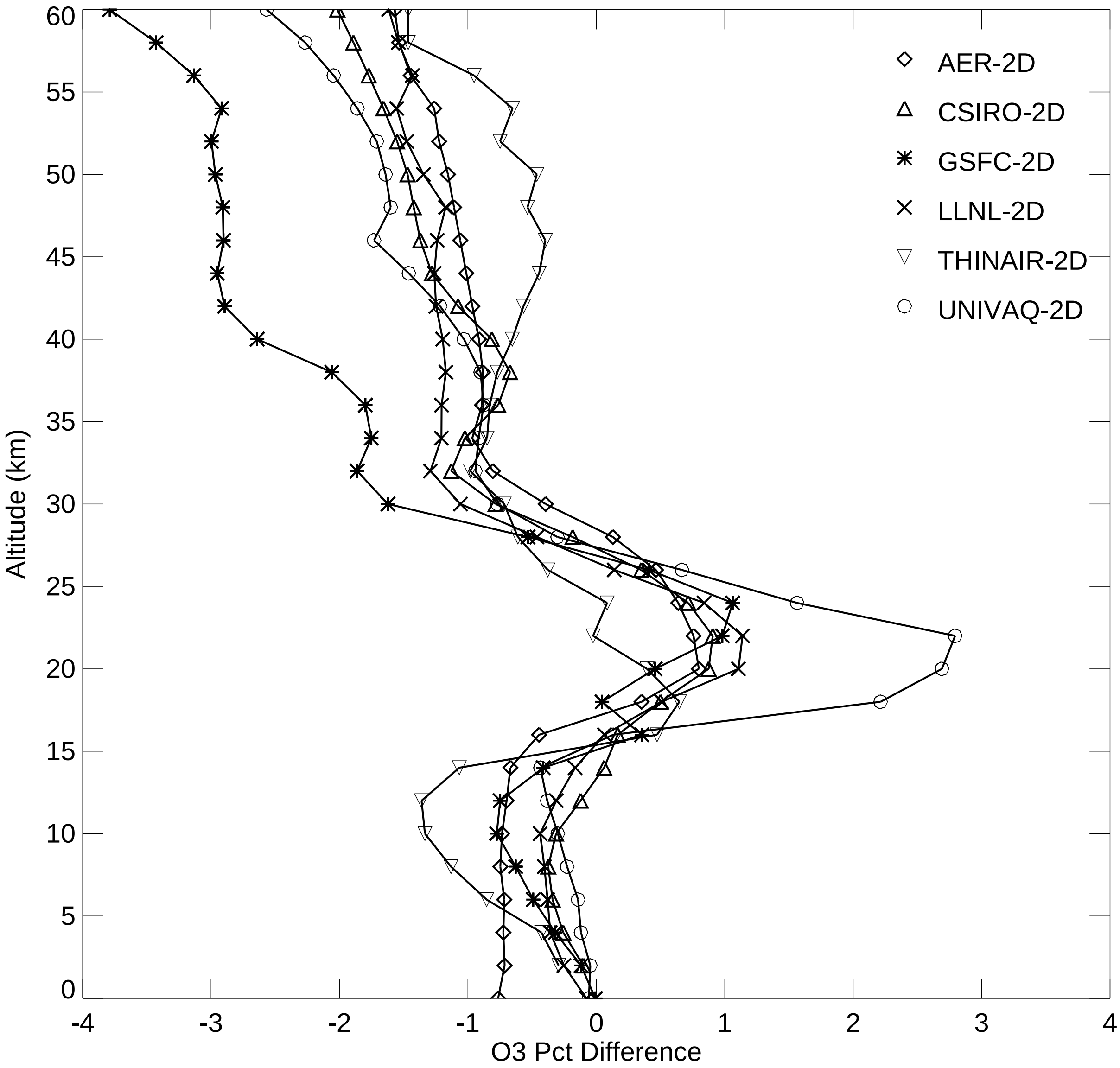

Figure 4.98: Calculated perturbations to O_3 (percent) as a function of altitude at the equator in June of 2015 due to emissions from a fleet of 1000 HSCT aircraft with EI(NO_x)=5 under Scenario S1i relative to Scenario D.

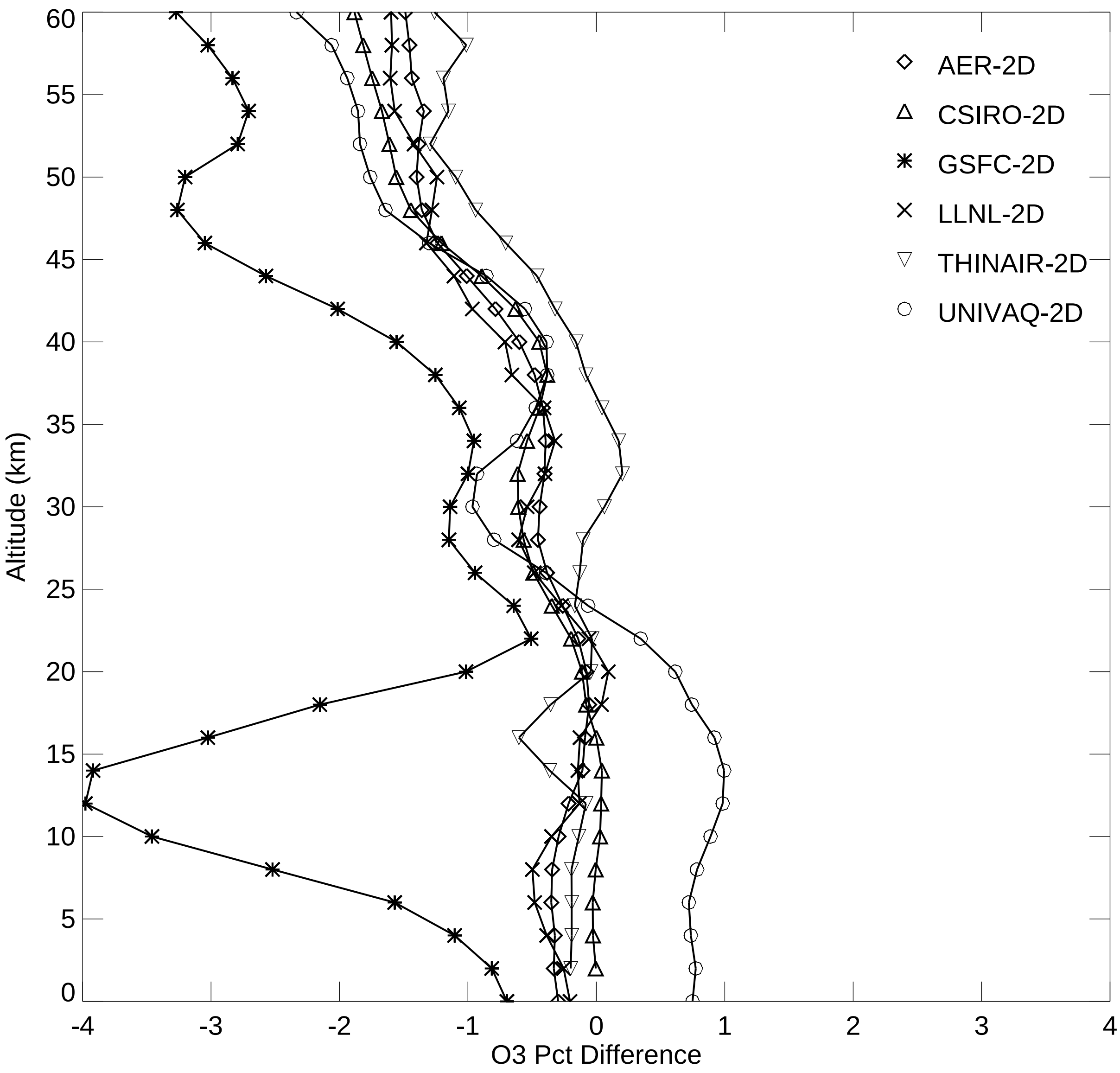

Figure 4.99: Calculated perturbations to O_3 (percent) as a function of altitude at 45^{o}S in June of 2015 due to emissions from a fleet of 1000 HSCT aircraft with EI(NO_x)=5 under Scenario S1i relative to Scenario D.

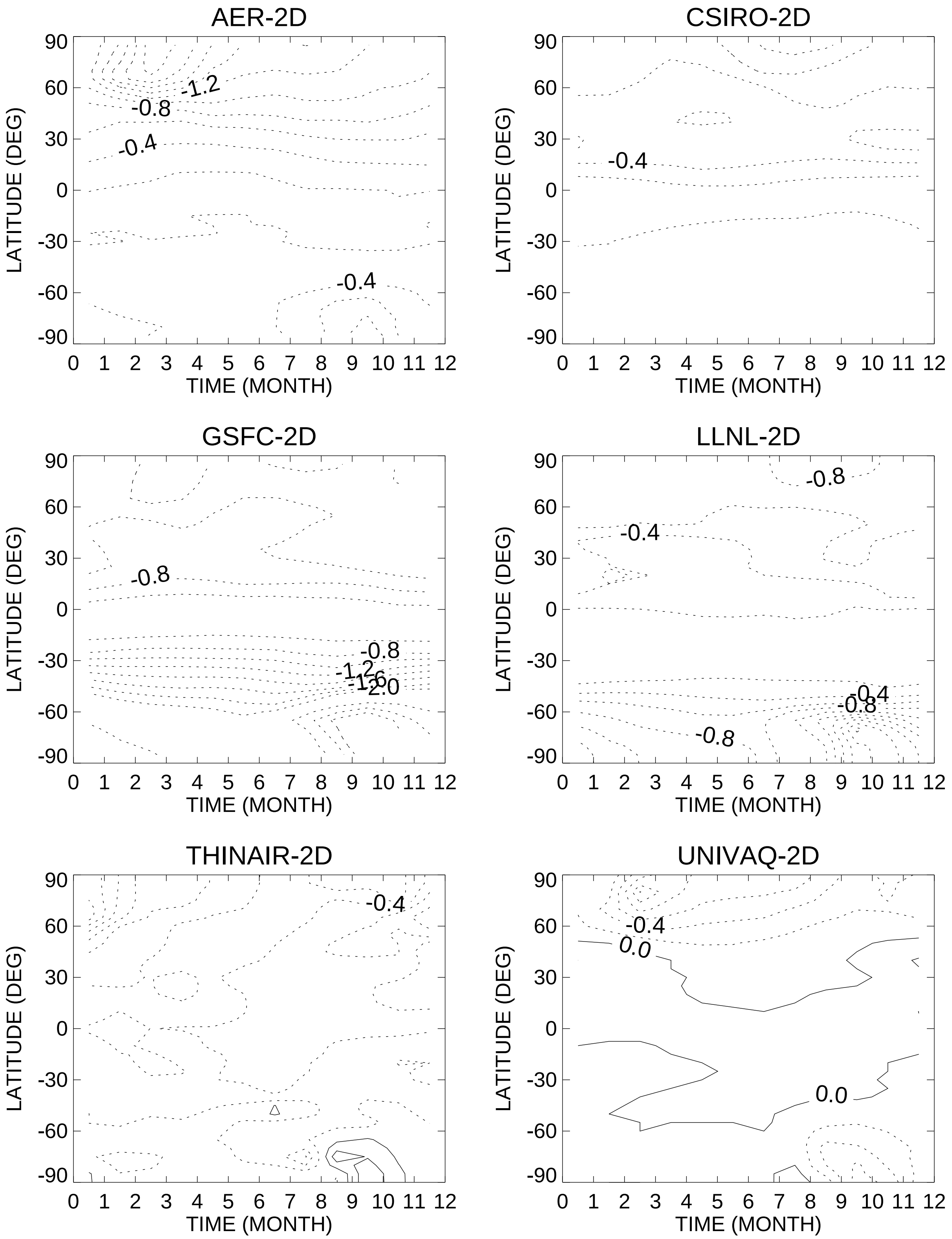

Figure 4.100: Calculated perturbations to column O_3 (percent) as a function of latitude and season in 2015 due to emissions from a fleet of 1000 HSCT aircraft with $EI(NO_x)=5$ under Scenario S1i relative to Scenario D. Contours are -5, -4, -3, and -2.0 to 0.2 by 0.2.

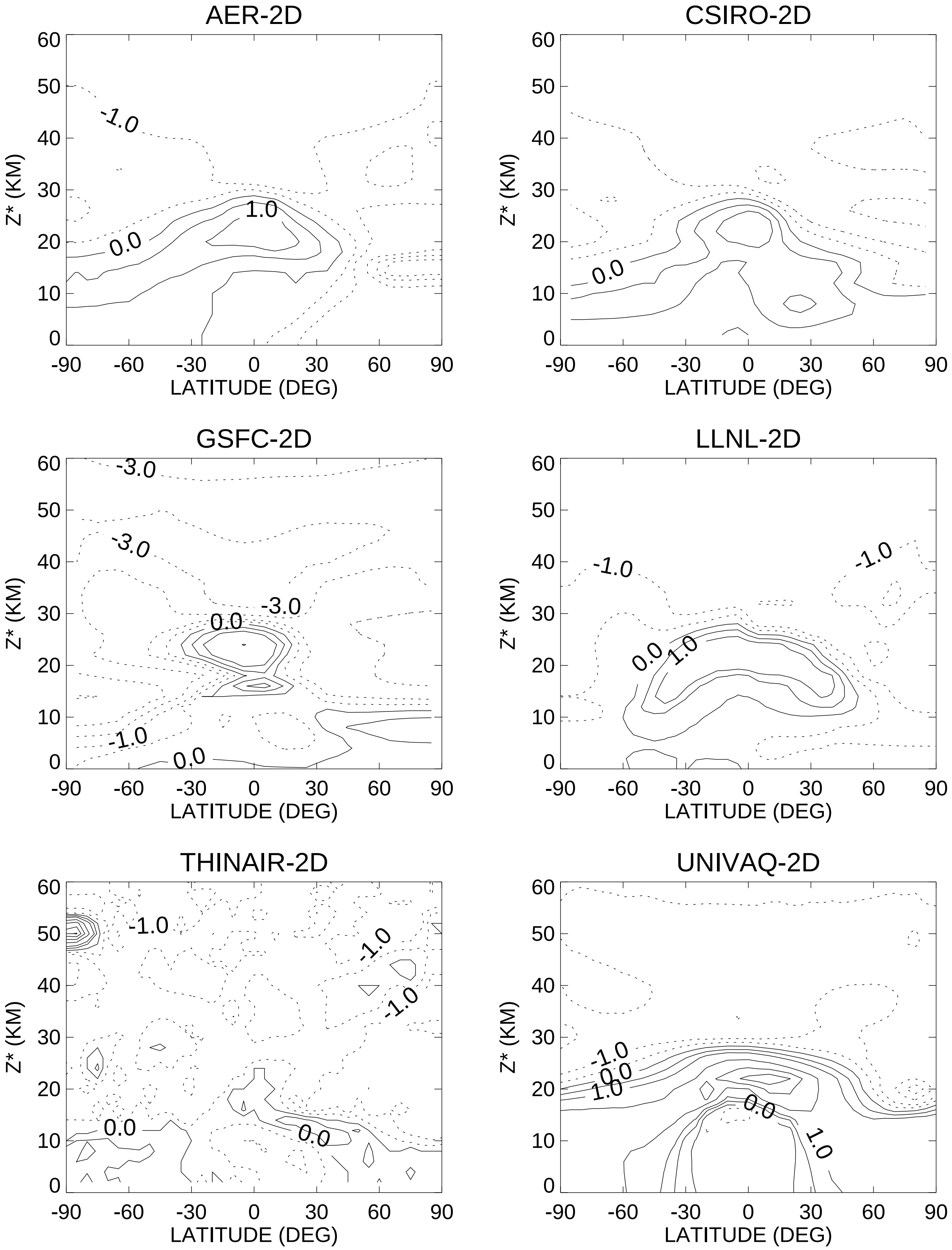

Figure 4.101: Calculated perturbations to O_3 (percent) as a function of latitude and altitude in March of 2015 due to emissions from a fleet of 1000 HSCT aircraft with $EI(NO_x)=10$ under Scenario S1j relative to Scenario D. Contours are -4, -3, -2, -1, -0.5, 0, 0.5, 1, 2, 3, 4.

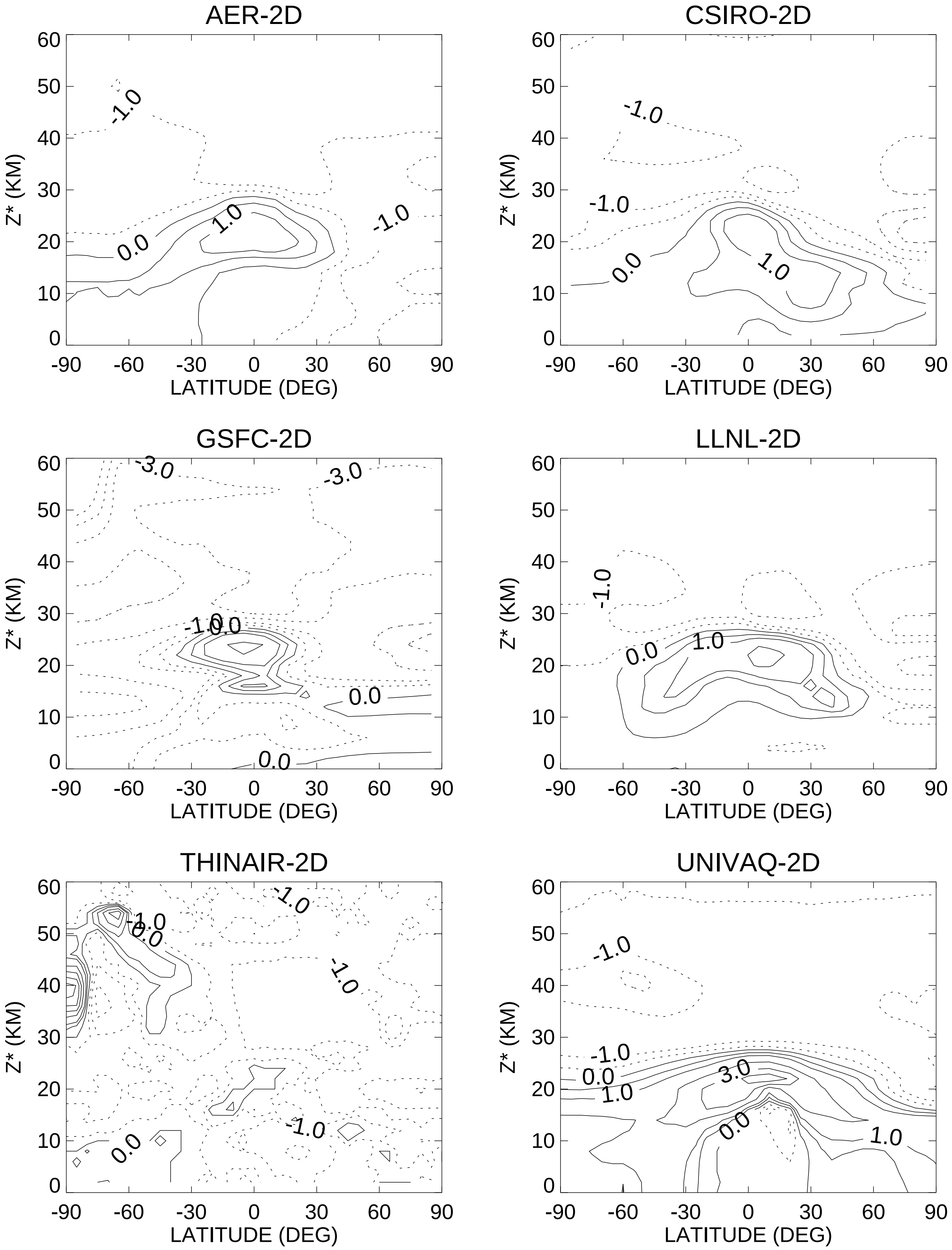

Figure 4.102: Calculated perturbations to O_3 (percent) as a function of latitude and altitude in June of 2015 due to emissions from a fleet of 1000 HSCT aircraft with EI(NO_x)=10 under Scenario S1j relative to Scenario D. Contours are -3, -2, -1, -0.5, 0, 0.5, 1, 2, 3, 4, 5.

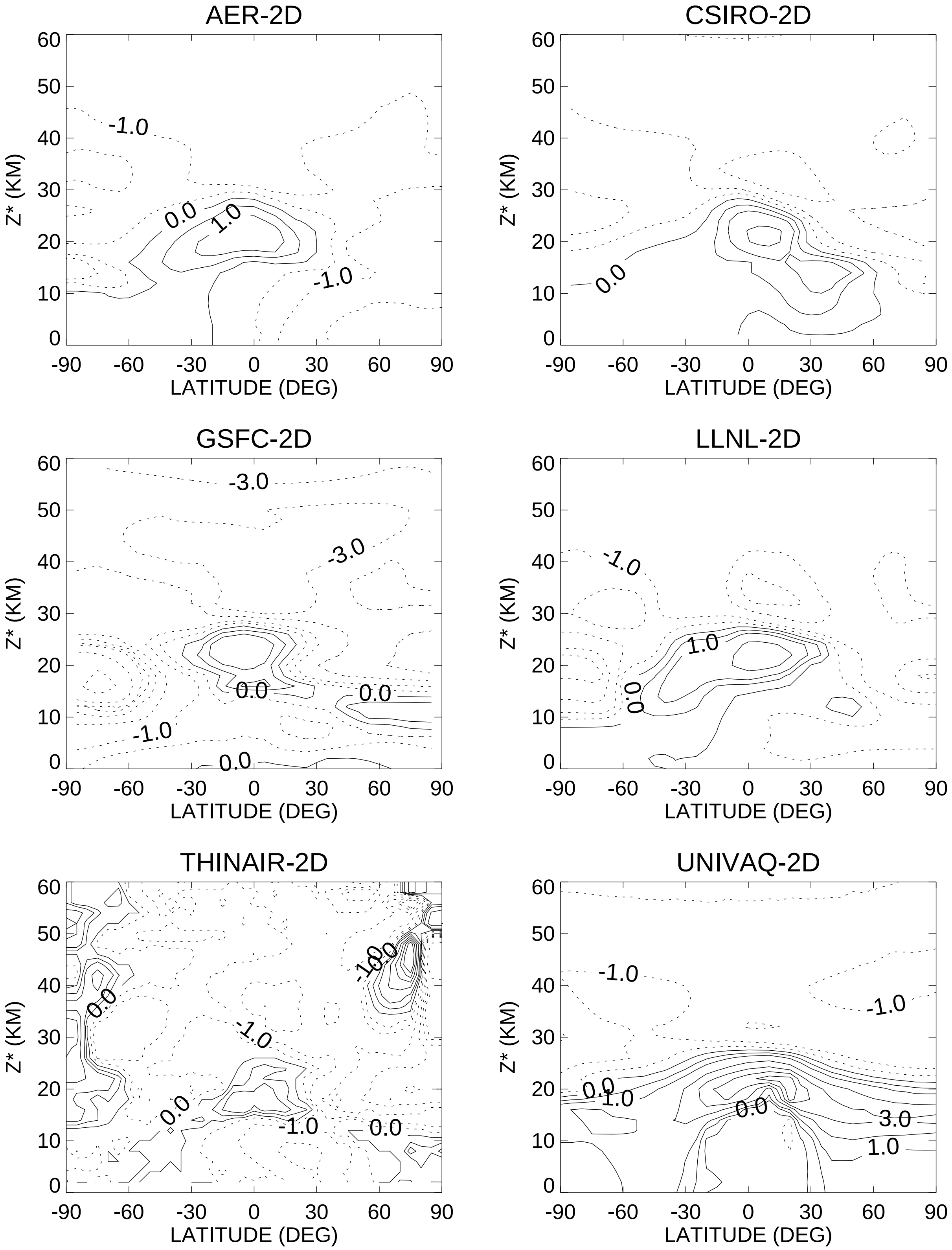

Figure 4.103: Calculated perturbations to O_3 (percent) as a function of latitude and altitude in October of 2015 due to emissions from a fleet of 1000 HSCT aircraft with EI(NO_x)=10 under Scenario S1j relative to Scenario D. Contours are -15, -10, -5, -4, -3, -2, -1, -0.5, 0, 0.5, 1, 2, 3, 4.

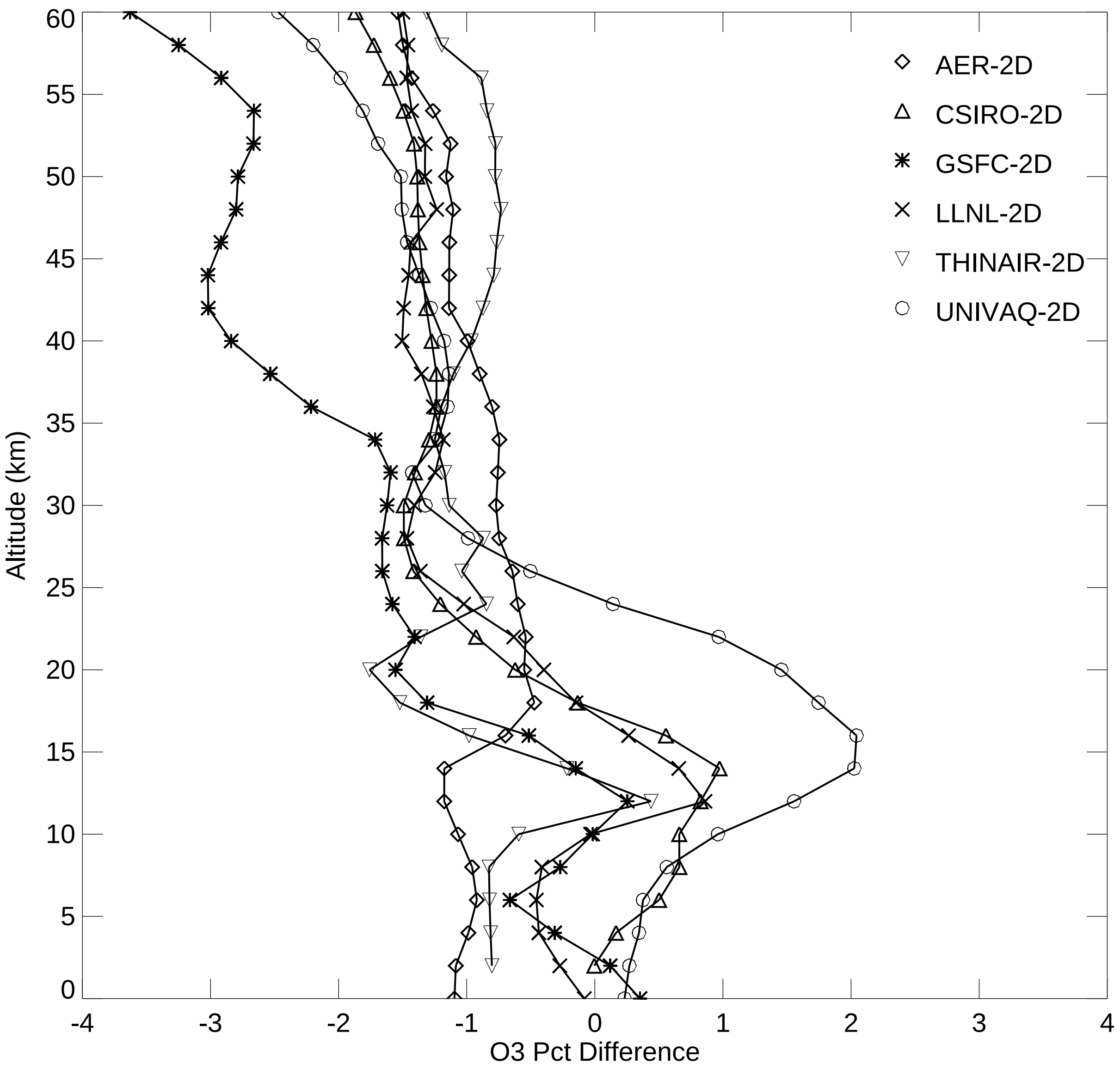

Figure 4.104: Calculated perturbations to O_3 (percent) as a function of altitude at 45^{o}N in June of 2015 due to emissions from a fleet of 1000 HSCT aircraft with EI(NO_x)=10 under Scenario S1j relative to Scenario D.

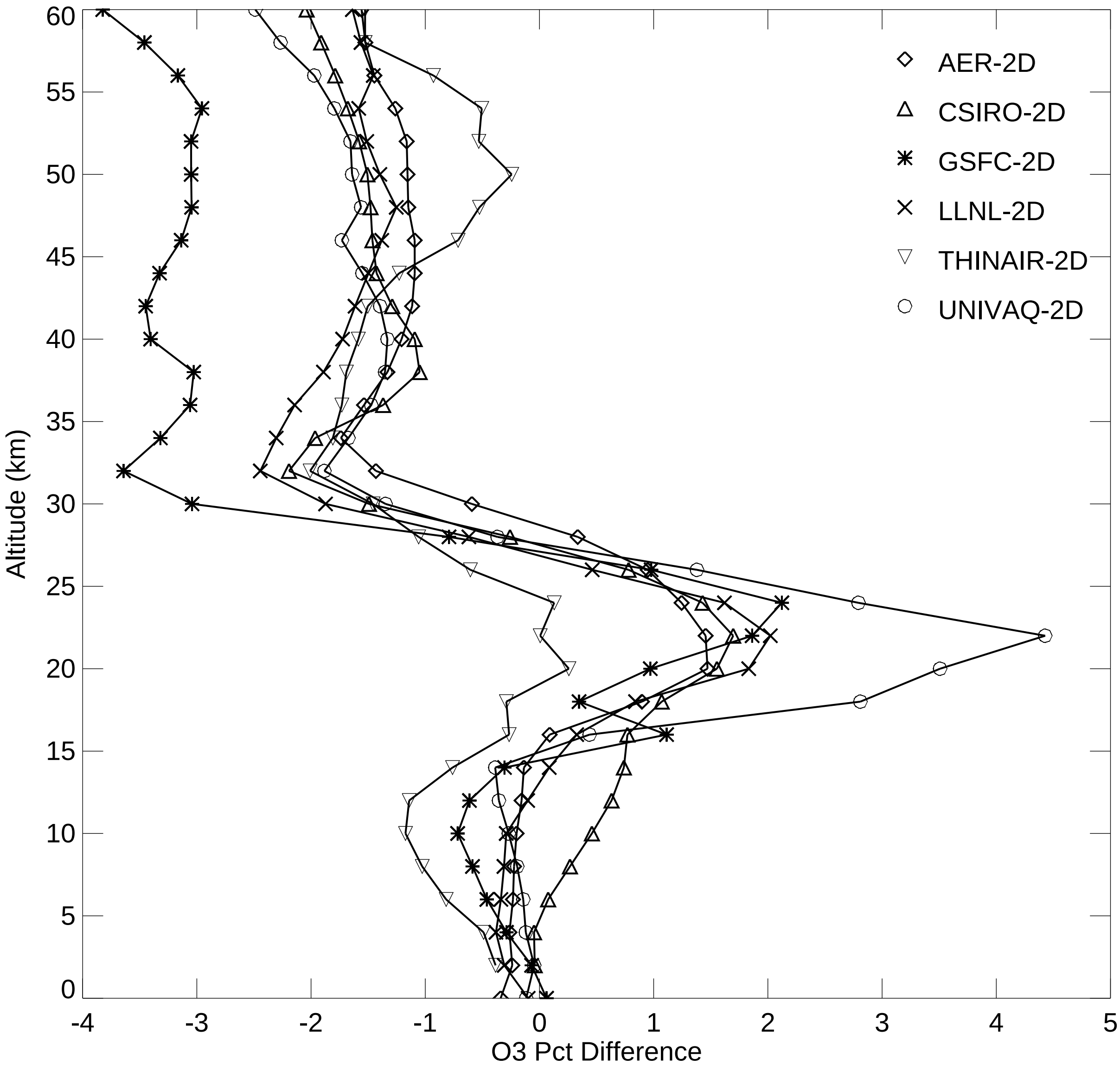

Figure 4.105: Calculated perturbations to O_3 (percent) as a function of altitude at the equator in June of 2015 due to emissions from a fleet of 1000 HSCT aircraft with $EI(NO_x)$=10 under Scenario S1j relative to Scenario D.

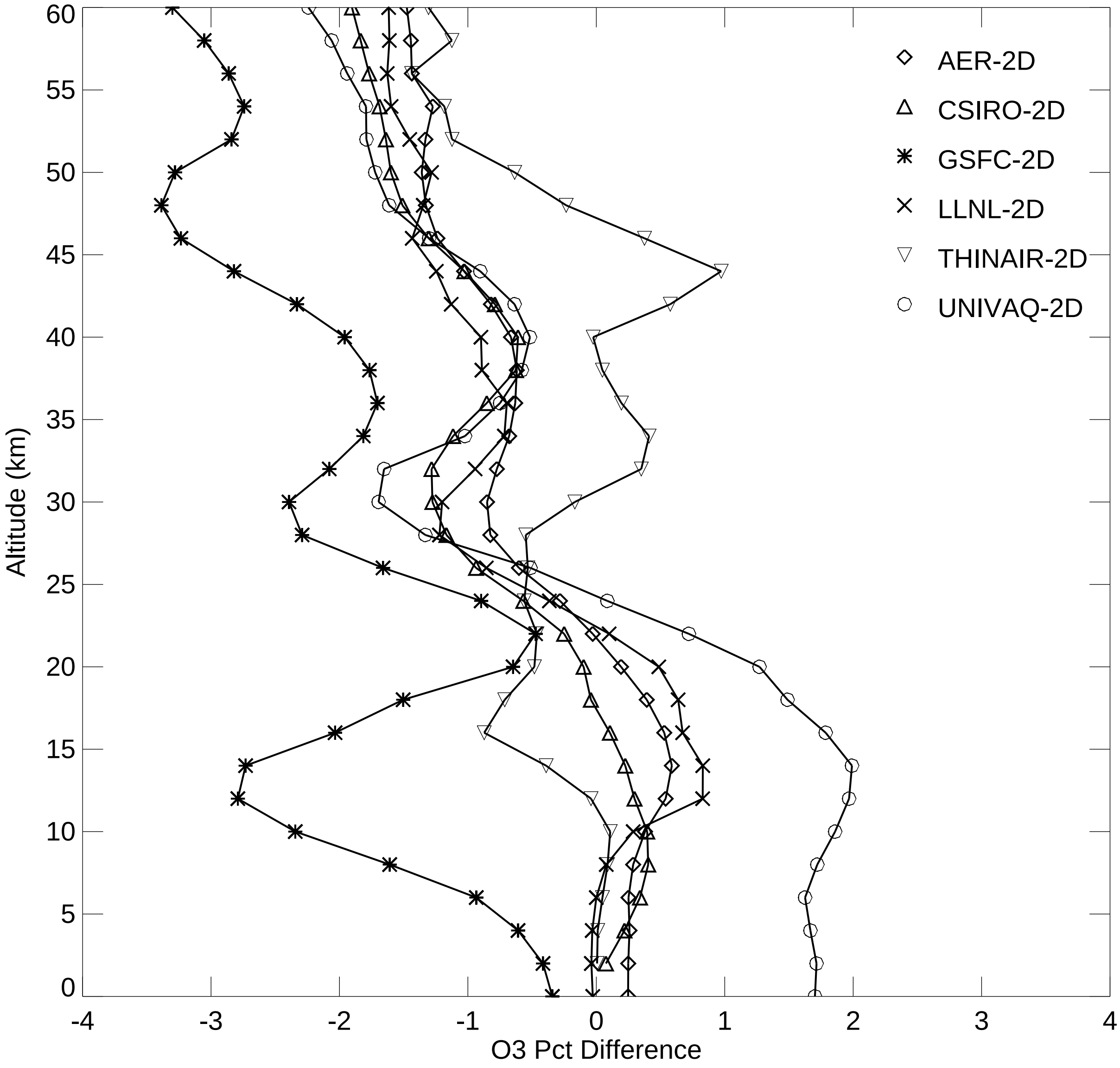

Figure 4.106: Calculated perturbations to O_3 (percent) as a function of altitude at 45^oS in June of 2015 due to emissions from a fleet of 1000 HSCT aircraft with EI(NO_x)=10 under Scenario S1j relative to Scenario D.

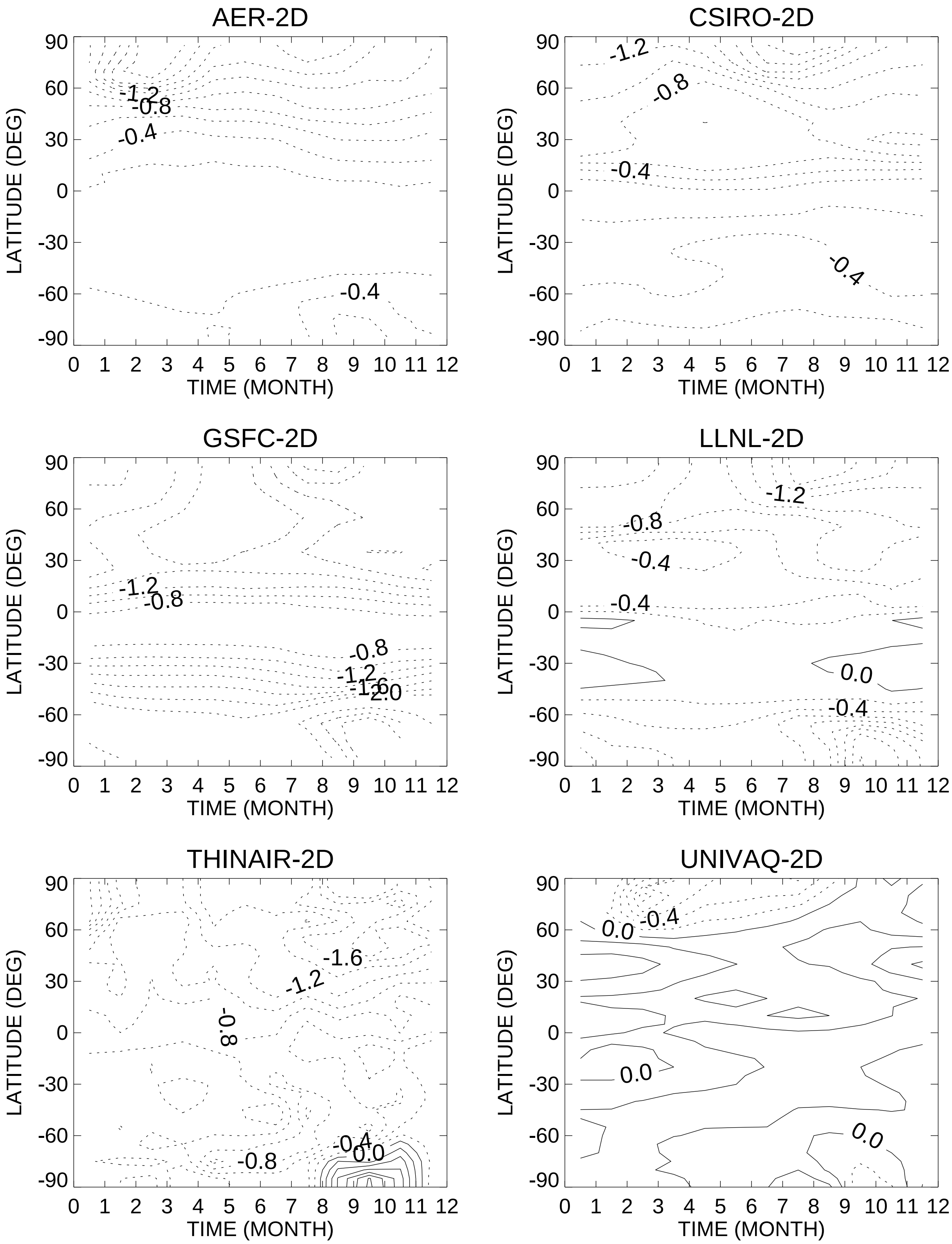

Figure 4.107: Calculated perturbations to column O_3 (percent) as a function of latitude and season in 2015 due to emissions from a fleet of 1000 HSCT aircraft with $EI(NO_x)=10$ under Scenario S1j relative to Scenario D. Contours are -5, -4, -3, and -2.0 to 1.0 by 0.2.

4.3.2 Scenarios with Sulfur Emissions (S1f-h,k,l)

Scenarios S1f, S1g, S1h, S1k, and S1l include emission of sulfur from a fleet of 500 HSCT aircraft, along with H_2O and NO_x emissions, in 2015. The sulfur emission scenarios are described in Section 2.3. They all assume an EI(SO_2) of 0.4 gm/(kg fuel) and that the new particles created in the plume reach a uniform radius of 10 nm when plume processing is complete. The fraction of sulfur emissions converted to particles within the plume is varied from 0% to 100%, with 10% taken as the most likely scenario and 50% a likely upper limit to the uncertainty. Aerosol surface area densities are specified as scenario input, based on calculations from the AER 2-D microphysical model. Table 2.3 describes the SAD designations used in these scenarios. Figures 2.12-2.16 show the SAD perturbations as a function of latitude and altitude for each of the scenarios. Aerosol surface area density for the subsonic-only background case (Scenario D) is SA0.

Scenario S1f uses the SA1 surface area density, which assumes 50% particle conversion, and EI(NO_x)=5. Changes in ozone relative to Scenario D for March, June, and October are shown in Figures 4.108, 4.109, and 4.110 as a function of latitude and altitude. Relative to Scenario S1c without sulfur emissions, ozone depletion is enhanced in all models below 25 km at middle and high latitudes. The AER and LLNL models show a region of ozone increase at near 25-30 km at high latitudes in October which were not present in Scenario S1c. The effect of added aerosol particles is to suppress NO_x and enhance HO_x, ClO_x, and BrO_x. The suppression of NO_x accounts for the ozone increase at 25 km in the AER and LLNL models, where the NO_x cycle represents a dominant removal cycle for ozone. Increases in HO_x, ClO_x, and BrO_x account for the additional ozone depletion below 25 km, where the HO_x cycle dominates ozone loss.

Figures 4.111, 4.112, and 4.113 show changes in ozone profile at 45^{o}N, the equator, and 45^{o}S for June. Local ozone depletions at 45^{o}N in June are as much as 3.5% for the AER and GSFC models for Scenario S1f, though they were below 1.5% for Scenario S1c. Changes at 45^{o}S are less dramatic. Changes in total ozone for Scenario S1f relative to Scenario D are shown in Figure 4.114. These column depletions are significantly larger than those for Scenario S1c without sulfur emissions. The UNIVAQ and LARC models, which showed mostly positive ozone change for Scenario S1c, show mostly negative ozone changes for Scenario S1f. The AER and GSFC models calculated northern hemisphere average ozone depletion of 1.0% and 1.1%, respectively, for this scenario.

Scenario S1g also uses SA1 aerosol surface area density, but with EI(NO_x)=10. Ozone change as a function of latitude and altitude for this scenario is shown in Figures 4.115-4.117. Ozone depletion below 25 km is somewhat reduced from Scenario S1f. Ozone depletion in the 25-30 km region is somewhat increased. Figures 4.118-4.120 show vertical profiles of ozone change for this scenario in June at 45^{o}N, the equator, and 45^{o}S. Changes in ozone column for Scenario S1g relative to Scenario D are shown in Figure 4.121. The AER and UNIVAQ models show less ozone depletion in the northern hemisphere with EI(NO_x)=10 than with EI(NO_x)=5 using SA1 surface area. The THINAIR model shows more ozone depletion with EI(NO_x)=10, and the GSFC, CSIRO, and LLNL models show little change with EI(NO_x).

The SA3 surface area distribution, representing 100% gas-to-particle conversion in the aircraft plume, is used in Scenario S1h, along with EI(NO_x)=5. Changes in ozone as a function of latitude and altitude for March, June, and October are shown in Figures 4.122, 4.123, and 4.124. The ozone depletion below 25 km is greater than that from Scenario S1f. Vertical profiles of ozone change are shown in Figures 4.125, 4.126, and 4.127 for 45^{o}N, the equator, and 45^{o}S, respectively, for this scenario. Ozone column changes, shown in Figure 4.128, are somewhat larger than for Scenario S1f for most models, though the CSIRO model shows little change.

An SO_2 gas-to-particle conversion ratio of 10% (SA5) is used in Scenario S1k, along with EI(NO_x)=5. Changes in ozone column for Scenario S1k relative to Scenario D are shown in Figures 4.129, 4.130, and 4.131 for March, June, and October. Vertical profiles of ozone change are shown in Figures 4.132, 4.133, and 4.134 for 45^{o}N, the equator, and 45^{o}S. Ozone depletion falls between that of Scenario S1c and Scenario S1f. Changes in total ozone are shown in Figure 4.135 as a function of latitude and season. Even for the SO_2 gas-to-particle conversion rate of 10%, ozone depletion is substantially increased over the case with no sulfur emissions (S1c). For the AER, LLNL, and CSIRO models, northern hemisphere average ozone depletion for Scenario S1k is double that for Scenario S1c.

A scenario with no SO_2 gas-to-particle conversion, ie. with all sulfur emitted as $SO2_2$ gas, was run by the AER model. Ozone changes for this scenario, designated S1l, are shown in Figures 4.136, 4.137, and 4.138 relative to Scenario D. Column ozone changes are shown in Figure 4.139. The average northern hemisphere ozone depletion is -0.6% and the average southern hemisphere ozone depletion of -0.3%. This shows that sulfur emissions may have a significant though reduced effect on ozone depletion from HSCT aircraft even if there is no gas-to-particle conversion in the plume.

The sensitivity of northern hemisphere ozone change to aircraft sulfur emissions is depicted graphically in Figure 4.140. The abscissa show percentage increase in SAD in the 14-21 km, 33-90^{o}N region due to HSCT emissions of sulfur relative to an SA0 background. Scenario S1c is used for the 0% change in SAD. Scenario S1l, with no gas-to-particle conversion, corresponds to a 27% increase in SAD. Scenario S1k, with 10% gas to particle conversion, corresponds to a 38% increase in SAD. Scenarios S1f and S1h, with 50% and 100% gas to particle conversion, correspond to 82% and 111% increases in SAD, respectively. All models show increased ozone depletion for increased SAD perturbations. The slopes are also fairly consistent among the models.

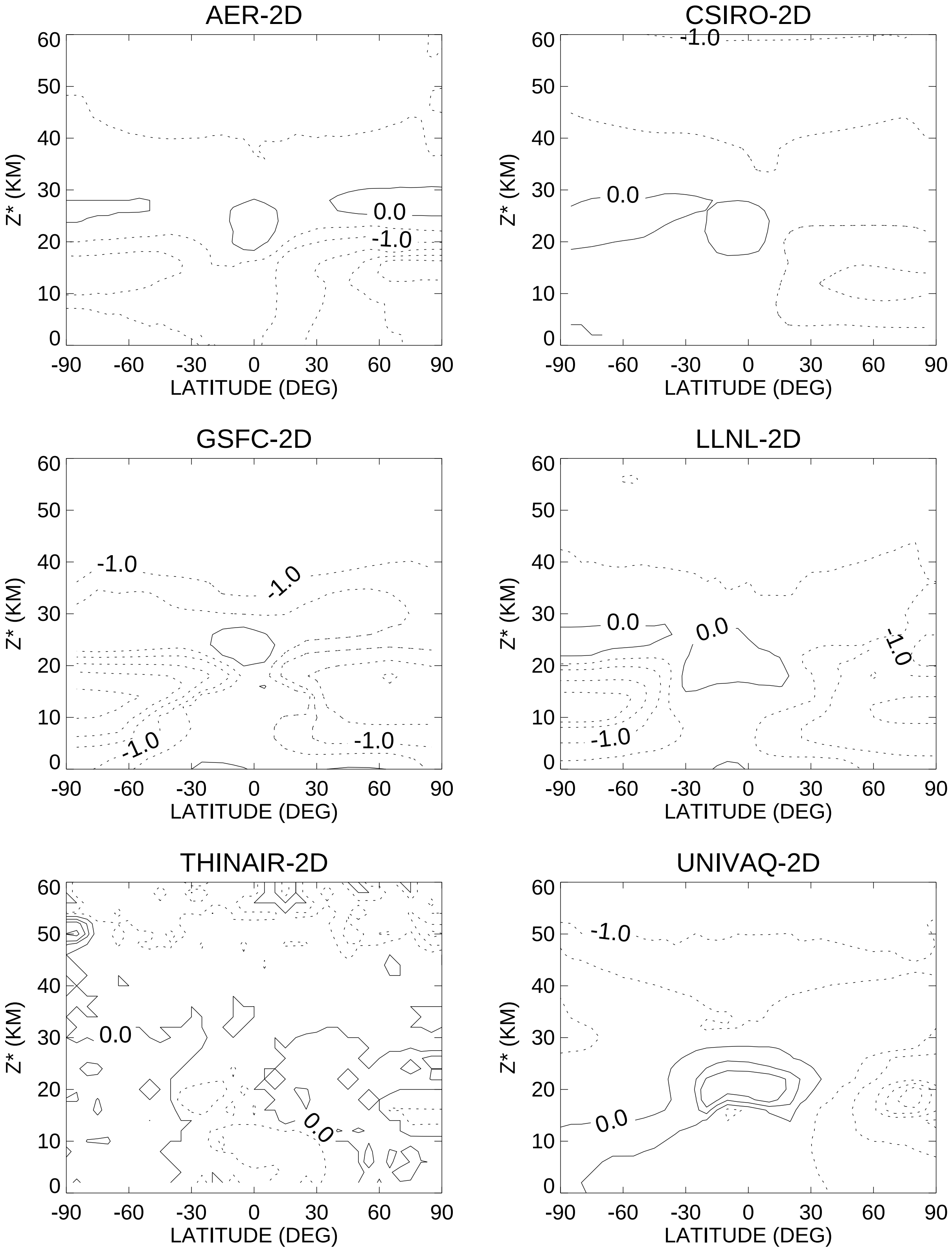

Figure 4.108: Calculated perturbations to O_3 (percent) as a function of latitude and altitude in March of 2015 due to emissions from a fleet of 500 HSCT aircraft with $EI(NO_x)=5$ and SA1 sulfate surface area under Scenario S1f relative to Scenario D. Contours are -4, -3, -2, -1, -0.5, 0, 0.5, 1.

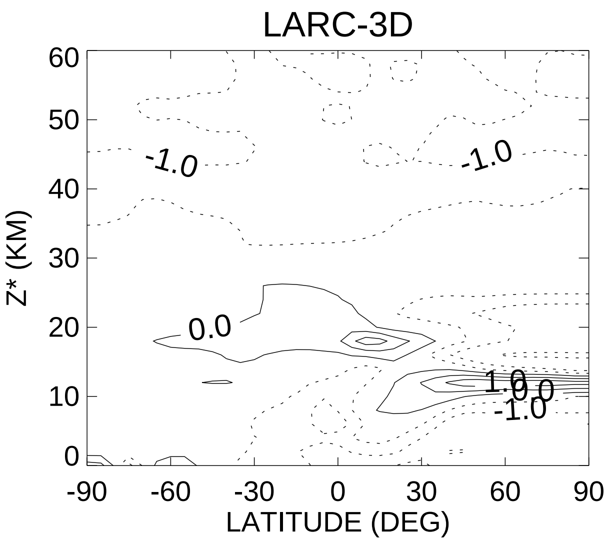

Figure 4.108: continued

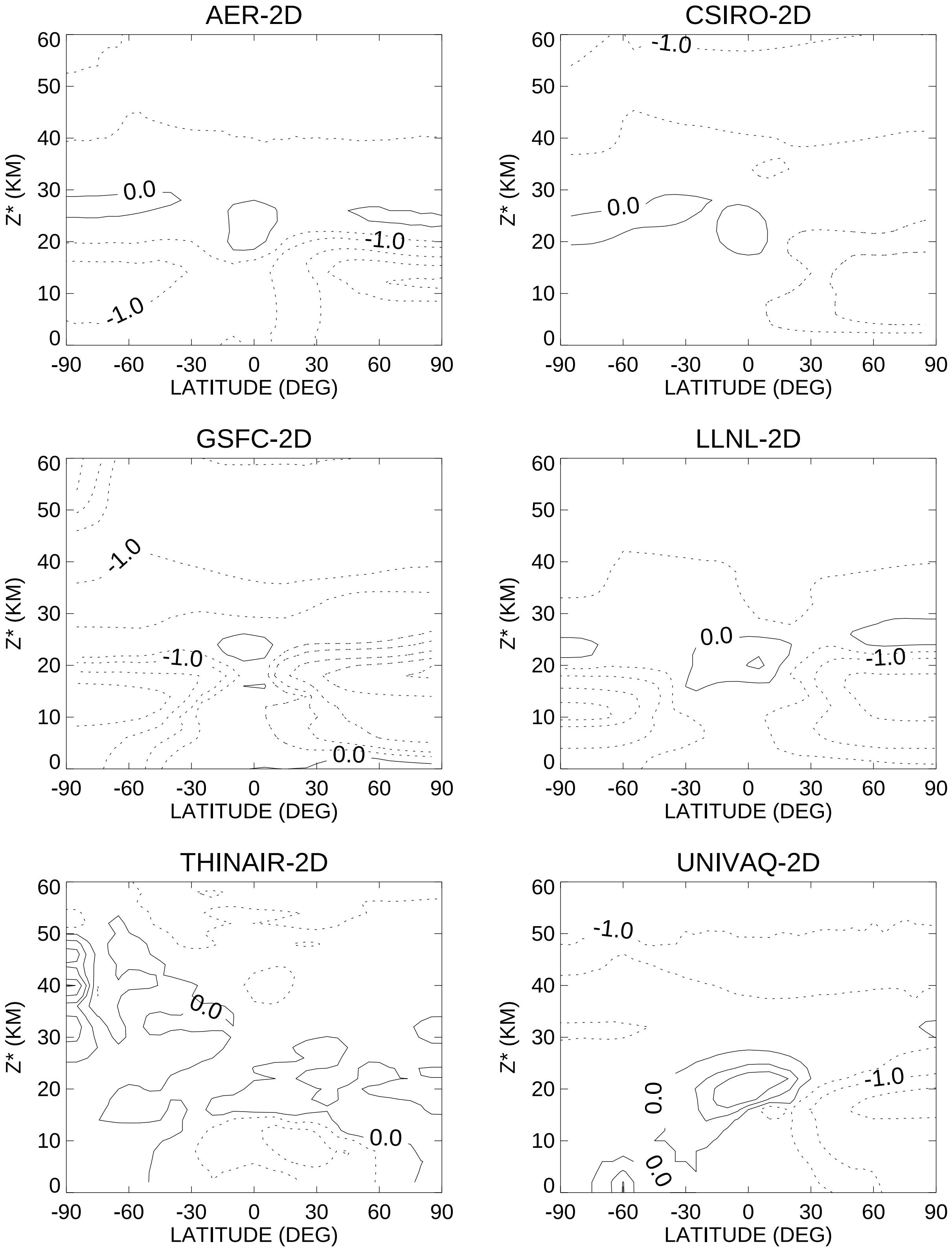

Figure 4.109: Calculated perturbations to O_3 (percent) as a function of latitude and altitude in June of 2015 due to emissions from a fleet of 500 HSCT aircraft with EI(NO_x)=5 and SA1 sulfate surface area under Scenario S1f relative to Scenario D. Contours are -4, -3, -2, -1, -0.5, 0, 0.5, 1.

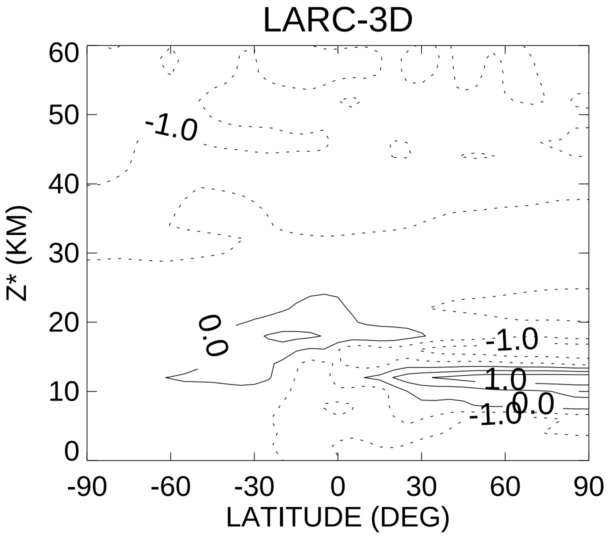

Figure 4.109: continued

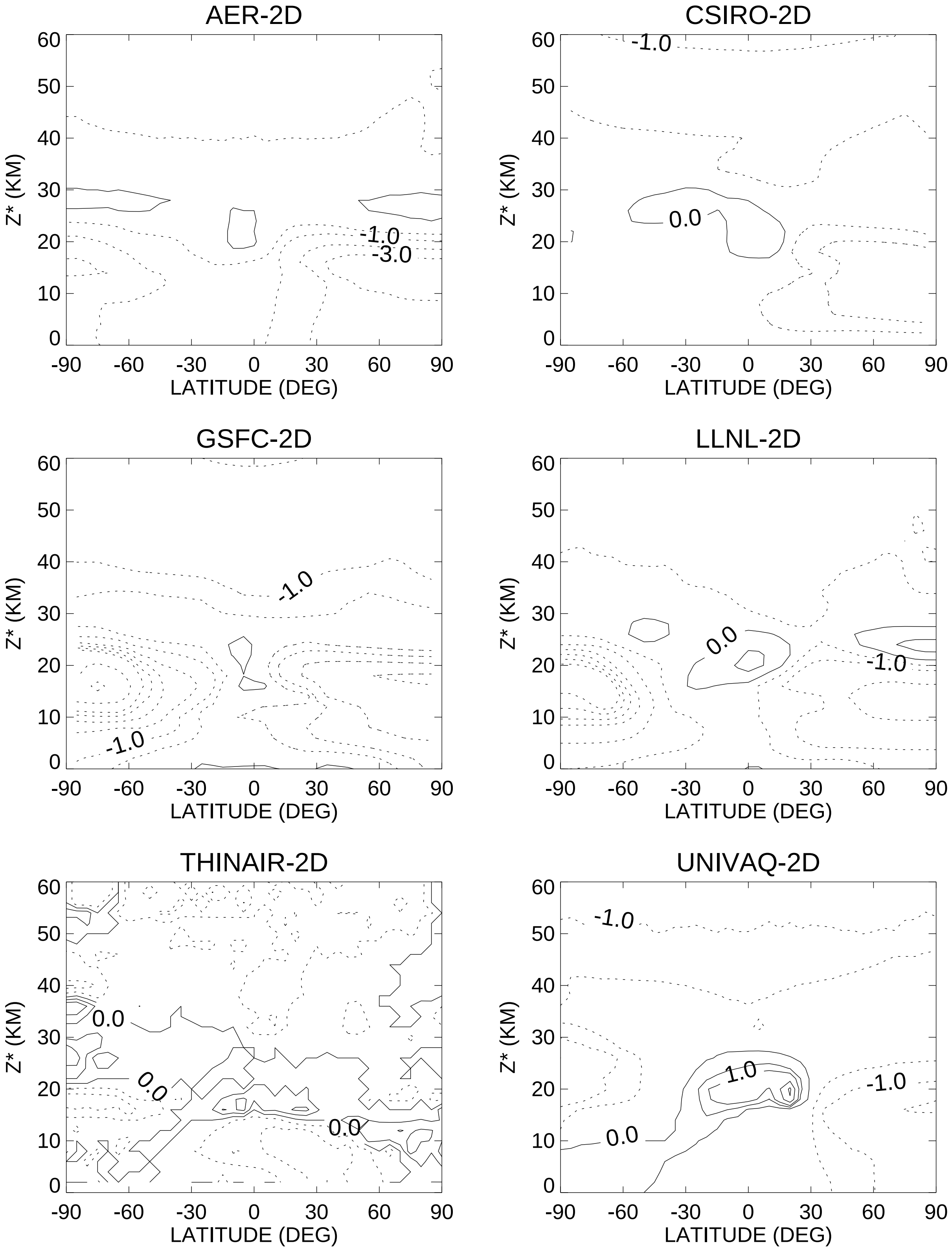

Figure 4.110: Calculated perturbations to O_3 (percent) as a function of latitude and altitude in October of 2015 due to emissions from a fleet of 500 HSCT aircraft with EI(NO_x)=5 and SA1 sulfate surface area under Scenario S1f relative to Scenario D. Contours are -15, -10, -5, -4, -3, -2, -1, -0.5, 0, 0.5, 1, 2, 3.

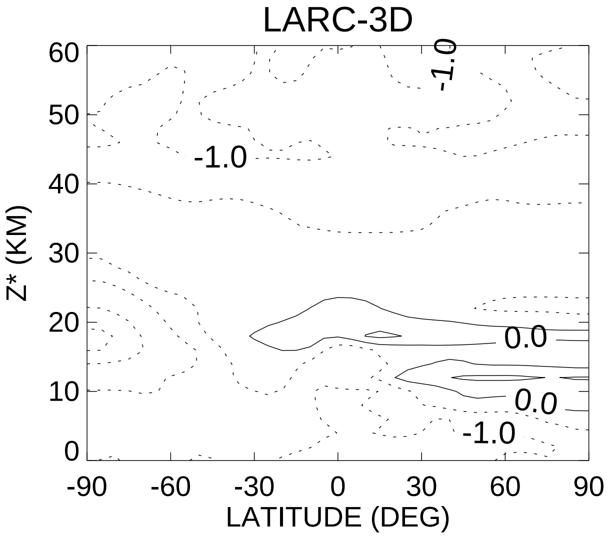

Figure 4.110: continued

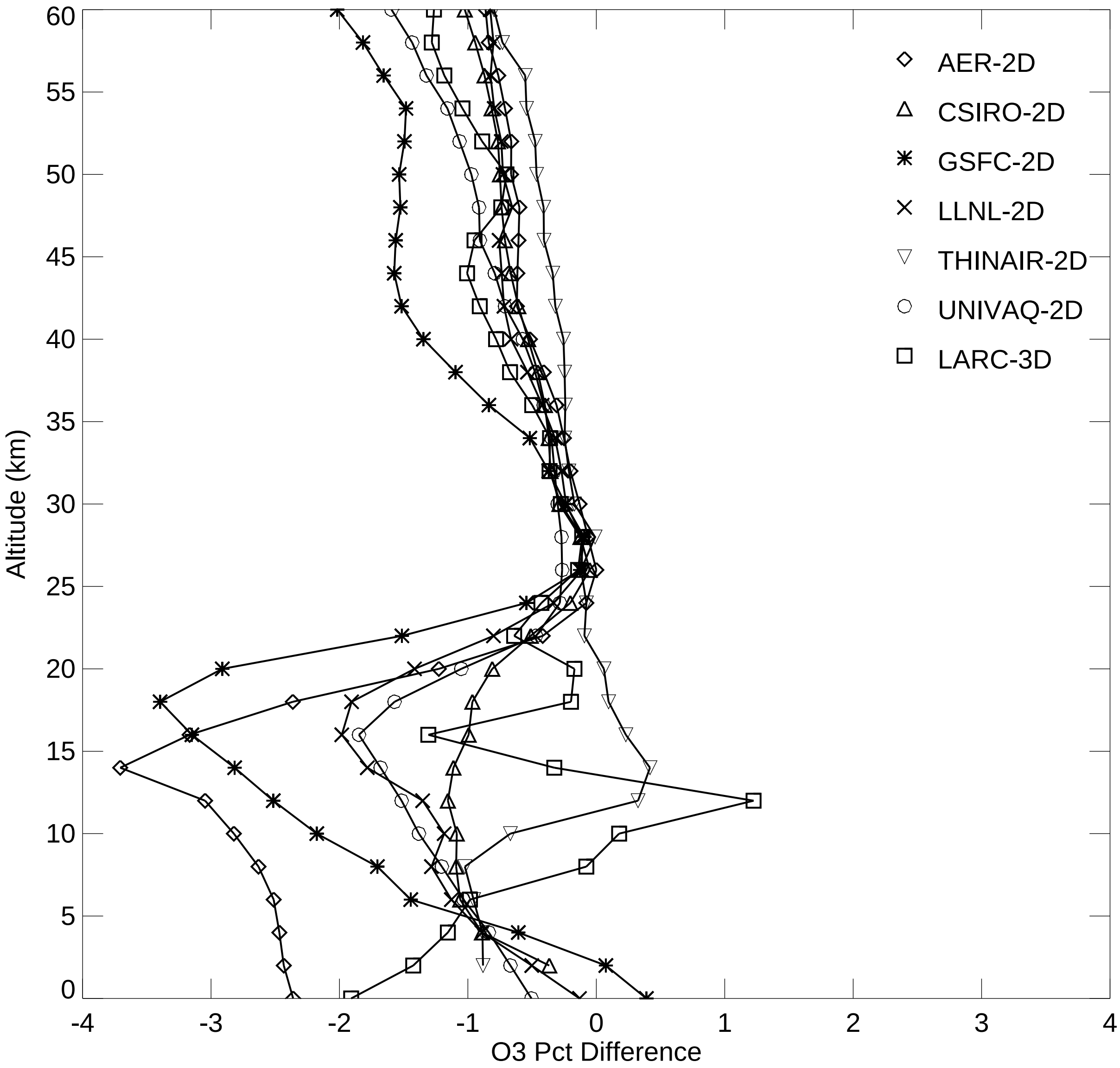

Figure 4.111: Calculated perturbations to O_3 (percent) as a function of altitude at 45^oN in June of 2015 due to emissions from a fleet of 500 HSCT aircraft with EI(NO_x)=5 and SA1 sulfate surface area under Scenario S1f relative to Scenario D.

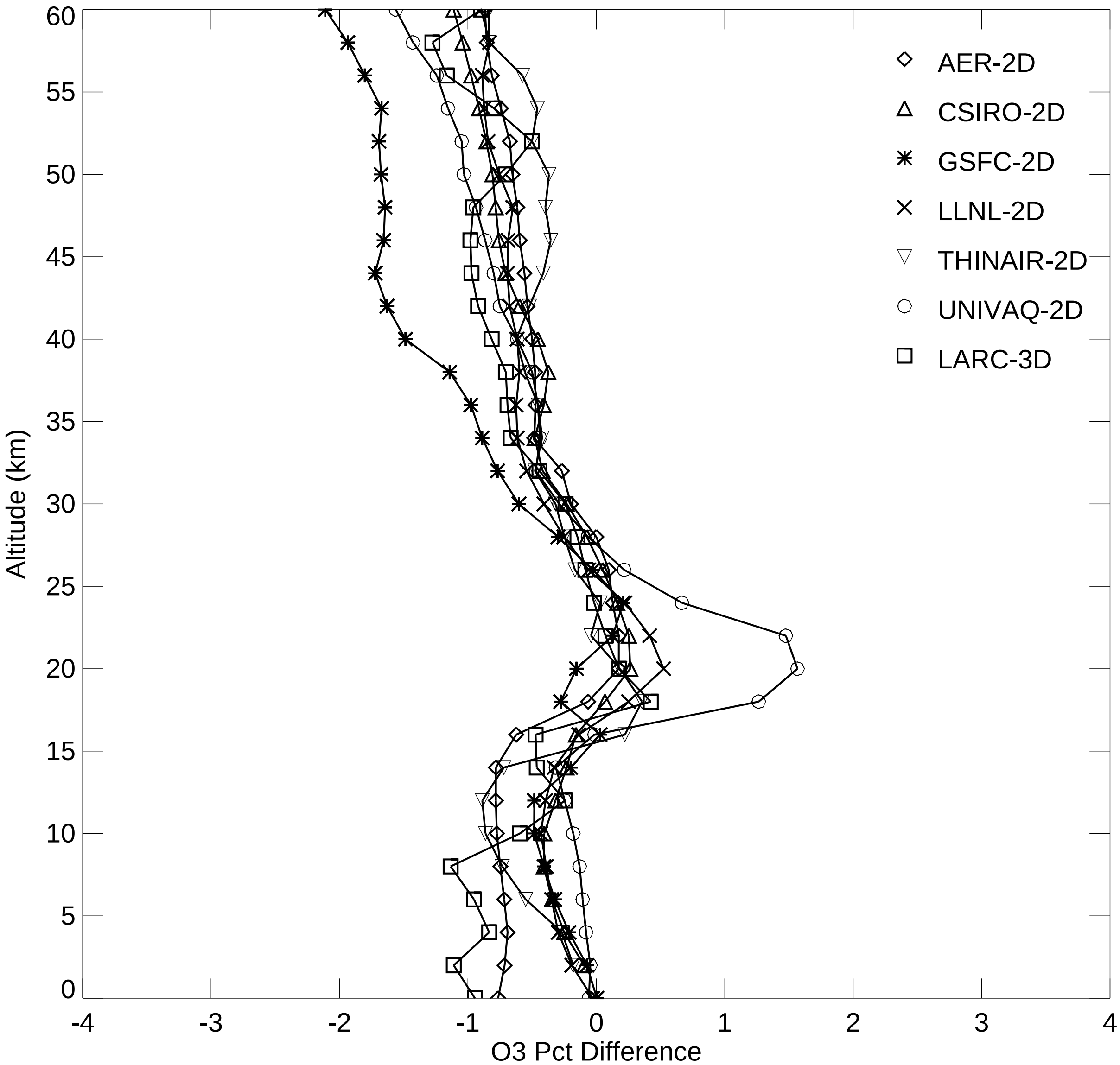

Figure 4.112: Calculated perturbations to O_3 (percent) as a function of altitude at the equator in June of 2015 due to emissions from a fleet of 500 HSCT aircraft with EI(NO_x)=5 and SA1 sulfate surface area under Scenario S1f relative to Scenario D.

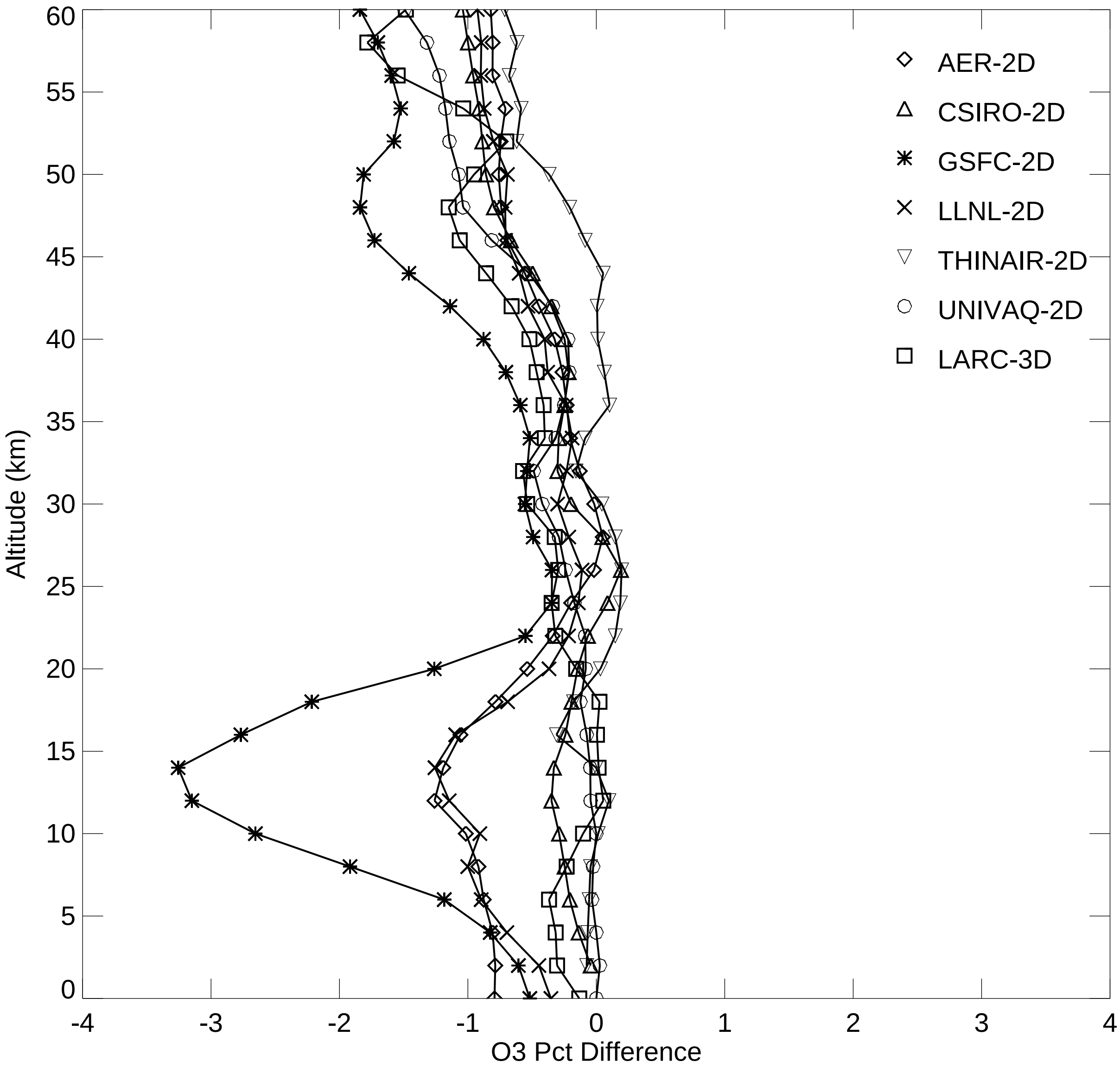

Figure 4.113: Calculated perturbations to O_3 (percent) as a function of altitude at 45^{o}S in June of 2015 due to emissions from a fleet of 500 HSCT aircraft with EI(NO_x)=5 and SA1 sulfate surface area under Scenario S1f relative to Scenario D.

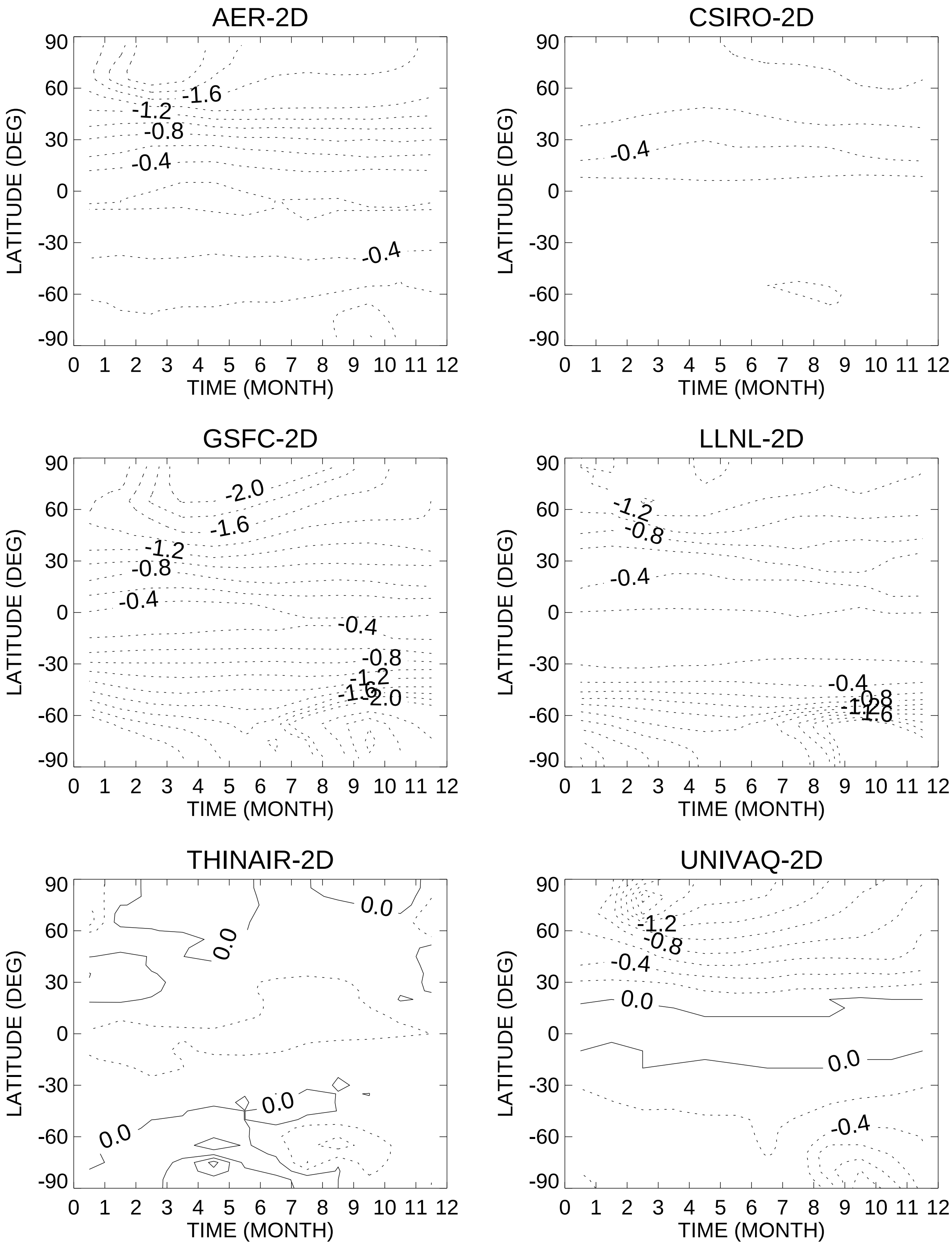

Figure 4.114: Calculated perturbations to column O_3 (percent) as a function of latitude and season in 2015 due to emissions from a fleet of 500 HSCT aircraft with $EI(NO_x)=5$ and SA1 sulfate surface area under Scenario S1f relative to Scenario D. Contours are -5, -4, -3, and -2.0 to 0.2 by 0.2.

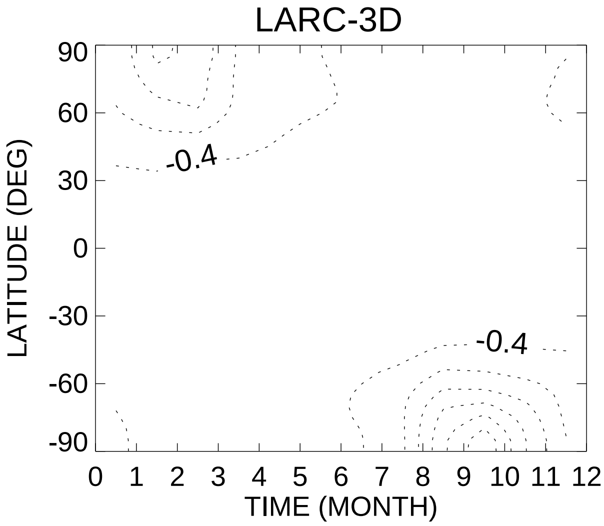

Figure 4.114: continued

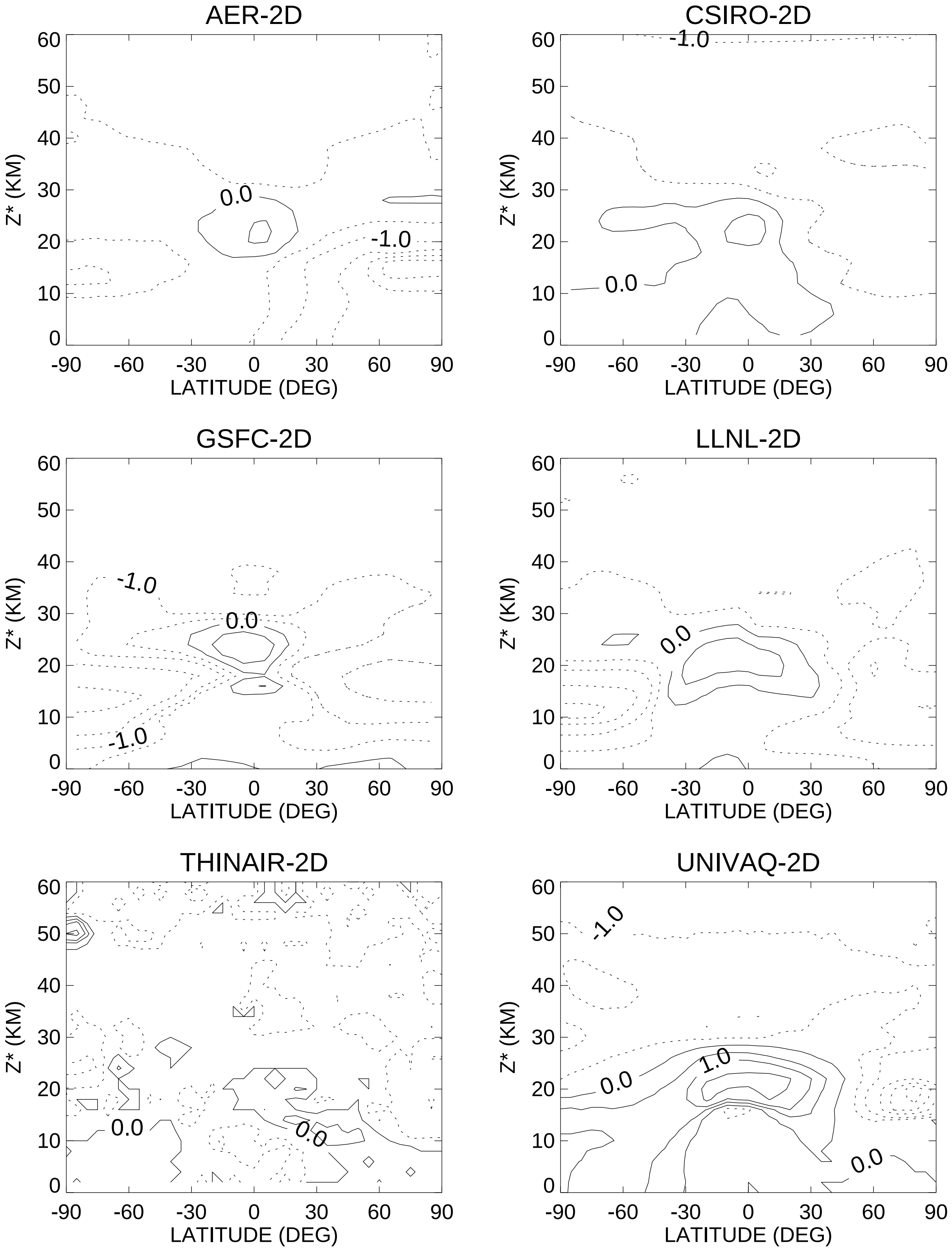

Figure 4.115: Calculated perturbations to O_3 (percent) as a function of latitude and altitude in March of 2015 due to emissions from a fleet of 500 HSCT aircraft with EI(NO_x)=10 and SA1 sulfate surface area under Scenario S1g relative to Scenario D. Contours are -4, -3, -2, -1, -0.5, 0, 0.5, 1, 2.

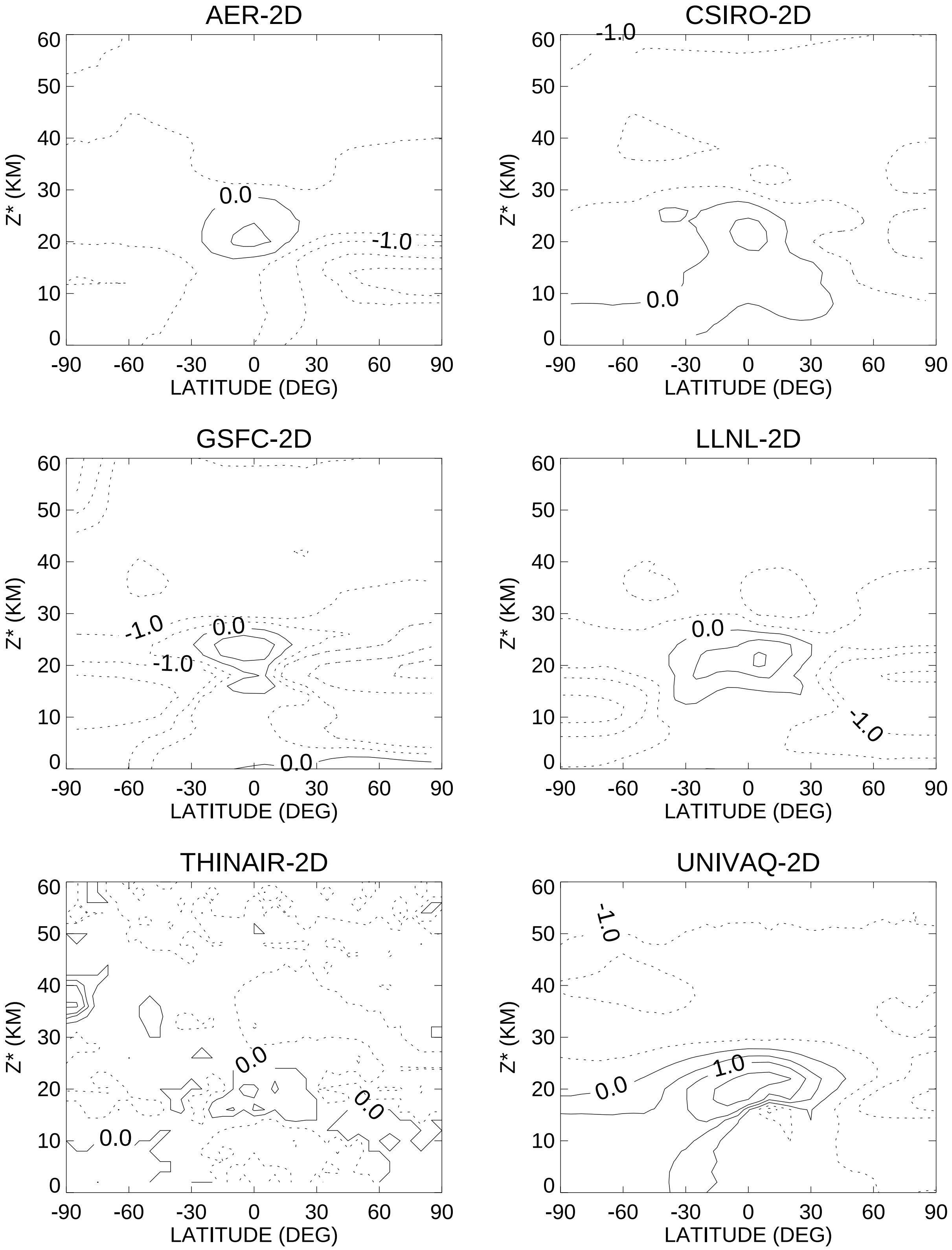

Figure 4.116: Calculated perturbations to O_3 (percent) as a function of latitude and altitude in June of 2015 due to emissions from a fleet of 500 HSCT aircraft with $EI(NO_x)=10$ and SA1 sulfate surface area under Scenario S1g relative to Scenario D. Contours are -3, -2, -1, -0.5, 0, 0.5, 1, 2.

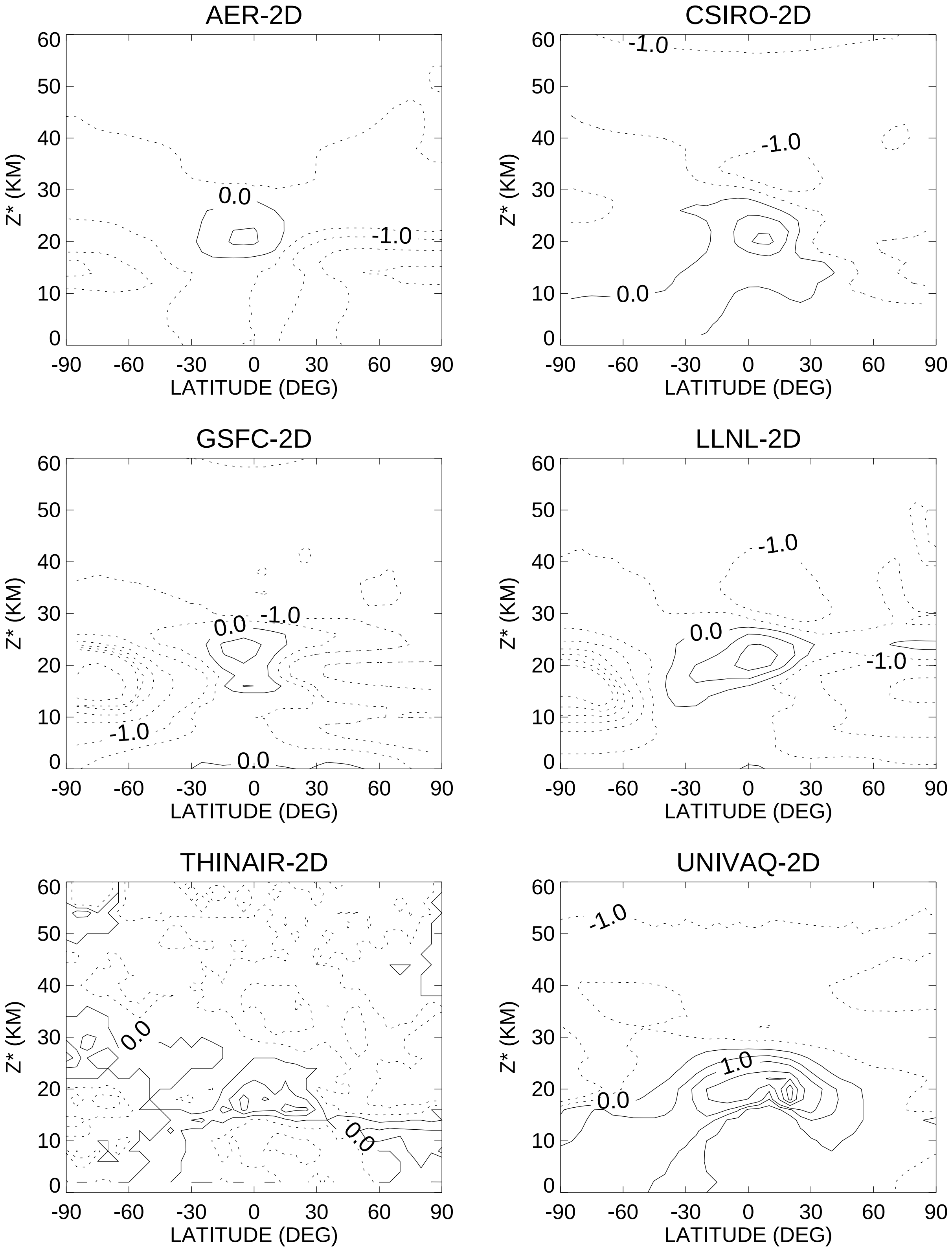

Figure 4.117: Calculated perturbations to O_3 (percent) as a function of latitude and altitude in October of 2015 due to emissions from a fleet of 500 HSCT aircraft with $EI(NO_x)=10$ and SA1 sulfate surface area under Scenario S1g relative to Scenario D. Contours are -10, -5, -4, -3, -2, -1, -0.5, 0, 0.5, 1, 2, 2, 3, 4.

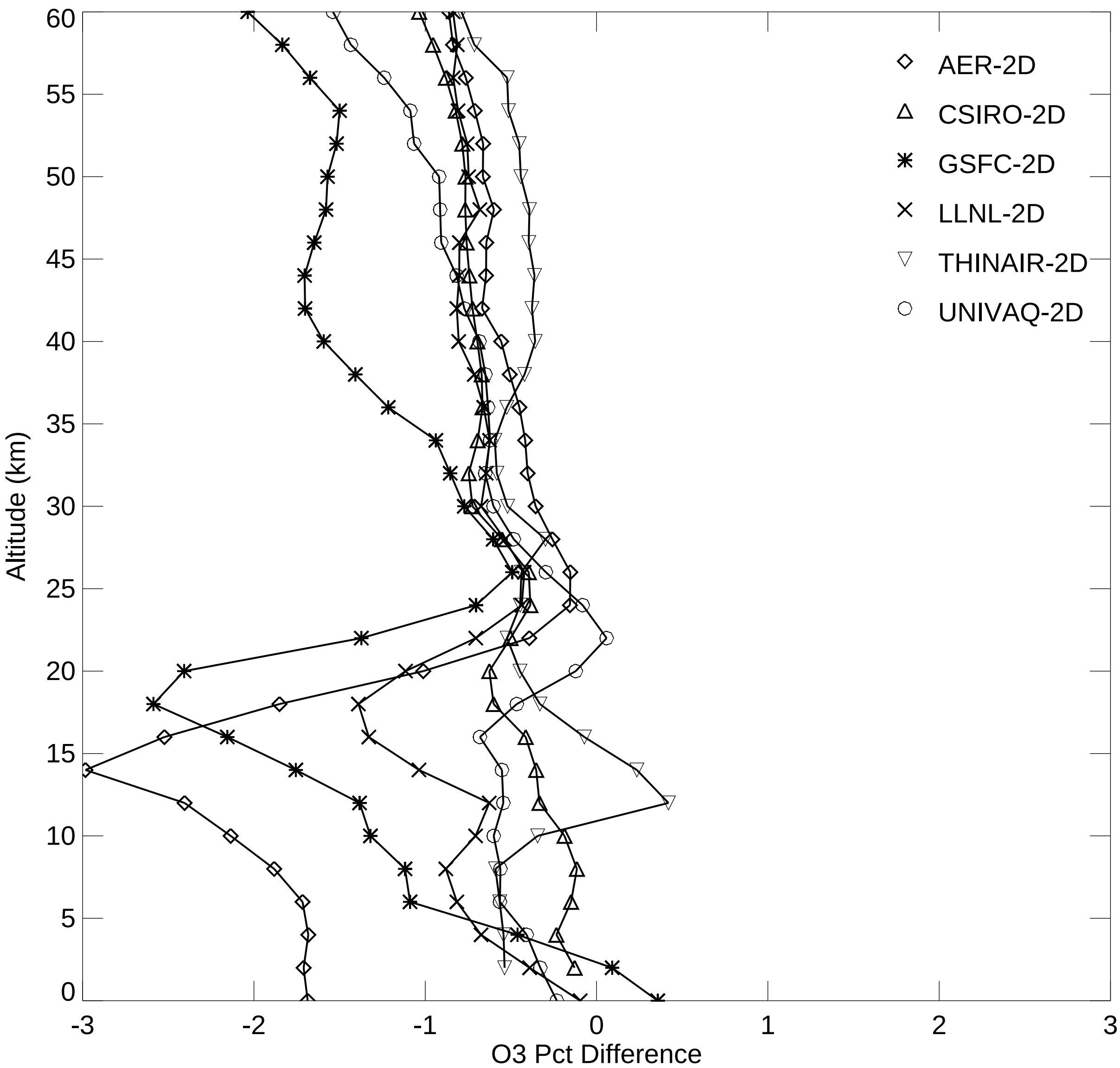

Figure 4.118: Calculated perturbations to O_3 (percent) as a function of altitude at 45^{o}N in June of 2015 due to emissions from a fleet of 500 HSCT aircraft with EI(NO_x)=10 and SA1 sulfate surface area under Scenario S1g relative to Scenario D.

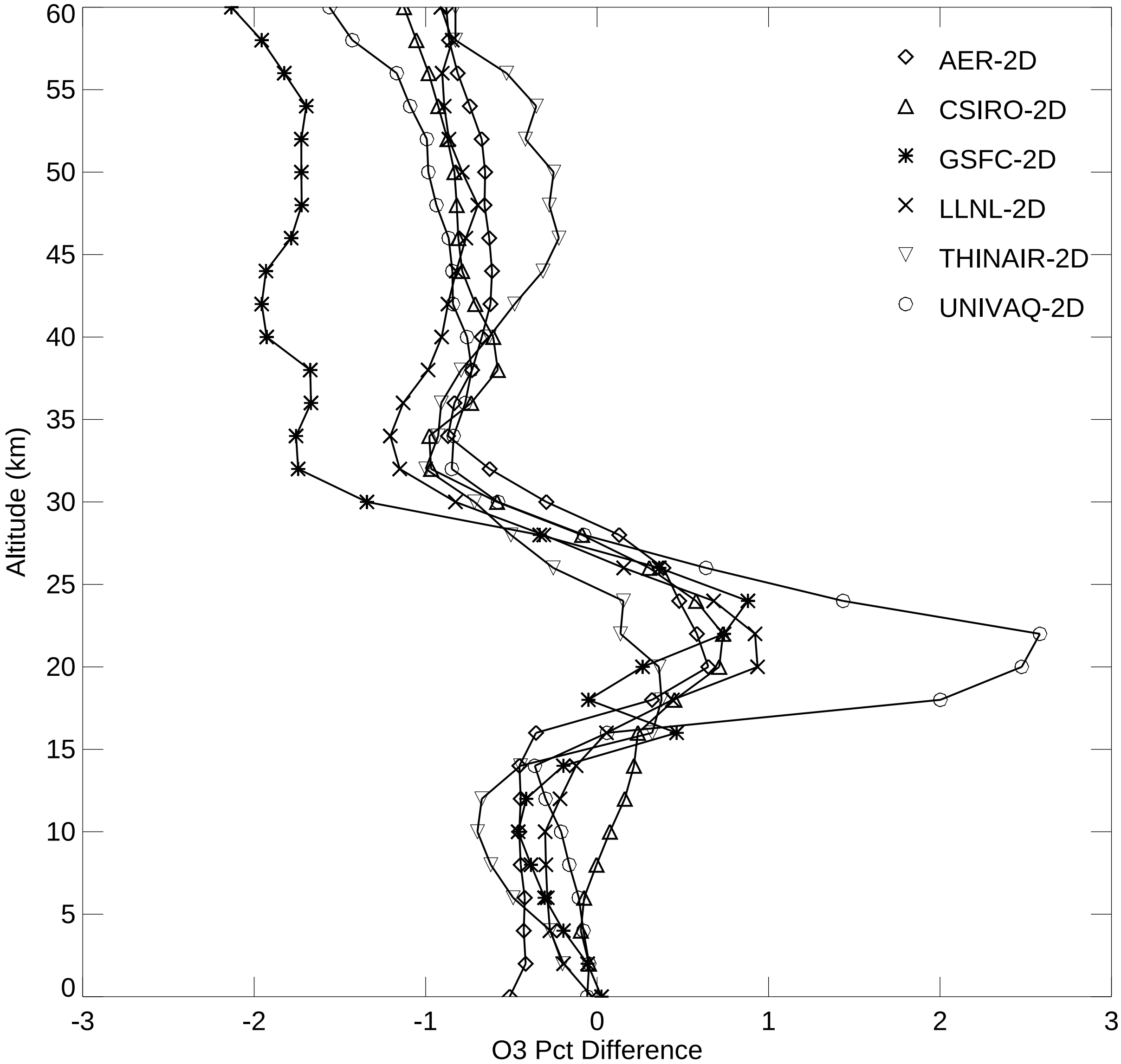

Figure 4.119: Calculated perturbations to O_3 (percent) as a function of altitude at the equator in June of 2015 due to emissions from a fleet of 500 HSCT aircraft with EI(NO_x)=10 and SA1 sulfate surface area under Scenario S1g relative to Scenario D.

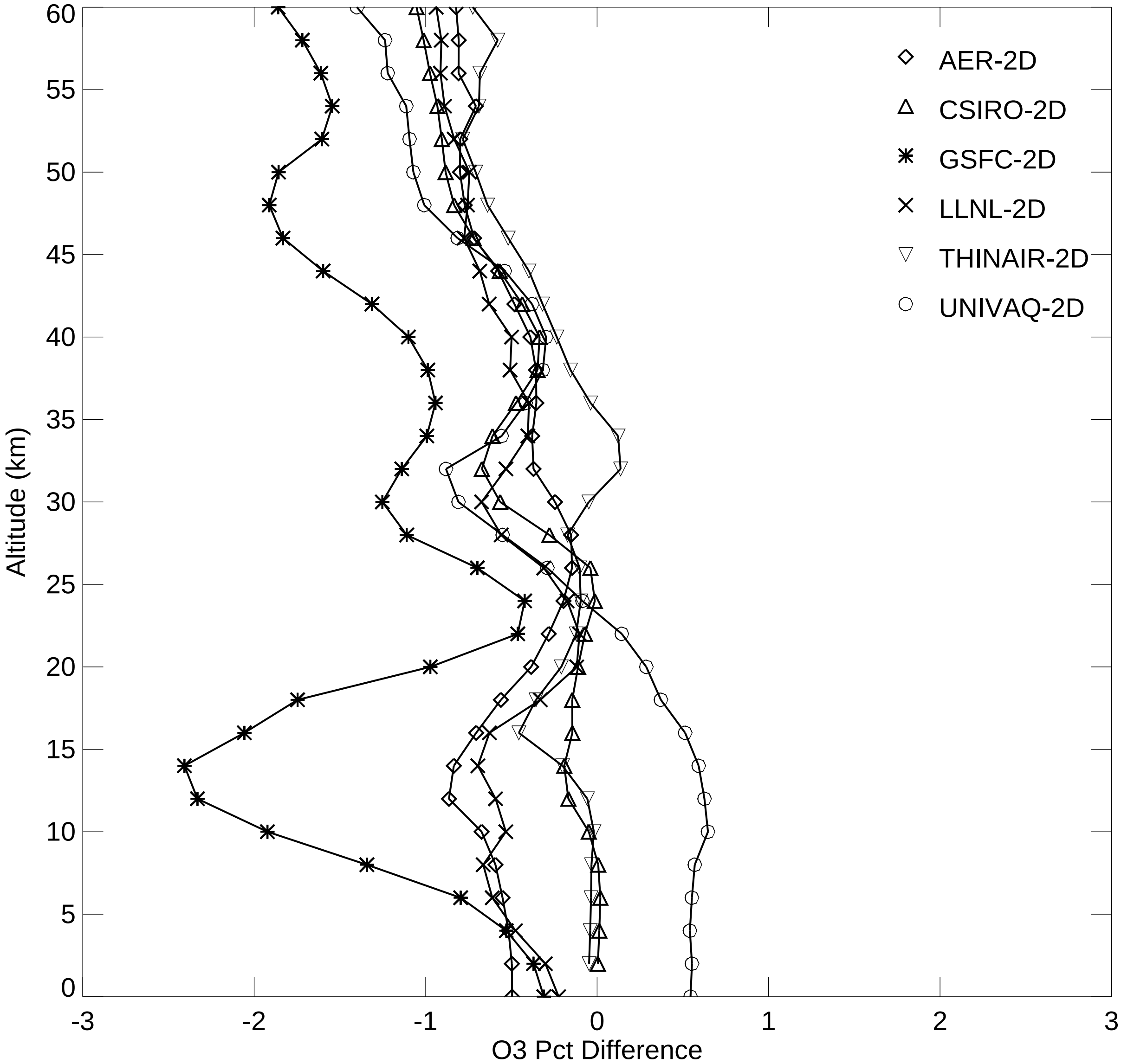

Figure 4.120: Calculated perturbations to O_3 (percent) as a function of altitude at 45^{o}S in June of 2015 due to emissions from a fleet of 500 HSCT aircraft with EI(NO_x)=10 and SA1 sulfate surface area under Scenario S1g relative to Scenario D.

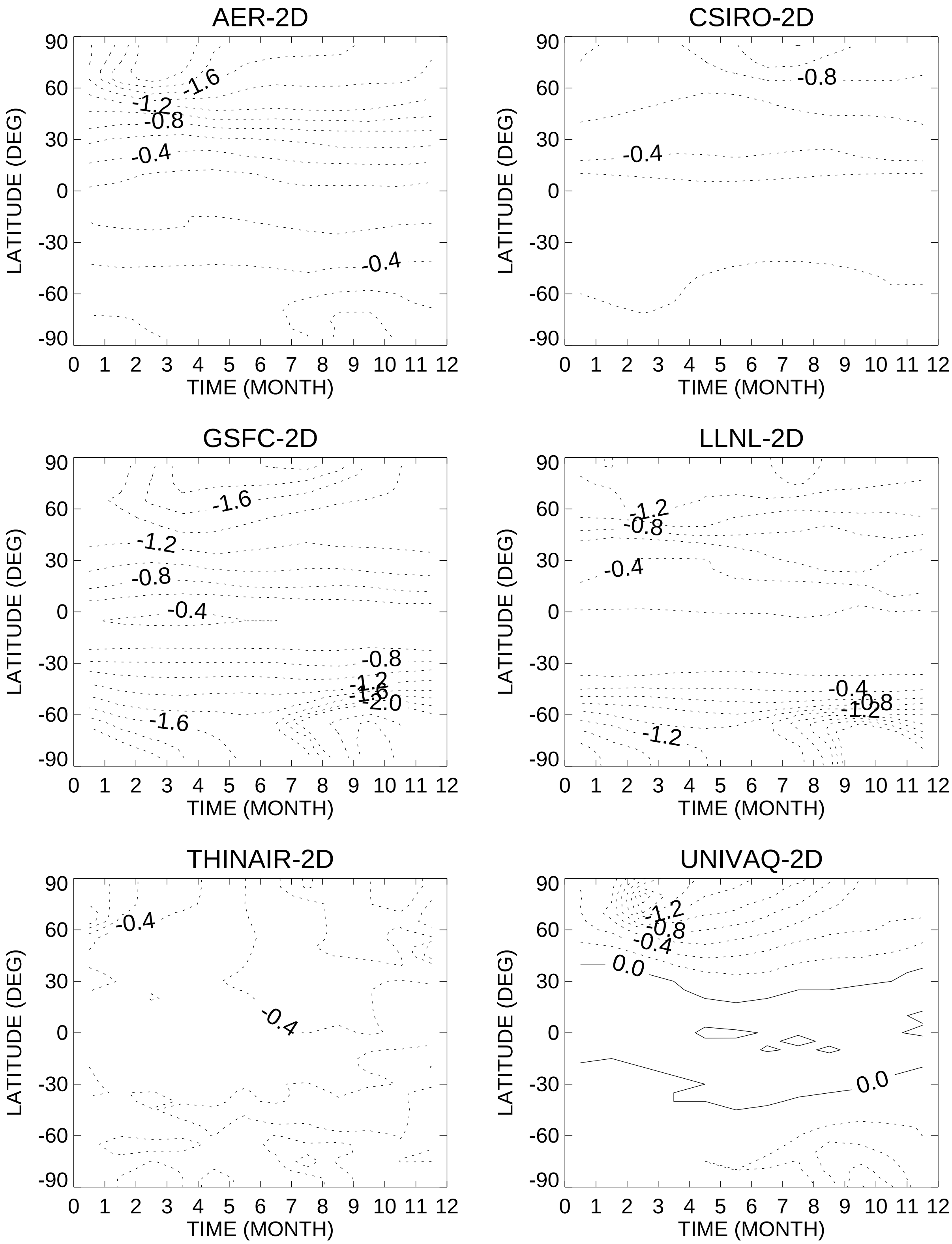

Figure 4.121: Calculated perturbations to column O_3 (percent) as a function of latitude and season in 2015 due to emissions from a fleet of 500 HSCT aircraft with EI(NO_x)=10 and SA1 sulfate surface area under Scenario S1g relative to Scenario D. Contours are -4, -3, and -2.0 to 0.2 by 0.2.

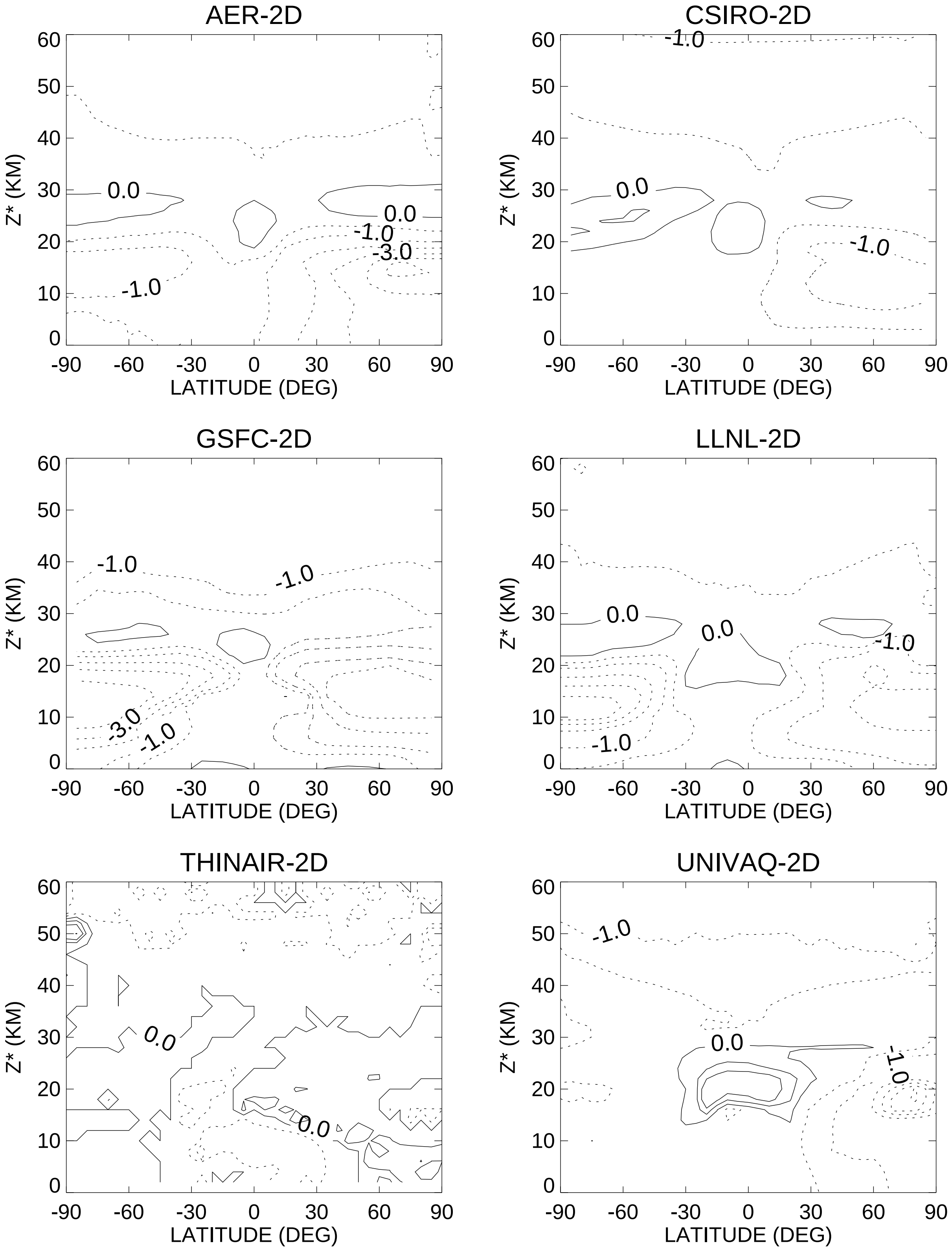

Figure 4.122: Calculated perturbations to O_3 (percent) as a function of latitude and altitude in March of 2015 due to emissions from a fleet of 500 HSCT aircraft with EI(NO_x)=5 and SA3 sulfate surface area under Scenario S1h relative to Scenario D. Contours are -5, -4, -3, -2, -1, -0.5, 0, 0.5, 1.

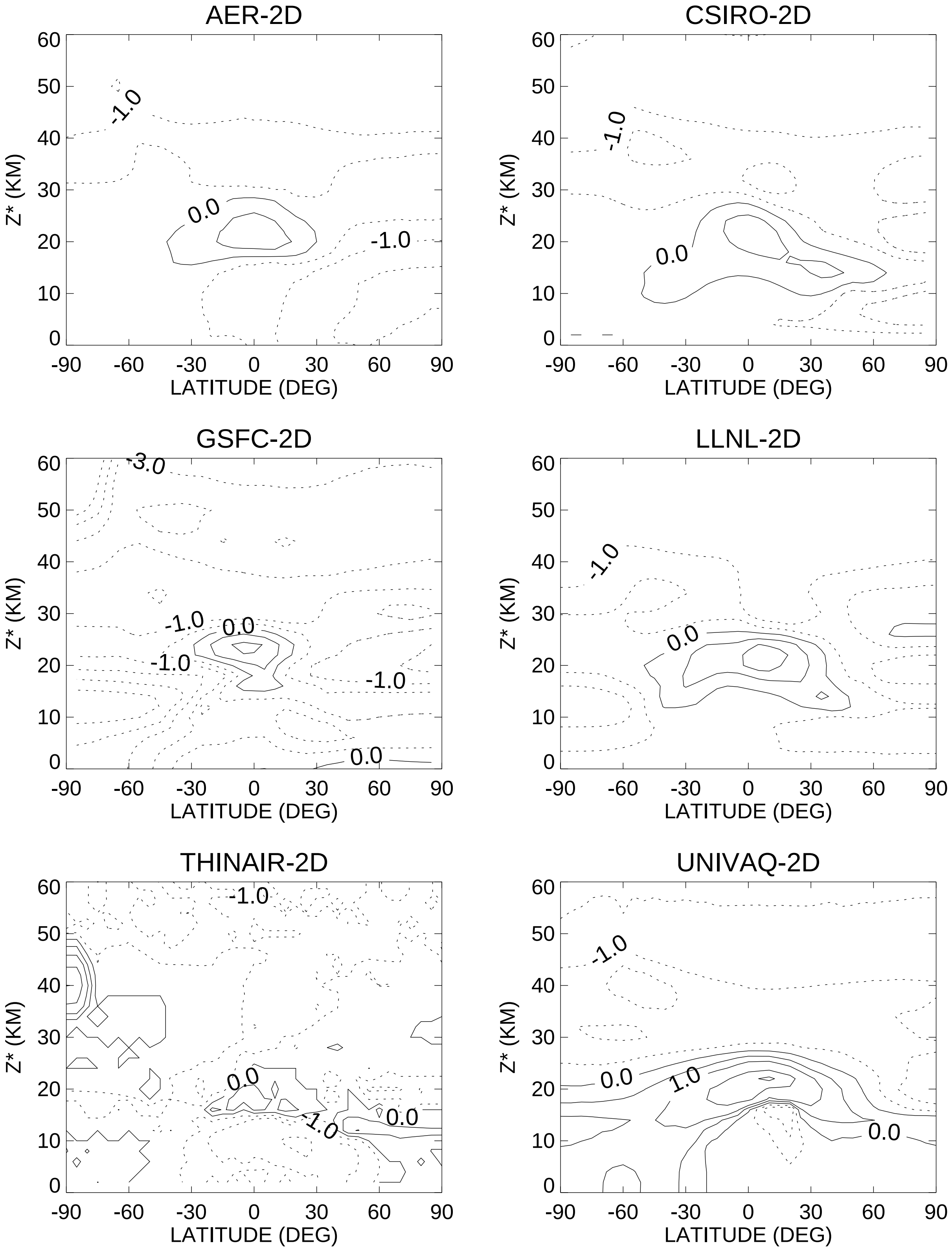

Figure 4.123: Calculated perturbations to O_3 (percent) as a function of latitude and altitude in June of 2015 due to emissions from a fleet of 500 HSCT aircraft with EI(NO_x)=5 and SA3 sulfate surface area under Scenario S1h relative to Scenario D. Contours are -4, -3, -2, -1, -0.5, 0, 0.5, 1, 2, 3.

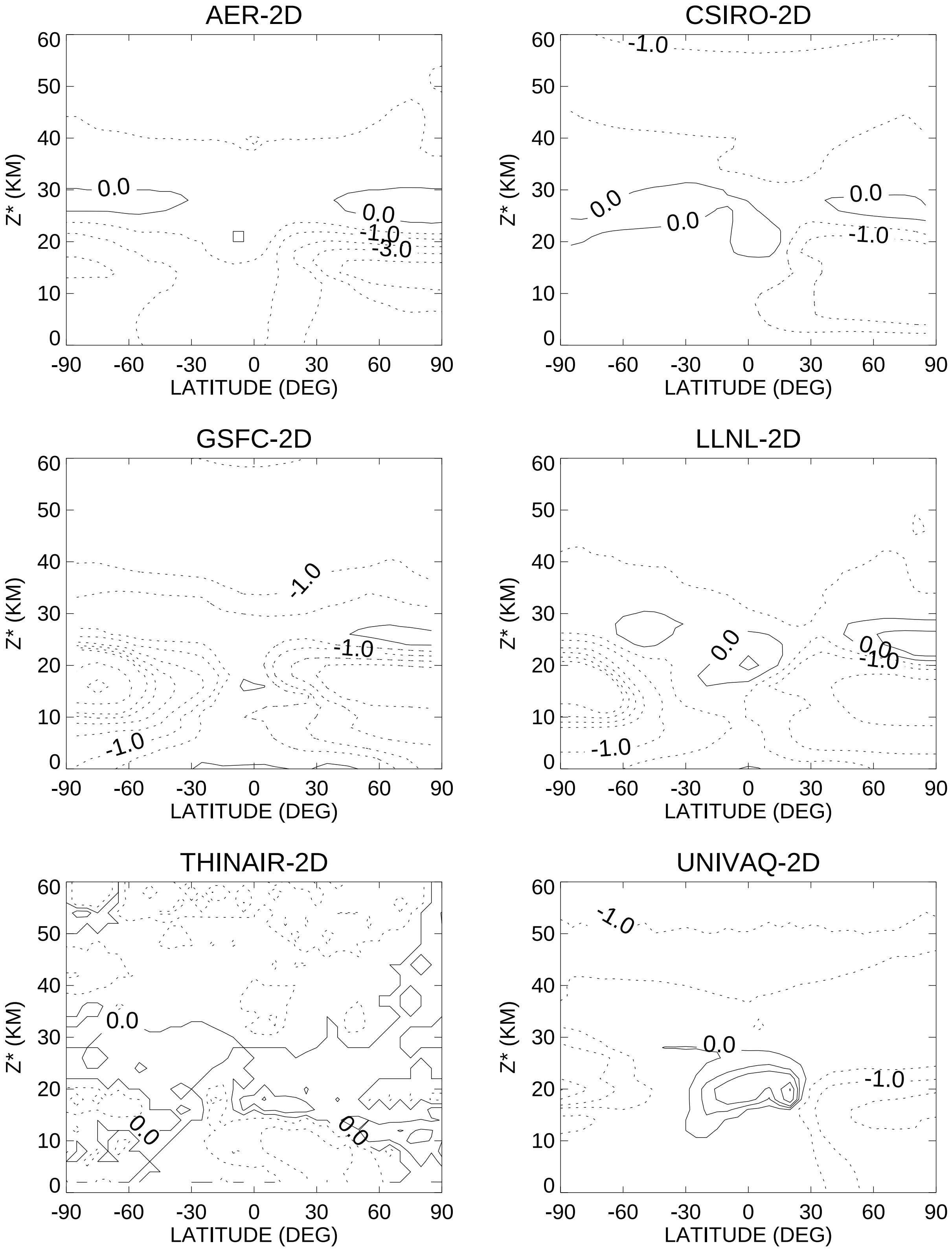

Figure 4.124: Calculated perturbations to O_3 (percent) as a function of latitude and altitude in October of 2015 due to emissions from a fleet of 500 HSCT aircraft with $EI(NO_x)=5$ and SA3 sulfate surface area under Scenario S1h relative to Scenario D. Contours are -15, -10, -5,-4, -3, -2, -1, -0.5, 0, 0.5, 1, 2, 3.

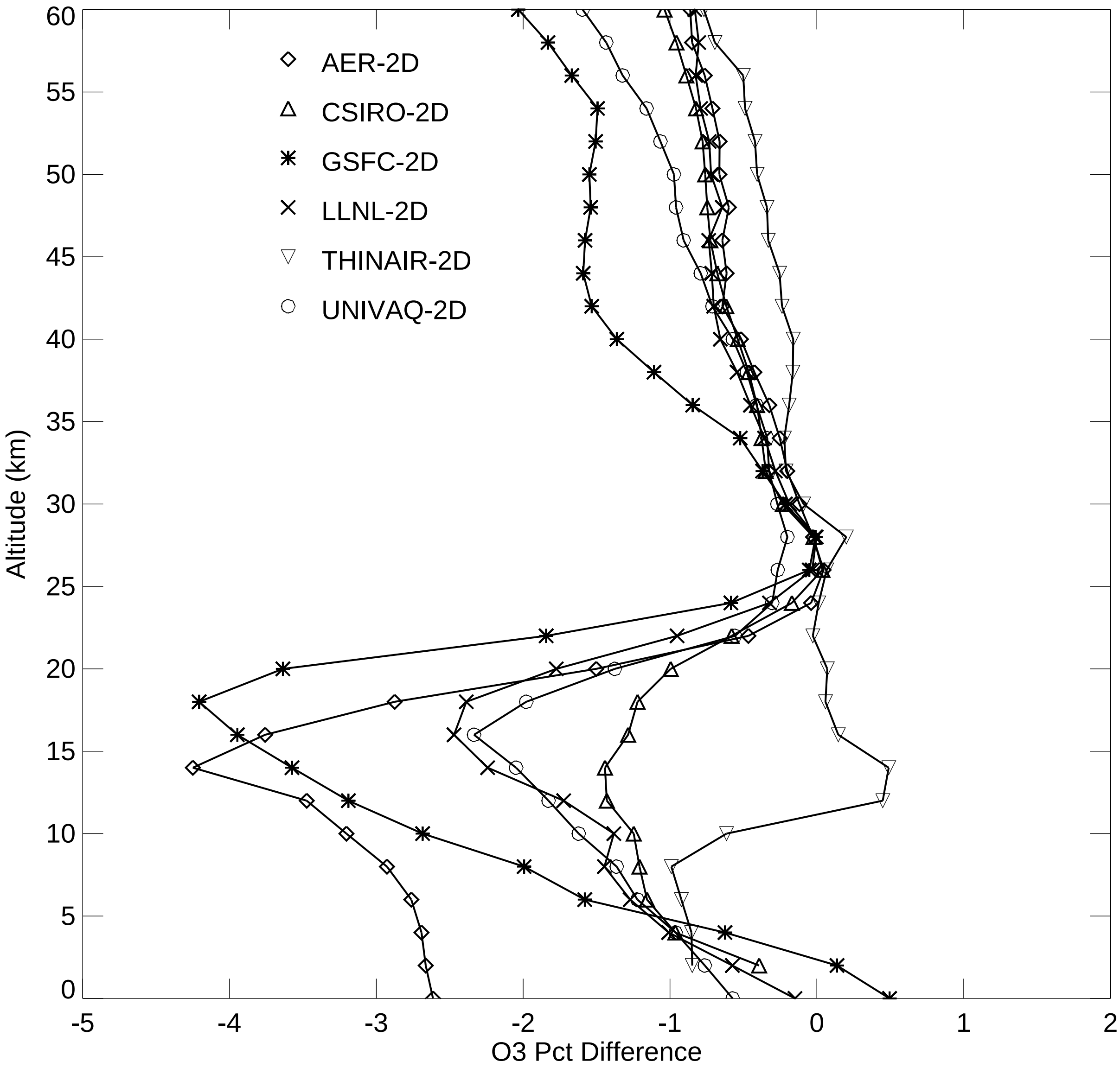

Figure 4.125: Calculated perturbations to O_3 (percent) as a function of altitude at 45^oN in June of 2015 due to emissions from a fleet of 500 HSCT aircraft with EI(NO_x)=5 and SA3 sulfate surface area under Scenario S1h relative to Scenario D.

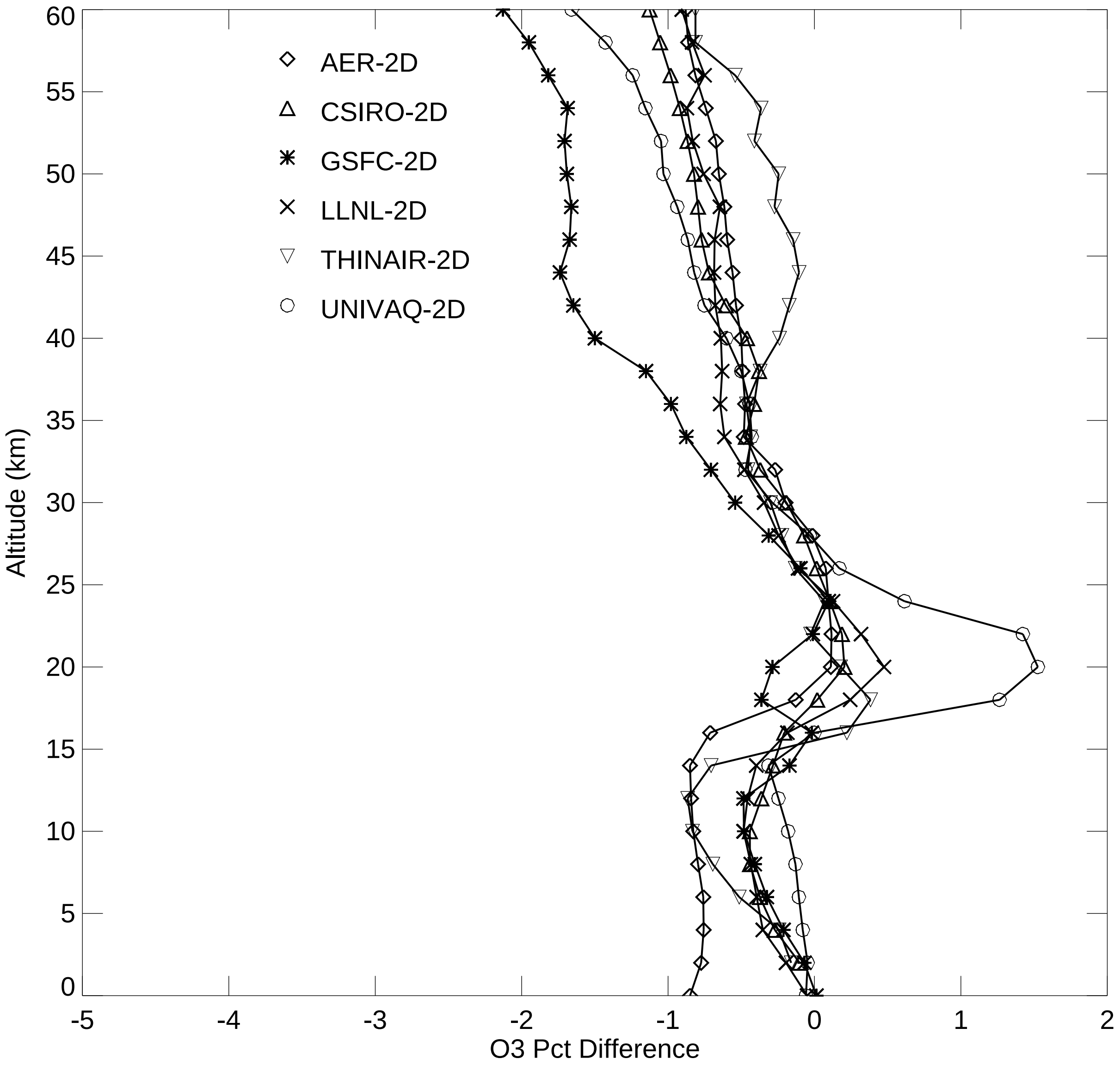

Figure 4.126: Calculated perturbations to O_3 (percent) as a function of altitude at the equator in June of 2015 due to emissions from a fleet of 500 HSCT aircraft with EI(NO_x)=5 and SA3 sulfate surface area under Scenario S1h relative to Scenario D.

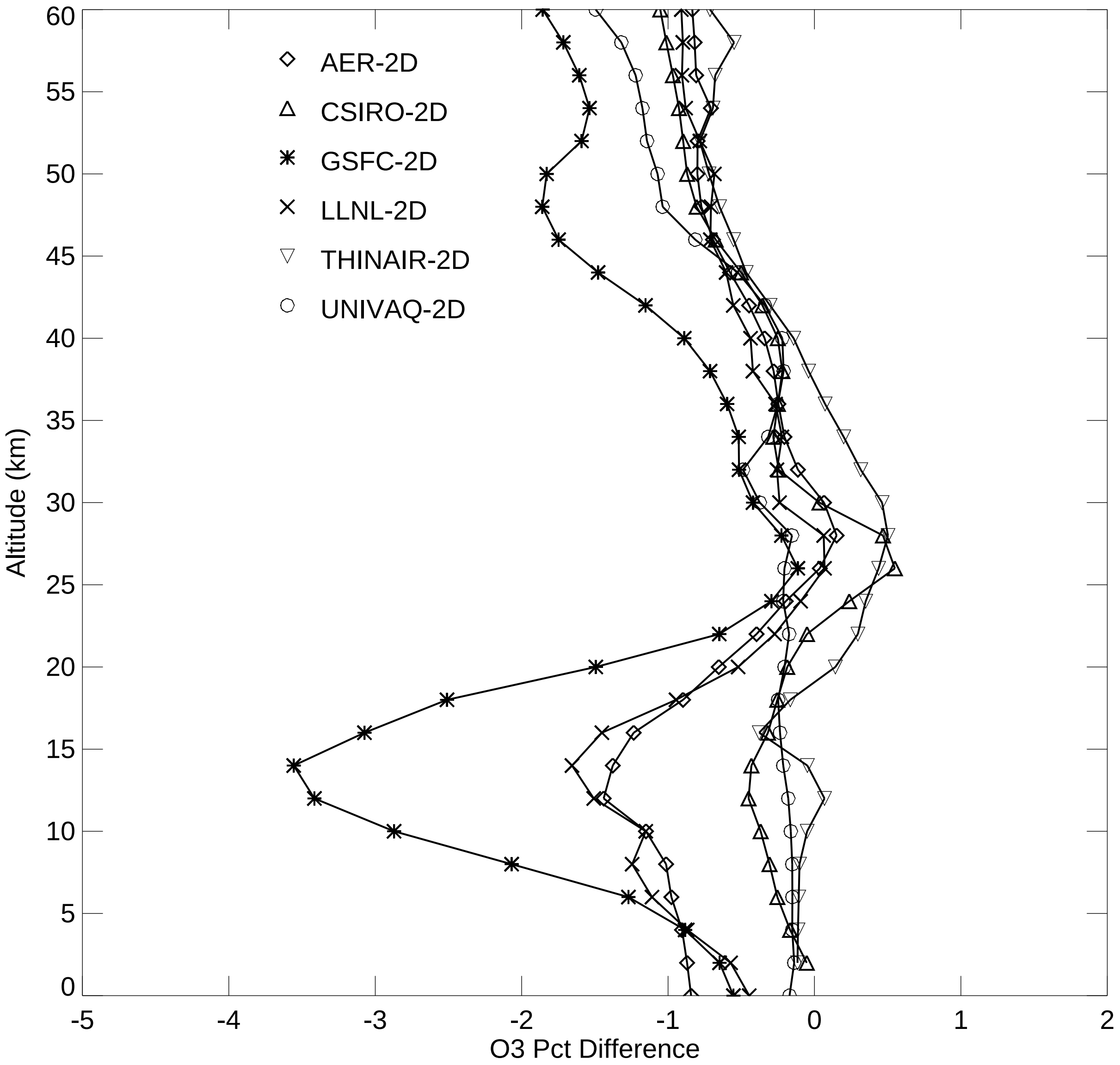

Figure 4.127: Calculated perturbations to O_3 (percent) as a function of altitude at 45^{o}S in June of 2015 due to emissions from a fleet of 500 HSCT aircraft with EI(NO_x)=5 and SA3 sulfate surface area under Scenario S1h relative to Scenario D.

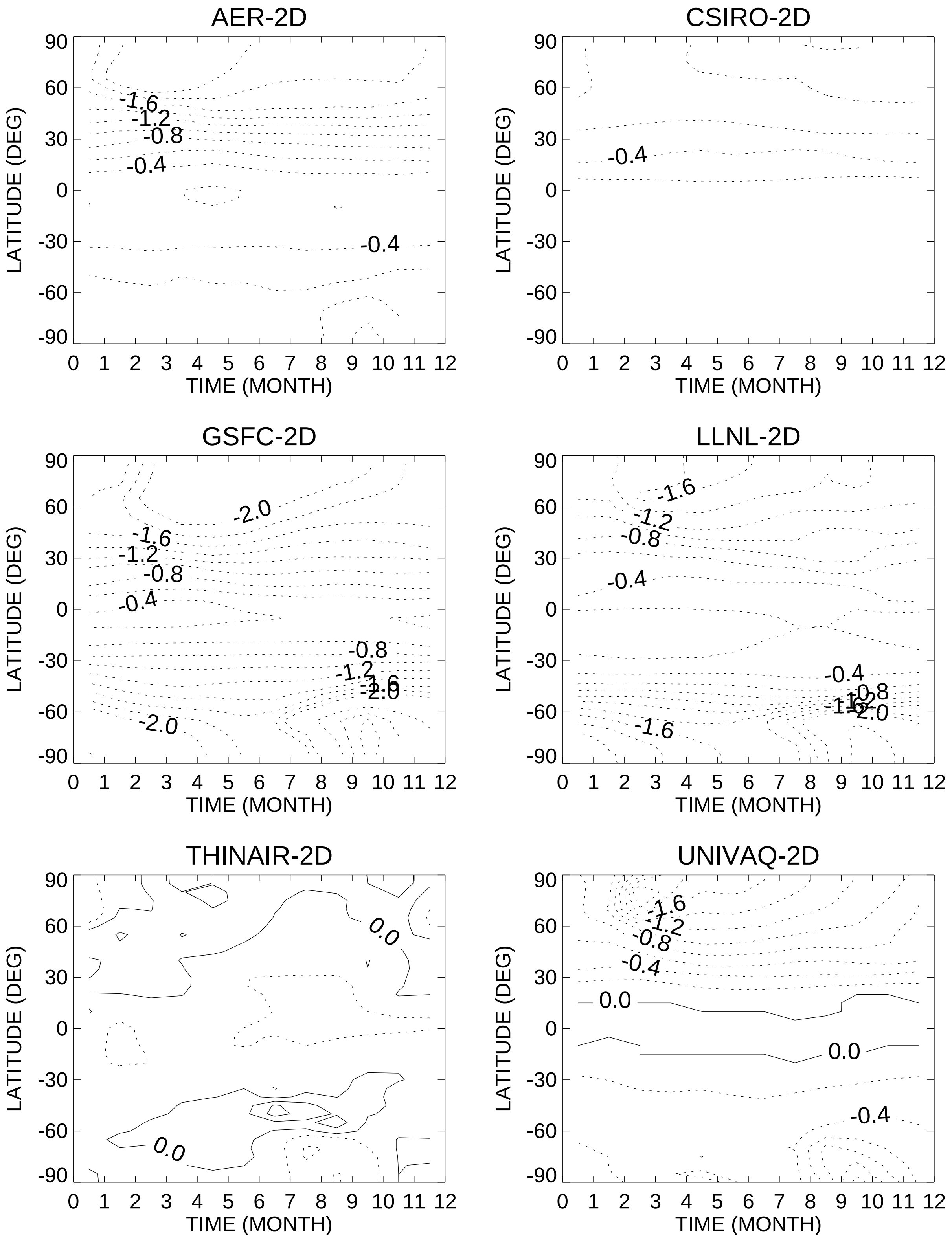

Figure 4.128: Calculated perturbations to column O_3 (percent) as a function of latitude and season in 2015 due to emissions from a fleet of 500 HSCT aircraft with $EI(NO_x)=5$ and SA3 sulfate surface area under Scenario S1h relative to Scenario D. Contours are -5, -4, -3, and -2.0 to 0.4 by 0.2.

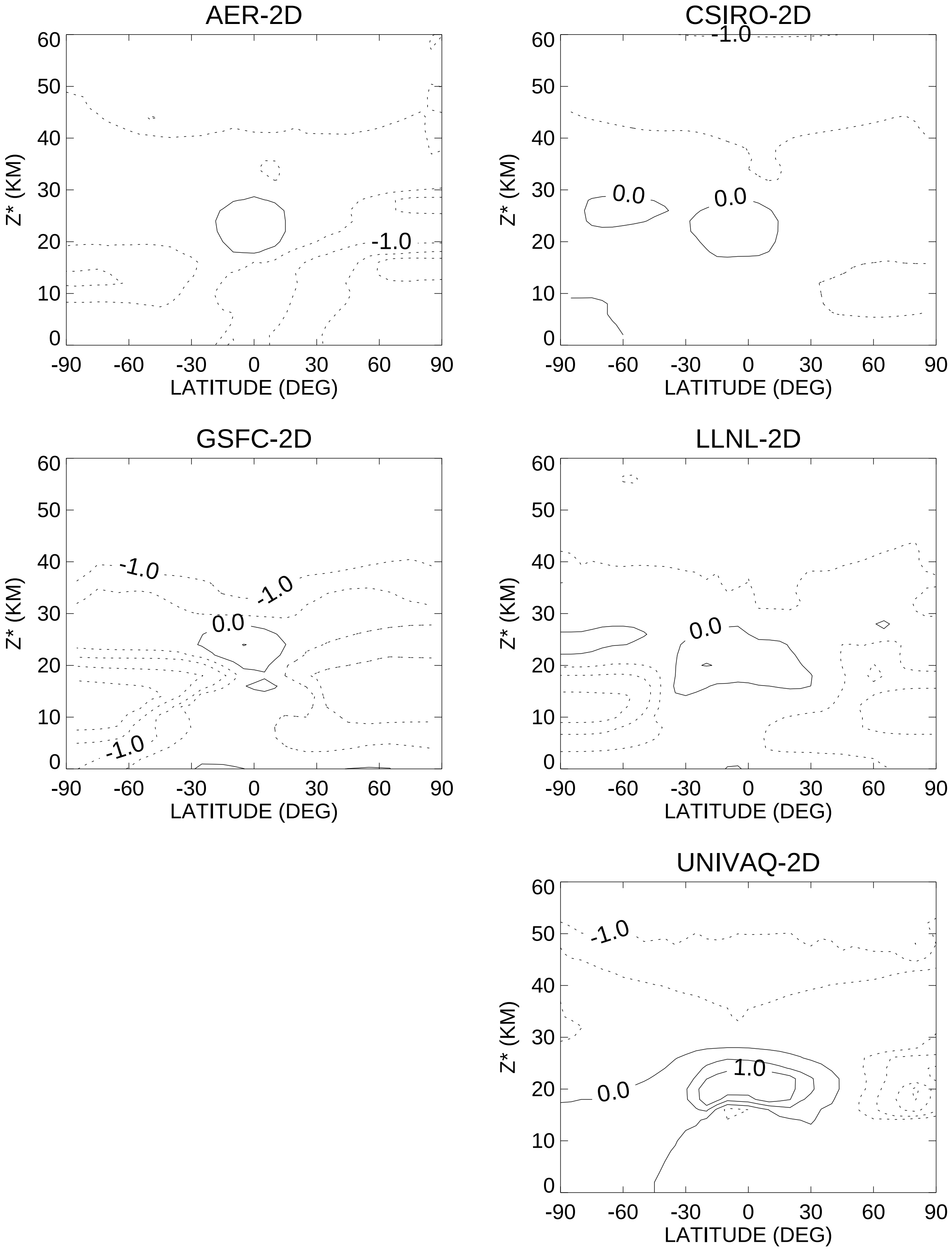

Figure 4.129: Calculated perturbations to O_3 (percent) as a function of latitude and altitude in March of 2015 due to emissions from a fleet of 500 HSCT aircraft with $EI(NO_x)=5$ and SA5 sulfate surface area under Scenario S1k relative to Scenario D. Contours are -3, -2, -1, -0.5, 0, 0.5, 1.

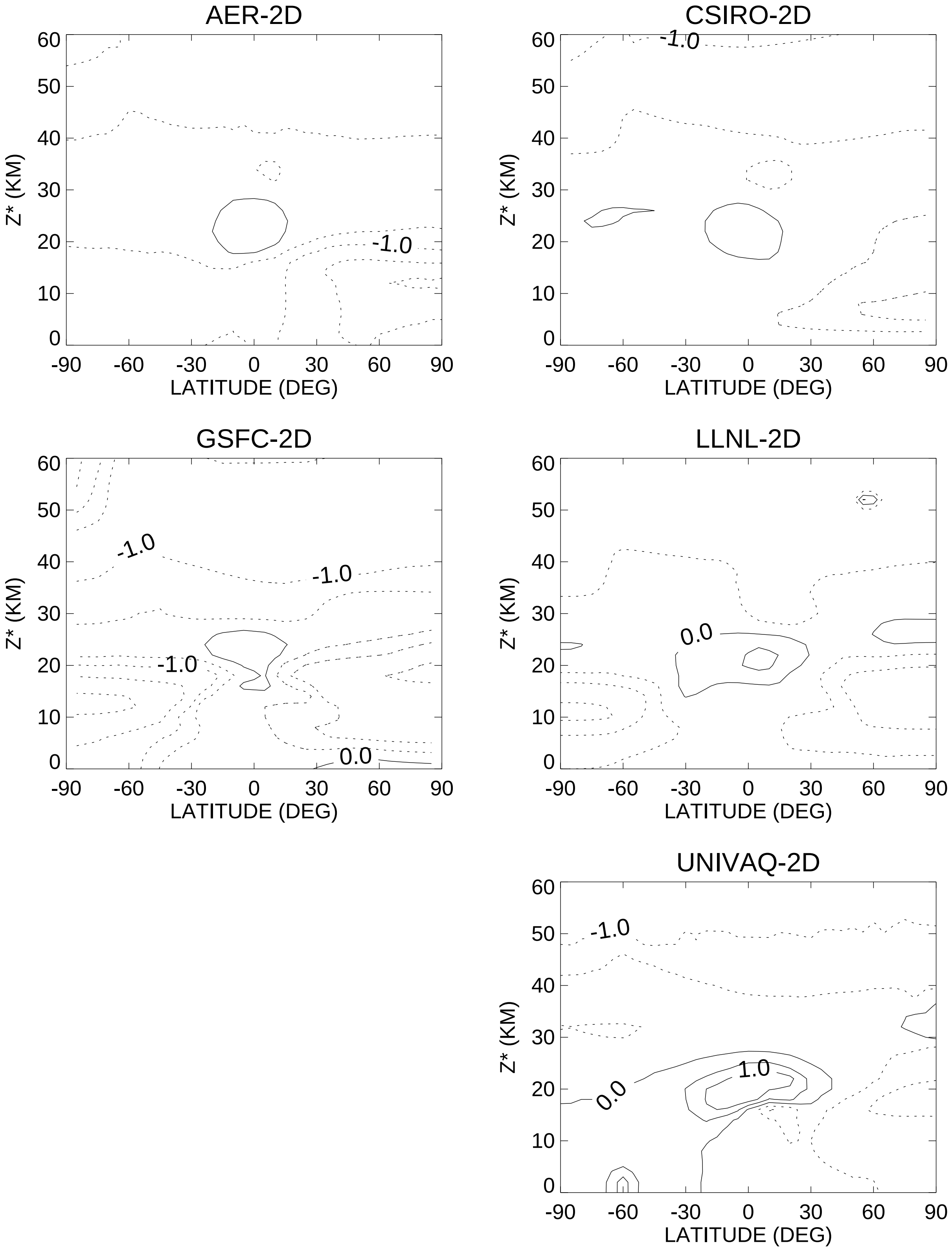

Figure 4.130: Calculated perturbations to O_3 (percent) as a function of latitude and altitude in June of 2015 due to emissions from a fleet of 500 HSCT aircraft with EI(NO_x)=5 and SA5 sulfate surface area under Scenario S1k relative to Scenario D. Contours are -3, -2, -1, -0.5, 0, 0.5, 1.

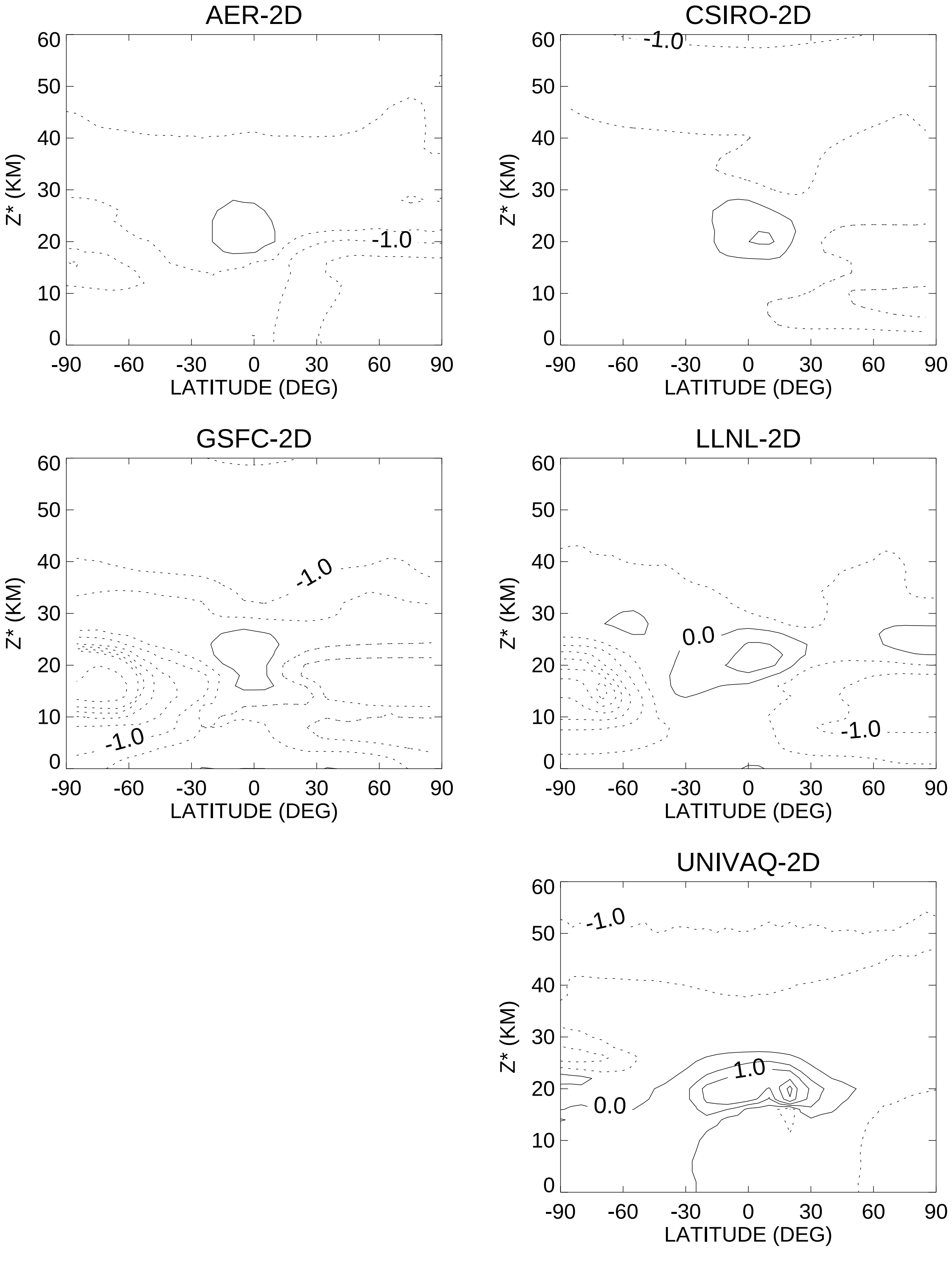

Figure 4.131: Calculated perturbations to O_3 (percent) as a function of latitude and altitude in October of 2015 due to emissions from a fleet of 500 HSCT aircraft with $EI(NO_x)=5$ and SA5 sulfate surface area under Scenario S1k relative to Scenario D. Contours are -10, -5, -4, -3, -2, -1, -0.5, 0, 0.5, 1, 2, 3.

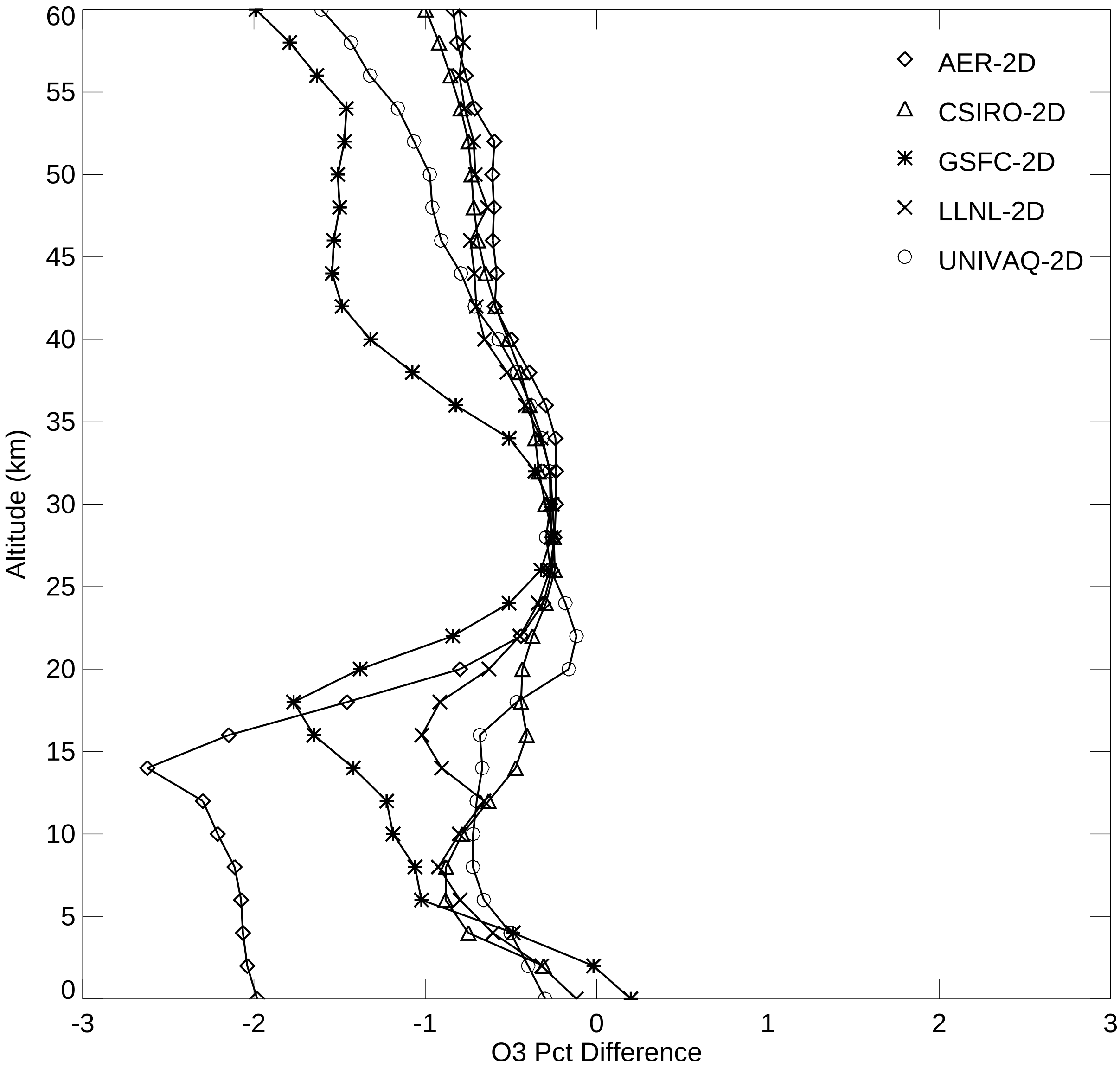

Figure 4.132: Calculated perturbations to O_3 (percent) as a function of altitude at 45^{o}N in June of 2015 due to emissions from a fleet of 500 HSCT aircraft with EI(NO_x)=5 and SA5 sulfate surface area under Scenario S1k relative to Scenario D.

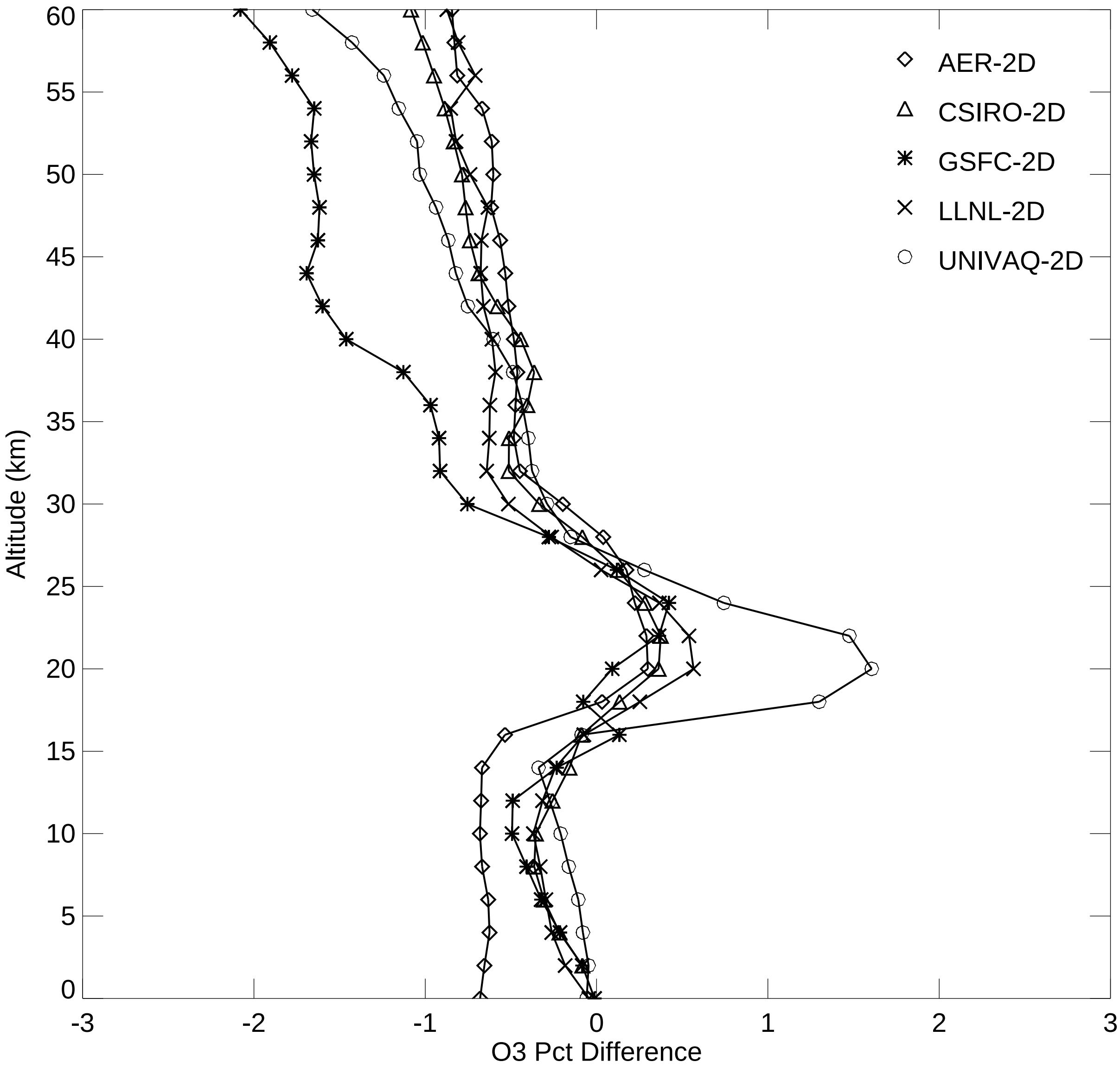

Figure 4.133: Calculated perturbations to O_3 (percent) as a function of altitude at the equator in June of 2015 due to emissions from a fleet of 500 HSCT aircraft with $EI(NO_x)=5$ and SA5 sulfate surface area under Scenario S1k relative to Scenario D.

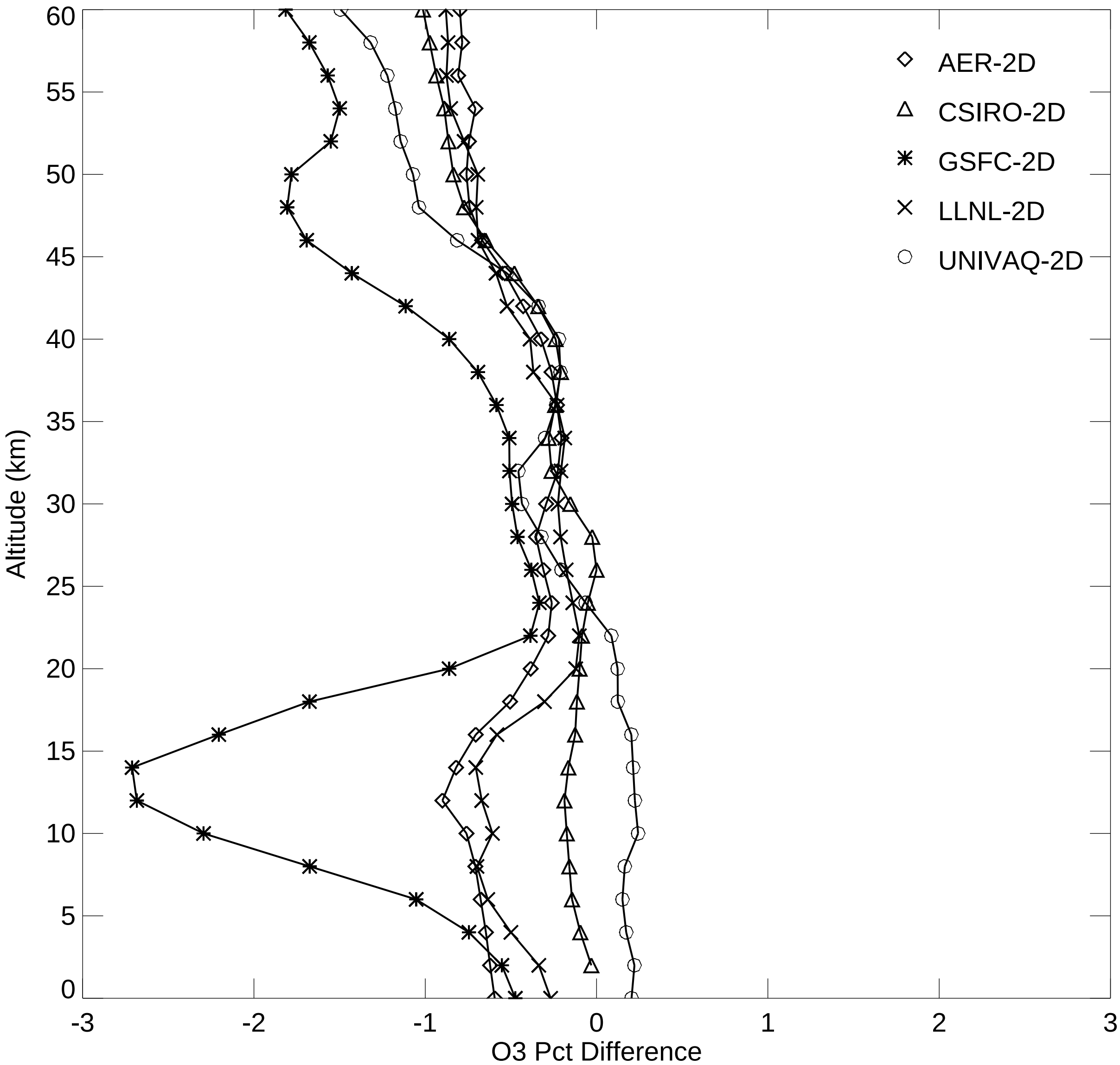

Figure 4.134: Calculated perturbations to O_3 (percent) as a function of altitude at 45^{o}S in June of 2015 due to emissions from a fleet of 500 HSCT aircraft with EI(NO_x)=5 and SA5 sulfate surface area under Scenario S1k relative to Scenario D.

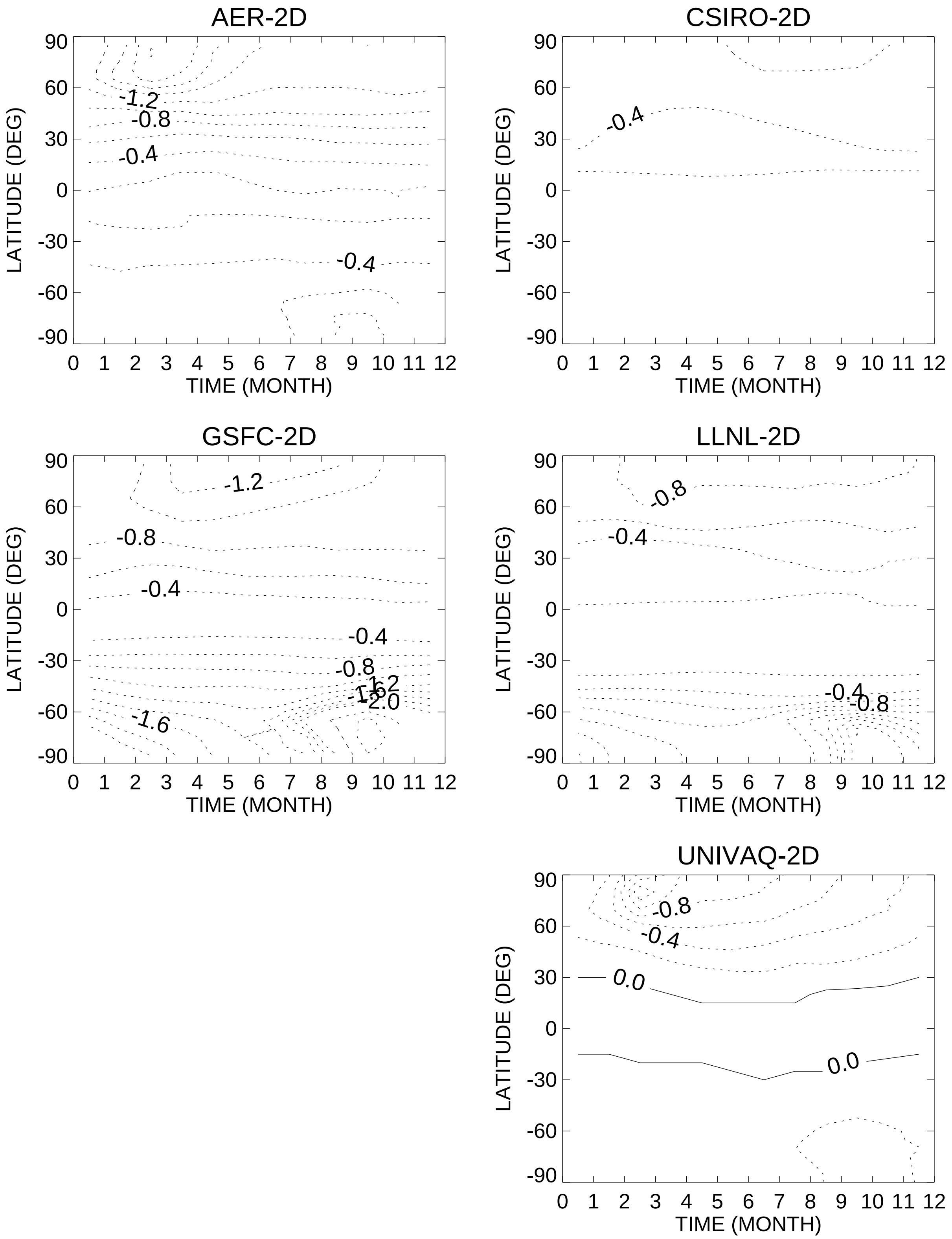

Figure 4.135: Calculated perturbations to column O_3 (percent) as a function of latitude and season in 2015 due to emissions from a fleet of 500 HSCT aircraft with EI(NO_x)=5 and SA5 sulfate surface area under Scenario S1k relative to Scenario D. Contours are -4, -3, and -2 to 0 by 0.2.

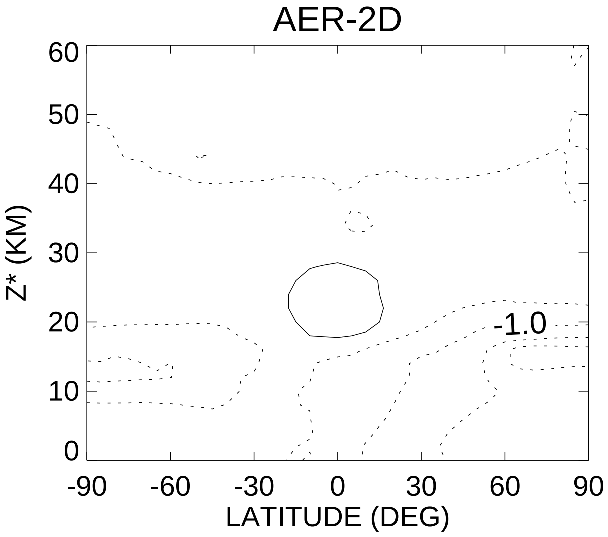

Figure 4.136: Calculated perturbations to O_3 (percent) as a function of latitude and altitude in March of 2015 due to emissions from a fleet of 500 HSCT aircraft with EI(NO_x)=5 and SA7 sulfate surface area under Scenario S1l relative to Scenario D. Contours are -3, -2, -1, -0.5, 0.

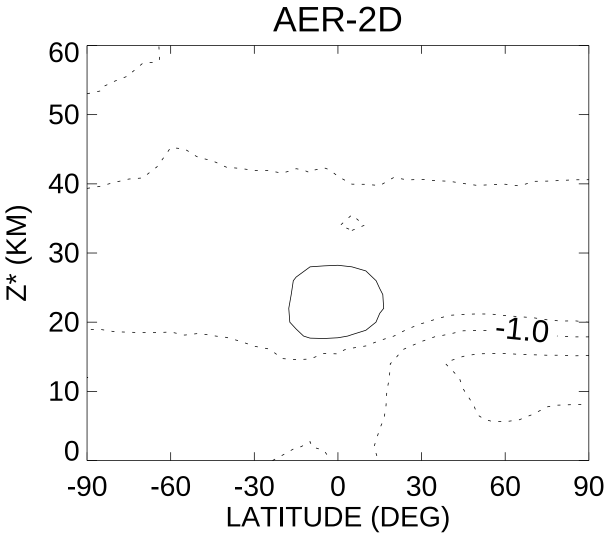

Figure 4.137: Calculated perturbations to O_3 (percent) as a function of latitude and altitude in June of 2015 due to emissions from a fleet of 500 HSCT aircraft with EI(NO_x)=5 and SA7 sulfate surface area under Scenario S1l relative to Scenario D. Contours are -2, -1, -0.5, 0.

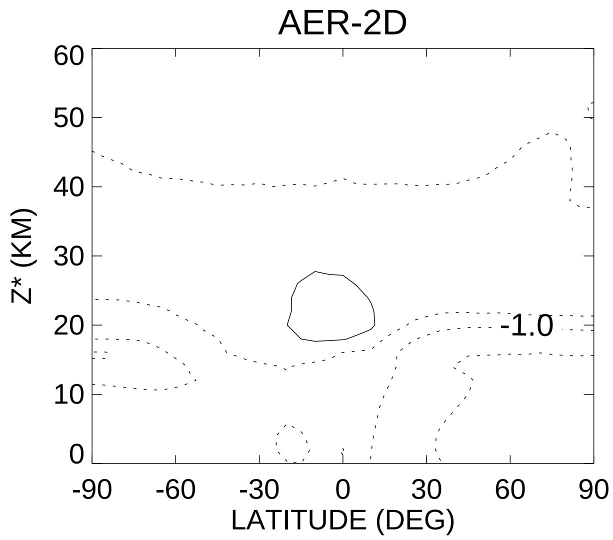

Figure 4.138: Calculated perturbations to O_3 (percent) as a function of latitude and altitude in October of 2015 due to emissions from a fleet of 500 HSCT aircraft with EI(NO_x)=5 and SA7 sulfate surface area under Scenario S1l relative to Scenario D. Contours are -2, -1, -0.5, 0.

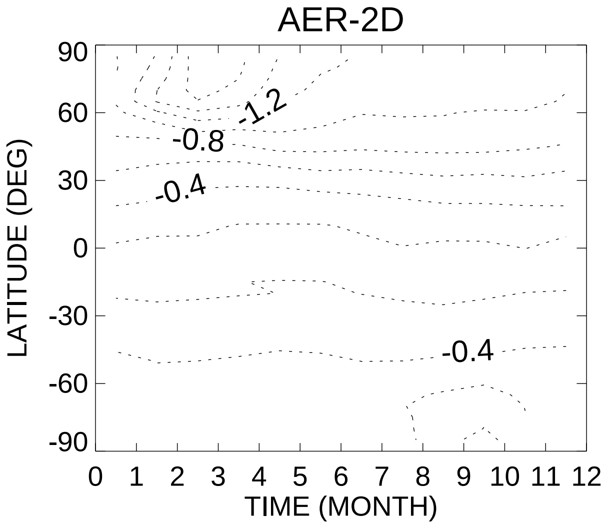

Figure 4.139: Calculated perturbations to column O_3 (percent) as a function of latitude and season in 2015 due to emissions from a fleet of 500 HSCT aircraft with EI(NO_x)=5 and SA7 sulfate surface area under Scenario S1l relative to Scenario D. Contours are -1.6 to -0.2 by 0.2.

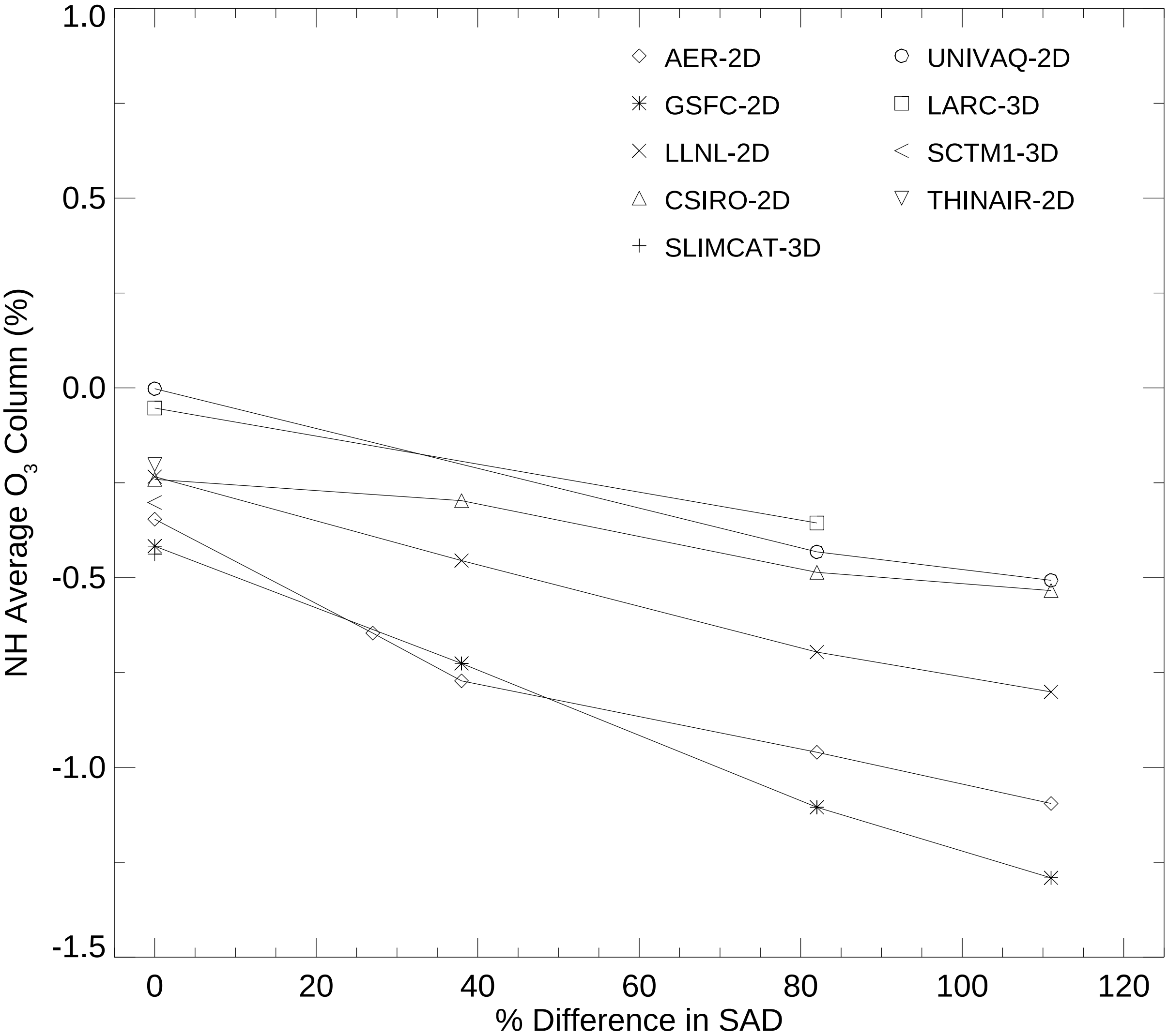

Figure 4.140: Northern hemisphere annual average total O_3 column change (percent) as a function of the percent change in aerosol surface area density in the region from 14 to 21 km and from 33^{o}N to 90^{o}N. The HSCT fleet consisted of 500 aircraft operating in 2015 with EI(NO_x)=5 and SA0 as the background surface area density.

4.3.3 Scenarios with Modified Cruise Altitude (S2a-e)

The impact of variations in cruise altitude on HSCT ozone perturbation is explored in this set of scenarios. Scenario S2a has the cruise altitude raised by 2 km, while Scenarios S2b-S2e have the cruise altitude lowered by 2 km. Based on the increased H_2O and NO_y perturbations found at higher cruise altitudes, the ozone response to HSCT should be larger for higher cruise altitudes and smaller for lower cruise altitudes.

Figures 4.141, 4.142, and 4.143 show ozone change as a function of latitude and altitude for March, June, and October for Scenario S2a relative to Scenario D. Scenario S2a includes 500 HSCT aircraft operating in 2015 with SA0 sulfate surface area density, no sulfur emissions, and a cruise altitude raised by 2 km above that used in the standard scenarios (S1a-S1l). Ozone depletion is increased in all models relative to Scenario S1c in both the lower and upper stratosphere. Figures 4.144, 4.145, and 4.146 show vertical profiles of ozone perturbation at 45^oN, the equator, and 45^oS in June. Changes in ozone column for Scenario S2a are shown in Figure 4.147. Ozone column depletion for Scenario S2a is greater than for Scenario S1c, though the THINAIR and UNIVAQ models still show regions of total ozone increase. For the AER, GSFC, LLNL, and CSIRO models, the northern hemisphere annual average percentage ozone depletion for Scenario S2a is more than double that of Scenario S1c.

Scenario S2b includes 500 HSCT aircraft in 2015 operating at 2 km below the standard cruise altitude with $EI(NO_x)=5$. This scenario produced smaller perturbations in H_2O and NO_y than a similar scenario (S1c) at the standard cruise altitude. Figures 4.148- 4.150 show ozone perturbations as a function of latitude and altitude for 3 months. Ozone depletion is considerably reduced compared with Scenario S1c. The CSIRO and LLNL models show depletion less than 0.5% everywhere in the stratosphere and ozone increases near the tropopause at all latitudes. Ozone changes as a function of altitude only for 45^oN, the equator, and 45^oS are shown in Figures 4.151-4.153. The large southern hemisphere ozone depletion calculated by the GSFC model is greatly reduced. Figure 4.154 shows changes in ozone column for Scenario S2b relative to Scenario D. Ozone column changes are less than 0.5% everywhere for all models except GSFC, which show a maximum 1% depletion near the south pole in September-October.

The sensitivity of ozone response to HSCT to changes in cruise altitude is depicted in Figures 4.155 and 4.156 for the northern and southern hemispheres, respectively. The annual average hemispheric ozone column perturbation is plotted against cruise altitude changes of -2 km (S2b-D), 0 km (S1c-D), and +2 km (S2a-D) with 500 HSCT aircraft, $EI(NO_x)=5$, and SA0. All models show a substantially more negative ozone response for higher cruise altitude in the northern hemisphere. For lower cruise altitudes, a reduced (near zero for -2 km cruise altitude) ozone response is seen. In the southern hemisphere, the GSFC model show a large sensitivity to cruise altitude and the LLNL model a moderate sensitivity. The other models show small sensitivity.

Scenario S2c is similar to Scenario S2b but with $EI(NO_x)=10$. Only the AER, CSIRO, GSFC, and LLNL models performed calculations for this case. Figures 4.157, 4.158, and 4.159 show changes in ozone as a function of latitude and altitude for this scenario for March, June, and October. The CSIRO, GSFC, and LLNL models show ozone increases in the troposphere due to substantial NO_x emissions at low altitude. Changes in ozone column for Scenario S2c relative to Scenario D are shown in Figure 4.160. All models show some areas of ozone increase. Ozone column depletion is greater than 0.5% only for the AER model at the springtime northern pole and the GSFC model at the springtime southern pole.

Scenario S2d is similar to S2b and S2c but with $EI(NO_x)=15$. Only the GSFC model performed this calculation. Figures 4.161, 4.162, and 4.163 show changes in ozone for March, June, and October from the GSFC model. Tropospheric ozone increases are as much as 6%. Stratospheric ozone depletions are up to 1%. Change in column ozone, shown in Figure 4.164, are mostly positive.

Sensitivity to aircraft NO_x emission index with 500 HSCT aircraft operating at 2 km below the standard cruise altitude in 2015 with SA0 sulfate surface area density is shown in Figures 4.165 and 4.166. These plots show annual average hemispheric ozone perturbation as a function of $EI(NO_x)$ for Scenarios S2b-S2d. The AER model shows slightly greater ozone depletion at $EI(NO_x)=10$ than at $EI(NO_x)=5$ in both hemispheres. The LLNL and CSIRO models show slightly less depletion or no change between $EI(NO_x)=5$ and $EI(NO_x)=10$. The GSFC model show a substantial reduction in ozone depletion from $EI(NO_x)=5$ to $EI(NO_x)=15$. In contrast, the GSFC model showed the opposite trend at the standard cruise altitude in the northern hemisphere.

Scenario S2e represents a fleet of 1000 HSCT aircraft operating at 2 km below the nominal cruise altitude in 2015 with $EI(NO_x)=5$. Changes in ozone as a function of latitude and altitude are shown in Figures 4.167-4.169. The HSCT NO_x emissions for this scenario are similar to S2c with 500 aircraft and $EI(NO_x)=10$, but the H_2O emissions are twice as large as that case. Stratospheric ozone depletion is greater than for Scenario S2c, and tropospheric ozone increases are much reduced. Figure 4.170 shows changes in ozone column for Scenario S2e relative to Scenario D. Ozone column depletion is greater for both Scenario S2b and S2c.

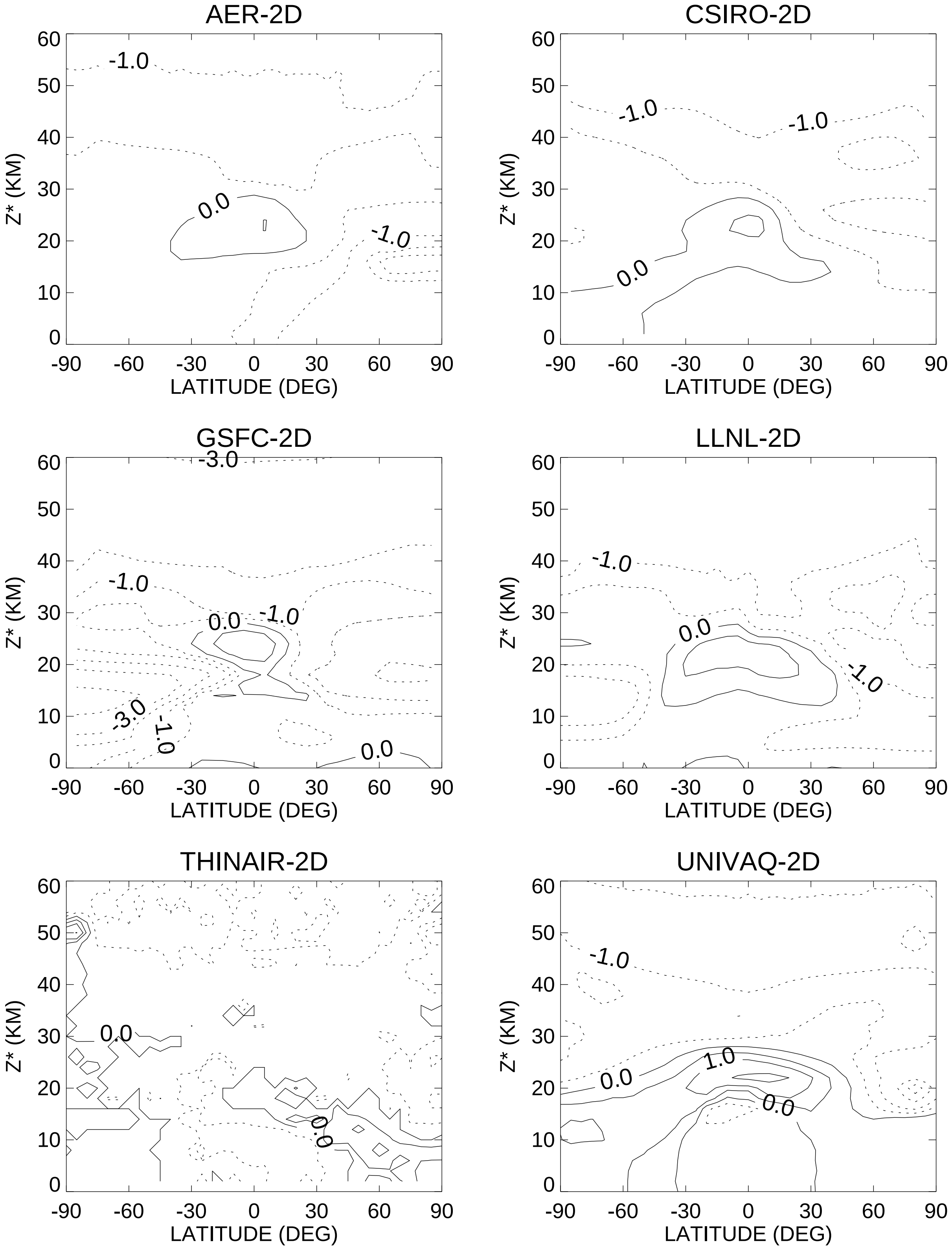

Figure 4.141: Calculated perturbations to O_3 (percent) as a function of latitude and altitude in March of 2015 due to emissions from a fleet of 500 HSCT aircraft operating at 2 km above nominal cruise altitude with EI(NO_x)=5 under Scenario S2a relative to Scenario D. Contours are -4, -3, -2, -1, -0.5, 0, 0.5, 1, 2.

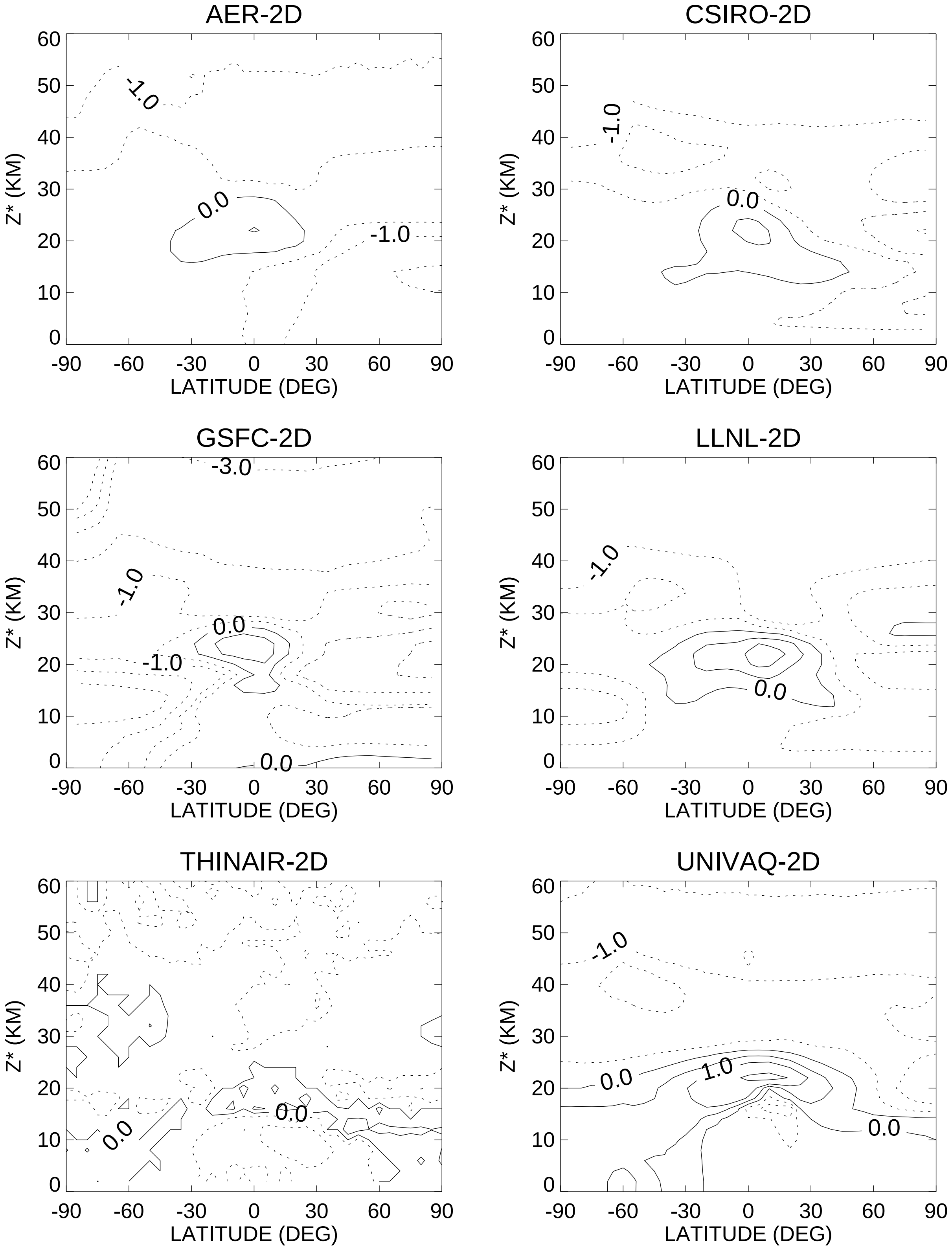

Figure 4.142: Calculated perturbations to O_3 (percent) as a function of latitude and altitude in June of 2015 due to emissions from a fleet of 500 HSCT aircraft operating at 2 km above nominal cruise altitude with $EI(NO_x)$=5 under Scenario S2a relative to Scenario D. Contours are -3, -2, -1, -0.5, 0, 0.5, 1, 2.

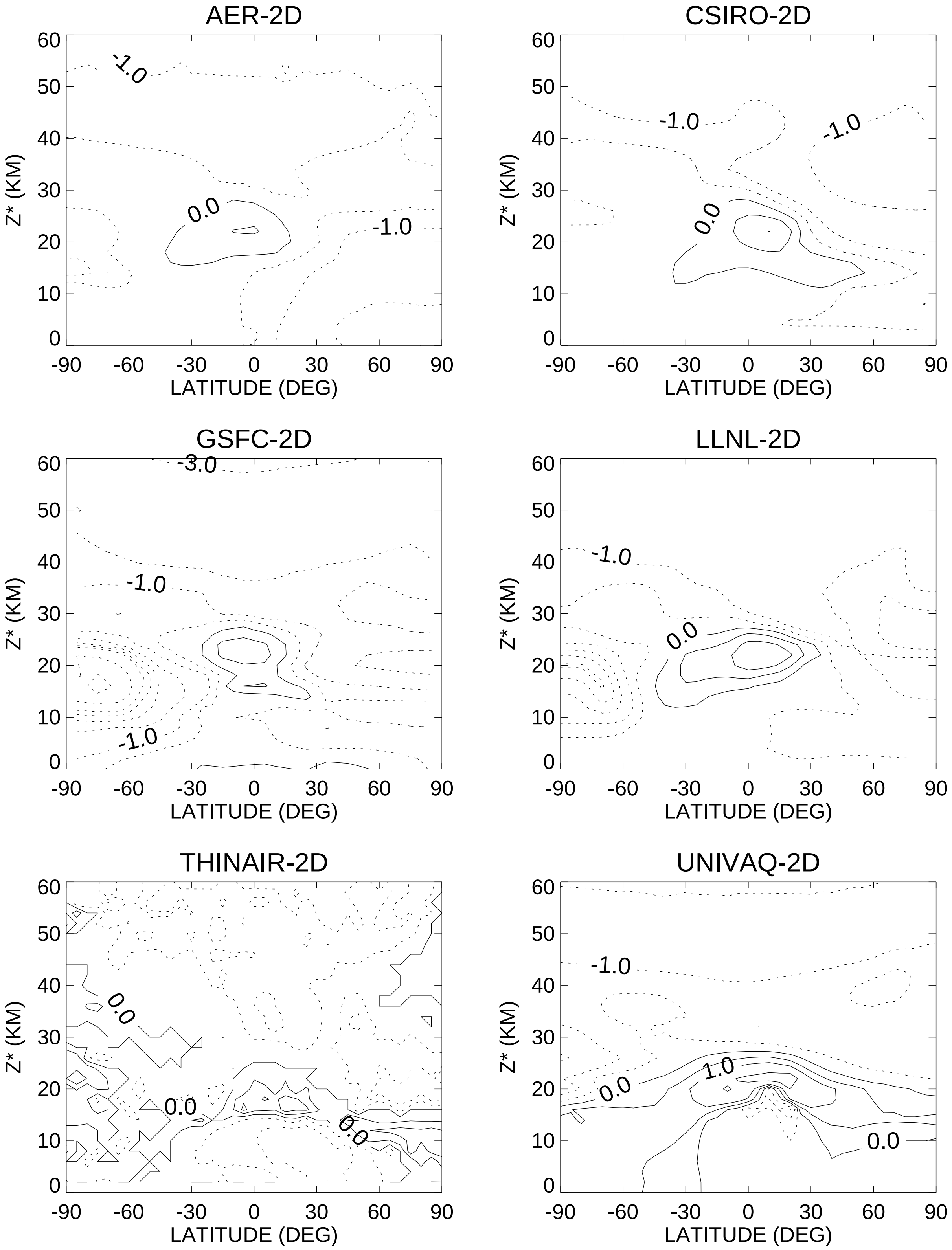

Figure 4.143: Calculated perturbations to O_3 (percent) as a function of latitude and altitude in October of 2015 due to emissions from a fleet of 500 HSCT aircraft operating at 2 km above nominal cruise altitude with EI(NO_x)=5 under Scenario S2a relative to Scenario D. Contours are -15, -10, -5, -4, -3, -2, -1, -0.5, 0, 0.5, 1, 2.

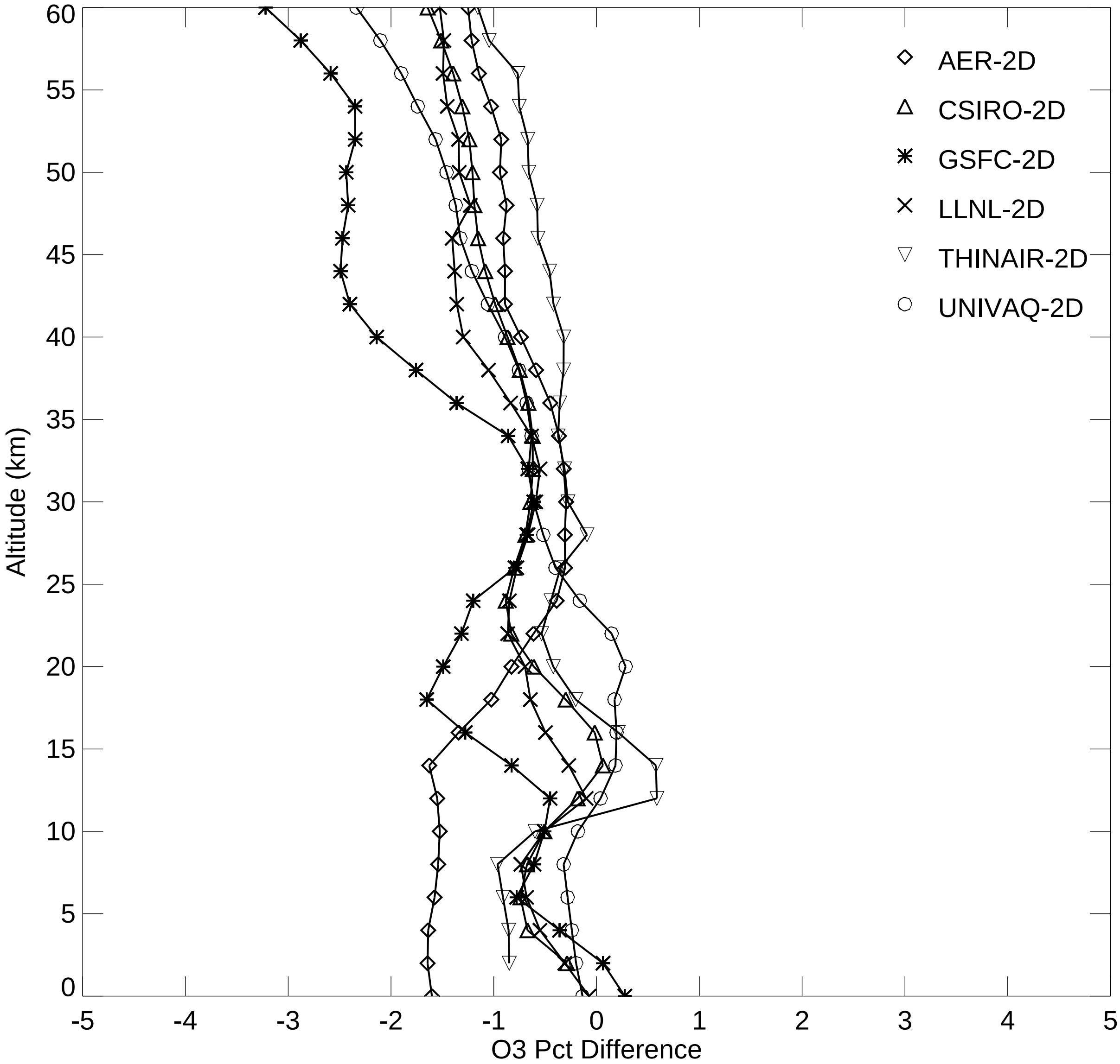

Figure 4.144: Calculated perturbations to O_3 (percent) as a function of altitude at 45^{o}N in June of 2015 due to emissions from a fleet of 500 HSCT aircraft operating at 2 km above nominal cruise altitude with EI(NO_x)=5 under Scenario S2a relative to Scenario D.

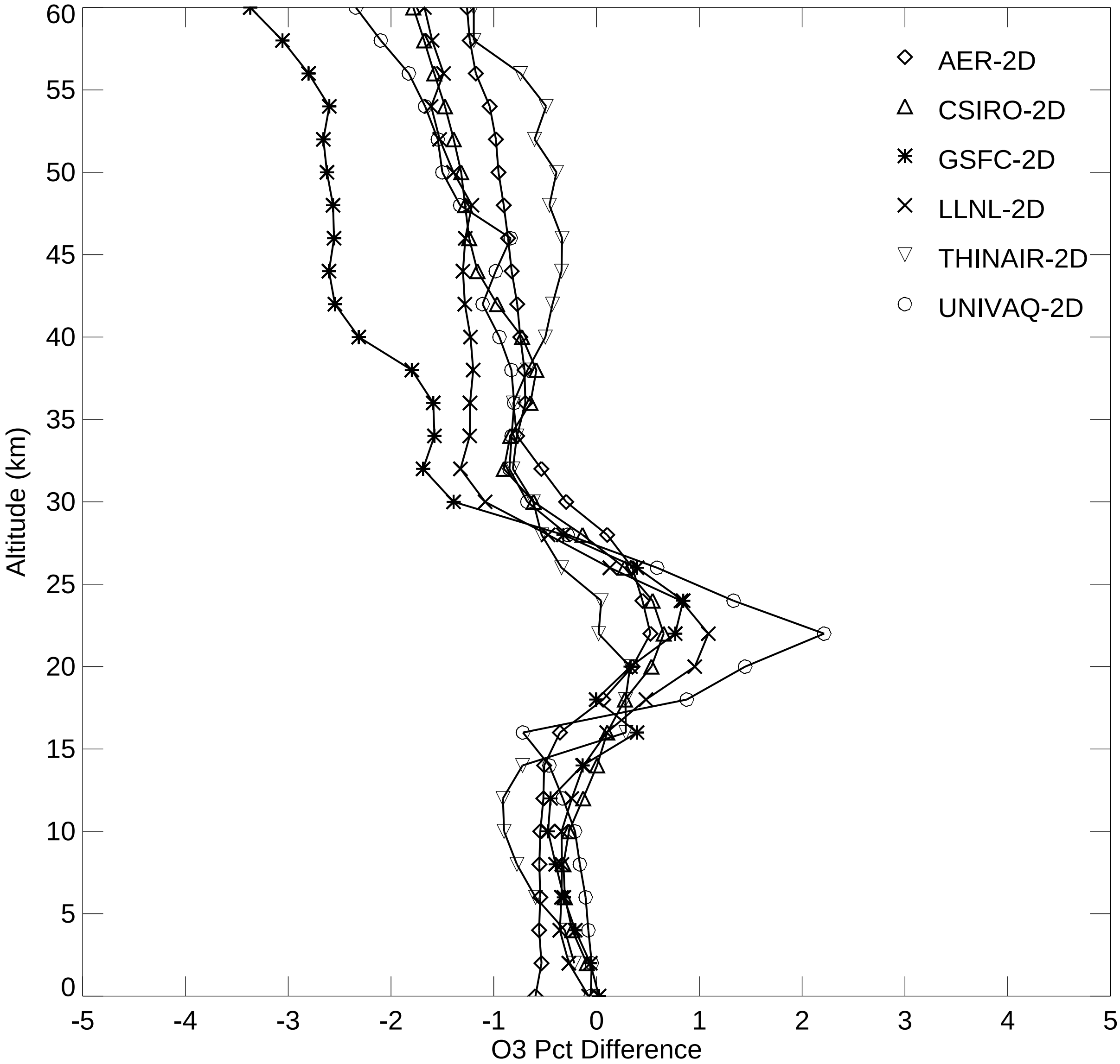

Figure 4.145: Calculated perturbations to O_3 (percent) as a function of altitude at the equator in June of 2015 due to emissions from a fleet of 500 HSCT aircraft operating at 2 km above nominal cruise altitude with EI(NO_x)=5 under Scenario S2a relative to Scenario D.

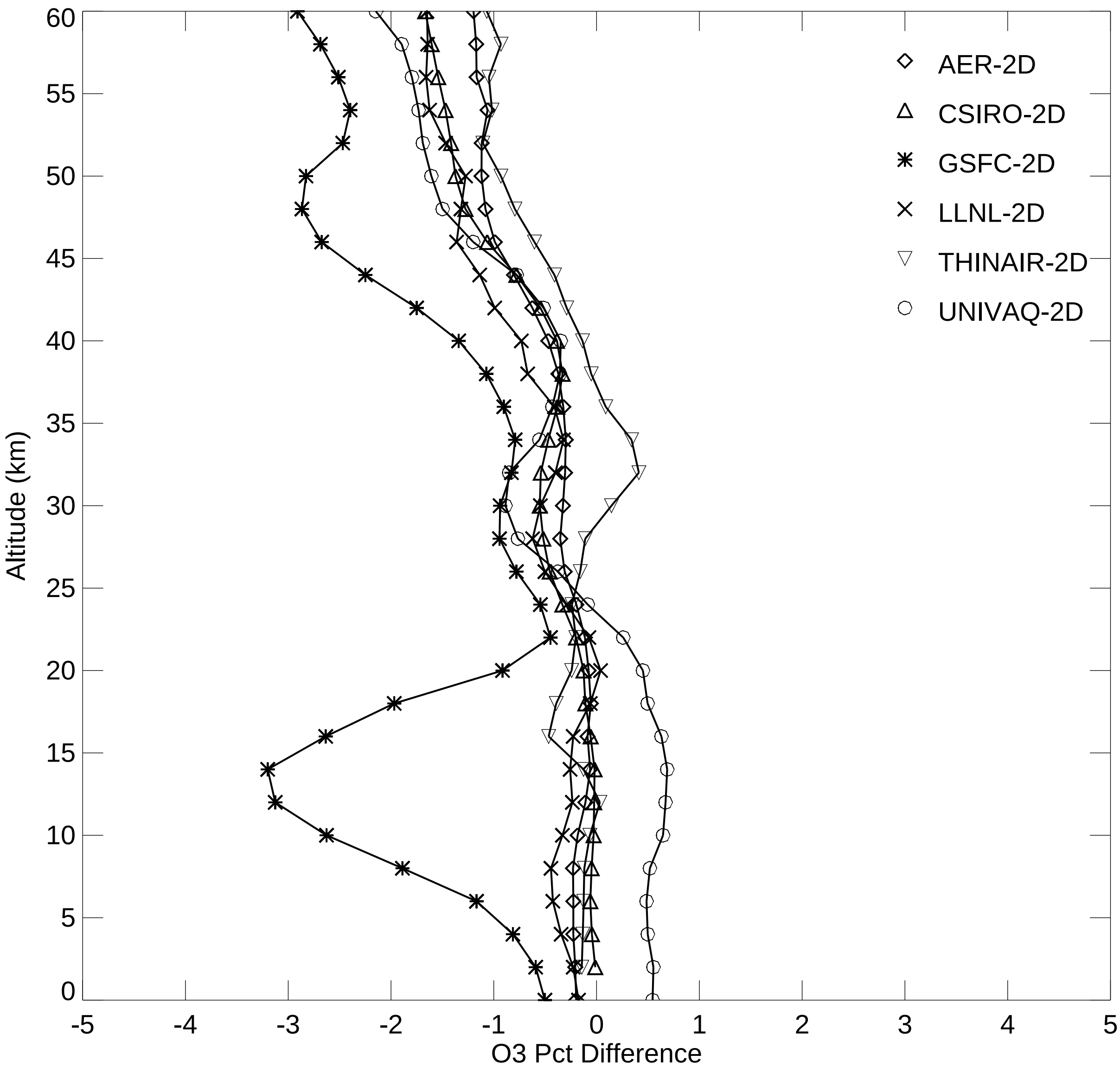

Figure 4.146: Calculated perturbations to O_3 (percent) as a function of altitude at 45^{o}S in June of 2015 due to emissions from a fleet of 500 HSCT aircraft operating at 2 km above nominal cruise altitude with EI(NO_x)=5 under Scenario S2a relative to Scenario D.

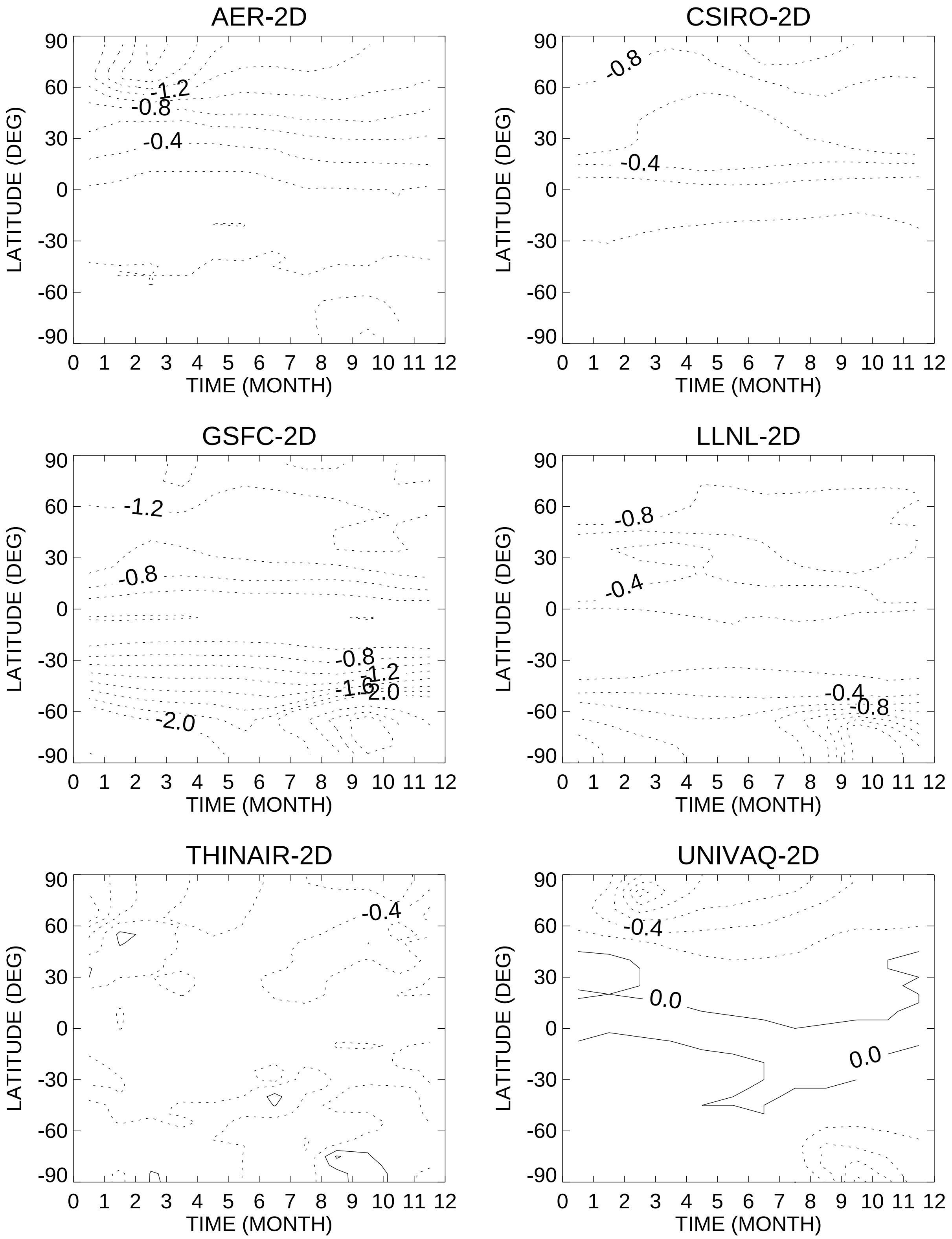

Figure 4.147: Calculated perturbations to column O_3 (percent) as a function of latitude and season in 2015 due to emissions from a fleet of 500 HSCT aircraft operating at 2 km above nominal cruise altitude with EI(NO_x)=5 under Scenario S2a relative to Scenario D. Contours are -5, -4, -3, and -2 to 0 by 0.2.

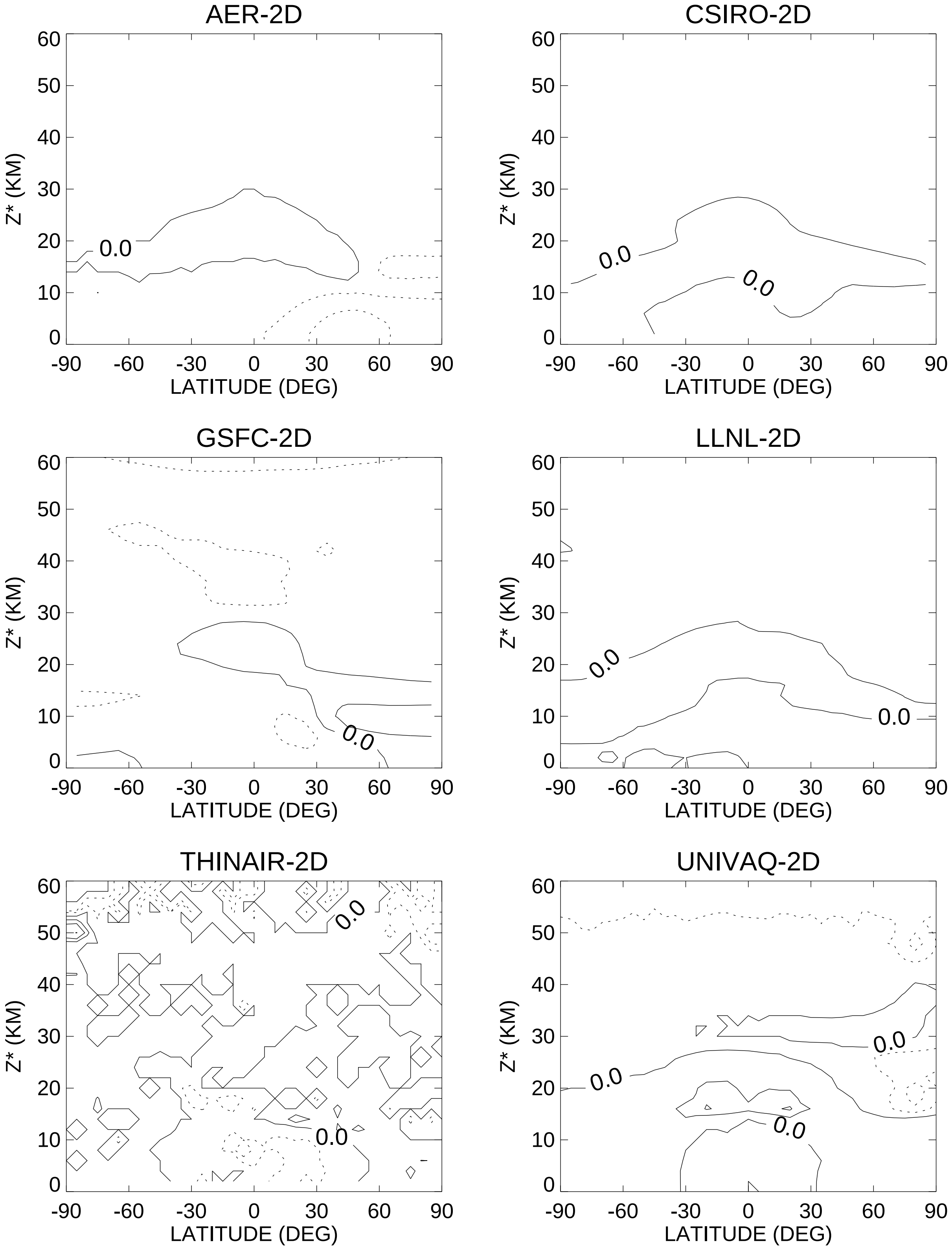

Figure 4.148: Calculated perturbations to O_3 (percent) as a function of latitude and altitude in March of 2015 due to emissions from a fleet of 500 HSCT aircraft operating at 2 km below nominal cruise altitude with EI(NO_x)=5 under Scenario S2b relative to Scenario D. Contours are -1, -0.5, 0, 0.5, 1.

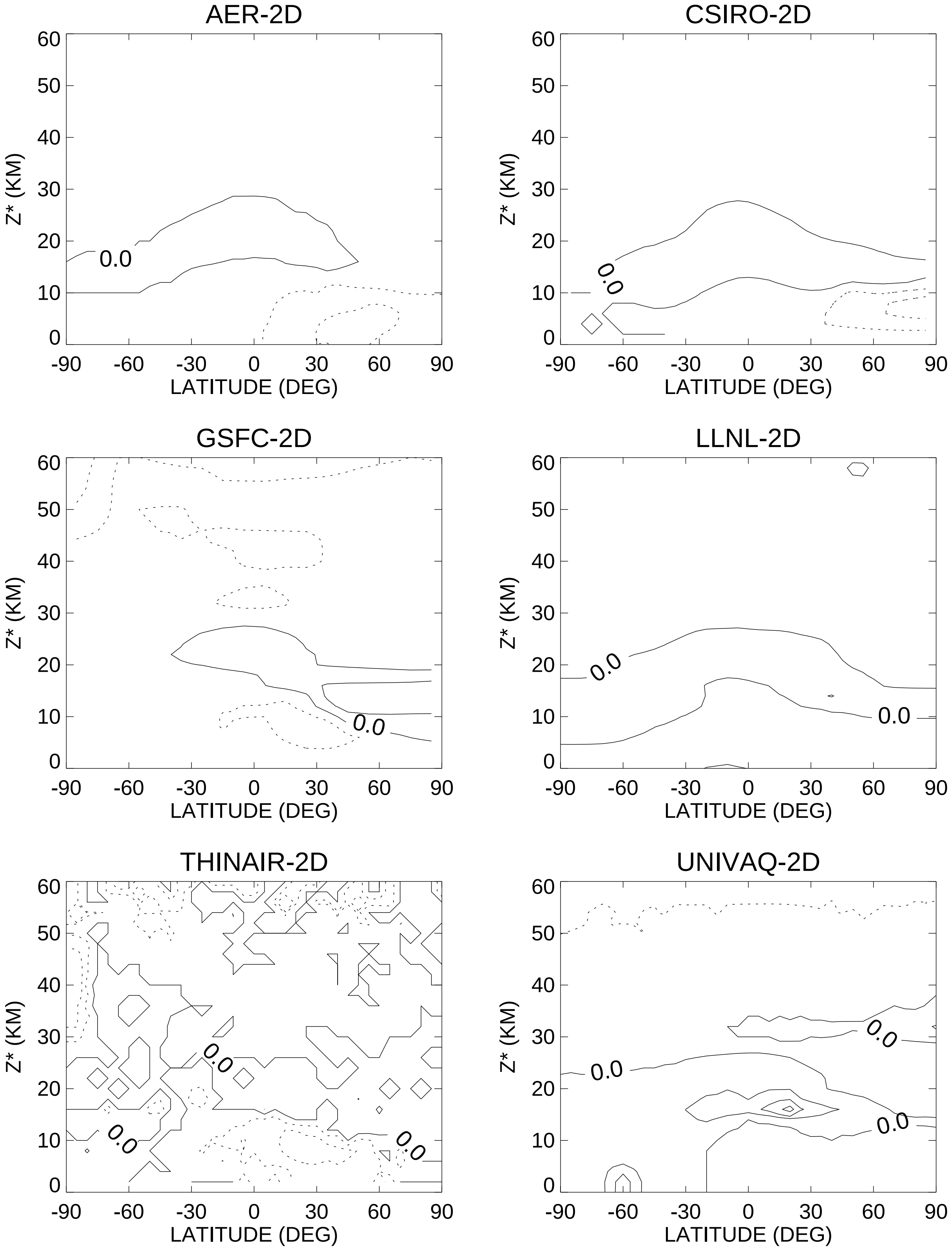

Figure 4.149: Calculated perturbations to O_3 (percent) as a function of latitude and altitude in June of 2015 due to emissions from a fleet of 500 HSCT aircraft operating at 2 km below nominal cruise altitude with $EI(NO_x)$=5 under Scenario S2b relative to Scenario D. Contours are -1, -0.5, 0, 0.5, 1, 2.

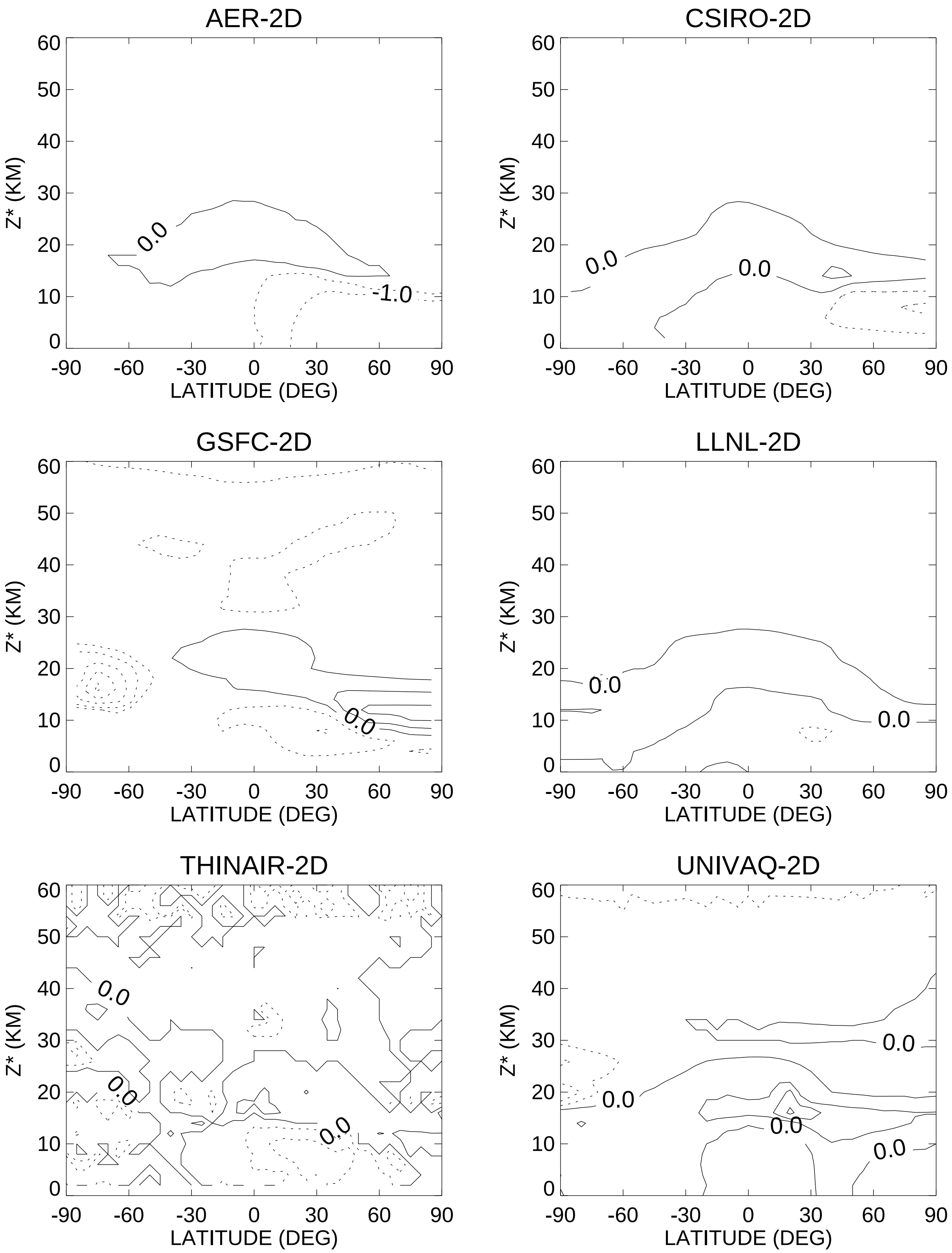

Figure 4.150: Calculated perturbations to O_3 (percent) as a function of latitude and altitude in October of 2015 due to emissions from a fleet of 500 HSCT aircraft operating at 2 km below nominal cruise altitude with EI(NO_x)=5 under Scenario S2b relative to Scenario D. Contours are -4, -3, -2,-1, -0.5, 0, 0.5, 1, 2.

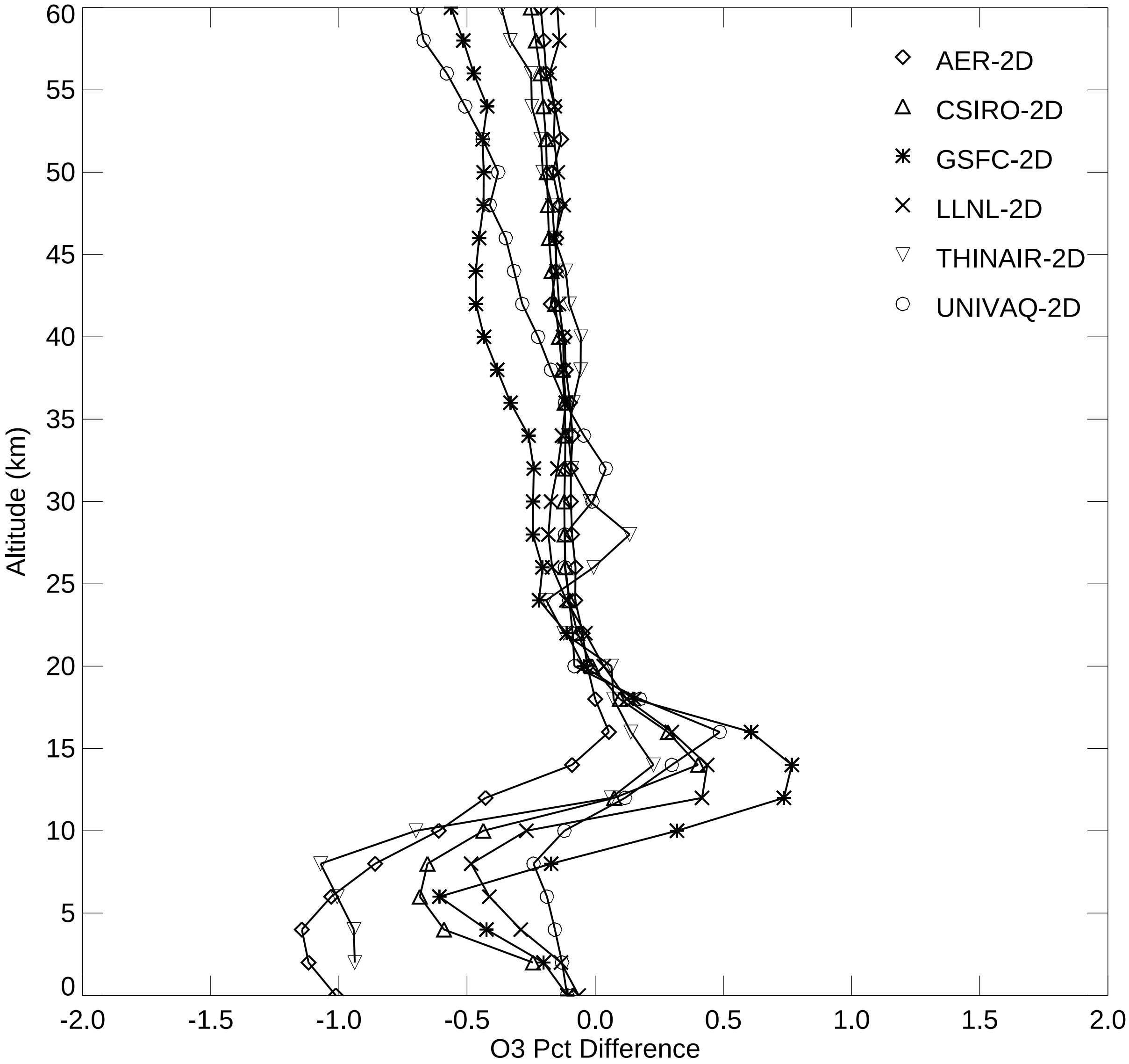

Figure 4.151: Calculated perturbations to O_3 (percent) as a function of altitude at 45^oN in June of 2015 due to emissions from a fleet of 500 HSCT aircraft operating at 2 km below nominal cruise altitude with EI(NO_x)=5 under Scenario S2b relative to Scenario D.

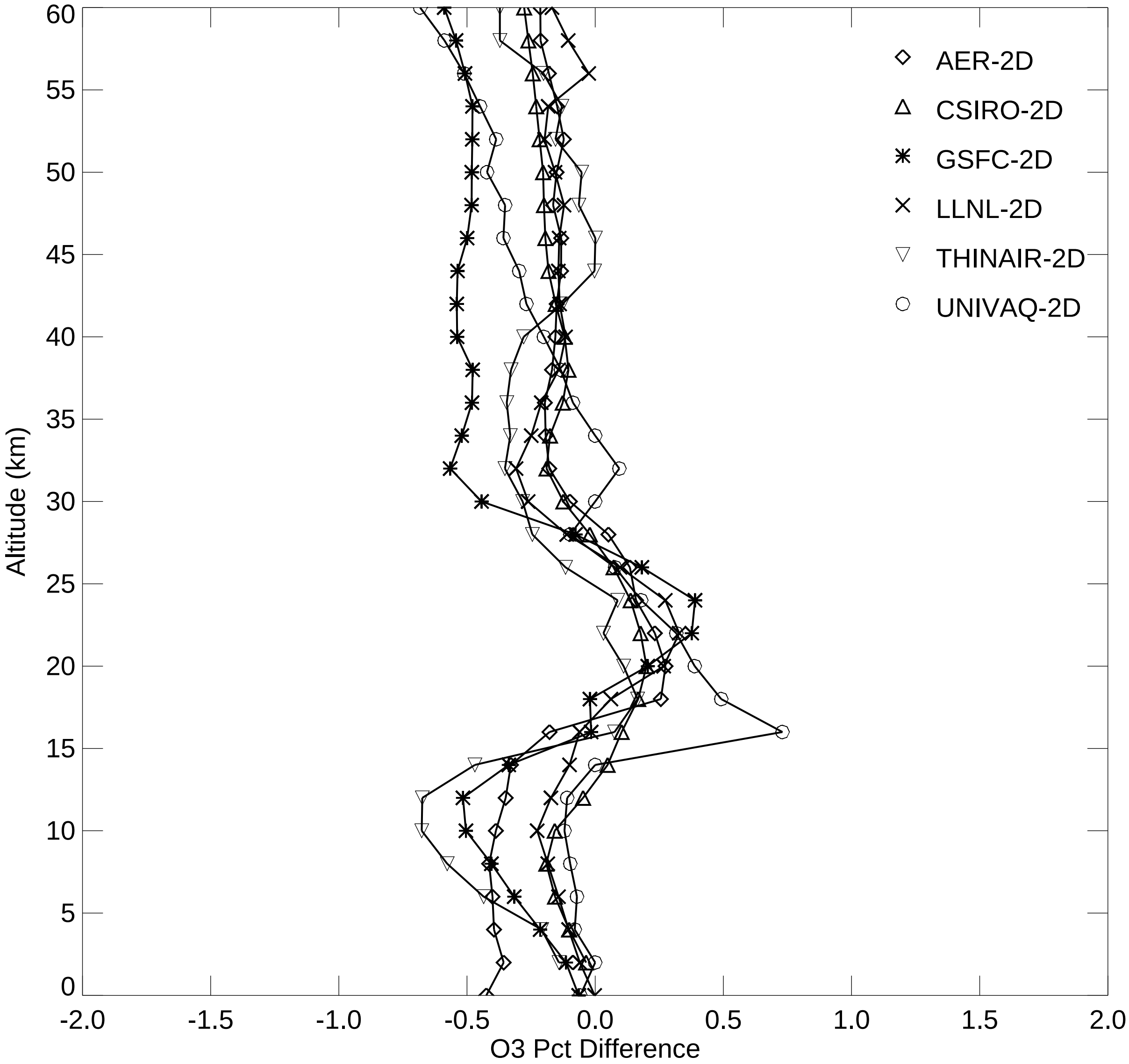

Figure 4.152: Calculated perturbations to O_3 (percent) as a function of altitude at the equator in June of 2015 due to emissions from a fleet of 500 HSCT aircraft operating at 2 km below nominal cruise altitude with $EI(NO_x)=5$ under Scenario S2b relative to Scenario D.

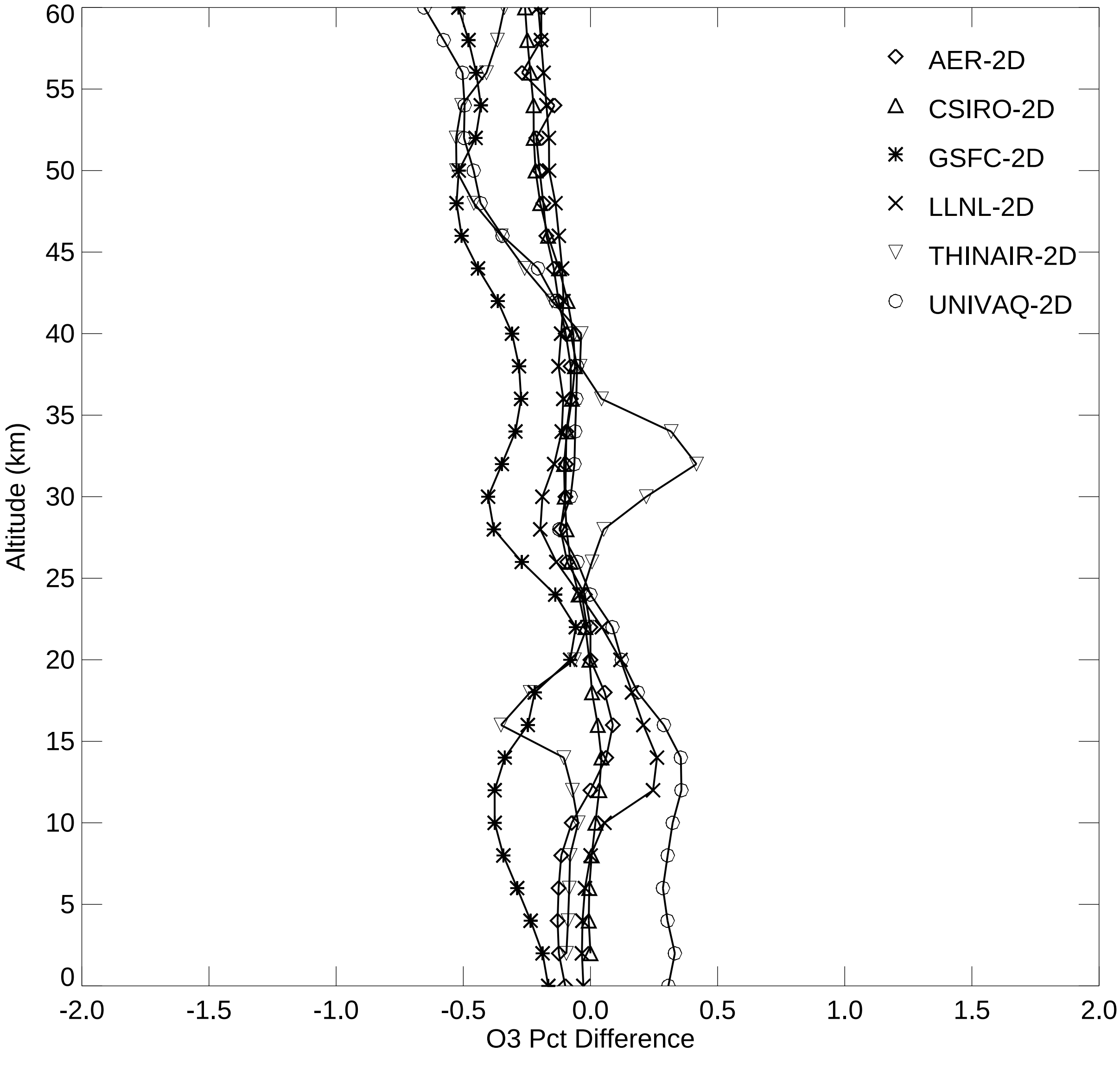

Figure 4.153: Calculated perturbations to O_3 (percent) as a function of altitude at 45^{o}S in June of 2015 due to emissions from a fleet of 500 HSCT aircraft operating at 2 km below nominal cruise altitude with EI(NO_x)=5 under Scenario S2b relative to Scenario D.

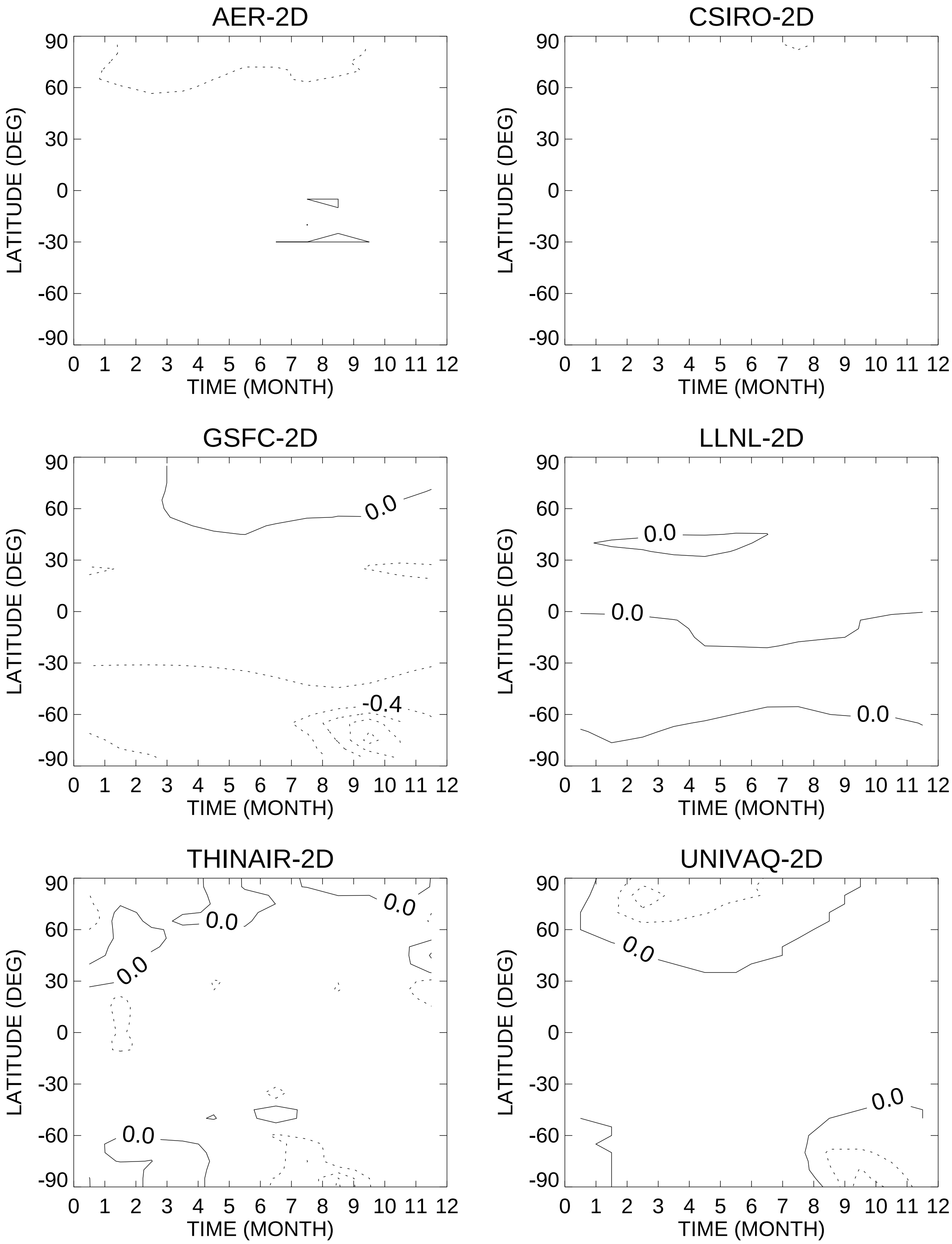

Figure 4.154: Calculated perturbations to column O_3 (percent) as a function of latitude and season in 2015 due to emissions from a fleet of 500 HSCT aircraft operating at 2 km below nominal cruise altitude with $EI(NO_x)=5$ under Scenario S2b relative to Scenario D. Contours are -1.0 to 0 by 0.2.

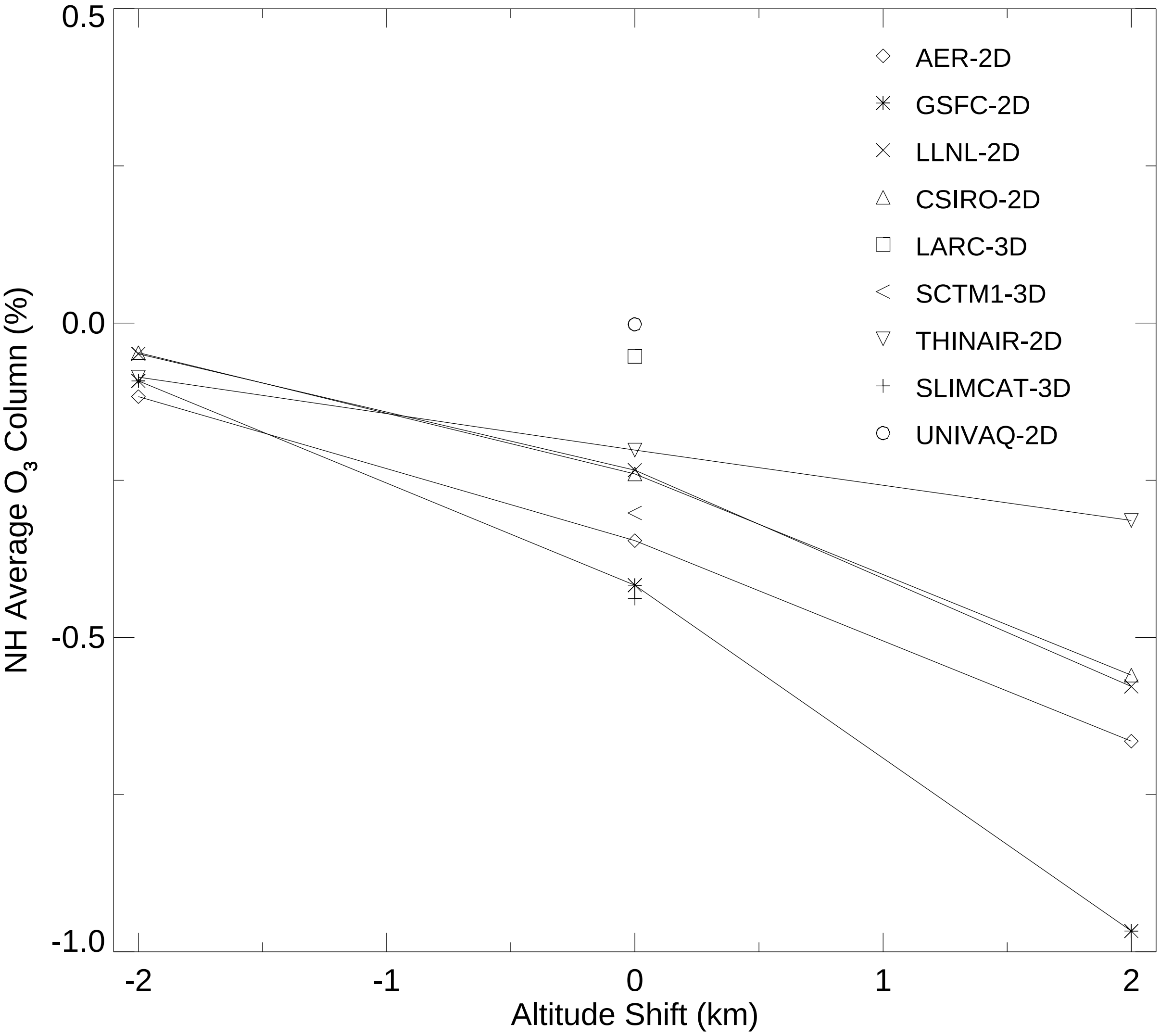

Figure 4.155: Northern hemisphere annual average total O_3 column change (percent) as a function of cruise altitude for an HSCT fleet of 500 aircraft operating in 2015 with $EI(NO_x)=5$ and SA0 sulfate surface area density.

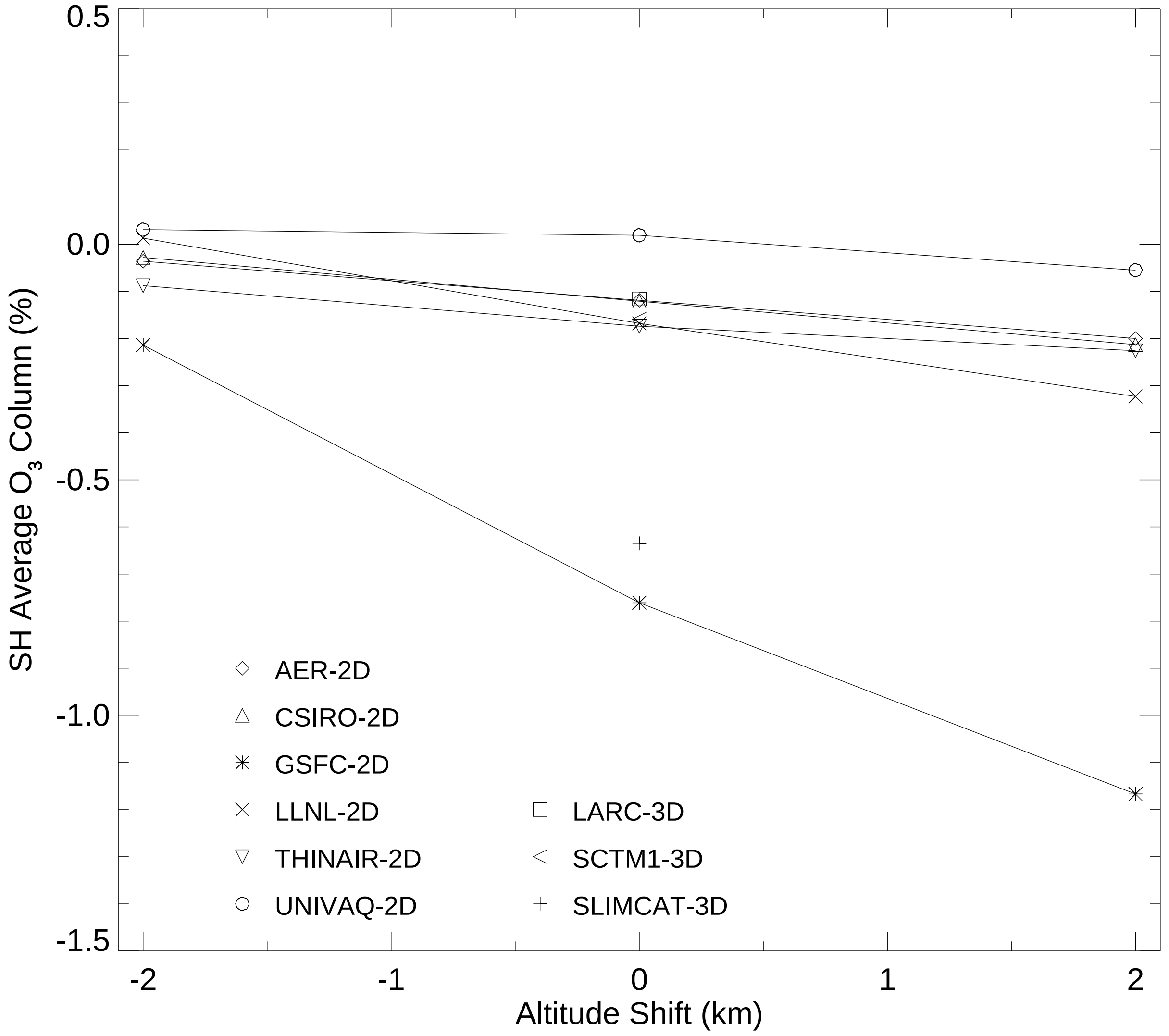

Figure 4.156: Southern hemisphere annual average total O_3 column change (percent) as a function of cruise altitude for an HSCT fleet of 500 aircraft operating in 2015 with $EI(NO_x)=5$ and SA0 sulfate surface area density.

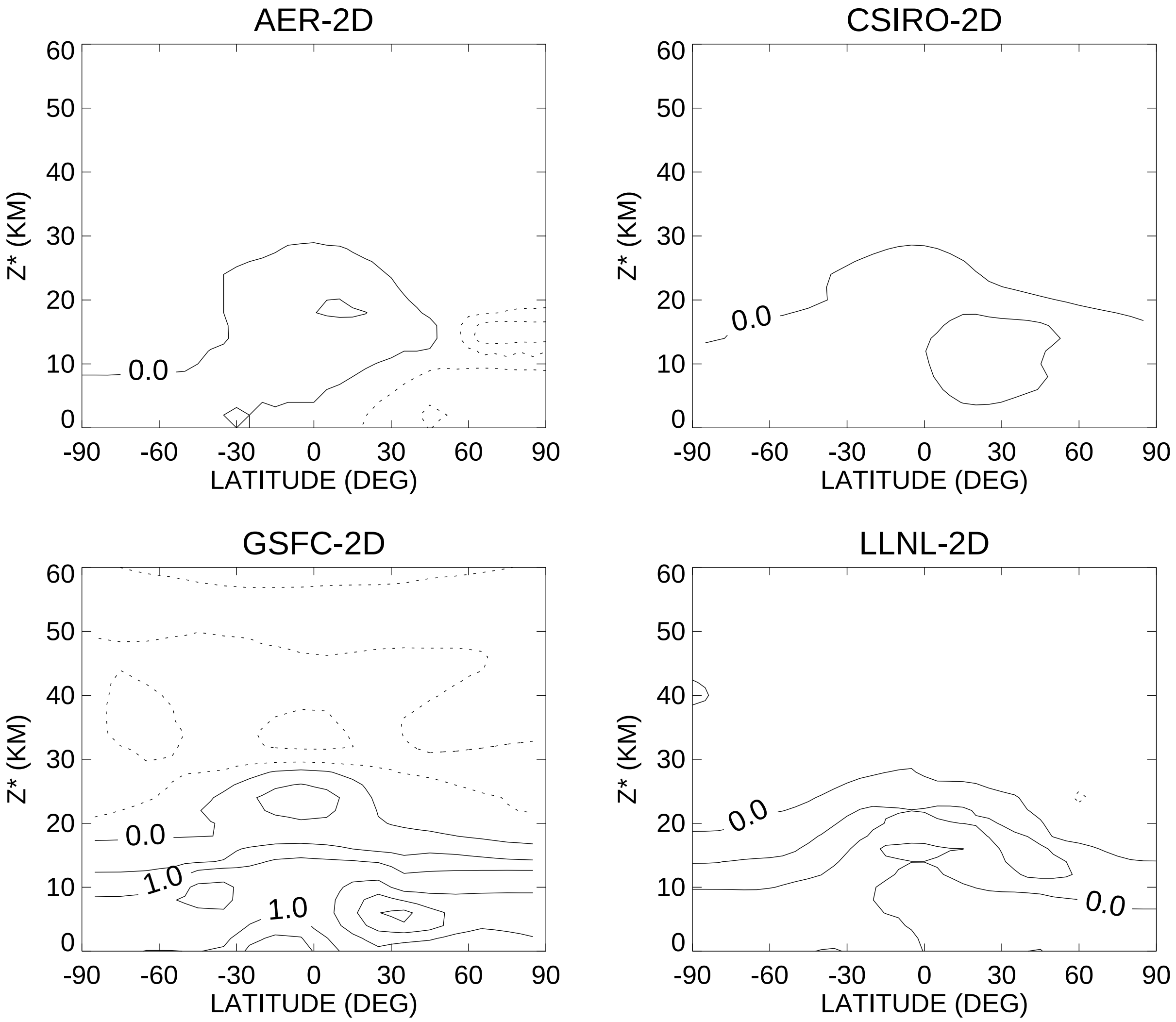

Figure 4.157: Calculated perturbations to O_3 (percent) as a function of latitude and altitude in March of 2015 due to emissions from a fleet of 500 HSCT aircraft operating at 2 km below nominal cruise altitude with EI(NO_x)=10 under Scenario S2c relative to Scenario D. Contours are -1, -0.5, 0, 0.5, 1, 2, 3, 4.

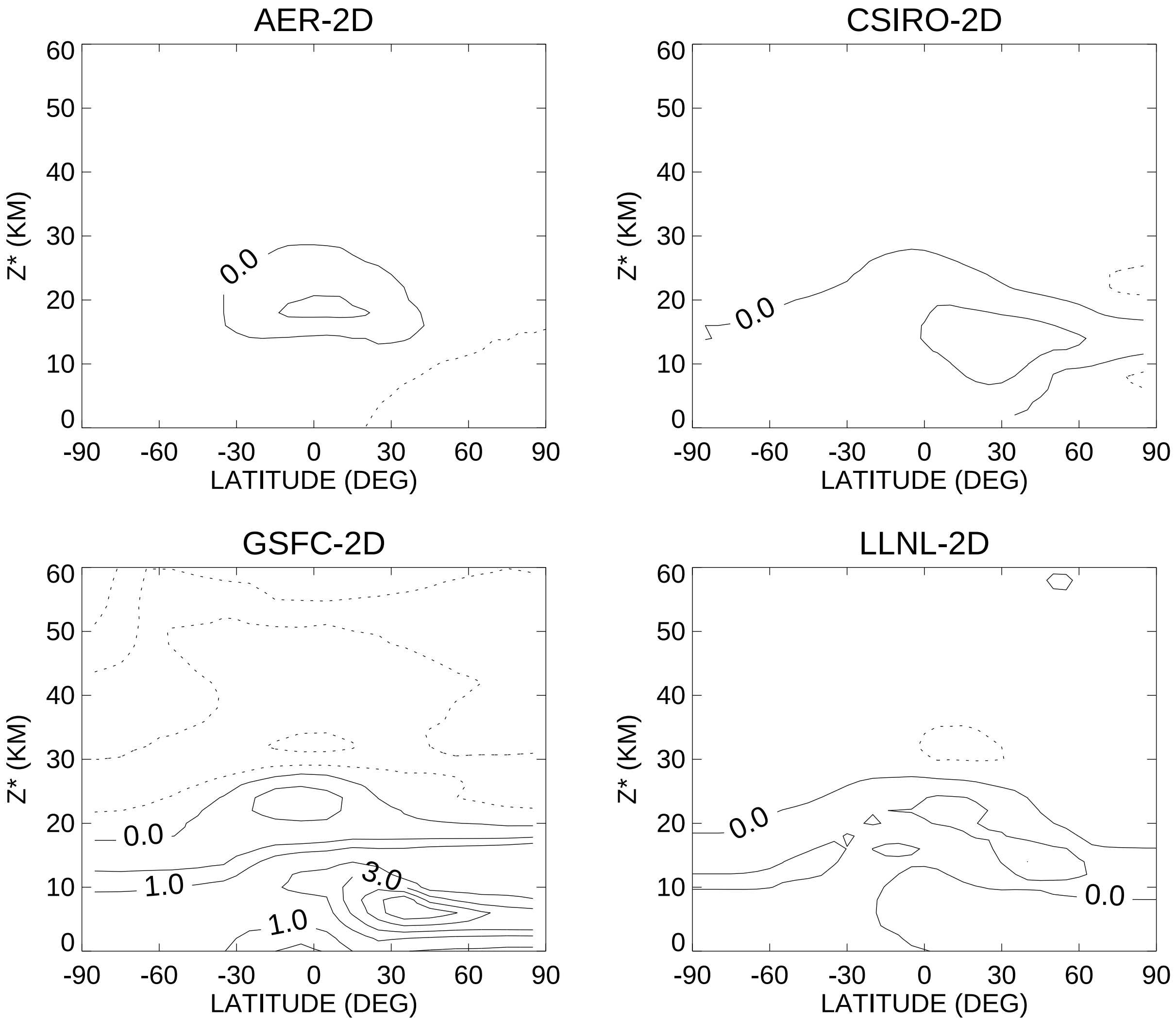

Figure 4.158: Calculated perturbations to O_3 (percent) as a function of latitude and altitude in June of 2015 due to emissions from a fleet of 500 HSCT aircraft operating at 2 km below nominal cruise altitude with $EI(NO_x)$=10 under Scenario S2c relative to Scenario D. Contours are -1, -0.5, 0, 0.5, 1, 2, 3, 4, 5.

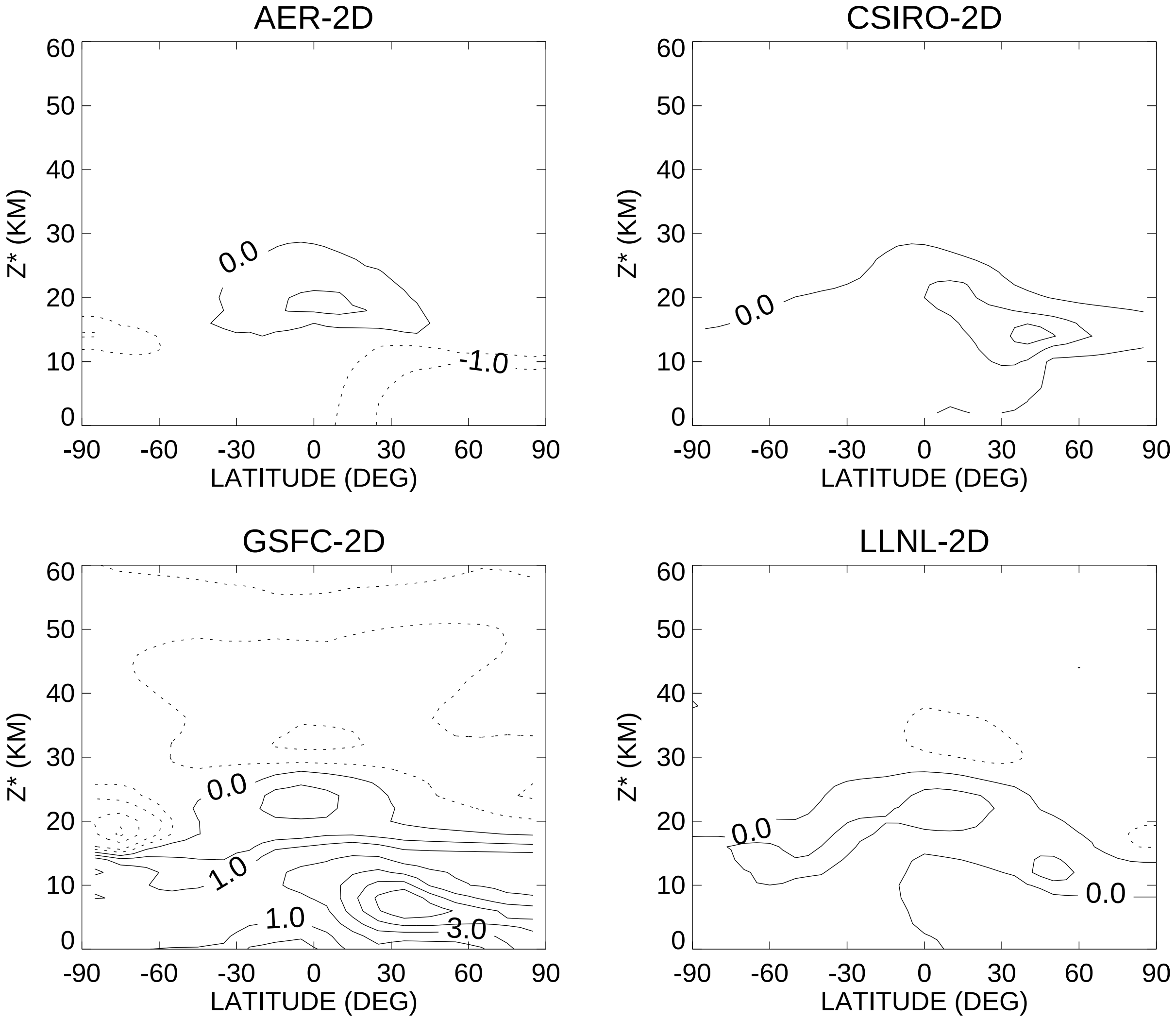

Figure 4.159: Calculated perturbations to O_3 (percent) as a function of latitude and altitude in October of 2015 due to emissions from a fleet of 500 HSCT aircraft operating at 2 km below nominal cruise altitude with EI(NO_x)=10 under Scenario S2c relative to Scenario D. Contours are -3, -2, -1, -0.5, 0, 0.5, 1, 2, 3, 4, 5.

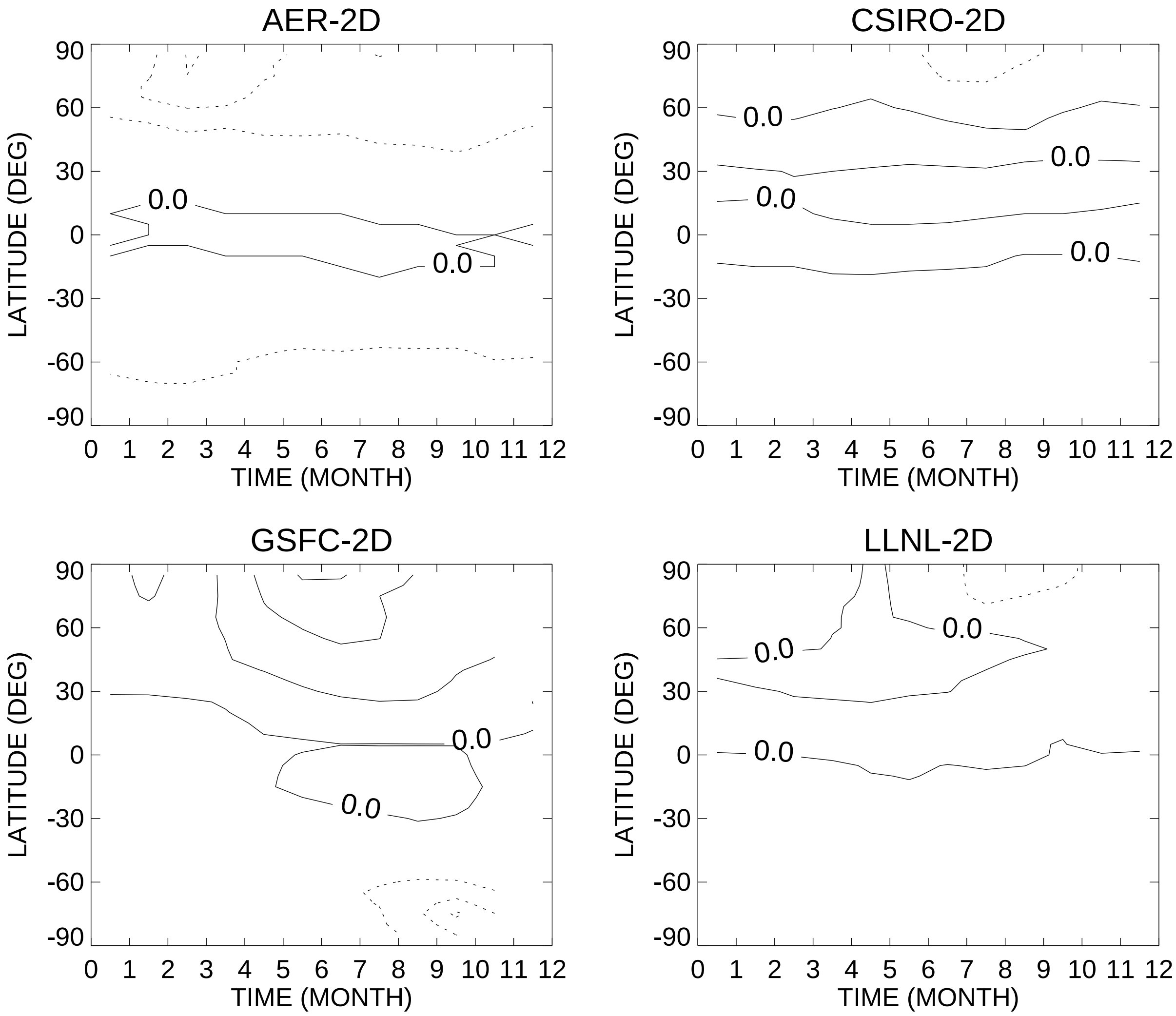

Figure 4.160: Calculated perturbations to column O_3 (percent) as a function of latitude and season in 2015 due to emissions from a fleet of 500 HSCT aircraft operating at 2 km below nominal cruise altitude with $EI(NO_x)=10$ under Scenario S2c relative to Scenario D. Contours are -0.6 to 0.6 by 0.2.

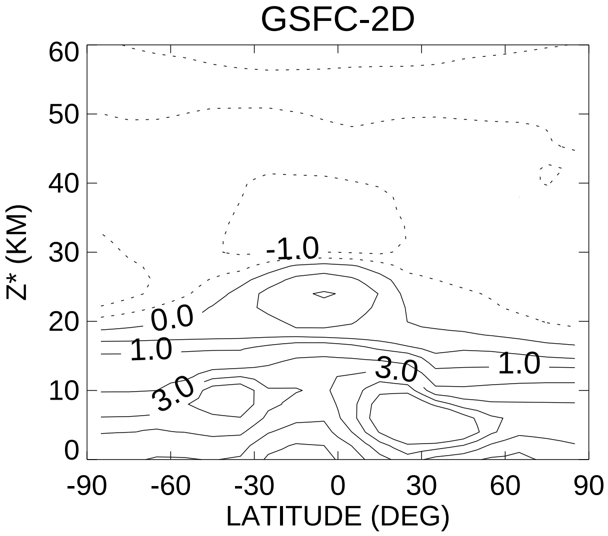

Figure 4.161: Calculated perturbations to O_3 (percent) as a function of latitude and altitude in March of 2015 due to emissions from a fleet of 500 HSCT aircraft operating at 2 km below nominal cruise altitude with $EI(NO_x)=15$ under Scenario S2d relative to Scenario D. Contours are -1, -0.5, 0, 0.5, 1, 2, 3, 4, 5.

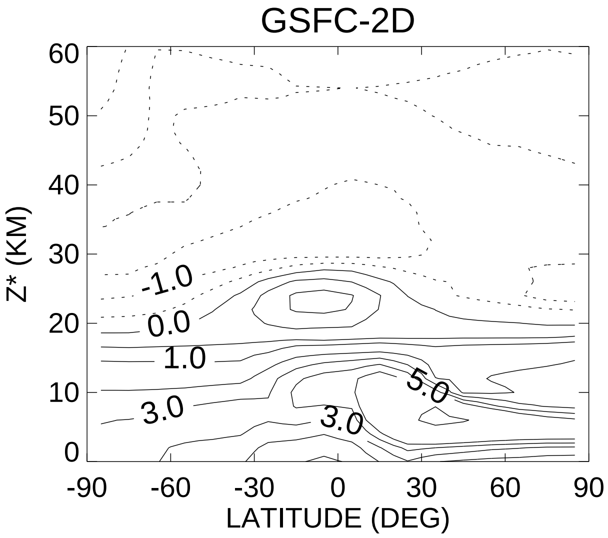

Figure 4.162: Calculated perturbations to O_3 (percent) as a function of latitude and altitude in June of 2015 due to emissions from a fleet of 500 HSCT aircraft operating at 2 km below nominal cruise altitude with $EI(NO_x)=15$ under Scenario S2d relative to Scenario D. Contours are -1, -0.5, 0, 0.5, 1, 2, 3, 4, 5, 10.

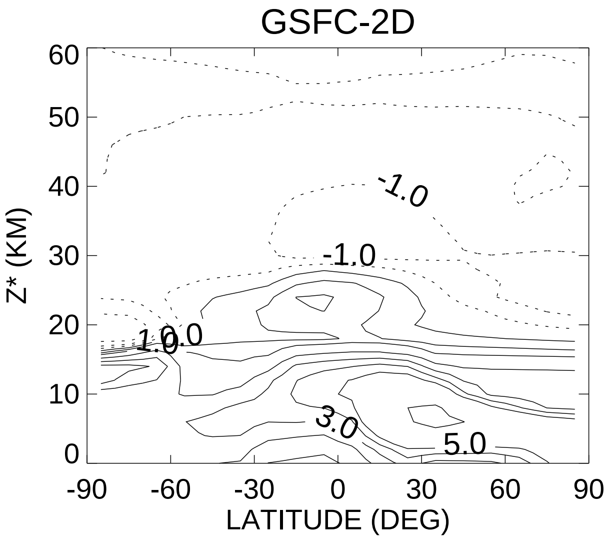

Figure 4.163: Calculated perturbations to O_3 (percent) as a function of latitude and altitude in October of 2015 due to emissions from a fleet of 500 HSCT aircraft operating at 2 km below nominal cruise altitude with EI(NO_x)=15 under Scenario S2d relative to Scenario D. Contours are -1, -0.5, 0, 0.5, 1, 2, 3, 4, 5, 10.

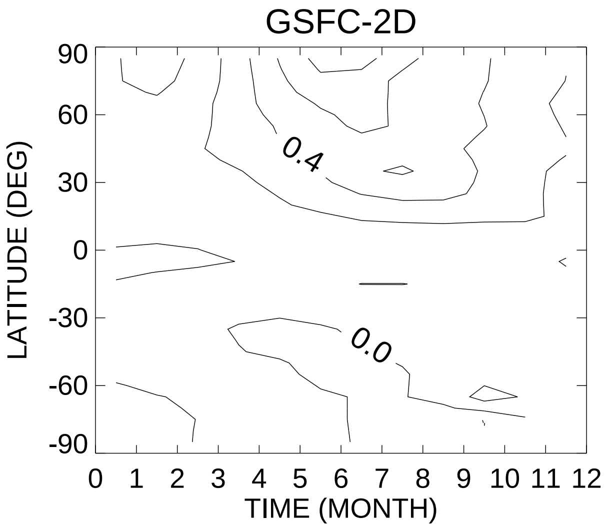

Figure 4.164: Calculated perturbations to column O_3 (percent) as a function of latitude and season in 2015 due to emissions from a fleet of 500 HSCT aircraft operating at 2 km below nominal cruise altitude with EI(NO_x)=15 under Scenario S2d relative to Scenario D. Contours are 0 to 0.8 by 0.2.

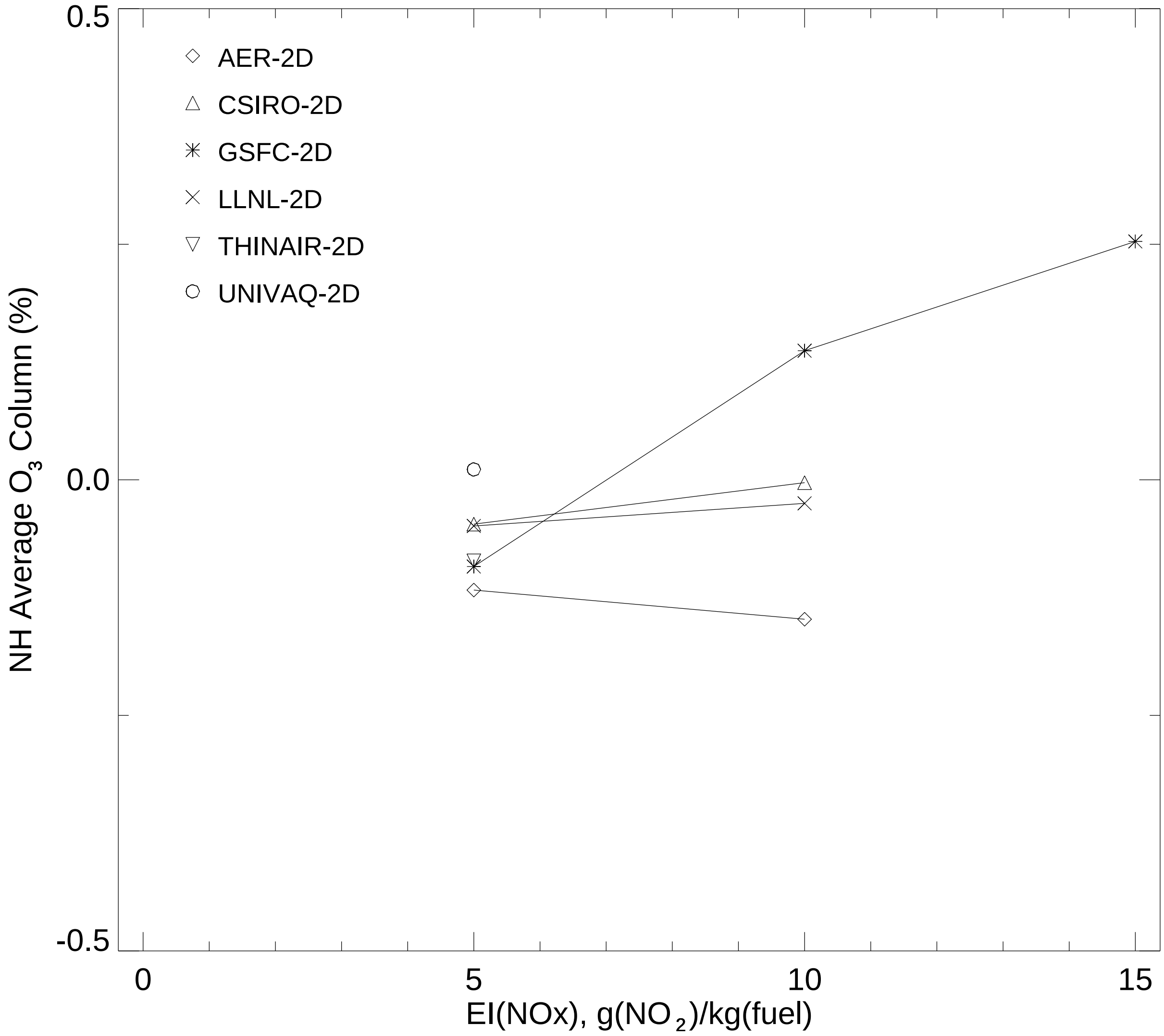

Figure 4.165: Northern hemisphere annual average total O_3 column change (percent) as a function of $EI(NO_x)$ for an HSCT fleet of 500 aircraft operating in 2015 at 2 km below nominal cruise altitude with SA0 sulfate surface area density.

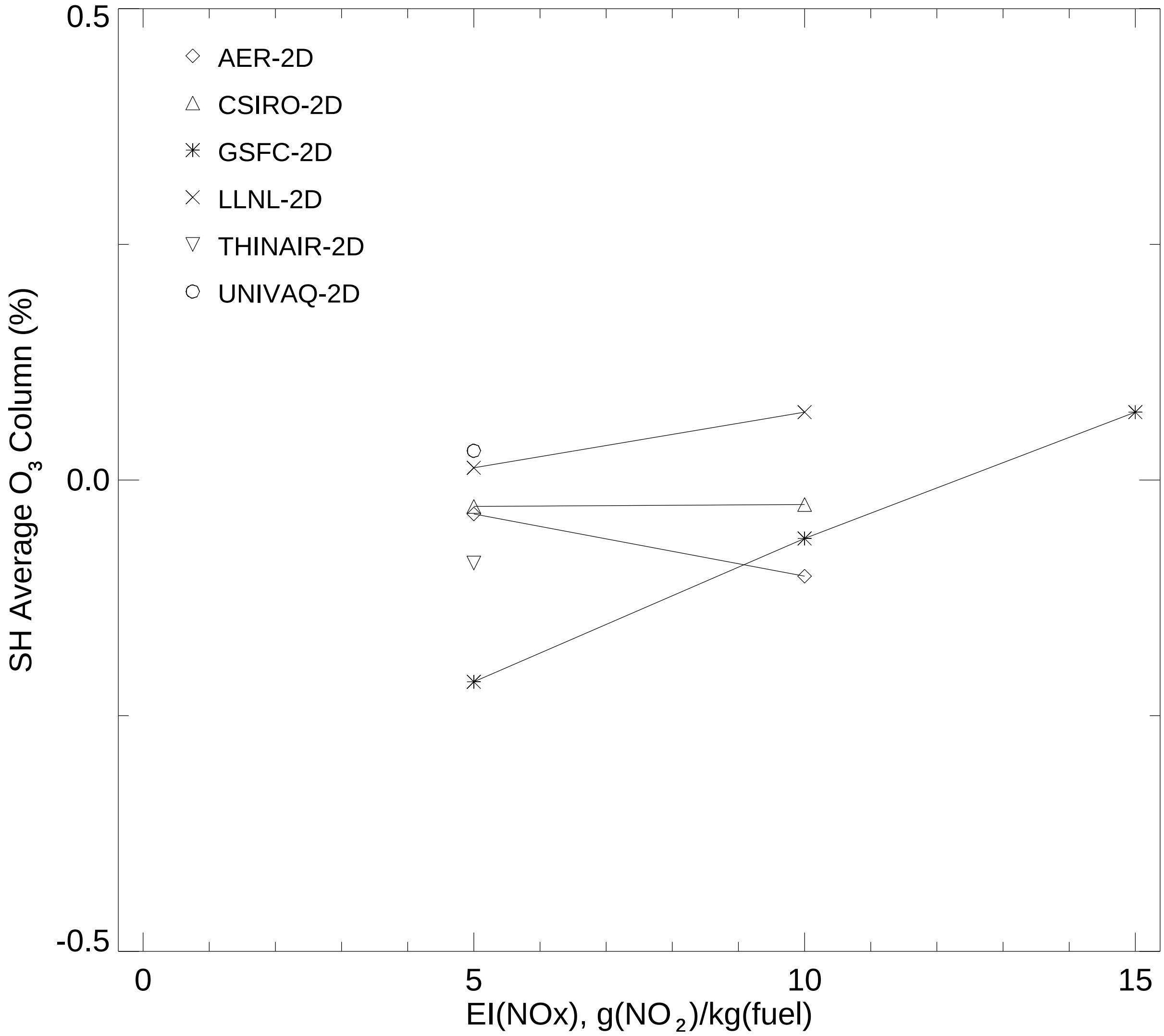

Figure 4.166: Southern hemisphere annual average total O_3 column change (percent) as a function of $EI(NO_x)$ for an HSCT fleet of 500 aircraft operating in 2015 at 2 km below nominal cruise altitude with SA0 sulfate surface area density.

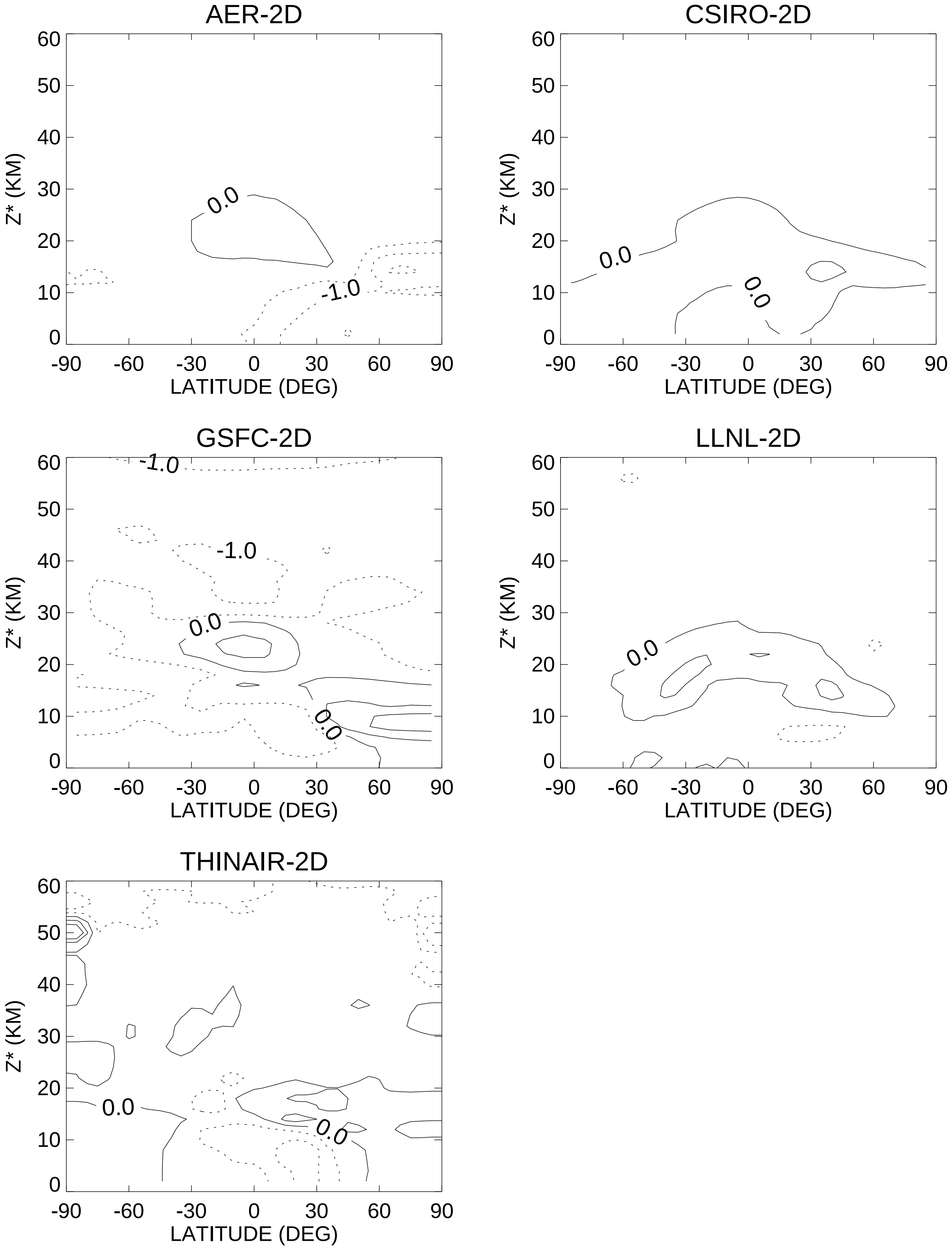

Figure 4.167: Calculated perturbations to O_3 (percent) as a function of latitude and altitude in March of 2015 due to emissions from a fleet of 1000 HSCT aircraft operating at 2 km below nominal cruise altitude with $EI(NO_x)=5$ under Scenario S2e relative to Scenario D. Contours are -2, -1, -0.5, 0, 0.5, 1.

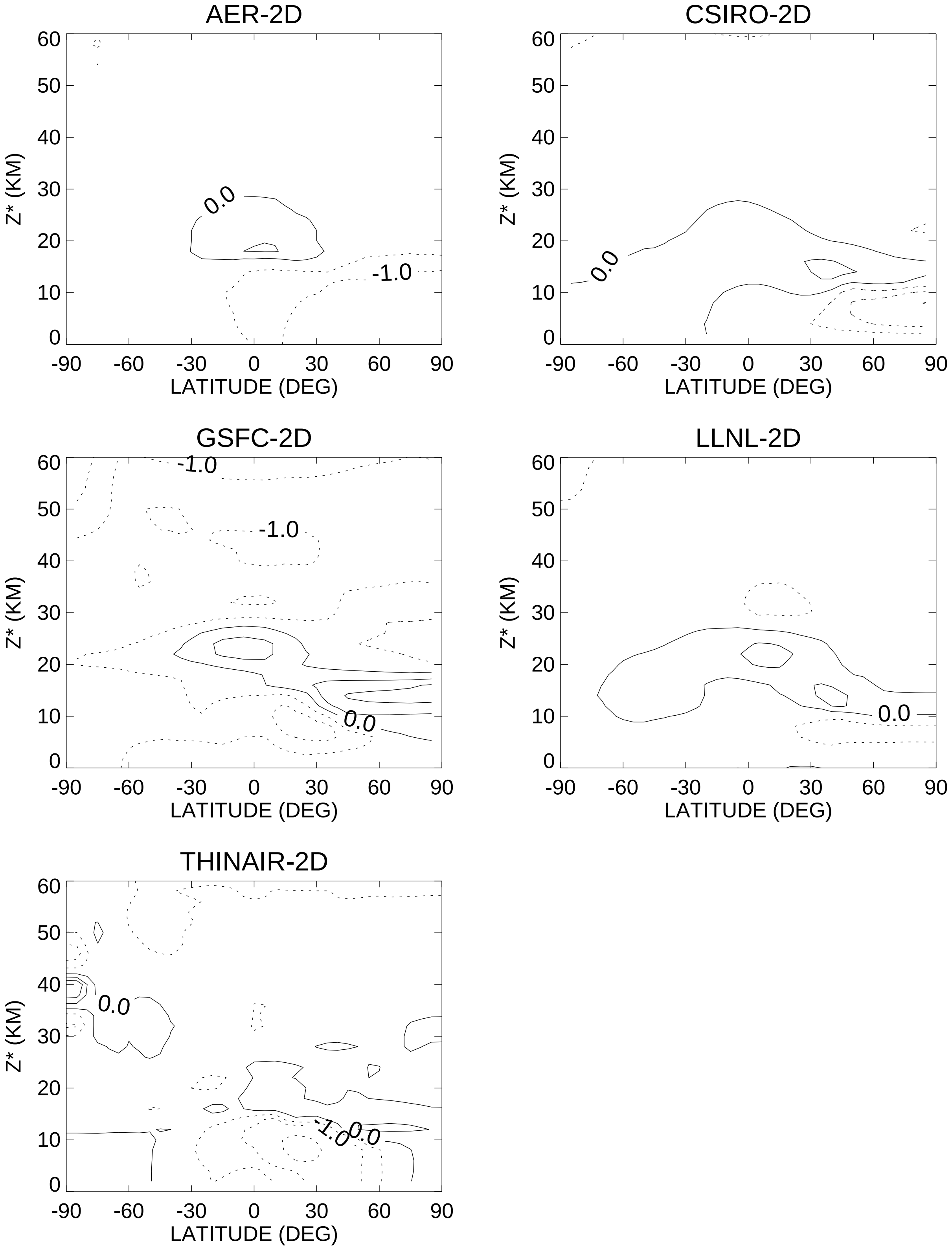

Figure 4.168: Calculated perturbations to O_3 (percent) as a function of latitude and altitude in June of 2015 due to emissions from a fleet of 1000 HSCT aircraft operating at 2 km below nominal cruise altitude with $EI(NO_x)=5$ under Scenario S2e relative to Scenario D. Contours are -1, -0.5, 0, 0.5, 1.

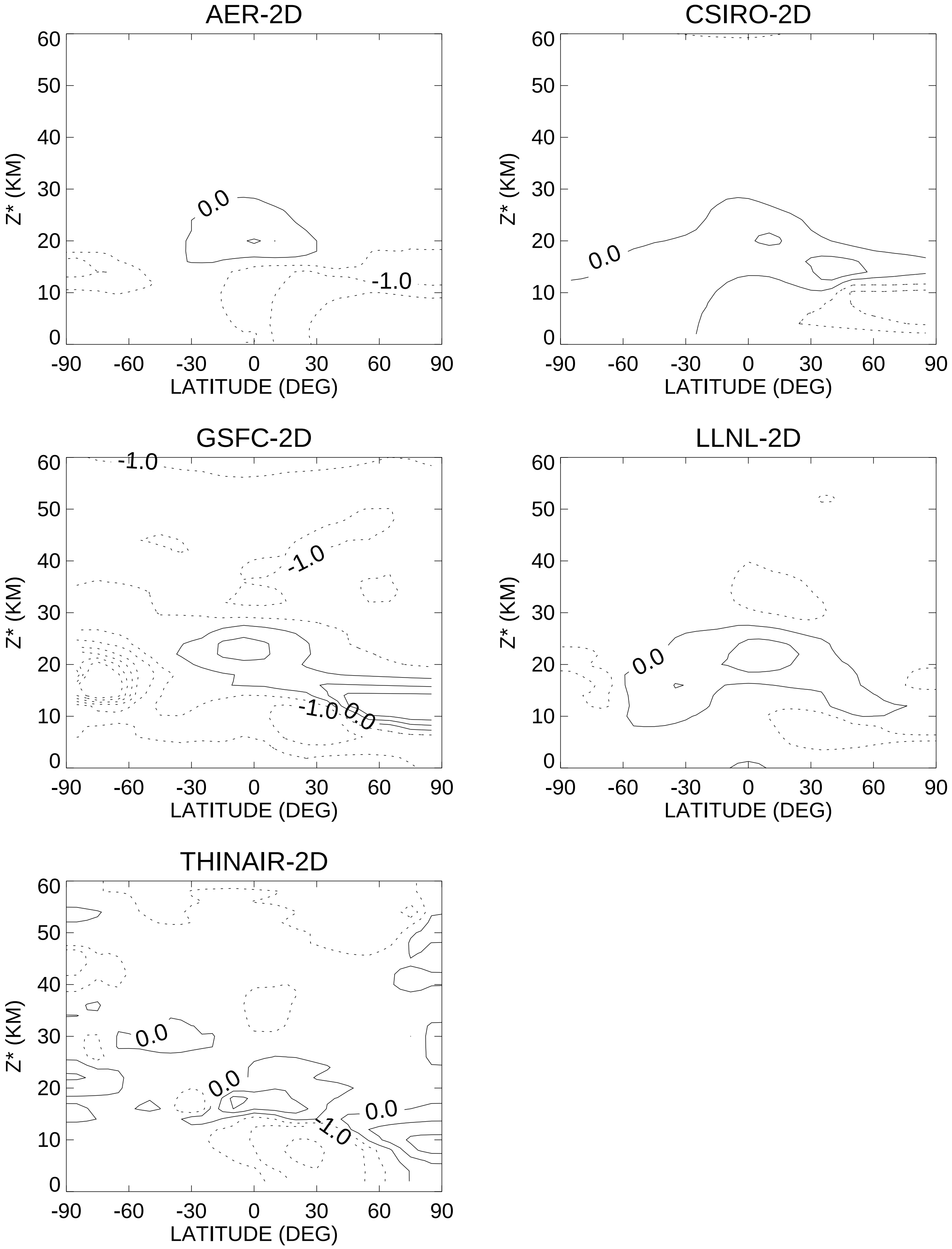

Figure 4.169: Calculated perturbations to O_3 (percent) as a function of latitude and altitude in October of 2015 due to emissions from a fleet of 1000 HSCT aircraft operating at 2 km below nominal cruise altitude with EI(NO_x)=5 under Scenario S2e relative to Scenario D. Contours are -5, -4, -3, -2, -1, -0.5, 0, 0.5, 1.

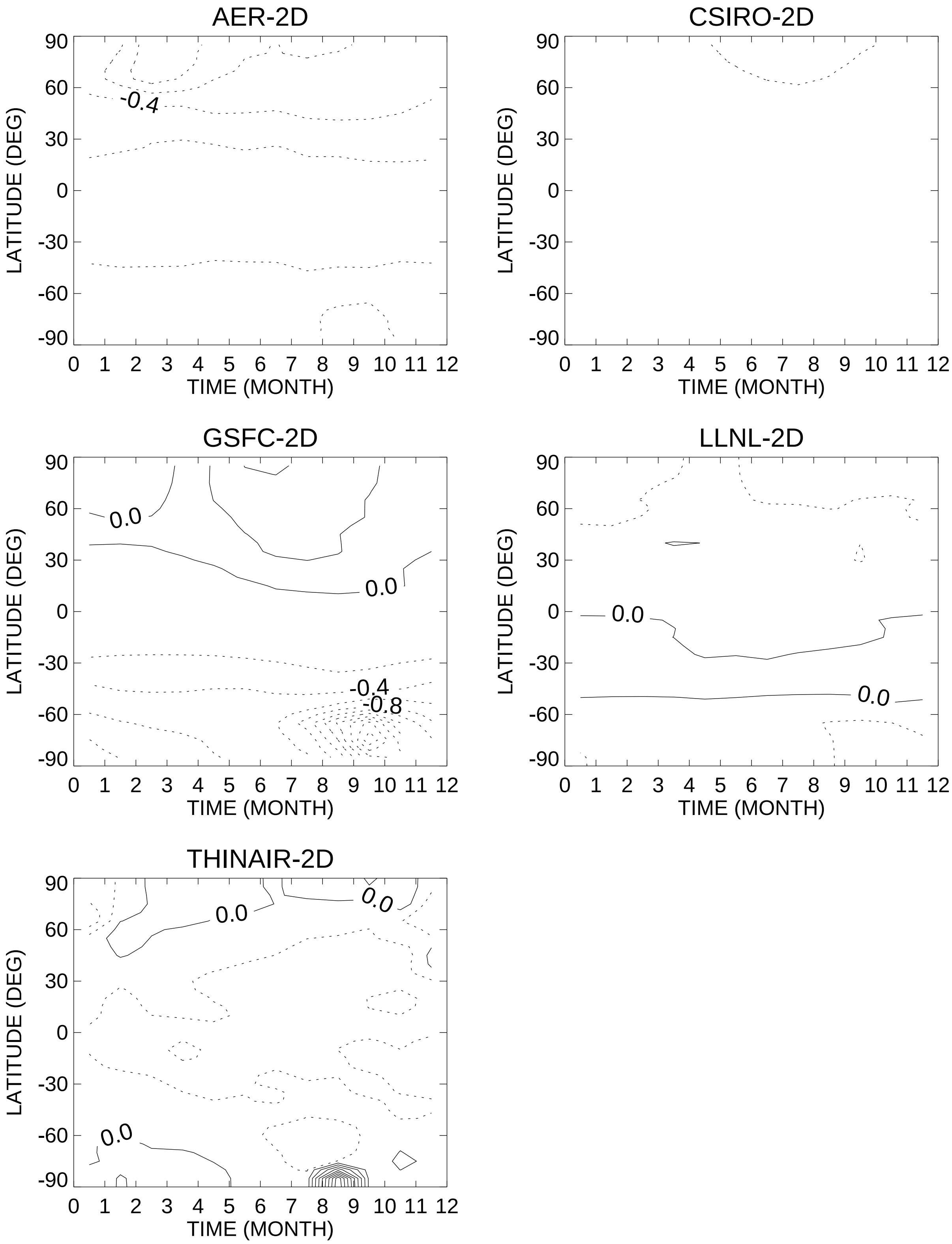

Figure 4.170: Calculated perturbations to column O_3 (percent) as a function of latitude and season in 2015 due to emissions from a fleet of 1000 HSCT aircraft operating at 2 km below nominal cruise altitude with $EI(NO_x)=5$ under Scenario S2e relative to Scenario D. Contours are -2.0 to 0.4 by 0.2.

4.3.4 Scenarios with Enhanced Background Aerosol (S3a-f)

This section will cover Scenarios S3a-S3f which use enhanced background surface area to simulate a volcanically active period. The background SAD is 4xSA0 for the HSCT scenarios in this section and the 2015 subsonic-only atmosphere (Scenario D3) with which they are compared. As discussed in Chapter 2.2, the increased aerosol SAD leads to reduced ozone below 20 km and increased ozone from 20-30 km for the D3 background atmosphere relative to Scenario D with SA0 sulfate surface area density. Total ozone amounts were several percent less with 4xSA0 than with SA0. For this sensitivity study, EI(NO_x) is varied from 0 to 15 in Scenarios S3a-S3d with no sulfur emitted by the 500 HSCT aircraft. Scenarios S3e and S3f do include aircraft sulfur emission with EI(NO_x)=5.

Scenario S3a represents 500 HSCT aircraft operating in 2015 with EI(NO_x)=0, no sulfur emissions, and a background sulfate surface area density of 4xSA0. Differences in ozone between this scenario and the 2015 background atmosphere with subsonic aircraft and sulfate surface area density of 4xSA0 (Scenario D3) are shown in Figures 4.171, 4.172, and 4.173 for March, June, and October. The models all show ozone depletion below 25 km and above 35 km due to the HSCT H_2O emissions. This is generally similar to the ozone response for Scenario S1b-D which includes the same HSCT fleet but for background surface area density of SA0. The GSFC show significantly less ozone depletion in the southern hemisphere lower stratosphere for this scenario than for S1b-D, while the LLNL model show somewhat more depletion in both hemispheres. Figure 4.174 shows changes in ozone column for Scenario S3a relative to Scenario D3. Ozone column depletions are less than 0.5% for the CSIRO model, up to 1% for the AER, LLNL, and UNIVAQ models, and up to 3% for the GSFC model.

Scenario S3b is identical to Scenario S1c except for the background sulfate SAD. This scenario includes 500 HSCTs operating in 2015 with EI(NO_x)=5 and background SAD of 4xSA0. Changes in ozone relative to background scenario D3 are shown in Figures 4.175, 4.176, and 4.177 for March, June, and October as functions of latitude and altitude. Again the GSFC model shows the greatest difference in ozone perturbation with elevated SAD (S3b-D3) versus with nonvolcanic SAD (S1c-D). The GSFC model shows a large region of ozone increase due to HSCT emissions under Scenario S3b, extending through the northern hemisphere and tropics near the tropopause. Other models also show some ozone increases in this region, and generally less depletion than in Scenario S1c. Changes in ozone for June at 45^{o}N, the equator, and 45^{o}S are shown in Figures 4.178, 4.179, and 4.180. Figure 4.181 shows changes in ozone column due to HSCT aircraft emissions for this scenario relative to Scenario D3. All models show less ozone depletion or more regions of ozone increase than for Scenario S1c, except for the LLNL model.

Scenario S3c uses an EI(NO_x) of 10 with background surface area density of 4xSA0. Calculated changes in ozone relative to Scenario D3 for March, June, and October are shown in Figures 4.182, 4.183, and 4.184. Ozone increases around the tropopause are of larger area and greater magnitude than for S3b-D3. Changes in total column ozone are shown in Figure 4.185 and reveal substantial ozone increases due to HSCT aircraft emissions for all models. The GSFC and LLNL models still show ozone reductions in the southern hemisphere, and the AER model shows ozone reductions in the northern polar region.

With EI(NO_x)=15, calculated ozone increases due to HSCT are even larger. Figures 4.186, 4.187, and 4.188 show ozone changes as a function of latitude and altitude for March, June, and October for Scenario S3d relative to Scenario D3. Ozone increases are as much as 5% in the GSFC model northern hemisphere lower stratosphere and up to 4% in the UNIVAQ model tropical lower stratosphere. Vertical profiles of ozone change are shown in Figures 4.189, 4.190, and 4.191 at 45^{o}N, the equator, and 45^{o}S in June. Changes in column ozone for this scenario are shown in Figure 4.192.

The sensitivity of the hemispheric annual average ozone column to EI(NO_x) in the 2015 environment with elevated sulfate SAD is shown in Figures 4.193 and 4.194. All models have a positive response to increases in EI(NO_x) in both the northern and southern hemispheres. This is in contrast to the sensitivity with nonvolcanic SAD (shown in Figures 4.92 and 4.93), in which some models showed positive sensitivity and some negative sensitivity. With EI(NO_x)=0, calculated changes in northern hemisphere column ozone range from -0.3% to -0.5%. With EI(NO_x)=15, calculated changes in northern hemisphere column ozone range from +0.1% to +0.6%. In the southern hemisphere, the spread among the models is larger. The GSFC and UNIVAQ models show the greatest positive sensitivity to EI(NO_x), while the CSIRO model shows almost no sensitivity.

The final two scenarios in this section include sulfur emission from HSCT aircraft with EI(NO_x)=5. The

SADs for Scenarios S3e and S3f were generated by adding the SAD perturbations calculated by the AER model for Scenarios S1f and S1h to the 4xSA0 elevated background SAD. The sulfate surface area density for S3e includes aircraft sulfur emissions assuming $EI(SO_2)=0.4$ and 50% gas to particle conversion in the plume and is designated 4xSA0+SA1-SA0. The sulfate surface area density for S3f assumes 100% gas to particle conversion and is designated 4xSA0+SA3-SA0.

Calculated changes in ozone as a function of latitude and altitude for March, June, and October for Scenario S3e relative to Scenario D3 are shown in Figures 4.195, 4.196, and 4.197. Ozone depletion is enhanced relative to S3b-D3 which does not include aircraft sulfur emissions. Vertical profiles of ozone change at 45^oN, the equator, and 45^oS in June are shown in Figures 4.198-4.200. Figure 4.201 shows changes in ozone column for Scenario S3e relative to Scenario D3. All models show more depletion in column ozone for this scenario than for a similar one without aircraft sulfur emissions. However, column ozone depletion is considerably less than (about half for most models) those for Scenario S1f-D, which included the same amount of sulfur emissions but with SA0 background SAD.

Calculated ozone perturbations for Scenario S3f are shown in Figures 4.202, 4.203, and 4.204 for March, June, and October. Results are not very different from S3e-D3. The change in ozone column for this scenario is shown in Figure 4.205. Ozone depletion is slightly larger than for S3e-D3. Figure 4.206 shows the sensitivity of northern hemisphere annual average column ozone response to HSCT to changes in sulfate surface area density in a background atmosphere with 4xSA0 surface area density. The abscissa shows the percent difference in SAD between the HSCT case and the baseline case in the 14-21 km, 33-90^oN region. All models show increases in ozone depletion with increasing SAD perturbation. The GSFC model shows the greatest sensitivity; the other models have similar sensitivities. Because the background SAD is elevated, the SAD perturbations are a factor of 4 smaller on a percentage basis than those shown in Figure 4.140 with SA0. The ozone sensitivities are similar to those for SA0 over the 0-28% SAD range.

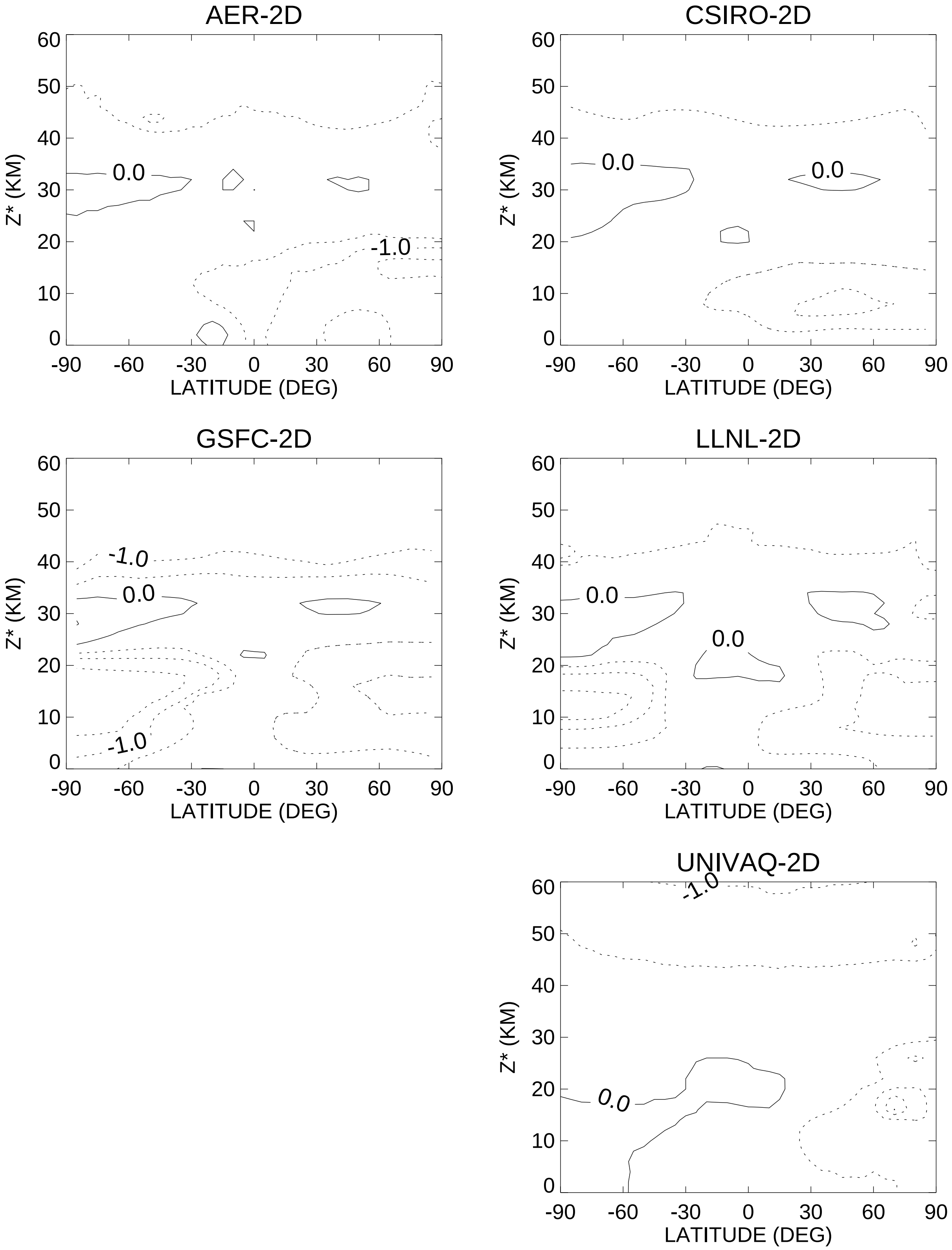

Figure 4.171: Calculated perturbations to O_3 (percent) as a function of latitude and altitude in March of 2015 due to emissions from a fleet of 500 HSCT aircraft with EI(NO_x)=0 and sulfate surface area of 4xSA0 under Scenario S3a relative to Scenario D3. Contours are -2, -1, -0.5, 0.

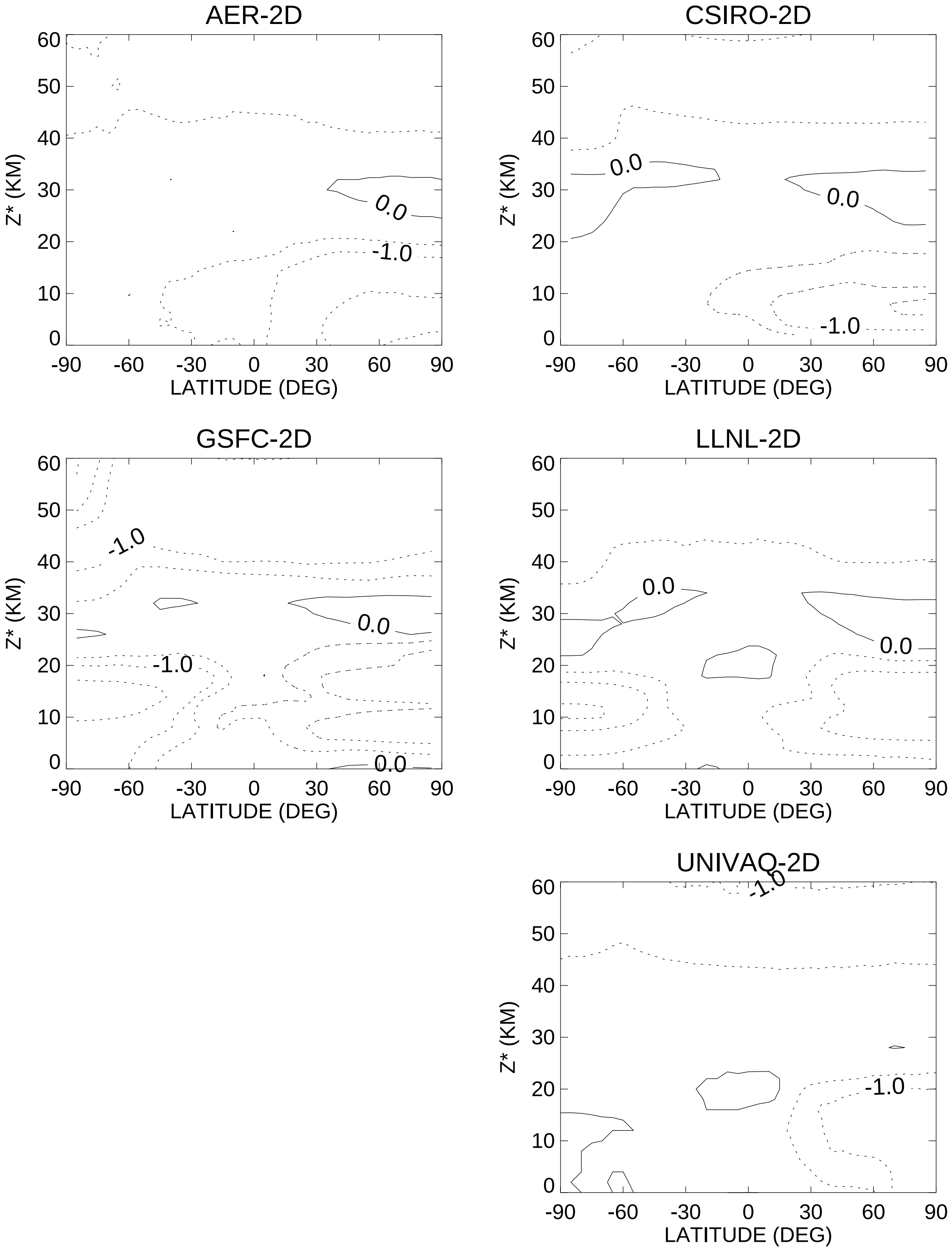

Figure 4.172: Calculated perturbations to O_3 (percent) as a function of latitude and altitude in June of 2015 due to emissions from a fleet of 500 HSCT aircraft with $EI(NO_x)=0$ and sulfate surface area of 4xSA0 under Scenario S3a relative to Scenario D3.. Contours are -3, -2, -1, -0.5, 0.

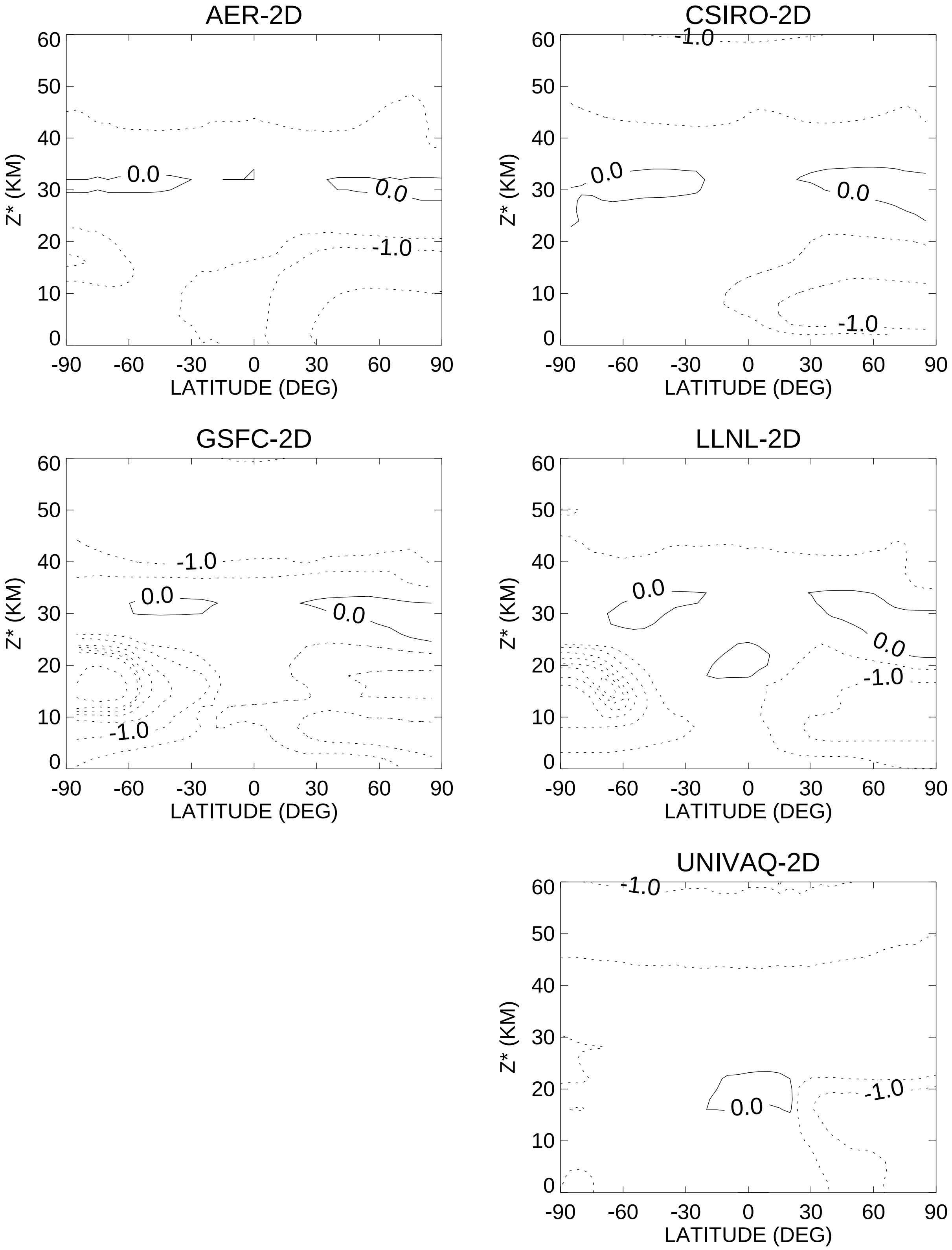

Figure 4.173: Calculated perturbations to O_3 (percent) as a function of latitude and altitude in October of 2015 due to emissions from a fleet of 500 HSCT aircraft with EI(NO_x)=0 and sulfate surface area of 4xSA0 under Scenario S3a relative to Scenario D3.. Contours are -10, -5, -4, -3, -2, -1, -0.5, 0.

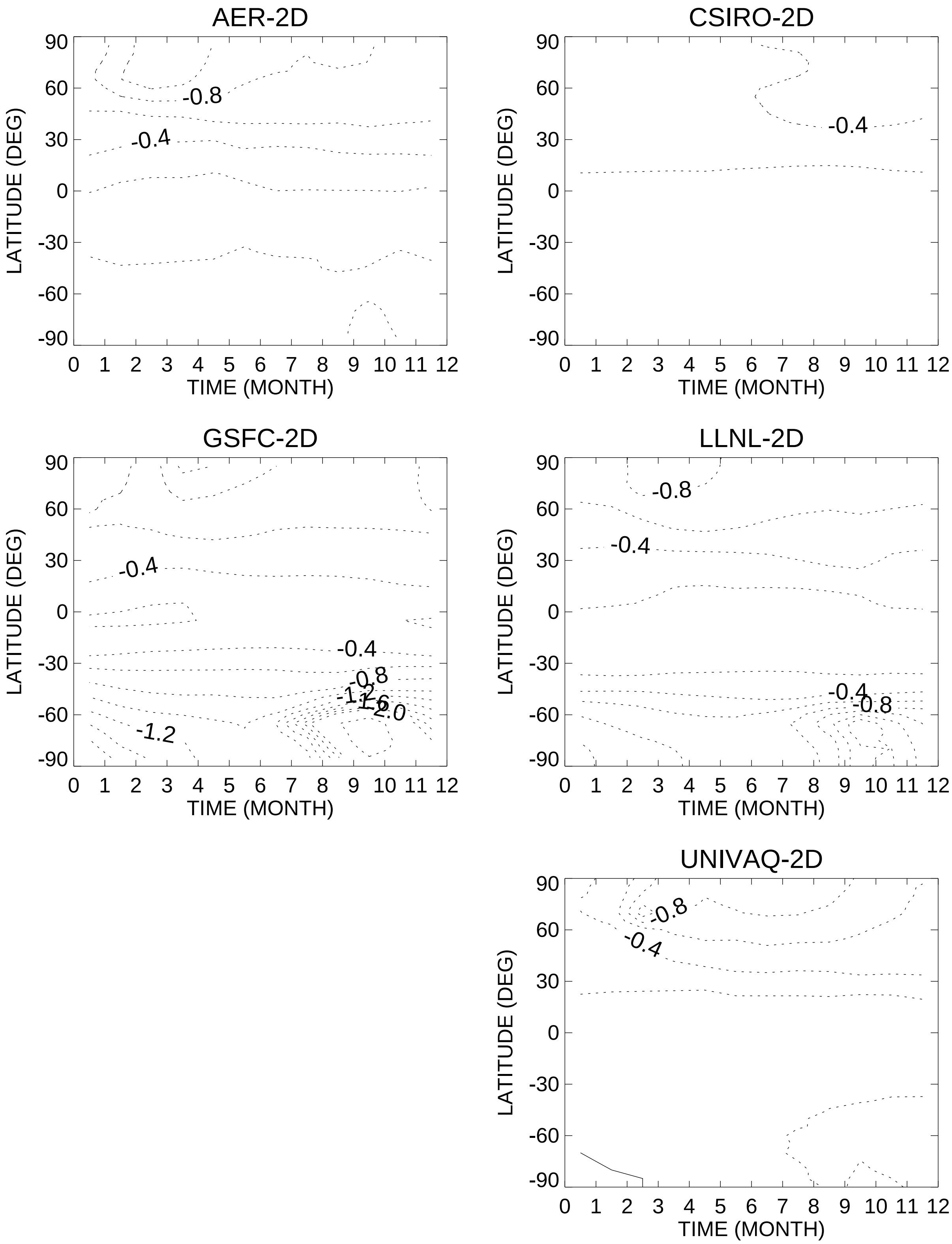

Figure 4.174: Calculated perturbations to column O_3 (percent) as a function of latitude and season in 2015 due to emissions from a fleet of 500 HSCT aircraft with $EI(NO_x)=0$ and sulfate surface area of 4xSA0 under Scenario S3a relative to Scenario D3. Contours are -3, and -2.0 to -0.2 by 0.2.

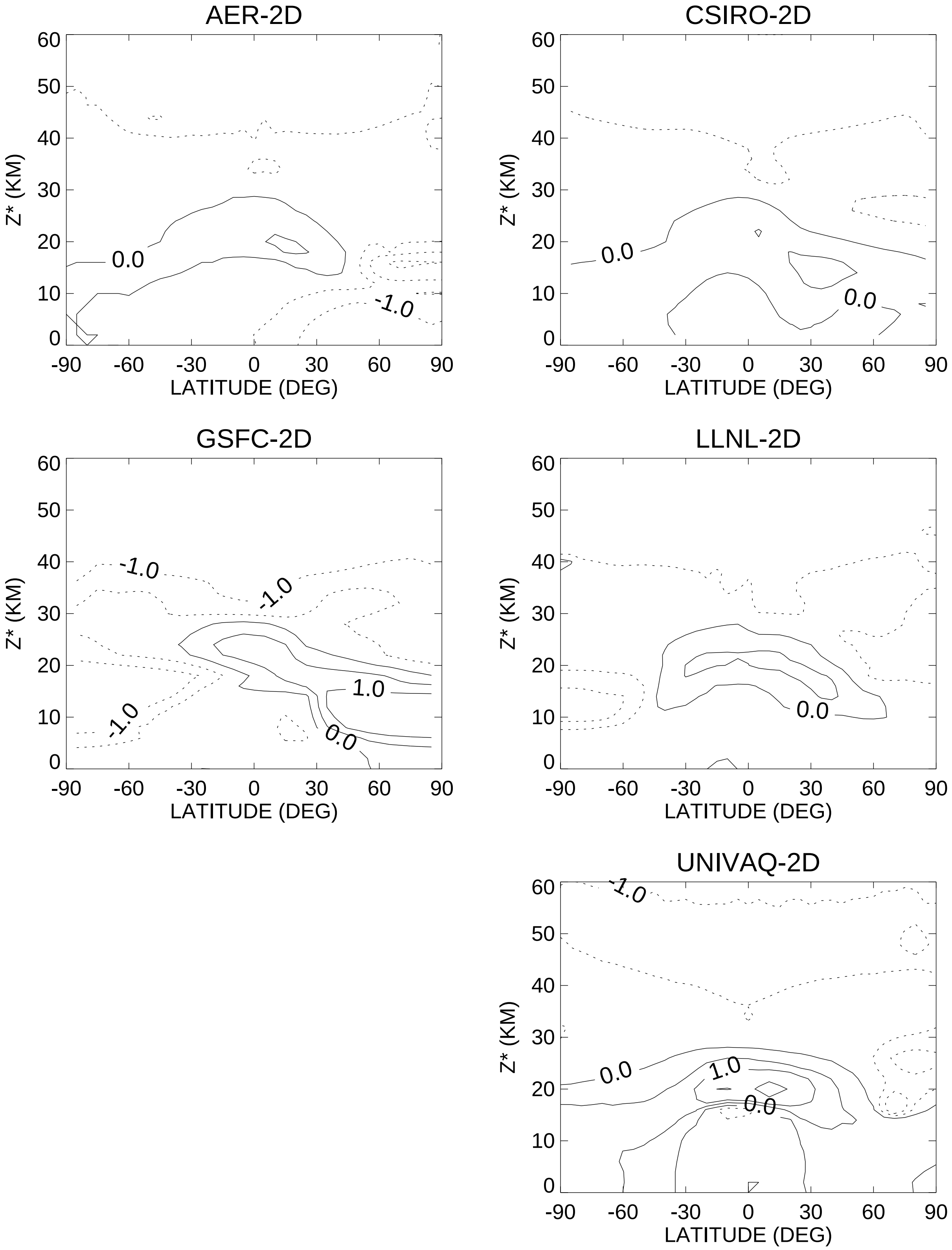

Figure 4.175: Calculated perturbations to O_3 (percent) as a function of latitude and altitude in March of 2015 due to emissions from a fleet of 500 HSCT aircraft with $EI(NO_x)$=5 and sulfate surface area of 4xSA0 under Scenario S3b relative to Scenario D3. Contours are -2, -1, -0.5, 0, 0.5, 1, 2.

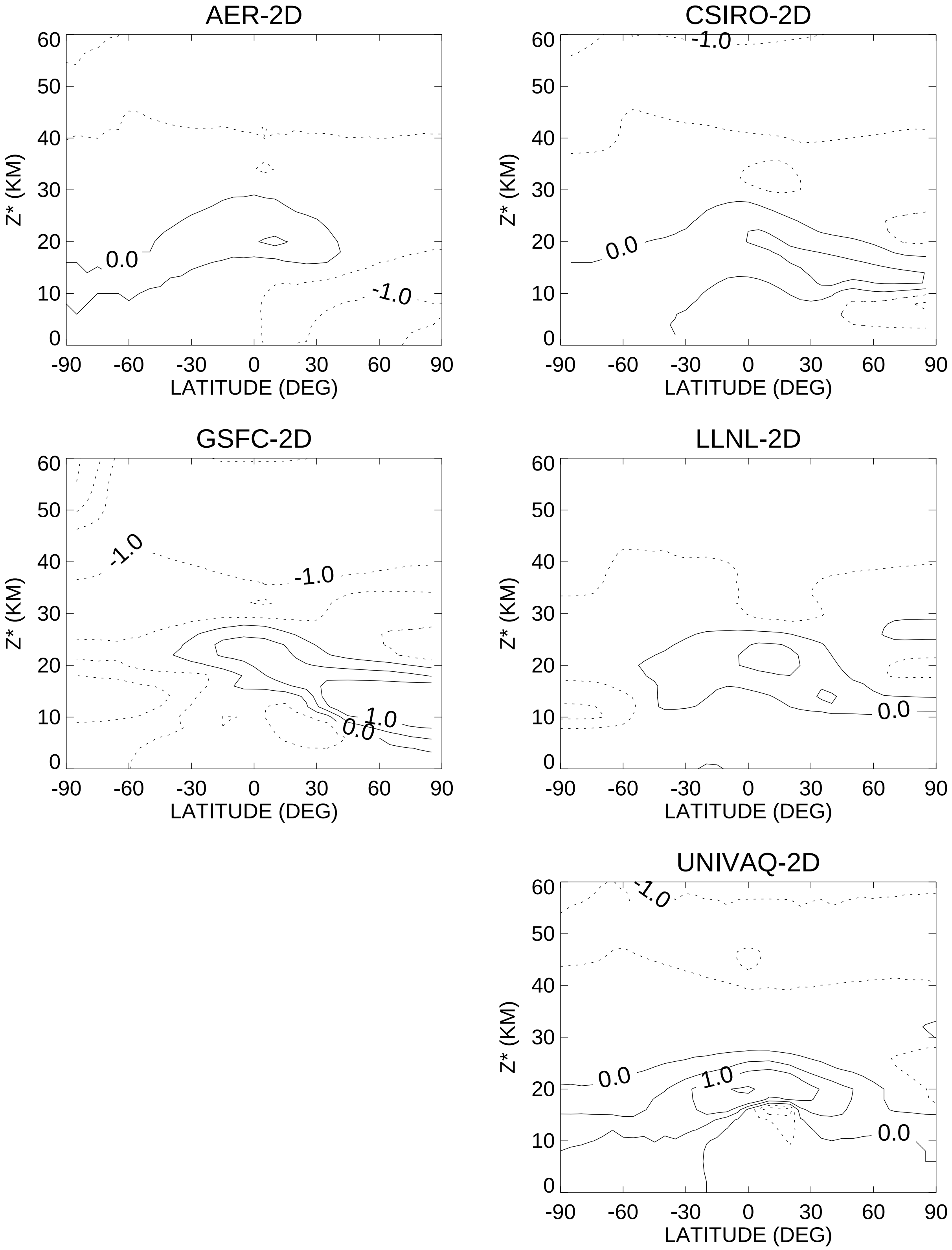

Figure 4.176: Calculated perturbations to O_3 (percent) as a function of latitude and altitude in June of 2015 due to emissions from a fleet of 500 HSCT aircraft with $EI(NO_x)=5$ and sulfate surface area of 4xSA0 under Scenario S3b relative to Scenario D3. Contours are -2, -1, -0.5, 0, 0.5, 1, 2.

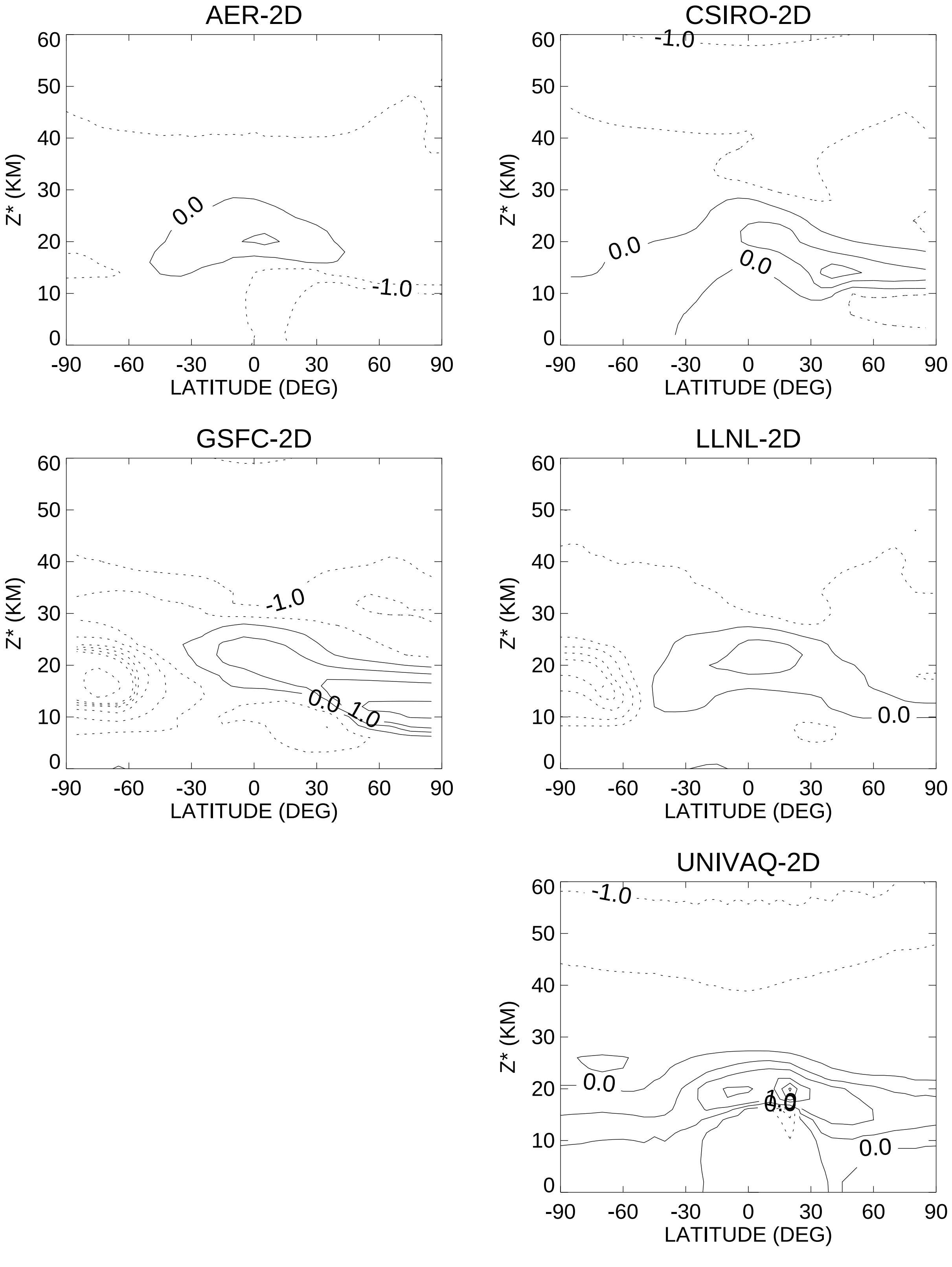

Figure 4.177: Calculated perturbations to O_3 (percent) as a function of latitude and altitude in October of 2015 due to emissions from a fleet of 500 HSCT aircraft with EI(NO_x)=5 and sulfate surface area of 4xSA0 under Scenario S3b relative to Scenario D3. Contours are -10, -5, -4, -3, -2, -1, -0.5, 0, 0.5, 1, 2, 3, 4.

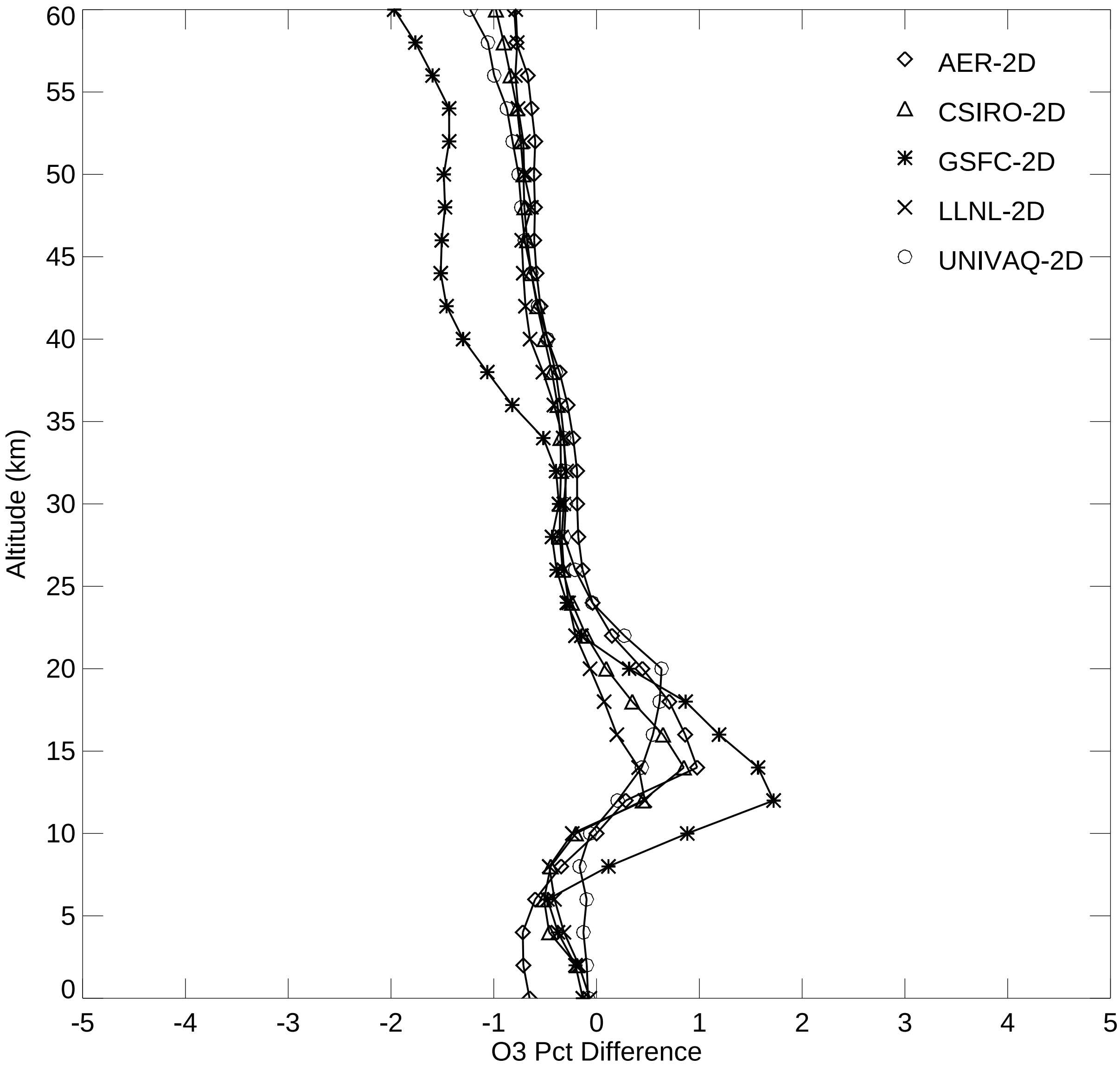

Figure 4.178: Calculated perturbations to O_3 (percent) as a function of altitude at 45^{o}N in June of 2015 due to emissions from a fleet of 500 HSCT aircraft with EI(NO_x)=5 and sulfate surface area of 4xSA0 under Scenario S3b relative to Scenario D3.

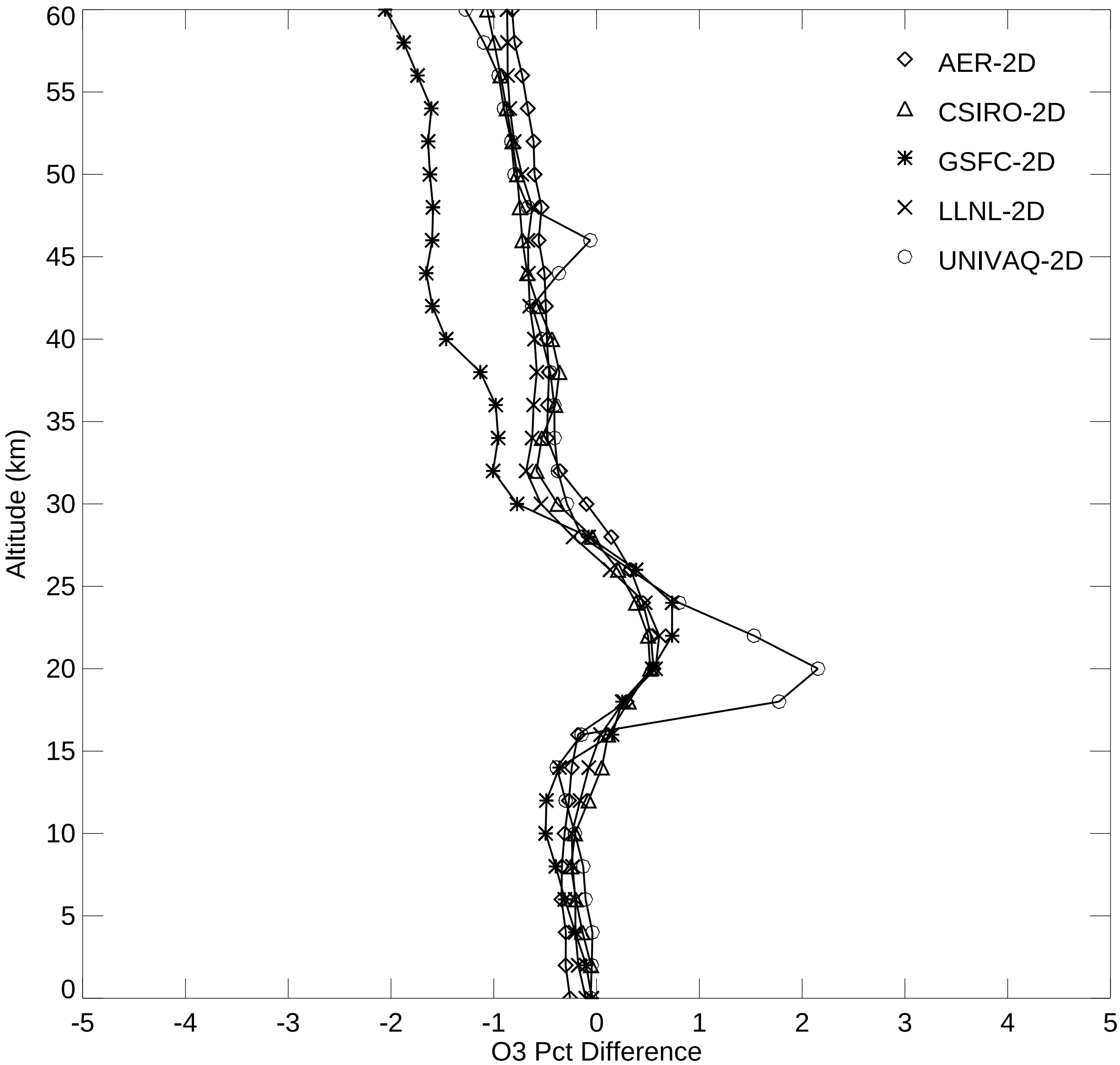

Figure 4.179: Calculated perturbations to O_3 (percent) as a function of altitude at the equator in June of 2015 due to emissions from a fleet of 500 HSCT aircraft with $EI(NO_x)=5$ and sulfate surface area of 4xSA0 under Scenario S3b relative to Scenario D3.

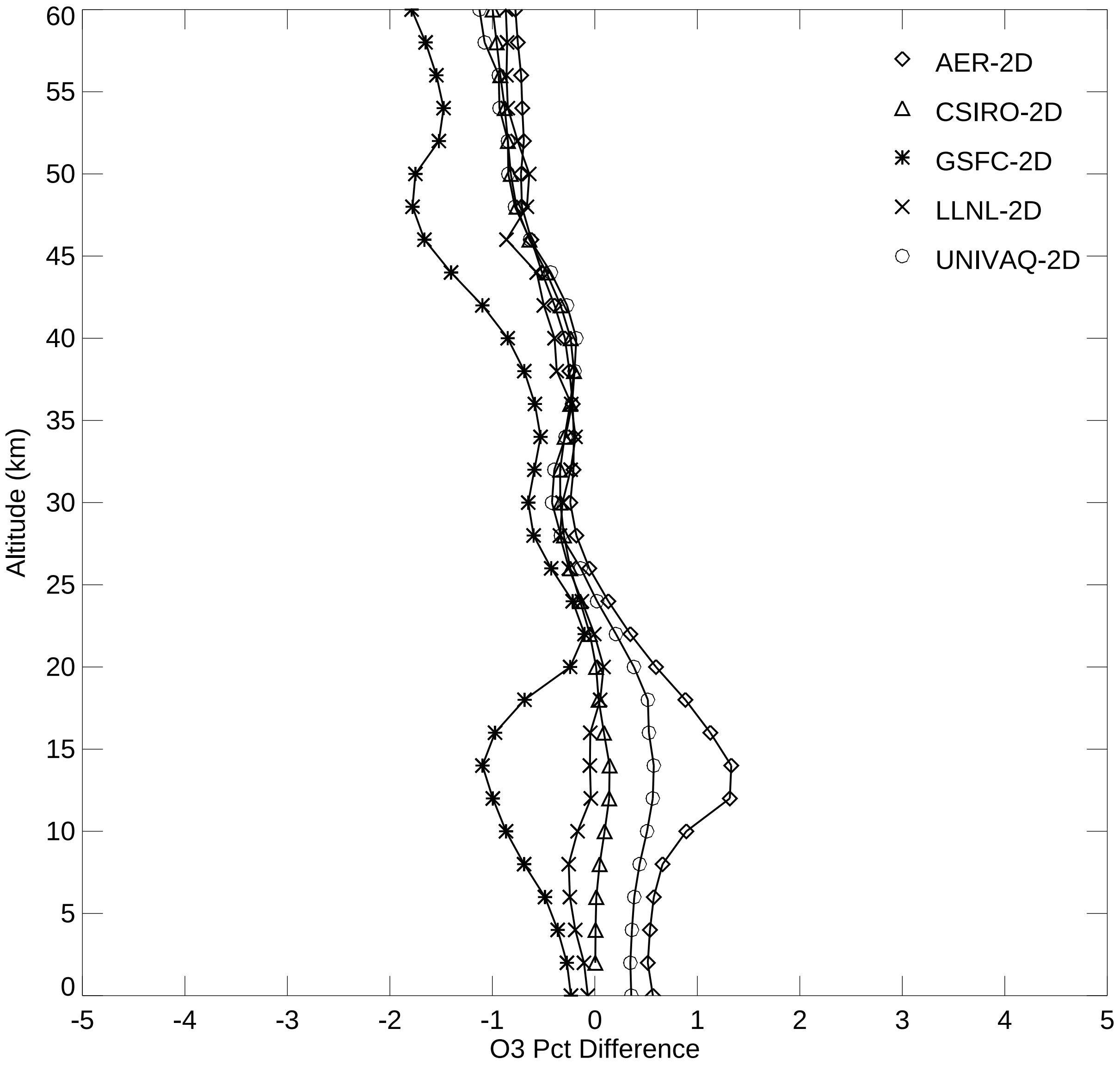

Figure 4.180: Calculated perturbations to O_3 (percent) as a function of altitude at 45^{o}S in June of 2015 due to emissions from a fleet of 500 HSCT aircraft with EI(NO_x)=5 and sulfate surface area of 4xSA0 under Scenario S3b relative to Scenario D3.

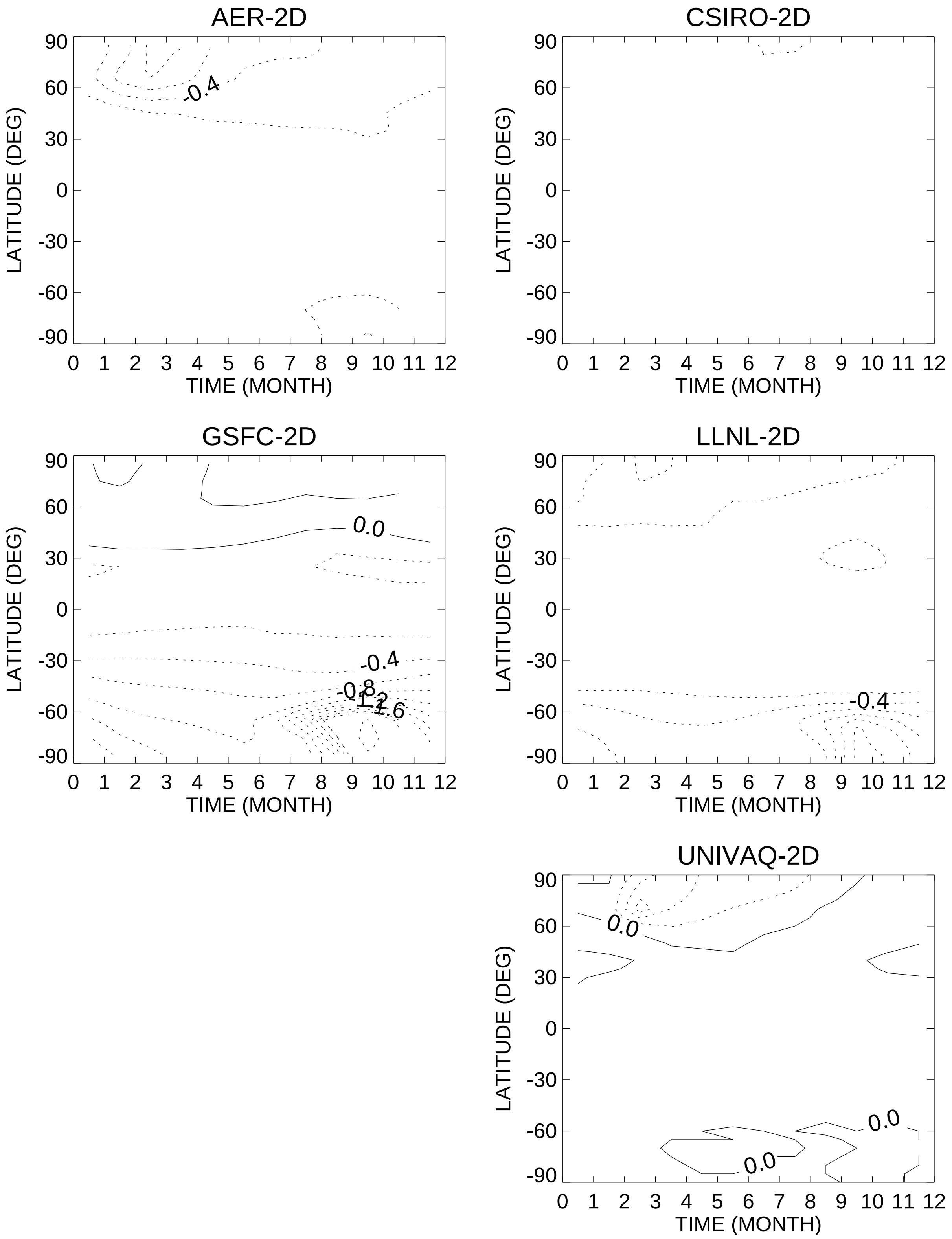

Figure 4.181: Calculated perturbations to column O_3 (percent) as a function of latitude and season in 2015 due to emissions from a fleet of 500 HSCT aircraft with EI(NO_x)=5 and sulfate surface area of 4xSA0 under Scenario S3b relative to Scenario D3. Contours are -3 and -2.0 to 0.2 by 0.2.

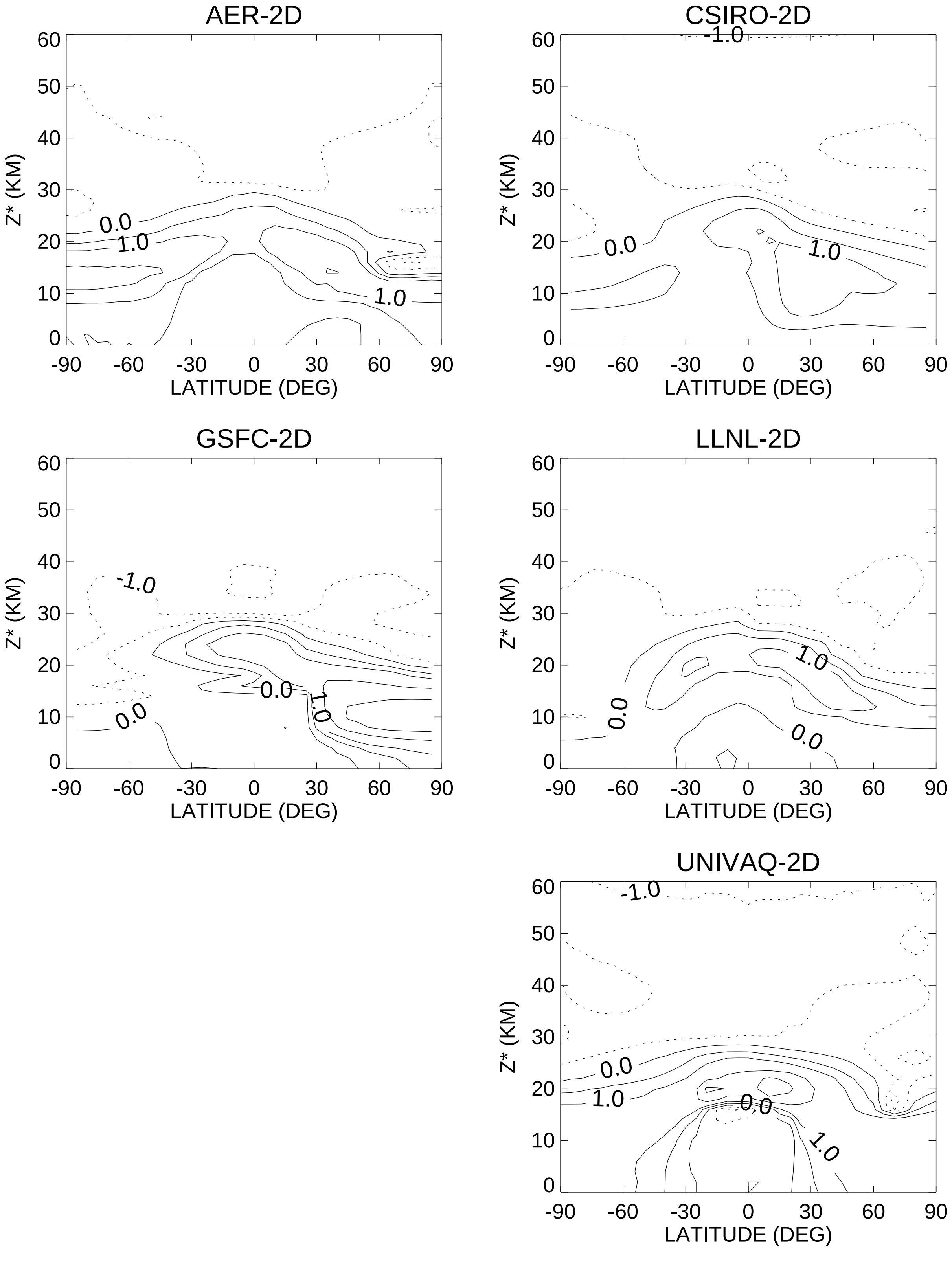

Figure 4.182: Calculated perturbations to O_3 (percent) as a function of latitude and altitude in March of 2015 due to emissions from a fleet of 500 HSCT aircraft with $EI(NO_x)=10$ and sulfate surface area of 4xSA0 under Scenario S3c relative to Scenario D3. Contours are -2, -1, -0.5, 0, 0.5, 1, 2, 3.

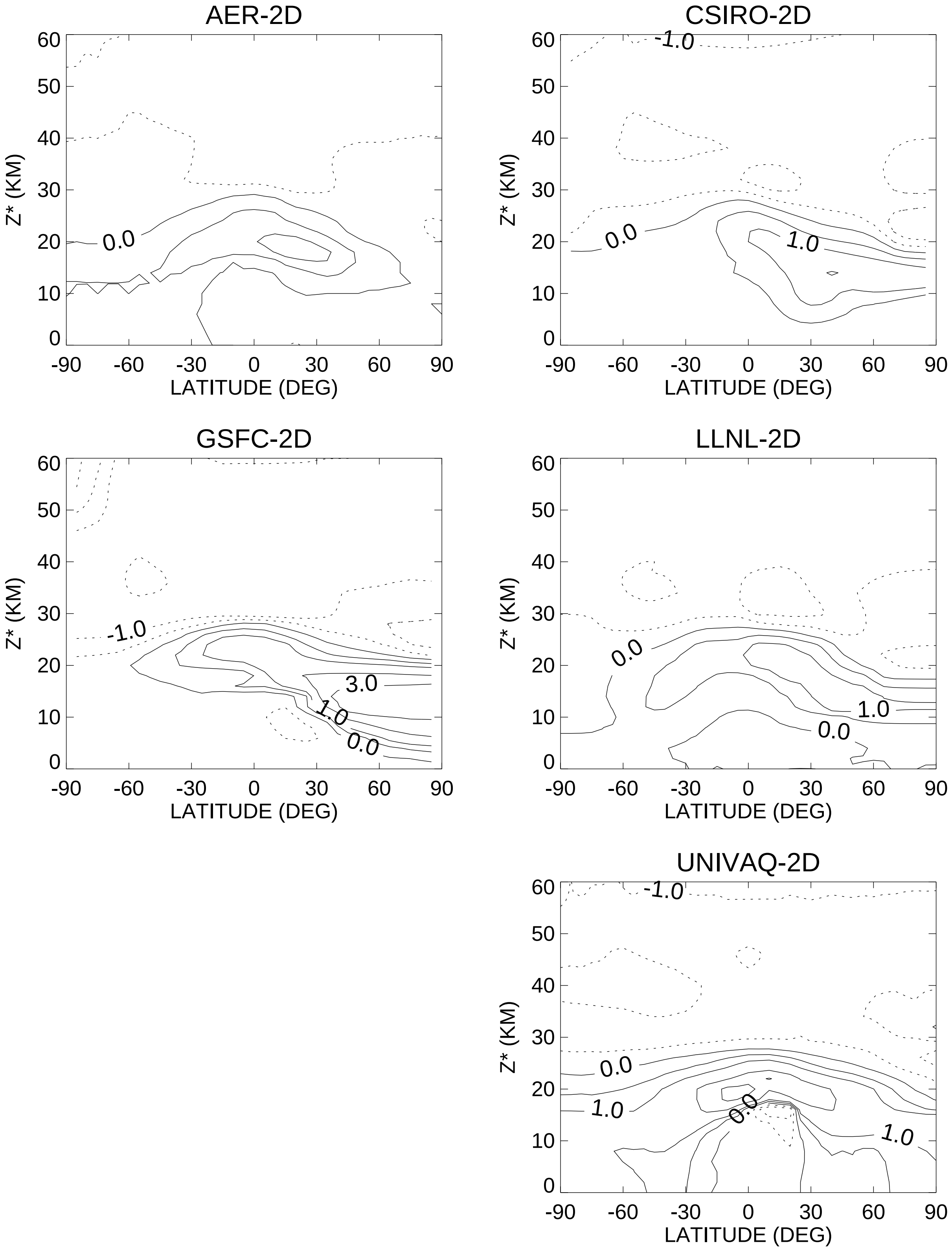

Figure 4.183: Calculated perturbations to O_3 (percent) as a function of latitude and altitude in June of 2015 due to emissions from a fleet of 500 HSCT aircraft with $EI(NO_x)=10$ and sulfate surface area of 4xSA0 under Scenario S3c relative to Scenario D3. Contours are -2, -1, -0.5, 0, 0.5, 1, 2, 3.

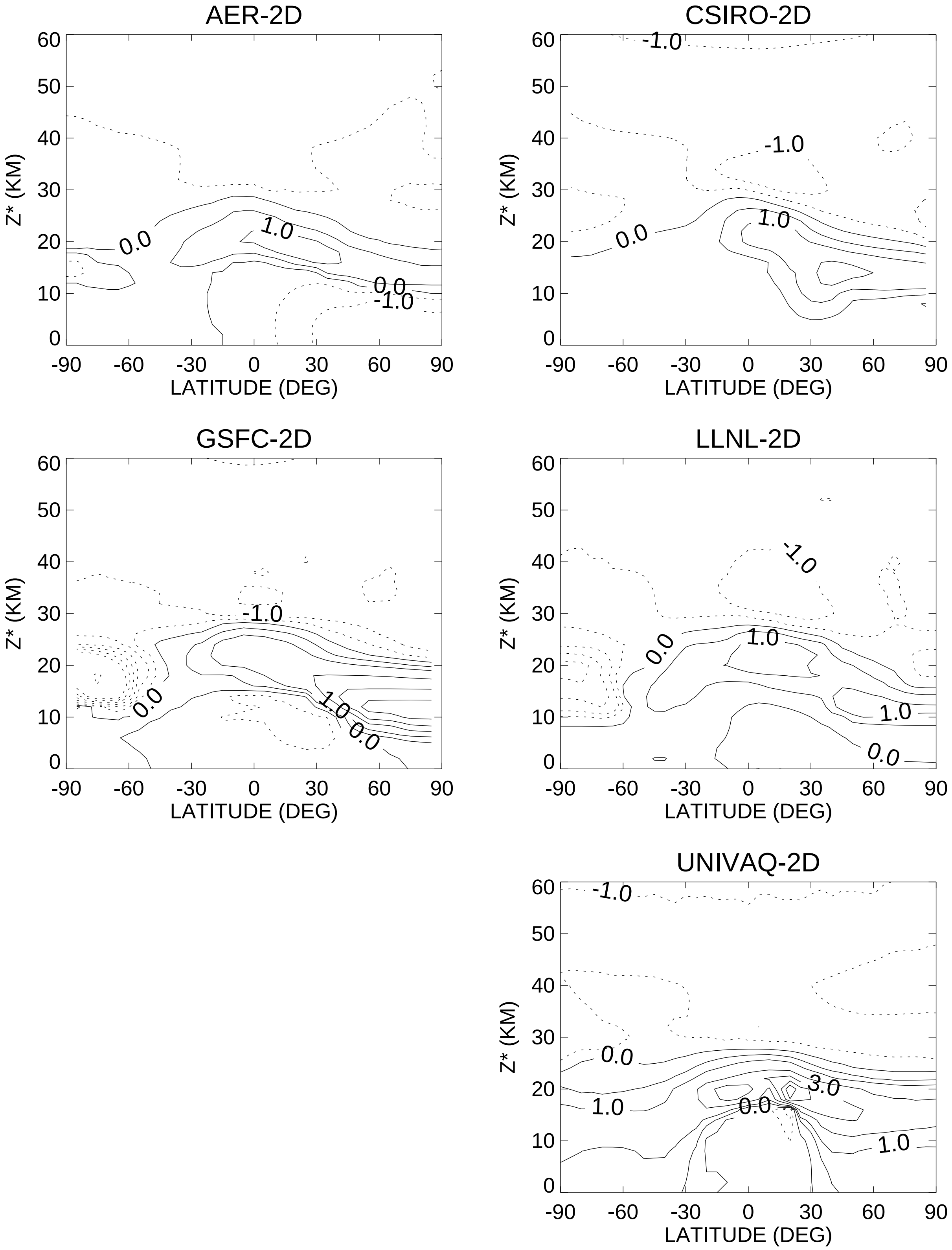

Figure 4.184: Calculated perturbations to O_3 (percent) as a function of latitude and altitude in October of 2015 due to emissions from a fleet of 500 HSCT aircraft with $EI(NO_x)=10$ and sulfate surface area of 4xSA0 under Scenario S3c relative to Scenario D3. Contours are -10, -5, -4, -3, -2, -1, -0.5, 0, 0.5, 1, 2, 3, 4, 5.

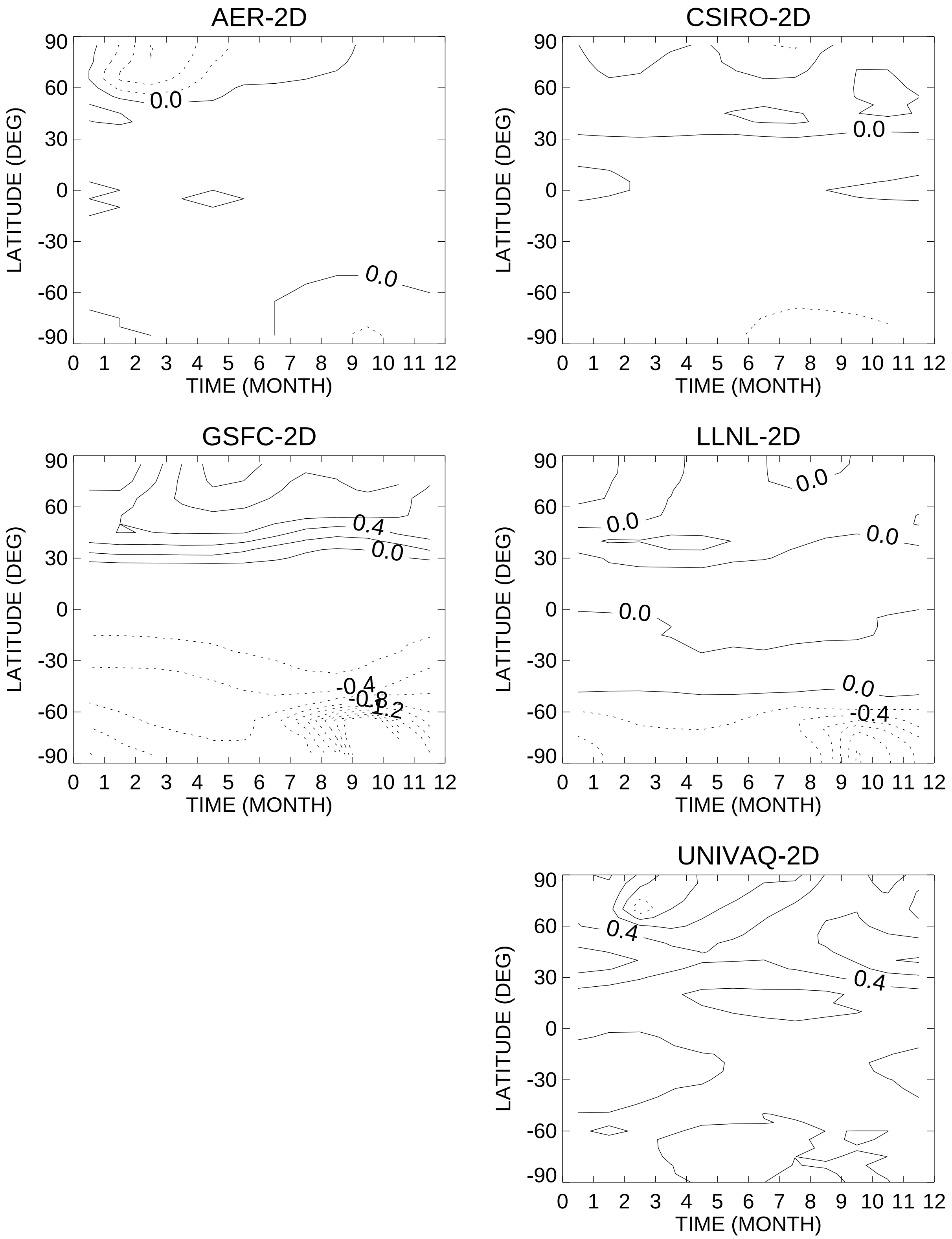

Figure 4.185: Calculated perturbations to column O_3 (percent) as a function of latitude and season in 2015 due to emissions from a fleet of 500 HSCT aircraft with EI(NO_x)=10 and sulfate surface area of 4xSA0 under Scenario S3c relative to Scenario D3. Contours are -2.0 to 1.0 by 0.2.

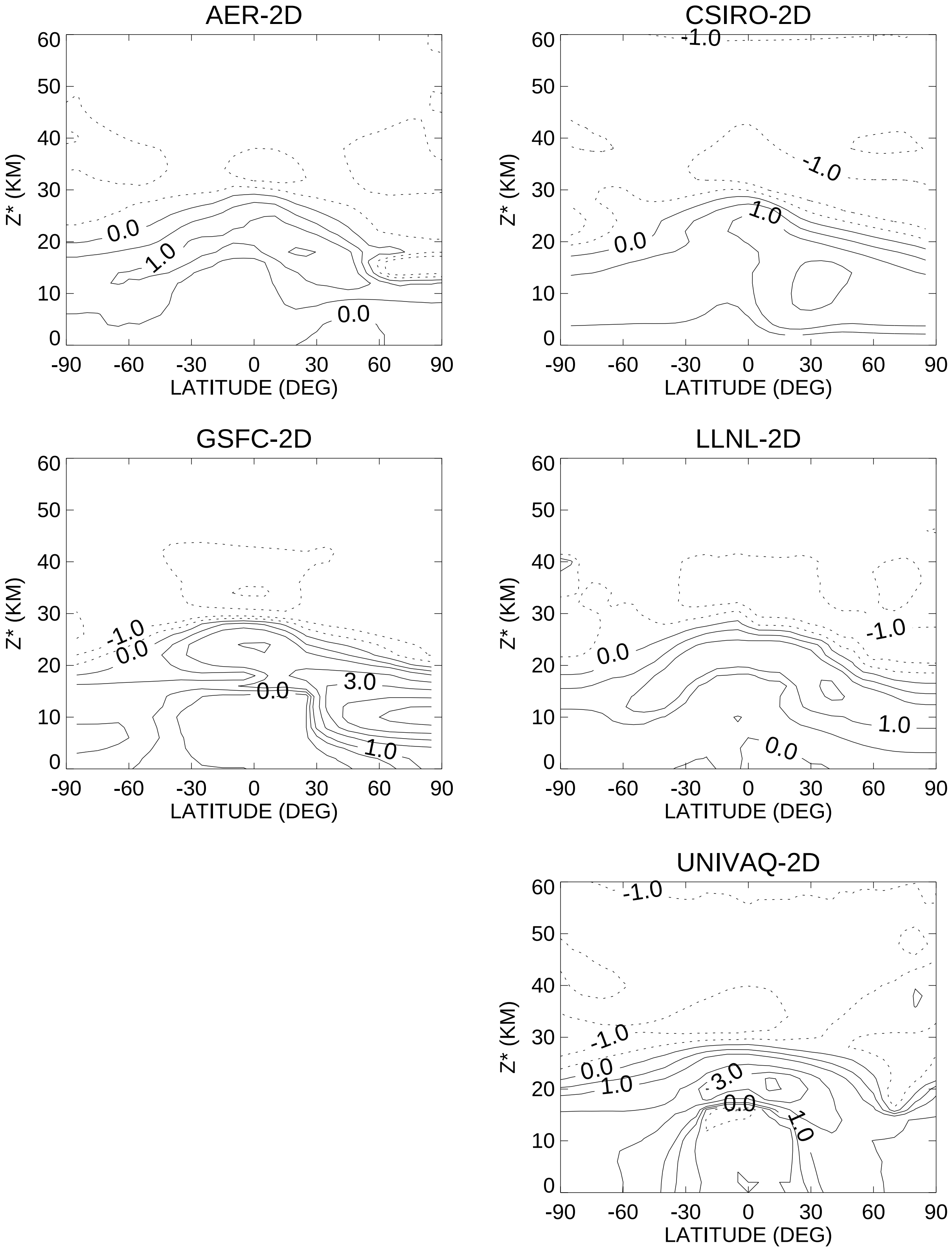

Figure 4.186: Calculated perturbations to O_3 (percent) as a function of latitude and altitude in March of 2015 due to emissions from a fleet of 500 HSCT aircraft with $EI(NO_x)=15$ and sulfate surface area of 4xSA0 under Scenario S3d relative to Scenario D3. Contours are -3, -2, -1, -0.5, 0, 0.5, 1, 2, 3, 4, 5.

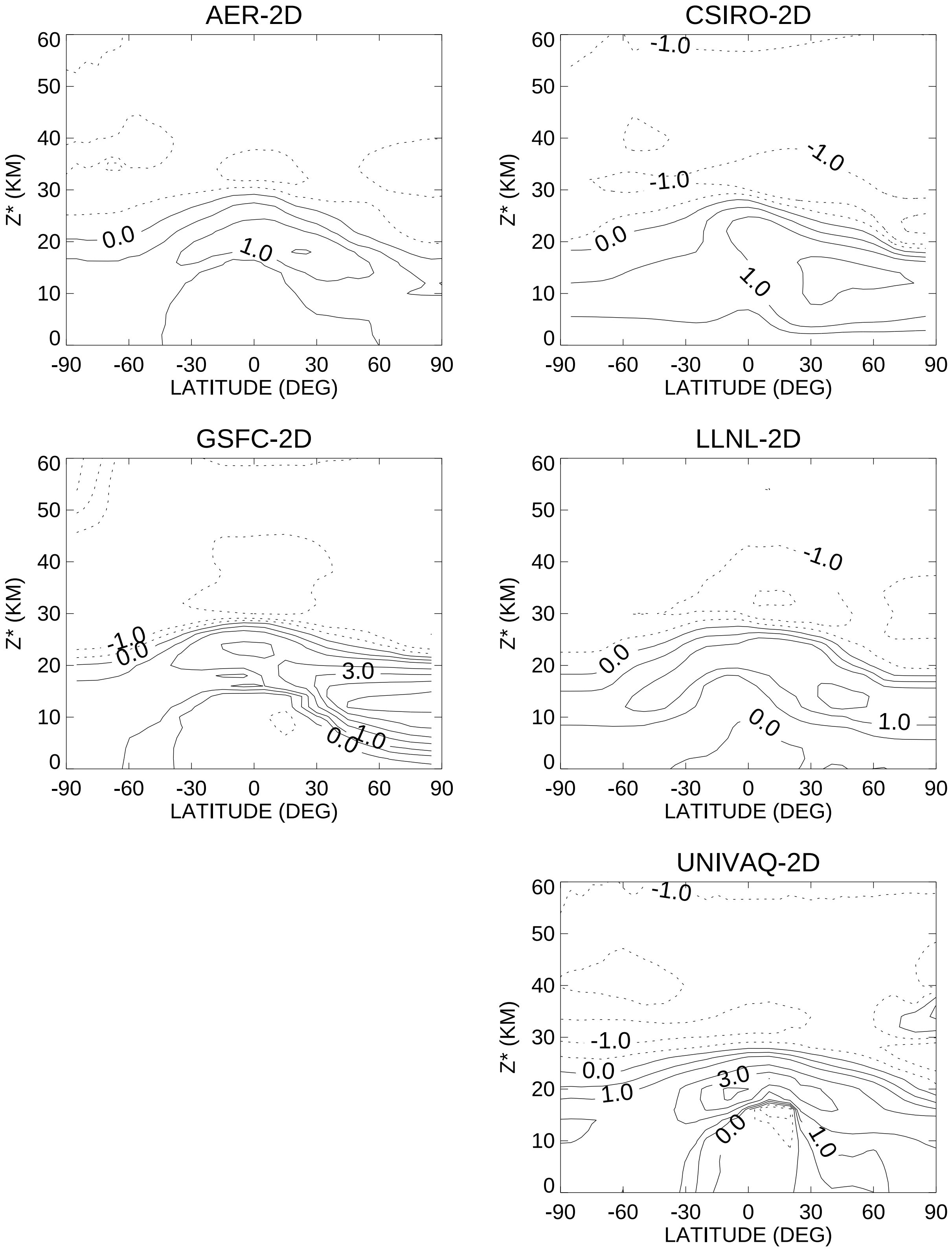

Figure 4.187: Calculated perturbations to O_3 (percent) as a function of latitude and altitude in June of 2015 due to emissions from a fleet of 500 HSCT aircraft with EI(NO_x)=15 and sulfate surface area of 4xSA0 under Scenario S3d relative to Scenario D3. Contours are -2, -1, -0.5, 0, 0.5, 1, 2, 3, 4, 5.

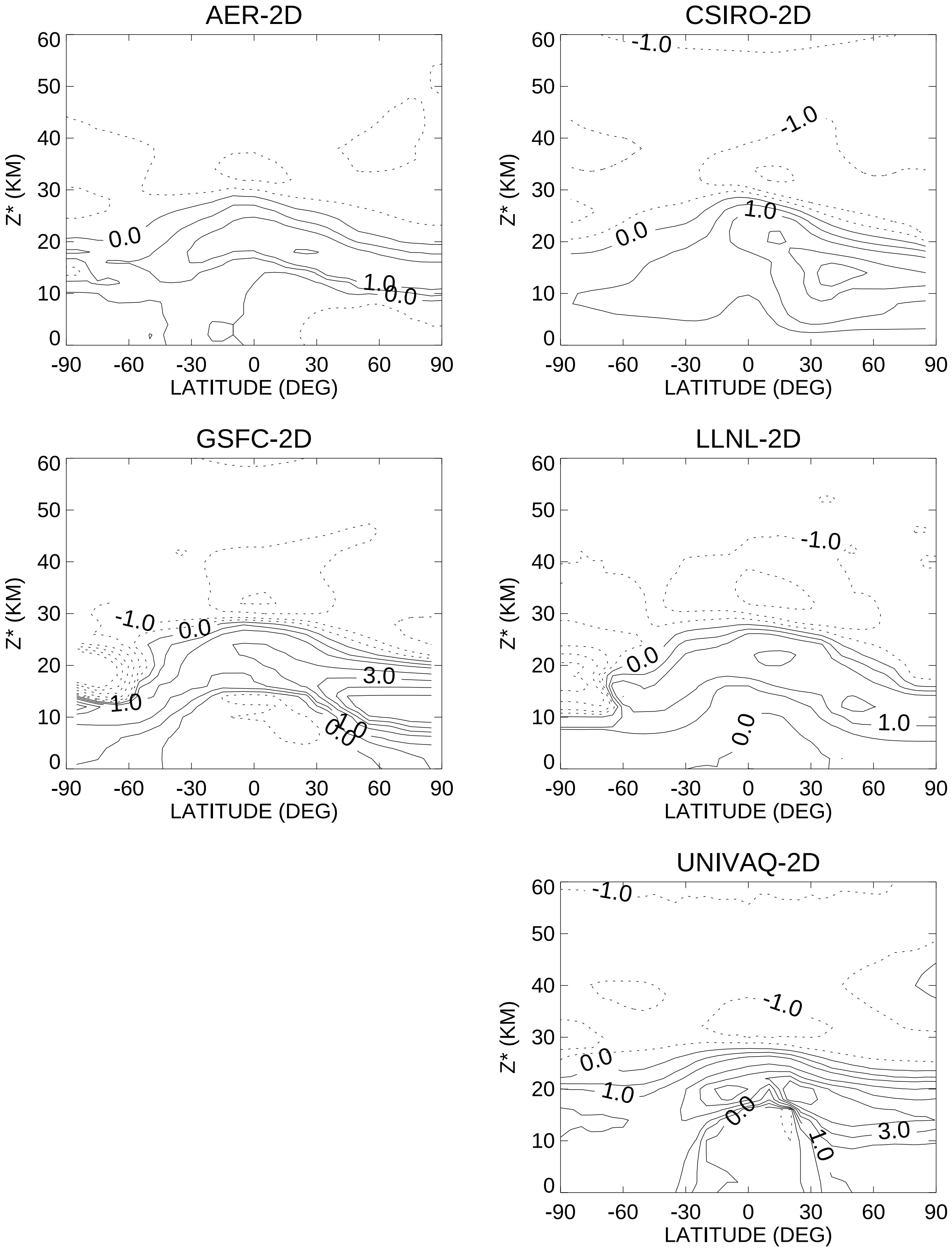

Figure 4.188: Calculated perturbations to O_3 (percent) as a function of latitude and altitude in October of 2015 due to emissions from a fleet of 500 HSCT aircraft with $EI(NO_x)=15$ and sulfate surface area of 4xSA0 under Scenario S3d relative to Scenario D3. Contours are -5, -4, -3, -2, -1, -0.5, 0, 0.5, 1, 2, 3, 4, 5.

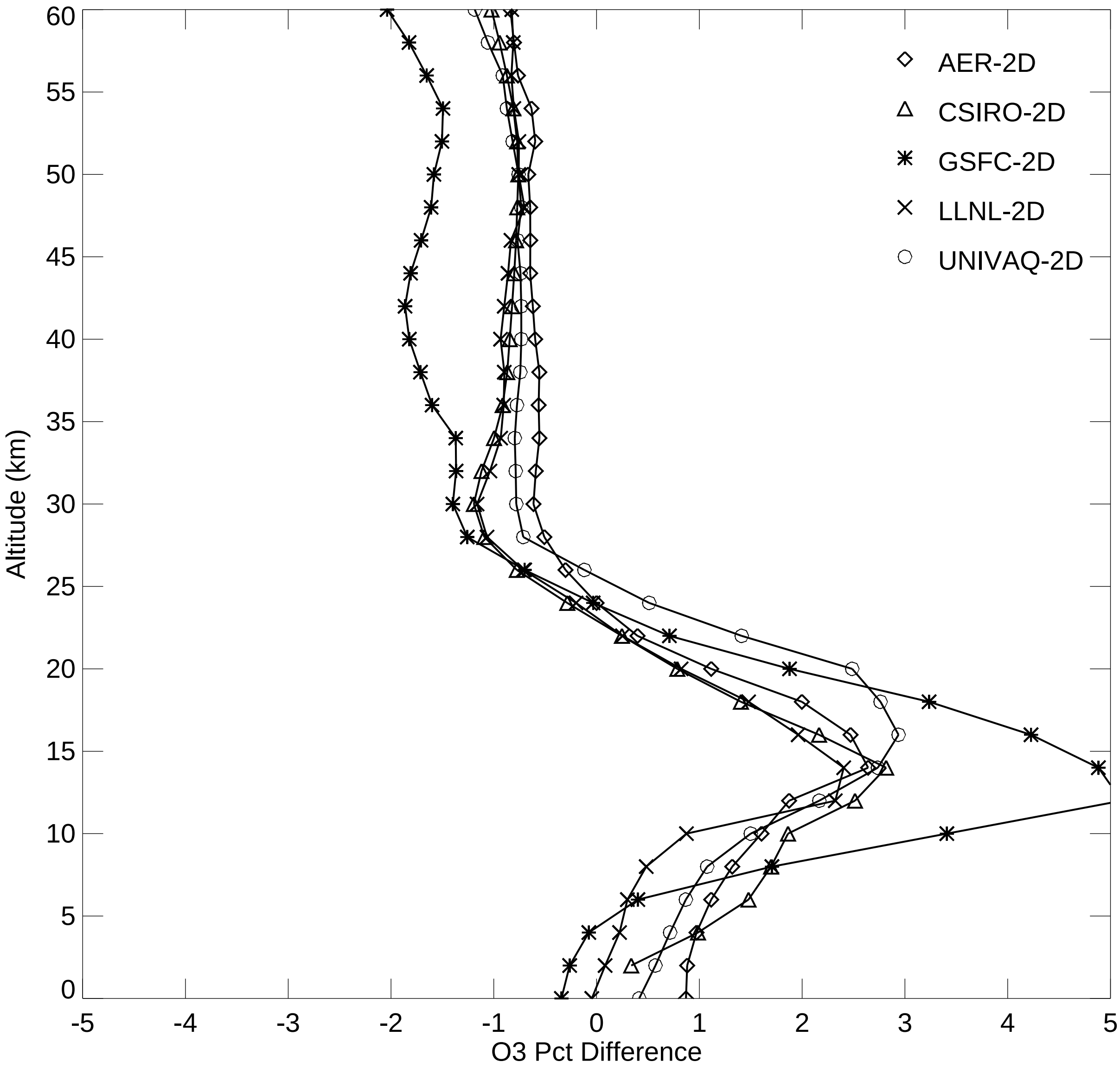

Figure 4.189: Calculated perturbations to O_3 (percent) as a function of altitude at 45^oN in June of 2015 due to emissions from a fleet of 500 HSCT aircraft with EI(NO_x)=15 and sulfate surface area of 4xSA0 under Scenario S3d relative to Scenario D3.

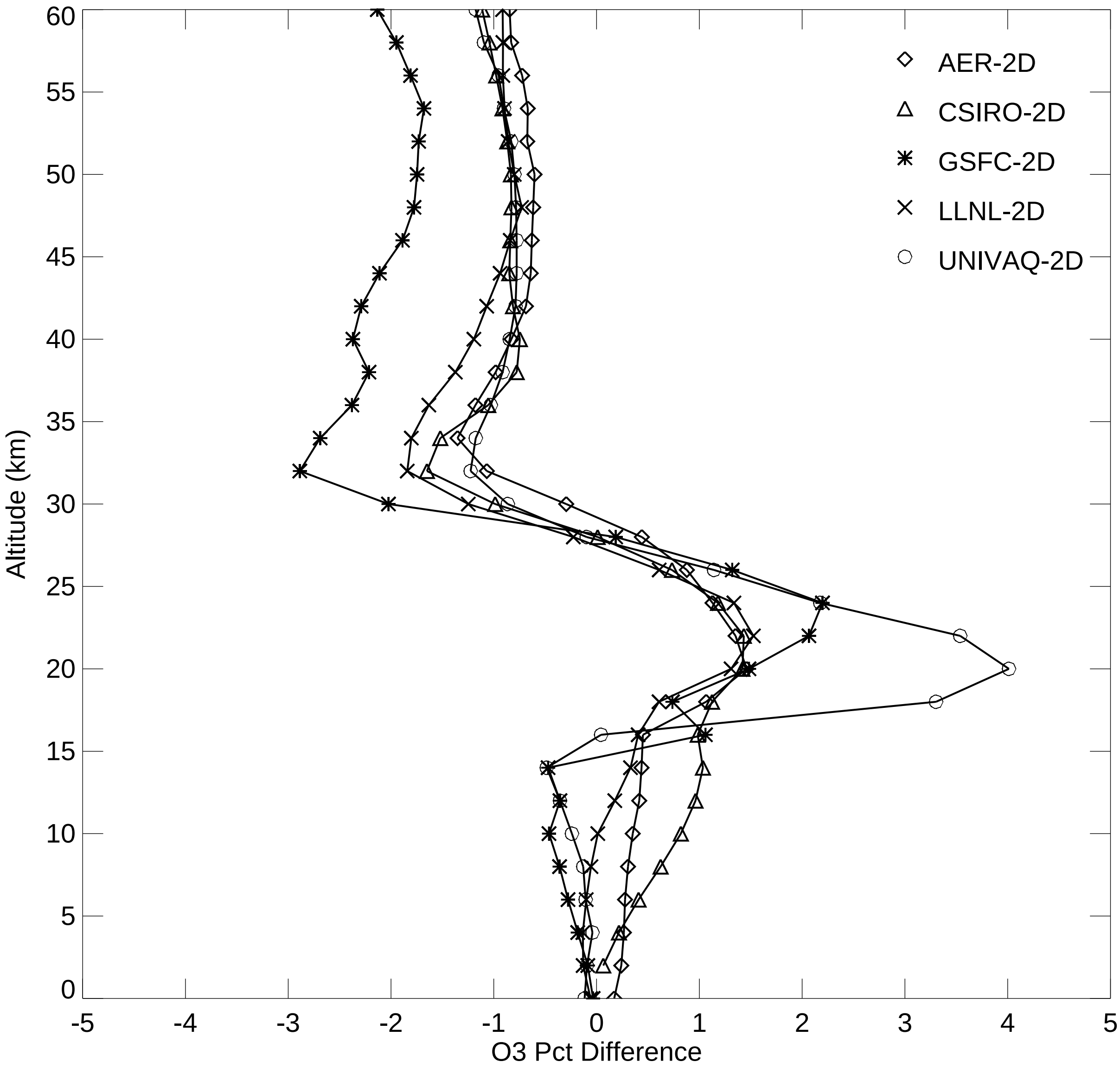

Figure 4.190: Calculated perturbations to O_3 (percent) as a function of altitude at the equator in June of 2015 due to emissions from a fleet of 500 HSCT aircraft with $EI(NO_x)=15$ and sulfate surface area of 4xSA0 under Scenario S3d relative to Scenario D3.

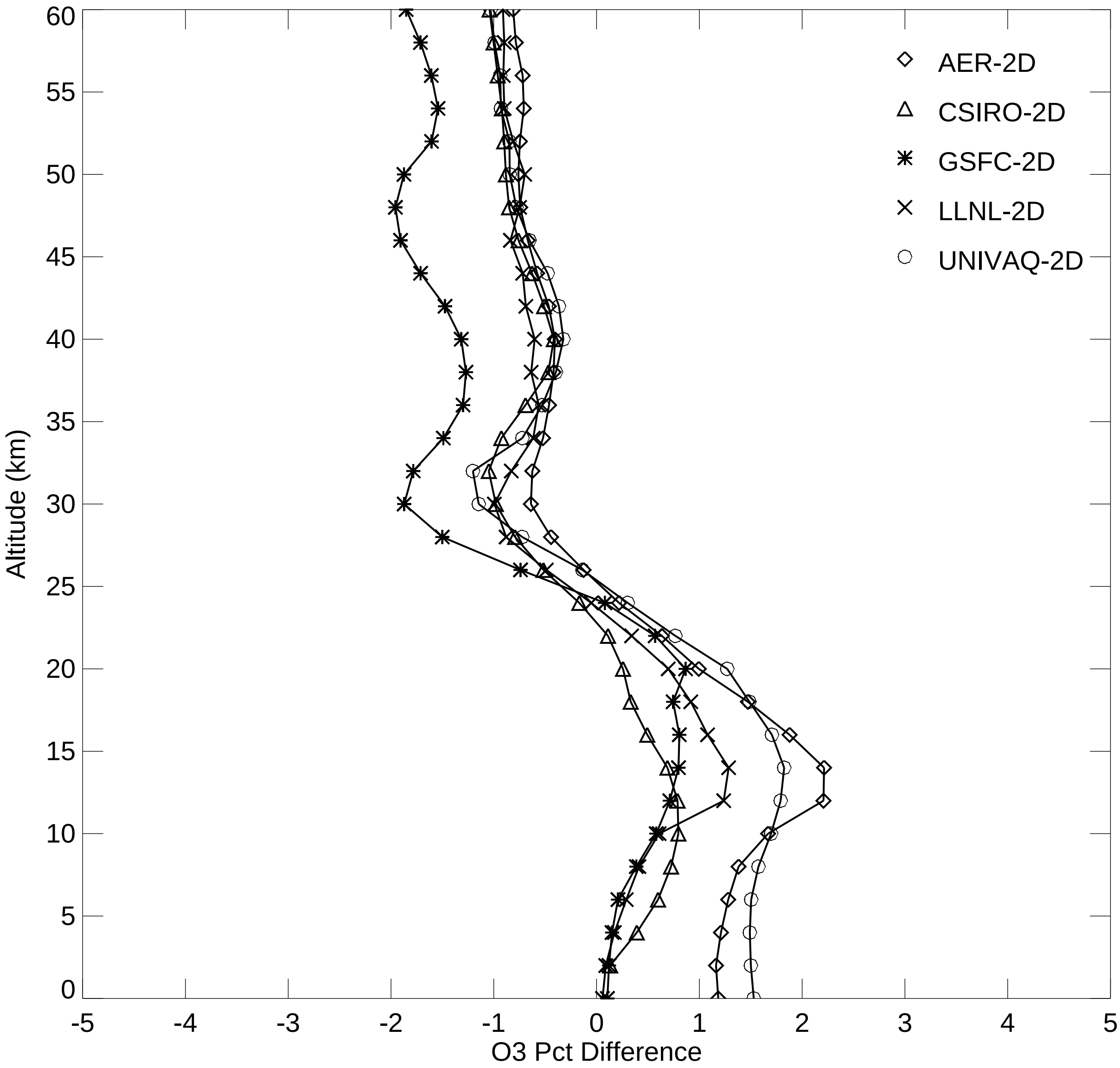

Figure 4.191: Calculated perturbations to O_3 (percent) as a function of altitude at 45^{o}S in June of 2015 due to emissions from a fleet of 500 HSCT aircraft with EI(NO_x)=15 and sulfate surface area of 4xSA0 under Scenario S3d relative to Scenario D3.

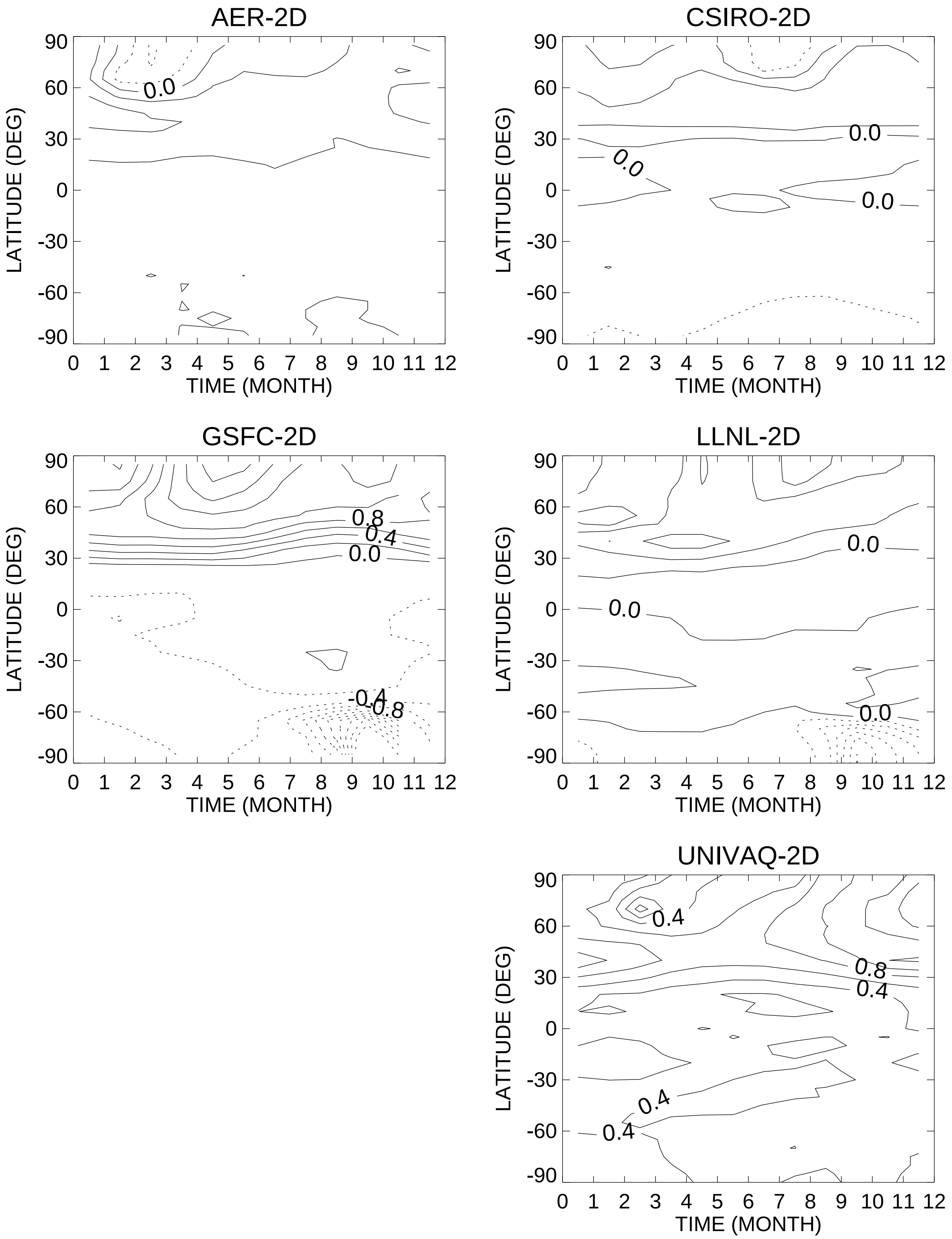

Figure 4.192: Calculated perturbations to column O_3 (percent) as a function of latitude and season in 2015 due to emissions from a fleet of 500 HSCT aircraft with $EI(NO_x)$=15 and sulfate surface area of 4xSA0 under Scenario S3d relative to Scenario D3. Contours are -2.0 to 1.6 by 0.2.

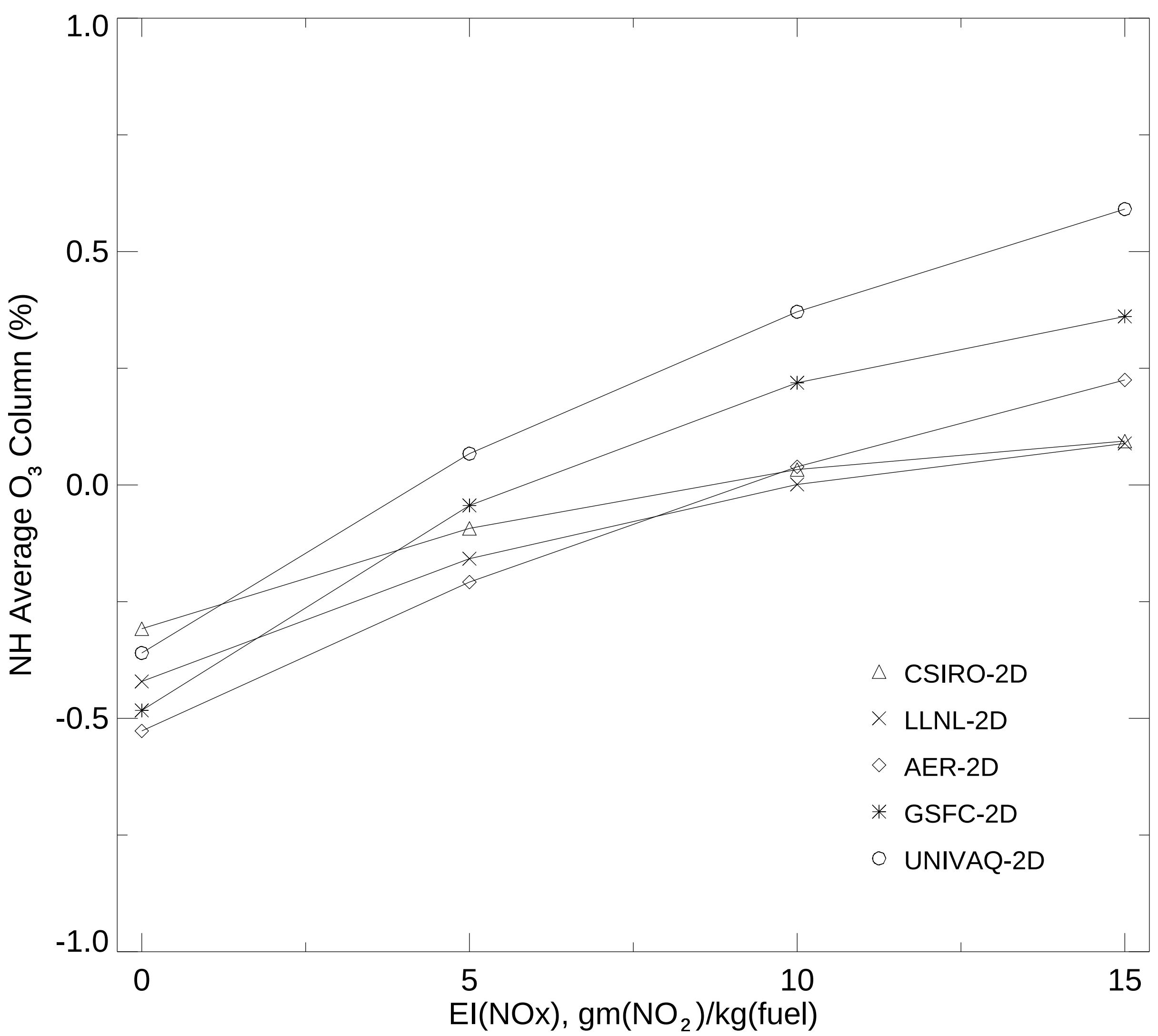

Figure 4.193: Northern hemisphere annual average total O_3 column change (percent) as a function of $EI(NO_x)$ for an HSCT fleet of 500 aircraft operating in 2015 with 4xSA0 sulfate surface area density.

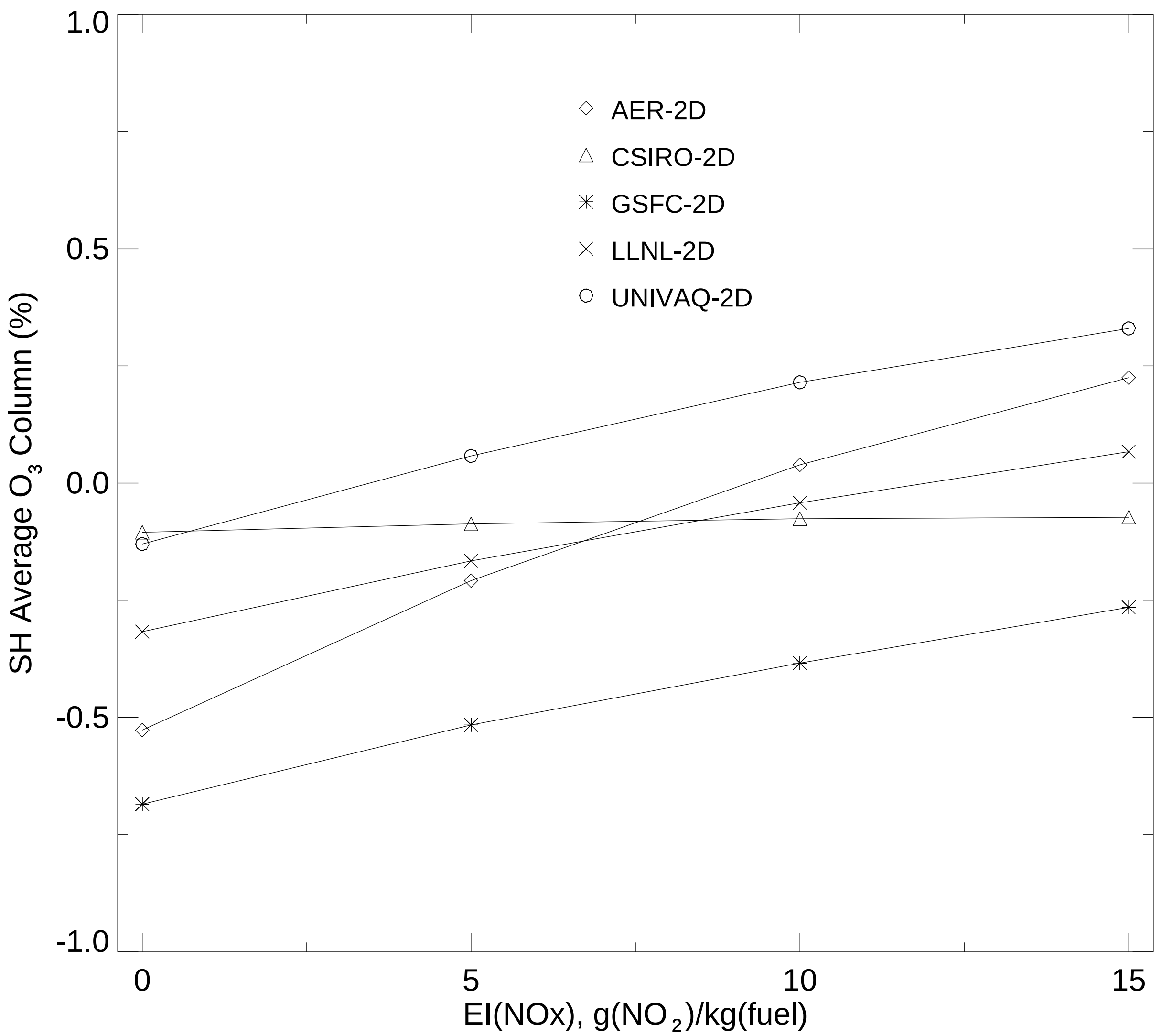

Figure 4.194: Southern hemisphere annual average total O_3 column change (percent) as a function of $EI(NO_x)$ for an HSCT fleet of 500 aircraft operating in 2015 with 4xSA0 sulfate surface area density.

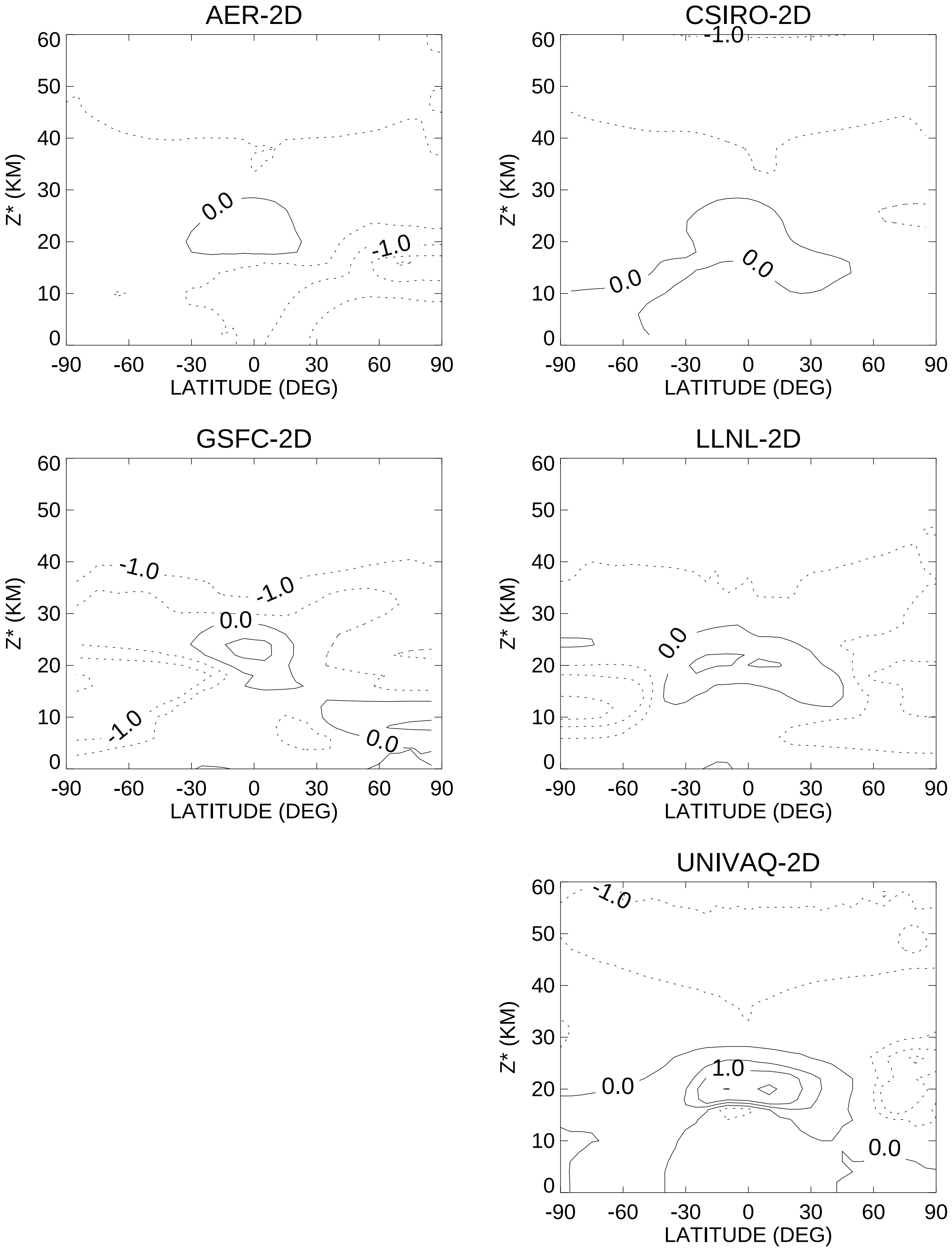

Figure 4.195: Calculated perturbations to O_3 (percent) as a function of latitude and altitude in March of 2015 due to emissions from a fleet of 500 HSCT aircraft operating with $EI(NO_x)=5$ and sulfate surface area of 4xSA0+SA1-SA0 under Scenario S3e relative to Scenario D3. Contours are -3, -2, -1, -0.5, 0, 0.5, 1, 2.

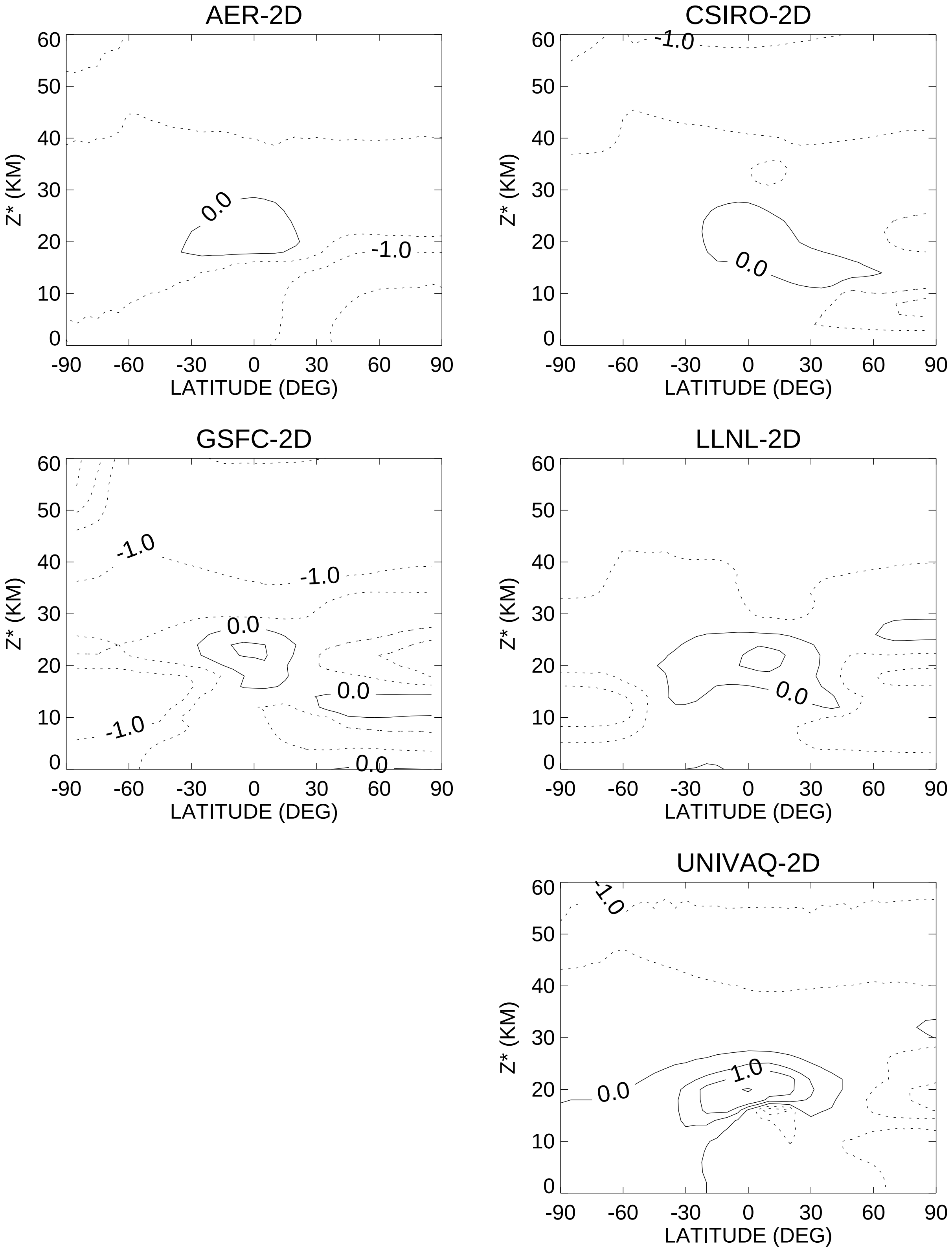

Figure 4.196: Calculated perturbations to O_3 (percent) as a function of latitude and altitude in June of 2015 due to emissions from a fleet of 500 HSCT aircraft with EI(NO_x)=5 and sulfate surface area of 4xSA0+SA1-SA0 under Scenario S3e relative to Scenario D3. Contours are -2, -1, -0.5, 0, 0.5, 1, 2.

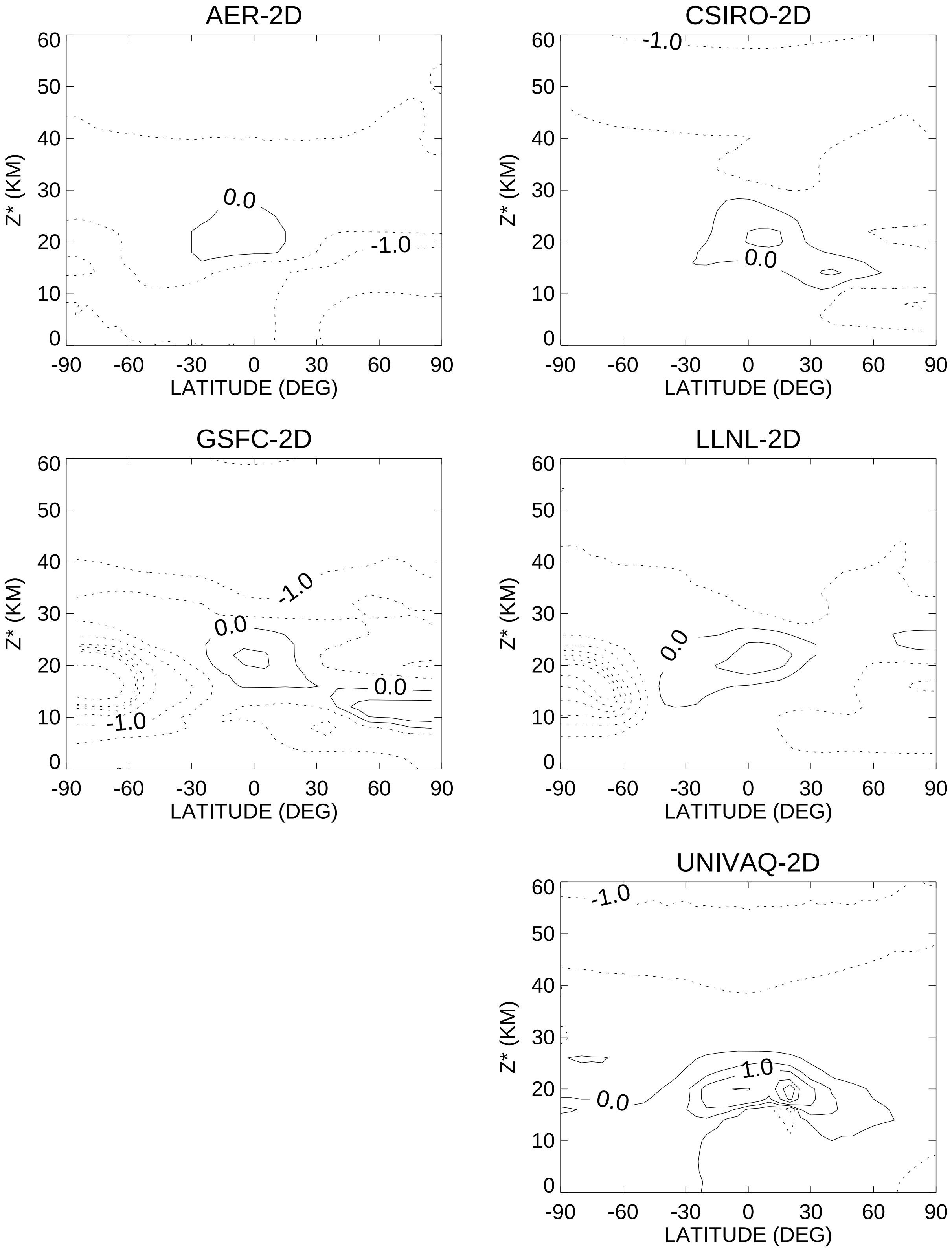

Figure 4.197: Calculated perturbations to O_3 (percent) as a function of latitude and altitude in October of 2015 due to emissions from a fleet of 500 HSCT aircraft with EI(NO_x)=5 and sulfate surface area of 4xSA0+SA1-SA0 under Scenario S3e relative to Scenario D3. Contours are -10, -5, -4, -3, -2, -1, -0.5, 0, 0.5, 1, 2, 3.

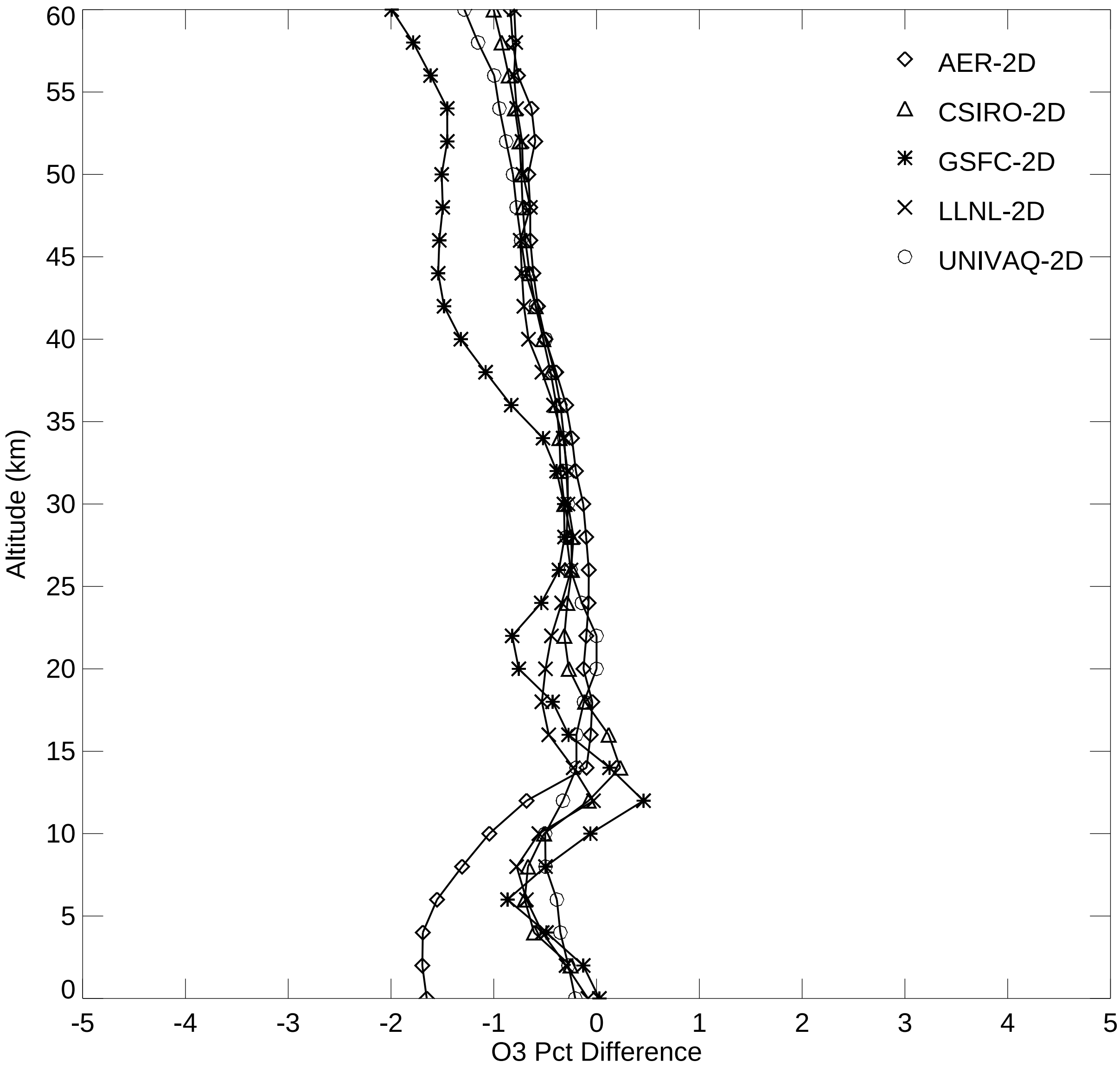

Figure 4.198: Calculated perturbations to O_3 (percent) as a function of altitude at 45^{o}N in June of 2015 due to emissions from a fleet of 500 HSCT aircraft with EI(NO_x)=5 and sulfate surface area of 4xSA0+SA1-SA0 under Scenario S3e relative to Scenario D3.

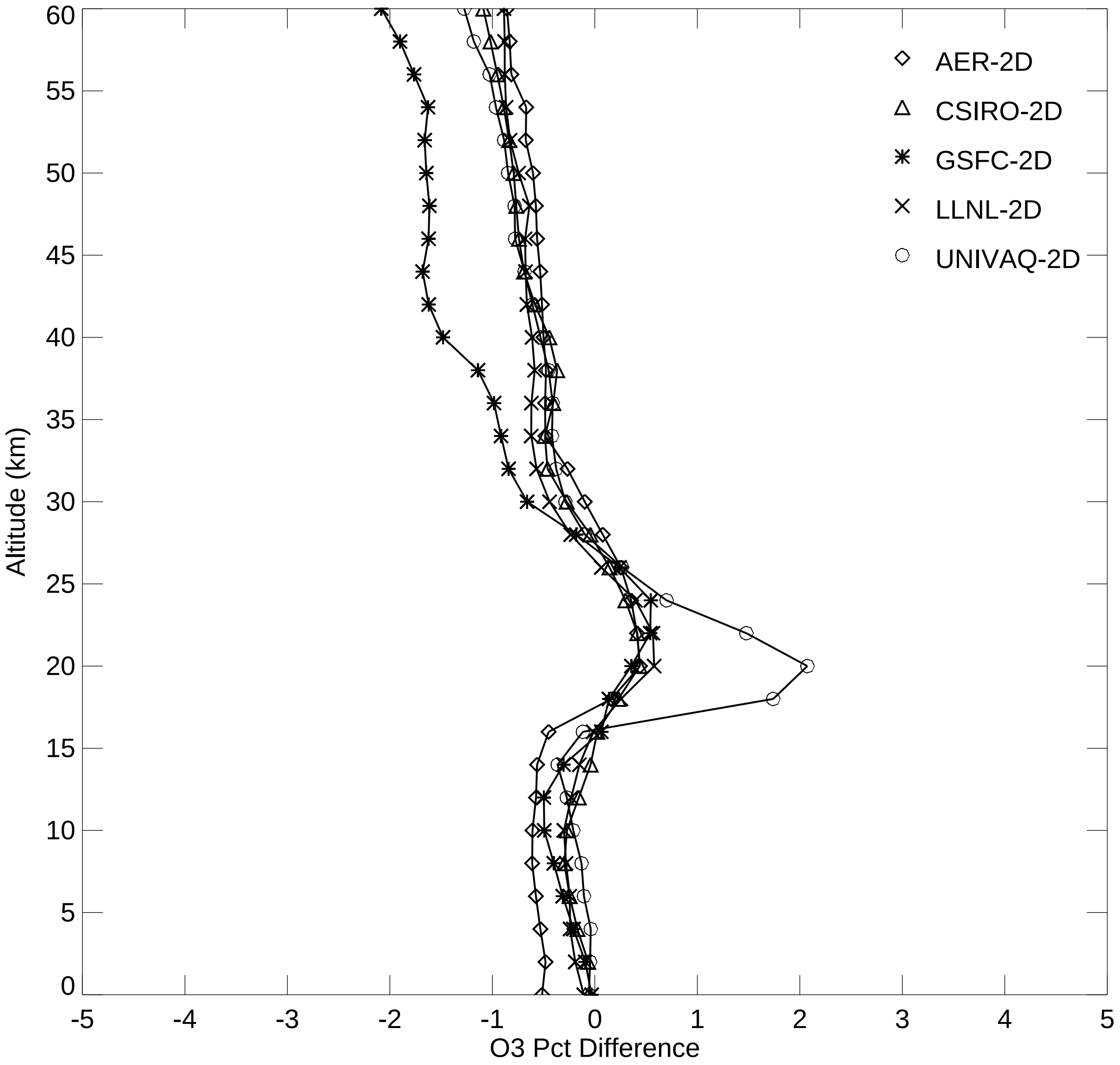

Figure 4.199: Calculated perturbations to O_3 (percent) as a function of altitude at the equator in June of 2015 due to emissions from a fleet of 500 HSCT aircraft with $EI(NO_x)=5$ and sulfate surface area of 4xSA0+SA1-SA0 under Scenario S3e relative to Scenario D3.

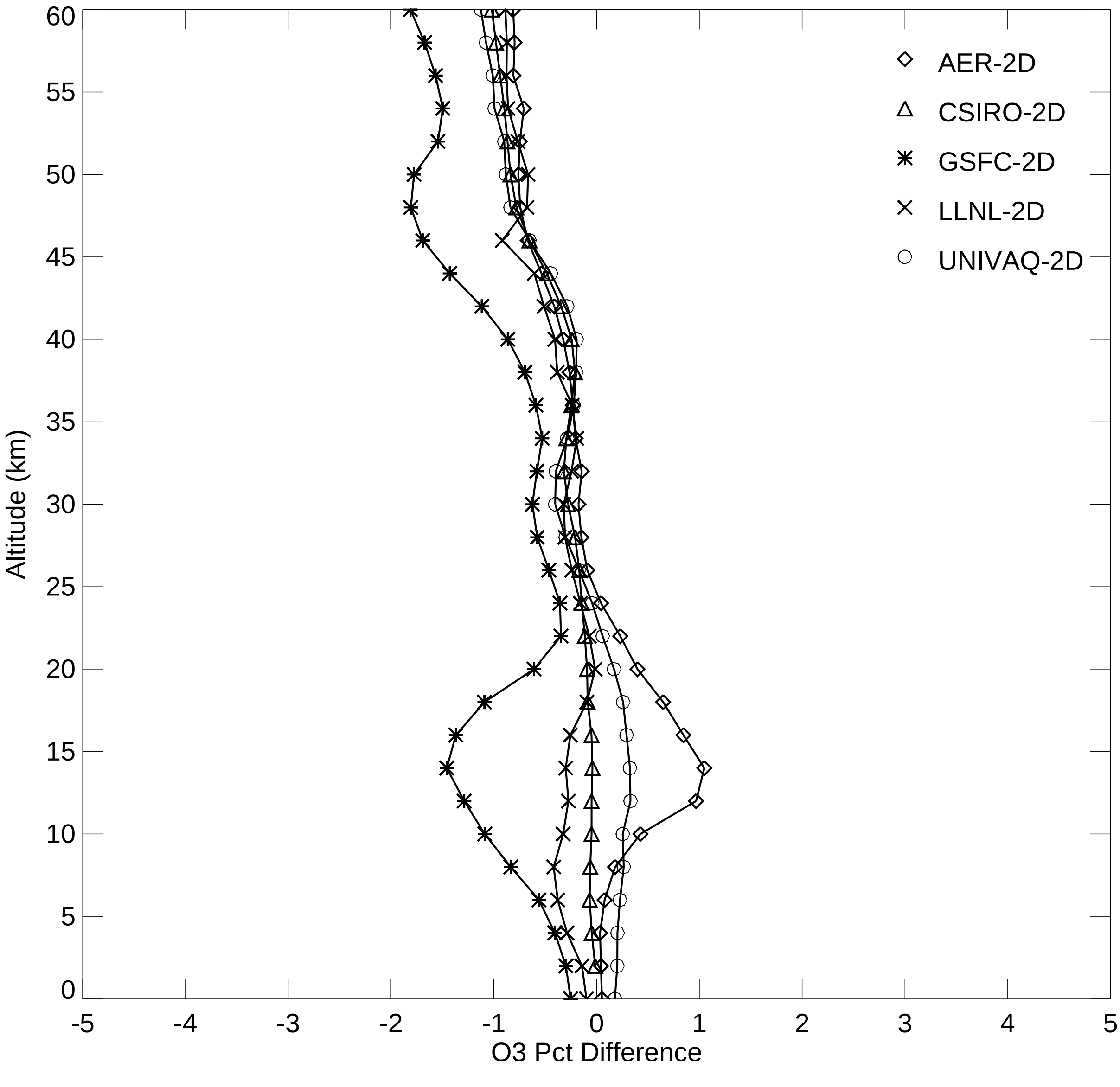

Figure 4.200: Calculated perturbations to O_3 (percent) as a function of altitude at 45^{o}S in June of 2015 due to emissions from a fleet of 500 HSCT aircraft with EI(NO_x)=5 and sulfate surface area of 4xSA0+SA1-SA0 under Scenario S3e relative to Scenario D3.

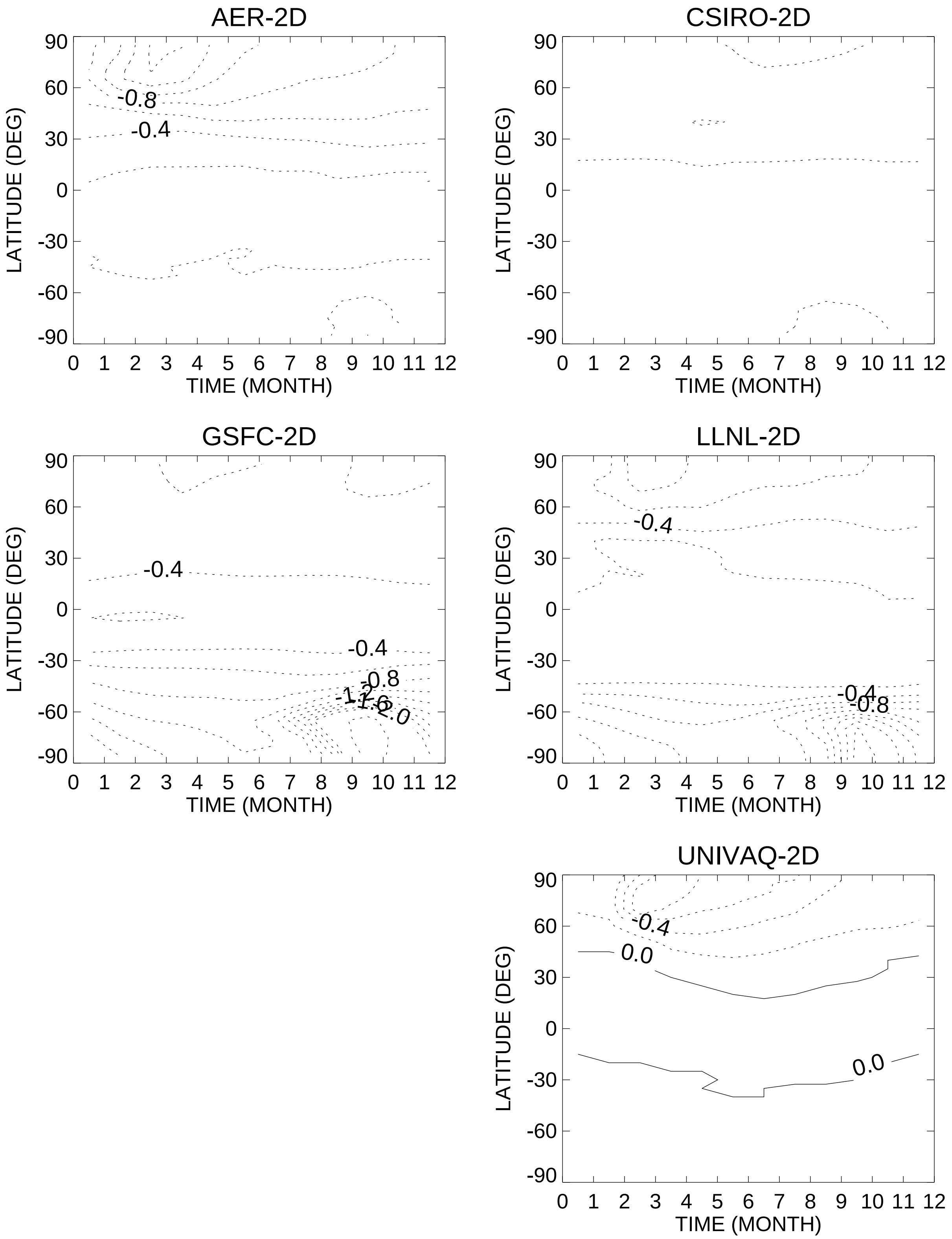

Figure 4.201: Calculated perturbations to column O_3 (percent) as a function of latitude and season in 2015 due to emissions from a fleet of 500 HSCT aircraft with $EI(NO_x)=5$ and sulfate surface area of 4xSA0+SA1-SA0 under Scenario S3e relative to Scenario D3. Contours are -3 and -2 to 0 by 0.2.

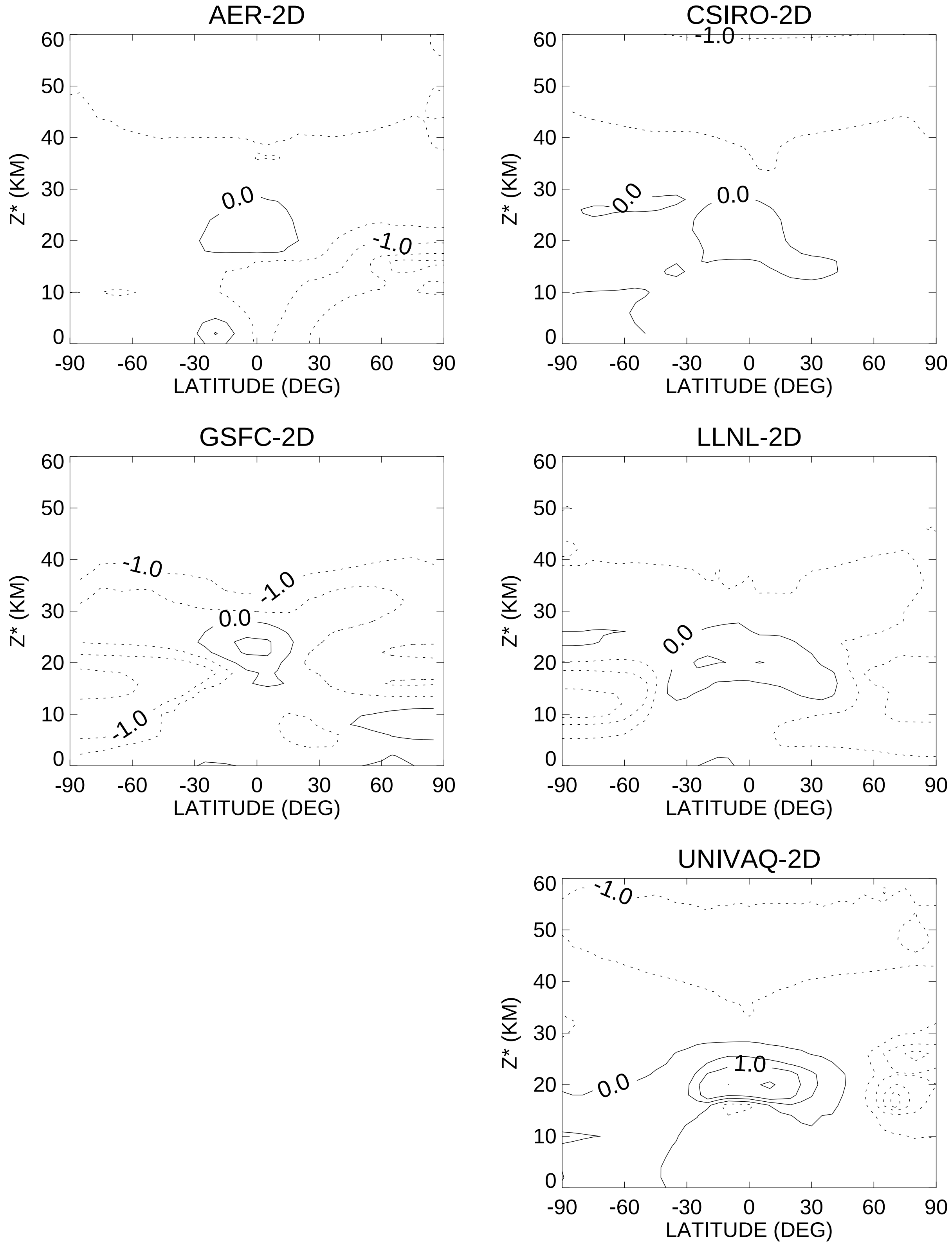

Figure 4.202: Calculated perturbations to O_3 (percent) as a function of latitude and altitude in March of 2015 due to emissions from a fleet of 500 HSCT aircraft with $EI(NO_x)=5$ and sulfate surface area of 4xSA0+SA3-SA0 under Scenario S3f relative to Scenario D3. Contours are -3, -2, -1, -0.5, 0, 0.5, 1, 2.

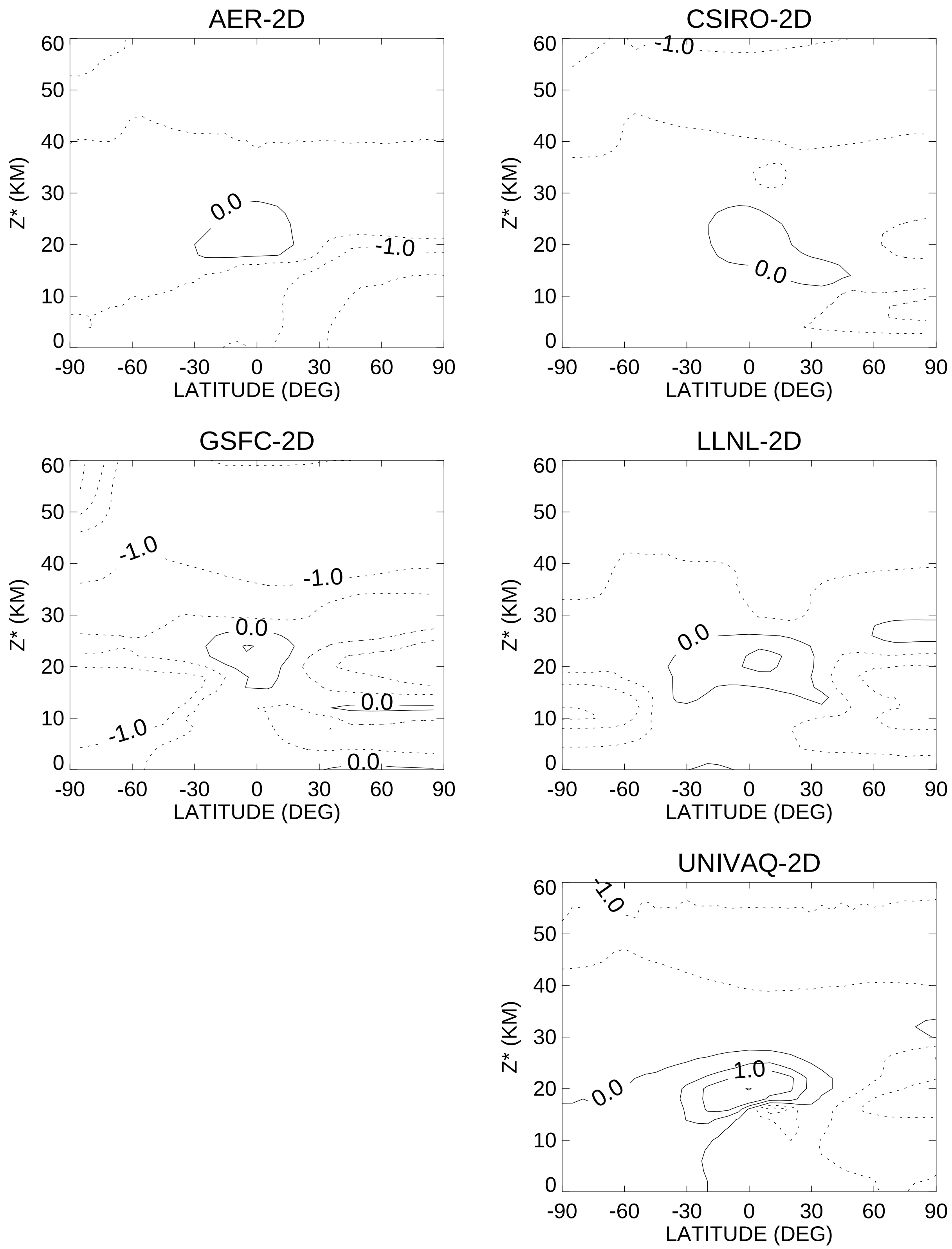

Figure 4.203: Calculated perturbations to O_3 (percent) as a function of latitude and altitude in June of 2015 due to emissions from a fleet of 500 HSCT aircraft with EI(NO_x)=5 and sulfate surface area of 4xSA0+SA3-SA0 under Scenario S3f relative to Scenario D3. Contours are -2, -1, -0.5, 0, 0.5, 1, 2.

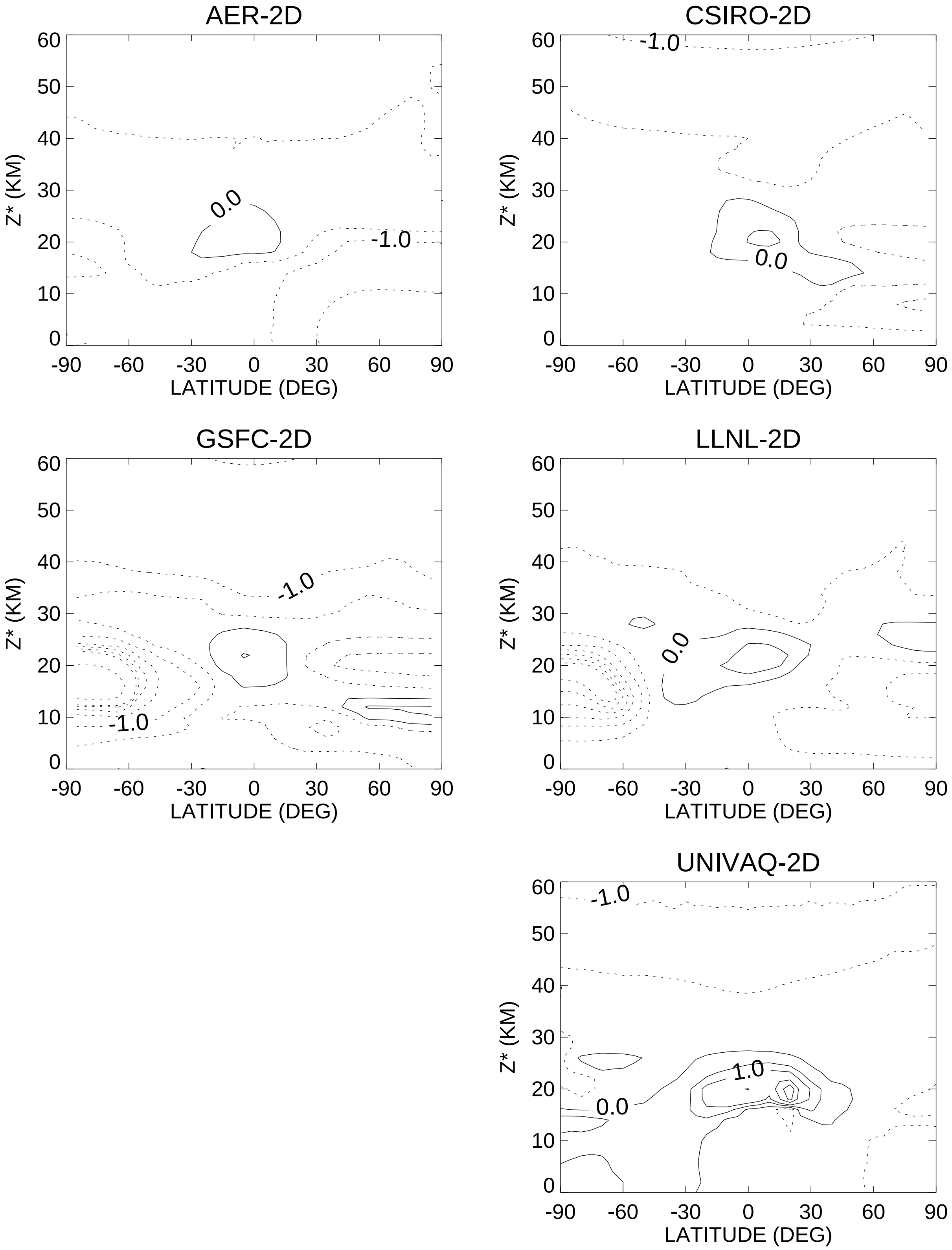

Figure 4.204: Calculated perturbations to O_3 (percent) as a function of latitude and altitude in October of 2015 due to emissions from a fleet of 500 HSCT aircraft with EI(NO_x)=5 and sulfate surface area of 4xSA0+SA3-SA0 under Scenario S3f relative to Scenario D3. Contours are -10, -5, -4, -3, -2, -1, -0.5, 0, 0.5, 1, 2, 3.

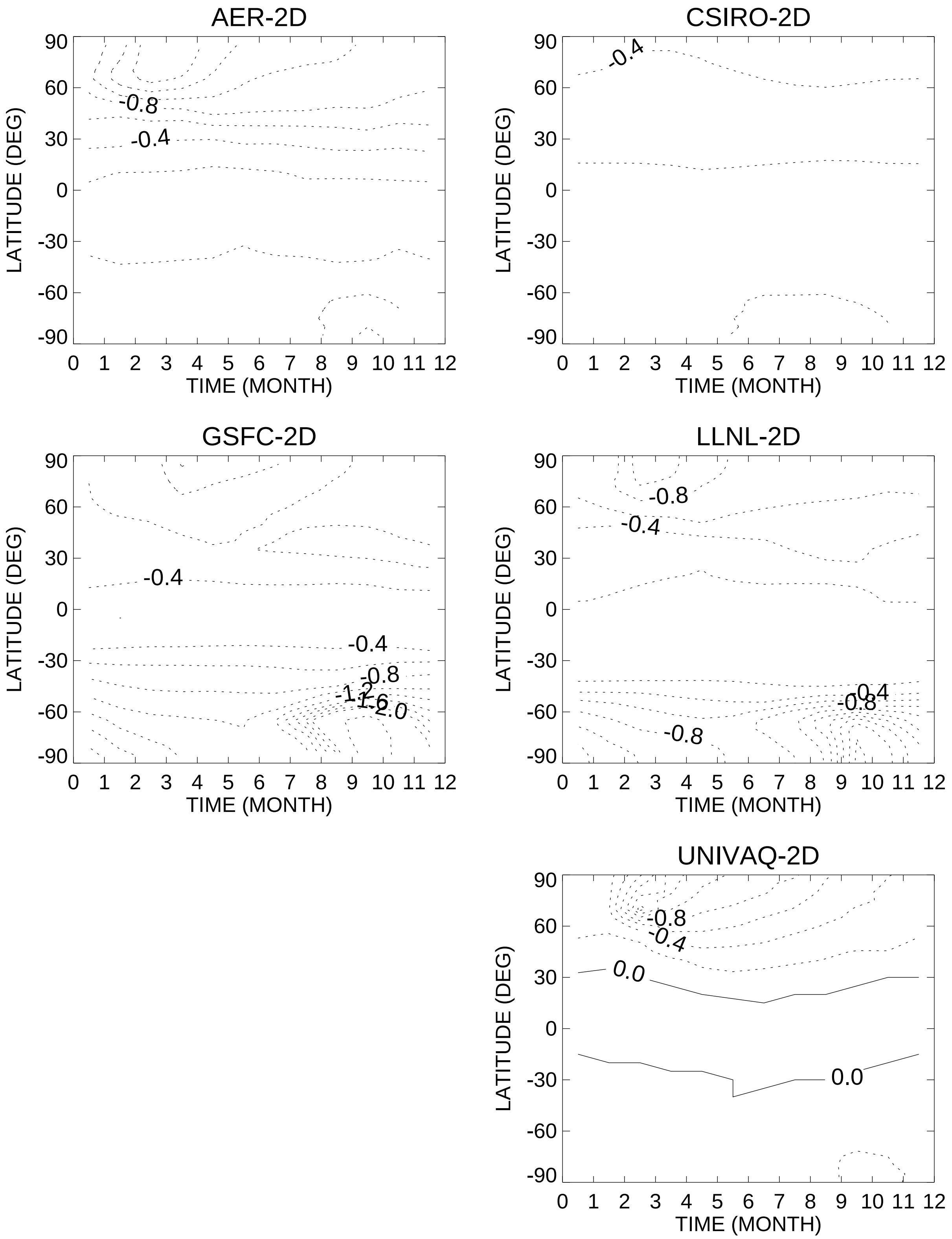

Figure 4.205: Calculated perturbations to column O_3 (percent) as a function of latitude and season in 2015 due to emissions from a fleet of 500 HSCT aircraft with EI(NO_x)=5 and sulfate surface area of 4xSA0+SA3-SA0 under Scenario S3f relative to Scenario D3. Contours are -3 and -2 to 0 by 0.2.

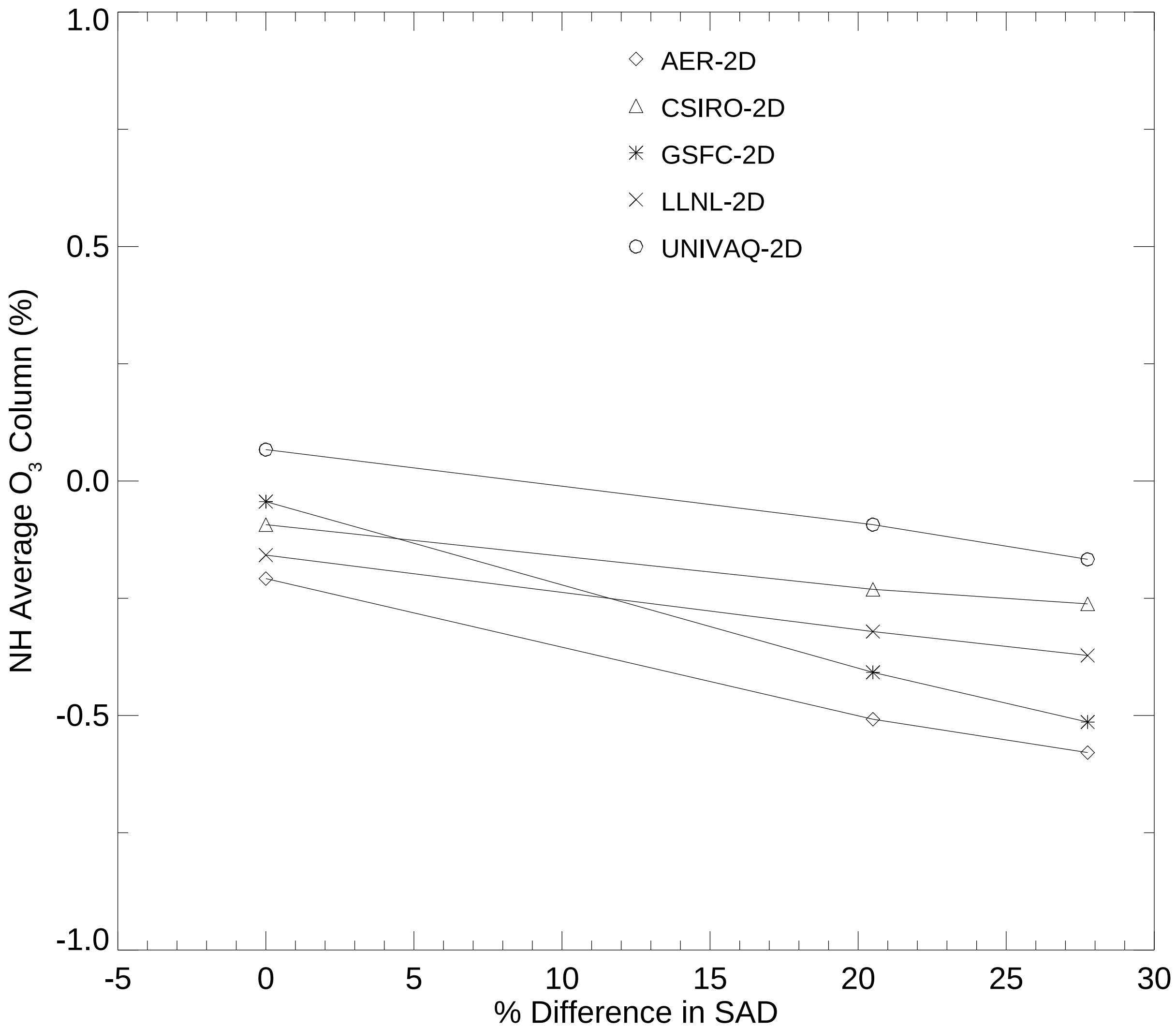

Figure 4.206: Northern hemisphere annual average total O_3 column change (percent) as a function of the percent change in aerosol surface area density in the region from 14 to 21 km and from 33^{o}N to 90^{o}N. The HSCT fleet consisted of 500 aircraft operating in 2015 with EI(NO_x)=5 and 4xSA0 as the background surface area density.

4.3.5 Scenarios without PSC Formulations (S4a-c)

This section will cover Scenarios S4a-S4c which omit the model PSC representation. Because the models use different representations of PSC processes, this is one aspect of modeling which may contribute substantially to intermodel differences. Removal of the PSC representations is found to considerably reduce the intermodel differences. It also allows us to evaluate the impact of each model's PSC representation on calculated ozone perturbation due to HSCT emissions. And it helps to provide a measurement of model uncertainty in evaluating HSCT impacts. Note that the CSIRO model does not include PSCs in its formulation, so Scenarios S1b, S1c, and S1a are identical to Scenarios S4a, S4b, and S4c, respectively.

Scenario S4a uses a 500 HSCT fleet with EI(NO_x)=0 in 2015 with nonvolcanic background sulfate surface area density SA0 and no aircraft sulfur emissions. This scenario is the same as Scenario S1b except that the PSC representations are omitted from the models. Changes in ozone for this scenario relative to background scenario D4 are shown in Figures 4.207, 4.208, and 4.209 for March, June, and October. The AER model is quite similar with and without PSCs for this scenario, but with northern hemisphere ozone depletion slightly smaller. The GSFC model shows much less ozone depletion in the southern hemisphere below 20 km without PSCs. The northern hemisphere also shows less ozone depletion below 20 km, but the 25-35 km region in both hemispheres shows more ozone depletion with PSCs. The UNIVAQ model shows slightly lower ozone depletion in both hemispheres without PSCs. Changes in ozone column as a function of latitude and season for S4a-D4 are shown in Figure 4.210.

Scenario S4b includes HSCT emissions with EI(NO_x)=5 and SA0 background SAD. Calculated ozone changes are shown in Figures 4.211, 4.212, and 4.213 for March, June, and October for S4b-D4. Ozone depletion is reduced relative to S4a-D4 in the AER, CSIRO, and UNIVAQ models below 25 km, but increased around 30 km. The GSFC model shows virtually no change due to the added HSCT NO_x emissions. Figure 4.214 shows changes in ozone column for Scenario S4b-D4. By comparison with Scenario S1c-D, ozone depletion is seen to be reduced in the southern hemisphere for the GSFC model when the PSC parameterizations are removed. Northern hemisphere ozone depletion is reduced for the AER model without PSCs.

Scenario S4c includes HSCT emissions of NO_x only (no H_2O emissions) with EI(NO_x)=5. Changes in ozone for S4c-D4 are shown in Figures 4.215-4.217. Ozone changes in the upper stratosphere are greatly reduced relative to S2b-D4 with H_2O emissions. All models show reduced ozone depletion relative to S2b-D4 in the troposphere and lower stratosphere as well, with the CSIRO, GSFC, and UNIVAQ models showing ozone increases relative to D4 in this region. Column ozone changes for S4c-D4 are shown in Figure 4.218. Ozone column changes are quite small for all models, between -0.4% and +0.4%. From comparison with S1a-D, which includes PSCs, we conclude that the PSC parameterizations have little impact without H_2O emissions.

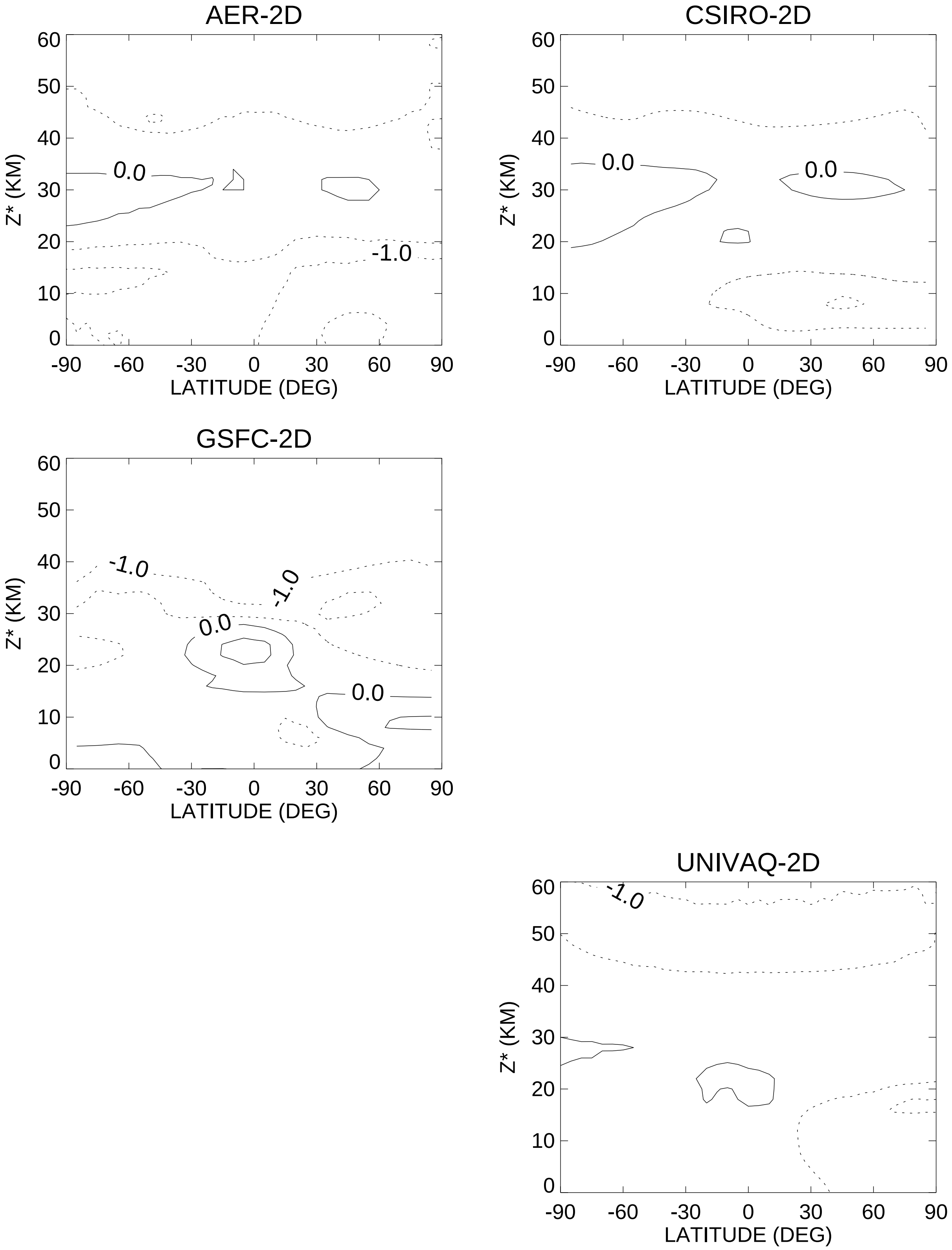

Figure 4.207: Calculated perturbations to O_3 (percent) as a function of latitude and altitude in March of 2015 due to emissions from a fleet of 500 HSCT aircraft with EI(NO_x)=0 and the model PSC parameterization removed under Scenario S4a relative to Scenario D4. Contours are -2, -1, -0.5, 0, 0.5.

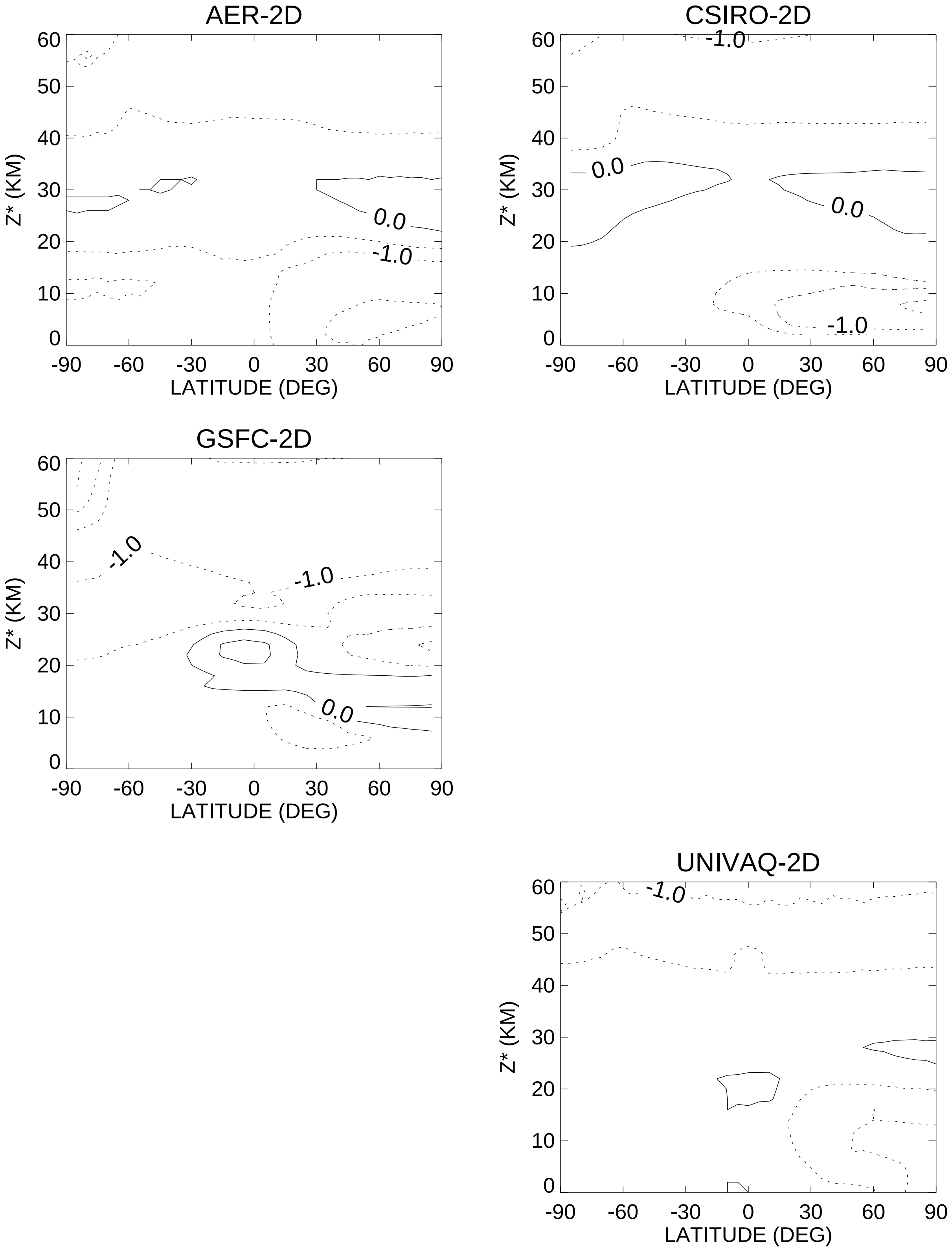

Figure 4.208: Calculated perturbations to O_3 (percent) as a function of latitude and altitude in June of 2015 due to emissions from a fleet of 500 HSCT aircraft with $EI(NO_x)=0$ and the model PSC parameterization removed under Scenario S4a relative to Scenario D4. Contours are -2, -1, -0.5, 0, 0.5.

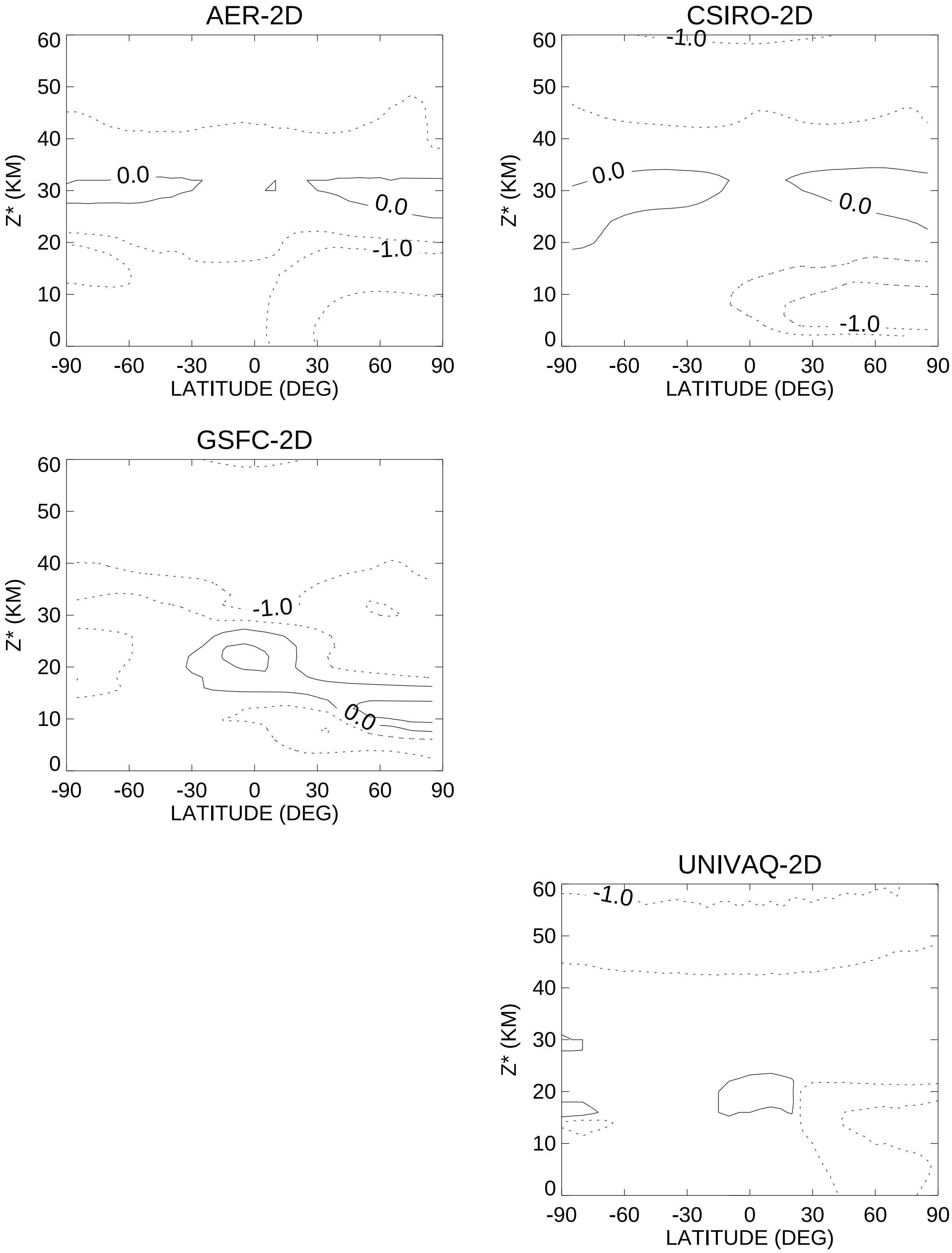

Figure 4.209: Calculated perturbations to O_3 (percent) as a function of latitude and altitude in October of 2015 due to emissions from a fleet of 500 HSCT aircraft with $EI(NO_x)=0$ and the model PSC parameterization removed under Scenario S4a relative to Scenario D4. Contours are -5, -4, -3, -2, -1, -0.5, 0, 0.5.

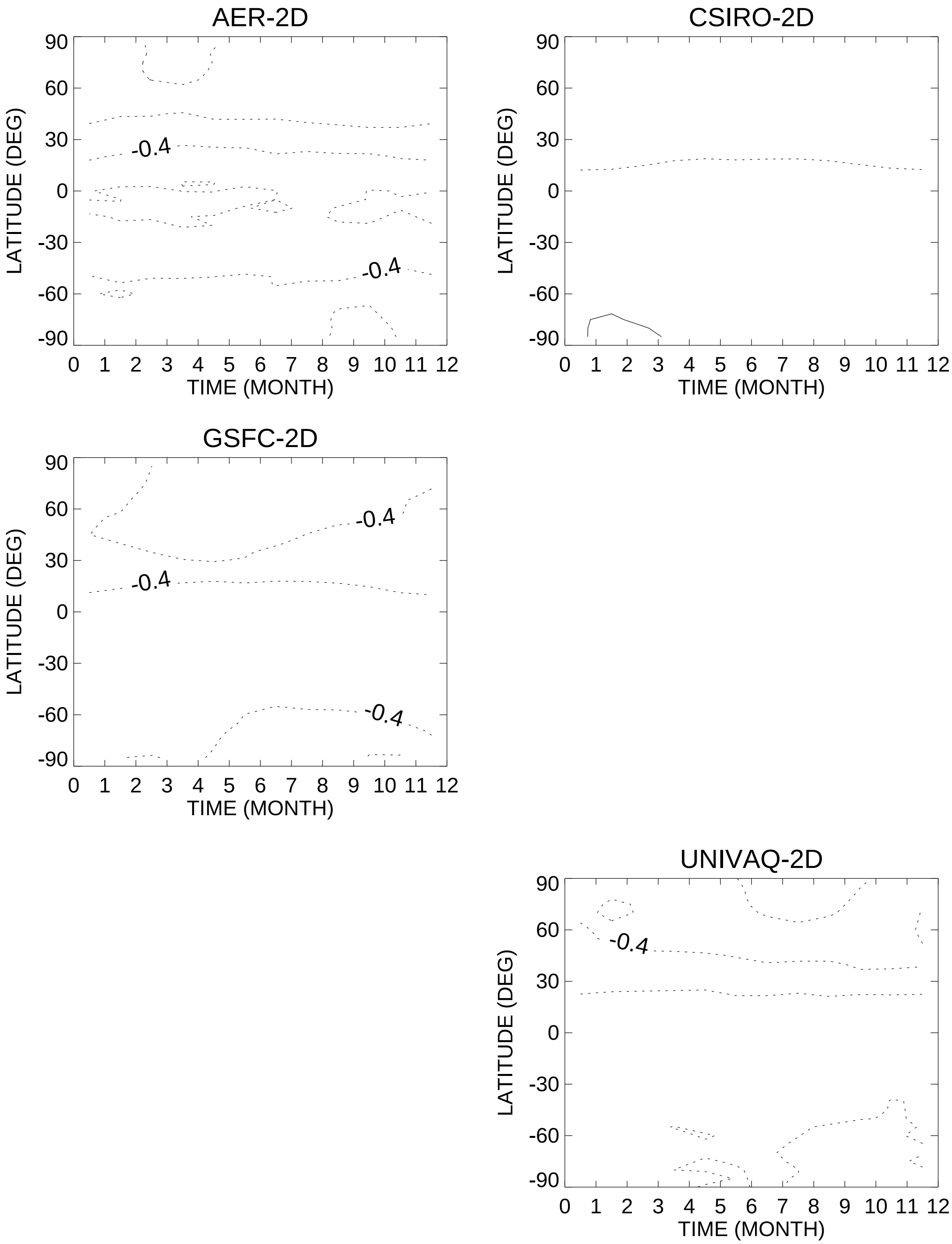

Figure 4.210: Calculated perturbations to column O_3 (percent) as a function of latitude and season in 2015 due to emissions from a fleet of 500 HSCT aircraft with EI(NO_x)=0 and the model PSC parameterization removed under Scenario S4a relative to Scenario D4. Contours are -1.2 to -0.2 by 0.2.

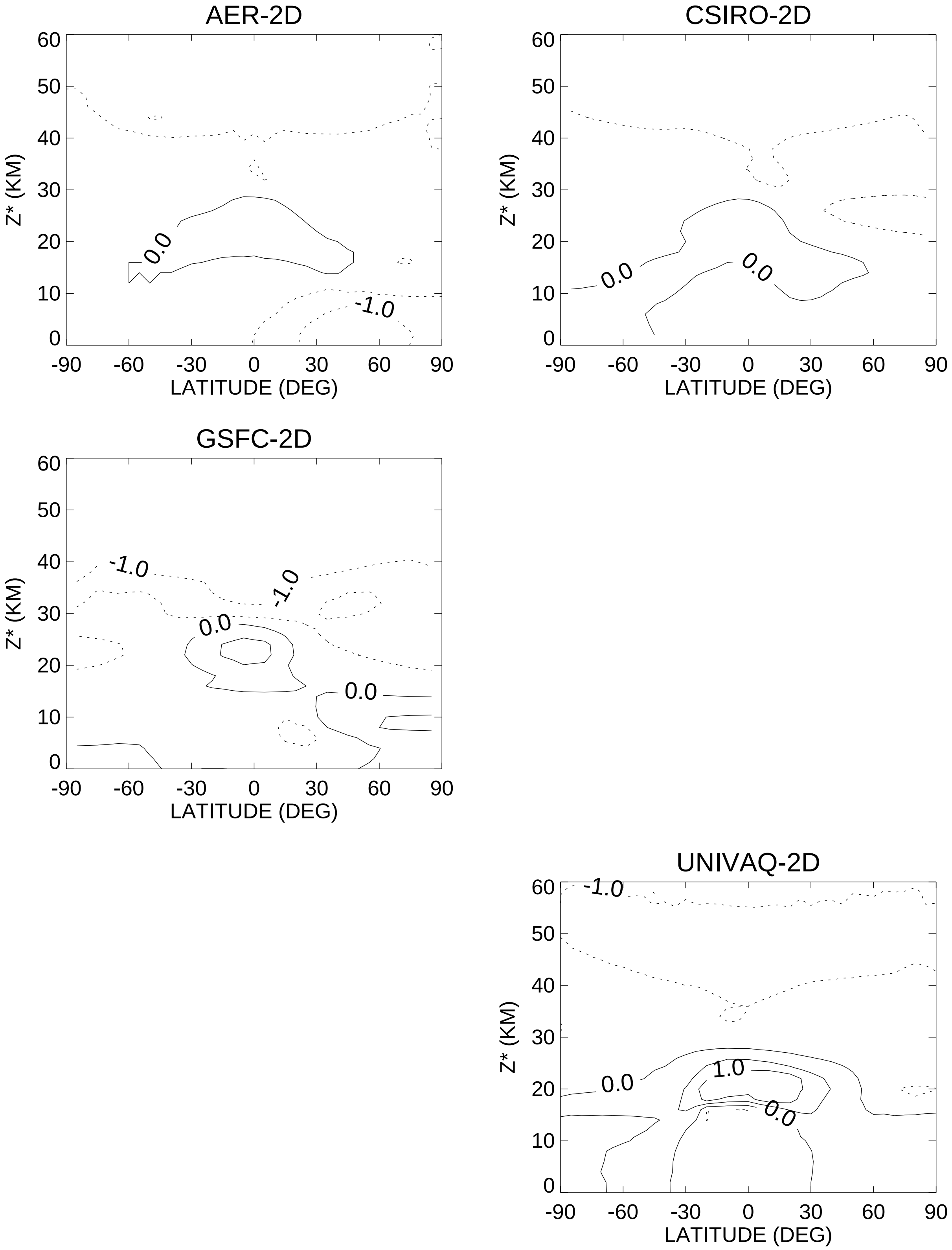

Figure 4.211: Calculated perturbations to O_3 (percent) as a function of latitude and altitude in March of 2015 due to emissions from a fleet of 500 HSCT aircraft with $EI(NO_x)=5$ and the model PSC parameterization removed under Scenario S4b relative to Scenario D4. Contours are -1, -0.5, 0, 0.5, 1.

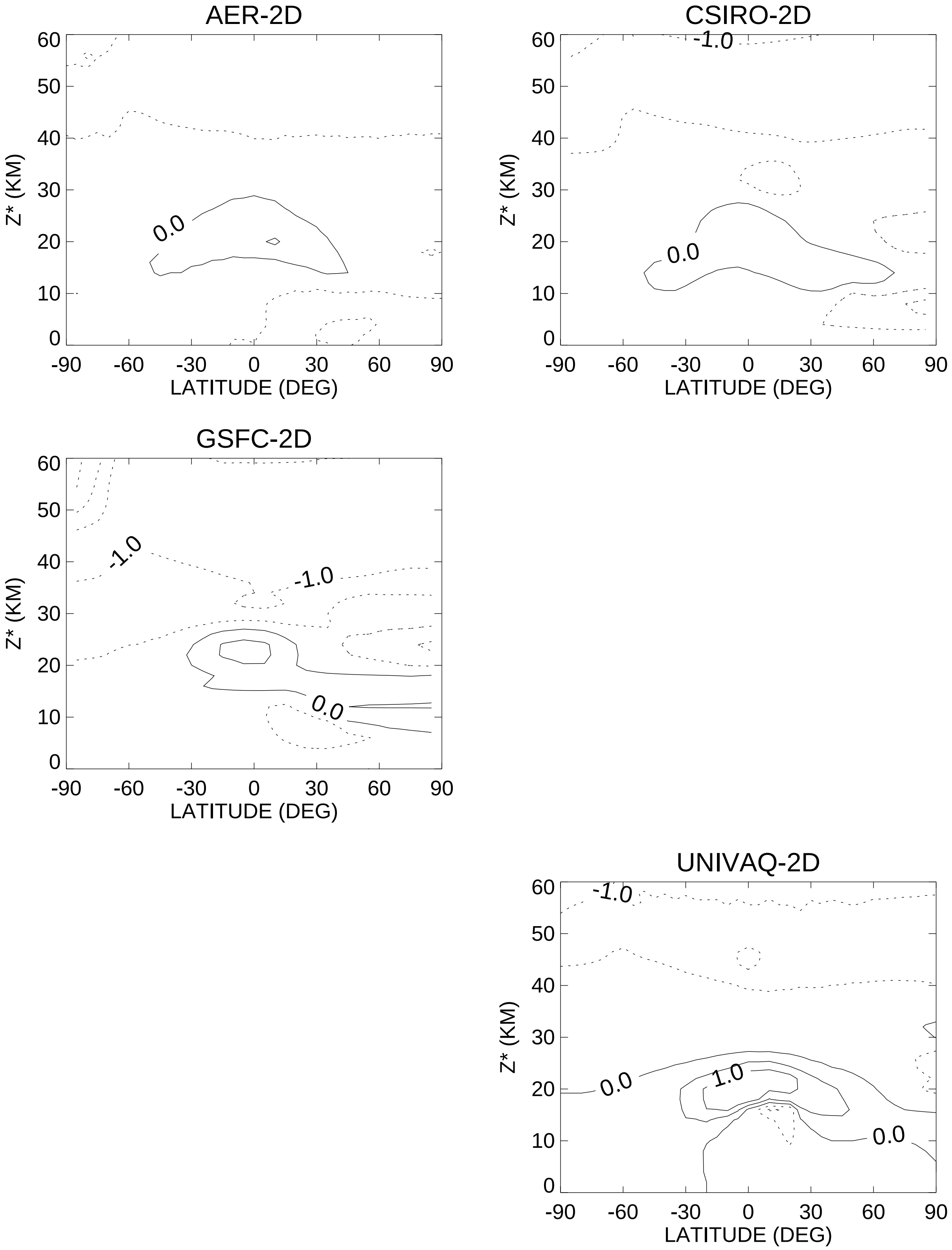

Figure 4.212: Calculated perturbations to O_3 (percent) as a function of latitude and altitude in June of 2015 due to emissions from a fleet of 500 HSCT aircraft with EI(NO_x)=5 and the model PSC parameterization removed under Scenario S4b relative to Scenario D4. Contours are -2, -1, -0.5, 0, 0.5, 1.

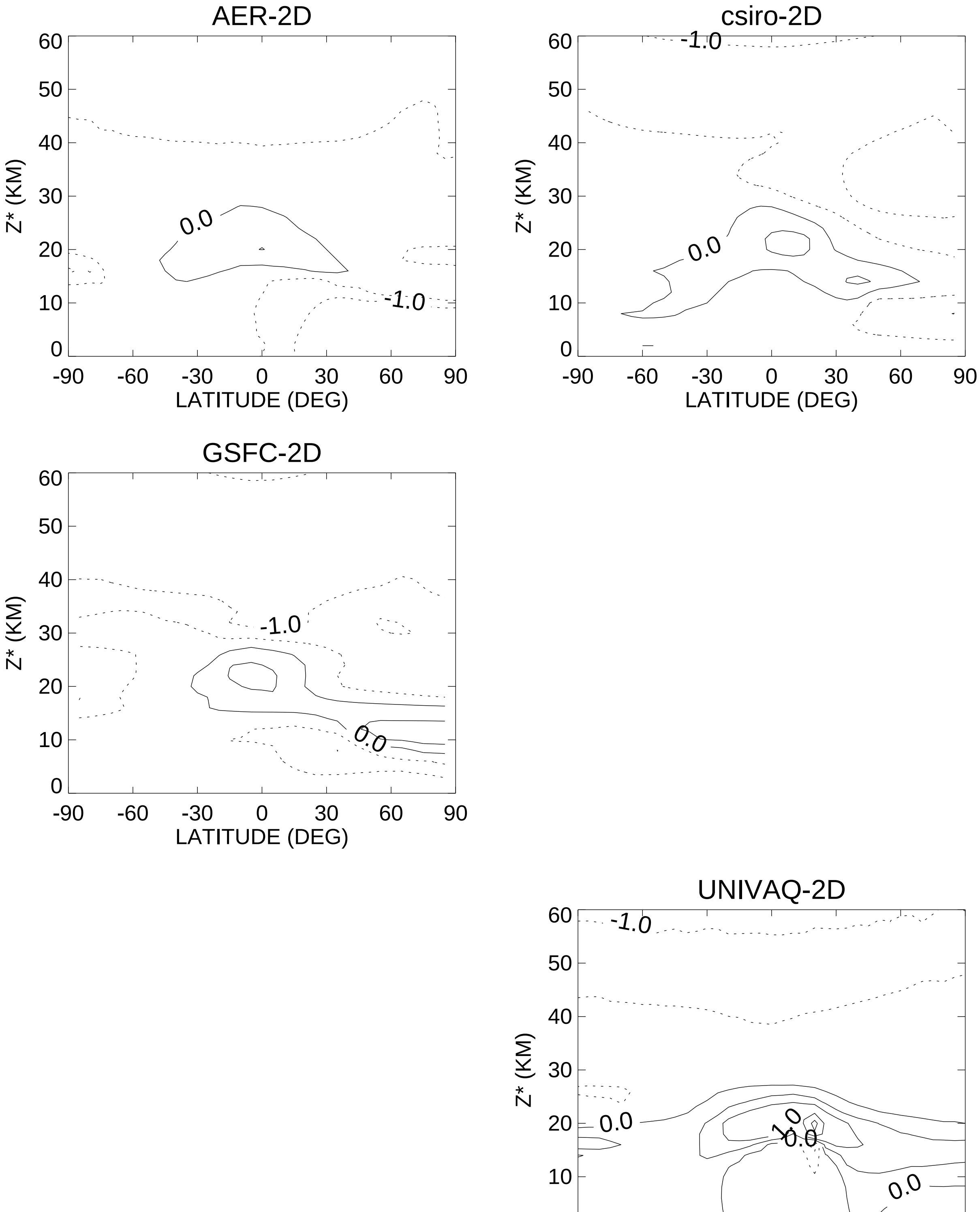

Figure 4.213: Calculated perturbations to O_3 (percent) as a function of latitude and altitude in October of 2015 due to emissions from a fleet of 500 HSCT aircraft with $EI(NO_x)=5$ and the model PSC parameterization removed under Scenario S4b relative to Scenario D4. Contours are -3, -2, -1, -0.5, 0, 0.5, 1, 2, 3.

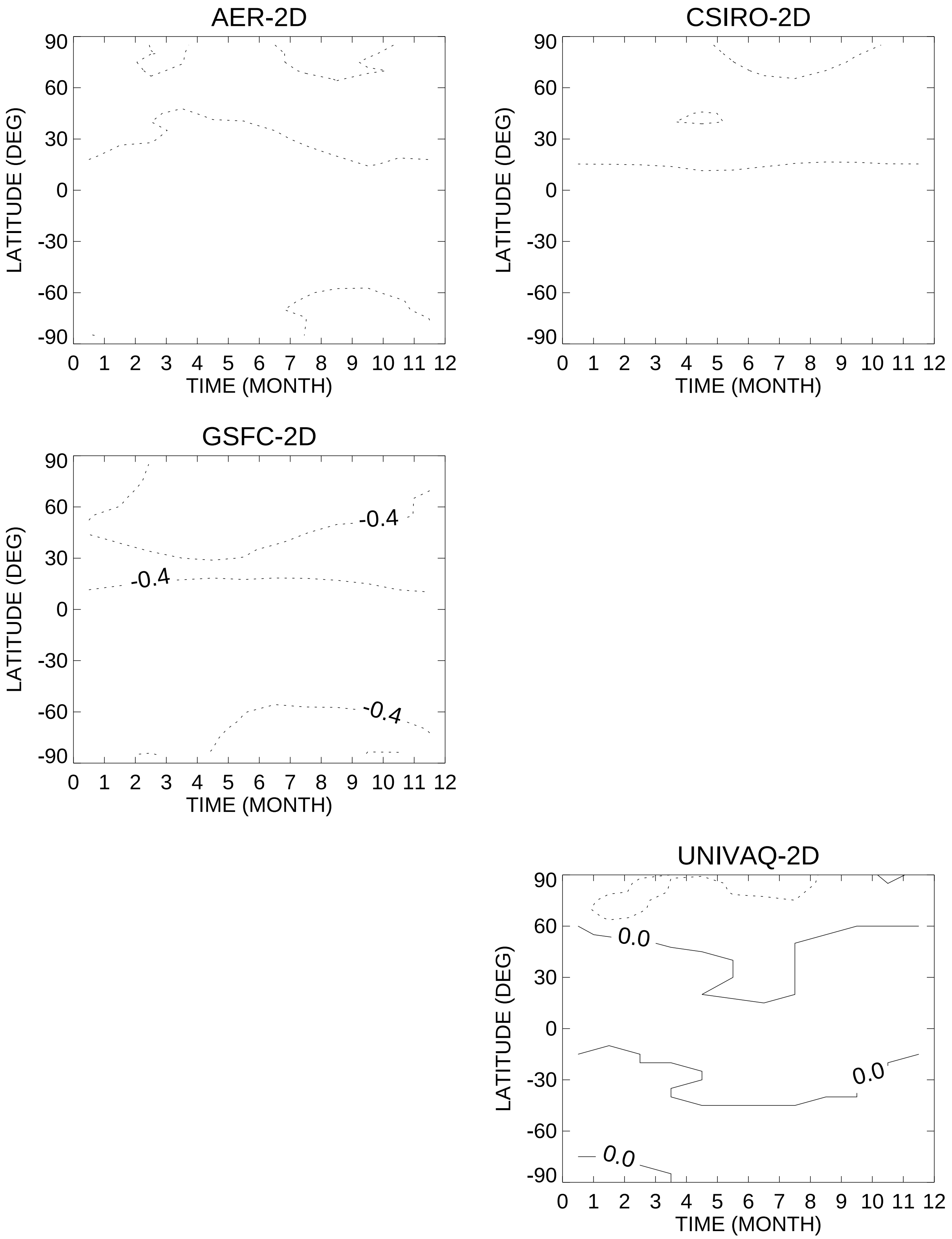

Figure 4.214: Calculated perturbations to column O_3 (percent) as a function of latitude and season in 2015 due to emissions from a fleet of 500 HSCT aircraft with $EI(NO_x)=5$ and the model PSC parameterization removed under Scenario S4b relative to Scenario D4. Contours are -0.6 to 0 by 0.2.

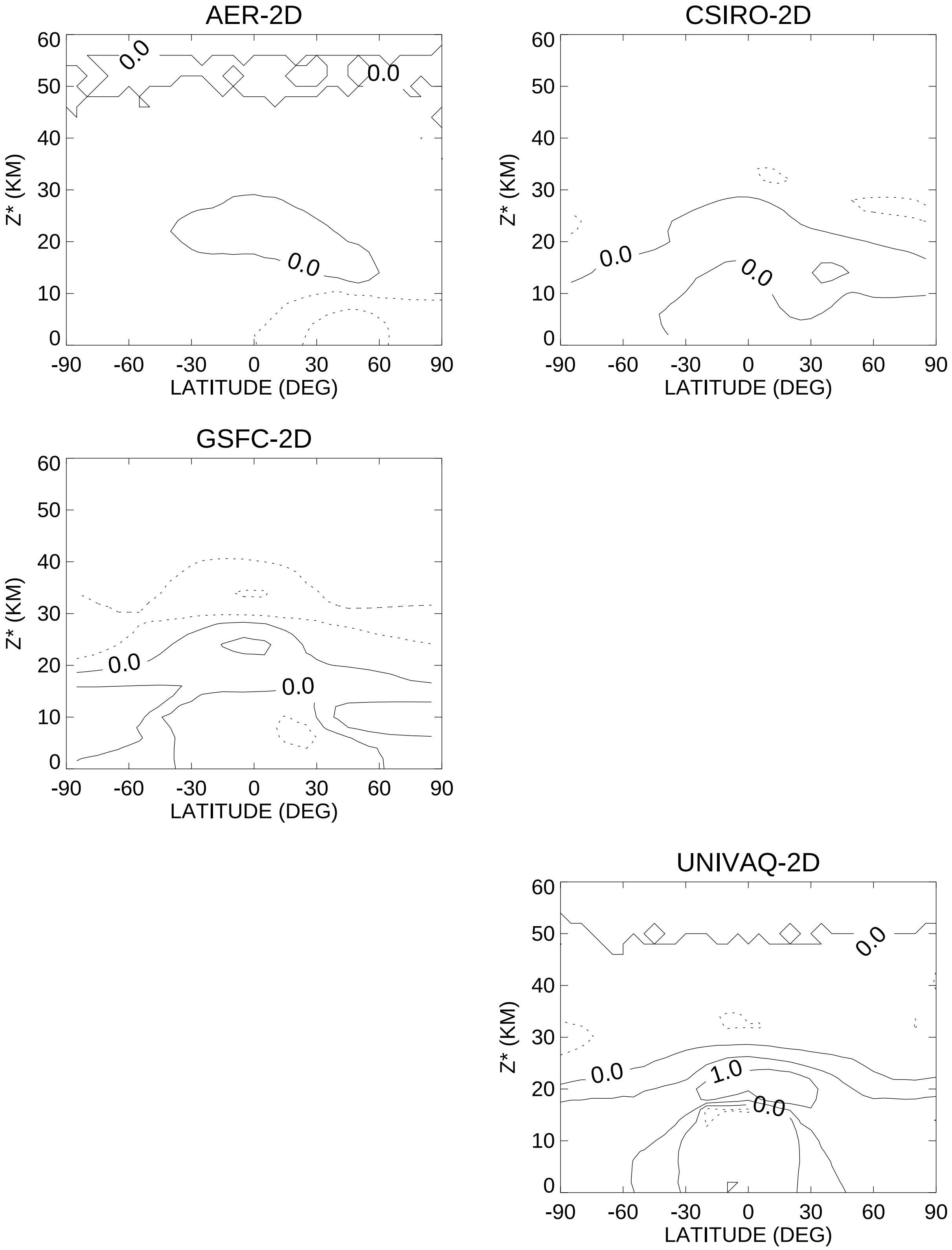

Figure 4.215: Calculated perturbations to O_3 (percent) as a function of latitude and altitude in March of 2015 due to emissions from a fleet of 500 HSCT aircraft with EI(NO_x)=5, no H_2O emissions, and the model PSC parameterization removed under Scenario S4c relative to Scenario D4. Contours are -1, -0.5, 0, 0.5, 1.

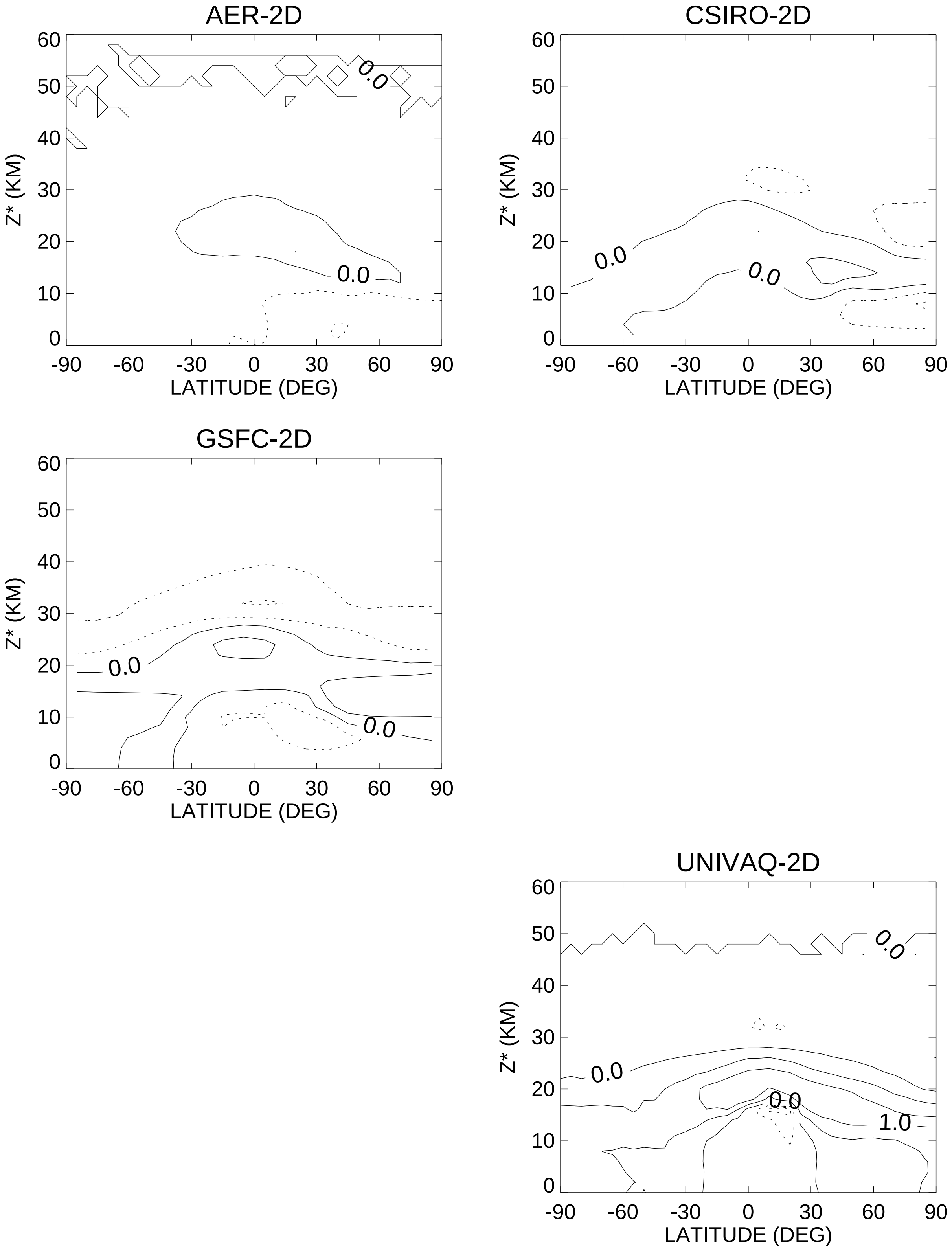

Figure 4.216: Calculated perturbations to O_3 (percent) as a function of latitude and altitude in June of 2015 due to emissions from a fleet of 500 HSCT aircraft with $EI(NO_x)=5$, no H_2O emissions, and the model PSC parameterization removed under Scenario S4c relative to Scenario D4. Contours are -1, -0.5, 0, 0.5, 1.

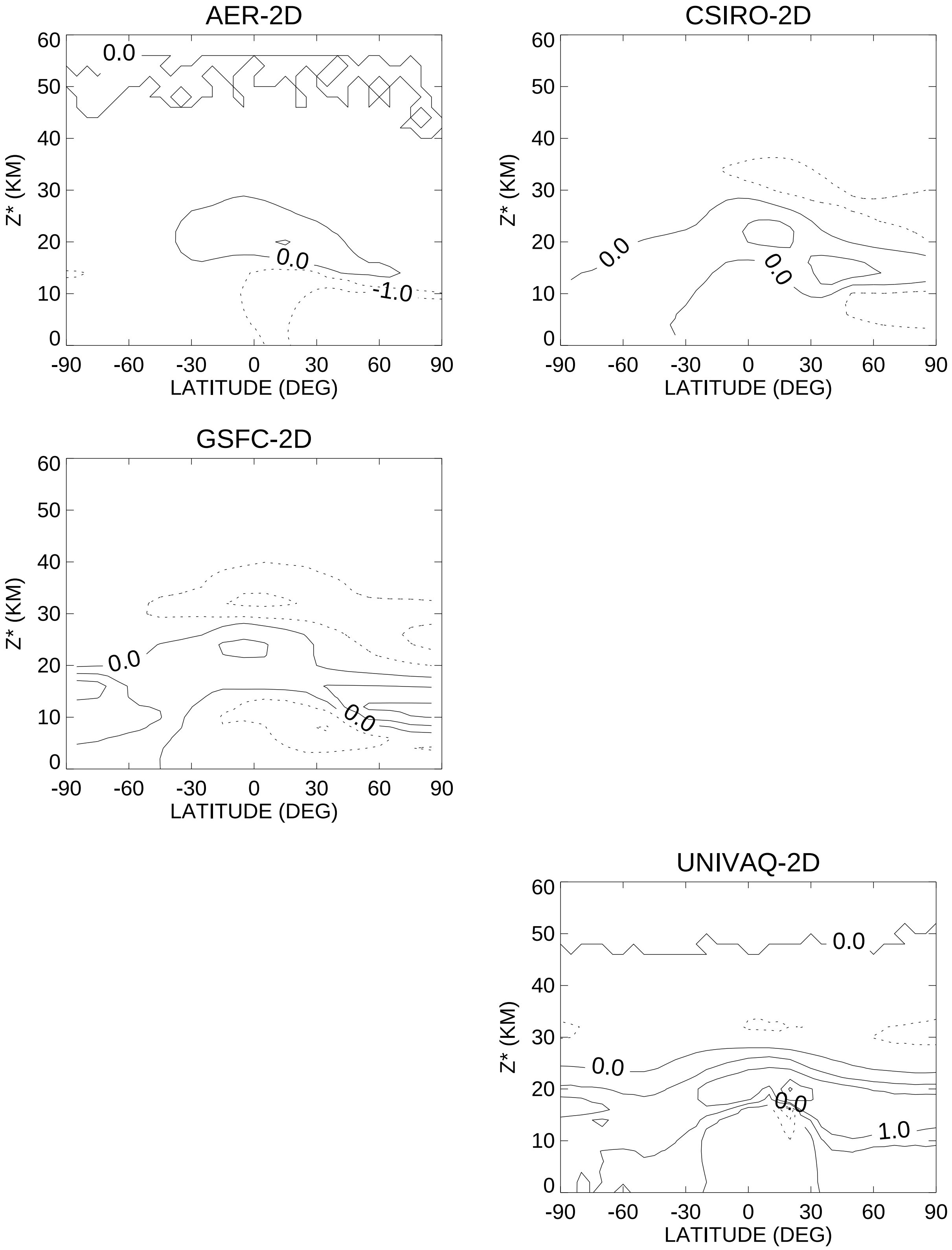

Figure 4.217: Calculated perturbations to O_3 (percent) as a function of latitude and altitude in October of 2015 due to emissions from a fleet of 500 HSCT aircraft with EI(NO_x)=5, no H_2O emissions, and the model PSC parameterization removed under Scenario S4c relative to Scenario D4. Contours are -1, -0.5, 0, 0.5, 1, 2, 3.

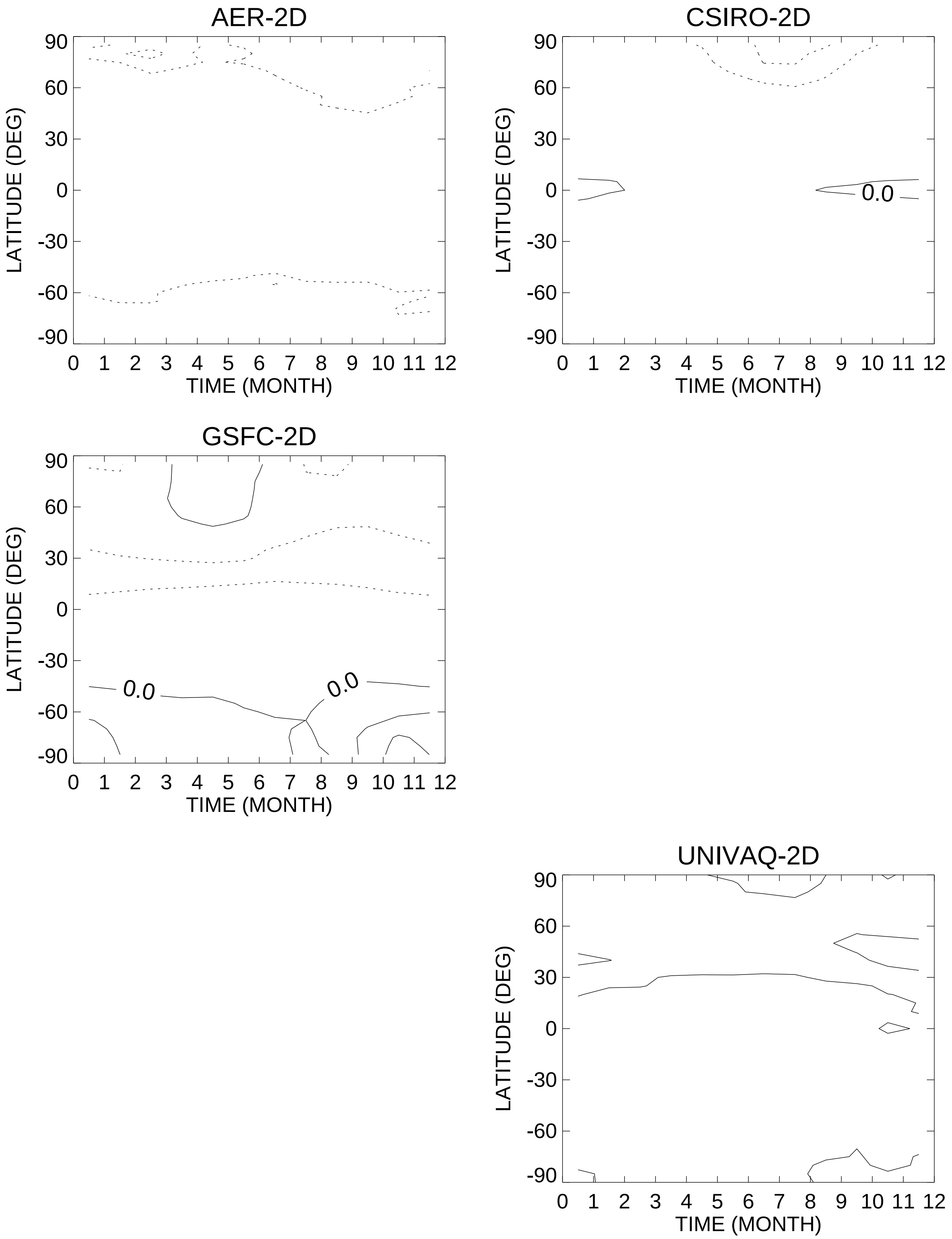

Figure 4.218: Calculated perturbations to column O_3 (percent) as a function of latitude and season in 2015 due to emissions from a fleet of 500 HSCT aircraft with EI(NO_x)=5, no H_2O emissions, and the model PSC parameterization removed under Scenario S4c relative to Scenario D4. Contours are -0.4 to 0.4 by 0.2.

4.3.6 Scenarios with Different Cl_y Loadings (S5a,b, S6a,b)

This section will cover Scenarios S5a-S6b which contain modified Cl_y background concentrations. Scenario S5a-S5b use 1.0 ppbv of Cl_y. Scenarios S6a-S6b use 4.0 ppbv of Cl_y. The standard 2015 scenarios use 3.0 ppbv of Cl_y and the 2050 scenarios use 2.0 ppbv of Cl_y. With these 4 alternate Cl_y loading levels, we can investigate the sensitivity of HSCT ozone impact to Cl_y loading, with and without aircraft sulfur emissions. The AER, GSFC, and UNIVAQ models performed these calculations.

Scenario S5a is identical to S1c except that the Cl_y loading is 1.0 ppbv instead of 3.0 ppbv. The scenario represents 500 HSCT aircraft with EI(NO_x)=5 and no sulfur emissions. Changes in ozone concentration for March, June, and October for S5a relative to D5 are shown in Figures 4.219, 4.220, and 4.221. The models show somewhat less ozone depletion in the extratropical lower stratosphere with S5a-D5 than with S1c-D, except for October, when the GSFC and UNIVAQ models show more depletion in the northern hemisphere lower stratosphere with S5a-D5. Figure 4.222 shows changes in ozone column for Scenario S5a relative to D5. The GSFC model shows much less springtime ozone column depletion in the southern polar region with 1 ppbv of Cl_y than with 3 ppbv of Cl_y. In the northern hemisphere, the GSFC model shows somewhat more depletion. The AER and UNIVAQ models show slightly less ozone column depletion in both hemispheres at high latitudes.

Scenario S5b includes sulfur emissions from HSCT aircraft assuming 50% gas to particle conversion (ie. using the SA1 surface area density) along with a Cl_y loading is 1 ppbv. The HSCT fleet includes 500 aircraft with EI(NO_x)=5. Changes in ozone relative to background scenario D5 are shown in Figures 4.223, 4.224, and 4.225 for March, June, and October. Ozone column depletion is increased relative to S5a-D5 by the addition of aircraft-emitted sulfur. However, the increase in ozone depletion is not as great as with a Cl_y loading of 3 ppbv (Scenarios S1c-D, S1f-D). Figure 4.226 shows changes in ozone column for this scenario. The ozone depletion calculated for S5b-D5 is reduced by 40-50% relative to S1f-D for the AER and GSFC models and by a lesser amount for the UNIVAQ model.

Scenarios S6a and S6b use a Cl_y loading of 4.0 ppbv. Both include HSCT fleets of 500 aircraft with EI(NO_x)=5. Scenario S6a includes no aircraft sulfur emissions. Ozone changes for Scenario S6a relative to D6 are shown in Figures 4.227, 4.228, and 4.229. The results for the AER and GSFC models with 4.0 ppbv of Cl_y are very similar to those with 3.0 ppbv of Cl_y. The UNIVAQ model results show less ozone depletion in the high latitude lower stratosphere and less of an ozone increase in the high latitude troposphere than for S1c-D. Changes in column ozone for S6a-D6 are shown in Figure 4.230. The AER and GSFC models show ozone column depletions at high latitudes which are slightly greater than for Scenario S1c-D. The UNIVAQ model shows slightly reduced ozone column depletion.

Sulfur emissions with 50% gas to particle conversion are included in Scenario S6b, using the SA1 surface area density. Figures 4.231, 4.232, and 4.233 show changes in ozone for Scenario S6b relative to Scenario D6. Compared with Scenario S1f-D, ozone depletion is about the same for the AER model, smaller for the GSFC model in the southern hemisphere, and slightly smaller at high latitudes in the lower stratosphere for the UNIVAQ model. Changes in column ozone for S6b-D6 are shown in Figure 4.234. The AER and GSFC models show slightly more ozone depletion in the southern polar springtime compared with S1f-D. The UNIVAQ model shows a bit less depletion in both hemispheres at high latitudes.

The sensitivity of ozone response to Cl_y loading without aircraft sulfur emissions is shown graphically in Figures 4.235 and 4.236 for the northern and southern hemisphere annual average ozone columns, respectively. The 2 ppb Cl_y loadings are from Scenarios S9a and S9c for 2050. These scenarios use the 2050 boundary conditions for N_2O and CH_4, and so differ slightly from the other scenarios included in the plots. Sensitivity to Cl_y is minor over the 1 ppb to 4 ppb range plotted, except for the GSFC model in the southern hemisphere, which shows greater ozone depletion at at 2 ppbv of Cl_y than at 1 ppbv.

Figures 4.237 shows Cl_y sensitivity in the northern hemisphere with aircraft sulfur emissions (SA1) included. In this case, all models show greater ozone depletion at 3 ppbv of Cl_y than at 2 ppbv of Cl_y. The AER model also shows a change in ozone depletion between 1 and 2 ppbv of Cl_y. Cl_y sensitivity in the southern hemisphere with sulfur emissions is shown in Figure 4.238. All models show a modest increase in ozone depletion between 2 ppbv and 3 ppbv of Cl_y. The GSFC and AER models also show increases in ozone depletion between 1 ppbv and 2 ppbv of Cl_y. In both hemispheres, increasing Cl_y from 3 ppbv to 4 ppbv has no influence on calculated ozone depletion.

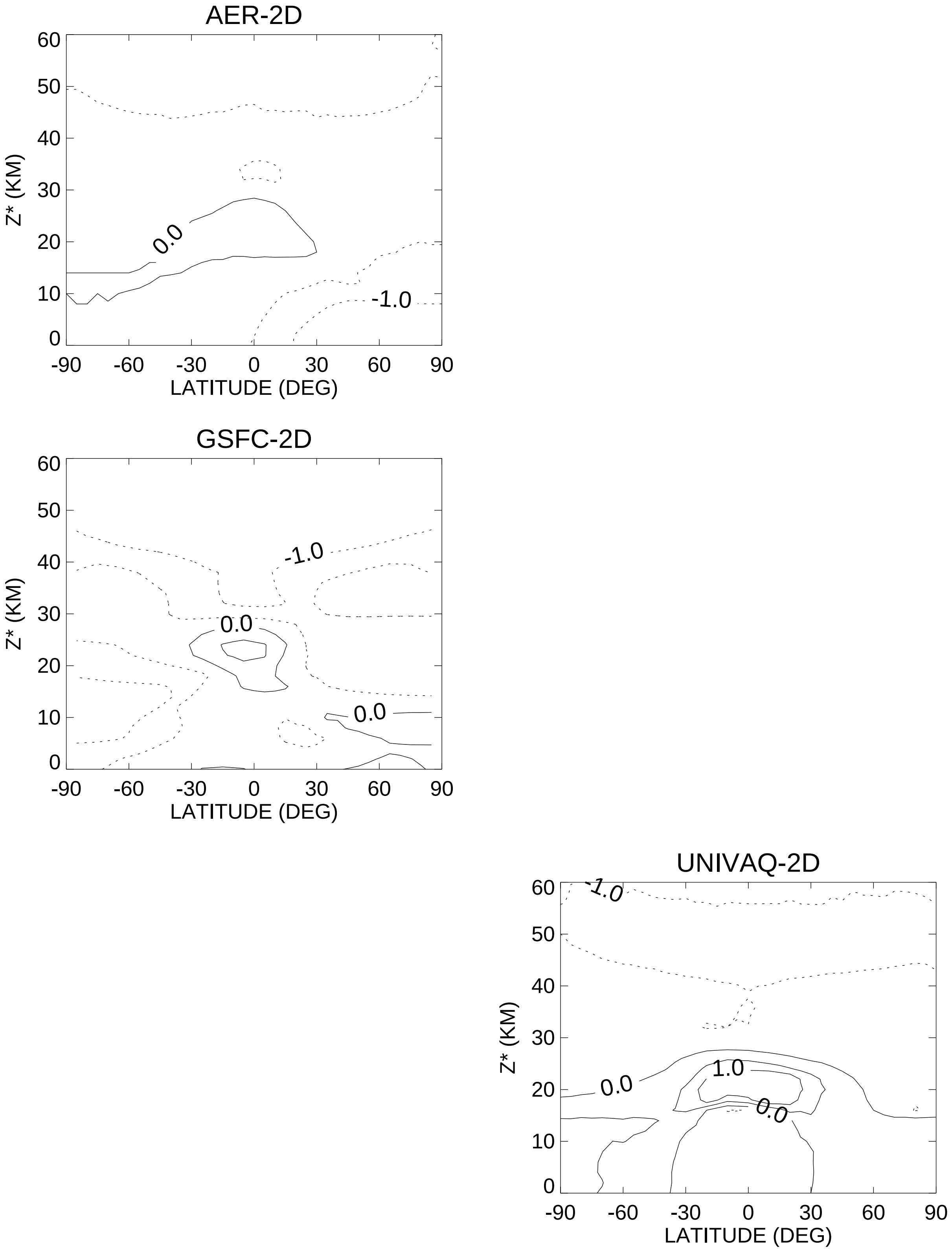

Figure 4.219: Calculated perturbations to O_3 (percent) as a function of latitude and altitude in March of 2015 due to emissions from a fleet of 500 HSCT aircraft with $EI(NO_x)=5$ and a background Cl_y concentration of 1.0 ppbv under Scenario S5a relative to Scenario D5. Contours are -1, -0.5, 0, 0.5, 1.

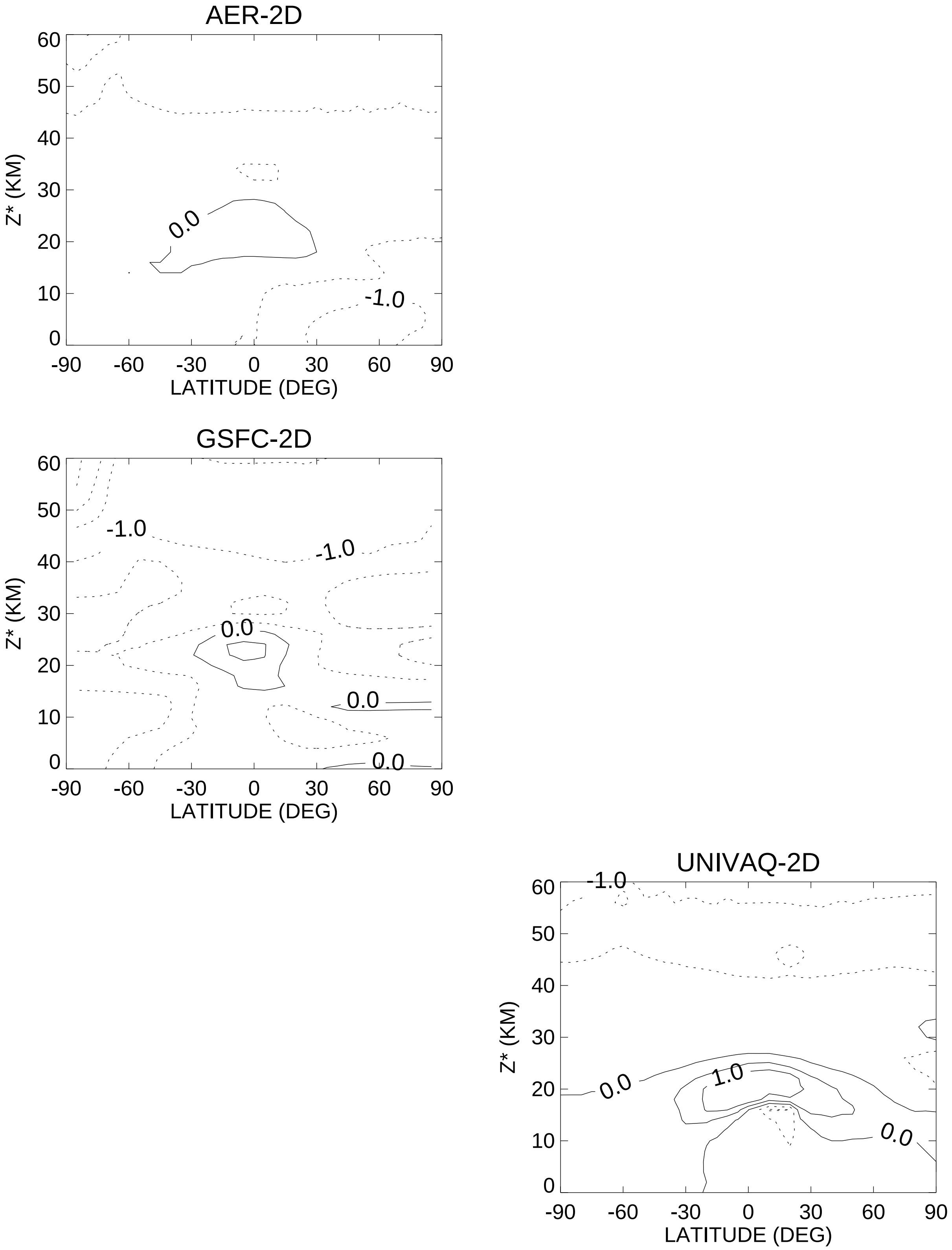

Figure 4.220: Calculated perturbations to O_3 (percent) as a function of latitude and altitude in June of 2015 due to emissions from a fleet of 500 HSCT aircraft with $EI(NO_x)=5$ and a background Cl_y concentration of 1.0 ppbv under Scenario S5a relative to Scenario D5. Contours are -1, -0.5, 0, 0.5, 1.

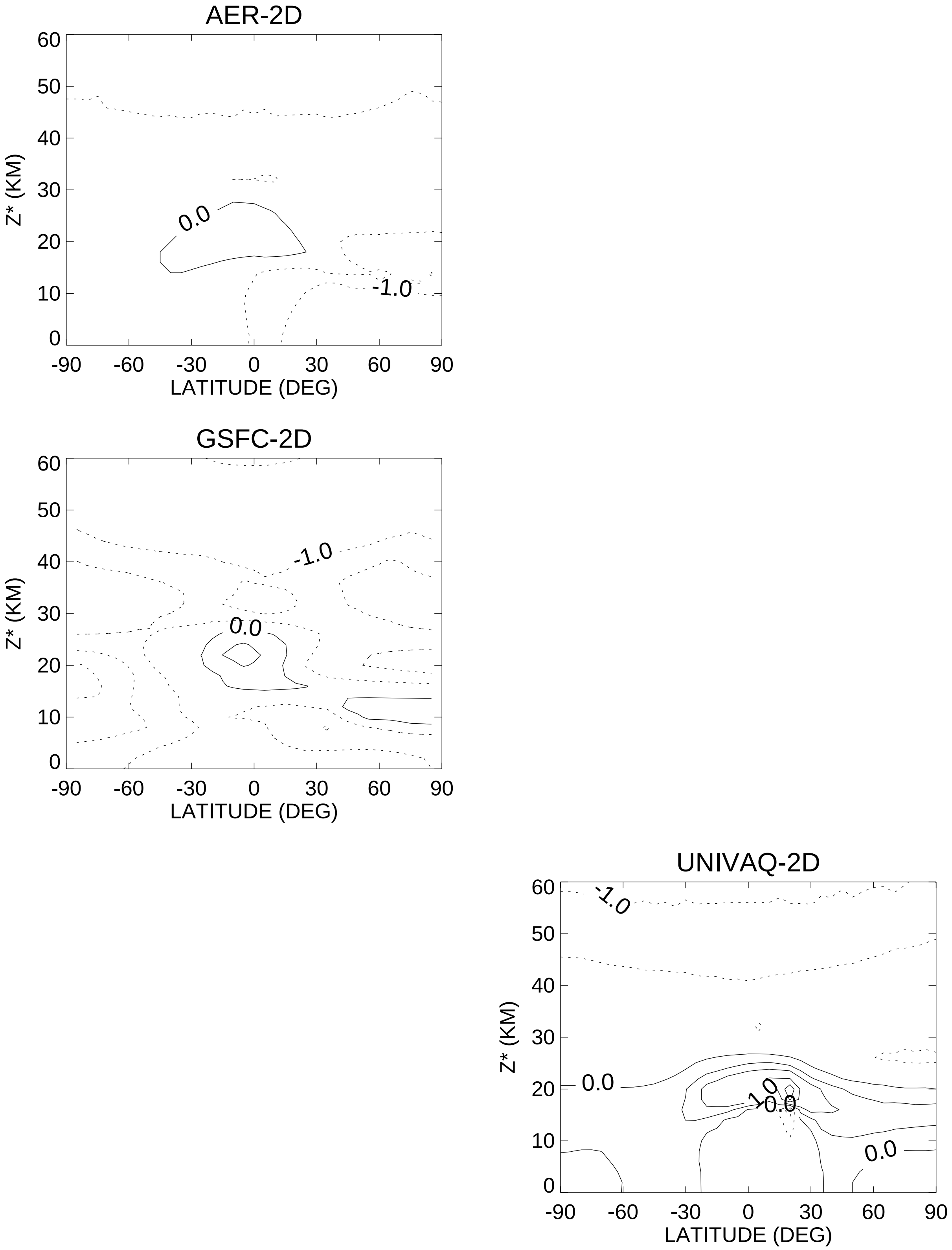

Figure 4.221: Calculated perturbations to O_3 (percent) as a function of latitude and altitude in October of 2015 due to emissions from a fleet of 500 HSCT aircraft with EI(NO_x)=5 and a background Cl_y concentration of 1.0 ppbv under Scenario S5a relative to Scenario D5. Contours are -2, -1, -0.5, 0, 0.5, 1, 2, 3.

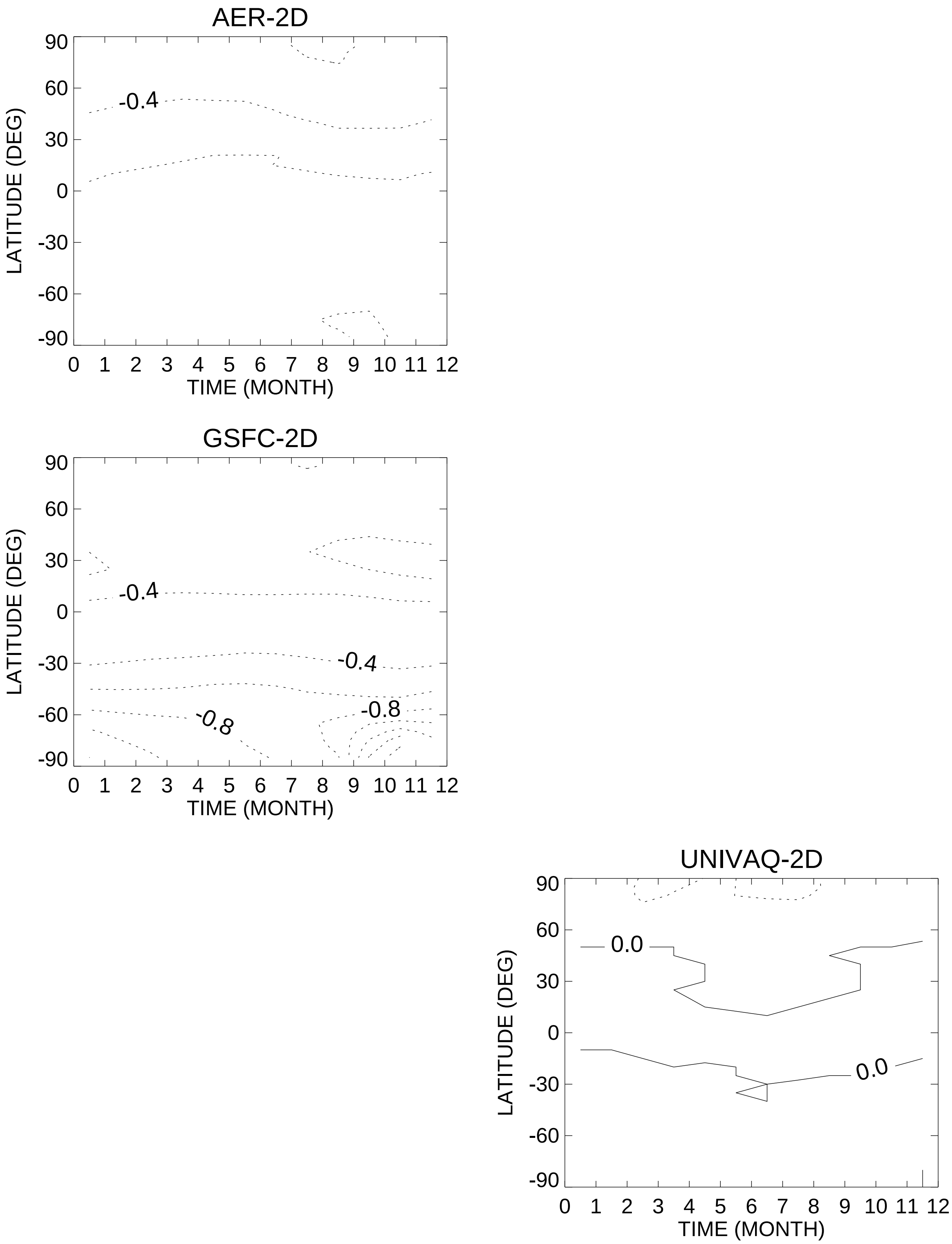

Figure 4.222: Calculated perturbations to column O_3 (percent) as a function of latitude and season in 2015 due to emissions from a fleet of 500 HSCT aircraft with EI(NO_x)=5 and a background Cl_y concentration of 1.0 ppbv under Scenario S5a relative to Scenario D5. Contours are -1.6 to 0 by 0.2.

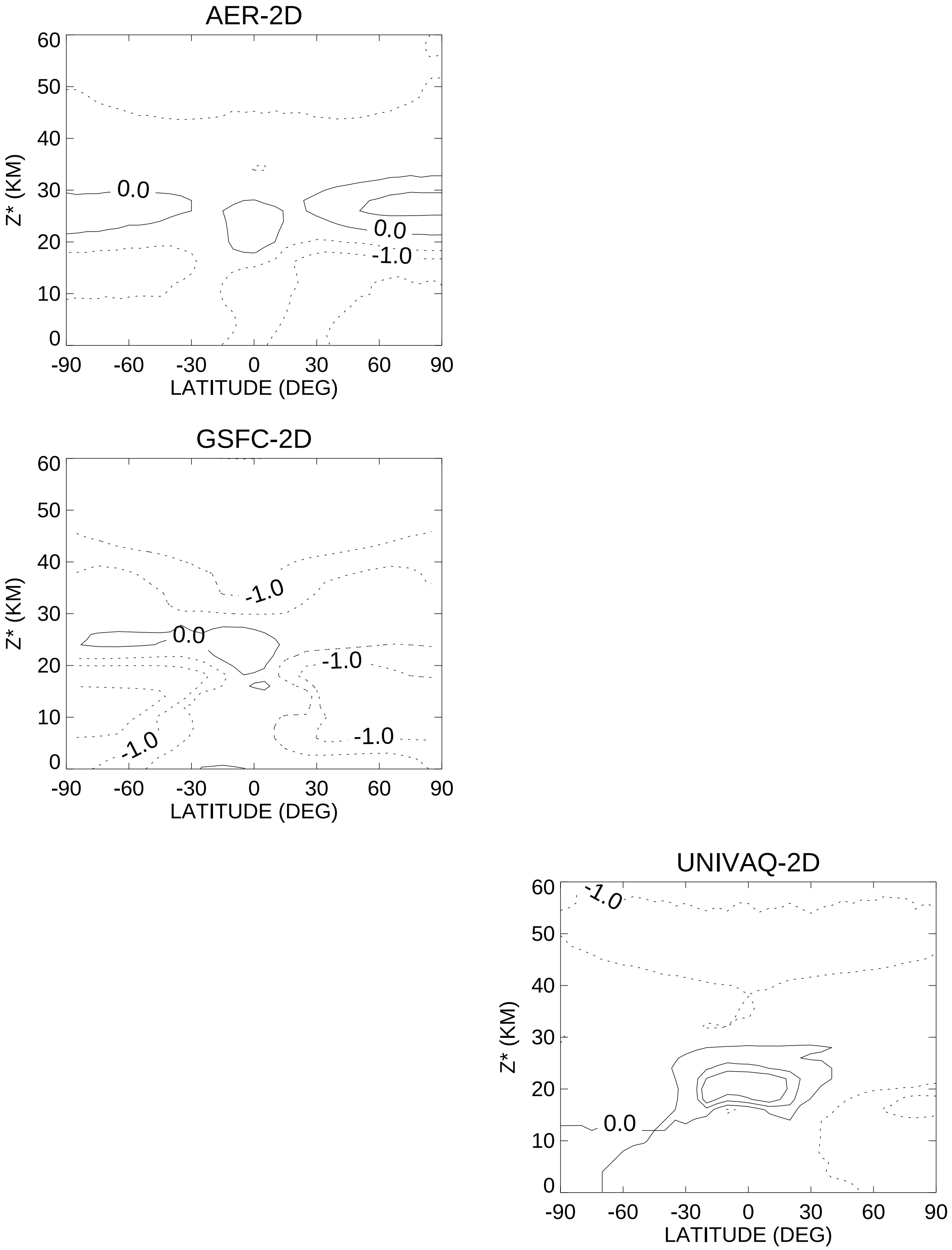

Figure 4.223: Calculated perturbations to O_3 (percent) as a function of latitude and altitude in March of 2015 due to emissions from a fleet of 500 HSCT aircraft with EI(NO_x)=5, SA1 sulfate surface area, and a background Cl_y concentration of 1.0 ppbv under Scenario S5b relative to Scenario D5. Contours are -2, -1, -0.5, 0, 0.5, 1.

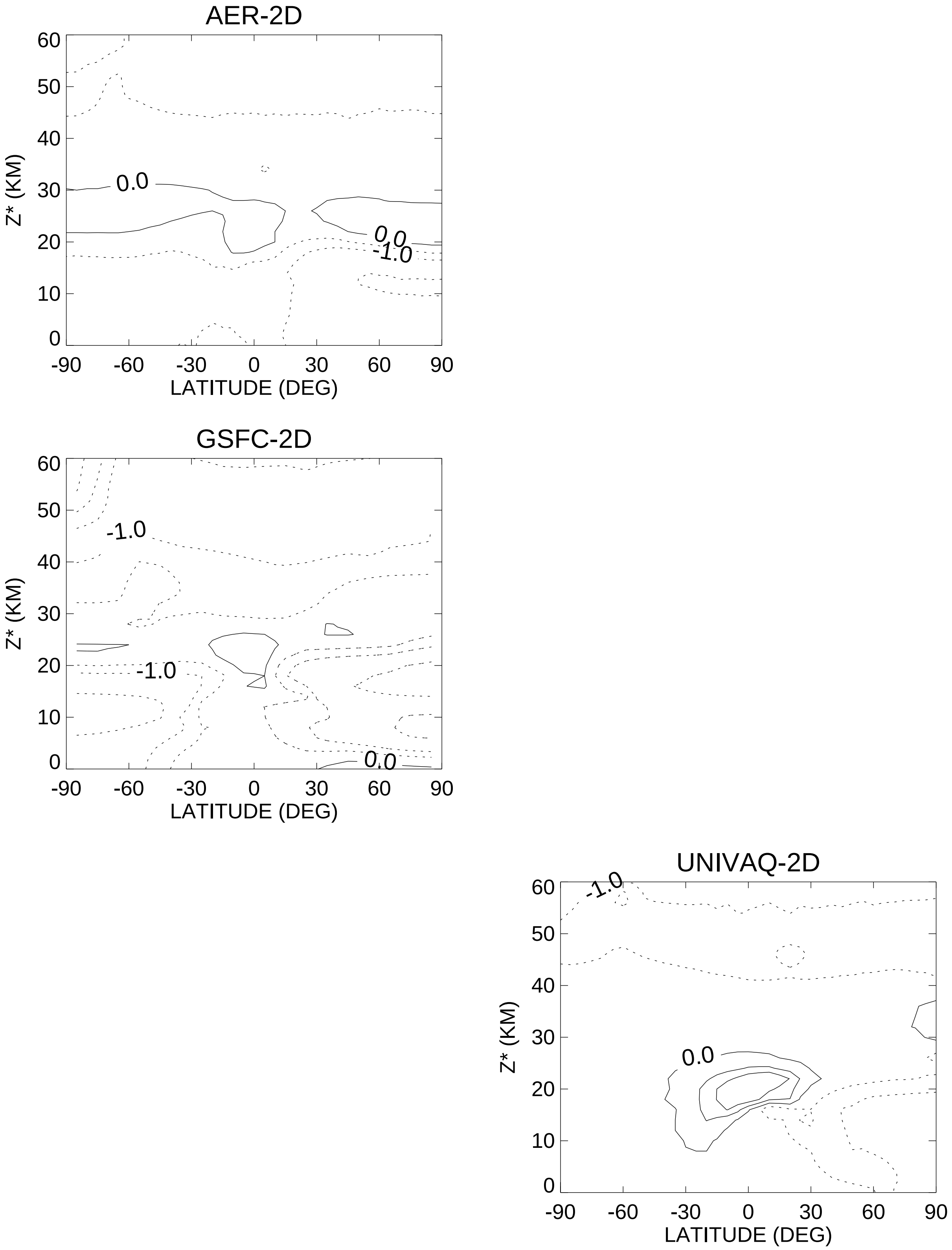

Figure 4.224: Calculated perturbations to O_3 (percent) as a function of latitude and altitude in June of 2015 due to emissions from a fleet of 500 HSCT aircraft with EI(NO_x)=5, SA1 sulfate surface area, and a background Cl_y concentration of 1.0 ppbv under Scenario S5b relative to Scenario D5. Contours are -2, -1, -0.5, 0, 0.5, 1.

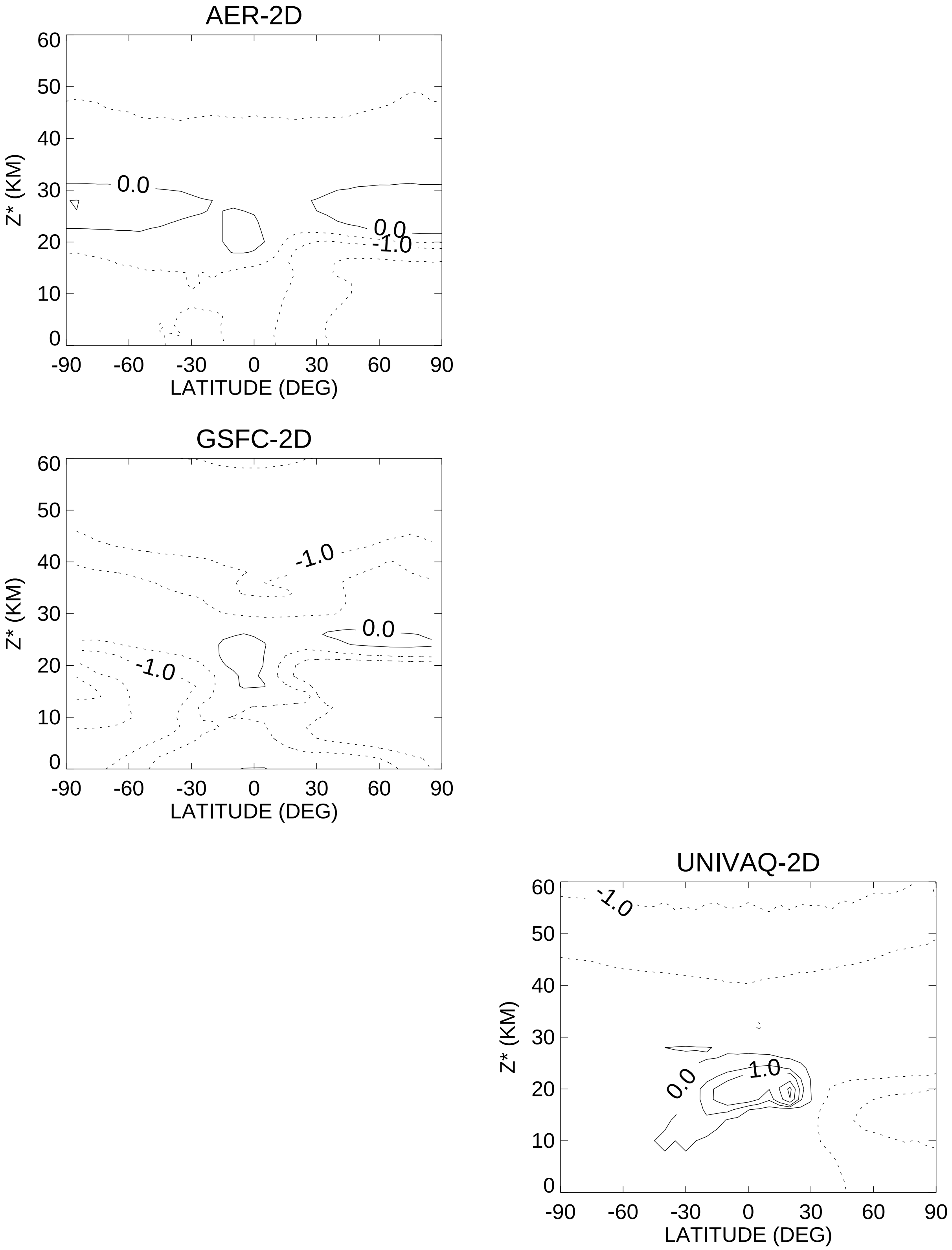

Figure 4.225: Calculated perturbations to O_3 (percent) as a function of latitude and altitude in October of 2015 due to emissions from a fleet of 500 HSCT aircraft with EI(NO_x)=5, SA1 sulfate surface area, and a background Cl_y concentration of 1.0 ppbv under Scenario S5b relative to Scenario D5. Contours are -3, -2, -1, -0.5, 0, 0.5, 1, 2, 3.

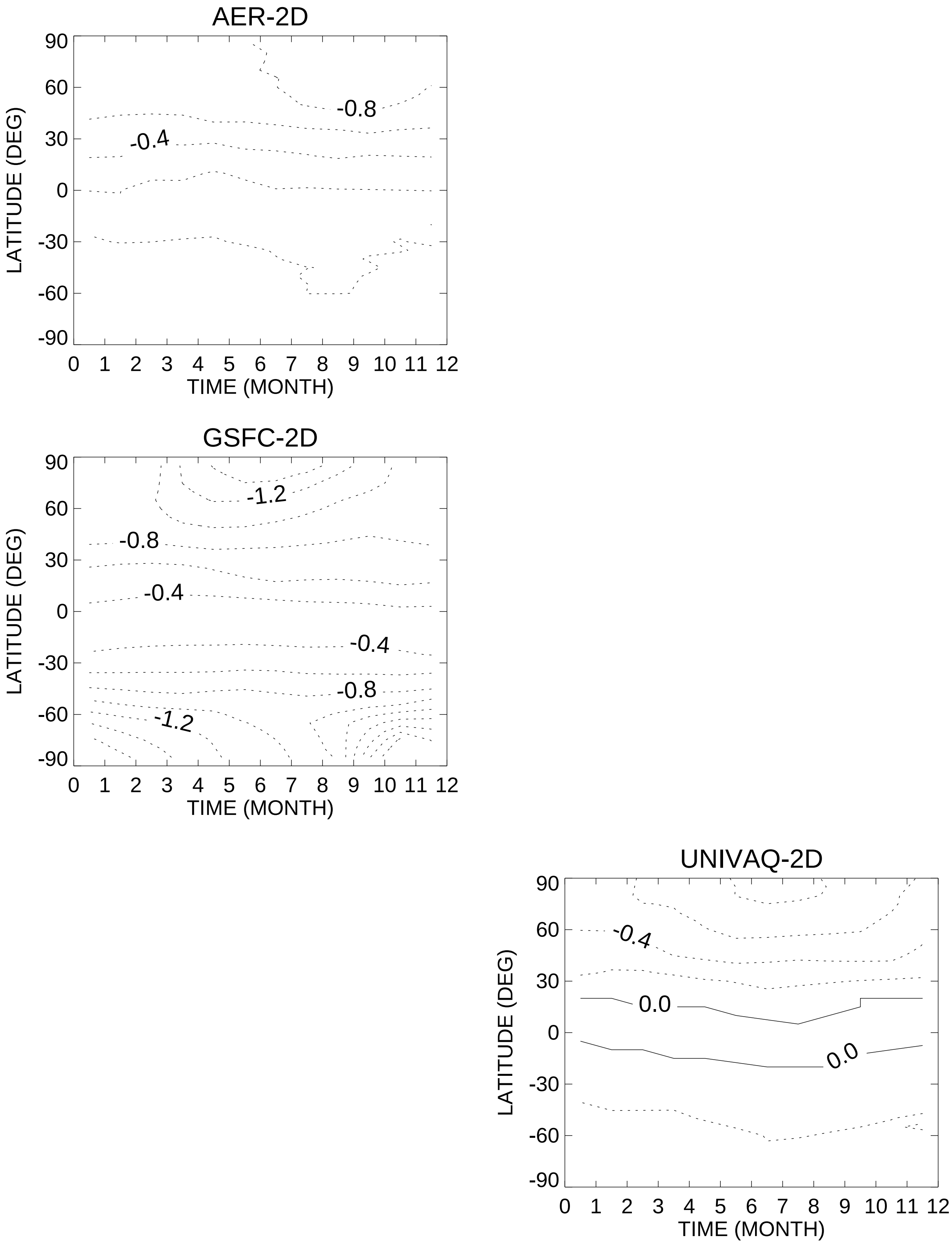

Figure 4.226: Calculated perturbations to column O_3 (percent) as a function of latitude and season in 2015 due to emissions from a fleet of 500 HSCT aircraft with EI(NO_x)=5, SA1 sulfate surface area, and a background Cl_y concentration of 1.0 ppbv under Scenario S5b relative to Scenario D5. Contours are -2.0 to 0 by 0.2.

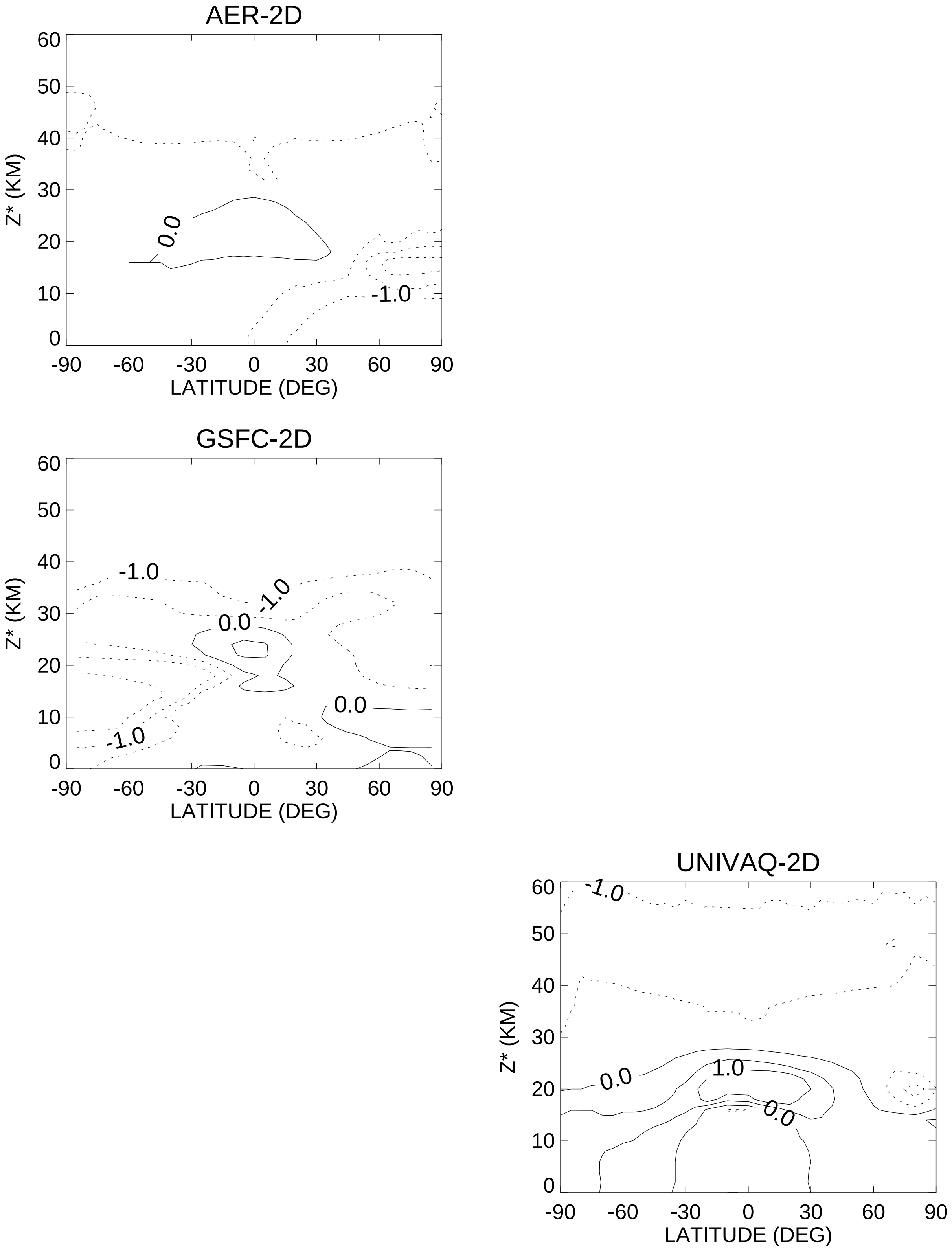

Figure 4.227: Calculated perturbations to O_3 (percent) as a function of latitude and altitude in March of 2015 due to emissions from a fleet of 500 HSCT aircraft with $EI(NO_x)=5$ and a background Cl_y concentration of 4.0 ppbv under Scenario S6a relative to Scenario D6. Contours are -2, -1, -0.5, 0, 0.5, 1.

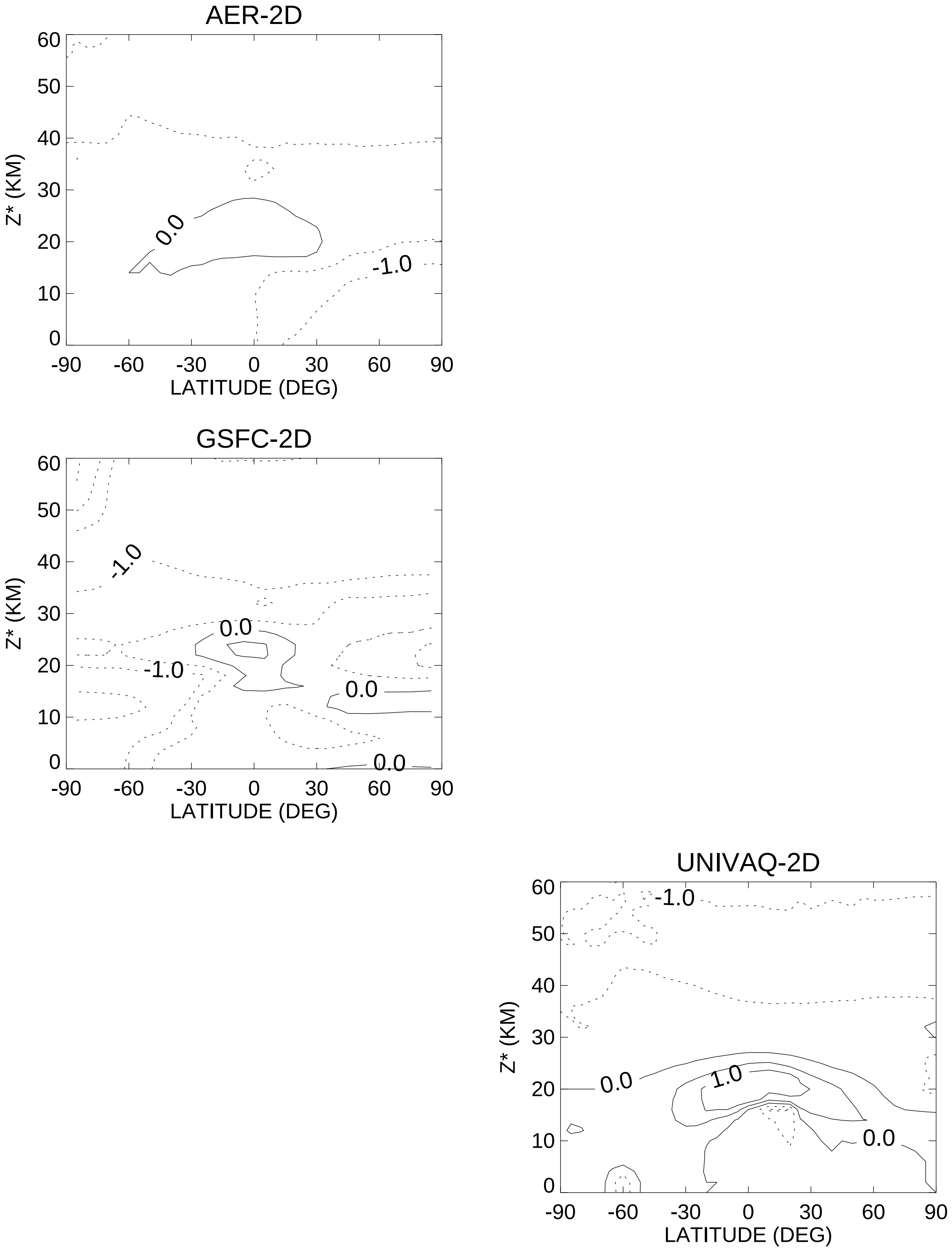

Figure 4.228: Calculated perturbations to O_3 (percent) as a function of latitude and altitude in June of 2015 due to emissions from a fleet of 500 HSCT aircraft with EI(NO_x)=5 and a background Cl_y concentration of 4.0 ppbv under Scenario S6a relative to Scenario D6. Contours are -2, -1, -0.5, 0, 0.5, 1.

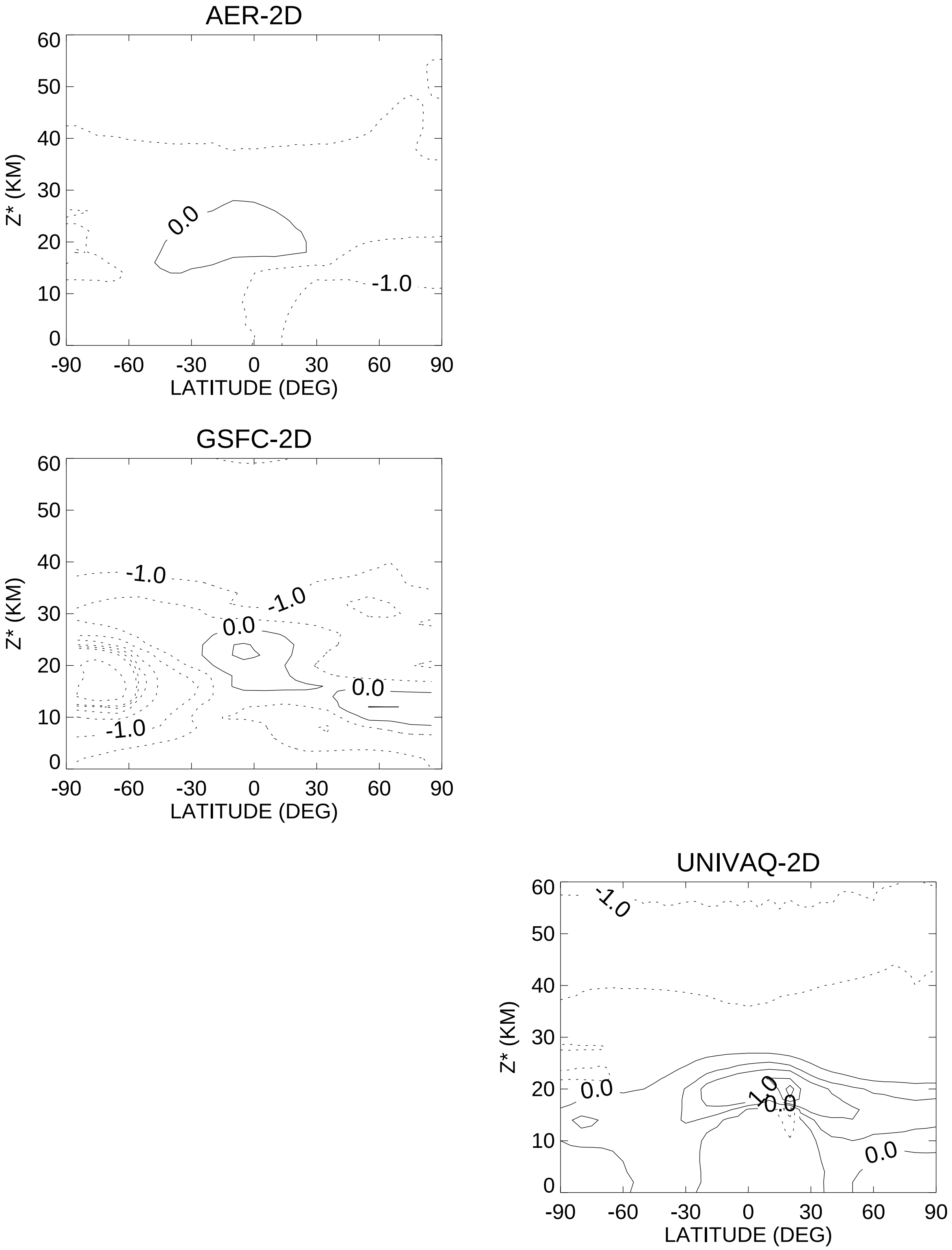

Figure 4.229: Calculated perturbations to O_3 (percent) as a function of latitude and altitude in October of 2015 due to emissions from a fleet of 500 HSCT aircraft with EI(NO_x)=5 and a background Cl_y concentration of 4.0 ppbv under Scenario S6a relative to Scenario D6. Contours are -10, -5, -4, -3, -2, -1, -0.5, 0, 0.5, 1, 2, 3.

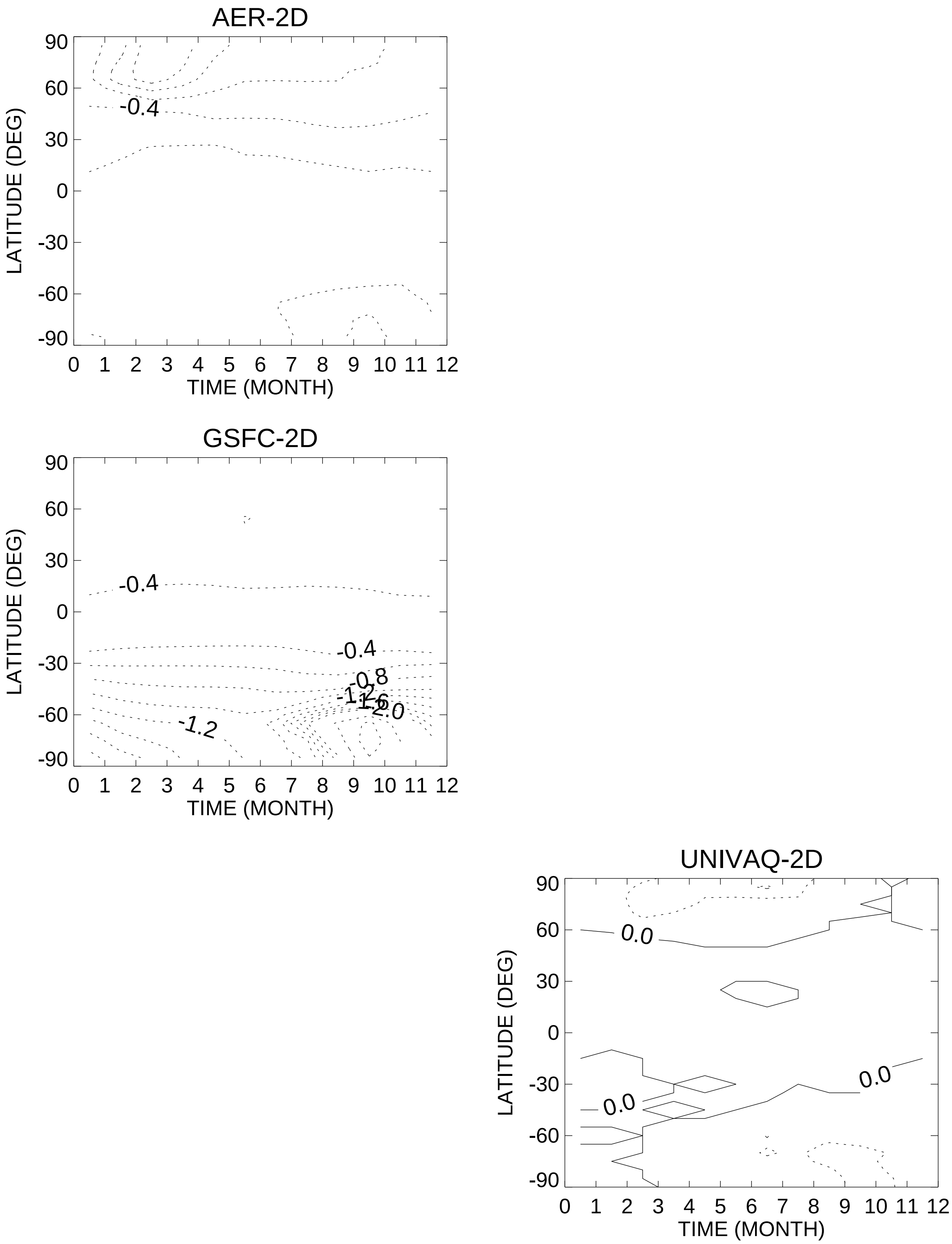

Figure 4.230: Calculated perturbations to column O_3 (percent) as a function of latitude and season in 2015 due to emissions from a fleet of 500 HSCT aircraft with $EI(NO_x)$=5 and a background Cl_y concentration of 4.0 ppbv under Scenario S6a relative to Scenario D6. Contours are -4, -3 and -2 to 0.2 by 0.2.

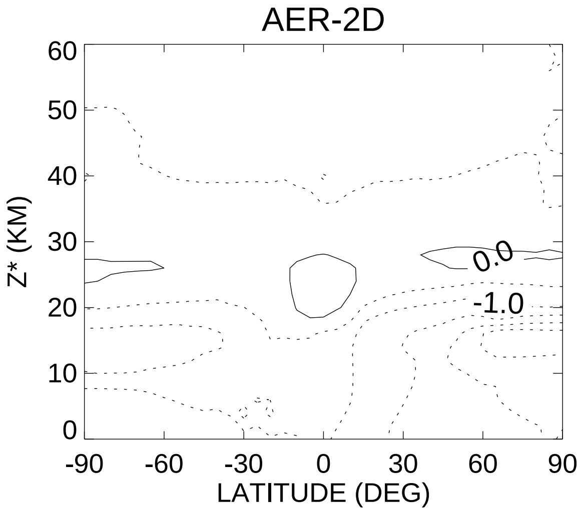

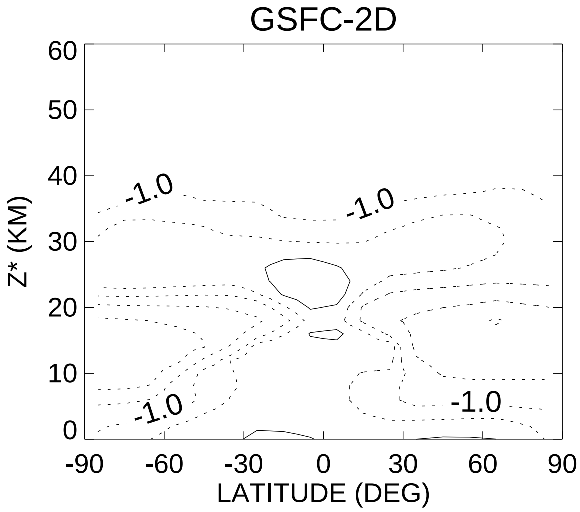

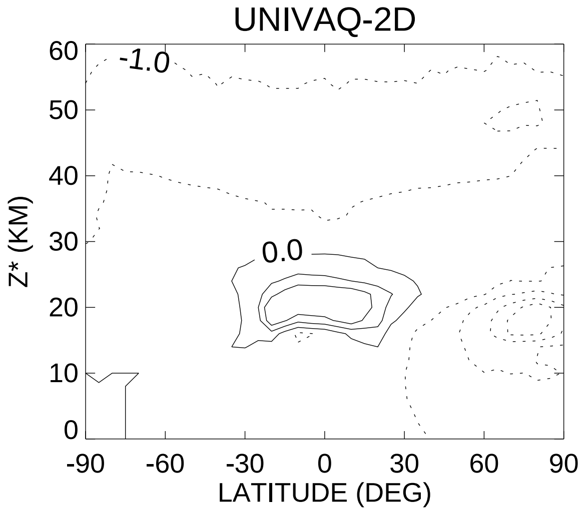

Figure 4.231: Calculated perturbations to O_3 (percent) as a function of latitude and altitude in March of 2015 due to emissions from a fleet of 500 HSCT aircraft with EI(NO_x)=5, SA1 sulfate surface area, and a background Cl_y concentration of 4.0 ppbv under Scenario S6b relative to Scenario D6. Contours are -4, -3, -2, -1, -0.5, 0, 0.5, 1.

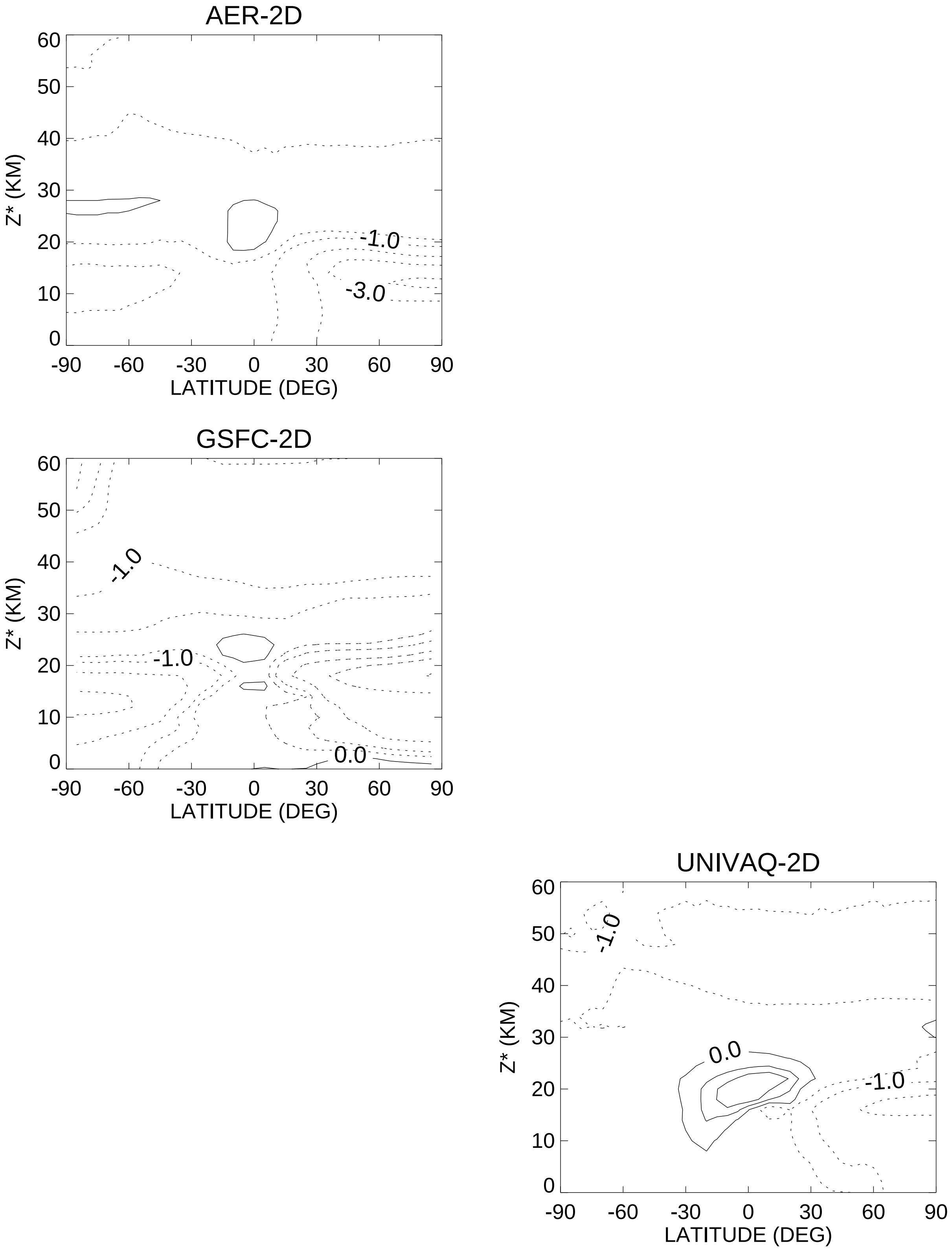

Figure 4.232: Calculated perturbations to O_3 (percent) as a function of latitude and altitude in June of 2015 due to emissions from a fleet of 500 HSCT aircraft with $EI(NO_x)$=5, SA1 sulfate surface area, and a background Cl_y concentration of 4.0 ppbv under Scenario S6b relative to Scenario D6. Contours are -4, -3, -2, -1, -0.5, 0, 0.5, 1.

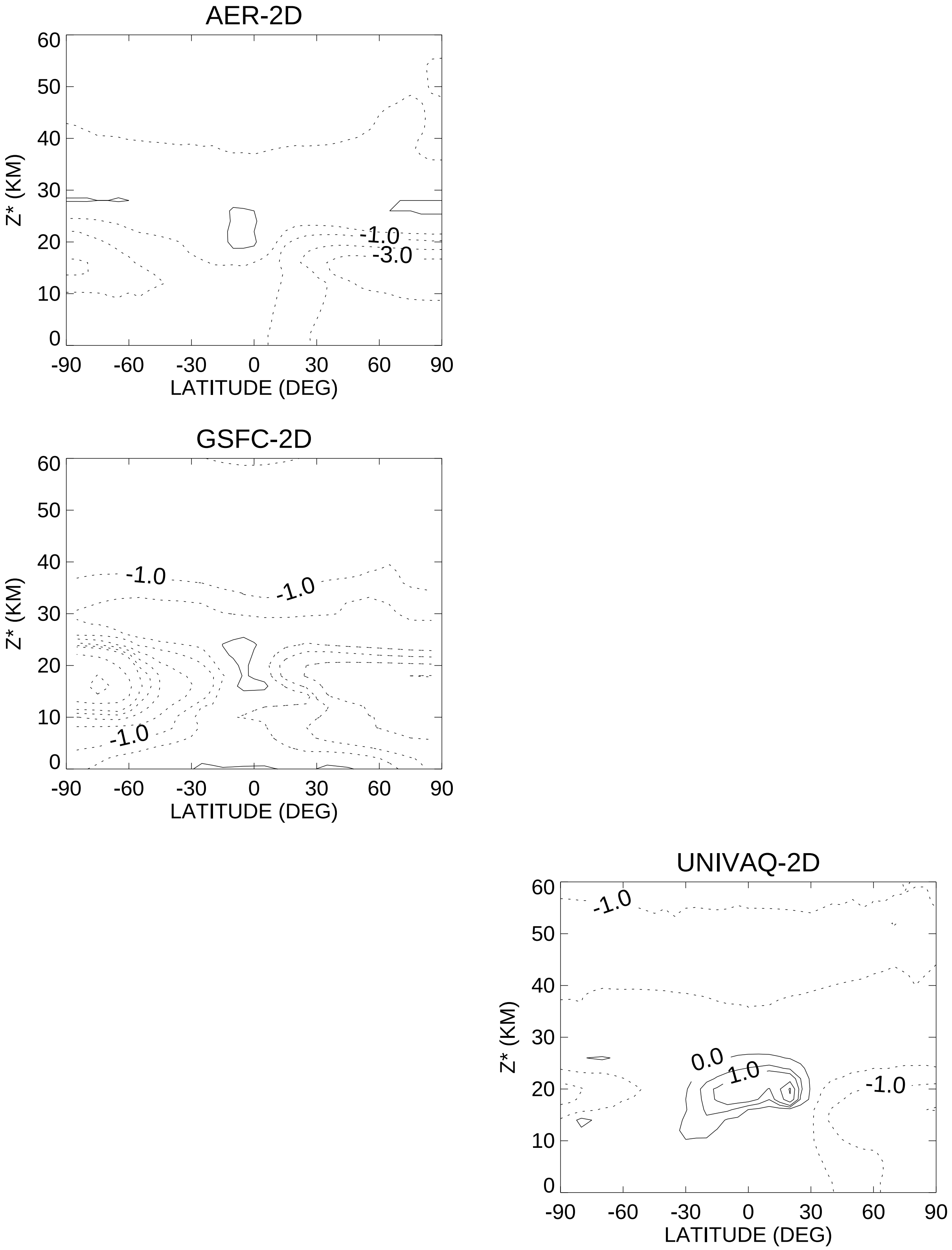

Figure 4.233: Calculated perturbations to O_3 (percent) as a function of latitude and altitude in October of 2015 due to emissions from a fleet of 500 HSCT aircraft with EI(NO_x)=5, SA1 sulfate surface area, and a background Cl_y concentration of 4.0 ppbv under Scenario S6b relative to Scenario D6. Contours are -15, -10, -5, -4, -3, -2, -1, -0.5, 0, 0.5, 1, 2, 3.

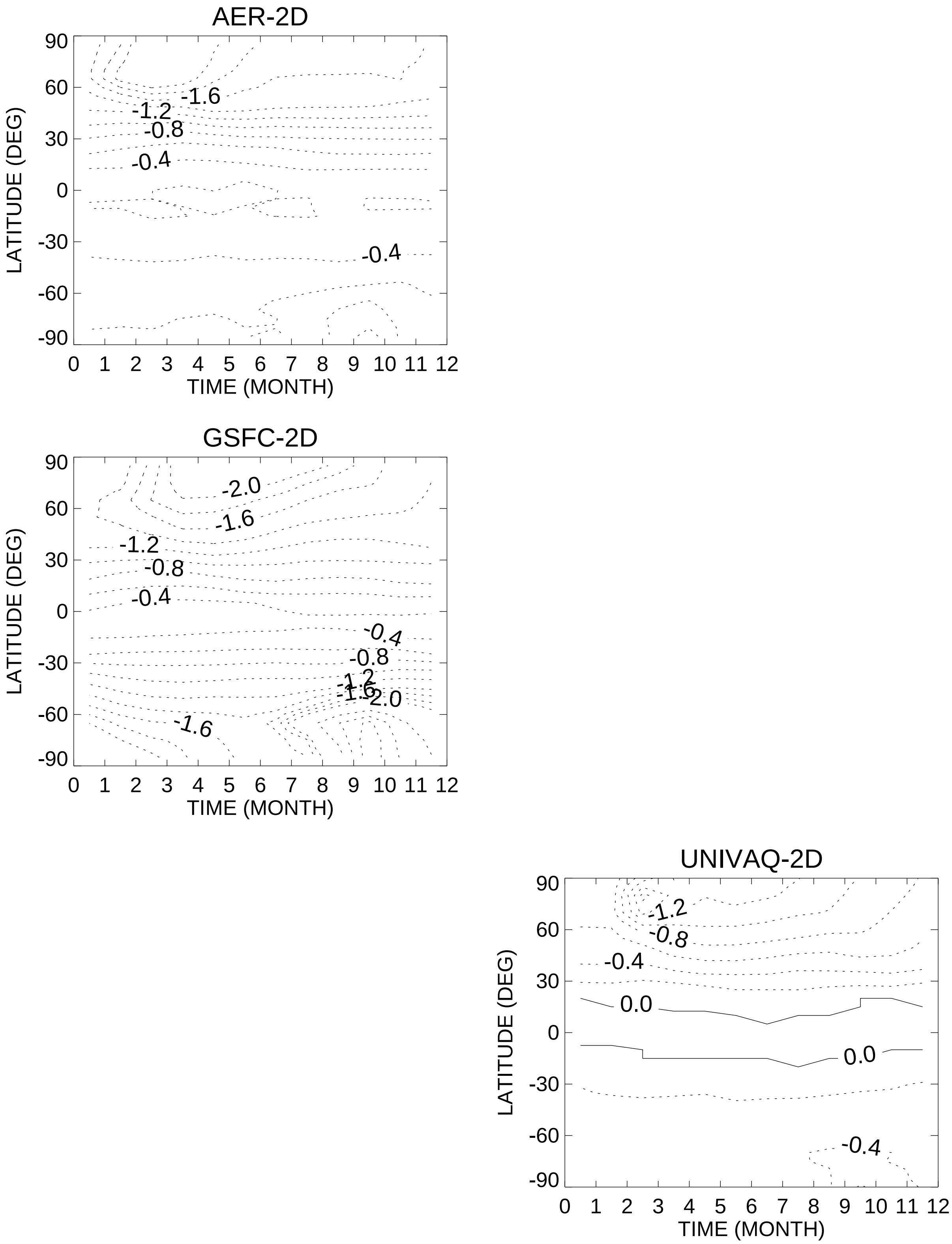

Figure 4.234: Calculated perturbations to column O_3 (percent) as a function of latitude and season in 2015 due to emissions from a fleet of 500 HSCT aircraft with $EI(NO_x)$=5, SA1 sulfate surface area, and a background Cl_y concentration of 4.0 ppbv under Scenario S6b relative to Scenario D6. Contours are -5, -4, -3 and -2 to 0 by 0.2.

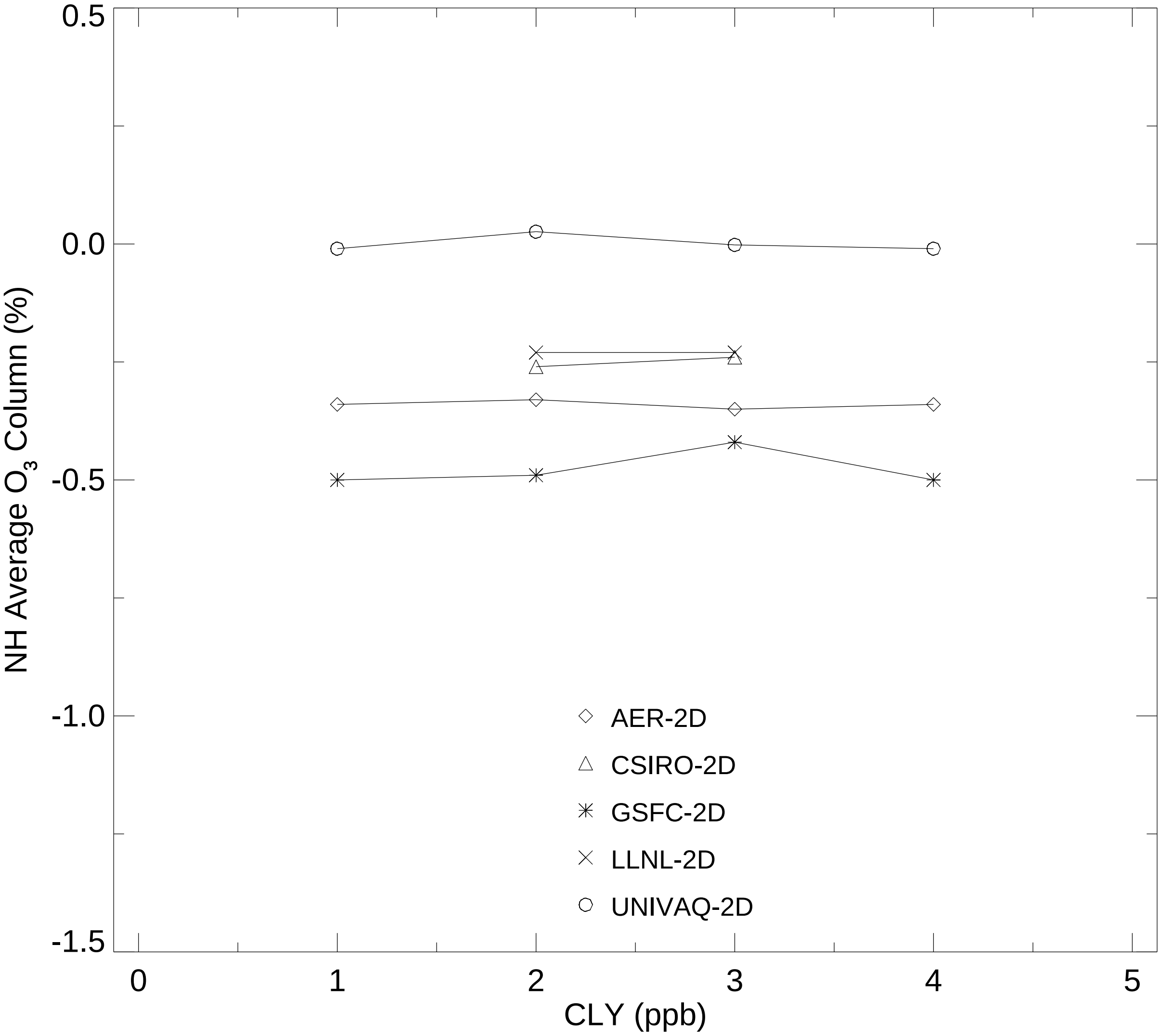

Figure 4.235: Northern hemisphere annual average total O_3 column change (percent) as a function of Cl_y loading for an HSCT fleet of 500 aircraft operating in 2015 with EI(NO_x)=5, no aircraft sulfur emissions, and SA0 sulfate surface area density. The 2 ppbv Cl_y scenarios use 2050 boundary conditions while the 1, 3, and 4 ppb Cl_y scenarios use 2015 boundary conditions.

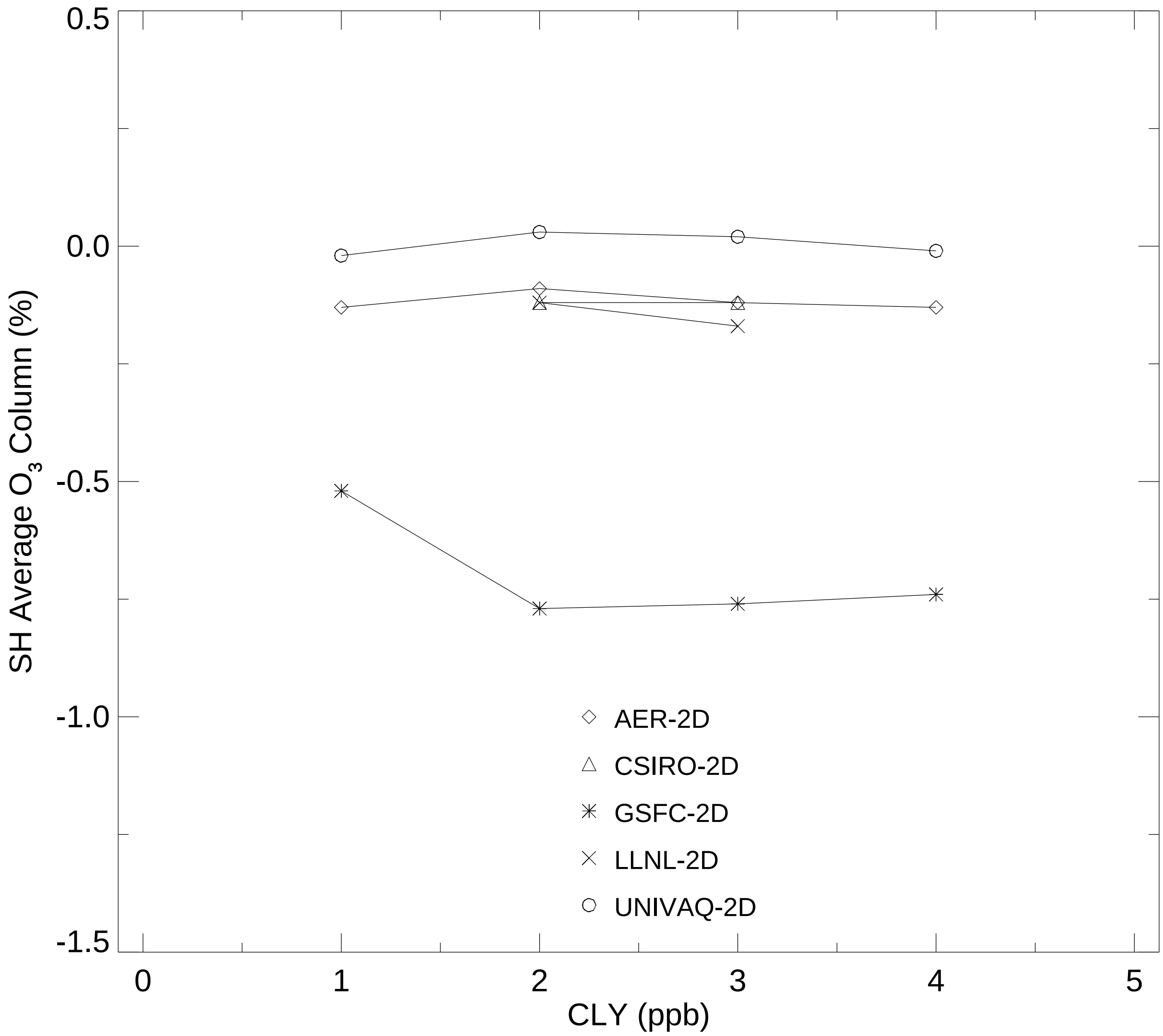

Figure 4.236: Southern hemisphere annual average total O_3 column change (percent) as a function of Cl_y loading for an HSCT fleet of 500 aircraft operating in 2015 with $EI(NO_x)=5$, no aircraft sulfur emissions, and SA0 sulfate surface area density. The 2 ppbv Cl_y scenarios use 2050 boundary conditions while the 1, 3, and 4 ppb Cl_y scenarios use 2015 boundary conditions.

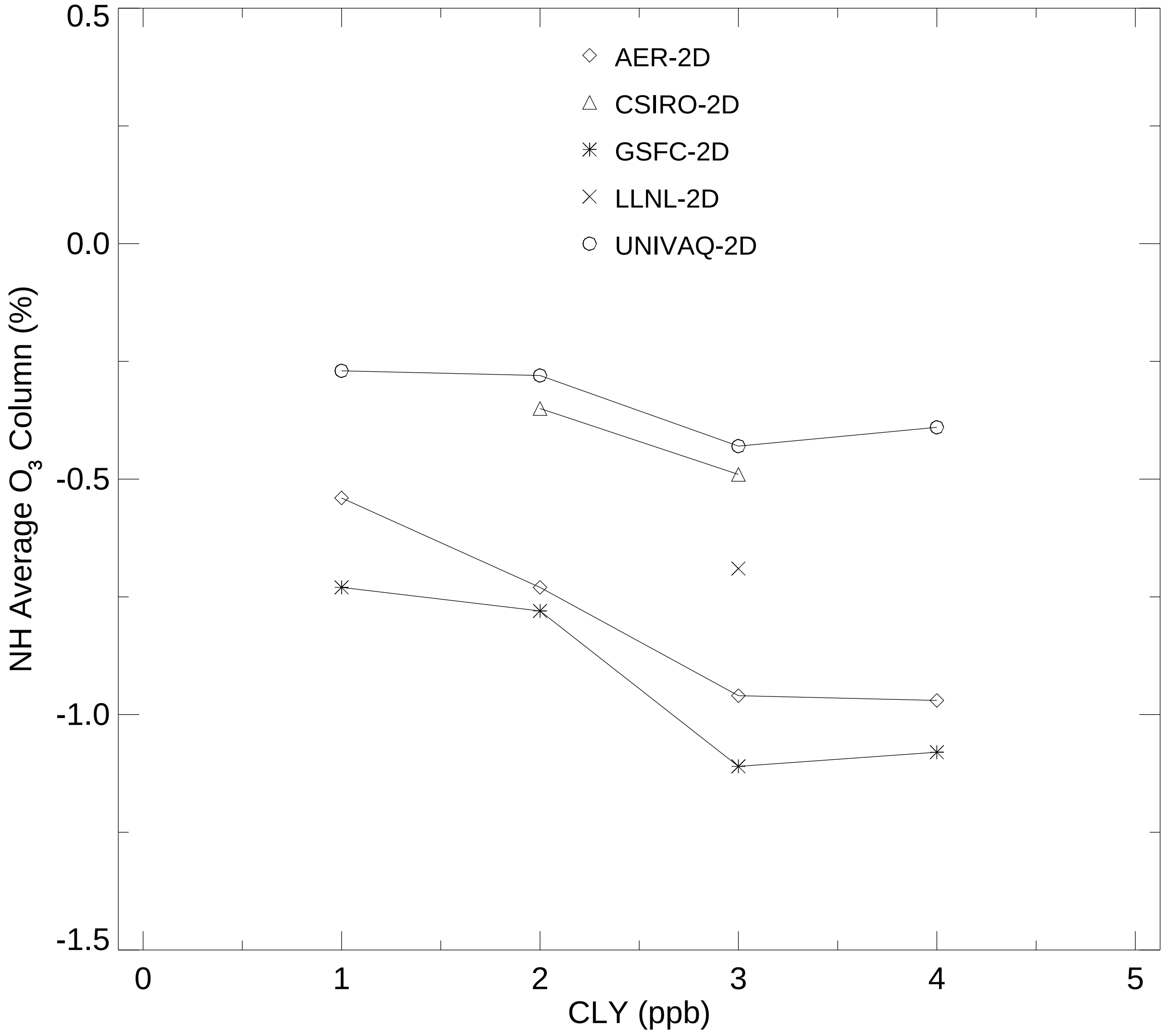

Figure 4.237: Northern hemisphere annual average total O_3 column change (percent) as a function of Cl_y loading for an HSCT fleet of 500 aircraft operating in 2015 with EI(NO_x)=5 and SA1 sulfate surface area density. The 2 ppbv Cl_y scenarios use 2050 boundary conditions while the 1, 3, and 4 ppb Cl_y scenarios use 2015 boundary conditions.

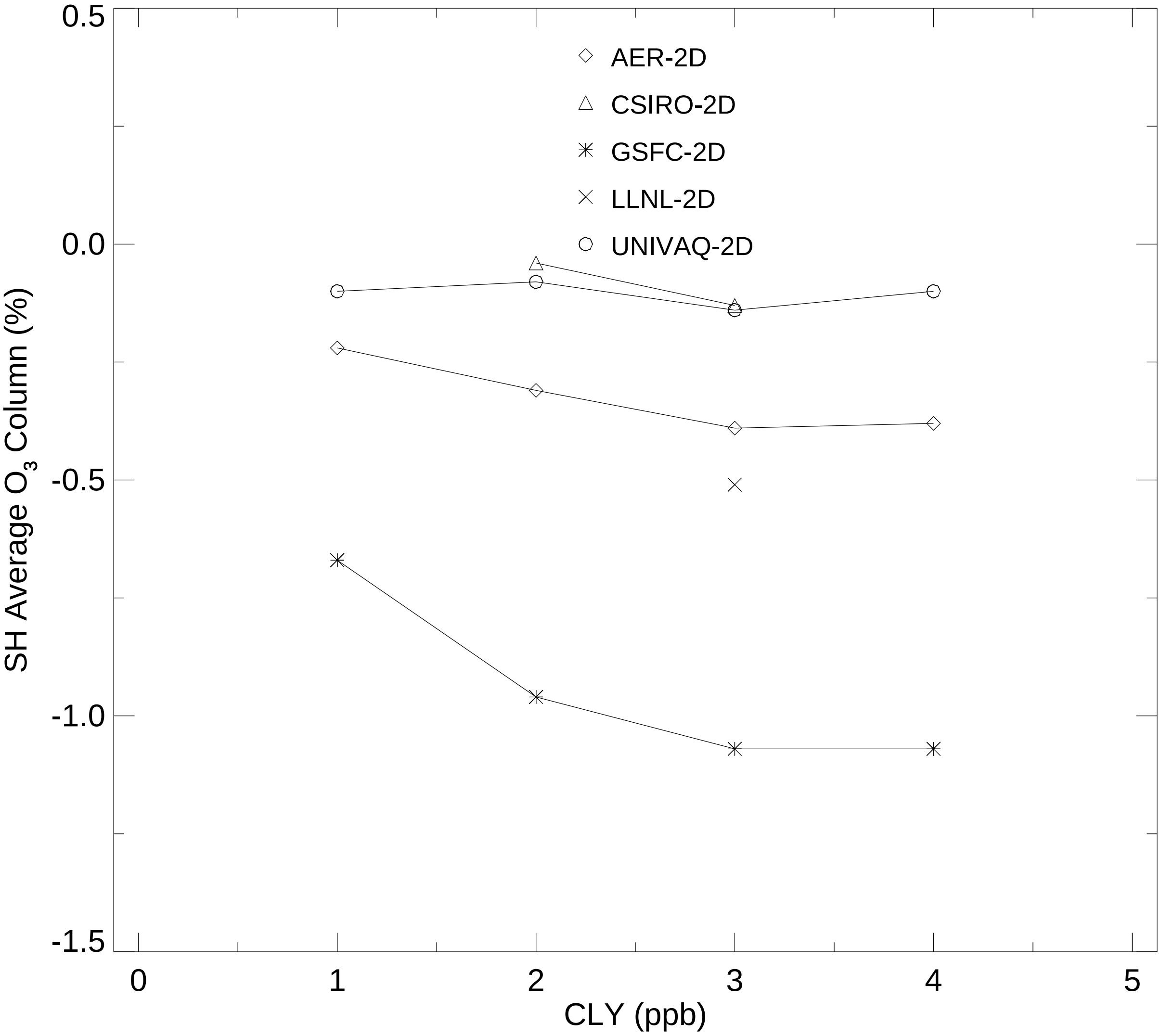

Figure 4.238: Southern hemisphere annual average total O_3 column change (percent) as a function of Cl_y loading for an HSCT fleet of 500 aircraft operating in 2015 with $EI(NO_x)$=5 and SA1 sulfate surface area density. The 2 ppbv Cl_y scenarios use 2050 boundary conditions while the 1, 3, and 4 ppb Cl_y scenarios use 2015 boundary conditions.

4.3.7 Scenarios with Interactive Microphysics (S7a-d, S8a)

This section will cover Scenarios S7a-S7d and S8a which include interactive sulfate aerosol microphysics. Only the AER and UNIVAQ models performed these simulations, as they were the only models with microphysics capabilities. The AER model calculations did not include aircraft emissions of sulfur below 13 km, due to uncertainties in modeling tropospheric sulfur. The UNIVAQ model did include these emissions, though they should have little impact on the perturbation which subtracts the HSCT+subsonic case from the subsonic-only case.

Scenario S7a includes 500 HSCT aircraft in 2015 with EI(NO_x)=5, EI(SO_2)=0.4, and 50% gas to particle conversion. It is identical to Scenario S1f except that instead of using the SA1 surface area density for the HSCT case, the SAD was calculated interactively by these models. Calculated perturbations in SAD are shown in Figure 4.239. Since the AER model provided the calculation of SA1, the only difference for AER is that the SAD perturbation is relative to the AER model's calculated background SAD rather than the SA0 surface area density provided by UNEP, and the values change monthly rather remaining fixed for 6 months at a time. Figures 4.240, 4.241, and 4.242 show changes in ozone between Scenario S7a and Scenario D7 (with subsonic aircraft only) for March, June, and October. The AER results is very similar to the AER results for S1f-D. The UNIVAQ result is quite different in the extra-tropical lower stratosphere. The ozone perturbation is zero at 30 km at all latitudes. In the 10-20 km region at mid and high latitudes, ozone depletion from S7a-D7 is somewhat larger than from S1f-D. Figure 4.243 shows the change in ozone column for this scenario. Both models show ozone depletion of up to 2% in the northern hemisphere high latitudes and up to 1% in the southern hemisphere high latitudes. This is slightly more depletion than was seen with S1f-D.

Scenario S7b is similar to S7a but with the HSCT emission altitude shifted upward by 2 km. The calculated surface area perturbation for this scenario is shown in Figure 4.244 for the AER model only. The peak surface area density perturbation has the same value as for S7a-D7, but occurs at a higher altitude. Figures 4.245, 4.246, and 4.247 show changes in ozone for Scenario S7b relative to Scenario D7 for March, June, and October. Ozone depletion for this scenario is greater than for S7a-D7 in both the upper and lower stratosphere, as the stratospheric residence time of H_2O, NO_y, and sulfur is increased by the higher altitude of emission. Changes in column ozone for this scenario are shown in Figure 4.248. Ozone depletions of up to 3% are seen at high northern latitudes for both models. Northern hemisphere annual average ozone depletion is 1.4% for the AER model and 0.7% for the UNIVAQ model. This is 40% greater than at the standard cruise altitude (S7a-D7) and double the depletion seen in Scenario S2a-D, which used the increased cruise altitude but no sulfur emissions.

Scenario S7c includes a downward shift of 2 km in the HSCT cruise altitude, but is otherwise similar to S7a and S7b. Figure 4.249 shows the change in aerosol surface area calculated by the AER model for this scenario. Ozone changes for this scenario are shown in Figures 4.250, 4.251, and 4.252. Ozone perturbations are significantly smaller than for S7a-D7, especially in the upper stratosphere and around 10-20 km in the mid to high latitudes. However, ozone depletion is significantly larger than for S2b-D, which includes HSCT emissions at the same altitude but without sulfur emissions. Figure 4.253 shows changes in ozone column as a function of latitude and season for this scenario. Ozone column changes range from -1.2% to -0.2% for the AER model and from -1.0% to 0% for the UNIVAQ model, with the UNIVAQ model showing larger column depletions in the southern springtime polar region. These results indicate the possible importance of aircraft sulfur emissions even with HSCT aircraft operating at reduced cruise altitude.

The sensitivity of annual average hemispheric ozone column change to cruise altitude for a fleet of 500 HSCT aircraft operating in 2015 with EI(NO_x)=5, EI(SO_2)=0.4, and 50% gas to particle conversion is shown in Figures 4.254 and 4.255. The change is calculated hemispheric ozone depletion over the -2 km to +2 km cruise altitude range is much greater than that seen without aircraft sulfur emissions (Figures 4.155 and 4.156), and the magnitude of the ozone depletion is larger for all altitudes.

Scenario S7d uses an EI(NO_x) of 10 with 50% gas to particle conversion and HSCT operation at the nominal cruise altitude. Figures 4.250, 4.251, and 4.252 show calculated ozone perturbations for this scenario. Ozone depletion is smaller than for S7a-D7 except near 30 km, where the depletion is larger with higher NO_x emissions. Changes in ozone column for this scenario are shown in Figure 4.259. Ozone depletion is slightly smaller than for S7a-D7 for both models. In the UNIVAQ model, northern hemisphere annual average ozone depletion is reduced from 0.5% for S7a-D7 to 0.2% for S7d-D7.

Scenario S8a includes 500 HSCT aircraft with EI(NO_x)=5 and EI(SO_2)=0.4. Sulfur emissions are assumed to be 100% particles of 10 nm radius. Figure 4.260 shows the change in aerosol surface area density calculated by the AER and UNIVAQ models for this scenario. SAD perturbations are 50% larger than for S7a-D7. Changes in calculated ozone for S8a-D8 are shown in Figures 4.261, 4.262, and 4.263. Due to the greater aerosol surface area perturbation with 100% gas to particle conversion in the plume, the models shows slightly greater ozone depletion in the lower stratosphere for this scenario than for S7a-D7. Ozone column perturbations, shown in Figure 4.264, are almost identical to S7a-D7 for the UNIVAQ model and just slightly greater for the AER model.

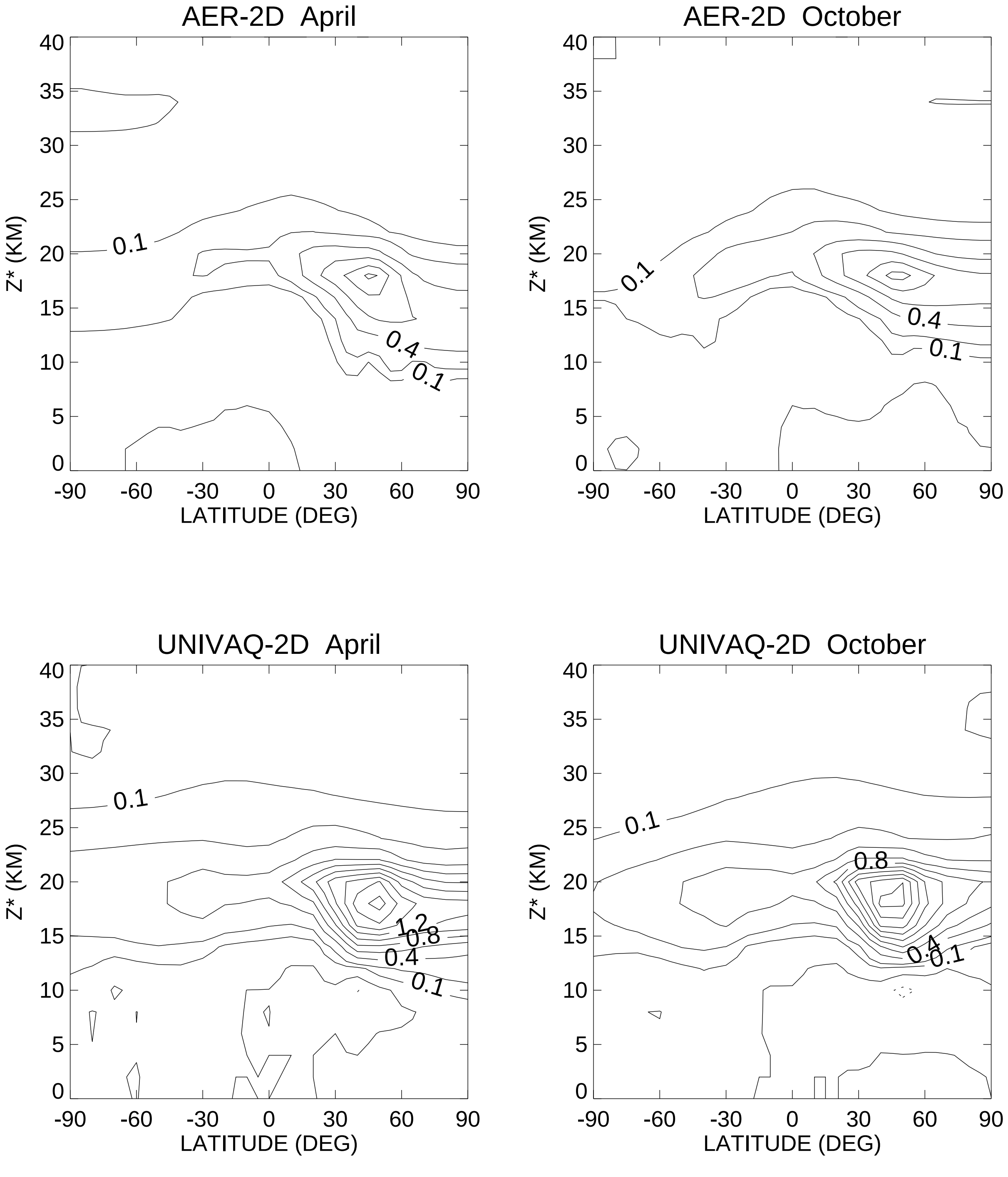

Figure 4.239: Calculated perturbations to aerosol surface area density ($\mu m^2/cm^3$) as a function of latitude and altitude in April and October due to emissions from a fleet of 500 HSCT aircraft with $EI(SO_2)$=0.4 and 50% gas to particle conversion under Scenario S7a relative to Scenario D7. Contours are -0.1, 0, 0.1, and 0.2 to 1.8 by 0.2.

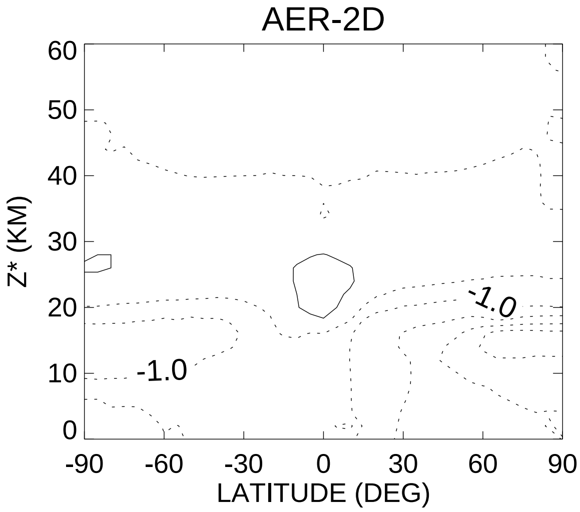

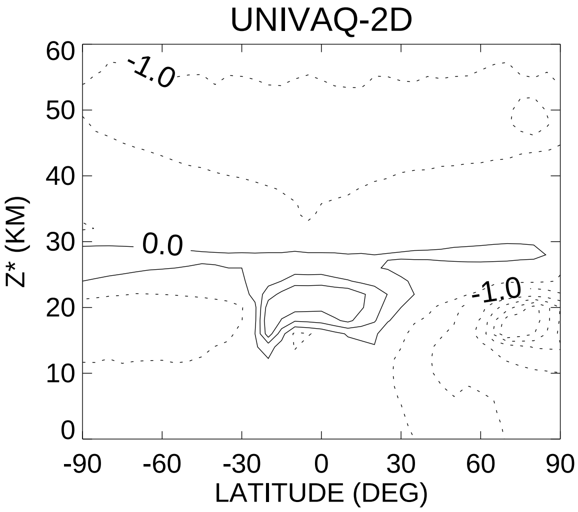

Figure 4.240: Calculated perturbations to O_3 (percent) as a function of latitude and altitude in March of 2015 due to emissions from a fleet of 500 HSCT aircraft with EI(NO_x)=5, EI(SO_2)=0.4, and 50% gas to article conversion under Scenario S7a relative to Scenario D7. Contours are -5, -4, -3, -2, -1, -0.5, 0, 0.5, 1.

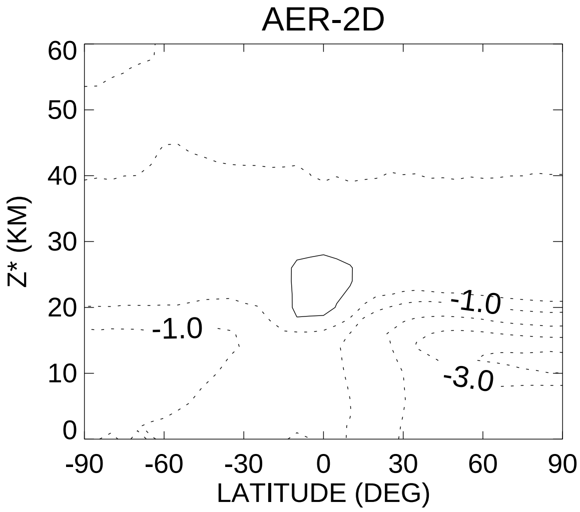

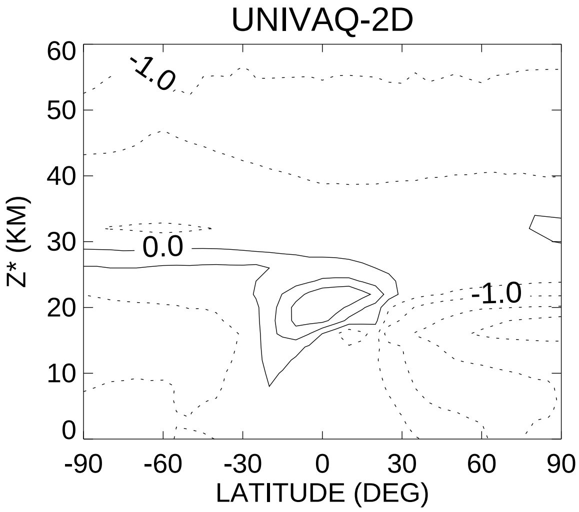

Figure 4.241: Calculated perturbations to O_3 (percent) as a function of latitude and altitude in June of 2015 due to emissions from a fleet of 500 HSCT aircraft with EI(NO_x)=5, EI(SO_2)=0.4, and 50% gas to particle conversion under Scenario S7a relative to Scenario D7. Contours are -4, -3, -2, -1, -0.5, 0, 0.5, 1.

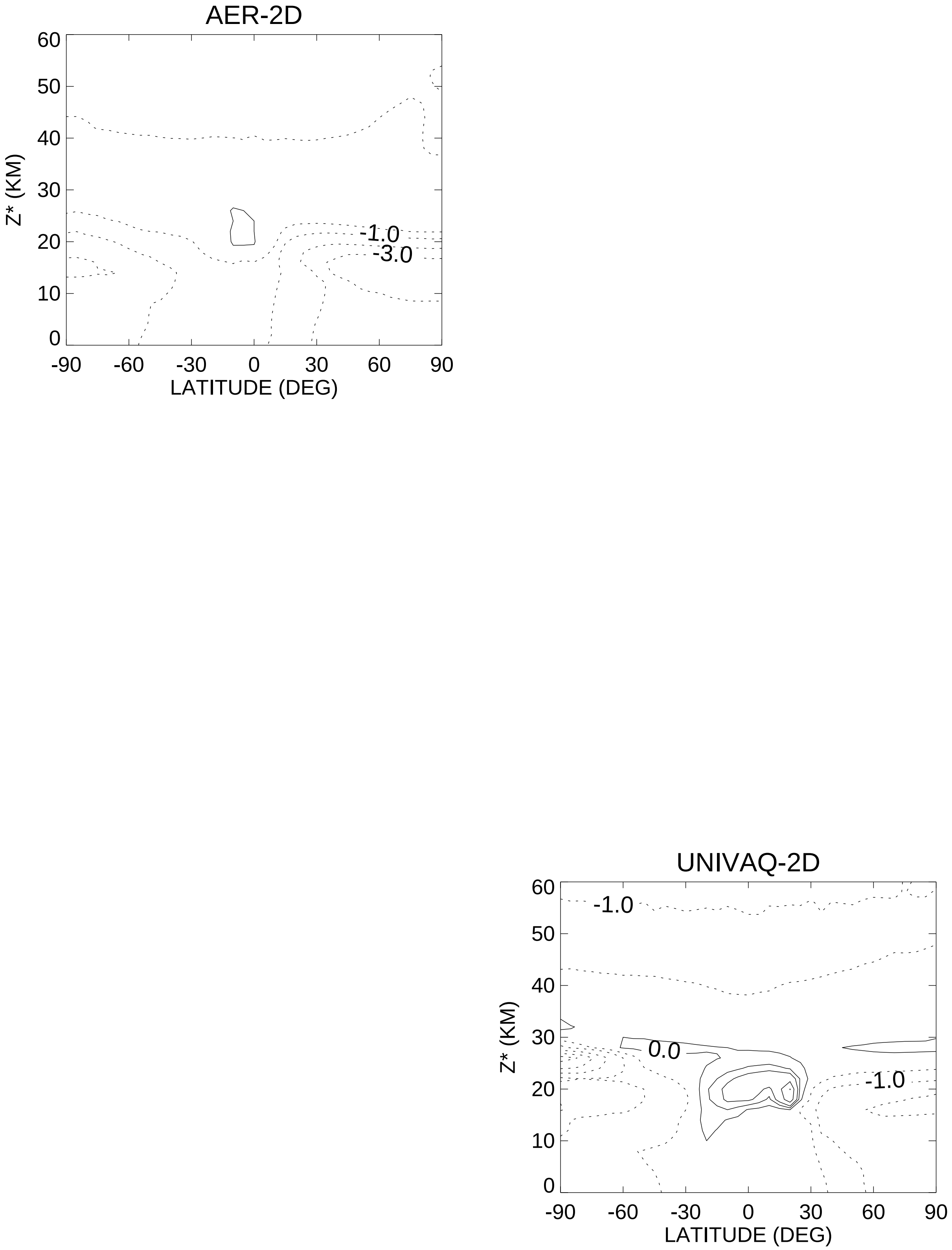

Figure 4.242: Calculated perturbations to O_3 (percent) as a function of latitude and altitude in October of 2015 due to emissions from a fleet of 500 HSCT aircraft with $EI(NO_x)=5$, $EI(SO_2)=0.4$, and 50% gas to particle conversion under Scenario S7a relative to Scenario D7. Contours are -3, -2, -1, -0.5, 0, 0.5, 1, 2, 3.

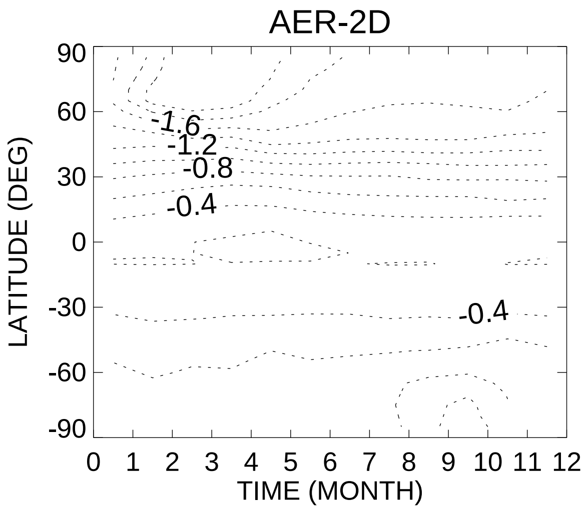

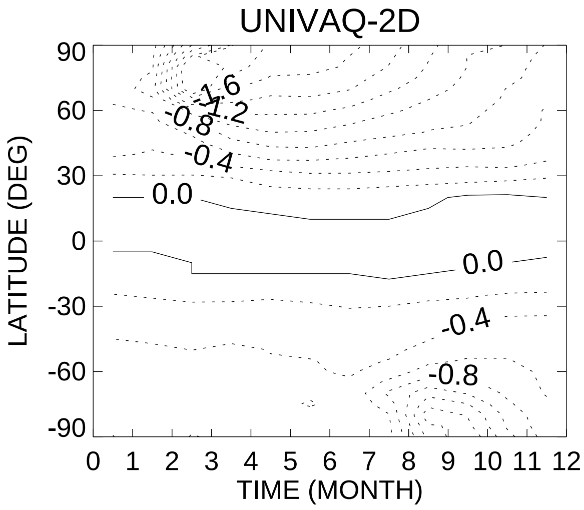

Figure 4.243: Calculated perturbations to column O_3 (percent) as a function of latitude and season in 2015 due to emissions from a fleet of 500 HSCT aircraft with EI(NO_x)=5, EI(SO_2)=0.4, and 50% gas to particle conversion under Scenario S7a relative to Scenario D7. Contours are -2 to 0 by 0.2.

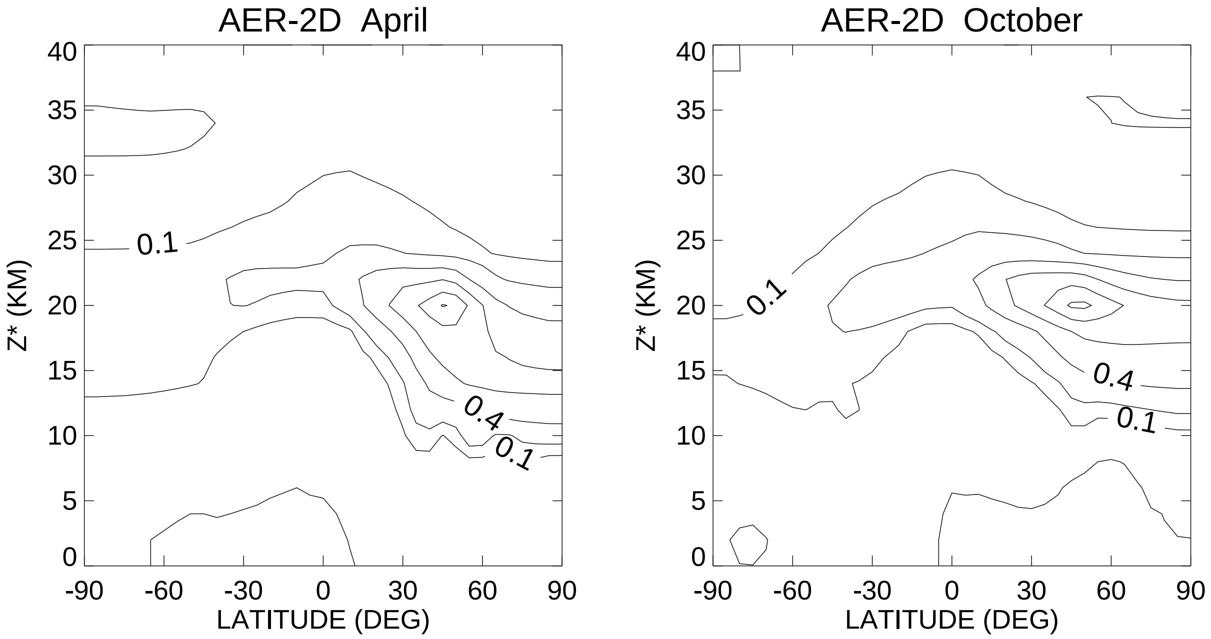

Figure 4.244: Calculated perturbations to aerosol surface area density ($\mu m^2/cm^3$) as a function of latitude and altitude in April and October due to emissions from a fleet of 500 HSCT aircraft operating at 2 km above the nominal cruise altitude with EI(SO_2)=0.4 and 50% gas to particle conversion under Scenario S7b relative to Scenario D7. Contours are -0.1, 0, 0.1, and 0.2, 0.4, 0.6, 0.8.

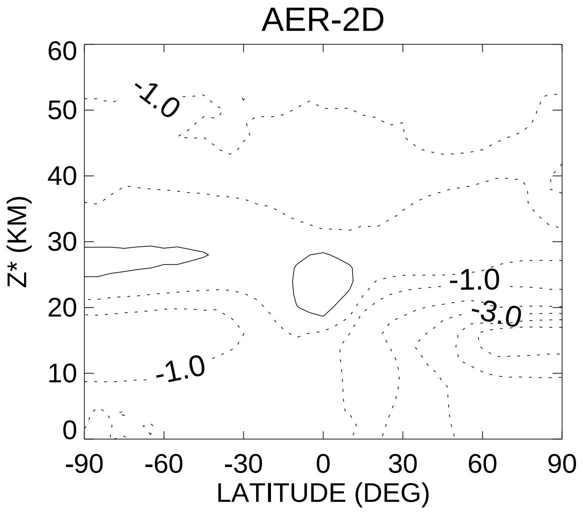

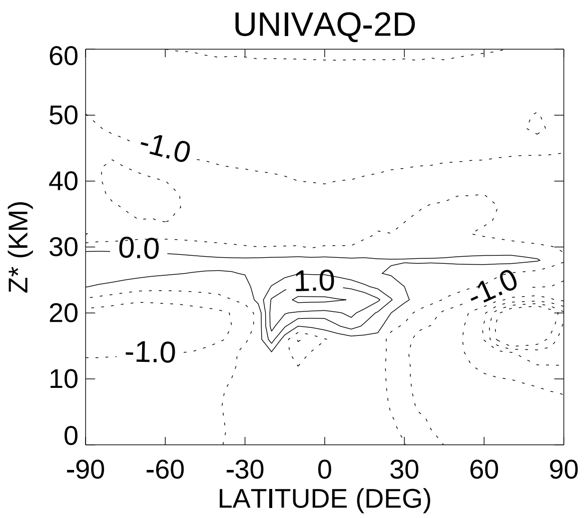

Figure 4.245: Calculated perturbations to O_3 (percent) as a function of latitude and altitude in March of 2015 due to emissions from a fleet of 500 HSCT aircraft operating at 2 km above the nominal cruise altitude with EI(NO_x)=5, EI(SO_2)=0.4, and 50% gas to particle conversion under Scenario S7b relative to Scenario D7. Contours are -5, -4, -3, -2, -1, -0.5, 0, 0.5, 1, 2.

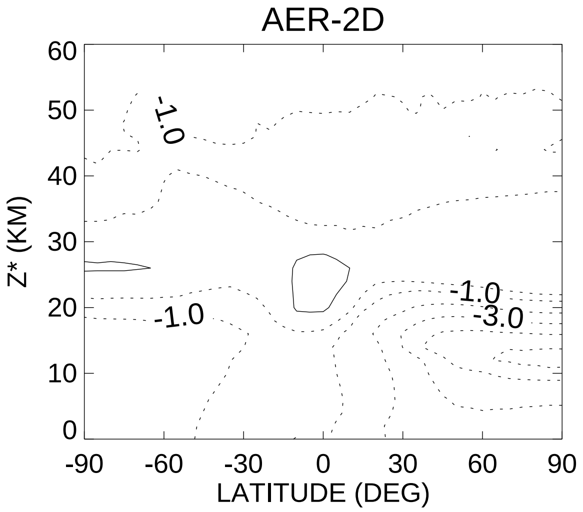

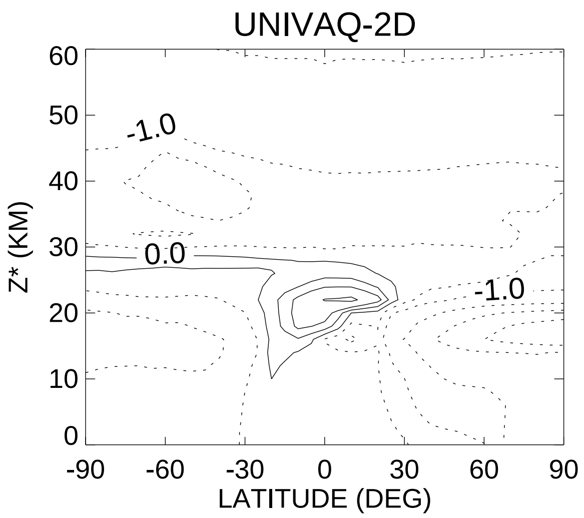

Figure 4.246: Calculated perturbations to O_3 (percent) as a function of latitude and altitude in June of 2015 due to emissions from a fleet of 500 HSCT aircraft operating at 2 km above the nominal cruise altitude with EI(NO_x)=5, EI(SO_2)=0.4, and 50% gas to particle conversion under Scenario S7b relative to Scenario D7. Contours are -5, -4, -3, -2, -1, -0.5, 0, 0.5, 1, 2.

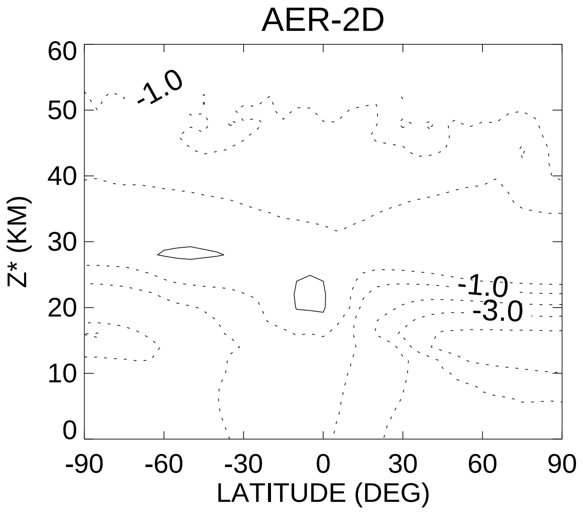

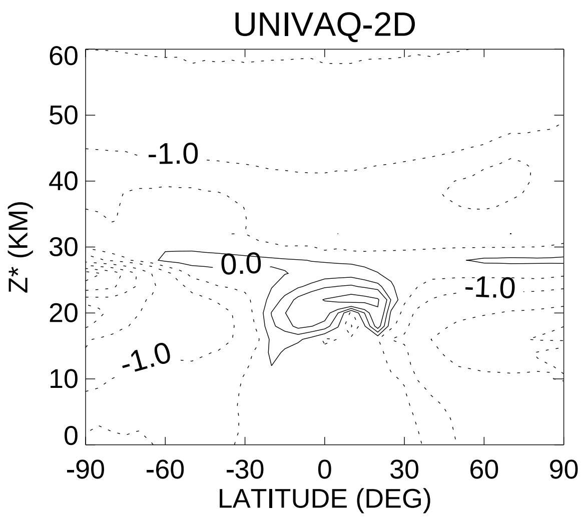

Figure 4.247: Calculated perturbations to O_3 (percent) as a function of latitude and altitude in October of 2015 due to emissions from a fleet of 500 HSCT aircraft operating at 2 km above the nominal cruise altitude with EI(NO_x)=5, EI(SO_2)=0.4, and 50% gas to particle conversion under Scenario S7b relative to Scenario D7. Contours are -5, -4, -3, -2, -1, -0.5, 0, 0.5, 1, 2.

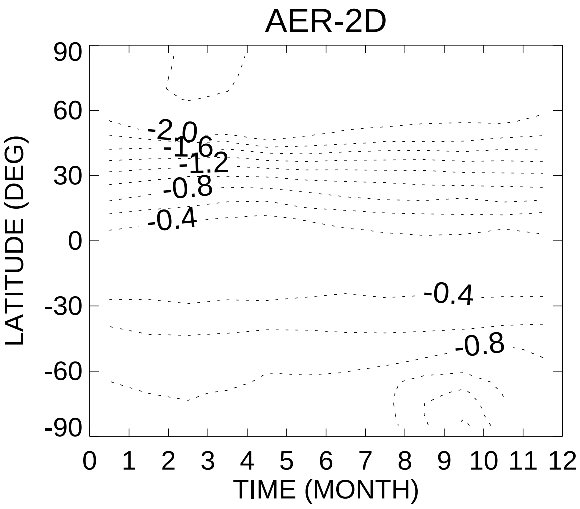

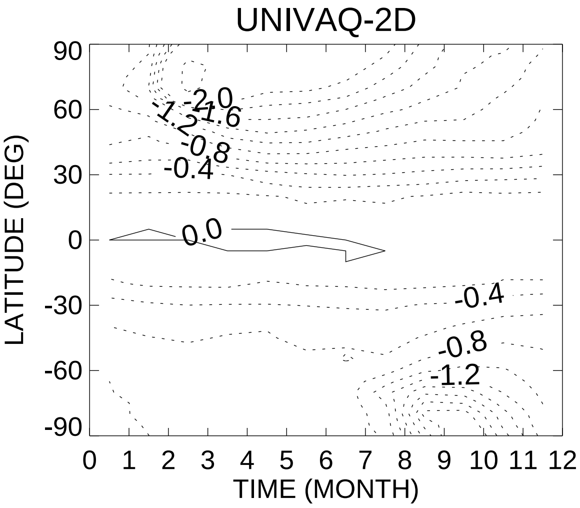

Figure 4.248: Calculated perturbations to column O_3 (percent) as a function of latitude and season in 2015 due to emissions from a fleet of 500 HSCT aircraft operating at 2 km above the nominal cruise altitude with $EI(NO_x)=5$, $EI(SO_2)=0.4$, and 50% gas to particle conversion under Scenario S7b relative to Scenario D7. Contours are -3 and -2 to 0 by 0.2.

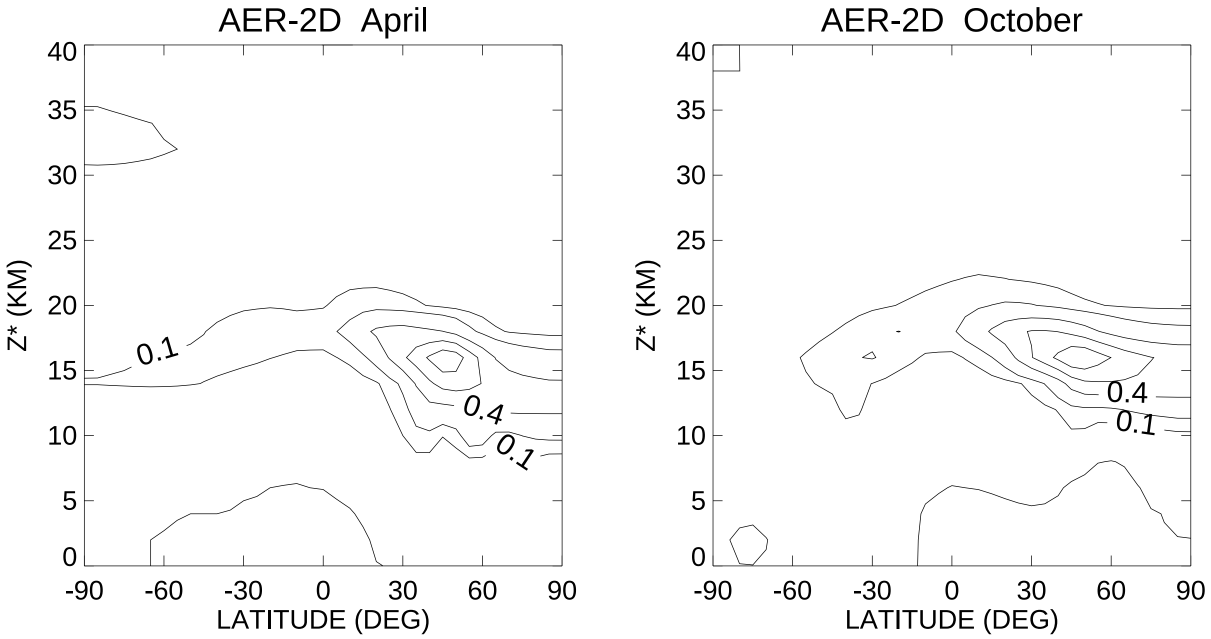

Figure 4.249: Calculated perturbations to aerosol surface area density ($\mu m^2/cm^3$) as a function of latitude and altitude in April and October due to emissions from a fleet of 500 HSCT aircraft operating at 2 km below the nominal cruise altitude with EI(SO_2)=0.4 and 50% gas to particle conversion under Scenario S7c relative to Scenario D7. Contours are -0.1, 0, 0.1, and 0.2, 0.4, 0.6, 0.8.

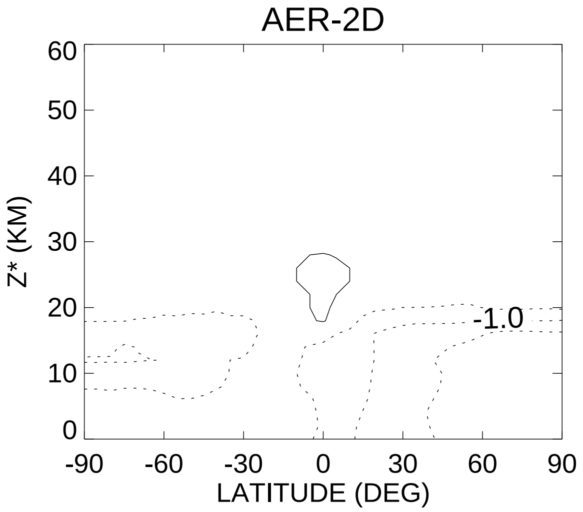

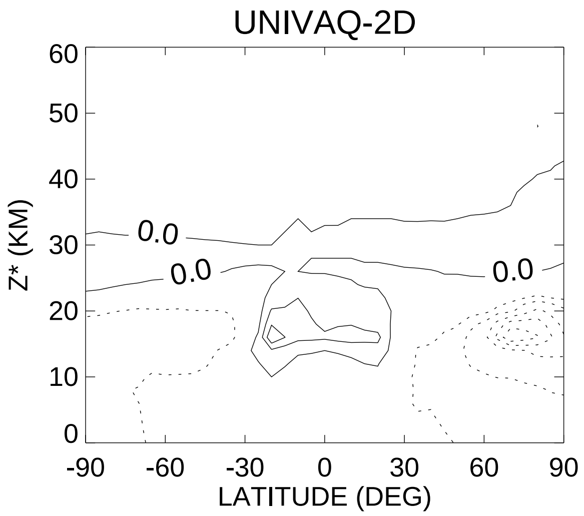

Figure 4.250: Calculated perturbations to O_3 (percent) as a function of latitude and altitude in March of 2015 due to emissions from a fleet of 500 HSCT aircraft operating at 2 km below the nominal cruise altitude with EI(NO_x)=5, EI(SO_2)=0.4, and 50% gas to particle conversion under Scenario S7c relative to Scenario D7. Contours are -4, -3, -2, -1, -0.5, 0, 0.5, 1.

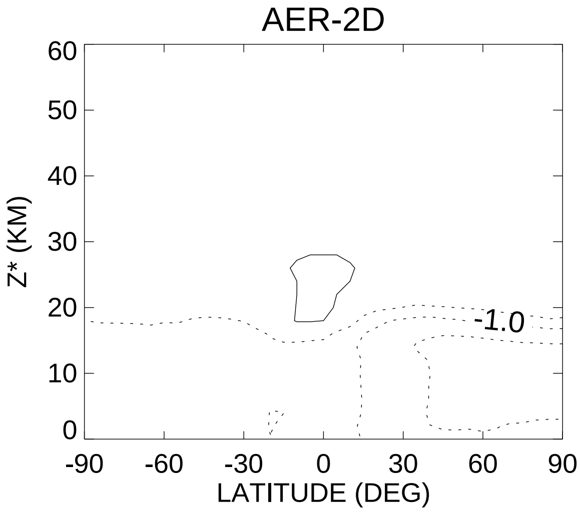

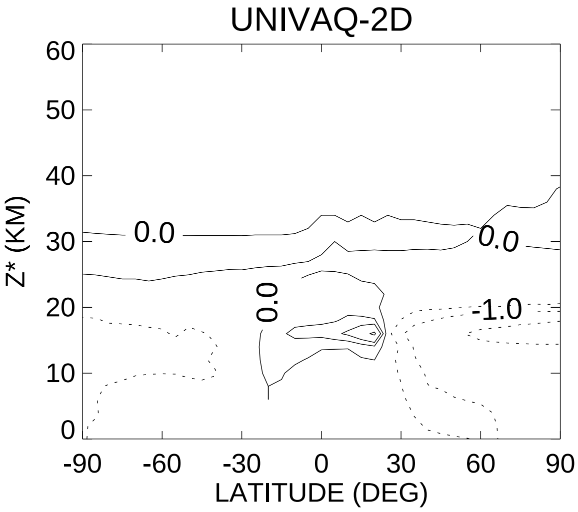

Figure 4.251: Calculated perturbations to O_3 (percent) as a function of latitude and altitude in June of 2015 due to emissions from a fleet of 500 HSCT aircraft operating at 2 km below the nominal cruise altitude with EI(NO_x)=5, EI(SO_2)=0.4, and 50% gas to particle conversion under Scenario S7c relative to Scenario D7. Contours are -2, -1, -0.5, 0, 0.5, 1, 2.

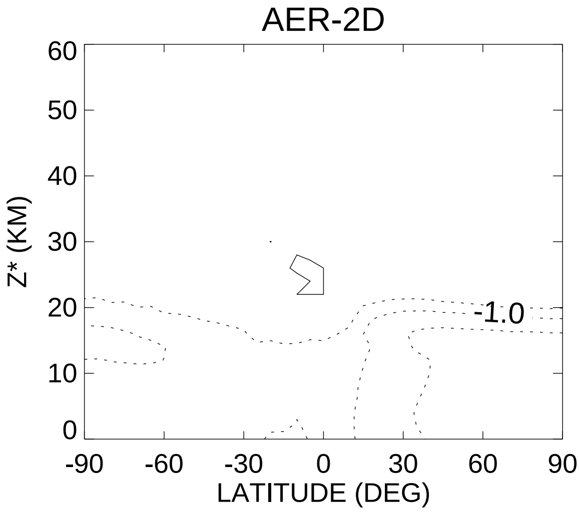

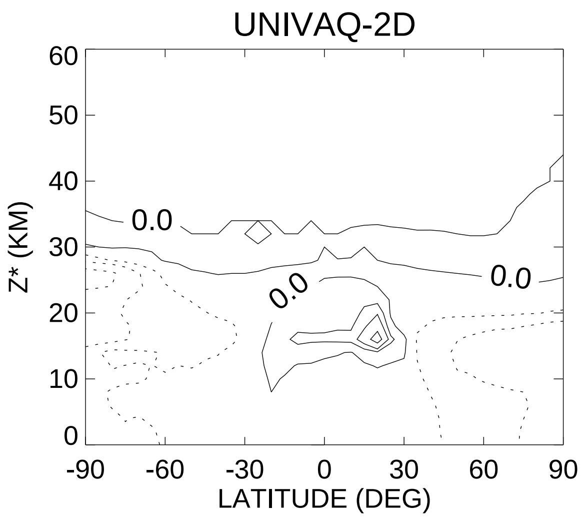

Figure 4.252: Calculated perturbations to O_3 (percent) as a function of latitude and altitude in October of 2015 due to emissions from a fleet of 500 HSCT aircraft operating at 2 km below the nominal cruise altitude with EI(NO_x)=5, EI(SO_2)=0.4, and 50% gas to particle conversion under Scenario S7c relative to Scenario D7. Contours are -2, -1, -0.5, 0, 0.5, 1, 2.

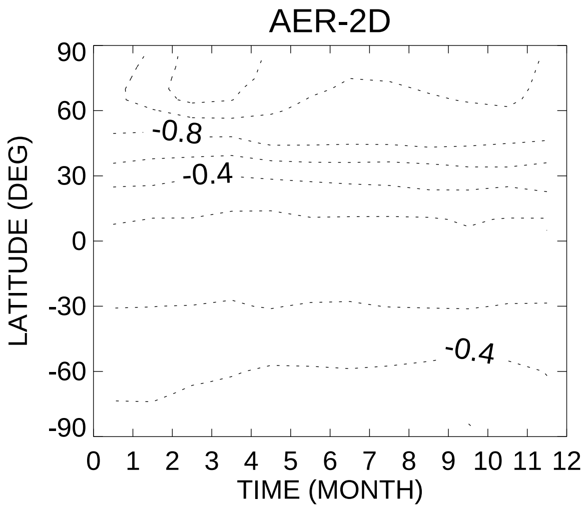

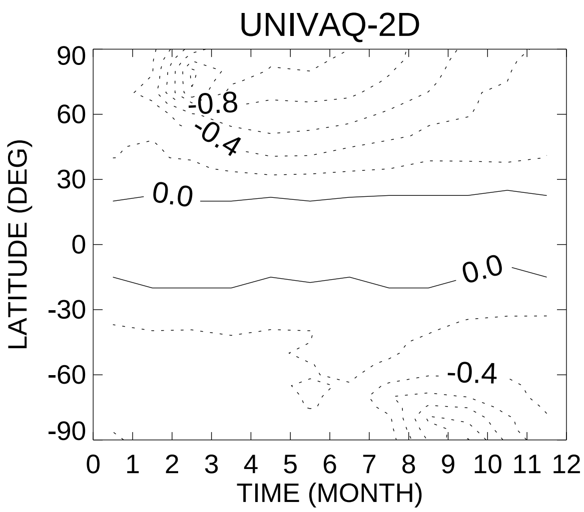

Figure 4.253: Calculated perturbations to column O_3 (percent) as a function of latitude and season in 2015 due to emissions from a fleet of 500 HSCT aircraft operating at 2 km below the nominal cruise altitude with EI(NO_x)=5, EI(SO_2)=0.4, and 50% gas to particle conversion under Scenario S7c relative to Scenario D7. Contours are -1.2 to 0 by 0.2.

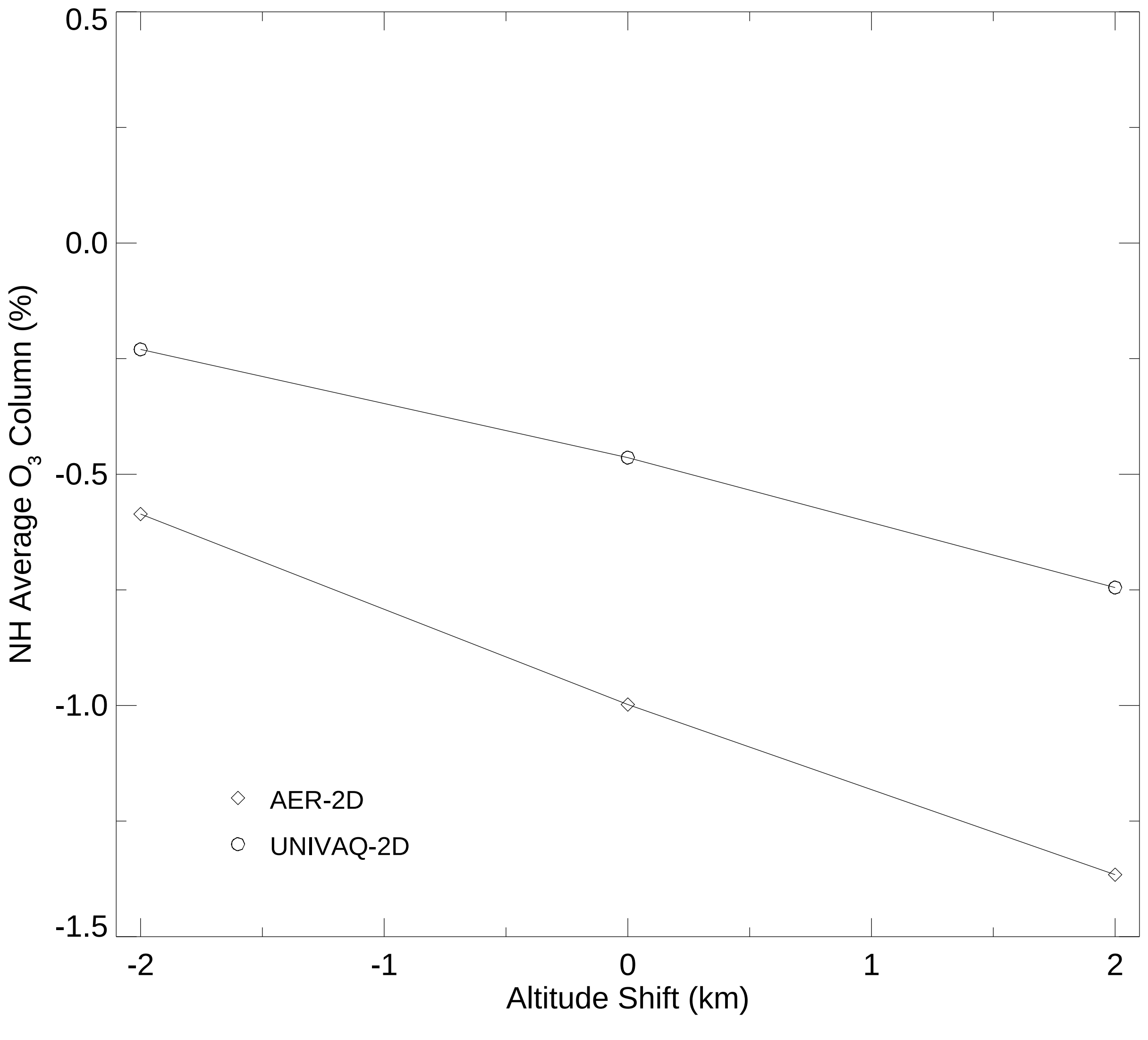

Figure 4.254: Northern hemisphere annual average total O_3 column change (percent) as a function of cruise altitude for an HSCT fleet of 500 aircraft operating in 2015 with $EI(NO_x)=5$ and sulfur emissions from aircraft assuming $EI(SO_2)=0.4$ and 50% particle conversion. These calculations were performed by the AER and UNIVAQ models with interactive microphysics.

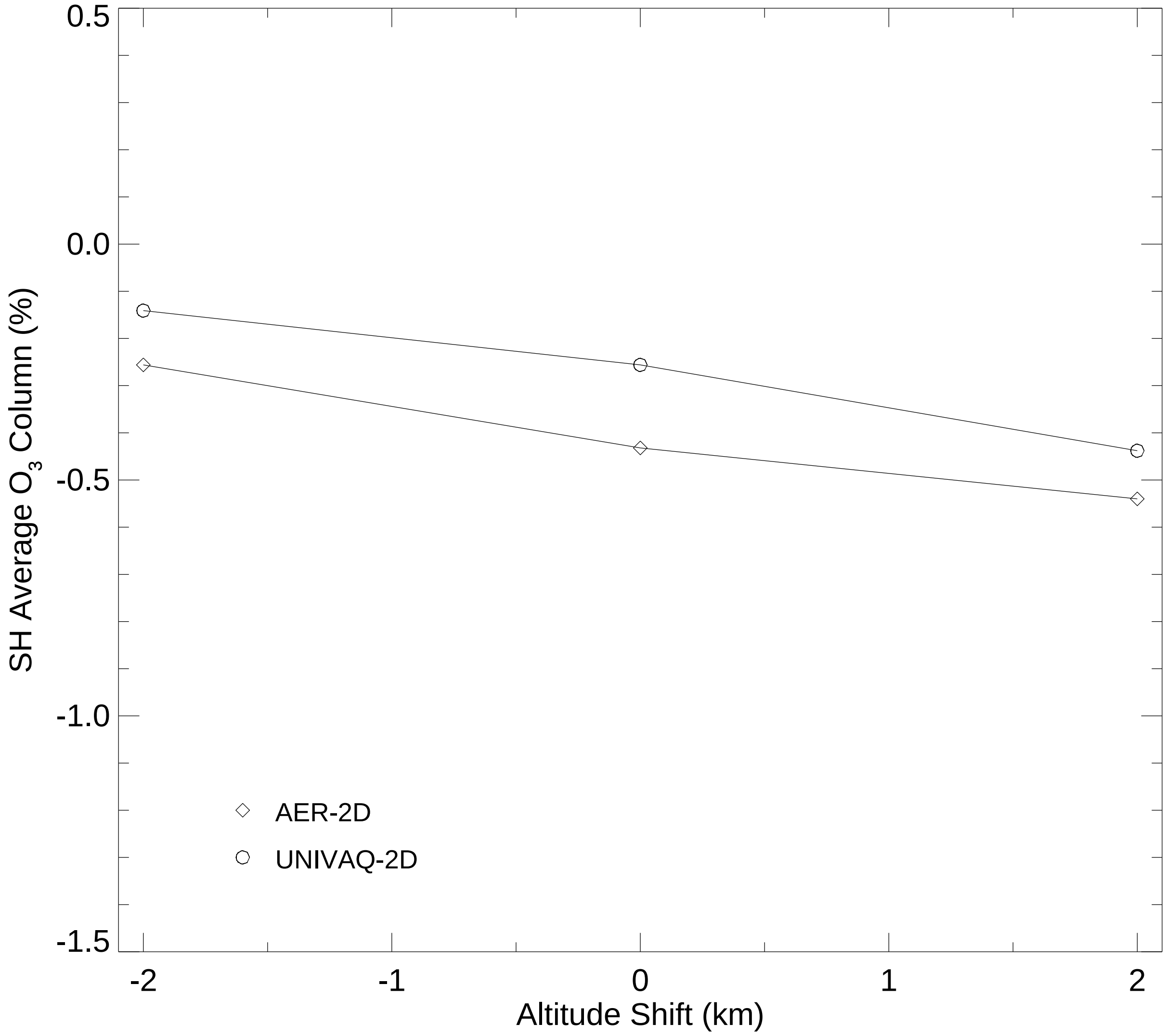

Figure 4.255: Southern hemisphere annual average total O_3 column change (percent) as a function of cruise altitude for an HSCT fleet of 500 aircraft operating in 2015 with EI(NO_x)=5 and sulfur emissions from aircraft assuming EI(SO_2)=0.4 and 50% particle conversion. These calculations were performed by the AER and UNIVAQ models with interactive microphysics.

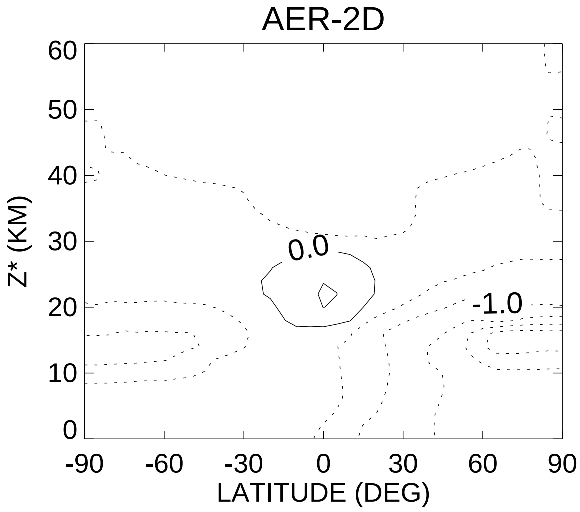

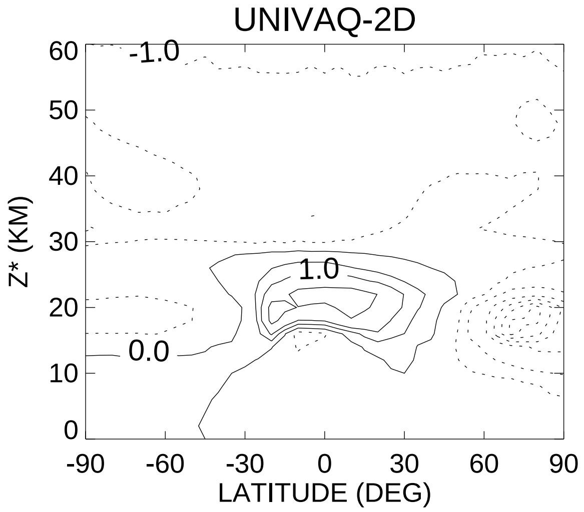

Figure 4.256: Calculated perturbations to O_3 (percent) as a function of latitude and altitude in March of 2015 due to emissions from a fleet of 500 HSCT aircraft with EI(NO_x)=10, EI(SO_2)=0.4, and 50% gas to particle conversion under Scenario S7d relative to Scenario D7. Contours are -3, -2, -1, -0.5, 0, 0.5, 1, 2.

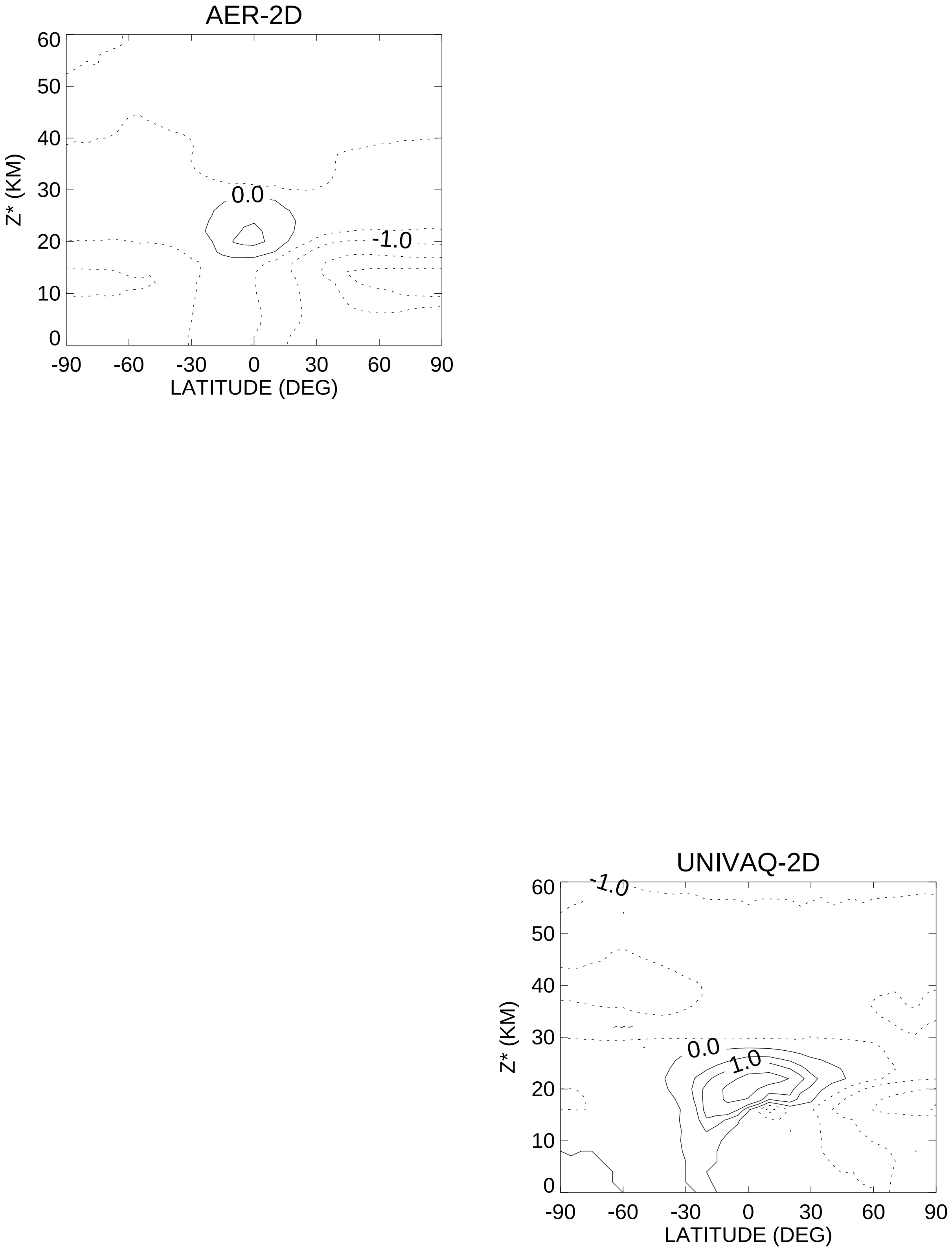

Figure 4.257: Calculated perturbations to O_3 (percent) as a function of latitude and altitude in June of 2015 due to emissions from a fleet of 500 HSCT aircraft with EI(NO_x)=10, EI(SO_2)=0.4, and 50% gas to particle conversion under Scenario S7d relative to Scenario D7. Contours are -3, -2, -1, -0.5, 0, 0.5, 1, 2.

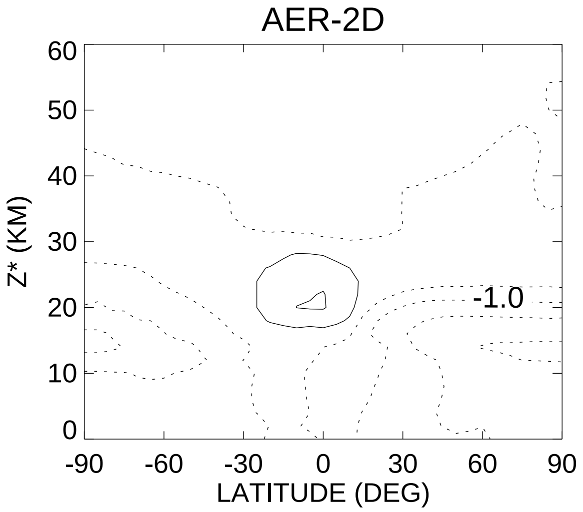

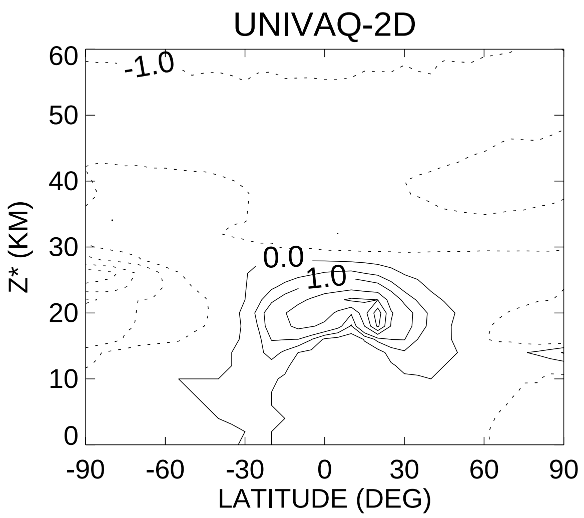

Figure 4.258: Calculated perturbations to O_3 (percent) as a function of latitude and altitude in October of 2015 due to emissions from a fleet of 500 HSCT aircraft with EI(NO_x)=10, EI(SO_2)=0.4, and 50% gas to particle conversion under Scenario S7d relative to Scenario D7. Contours are -3, -2, -1, -0.5, 0, 0.5, 1, 2, 3, 4.

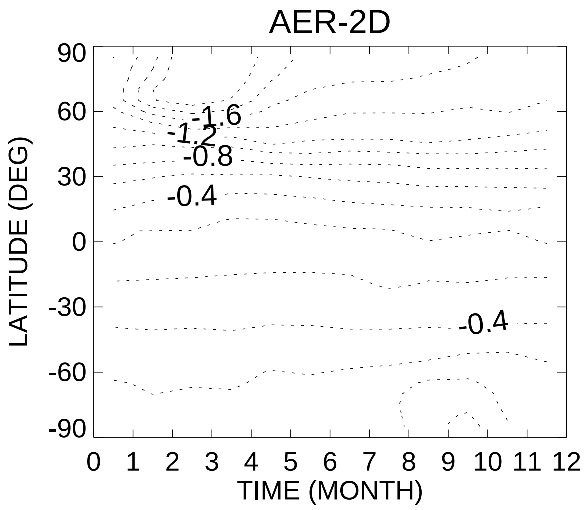

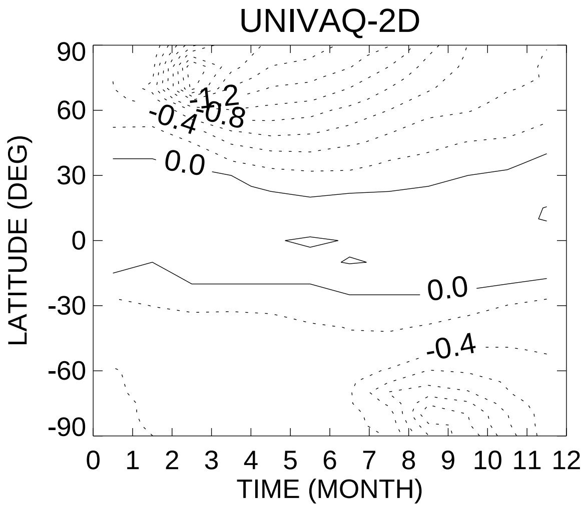

Figure 4.259: Calculated perturbations to column O_3 (percent) as a function of latitude and season in 2015 due to emissions from a fleet of 500 HSCT aircraft with EI(NO_x)=10, EI(SO_2)=0.4, and 50% gas to particle conversion under Scenario S7d relative to Scenario D7. Contours are -2 to +0.2 by 0.2.

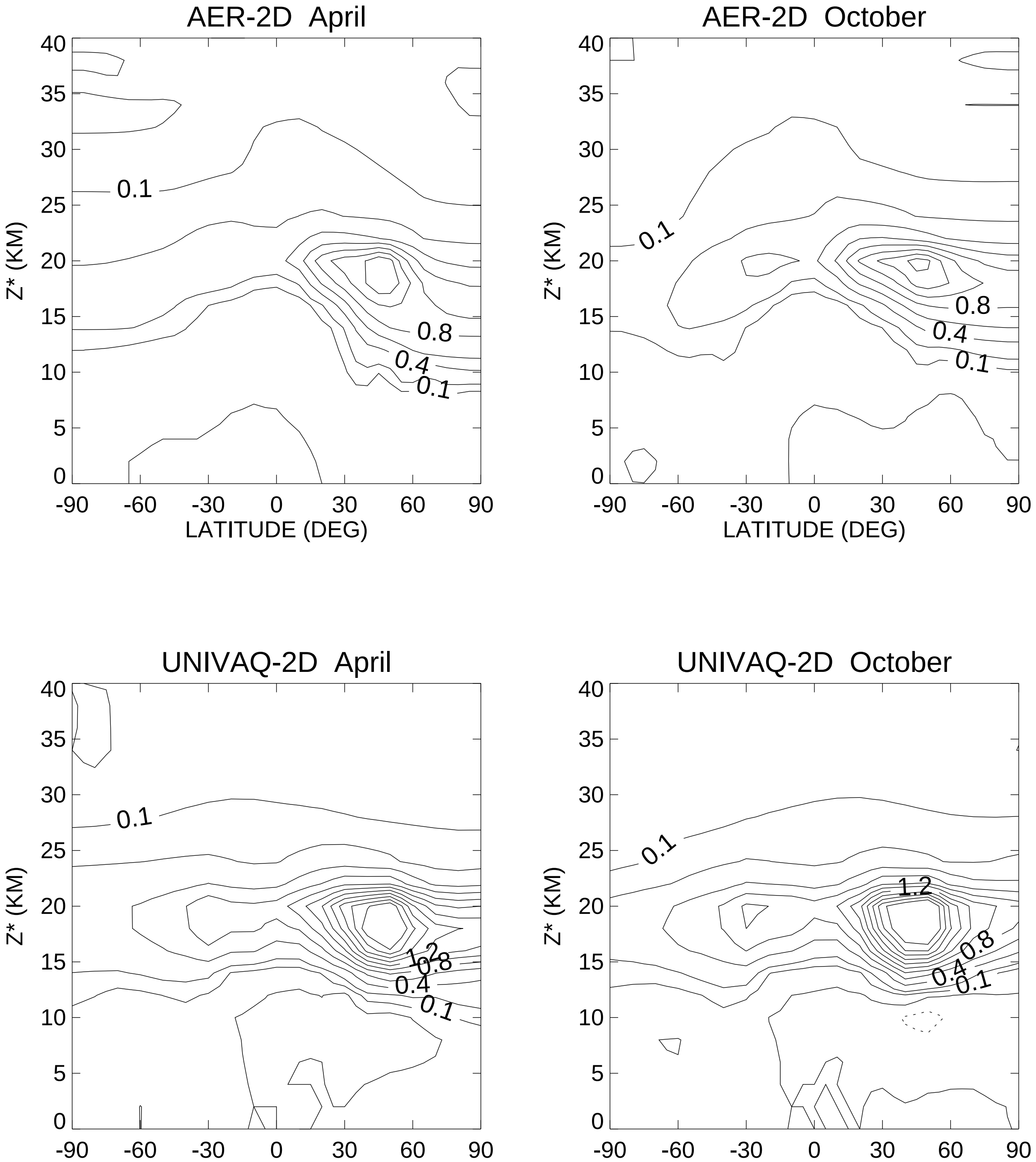

Figure 4.260: Calculated perturbations to aerosol surface area density ($\mu m^2/cm^3$) as a function of latitude and altitude in April and October due to emissions from a fleet of 500 HSCT aircraft with EI(SO_2)=0.4 and 100% gas to particle conversion under Scenario S8a relative to Scenario D8. Contours are -0.1, 0, 0.1, and 0.2 to 2.0 by 0.2.

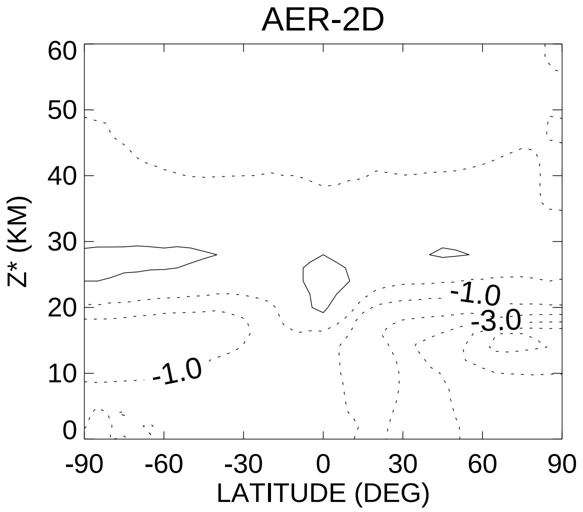

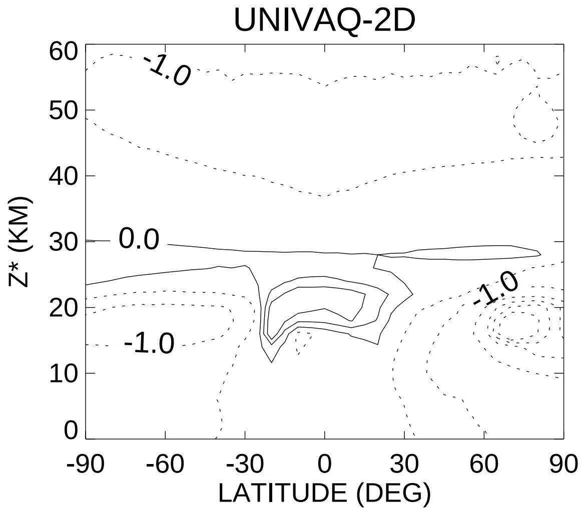

Figure 4.261: Calculated perturbations to O_3 (percent) as a function of latitude and altitude in March of 2015 due to emissions from a fleet of 500 HSCT aircraft with EI(NO_x)=5, EI(SO_2)=0.4, and 100% gas to particle conversion under Scenario S8a relative to Scenario D8. Contours are -5, -4, -3, -2, -1, -0.5, 0, 0.5, 1.

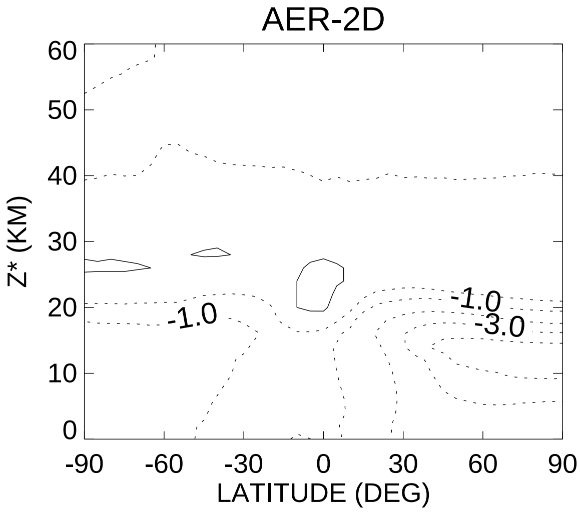

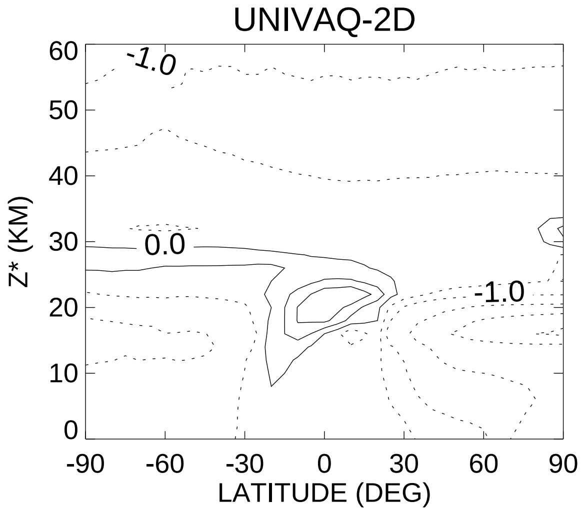

Figure 4.262: Calculated perturbations to O_3 (percent) as a function of latitude and altitude in June of 2015 due to emissions from a fleet of 500 HSCT aircraft with $EI(NO_x)=5$, $EI(SO_2)=0.4$, and 100% gas to particle conversion under Scenario S8a relative to Scenario D8. Contours are -4, -3, -2, -1, -0.5, 0, 0.5, 1.

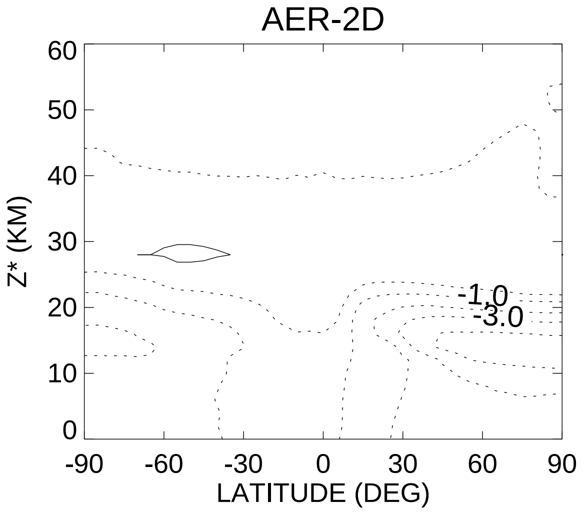

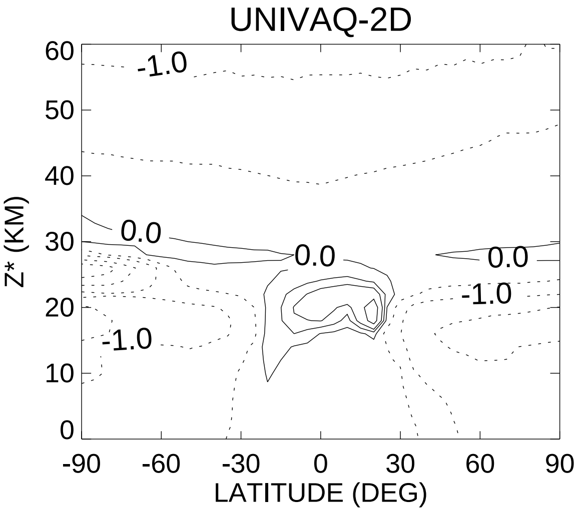

Figure 4.263: Calculated perturbations to O_3 (percent) as a function of latitude and altitude in October of 2015 due to emissions from a fleet of 500 HSCT aircraft with EI(NO_x)=5, EI(SO_2)=0.4, and 100% gas to particle conversion under Scenario S8a relative to Scenario D8. Contours are -4, -3, -2, -1, -0.5, 0, 0.5, 1, 2.

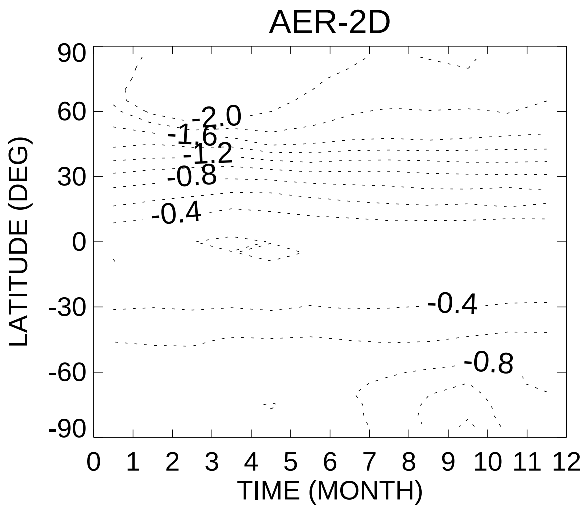

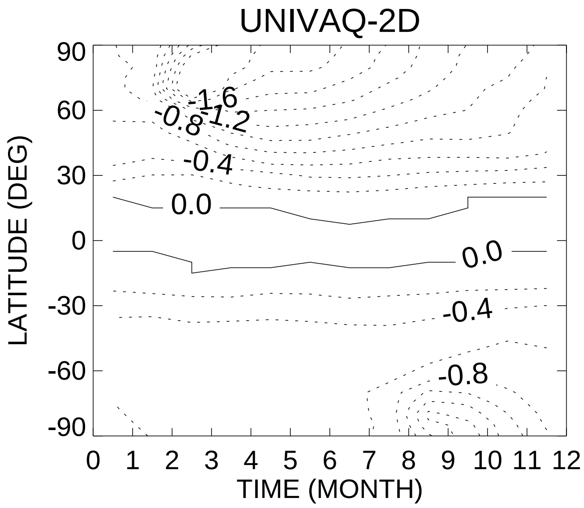

Figure 4.264: Calculated perturbations to column O_3 (percent) as a function of latitude and season in 2015 due to emissions from a fleet of 500 HSCT aircraft with $EI(NO_x)=5$, $EI(SO_2)=0.4$, and 100% gas to particle conversion under Scenario S8a relative to Scenario D8. Contours are -2 to 0 by 0.2.